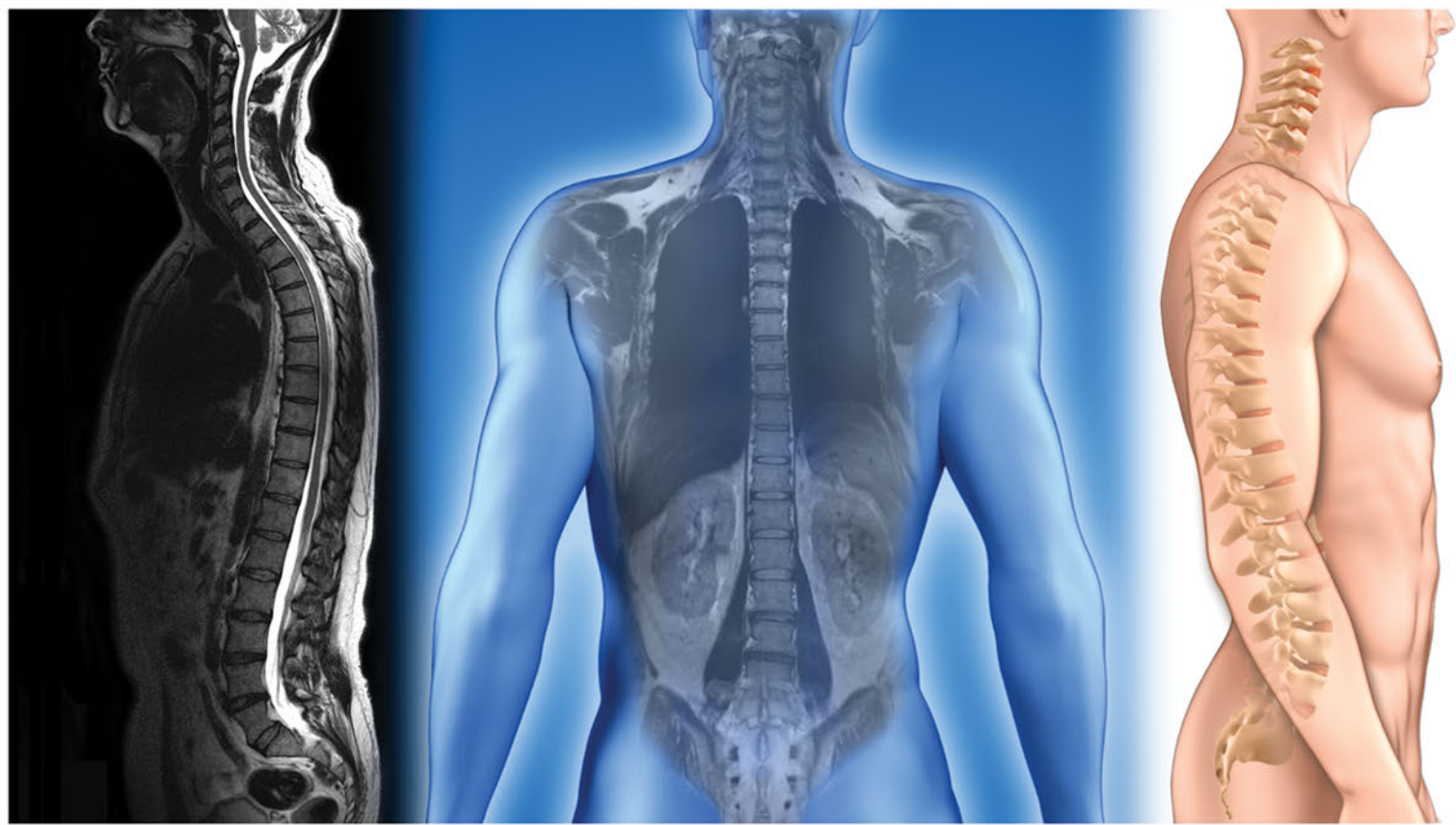


MRI Essentials for the Spine Specialist

A. Jay Khanna



MRI Essentials for the Spine Specialist

MRI Essentials for the Spine Specialist

A. Jay Khanna, MD, MBA

Associate Professor

Departments of Orthopaedic Surgery and Biomedical Engineering

The Johns Hopkins University School of Medicine

Baltimore, Maryland

Division Chief

Johns Hopkins Orthopaedic and Spine Surgery–National Capital Region

Bethesda, Maryland

Thieme

New York • Stuttgart • Delhi • Rio de Janeiro

Thieme Medical Publishers, Inc.
333 Seventh Ave.
New York, NY 10001

Executive Editor: Kay Conerly
Managing Editor: Judith Tomat
Editorial Assistant: Nikole Connors
Senior Vice President, Editorial and Electronic Product Development: Cornelia Schulze
Production Editor: Kenneth L. Chumbley
International Production Director: Andreas Schabert
Vice President, Finance and Accounts: Sarah Vanderbilt
President: Brian D. Scanlan
Printer: Replika Press

Library of Congress Cataloging-in-Publication Data

MRI for spine surgeons and specialists / [edited by] A. Jay Khanna.

p. ; cm.

Includes bibliographical references.

ISBN 978-1-60406-877-1 (alk. paper)—ISBN 978-1-60406-878-8 (eISBN)

I. Khanna, A. Jay., editor of compilation.

[DNLM: 1. Spinal Diseases—surgery. 2. Spine—surgery. 3. Magnetic Resonance Imaging—methods. 4. Spine—
anatomy & histology. WE 725]

RD768

617.5'607548--dc23

2014002562

Copyright © 2014 by Thieme Medical Publishers, Inc.

Thieme Publishers New York 333 Seventh Avenue, New York, NY 10001 USA, 1-800-782-3488, customerservice@thieme.com; Thieme Publishers Stuttgart Rüdigerstrasse 14, 70469 Stuttgart, Germany, +49 [0]711 8931 421, customerservice@thieme.de; Thieme Publishers Delhi A-12, Second Floor, Sector -2, NOIDA -201301, Uttar Pradesh, India +91 120 45 566 00, customerservice@thieme.in; Thieme Publishers Rio, Thieme Publicações Ltda. Argentina Building 16th floor, Ala A, 228 Praia do Botafogo Rio de Janeiro 22250-040 Brazil, +55 21 3736-3631

This book, including all parts thereof, is legally protected by copyright. Any use, exploitation, or commercialization outside the narrow limits set by copyright legislation without the publisher's consent is illegal and liable to prosecution. This applies in particular to photostat reproduction, copying, mimeographing or duplication of any kind, translating, preparation of microfilms, and electronic data processing and storage.

Important note: Medical knowledge is ever-changing. As new research and clinical experience broaden our knowledge, changes in treatment and drug therapy may be required. The authors and editors of the material herein have consulted sources believed to be reliable in their efforts to provide information that is complete and in accord with the standards accepted at the time of publication. However, in view of the possibility of human error by the authors, editors, or publisher of the work herein or changes in medical knowledge, neither the authors, editors, nor publisher, nor any other party who has been involved in the preparation of this work, warrants that the information contained herein is in every respect accurate or complete, and they are not responsible for any errors or omissions or for the results obtained from use of such information. Readers are encouraged to confirm the information contained herein with other sources. For example, readers are advised to check the product information sheet included in the package of each drug they plan to administer to be certain that the information contained in this publication is accurate and that changes have not been made in the recommended dose or in the contraindications for administration. This recommendation is of particular importance in connection with new or infrequently used drugs.

Some of the product names, patents, and registered designs referred to in this book are in fact registered trademarks or proprietary names even though specific reference to this fact is not always made in the text. Therefore, the appearance of a name without designation as proprietary is not to be construed as a representation by the publisher that it is in the public domain.

Printed in India

5 4 3 2 1

ISBN 978-1-60406-877-1

Also available as an ebook:
eISBN 978-1-60406-878-8



I dedicate this book to the most precious people in my life—my wife, Roma, and our children, Rajan and Priya.

Contents

Foreword	ix
Preface	xi
Acknowledgments	xiii
Contributors	xv
I Initial Considerations	
1 Essentials of MRI Physics and Pulse Sequences	3
<i>Shivani Ahlawat, Rick W. Obray, Douglas P. Beall, John D. Reeder, John A. Carrino, and Laura M. Fayad</i>	
2 Normal Spine MRI Anatomy	19
<i>Swati Deshmukh, John A. Carrino, J. Dana Dunleavy, and A. Jay Khanna</i>	
3 Common Clinical and Correlative Pain Generators of the Cervical and Lumbosacral Spine	45
<i>Josemaria Paterno, Chad M. Silverberg, A. Jay Khanna, and Aneesh K. Singla</i>	
4 A Systematic Approach to the Review of Spine MRI Studies	68
<i>A. Jay Khanna</i>	
II Spine	
5 The Occipitocervical Junction	87
<i>Colin M. Haines, A. Jay Khanna, John A. Carrino, Shih-Chun David Lin, and Joseph R. O'Brien</i>	
6 The Cervical Spine	111
<i>Lukas P. Zebala, Jacob M. Buchowski, Aditya Daftary, Joseph R. O'Brien, John A. Carrino, and A. Jay Khanna</i>	
7 The Lumbar and Thoracic Spine	155
<i>Gbolahan O. Okubadejo, Aditya Daftary, Jacob M. Buchowski, John A. Carrino, and A. Jay Khanna</i>	
8 Tumors of the Spine	211
<i>Daniel M. Sciubba, Patricia L. Zadnik, Bruce A. Wasserman, and Ziya L. Gokaslan</i>	
9 MRI of the Pediatric Spine	237
<i>A. Jay Khanna, Bruce A. Wasserman, and Paul D. Sponseller</i>	
III Special Conditions	
10 Advanced Techniques in Spine MRI	253
<i>Joseph P. Gjolaj and John A. Carrino</i>	

11	Correlation of MRI with Other Imaging Studies	267
	<i>Shivani Ahlawat, Uma Srikumaran, A. Jay Khanna, and Laura M. Fayad</i>	
12	MRI Safety Considerations for the Referring Clinician	280
	<i>Monica D. Watkins and Bruce A. Wasserman</i>	
	Glossary	289
	Index	291

Foreword

Given the large number of publications, journals, and textbooks available in the area of spinal disorders, it is refreshing to see a practical, focused text on a topic that is universally critical to all practitioners who care for patients with spinal pathologies. The introduction of MRI technology revolutionized all medical diagnostics, but it arguably is the single most important advancement in the evaluation of spinal pathology. The ability to interpret and relate spinal abnormalities, detected on the MRI study, into the treatment algorithms for our patients is an essential element in the successful clinical treatment of patients with a broad range of spinal pathologies. It is important for any practitioner to be able to accurately interpret an MRI study because, although some findings can be quite subtle, the consequences of making inaccurate interpretations or “missing” significant pathology can have catastrophic effects on the ultimate outcome of our patients. In addition, many studies have shown that the sensitivity of MRI technology and the presence of age-appropriate degenerative changes that occur normally in patients with increasing age should be considered. The ability to detect spinal pathology, put it in the appropriate clinical context, and minimize the treatment of nonrelevant pathology is truly an art form in the treatment of our patients. The lower success rates of spinal interventions and surgery may arguably be the result, at least in part, of “over-reading” or over-emphasizing the significance of some MRI findings. Regardless, the ability to accurately interpret spinal MRI studies is critical, and this textbook is an extremely valuable resource for all spinal practitioners.

MRI for Spine Surgeons and Specialists is a textbook written by spine surgeons, spine specialists, and radiologists to detail the relatively complex MRI anatomy of the spine and the spectrum of pathological findings in spinal disorders. I congratulate the editor and all the authors of this text for putting forth

the core concepts of MRI technology as they relate to the spine, with correlative chapters on anatomic pain generators and MRI findings. The second part of the text is focused on the different anatomic areas of the spine from the occiput to the sacrum. The last portion of the text explores more advanced concepts and special considerations for pediatric patients, tumors, MRI safety, and the correlation of MRI studies with other imaging studies. Taken as a whole, this is a comprehensive compilation of all aspects of the use of MRI for imaging the spine and spinal pathologies.

The editor of this textbook, Dr. Jay Khanna, has great experience in MR imaging and is a passionate educator on this topic. He has created several educational efforts in this specific area and has taught several courses, conducted meetings, and edited other texts on MR imaging. As a noted expert in the field, he has constantly striven to create new resources to help spine surgeons and specialists utilize this technology in order to ultimately help with better care for our patients.

I believe this text is a crucial collection of information that all spine practitioners should read and utilize as a resource in the diagnosis and treatment of our patients with spinal disorders. I commend the editor and all the authors for their commitment to this educational endeavor and anticipate that this text will be well received by all spine specialists, both operative and nonoperative.

Jeffrey C. Wang, MD
Co-Director, University of Southern California
Spine Institute
Chief, Orthopaedic Spine Service
Professor of Orthopaedic Surgery and Neurosurgery
University of Southern California
Department of Orthopaedic Surgery
Los Angeles, California

Preface

Although the ability to evaluate MRI studies is critical to the clinical and surgical care of patients with spine pathology, most clinicians learn this skill in an informal fashion, by experience gained throughout their training and in clinical practice. As a result, we may not have (or need) a thorough understanding of the science and physics of MR imaging and the various pulse sequences that are available for obtaining the images. Many of us clinicians prefer to read our patients' MR imaging studies ourselves rather than rely solely on the "official" radiologist's report. We learn to make preoperative, intraoperative, and postoperative decisions based on those readings. However, unlike radiologists who are trained to evaluate MRI studies in a systematic fashion, we may be more likely to evaluate the images in a less organized manner and to rely on our anatomic expertise and experience, which may not be the most effective method.

This text, *MRI Essentials for the Spine Specialist*, will teach the reader how to systematically evaluate and interpret MR imaging studies of the spine. Specialists who may benefit from reading and referencing this book include spine surgeons, interventional and noninterventional pain specialists, interventional radiologists, physiatrists, rheumatologists, neurologists, sports medicine specialists, and any other physicians or allied health professionals who have an interest or expertise in the management of patients with spinal disorders. This book is also an excellent reference for diagnostic radiologists who interpret spine MRI studies and would like to gain a better appreciation of the associated clinical aspects.

Although there are many excellent books that focus on MR imaging of the spine, this one is unique in that it is written by spine surgeons (with both orthopaedic and neurosurgical backgrounds), interventional pain specialists, and radiologists specifically for clinicians. As such, it is clinically oriented and presents the information from a perspective that a spine surgeon or specialist will appreciate.

My desire to create this book stems from my interest and background in musculoskeletal imaging and from my recognition of the fact that the ability to accurately evaluate MR imaging studies is critical to the care of patients with spinal pathology. Along these lines, over the last several years, I have helped develop and deliver several courses for spine surgeons in practice and in training that teach them how to systematically evaluate MR imaging studies of the spine. In doing so, I realized that many of the text-

books and other resources on the topic of spine MRI are written by radiologists and directed toward radiologists and radiologists in training. This perceived void of imaging resources for clinicians who care for patients with spine and other musculoskeletal pathologies led me to compile and edit the predecessor of this book, *MRI for Orthopaedic Surgeons*, which was also published by Thieme Medical Publishers. That textbook provided an overview of MR imaging of the entire musculoskeletal system by anatomic region. Given the success of that book and my personal interest in providing a more in-depth evaluation of my primary area of clinical interest, the spine, we decided to create this textbook. Thieme Medical Publishers has graciously allowed me to reuse some of the relevant text, images, and drawings from *MRI for Orthopaedic Surgeons*, and I have built upon that content with current theories and practices, contributions authored by acknowledged experts, and additional illustrative material.

The chapters of *MRI Essentials for the Spine Specialist* are organized into three sections: (1) Core Concepts, (2) Anatomical Regions of the Spine: Spectrum of Disease, and (3) Advanced Concepts and Special Considerations. Each of these three sections, or each chapter, can be read independently, but the textbook is best read in sequential chapter order. In particular, before reading the chapters on individual spinal regions, the clinician should review Chapter 2, "Normal Spine MRI Anatomy," and Chapter 3, "Common Clinical and Correlative Pain Generators of the Cervical and Lumbosacral Spine." These two chapters provide a moderately comprehensive evaluation of the key anatomic structures and concepts with which one should be familiar when reviewing an MR imaging study of the occipitocervical, cervical, thoracolumbar, and lumbosacral spine; they also serve as a reference point when evaluating the pathologic images in a region-specific chapter.

This book features two different types of chapters: region-specific and concept-specific. The region-specific chapters (e.g., Chapter 6, "The Cervical Spine," and Chapter 7, "The Lumbar and Thoracic Spine") share a common organization, with sections on specialized pulse sequences and protocols, traumatic pathology, degenerative pathology, infectious conditions, and postoperative findings. The concept-specific chapters (e.g., Chapter 10, "Advanced Techniques in Spine MRI") are organized in a fashion that best suits the individual chapter's content and the goal

of providing spine surgeons and specialists with the information they need to maximize their proficiency in evaluating and interpreting MR imaging studies.

MRI Essentials for the Spine Specialist contains nearly 450 MR images and approximately 150 artist's drawings that have been carefully selected and created to help illustrate and teach the essential anatomy and pathology that a spine surgeon, other clinician, or radiologist should be able to recognize and define when evaluating an MRI study of the spine. As such, much of the material can be reviewed effectively by evaluating the images and illustrations along with the associated figure legends. In addition, this book contains a new feature, which is a set of Common Clinical Questions (with answers and explanations) for each chapter. These questions will also allow the reader to review the material efficiently and test his or her comprehension of some of the key concepts from each chapter.

Most of the chapters have been authored by spine surgeons, interventional pain specialists, and radiologists. Some, such as the region-specific chapters, have spine surgeons as the primary authors, with radiologists as co-authors for accuracy and clarity from their standpoint. Others (e.g., "Essentials of MRI Physics and Pulse Sequences") were written solely by radiologists, but the presentation of the material was specifically designed with a clinician audience in mind. The collaboration between clinicians and radiologists that has been used to produce this textbook emulates the optimal relationship between these two groups of physicians in clinical practice.

This book was envisioned to be a practical aid to develop and/or refine the skills needed to effectively and systematically evaluate MR imaging studies of the spine. I hope that it accomplishes this goal for you.

A. Jay Khanna, MD, MBA

† added to figure legend or table title indicates that the figure or table was borrowed from Dr. Khanna's book, *MRI for Orthopaedic Surgeons*.

Acknowledgments

First and foremost, I would like to thank the many contributors to this text. They have given generously of their time and willingly shared their knowledge gained from years of clinical and research experience, which has culminated in the information-packed pages of this book.

Next, a sincere thank you to Kay Conerly, executive editor at Thieme, for inviting me to help create this book under the Thieme banner and for allowing us to follow in the success of our previous book together, *MRI for Orthopaedic Surgeons*. Thanks, as well, to Judith Tomat at Thieme for her outstanding efforts in bringing this book through the publishing process and helping us navigate our way through the various steps from concept to final product. Thanks, also, to Kenneth Chumbley, production editor, for his meticulous work during the final phase of the book and specifically for helping us solve the puzzle of merging numerous images and illustrations with the text to create a beautiful layout. A very special thank

you to Tony Pazos, medical illustrator extraordinaire, for his skill, attention to detail, and willingness to work through many rounds of revisions. Thanks also to Jennifer Pryll for conceptualizing and creating the cover art, which creatively illustrates the intention of this book, which is to focus on the convergence of the clinical presentation of our patients and the radiographic manifestations of their spinal conditions.

Finally, I would like to express my greatest appreciation to Elaine Henze, medical editor for The Johns Hopkins University's Department of Orthopaedic Surgery. She, with the support of Jenni Weems, has spent countless hours on this project at work and on her own time during an especially challenging personal year. I thank Elaine for helping me with the multiple rounds of edits and revisions for every chapter, table, image, figure, and legend. Her commitment to accuracy and focus on quality have helped ensure this book is the excellent product you see today.

Contributors

Shivani Ahlawat, MD

Clinical Instructor
Department of Radiology, Musculoskeletal Section
The Johns Hopkins University School of Medicine
Baltimore, Maryland

Douglas P. Beall, MD

Chief of Radiology Services
Clinical Radiology of Oklahoma
Oklahoma City, Oklahoma
Chief of Radiology Services
Summit Medical Center
Edmond, Oklahoma
Adjunct Faculty
Department of Orthopedics Bone and Joint Hospital
at St. Anthony
Oklahoma City, Oklahoma

Jacob M. Buchowski, MD, MS

Associate Professor of Orthopaedic Surgery and
Neurological Surgery
Department of Orthopaedic Surgery
Washington University in St. Louis
St. Louis, Missouri

John A. Carrino, MD, MPH

Associate Professor of Radiology and Orthopaedic
Surgery
The Johns Hopkins University School of Medicine
Section Chief, Musculoskeletal Radiology
Russell H. Morgan Department of Radiology and
Radiological Science
Baltimore, Maryland

Aditya Daftary, MBBS

Consultant Radiologist
InnoVision Imaging and SportsMed Mumbai
Mumbai, India

Swati Deshmukh, MD

Department of Radiology
Johns Hopkins Hospital
Baltimore, Maryland

J. Dana Dunleavy, MD

Director of Interventional Radiology
Windsong Radiology Group
Buffalo, New York

Laura M. Fayad, MD

Associate Professor of Radiology, Orthopaedic
Surgery, and Oncology
Director of Translational Research for Advanced
Imaging
The Russell H. Morgan Department of Radiology
and Radiological Science
The Johns Hopkins University School of Medicine
Baltimore, Maryland

Joseph P. Gjolaj, MD

Assistant Professor
Department of Orthopaedics and Rehabilitation
University of Miami Miller School of Medicine
Miami, Florida

Ziya L. Gokaslan, MD, FACS

Donlin M. Long Professor
Professor of Neurosurgery, Oncology and
Orthopaedic Surgery
Vice Chairman, Department of Neurosurgery
Director, Neurosurgical Spine Program
Director, Neurosurgical Spine Metastasis Center
Department of Neurosurgery
The Johns Hopkins University School of Medicine
Baltimore, Maryland

Colin M. Haines, MD

Department of Orthopaedic Surgery
George Washington University
Washington, DC

A. Jay Khanna, MD, MBA

Associate Professor
Departments of Orthopaedic Surgery and
Biomedical Engineering
The Johns Hopkins University School of Medicine
Baltimore, Maryland
Division Chief
Johns Hopkins Orthopaedic and Spine Surgery–
National Capital Region
Bethesda, Maryland

Shih-Chun David Lin, MD, PhD

Neurosurgeon
Suburban Hospital
Johns Hopkins Medicine
Bethesda, Maryland

Joseph R. O'Brien, MD, MPH

Associate Professor of Orthopaedic Surgery and
Neurological Surgery
George Washington University School of Medicine
and Health Sciences
Washington, DC

Rick W. O Bray, MD

Southwest Spine and Pain Center
Director
Spine and Pain Medicine—Dixie Regional Medical
Center
St. George, Utah

Gbolahan O. Okubadejo, MD, FAAOS

Spine Surgeon
The Institute for Comprehensive Spine Care
New York, New York

Josemaria Paterno, MD

Interventional Pain Fellow
Brigham and Women's Hospital
Department of Anesthesiology and Pain Medicine
Harvard Medical School
Boston, Massachusetts

John D. Reeder, MD, FACR

Director of Imaging
Proscan Imaging Columbia
Columbia, Maryland

Daniel M. Sciubba, MD

Assistant Professor of Neurosurgery
Department of Oncology and Orthopaedic Surgery
The Johns Hopkins University School of Medicine
Baltimore, Maryland

Chad M. Silverberg, DO

Musculoskeletal Radiologist and Interventionalist
Progressive Radiology
Washington, DC

Aneesh K. Singla, MD, MPH

Physician and Partner
National Spine and Pain Centers
Bethesda, Maryland
Lecturer
Harvard Medical School
Boston, Massachusetts

Paul D. Sponseller, MD, MBA

Professor and Head
Department of Pediatric Orthopaedics
Johns Hopkins Bloomberg Children's Hospital
Baltimore, Maryland

Uma Srikumaran, MD

Assistant Professor of Orthopaedic Surgery
Johns Hopkins Shoulder and Sports Medicine
Johns Hopkins Community Physicians
Baltimore, Maryland

Bruce A. Wasserman, MD

Professor of Radiology
Director of Diagnostic Neurovascular Imaging
Russell H. Morgan Department of Radiology and
Radiological Sciences
The Johns Hopkins University School of Medicine
Baltimore, Maryland

Monica D. Watkins, MD

Neuroradiologist
American Radiology
Howard County General Hospital (a Johns Hopkins
affiliate)
Columbia, Maryland

Patricia L. Zadnik, BA

Department of Neurosurgery
The Johns Hopkins University School of Medicine
Baltimore, Maryland

Lukas P. Zebala, MD

Assistant Professor
Department of Orthopaedic Surgery
Washington University in St. Louis
St. Louis, Missouri

I Initial Considerations

1 Essentials of MRI Physics and Pulse Sequences

Shivani Ahlawat, Rick W. Obray, Douglas P. Beall, John D. Reeder, John A. Carrino, and Laura M. Fayad

CHAPTER OUTLINE

- I. Fundamentals of MRI
 - A. Magnetization of Nuclei and Tissues and the Larmor Equation
 - B. T1, T2, and T2*
 - C. Gradient Coils and Signal Localization
 - D. MRI Pulse Sequence and TE, TR, and TI
- II. MRI Applications
 - A. Standard Sequences
 - 1. T1-Weighted SE
 - 2. T2-Weighted SE and T2-Weighted FSE
 - 3. Fat Suppression with T1-Weighted and T2-Weighted
 - 4. STIR
 - 5. Gradient Echo, 3D Gradient Echo
 - B. Contrast-Enhanced Imaging
- III. Artifacts
- IV. Summary

MRI is an essential tool in the accurate diagnosis and treatment of spine disease. The number of MRI applications has increased dramatically over the past two decades and will likely continue to increase. A detailed understanding of the fundamentals of MRI physics is not required to review images, although a basic working knowledge of certain key principles is important for the accurate utilization of the technology. This chapter provides the reader with a basic understanding of the physics behind MRI by addressing its specific applications for the spine, by emphasizing how an MR image is generated, and by describing what basic sequences are important for optimally showing spine anatomy. The intent is to provide the reader with a sufficient working knowledge of the technology to enable the reader to acquire and in-

terpret high-quality images in a reasonable amount of time. This chapter is only a brief introduction to what most would consider a complex technology, and the reader is referred to additional sources for more detailed explanations.¹⁻⁶

■ Fundamentals of MRI

Magnetization of Nuclei and Tissues and the Larmor Equation

Understanding how an MR image is generated requires some knowledge of the basic physical properties of the nucleus of an atom and its components, that is, neutrons and protons. All neutrons and protons within the nucleus spin about their axes and generate a magnetic field called a magnetic dipole (**Fig. 1.1**). When the total number of protons and neutrons is even, their magnetic dipoles cancel each other out. However, nuclei with an odd total number of protons and neutrons generate a net magnetic moment, which can be represented as a vector. When placed in a magnetic field, odd-numbered nuclei, because of their magnetic moments, align parallel to the external magnetic field in one of two orientations: spin-up (in the same direction as the field) or spin-down (in the opposite direction to the field; **Fig. 1.2**). A small excess of nuclei align in a spin-up orientation (because it has slightly greater stability) and generate an overall small net magnetization vector (**Fig. 1.3**). Conveniently, the human body is replete with hydrogen, whose nucleus consists of one proton and no neutrons. This hydrogen is most common in water (which makes up the majority of the body's mass) and in fat. The body also contains a lesser amount of fluorine, whose nucleus contains 9 protons and 10 neutrons. It is the manipulation within an external magnetic field of this small number of excess spin-up, odd-numbered nuclei that is the basis for the signal that ultimately generates an MR image.^{1,2}

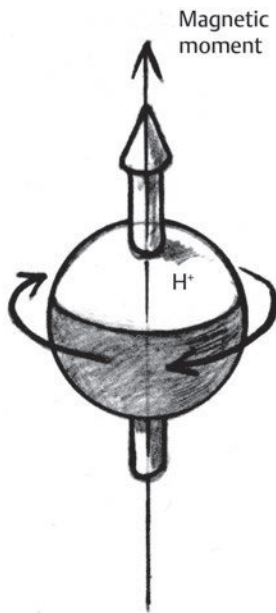


Fig. 1.1 Neutrons and protons within the nucleus spin about their axes and generate a directional magnetic field called a magnetic dipole. In this illustration, the dipole is pointing upward.[†]

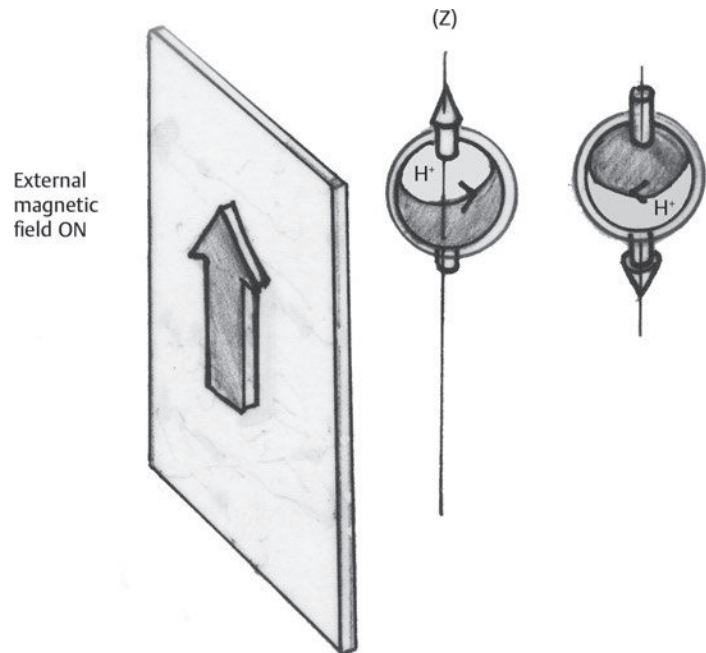


Fig. 1.2 Odd-numbered nuclei may exist in one of two energy states when placed in an external magnetic field: spin-up or spin-down orientation, that is, parallel to and aligned with the external magnetic field (*large arrow*) or parallel to and in an opposite direction to the external magnetic field. The spin-up orientation (z) is a slightly more stable energy state.[†]

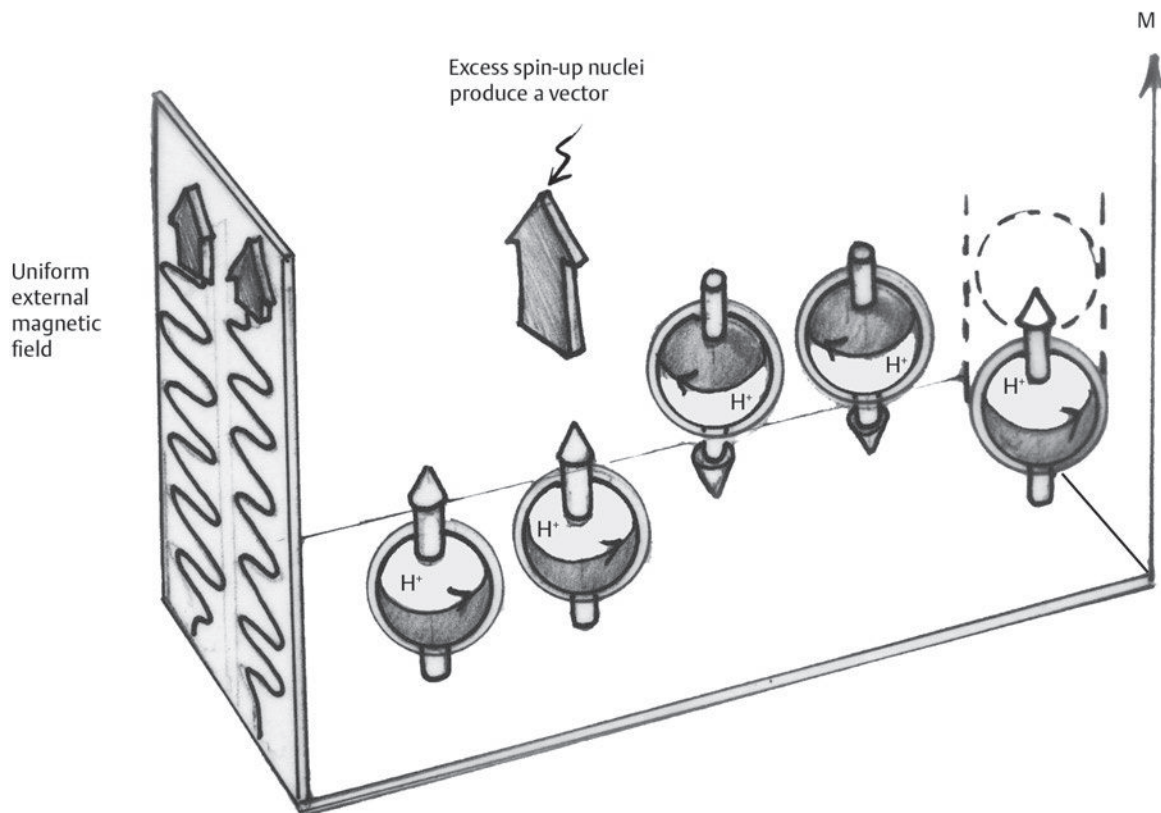


Fig. 1.3 The slight excess of nuclei in the spin-up orientation is the result of the increased stability of the spin-up orientation relative to the spin-down orientation, and it produces a net magnetization vector (*large arrow*) that can be manipulated to create an RF signal, which in turn can be used to create an MR image. The two *smaller arrows* depict the direction of the external magnetic field (M).[†]

When spinning nuclei are exposed to an external magnetic field, the magnetic fields of the spinning nuclei and the external magnetic field interact and cause the nuclei to precess, or “wobble” (**Fig. 1.4**). The frequency of precession can be described by the Larmor equation:

Equation 1:

$$\omega_0 = B_0 \times \gamma$$

where ω_0 is the precessional frequency, B_0 is the external magnetic field strength measured in tesla (T) units, and γ is the gyromagnetic ratio measured in megahertz per tesla unit. Conveniently, the ω_0 is constant for every atom of a particular element at a particular magnetic field strength, and it is key for the localization of the MRI signal within space (see details below).

When an RF pulse (at the Larmor frequency for hydrogen at a given field strength) is applied within an external magnetic field, the net magnetization vector flips from its longitudinal direction by a certain angle (flip angle). This flipping process produces a transverse magnetization vector (perpendicular to the external magnetic field) and a longitudinal magnetization vector (parallel to the external magnetic field) (**Fig. 1.5**). The magnitude of the flip angle is determined by the strength and duration of the RF pulse applied. A 90-degree RF pulse, for instance, aligns the magnetization vector in a plane perpendicular to the external magnetic field, whereas a 180-degree RF pulse aligns the magnetization vector in a plane parallel to, but in a direction opposite to that of, the external magnetic field. After the RF pulse, the pre-

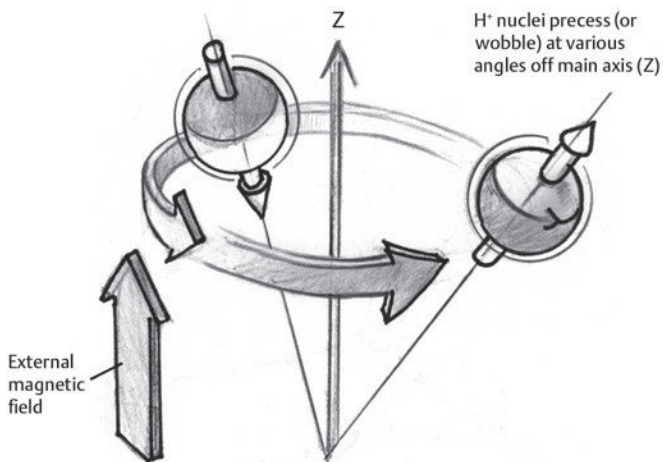


Fig. 1.4 All nuclei, including hydrogen nuclei, precess (wobble) about their axes when placed in an external magnetic field, similarly to the way a spinning top standing on its point wobbles under the influence of the gravity field. The frequency of precession is related to the strength of the external magnetic field as determined by the Larmor equation ($\omega_0 = B_0 \times \gamma$).[†]

cessing nuclei initially are also “in phase” with one another; that is, they are precessing in synch with one another. This synchronized precession maximizes the transverse magnetization vector (additive effect). Once the RF pulse is turned off, the precessing nuclei relax, that is, they return to their original orientation, the longitudinal vector returns, and the transverse vector dissipates (**Fig. 1.6**). As the nuclei relax, the transverse magnetization vector produces a signal as it precesses around a receiver coil; this signal can be optimized, recorded, and ultimately transformed into MR images by Fourier analysis.¹

In summary, by using an RF pulse to flip the excess spin-up hydrogen nuclei and ultimately transform the longitudinal magnetization vector within a sample or tissue into a transverse magnetization vector, an RF signal can be generated and subsequently used to create an image.

T1, T2, and T2*

The terms T1, T2, and T2* pertain to the times the transverse and longitudinal magnetization vectors take to relax and generate the MRI signal. As stated, when an RF pulse that is interacting with nuclei in an external magnetic field is turned off, the precessing nuclei return to their original equilibrium state and realign with the external magnetic field. As one might expect, the longitudinal magnetization vector returns to equilibrium value before the RF pulse does. The return or recovery of the longitudinal magnetization is known as *T1 recovery*, with T1 being defined as the time constant representing 63% recovery of the equilibrium longitudinal magnetization vector.² On the other hand, after the RF pulse is turned off, the transverse magnetization vector decays exponentially because of spin dephasing as the local magnetic fields of the individual nuclei interact with each other. This is known as *T2 decay* or *T2 relaxation*, in which T2 is defined as the time in which the transverse magnetization vector has decayed by 63% of its maximum. The T1 relaxation time is also known as the *longitudinal* or *spin-lattice* relaxation time, and T2 is also known as the *transverse* or *spin-spin* relaxation time. The T2* relaxation time represents the loss of the transverse magnetization vector due to both T2 effects and the spin dephasing caused by local magnetic field inhomogeneities. Therefore, the T2* relaxation time is always shorter than the T2 relaxation time. As would be expected, T1, T2, and T2* differ for individual tissues. Tissues with a long T1 include water and large protein molecules, and tissues with a short T1 include fats and intermediate-size molecules. Tissues with a long T2 include liquids, whereas large molecules and solids generally have short T2 times. The T2* relaxation time usually is short for fat and water.^{2,3}

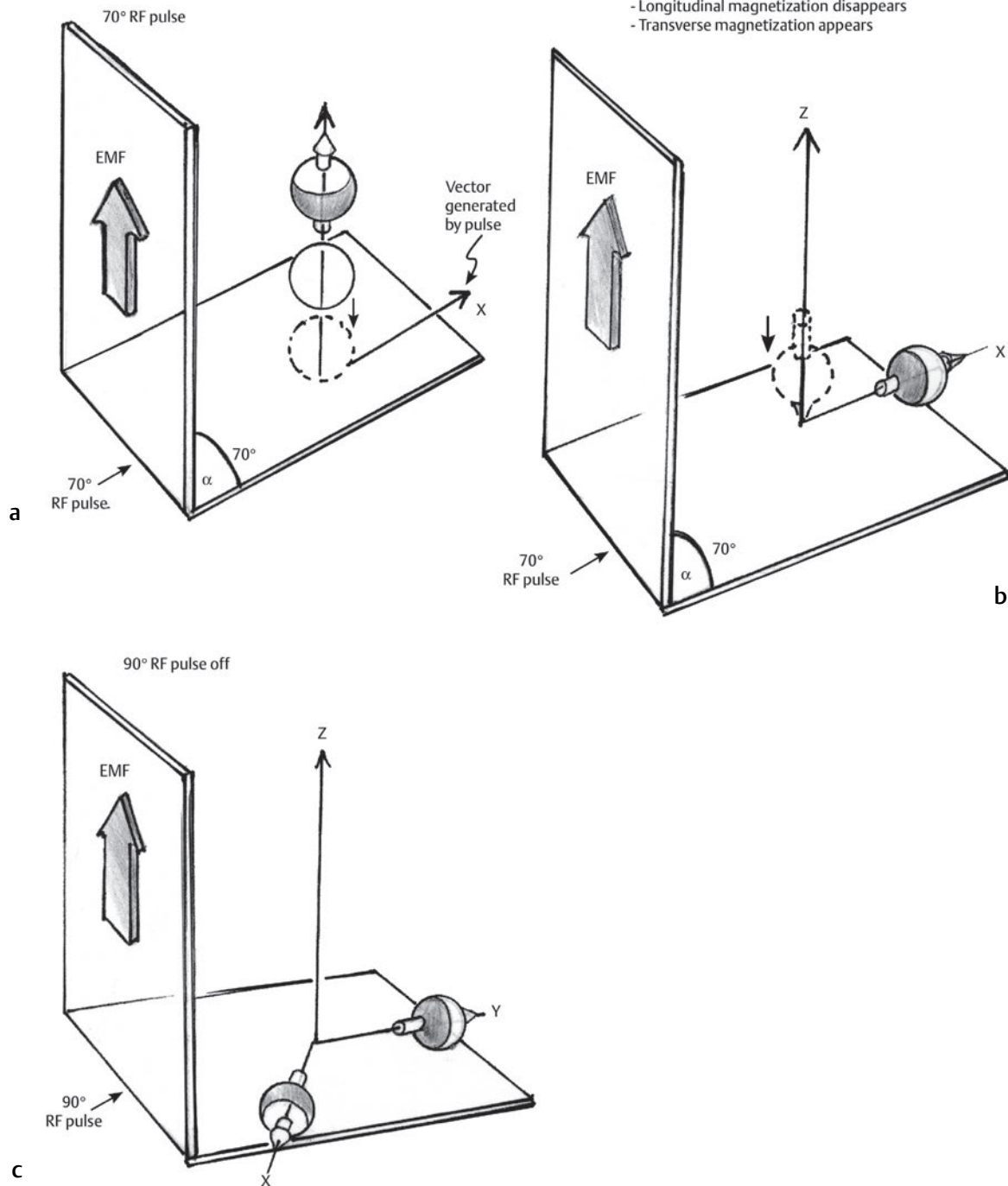


Fig. 1.5 Manipulation of the magnetization vector (EMF, external magnetic field). **(a)** An external RF pulse administered at the Larmor frequency can flip the direction of the magnetization vector from the longitudinal to the transverse direction. **(b)** The longitudinal component of the magnetization vector decreases and the transverse component of the magnetization vector increases, based on the strength and duration of the applied RF pulse. The angle the net magnetization vector makes with the longitudinal axis, that is, the external magnetic field, is called the flip angle. **(c)** A 90-degree RF pulse, for instance, will flip the direction of the net magnetization vector 90 degrees relative to the external magnetic field.[†]

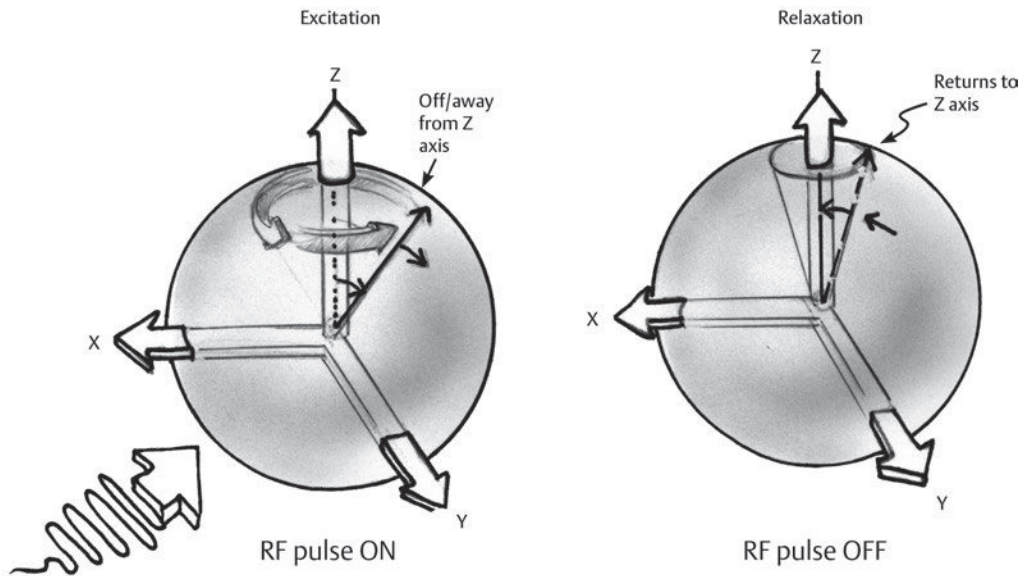


Fig. 1.6 After the discontinuation of an RF pulse, the net magnetization vector will relax, or return, to a more stable energy state, with recovery of the longitudinal component and loss of the transverse component of the magnetization vector. The strength of the transverse component of the magnetization vector is what is ultimately used to generate the MR image.[†]

In summary, individual tissues, such as fat and water, have reasonably well-defined T1, T2, and T2* time constants related to the recovery of the longitudinal magnetization signal (T1) and the decay of the transverse magnetization signal (T2, T2*) after an RF pulse. These differences in T1, T2, and T2* directly affect the strength of the RF signal emitted from a particular type of tissue (e.g., fat or water) at a given time and ultimately can be converted to visual differences in tissue contrast on the final image.^{2,3} It is MRI's ability to resolve subtle differences in the T1, T2, and T2* characteristics of various tissues and assign the differences to a discrete location (pixel/voxel, see below) within the patient that enables this technique to produce images of such high spatial resolution and to provide information about the anatomy and pathology within the musculoskeletal system.

Gradient Coils and Signal Localization

The transverse magnetization signal is localized within tissue via the use of gradient coils. As previously stated, nuclei in an external magnetic field precess at a particular frequency when subjected to an RF pulse, as described by the Larmor equation. By altering the external magnetic field and creating gradients in the x, y, and z planes, it is possible to identify the location of signal within tissue based on its emitted RF and phase. Gradient coils superimpose small field gradients in the x, y, and z directions on the main magnetic field and include section-selection gradients, phase-encoding gradients, and frequency-encoding gradients.¹ *Section-selection* (or slice-selection) gradients select the section to be imaged.¹ The *phase-encoding* gradient causes a phase shift

that enables localization of the signal by its phase. A *frequency-encoding* gradient causes a frequency shift, enabling localization by frequency.¹ The determination of the direction (i.e., x, y, z) in which each gradient is applied depends on the orientation of the image (i.e., axial, sagittal, coronal) and the structures involved; typically the gradients are applied to minimize artifacts in the region of interest.^{1,5}

Data within the MR image are divided into *pixels* and *voxels*, which localize the signal in two or three dimensions, respectively. A pixel is a 2D unit in the xy, xz, or yz plane, whereas a voxel is a 3D unit, representing a unit of volume within the dataset/image.

MRI Pulse Sequence and TE, TR, and TI

An *MRI pulse sequence* is the sequence of RF pulses and magnetic field gradients used to generate an image. Several concepts in addition to those discussed above are important when interpreting an MRI pulse sequence: TE, TR, and TI.

In conventional SE and *gradient-echo* sequences, the TE is the time from the initial RF pulse (used to flip the longitudinal magnetization vector into the transverse plane/transverse magnetization vector) to the center of the echo signal (time when signal is at its maximum) (**Fig. 1.7**). In conventional SE sequences, a phase-encoding gradient is applied at TE/2 to allow for spin rephasing at TE. This technique maximizes the recorded signal at readout (**Fig. 1.7**). In gradient-echo sequences, gradients are used to “recall the echo” at TE and use a negative gradient followed by a positive gradient (gradient echo) to refocus the signal at readout (**Fig. 1.8**). One might question why it is necessary to refocus at all. As previously

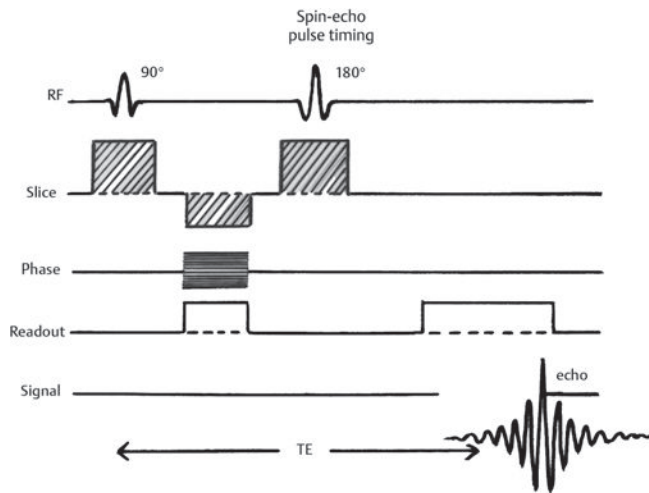


Fig. 1.7 In this example of a conventional SE pulse sequence, the top line shows an RF pulse sequence consisting of a 90-degree pulse followed by a 180-degree refocusing pulse. Section-selection gradients, a phase-encoding gradient, and a readout or frequency-encoding gradients are also shown. The bottom line depicts the RF signal or “echo” recorded at TE. The 180-degree pulse is responsible for the echo at a specific time, that is, TE.[†]

described, the transverse magnetization degrades because of dephasing effects on time scales represented quantitatively by T2 and T2*. Dephasing weakens the transverse magnetization vector/signal, and rephasing (using a perfectly timed gradient echo) rephases, or resynchronizes, the precessing nuclei. When all the nuclei are in phase, or precessing in synch (i.e., vectors pointing in the same direction), the recorded signal is at a maximum. TE primarily affects T2 in conventional SE sequences and T2* in gradient-echo sequences.^{1,2}

TR is the time interval between the initial RF pulse of the basic pulse sequence and the subsequent repetition of the initial RF pulse.¹ In conventional SE sequences, TR primarily affects T1, or the recovery of the longitudinal magnetization vector.

TE and TR can be manipulated to visualize the inherent differences in T1 and T2 among tissues on MRI sequences. For example, in conventional SE sequences, a short TE (<30 ms) and a short TR (<1000 ms) result in *T1-weighted* images (T1 effects maximized and T2 effects minimized). A long TE (>60 ms) and a long TR (>2000 ms) result in *T2-weighted* images on the T2 SE sequences (i.e., T2 effects maximized and T1 effects minimized). An intermediate TR (>1000 ms but <2000 ms) and a short TE (<30 ms) minimize differences in T1 and T2 within tissues and result in an image based primarily on the density of the protons within that tissue on conventional SE sequences. This minimalization of the differences in T1 and T2 effects within tissue

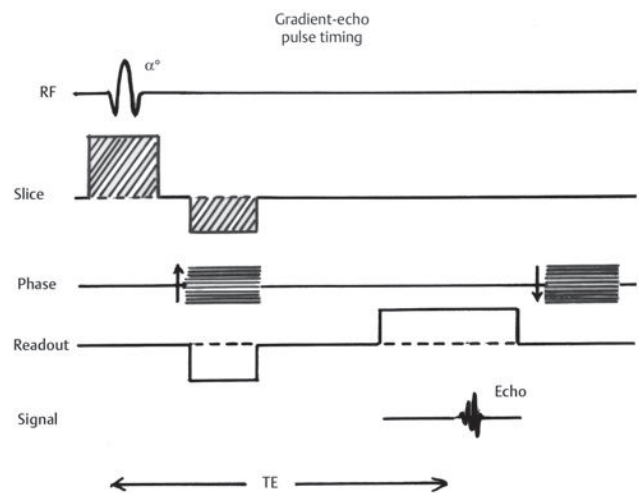


Fig. 1.8 In this example of a standard gradient-echo pulse sequence, the top line shows the RF pulse resulting in a pre-determined flip angle. Section-selection gradients, a phase-encoding gradient, and readout or frequency-encoding gradients also are shown. A refocusing gradient (readout or frequency selection gradient sequence), which refocuses signal, produces an echo at TE, hence the name “gradient echo.”[†]

when creating an MR image is known as *intermediate weighting*. In gradient-echo sequences, TR varies and is related to the flip angle and the TE. A larger flip angle (70 to 110 degrees) and a short TE favor T1 weighting, whereas a smaller flip angle (5 to 20 degrees) and a larger TE favor T2* weighting. A low flip angle and a short TE result in an intermediate-weighted image.¹⁻³

TI is the time to inversion used in inversion recovery MRI pulse sequences, such as STIR and fluid-attenuated inversion recovery. More specifically, it represents the time interval between the initial 180-degree pulse used to invert the longitudinal magnetization vector and the subsequent 90-degree pulse used to convert the longitudinal magnetization vector into the transverse plane. A second 180-degree pulse is used at TE/2 that generates an echo at TE, at which time the signal is recorded. Why use a 180-degree pulse followed by a 90-degree pulse? By applying a 90-degree pulse as the longitudinal vector of a certain tissue (e.g., water) crosses from a negative to a positive value (near zero), the transverse magnetization vector generated by the RF pulse from that type of tissue is very small or zero,^{1,2,5} which essentially nulls the signal from that tissue. The most common tissue that is suppressed is fat, and STIR sequences are commonly used in musculoskeletal radiology for this purpose.¹⁻³

In summary, it is important to note that occasionally there is confusion regarding the terms T1, T2, TR, and TE. T1 and T2 relaxation properties are

characteristics of a given tissue and are intrinsic to that tissue. Conversely, TR and TE are parameters of the pulse sequence and, as such, are extrinsic to the tissue and may be modified by the radiologist. By altering the TE and TR in a pulse sequence, it is possible to manipulate the visually perceived differences within tissue and therefore the MR image generated from that tissue. MR pulse sequences are, in fact, designed to take advantage of the intrinsic differences within tissue, that is, differences in T1, T2, and T2*, to create an image that allows these differences to be perceptible visually. The fact that disease processes often alter the intrinsic properties of the affected tissue and subsequently alter the T1, T2, and T2* effects is the reason that MRI is helpful in the detection of pathology.

■ MRI Applications

Standard Sequences

Standard MRI pulse sequences used in spine imaging include T1-weighted, T2-weighted, and STIR-weighted sequences; T2* gradient-echo sequences; 3D imaging techniques; and contrast-enhanced imaging techniques. For the purposes of this text, the nomenclature as it relates to the “standard” pulse sequences used for most musculoskeletal MRI has been simplified by using the following terms:

- T1-weighted image
- T2-weighted image
- Fluid-sensitive sequence, such as STIR or fat-suppressed T2-weighted image
- Gradient-echo image
- Postgadolinium T1-weighted image

Various other proprietary terms and acronyms (such as FLASH, GRASS, or FLAIR), commonly used primarily in the radiologic literature, have been avoided.

In contrast to imaging techniques based on X-ray absorption, such as conventional radiography and CT, the appearance of biologic tissue with MRI, that is, its relative brightness or darkness, is determined to a great extent by the operator-chosen parameters of the MR pulse sequence used to acquire the images. Thus, CSF may appear bright, dark, or intermediate in signal intensity, depending on the MR pulse sequence and the selective parameters in that sequence. Each MR pulse sequence has its own specific strengths and weaknesses, and typically a combination of pulse sequences is used in a standard examination.

Conventional SE (and FSE) sequences make up the bulk of sequences in the MRI assessment of

spine anatomy. Intermediate-weighted sequences are useful because they produce images with the highest signal-to-noise ratio and, therefore, provide better resolution than T2-weighted FSE images do. T1-weighted images, which provide nearly as high a signal-to-noise ratio, are also useful in showing musculoskeletal anatomy. T2-weighted sequences tend to have the poorest signal-to-noise ratio, and therefore the poorest resolution, but they are used primarily for their fluid sensitivity and their ability to detect pathology that has a high fluid content (e.g., ligament tears, bone-marrow edema, or tumors). T2 sequences can also give a rough depiction of anatomy, although it is inferior to that of intermediate-weighted and T1-weighted sequences.

Fluid-sensitive sequences include T2, fat-suppressed T2-weighted, and STIR sequences. Depending on the clinical situation, each specific MRI sequence has some optimal and some less than optimal characteristics (**Table 1.1**).

T1-Weighted SE

Standard T1-weighted SE sequences use a short TR (250 to 700 ms) and a short TE (10 to 25 ms) to maximize T1 differences of the tissues being imaged.¹ The ability to depict anatomic detail, bone-marrow abnormalities (including marrow-infiltrating processes and fractures), blood products, melanin, and enhancement after the administration of gadolinium are the strengths of T1-weighted SE sequences.³ Proton-poor substances, such as air, and substances that do not have mobile protons, such as cortical bone or other calcified structures (e.g., calcific tendinitis), produce no detectable signal and produce a relative signal void. Fast-flowing blood may generate a flow void and appear dark on T1-weighted sequences, mostly because of a lack of refocusing of the blood, which is excited by the 90-degree pulse but not by the 180-degree pulse. Other tissues, such as fat, melanin, fatty bone marrow, and certain blood products (intracellular and extracellular methemoglobin), appear bright on T1-weighted images (**Figs. 1.9** and **1.10**). Fluids, such as CSF, reactive edema, and simple cysts, show low signal on standard T1-weighted sequences (**Fig. 1.11**). Tissues with mixed characteristics (with some fluid and some collagenous tissue), such as abscesses, synovium, and complex cysts, tend to show intermediate signal intensity that is somewhere between that of collagenous tissue and fat. Usually, the higher the protein content of the fluid, the brighter the fluid appears on T1-weighted images. For the assessment of tumors or infection, fat-suppressed T1-weighted imaging after gadolinium contrast administration represents the sequence of choice because the high signal from

Table 1.1 Basic pulse sequences for MRI

Image Type	TR	TE	Signal Intensity		Advantages	Disadvantages
			Fat	Water		
T1	Short	Short	High	Low	Best anatomic detail; rapid acquisition	Poor visualization of pathology/edema
T2	Long	Long	Intermediate	High	Moderately sensitive for pathology/edema	Poor spatial resolution, time-consuming
Fat-suppressed T2	Long	Short	Very low	Very high	Most sensitive for pathology/edema	Susceptible to artifacts related to magnetic field inhomogeneity
Gradient echo	Short	Short	Intermediate	Intermediate/high	Excellent for evaluation of articular cartilage, PVNS, and blood	Very susceptible to metallic artifacts (prostheses)
Intermediate-weighted	Long	Short	Intermediate/high	Intermediate	Excellent for evaluation of meniscal pathology	

Source: From Khanna AJ, Cosgarea AJ, Mont MA, et al. Magnetic resonance imaging of the knee: current techniques and spectrum of disease. J Bone Joint Surg Am 2001;83A(suppl 2, part 2):128–141. Adapted with permission.



Fig. 1.9 Sagittal T1-weighted images of vertebral marrow in the thoracic spine. **(a)** This image shows normal bone marrow, which is seen as a mixture of fatty marrow (which appears as bright signal) and red marrow (which appears as intermediate signal, brighter than the adjacent intervertebral disc). **(b)** This image from a different patient (with metastatic breast cancer) shows vertebral bodies that are diffusely dark (hypointense) because of marrow replacement (abnormal bone marrow).

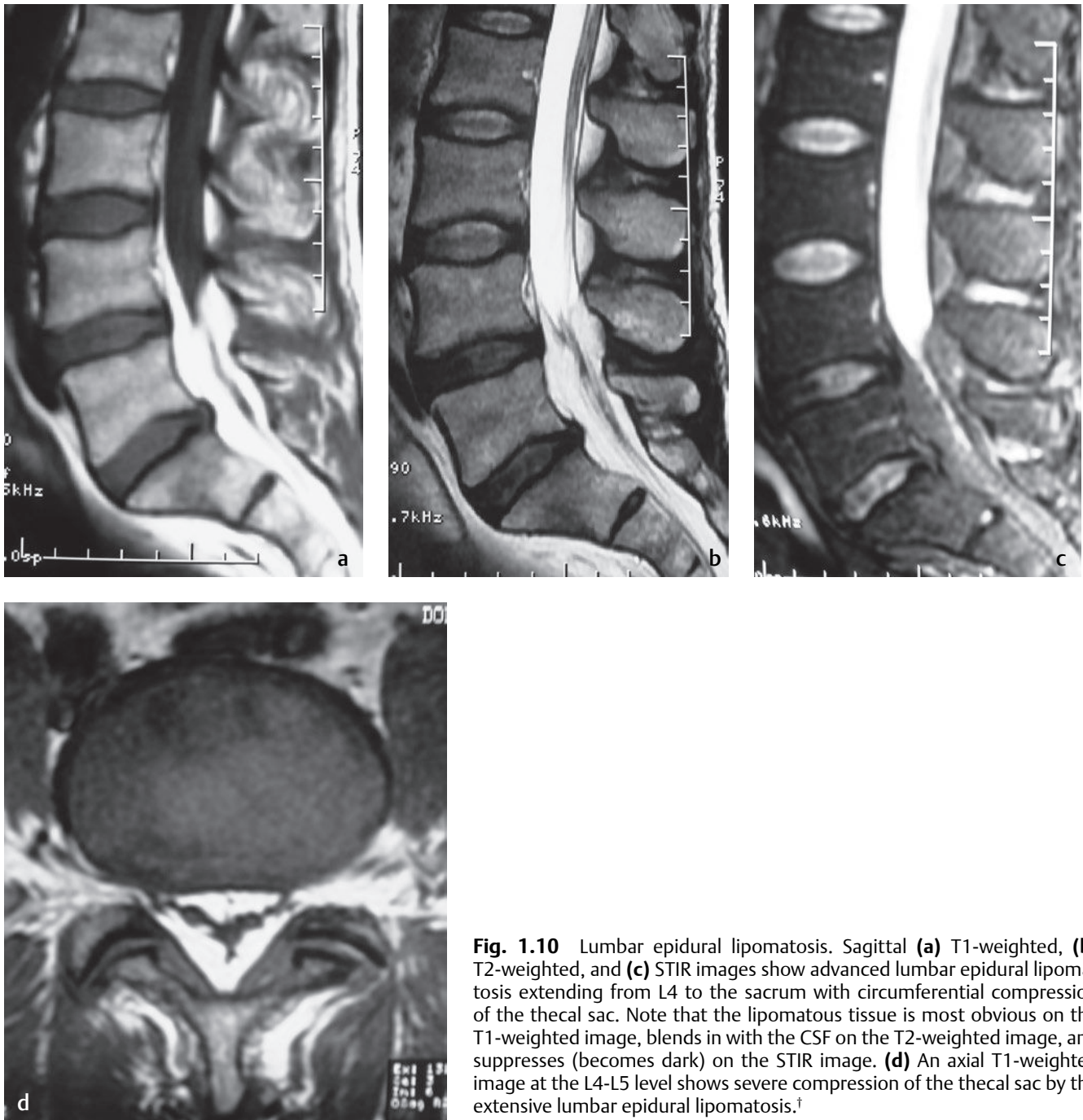


Fig. 1.10 Lumbar epidural lipomatosis. Sagittal (a) T1-weighted, (b) T2-weighted, and (c) STIR images show advanced lumbar epidural lipomatosis extending from L4 to the sacrum with circumferential compression of the thecal sac. Note that the lipomatous tissue is most obvious on the T1-weighted image, blends in with the CSF on the T2-weighted image, and suppresses (becomes dark) on the STIR image. (d) An axial T1-weighted image at the L4-L5 level shows severe compression of the thecal sac by the extensive lumbar epidural lipomatosis.[†]

fat is suppressed, making enhancement of abnormal tissue more conspicuous. Short scan times (because of the relatively short TRs) and excellent spatial resolution and depiction of anatomic detail are the major advantages of a T1-weighted pulse sequence. An additional strength of T1-weighted imaging remains its ability to show marrow replacement processes. Its major weakness is the relatively lower sensitivity for detecting soft-tissue edema compared with fluid-sensitive sequences such as fat-suppressed T2-weighted and STIR sequences.³

T2-Weighted SE and T2-Weighted FSE

T2-weighted SE and FSE sequences use a relatively long TE and long TR to maximize the T2 differences in the tissues. Both sequences, when combined with fat suppression, are excellent for detecting edema/fluid, which appears bright and is often associated with pathologic processes such as tumors, infection, fractures, and ligamentous injury (**Fig. 1.12**). The T2-weighted SE and FSE sequences are also good for evaluating ligaments and fluid-filled structures such



Fig. 1.11 Note the dark (hypointense) CSF on this sagittal T1-weighted image.

as cysts. As on T1-weighted SE sequences, air, cortical bone, calcified structures, and fast-flowing blood appear dark on T2-weighted sequences. Hyperacute blood (oxyhemoglobin) and subacute blood (extracellular methemoglobin) are bright on T2-weighted SE and FSE sequences. These sequences also have been shown to be useful for differentiating between fluid and tissue with a high fluid content.

One of the limitations of standard T2-weighted SE sequences is the relatively long image acquisition times. FSE imaging represents a technical innovation



Fig. 1.12 A sagittal T2-weighted image of the lumbar spine shows loss of normal bright signal at the L4-L5 intervertebral disc, representing desiccation. A focal, linear region of increased T2-weighted signal at the posterior aspect of the disc represents a high-intensity zone or an annular fissure (arrow).

that permits much more rapid imaging by using T2 contrast⁷ and multiple 180-degree RF pulses to create multiple echoes during a single TR period. The series of echoes is called the *echo train*, and the number of echoes produced in a single TR period is known as the *echo train length*. Because of their fast acquisition times, T2-weighted FSE sequences have largely replaced standard T2-weighted SE sequences.^{1,8}

The major weakness of T2-weighted SE and T2-weighted FSE sequences is their inability to detect marrow pathology when not combined with

fat-suppression techniques. This limitation is due to fat and water both being bright on non-fat-suppressed T2-weighted FSE and SE sequences.³

Fat Suppression with T1-Weighted and T2-Weighted Images

Fat suppression commonly is achieved by spectral fat suppression or a STIR technique.⁹ Spectral fat-suppression imaging is restricted to MRI systems with midlevel and high magnetic field strength because of the necessity of identifying distinct fat and water resonance peaks and selectively suppressing the signal arising from adipose tissue, a process that depends on the presence of a relatively strong magnetic field. Combined with T2-weighted or intermediate-weighted imaging, this technique is particularly useful in detecting bone bruises and osseous stress injury; the hyperintense intraosseous fluid that accumulates secondary to osseous contusion and microtrabecular fractures appears particularly conspicuous in contrast to the adjacent suppressed normal marrow fat signal.

On T1-weighted images, fat suppression can enable the differentiation of fat-containing masses (e.g., lipoma/liposarcoma) from other tissue that may contain elements of increased signal (e.g., hemorrhage within tissue). Additionally, it can be used to verify the presence of fat within a lesion and to increase the conspicuity of enhancing masses on contrast-enhanced T1-weighted images.

One of the disadvantages of T2 and T1 sequences is incomplete suppression of the signal from fat, due to local magnetic field inhomogeneities and susceptibility effects.³ This effect is most prominent with images of curved surfaces, such as in the shoulder and ankle, or of any body part in the presence of metal or air. Additionally, as just mentioned, fat suppression requires higher-strength magnets (>1 T) to ensure proper fat suppression than is generally required for non-fat-suppressed MRI. STIR sequences often are used to overcome the effects of magnetic field inhomogeneities seen with fat-suppression techniques (see the following section).

STIR

STIR is another MRI pulse sequence commonly used in spine imaging and, like T2-weighted sequences with fat suppression, is excellent for detecting fluid and edema when administered with a long TE. STIR can be used as an alternative to T2-weighted imaging (**Fig. 1.13**). On fluid-sensitive images such as STIR, fluid appears bright and makes the edema and fluid associated with certain types of pathology more conspicuous than they are on non-fluid-sensitive

sequences (**Fig. 1.14**). Such pathology includes osteomyelitis, abscesses, metastases, primary bone tumors, fractures, ligament tears, and bone contusions. Unlike T1-weighted and T2-weighted fat-suppressed sequences, STIR uses a 180-degree RF inversion pulse, followed by a 90-degree RF pulse after TI to nullify the signal from fat. Because of this phase-refocusing inversion pulse, STIR sequences are less susceptible to magnetic field inhomogeneities and subsequent susceptibility effects, which often result in inhomogeneous fat suppression on SE and FSE sequences. The STIR FSE technique has been shown to be superior to the fat-suppressed FSE technique for cervical and thoracic MR imaging.¹⁰ One of the major weaknesses of the STIR sequence, however, is that it suppresses the signal from all tissue with T1 signal characteristics similar to those of fat. Therefore, STIR pulse sequences should not be used with gadolinium contrast because gadolinium has relaxation properties similar to those of fat tissue, and thus all tissue with the same T1 as fat (e.g., certain types of hemorrhage, melanin, and proteinaceous fluid) will also have its signal suppressed.³

Gradient Echo, 3D Gradient Echo

As indicated above, gradient-echo MRI pulse sequences use gradients to recall the echo at TE. Specifically, a negative gradient is followed by a positive gradient to refocus the signal at readout. As described above, in gradient-echo sequences, the TR varies and is related to the flip angle and the TE. A large flip angle (70 to 110 degrees) and a short TE favor T1 weighting, whereas a small flip angle (5 to 20 degrees) and a large TE favor T2* weighting. A low flip angle and a short TE result in an intermediate-weighted image.

Gradient-echo sequences are more sensitive than SE sequences to local magnetic field inhomogeneities. These inhomogeneities can be created by blood, air, or calcium within tissue or can be intrinsic to the MRI unit itself. As a result, gradient-echo sequences are very sensitive for the detection of certain types of tissue, such as calcification, focal air collections, and blood products, which produce magnetic field inhomogeneity. Similarly, gradient-echo sequences of tissue that contains surgical instrumentation (metal) tend to produce substantial artifact due to the disturbance in the local magnetic field created by that instrumentation. Because of the susceptibility effects of the trabecular bone, gradient-echo images also tend to overestimate the size or prominence of osteophytes within the spine and marrow pathology when the trabecular bone is not destroyed (**Fig. 1.15**).³ Gradient-echo sequences may be T2*-weighted, T1-weighted, or intermediate-weighted, depending on what tissue is being evaluated.

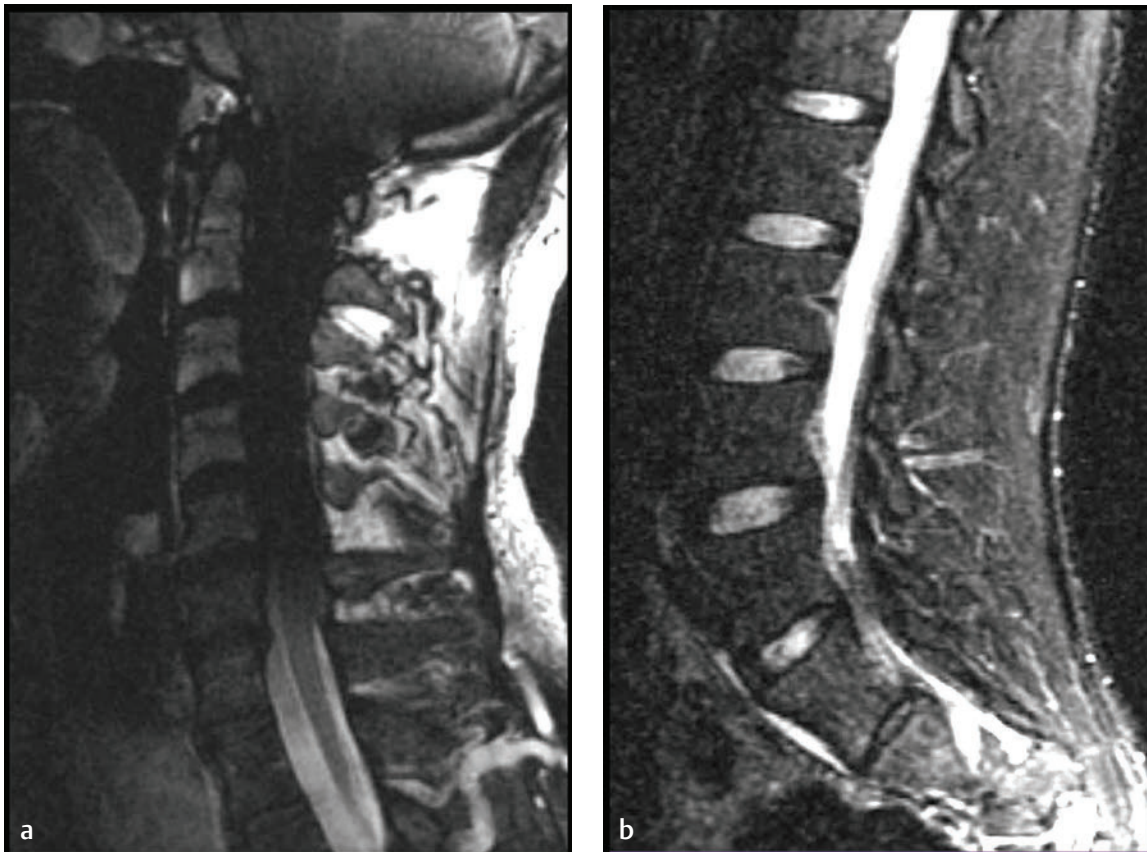


Fig. 1.13 Comparison of fluid-sensitive techniques. **(a)** A T2-weighted image of the cervical spine with frequency-selective fat suppression shows heterogeneous signal, especially through the cervical spinal canal, due to failure of fat suppression. **(b)** A sagittal STIR image through the lumbar spine shows homogeneous fat signal because it is an inversion recovery sequence rather than a frequency-selective method of suppression.

In 3D gradient-echo sequences, signal from an entire volume of tissue (i.e., in the xy , yz , and xz planes) is acquired at the same time. This volume of tissue then may be partitioned into sections in any plane. These sections obtained from the 3D volume dataset may be isotropic, or nearly so, and can be oriented in any way that is helpful for interpreting the dataset. In general, 3D sequences (also known as volume acquisitions) have a higher signal-to-noise ratio because an entire volume of tissue is sampled rather than a single thin section. This optimal signal-to-noise ratio makes the 3D acquisition pulse sequences especially useful at low field strengths.⁵ The major disadvantages of 3D gradient-echo pulse sequences are the relatively long acquisition times and the tendency toward susceptibility and motion artifacts.

Contrast-Enhanced Imaging

Gadolinium is commonly used as an intravenous contrast agent in spine imaging. Its function in intravenous imaging is analogous to that of the iodinated contrast agent used in CT, and tissues that show in-

creased vascularity generally show enhancement on postcontrast T1-weighted images. Fat-suppression techniques are commonly used with gadolinium because of their sensitivity to detecting gadolinium.¹¹ Areas in which there is breakdown of the blood-brain barrier also show enhancement. Specific uses for intravenous contrast include the evaluation of spinal lesions and differentiation of the following^{3,11}:

- Solid from cystic lesions
- Soft-tissue phlegmon from inflammation from abscess
- Surgical scars from disc fragments (**Fig. 1.16**)

Artifacts

Common artifacts seen in MRI include motion artifacts, truncation artifacts, and susceptibility effects.

Motion artifacts in MRI are common and are directly related to patient motion within the scanner. Patient motion results in misregistration of the MR signal and subsequent blurring of the MR image. Motion from the

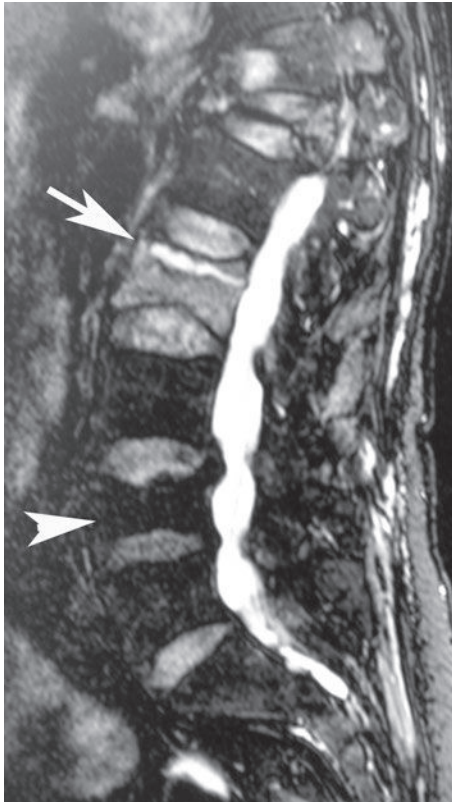


Fig. 1.14 A sagittal STIR image shows a linear region of increased signal intensity compatible with edema in the L2 vertebral body (*arrow*), which is compatible with an acute fracture. Note the diffuse edema in the vertebral body, which could be mistaken for diffuse bone-marrow involvement by a neoplastic process. There is no increase in signal intensity in the L4 vertebral body (*arrowhead*), which is compatible with a chronic fracture.[†]

pulsation of arteries results in a particular type of motion artifact or pulsation artifact. This type of artifact produces partial reproductions of the pulsating vessel in the phase-encoding direction.

Truncation artifacts occur in MRI and are related to the way the MR signal is processed during image creation and, in particular, to the Fourier transformation method used to process the MR signal data.¹² Truncation artifacts that can be seen include ring artifacts, artificial edge widening at parallel high-contrast interfaces, interface edge enhancement, and distortion of adjacent tissues at parallel high-contrast interfaces.¹²

Susceptibility artifacts seen in MRI, and briefly discussed previously, are the result of local field inhomogeneities within the scan field that create areas of focal signal loss (**Fig. 1.17**). These magnetic field inhomogeneities can be related to the magnet or to metal, air, calcium, or blood products within the tissues being imaged.^{3,5}

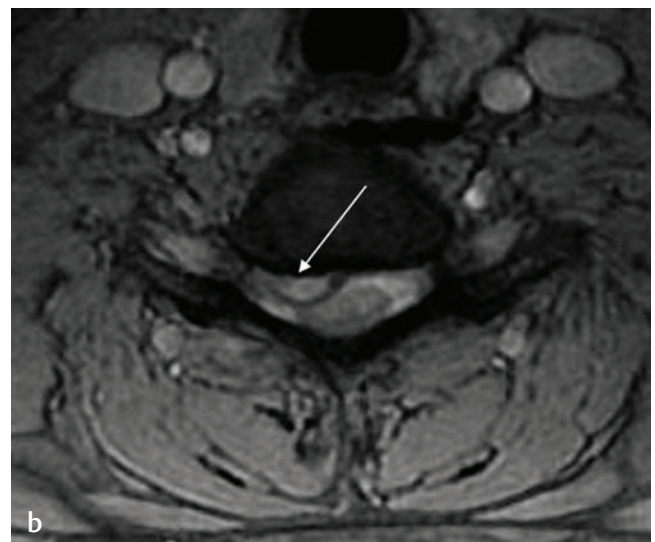
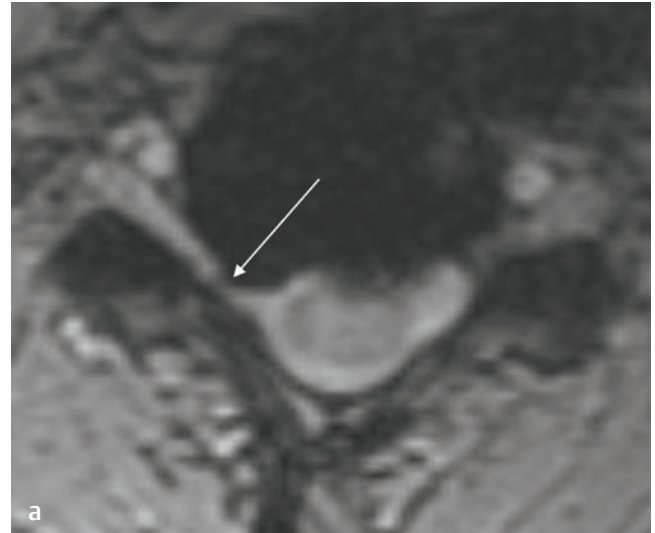


Fig. 1.15 Cervical spine imaging. **(a)** An axial gradient-echo image shows the posterior osteophyte to a better advantage than SE imaging does, but it also exaggerates the degree of foraminal stenosis (*arrow*); these phenomena are due to the presence of susceptibility artifact. **(b)** An axial gradient-echo image (different patient) shows a prominent right paracentral disc protrusion (*arrow*); note the high-intensity disc herniation compared with the low signal of the osteophyte in part **a**.

■ Summary

A fundamental knowledge base of MRI physics is important for the optimal use of MRI technology. This imaging modality is well suited for evaluating spine abnormalities because it provides an accurate anatomic assessment, which is of paramount importance. RF pulses, appropriately applied within a graded magnetic field, can localize the tissue of interest, and the signal produced can be Fourier-transformed

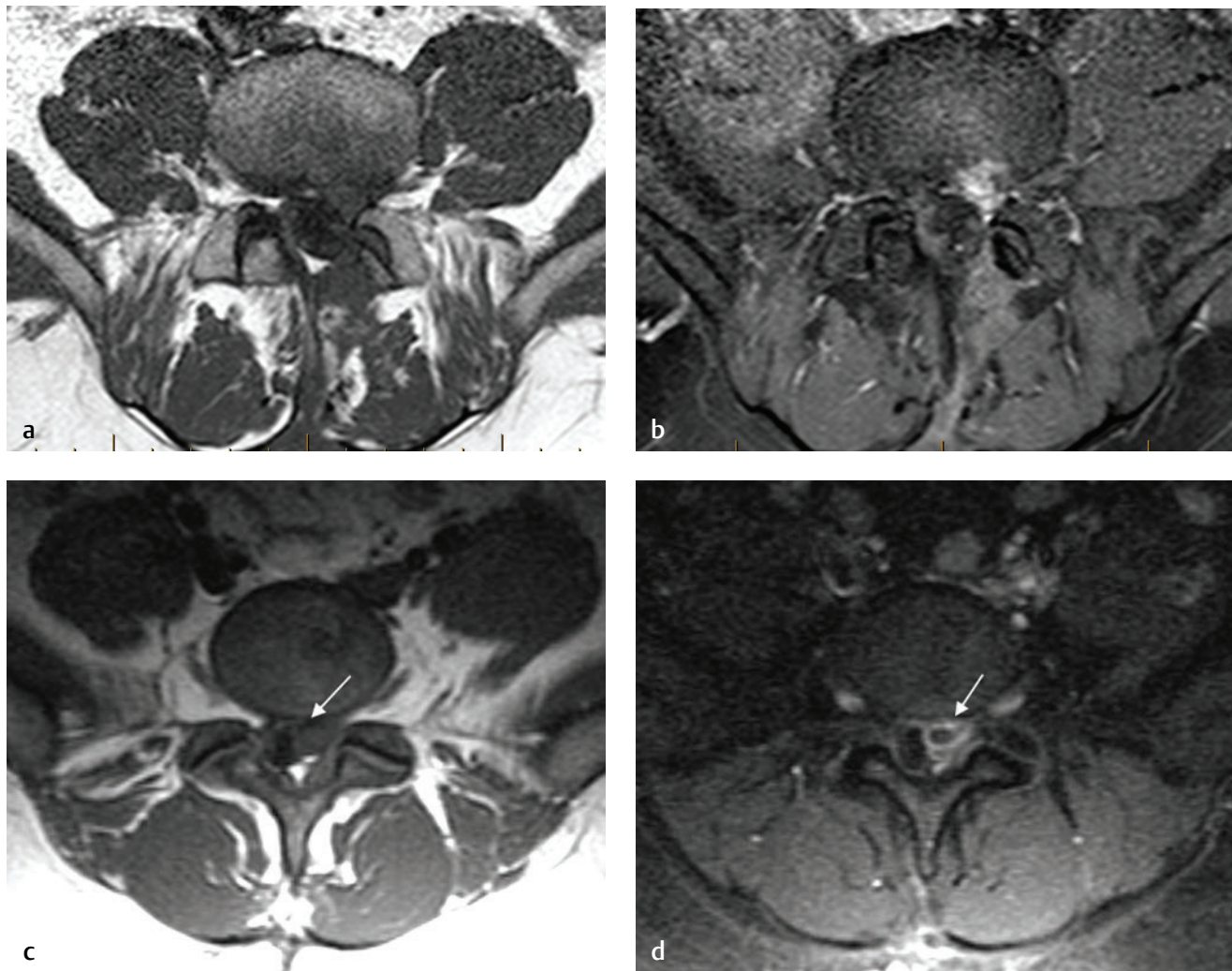


Fig. 1.16 (a) Axial, noncontrast and (b) postcontrast fat-suppressed T1-weighted images show a left paracentral abnormality with homogeneous delayed enhancement, consistent with epidural fibrosis. In contradistinction, (c) axial noncontrast and (d) postcontrast fat-suppressed T1-weighted images show a left paracentral abnormality with thin peripheral enhancement (arrow on both) consistent with a recurrent disc herniation.

into an image. This image is defined not only by the T1, T2, and T2* relaxation time constants of the specific tissue but also by the parameters that are used to assess the region of interest.

The primary pulse sequence parameters in MRI are TE, TR, and TI, and these values determine the weighting of the image (e.g., T1, T2, or intermediate weighting), the strength of the signal, and whether a certain type of tissue (e.g., fat) is suppressed. Each of the standard pulse sequences used in musculoskeletal imaging (SE, FSE, STIR, and gradient echo) has its own strengths and weaknesses, and a combination of various sequences is typical for the evaluation of the joints and spine. T1-weighted images are optimal for showing anatomic detail and bone/bone-marrow abnormalities, and they

are excellent, when combined with fat suppression, for showing abnormal contrast enhancement. Conversely, T1-weighted images are not optimal for showing soft-tissue edema. T2-weighted images are excellent for detecting edema/fluid and processes associated with an increased fluid content, such as trauma and tumors. They also may be useful for articular cartilage evaluation but are relatively insensitive to marrow fluid unless combined with a fat-suppression technique. Intermediate-weighted images provide the highest signal-to-noise ratio and are excellent for showing anatomic detail. The primary disadvantage of intermediate-weighted sequences is the lack of pure contrast compared with that of T1-weighted and T2-weighted images. Gradient-echo sequences are useful for identifying

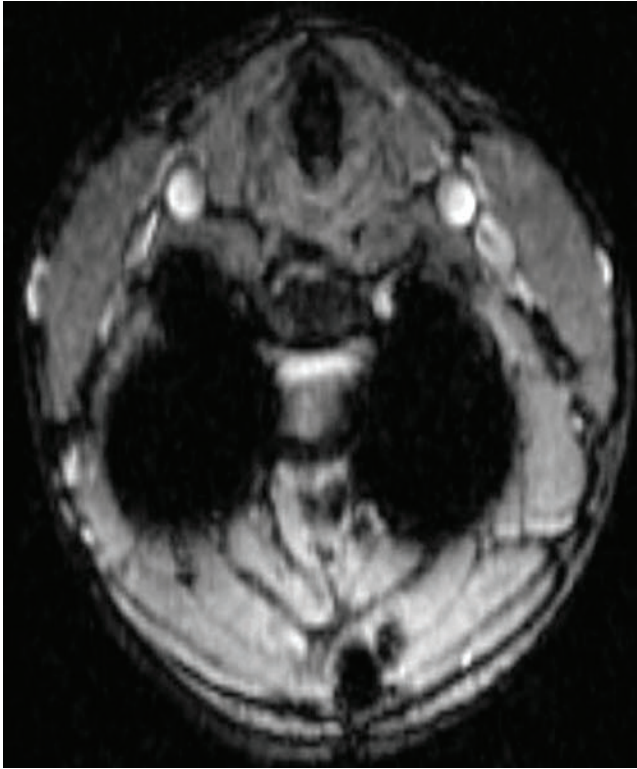


Fig. 1.17 An axial gradient-echo image through a postoperative cervical spine shows marked susceptibility artifact around the lateral mass screws; the susceptibility artifact is exaggerated on gradient-echo images compared with SE images.

blood products or metal that causes magnetic inhomogeneity. 3D gradient-echo sequences can be obtained in one sequence and examined in any plane as a volume of tissue. The primary disadvantage of 3D gradient-echo imaging is the long acquisition time; the same susceptibility to magnetic field inhomogeneity that may be useful is also a disadvantage when it obscures the tissue of interest. Fat suppression may be accomplished by frequency-specific suppression or by inversion recovery techniques. Frequency-specific suppression is useful but may be affected by magnetic field heterogeneity. Inversion recovery fat suppression is homogeneous but also suppresses tissue with the same T1 as fat. Gadolinium is used as a contrast agent, most often with frequency-specific fat suppression (because inversion recovery techniques may suppress the signal from

the gadolinium). Intravenous injections also may be used for indirect arthrography, although direct injection of gadolinium may often be necessary to achieve optimal joint distension and visualization of the appropriate anatomy.

It is frequently said that MRI is a compromise and that no gain in image quality is obtained without sacrificing some other portion of the sequence or the examination. A clear understanding of the basic elements of MRI, along with how these elements interact, enables the imager to adjust the scanning techniques and image protocols to obtain the highest-quality images possible. This optimization is important in all subspecialty imaging but is especially so in musculoskeletal imaging, where elucidating the anatomy is fundamental to analyzing the structure for the presence of pathology.

COMMON CLINICAL QUESTIONS

- Which sequence is best used for assessment of marrow replacement process in the spine?
 - T1-weighted image
 - T2-weighted image
 - STIR
 - Contrast-enhanced T1-weighted image
- Epidural lipomatosis is seen as bright signal on T1-weighted images and on T2-weighted images without fat suppression. True or false?
- Gradient-echo sequences are very sensitive for the detection of certain types of tissue, such as calcification, focal air collections, and blood products, that produce magnetic field inhomogeneity. True or false?
- In the presence of metal, frequency-selective fat-suppression techniques should be used instead of STIR techniques. True or false?
- Which sequence is best used for distinguishing recurrent disc herniation from epidural fibrosis in the postoperative spine?
 - T1-weighted image
 - T2-weighted image
 - STIR
 - Postcontrast T1-weighted image

References

1. Bitar R, Leung G, Perng R, et al. MR pulse sequences: what every radiologist wants to know but is afraid to ask. *Radiographics* 2006;26(2):513–537 PubMed
2. Huda W, Slone RM. Review of Radiologic Physics. Philadelphia, PA: Lippincott William & Wilkins; 2003
3. Kaplan PA, Helms CA, Dussault R, Anderson MW, Major NM. Basic principles of musculoskeletal MRI. In: Kaplan PA, Helms CA, Dussault R, Anderson MW, Major NM, eds. *Musculoskeletal MRI*. Philadelphia, PA: WB Saunders; 2001:1–21
4. Lejay H, Holland BA. Technical advances in musculoskeletal imaging. In: Stoller DW, ed. *Magnetic Resonance Imaging in Orthopaedics and Sports Medicine*. Baltimore, MD: Lippincott Williams & Wilkins; 2007:1–28
5. Runge VM, Nitz WR, Schmeets SH, Faulkner WH Jr, Desai NK. The Physics of Clinical MR Taught through Images. New York, NY: Thieme; 2005
6. Wehrli FW, Shaw D, Kneeland JB, Eds. *Biomedical Magnetic Resonance Imaging: Principles, Methodology, and Applications*. New York, NY: VCH Publishers; 1988
7. Mirowitz SA. Fast scanning and fat-suppression MR imaging of musculoskeletal disorders. *AJR Am J Roentgenol* 1993;161(6):1147–1157 PubMed
8. Escobedo EM, Hunter JC, Zink-Brody GC, Wilson AJ, Harrison SD, Fisher DJ. Usefulness of turbo spin-echo MR imaging in the evaluation of meniscal tears: comparison with a conventional spin-echo sequence. *AJR Am J Roentgenol* 1996;167(5):1223–1227 PubMed
9. Potter HG, Linklater JM, Allen AA, Hannafin JA, Haas SB. Magnetic resonance imaging of articular cartilage in the knee. An evaluation with use of fast-spin-echo imaging. *J Bone Joint Surg Am* 1998;80(9):1276–1284 PubMed
10. Delfaut EM, Beltran J, Johnson G, Rousseau J, Marchandise X, Cotten A. Fat suppression in MR imaging: techniques and pitfalls. *Radiographics* 1999;19(2):373–382 PubMed
11. Stoller DW, Ed. *Magnetic Resonance Imaging in Orthopaedics and Sports Medicine*. Philadelphia, PA: Lippincott Williams & Wilkins; 2007
12. Czervionke LF, Czervionke JM, Daniels DL, Haughton VM. Characteristic features of MR truncation artifacts. *AJR Am J Roentgenol* 1988;151(6):1219–1228 PubMed

ANSWERS TO COMMON CLINICAL QUESTIONS

1. A
Explanation: T1-weighted images are best used for the assessment of marrow replacement processes in the spine. On the T1-weighted images, the marrow fat remains bright, whereas a marrow-replacing process, such as metastasis, has low signal intensity. T2-weighted images and STIR images are more sensitive to the edema that is seen with most pathology, including nonmalignant processes such as fracture and infection as well as malignancies. Contrast-enhanced T1-weighted images are useful for the evaluation of infection, tumors, and the postoperative spine.
2. True
Explanation: Epidural lipomatosis follows the signal of subcutaneous fat on all pulse sequences, including fat-suppression pulse sequences.
3. True
Explanation: Gradient-echo sequences are very sensitive in the detection of certain types of tissue, such as calcification and blood products, because of the susceptibility artifact generated by ferromagnetic substances.
4. False
Explanation: One of the disadvantages of frequency-selective fat-suppression sequences is incomplete suppression of the signal from fat because of local magnetic field inhomogeneities and susceptibility effects, which alter the frequency at which protons in fat precess. Failure of fat suppression is prominent in the presence of metal or air. Unlike T2-weighted fat-suppressed sequences, STIR uses a 180-degree RF inversion pulse before the 90-degree RF pulse to null the signal from fat. Because of this phase-refocusing inversion pulse, STIR sequences are less susceptible to magnetic field inhomogeneities.
5. D
Explanation: Comparison of pre- and post-contrast T1-weighted images enables the differentiation of recurrent disc herniation from epidural fibrosis in the postoperative spine.

2

Normal Spine MRI Anatomy

Swati Deshmukh, John A. Carrino, J. Dana Dunleavy, and A. Jay Khanna

CHAPTER OUTLINE

- I. General Spine Anatomy
 - A. Vertebral Bodies
 - B. Intervertebral Discs
 - C. Epidural Space
 - D. CSF
 - E. Spinal Cord
 - F. Ligaments
 - G. Roots and Foramina
 - H. Facet Joints
 - I. Vascular Structures
 - J. Muscles
- II. Cervical Spine
 - A. Anatomy
 - B. Sagittal MRI
 - C. Axial MRI
 - D. Coronal MRI
- III. Thoracic Spine
- IV. Lumbar Spine
 - A. Anatomy
 - B. Sagittal MRI
 - C. Axial MRI
 - D. Coronal MRI
- V. Sacrum and Coccyx

To evaluate an MRI examination of the spine effectively, it is essential to have a basic understanding of its normal anatomy and appearance under MRI. This chapter provides an overview of the normal MRI appearance of the spine. The figures and line drawings serve to highlight the structures with which the spine specialist or radiologist should be familiar

before interpreting an imaging examination of the spine. Fully understanding the normal MRI appearance of the spine will enhance the clinician's understanding of the relevant pathologic conditions and facilitate recognition and differentiation of the subtle regional anatomic alterations that represent various pathologic conditions.

■ General Spine Anatomy

The spinal column is a series of vertebrae, ligaments, and articulations that provides a flexible support structure for the cranium, thorax, abdomen, and pelvis. The spinal column also serves as protection for the spinal cord and nerve roots. There are three primary ossification centers of the vertebrae: one ossification center for the vertebral body, which develops by the eighth week of life, and one ossification center for each vertebral arch, which develops by the seventh or eighth week. There are multiple secondary ossification centers. The spinal column shows a longitudinal growth pattern during childhood and adolescence.

The spinal column is typically composed of 7 cervical vertebrae, 12 thoracic vertebrae, 5 lumbar vertebrae, the sacrum, and the coccyx. The spine (C2 through the sacrum) includes three different types of joints:

- Intervertebral discs
- Facet joints (zygapophyseal joints)
- Fibrous joints

The intervertebral discs represent fibrocartilaginous symphyses between vertebrae. The facet joints are synovial joints between the superior and inferior articular processes. The fibrous joints include the ligamentum flavum, interspinous ligaments, and supraspinous ligaments.

Vertebral Bodies

Normal lordosis should be seen in the cervical and lumbar spine, and normal kyphosis should be present in the thoracic spine. The superior and inferior end plates should be intact and parallel to one another in the absence of vertebral compression fractures, other fractures, tumors, or infection. A limbus vertebra is a defect within a vertebral body caused by intraosseous disc herniation (**Fig. 2.1**). The most common location is within the anterior superior corner of the vertebral body.

The subaxial cervical vertebral bodies all have a similar appearance (**Fig. 2.2**), whereas the atlas (C1) has no vertebral body and the axis (C2) has an odontoid process. Each of the lumbar vertebral bodies also has a similar appearance (**Fig. 2.3**), as do the thoracic vertebral bodies (**Fig. 2.4**). The anterior and posterior longitudinal ligaments, seen along the vertebral bodies, have low signal intensity. The entry site of the basivertebral veins is seen at the midportion of the posterior vertebral bodies. The spinal and radicular arteries course around the cord's anterior, posterior, and lateral aspects within the vertebral canal (**Fig. 2.5**). Fat-suppression techniques can be used to nullify marrow signal and increase the sensitivity in the evaluation of neoplastic and infiltrative processes.

Intervertebral Discs

Intervertebral discs are present between each of the vertebral bodies from the axis to the sacrum. They are immensely strong fibrocartilaginous structures



Fig. 2.1 A sagittal T1-weighted image of the lumbar spine shows a normal variant limbus vertebra. A limbus vertebra is a defect within a vertebral body caused by intraosseous disc herniation, most commonly within the anterior superior corner of the vertebral body.

that form the strongest bond between adjacent vertebrae. The normal discovertebral complex has three components:

- Cartilaginous end plate
- Annulus fibrosus
- Nucleus pulposus

Overall, the intervertebral discs show intermediate signal intensity on T1-weighted images and high signal intensity on T2-weighted images. The outer annulus appears hypointense on T2-weighted images, whereas the inner annulus, which is composed of fibrocartilage and a high proportion of type-II collagen, is indistinguishable from the hyperintense nucleus pulposus. Compared with normal vertebral marrow, the nucleus pulposus, which is composed of a proteoglycan matrix and type-II collagen, appears hyperintense on T2-weighted images and hypointense on T1-weighted images.¹ As the disc degenerates and as patients age, the signal intensity of the nucleus pulposus decreases on T2-weighted images, and the structure becomes dark on all pulse sequences. Additional pulse sequences, such as fat-suppressed T2-weighted images, are useful for accentuating fluid and edema, which may help in delineating spine pathology. Special attention should be given to the posterior aspect of the disc on sagittal and axial T2-weighted images to evaluate for disc protrusion, extrusion, sequestration, or other pathology that may be contributing to central canal or neural foraminal stenosis.

The end plate is a flat, osseous disc with a slightly elevated rim secondary to the attached ring apophysis, which produces a central depression in the end plate that is occupied by hyaline cartilage.¹ A Schmorl node results from protrusion of the cartilage of intervertebral discs through the vertebral end plate and into the adjacent vertebra (**Fig. 2.6**).

The annulus is composed of type-I collagen fibers (Sharpey fibers) that are attached to the ring apophysis periosteum. The annulus also blends with the anterior and posterior longitudinal ligaments. T1-weighted images provide optimal evaluation of anatomy, fracture lines, and other osseous detail. T1-weighted images also clearly delineate the relationships of the vertebral bodies, intervertebral discs, central canal, and posterior elements.

In the cervical spine, the annulus fibrosus is much thicker anteriorly with a crescentic mass of collagen.² The annulus fibrosus is essentially deficient posterolaterally. In the lumbar spine, disc height gradually increases inferiorly except at L5-S1. The posterior margin is concave in the upper lumbosacral spine and straight or convex at L4-L5 and L5-S1. The posterior margin should project no more than 1 mm beyond the end plate.

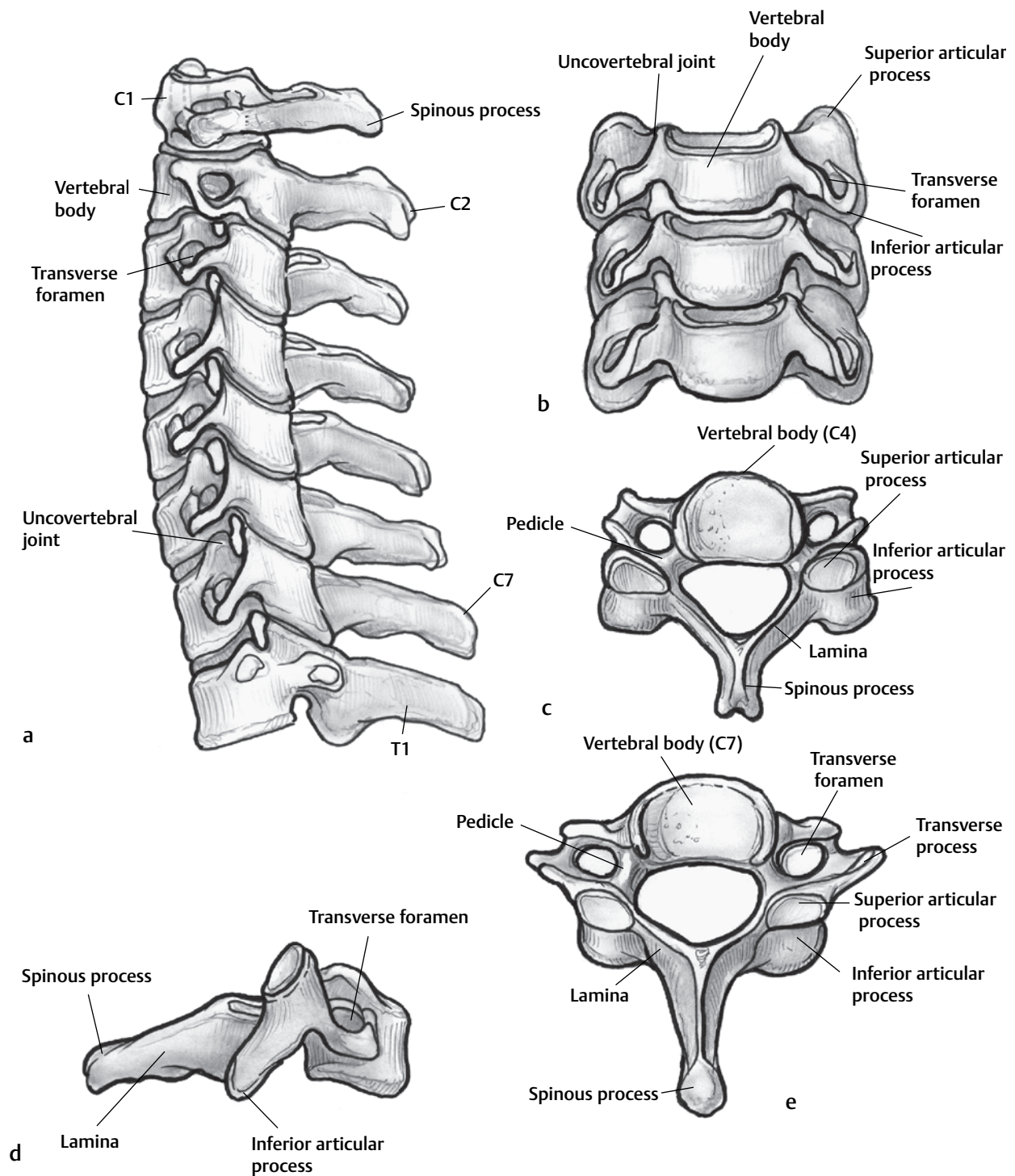


Fig. 2.2 Artist's sketches of the cervical vertebral bodies: **(a)** lateral vertebral bodies from C1-T1, **(b)** AP vertebral bodies from C4-C7, **(c)** axial vertebral body at C4, **(d)** lateral vertebral body at C7, and **(e)** axial vertebral body at C7.[†]

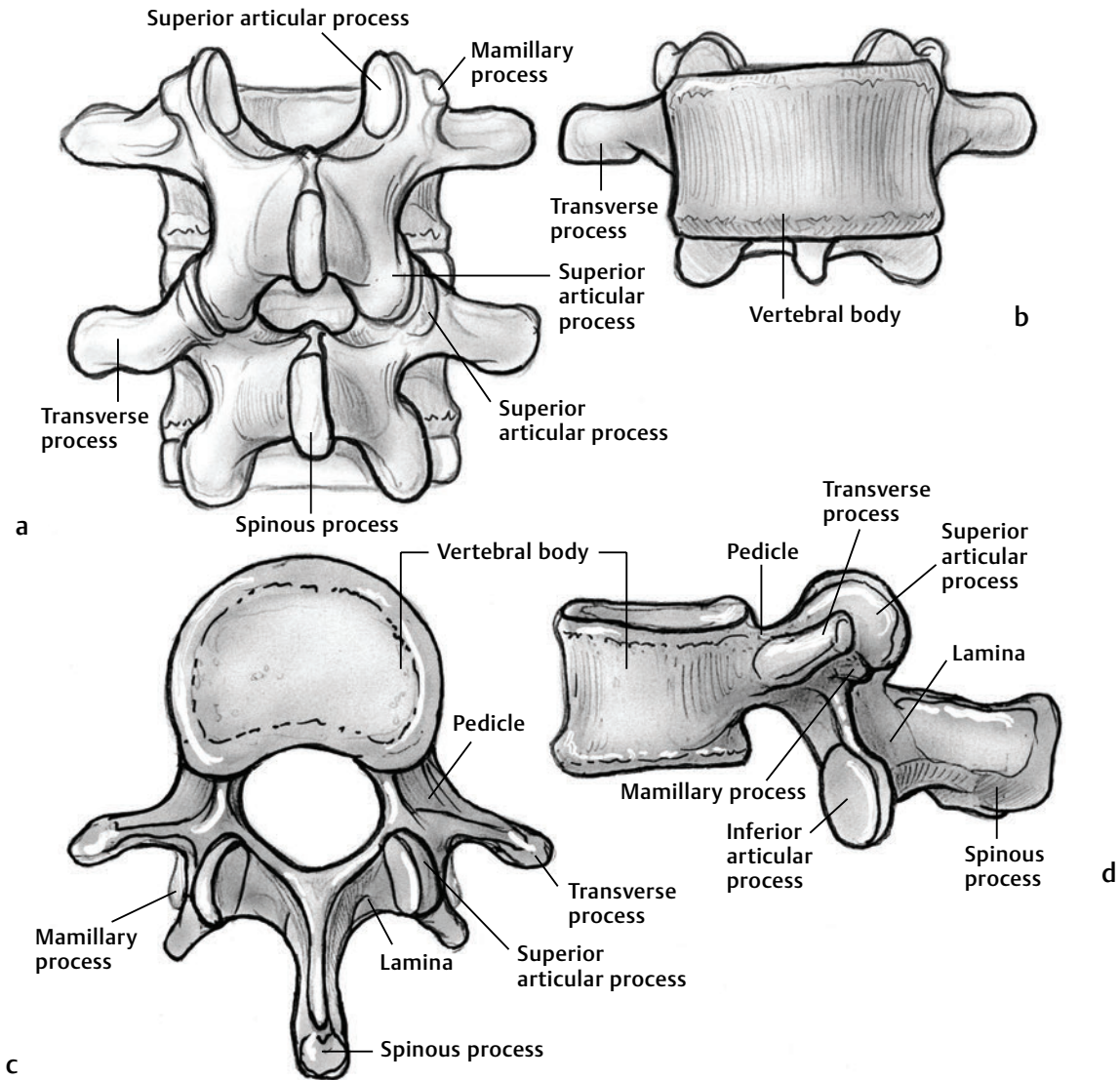


Fig. 2.3 Artist's sketches of the L3 and L4 lumbar vertebral bodies: (a) posterior, (b) anterior, (c) axial, and (d) lateral views.[†]

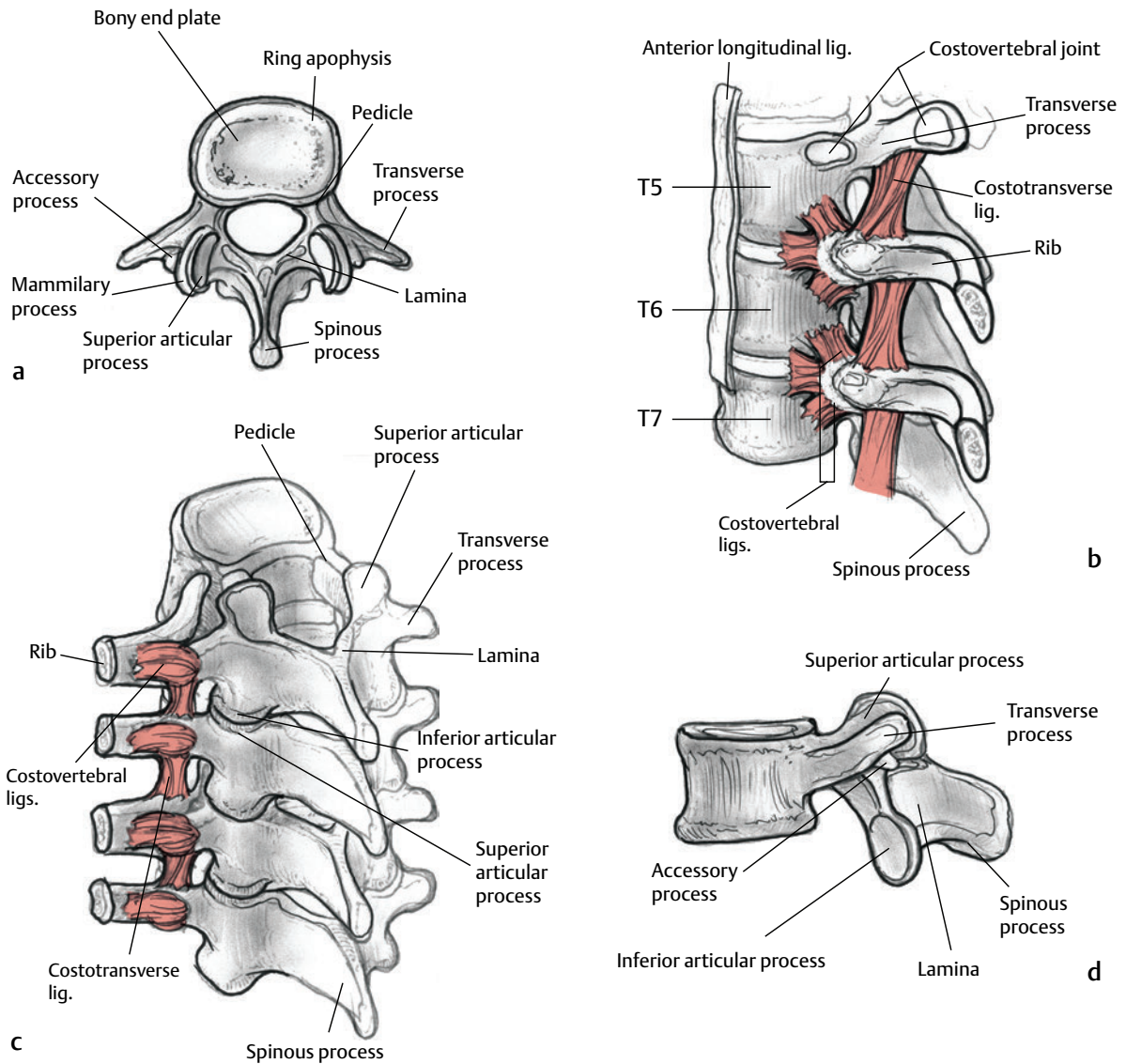


Fig. 2.4 Artist's sketches of the osseous structures of the thoracic spine, the costovertebral joints, and the costotransverse and costovertebral ligaments: **(a)** axial, **(b)** lateral, **(c)** posterior oblique, and **(d)** lateral views.[†]

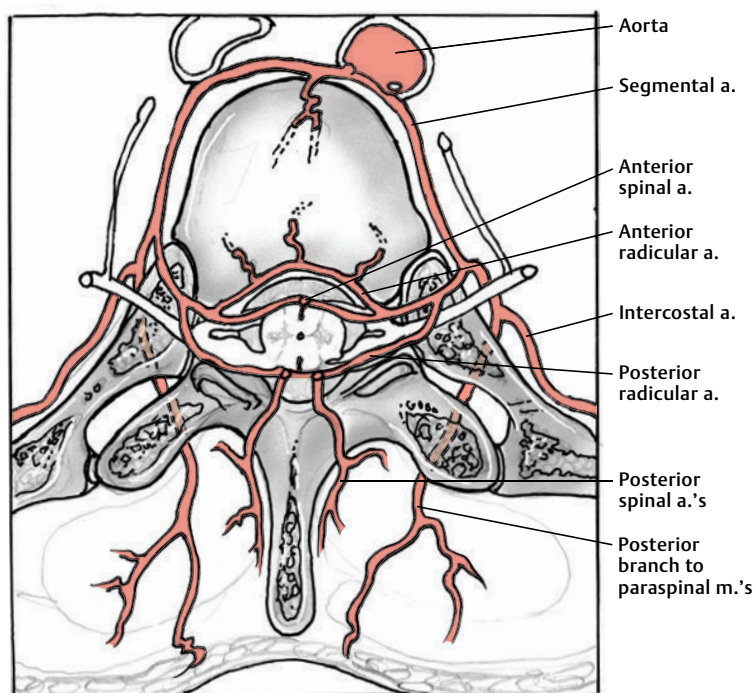


Fig. 2.5 A 3D artist's sketch (axial view) of the spinal, intercostal, and other arteries that supply the thoracic spine.

Epidural Space

The epidural space in the spinal canal is the true space between the dura and bone. Contents include epidural fat, nerves, blood vessels, the ligamentum flavum, and the posterior longitudinal ligament. The dura extends caudally to S2 and has lateral out-pouchings to the nerve roots. At L5-S1, the thecal sac enlarges, and usually no epidural fat is seen on MRI. Tarlov cysts are common extradural CSF-filled sacs that occur in the S1-S4 region of the spinal cord and are often asymptomatic (**Fig. 2.7**).

CSF

Like other fluids, CSF has low signal intensity on T1-weighted images and high signal intensity on T2-weighted images. On sagittal and axial images, CSF is seen surrounding the spinal cord in the cervical, thoracic, and lumbar spine and around the cauda equina in the lower lumbar spine. Thus, T2-weighted images provide a myelographic appearance that allows for the detection of spinal stenosis. One should be aware of the potential for imaging artifacts relating to CSF flow, which are most commonly seen in the thoracic spine and can be mistaken for multiple intradural-extramedullary lesions.



Fig. 2.6 A sagittal T2-weighted image shows multiple Schmorl nodes in the lumbar spine. A Schmorl node results from protrusion of the cartilage of intervertebral discs through the vertebral end plate and into the adjacent vertebra.

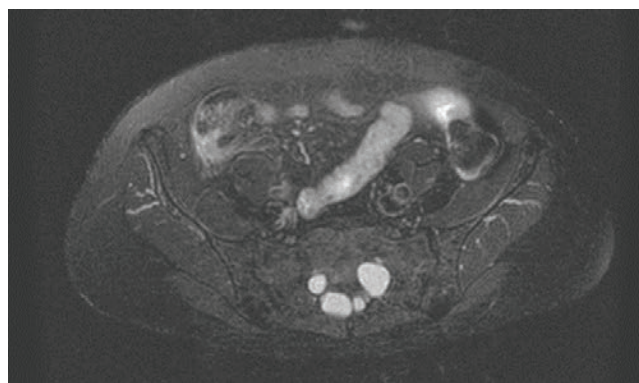


Fig. 2.7 An axial fat-suppressed T2-weighted image shows multiple Tarlov cysts in the sacrum. Tarlov cysts are extradural CSF-filled sacs that occur in the S1-S4 region of the spine and are often asymptomatic.

Spinal Cord

As noted above, the sagittal T2-weighted images provide a myelographic effect that allows the evaluation of spinal cord morphology and the presence of extrinsic compression. The cord should have homogeneous signal intensity in the absence of intrinsic pathology. On axial T2-weighted images, the central gray matter can be faintly identified. Specialized sequences obtained with high-field magnets enable detailed evaluation of central gray matter (**Fig. 2.8**). The spinal cord should terminate at or above the L1-L2 level in adults.

Ligaments

Normal ligaments should have low signal intensity on all pulse sequences. The transverse ligament can be seen posterior to the odontoid process (**Fig. 2.9**) and is best visualized on axial images. The ligamentum flavum connects the lamina of adjacent vertebrae and is seen as a hypointense band posterior to the dura. The ligamentum flavum blends with capsules of facet joints. In the cervical spine, the ligamentum flavum is typically 1.5 mm in thickness. In the lumbar spine, the ligamentum flavum is 4 to 6 mm in thickness. The ligamentum flavum may also calcify and lead to osseous spur formation and resultant neuroforaminal stenosis.

The anterior longitudinal ligament extends from the anterior margin of the foramen magnum to S1. The anterior longitudinal ligament is broad, thick, and adherent to the anterior vertebral bodies. It is loosely attached to the intervertebral discs. Although deep fibers span one intervertebral articulation, superficial fibers span up to four articulations. The anterior longitudinal ligament is narrow in the cervical spine and broad in the lumbar spine. The low signal on MRI blends with the peripheral portion of the annulus fibrosus and cortical bone.

The posterior longitudinal ligament extends from the body of the axis to the sacrum. The posterior longitudinal ligament is thin, attached to the posterior vertebral cortex via the midline septum, and defines the anterior margin of the anterior epidural space at the midline (**Fig. 2.10**). The anterior epidural space is not apparent at the disc level because the posterior longitudinal ligament fuses to the discs. Visualization of these structures may be limited with MRI because of partial volume averaging with the adjacent vertebral body.³ The posterior longitudinal ligament is attached to the intervertebral discs and margins of the adjacent vertebral bodies. There is no attachment at the center of the vertebral bodies. Deep fibers extend between adjacent vertebrae, whereas superficial fibers bridge three to four bodies. The posterior longitudinal ligament, like most ligaments, has low signal on both T1- and T2-weighted images.

Roots and Foramina

The neuroforamina or neural canals are bordered anteriorly by the vertebral bodies and discs, posteriorly by the facet joint and articular processes, and superiorly and inferiorly by pedicles. Nerve roots pass laterally through the neuroforamen. The dorsal and ventral nerve roots can be identified within the neural foramina on the parasagittal images and the axial images. The exiting nerve root is located just posterior to the vertebral artery in the cervical spine (**Fig. 2.11**). Additional neural structures, including the sympathetic chain, are located in and around the cervical vertebral bodies (**Fig. 2.12**). The eight cervical nerve roots exit above the similarly numbered vertebral bodies. It should be noted that the C2 nerve root exits the spine above the C2 pedicle and runs parallel to the C1-C2 facet joint (**Fig. 2.13**). The 12 thoracic and 5 lumbar nerve roots exit below the similarly numbered vertebrae. The nerve roots have intermediate signal intensity and are surrounded by high-signal-intensity fat on T1-weighted images and by high-signal-intensity CSF on T2-weighted images. On gadolinium-enhanced MRI, there is normal enhancement of the dorsal root ganglion. The normal conus medullaris ends around the level of the inferior end plate of L1 in adults.

Facet Joints

The facet joint is the articulation of the inferior articular process of the posterior elements of a vertebra with the superior articular process of the posterior elements of the next vertebra (**Fig. 2.14**). It is a synovial-type joint that consists of a capsule, synovium, menisci, and hyaline (articular) cartilage lining the reciprocating surfaces. Because the term “facet” actually represents only the articular cartilage surface of the joint, a more appropriate term is zygapophyseal joint or “z-joint.”

The anatomy of the zygapophyseal joint is oriented differently throughout the spine because of varying biomechanical stress. In the cervical spine, the zygapophyseal joint is oriented in a transverse/oblique plane. In the thoracic spine, the zygapophyseal joint is oriented coronally. In the lumbar spine, the zygapophyseal joint is typically oriented in the sagittal/oblique plane.

Vascular Structures

Normal vascular anatomy is important to recognize when evaluating MRI studies of the spine and spinal cord (even when evaluating for nonvascular diagnoses) (**Fig. 2.15**). The superior cord is supplied by the anterior spinal artery and two posterior spinal arteries that originate from the vertebral arteries.

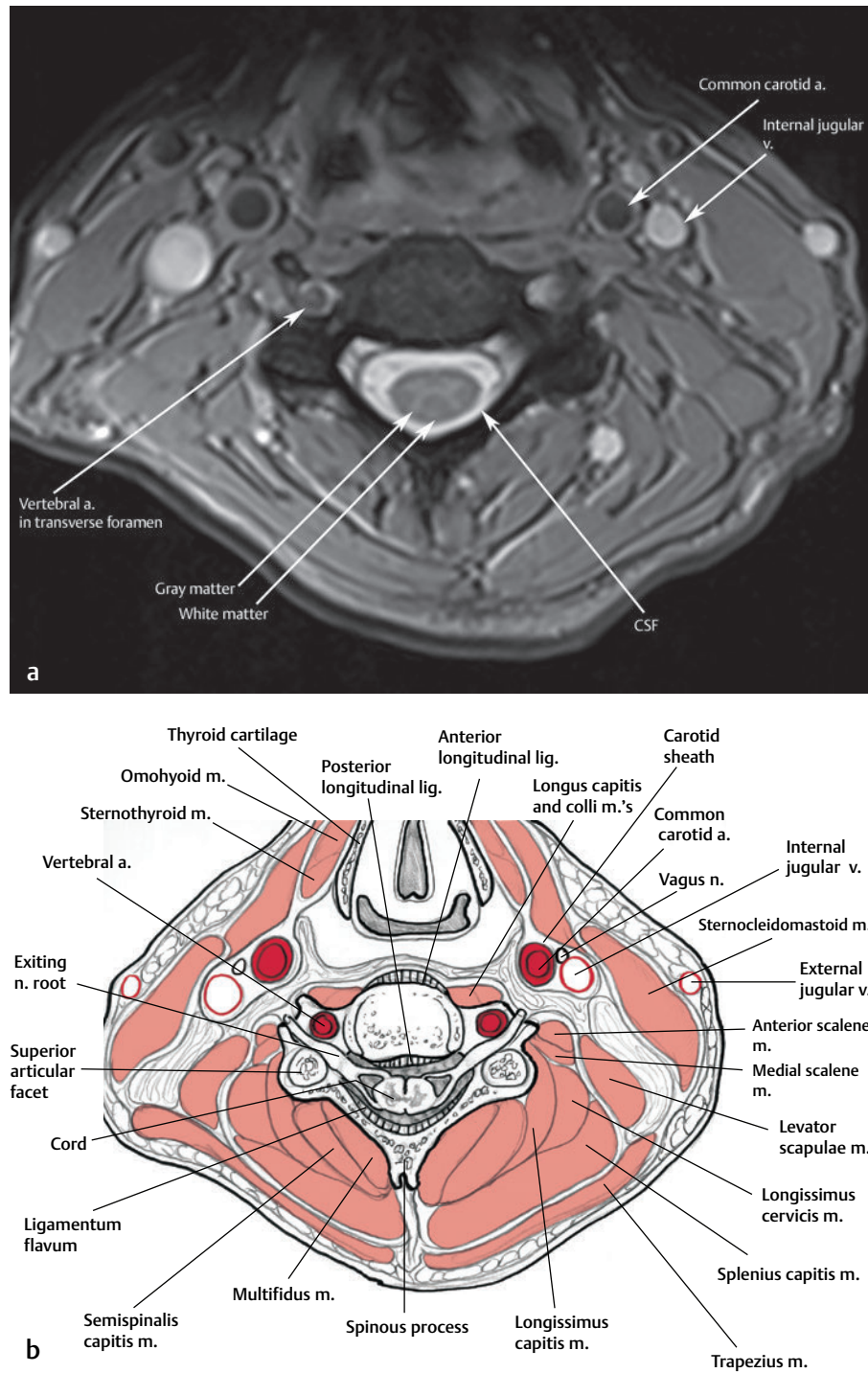


Fig. 2.8 This (a) axial T2-weighted image and (b) artist's sketch clearly define the gray and white matter of the cervical spinal cord, the CSF within the subarachnoid space, and epidural fat. Normal flow voids are seen within the carotid and vertebral arteries.[†]

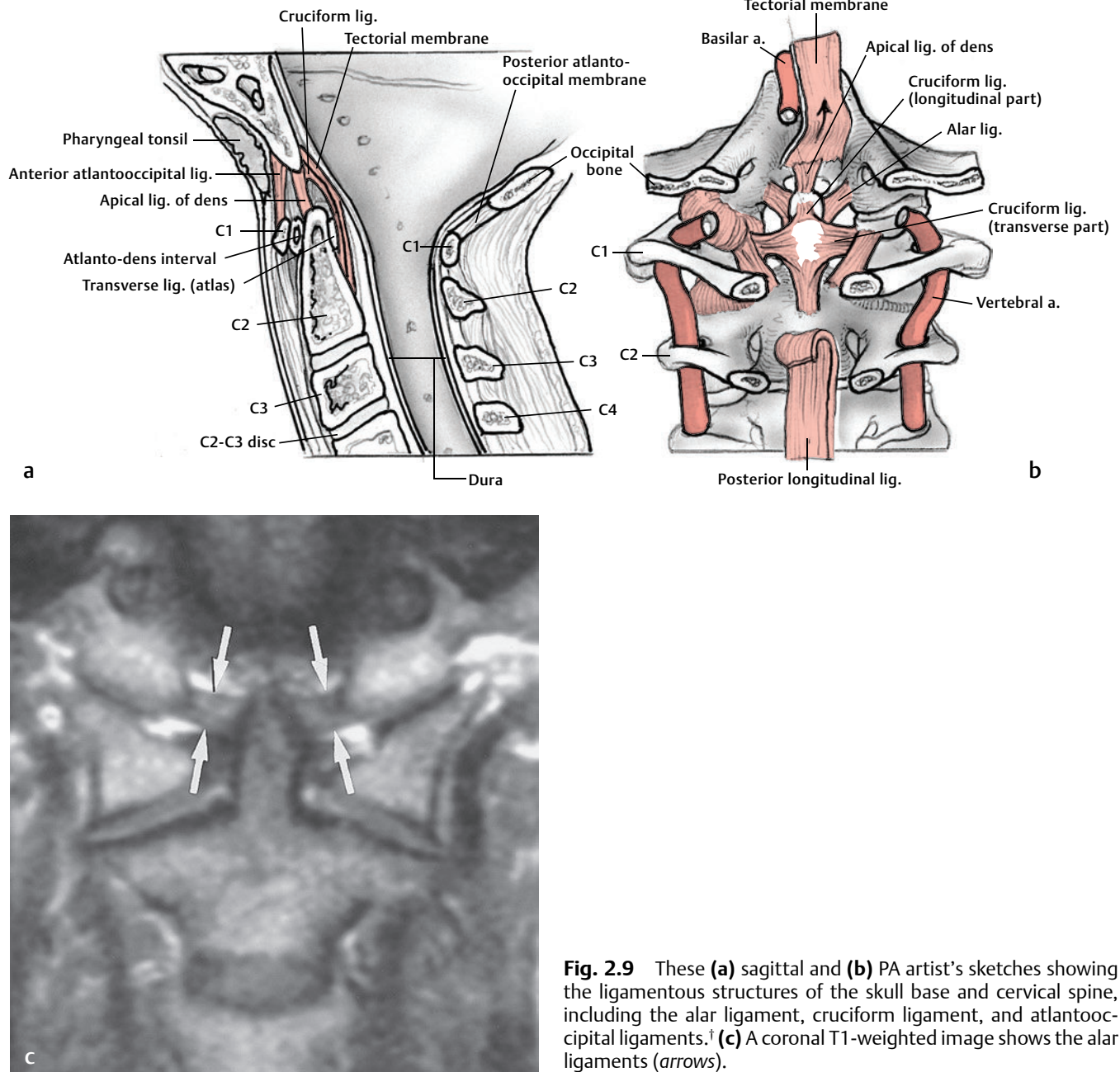


Fig. 2.9 These **(a)** sagittal and **(b)** PA artist's sketches showing the ligamentous structures of the skull base and cervical spine, including the alar ligament, cruciform ligament, and atlantooccipital ligaments.[†] **(c)** A coronal T1-weighted image shows the alar ligaments (arrows).

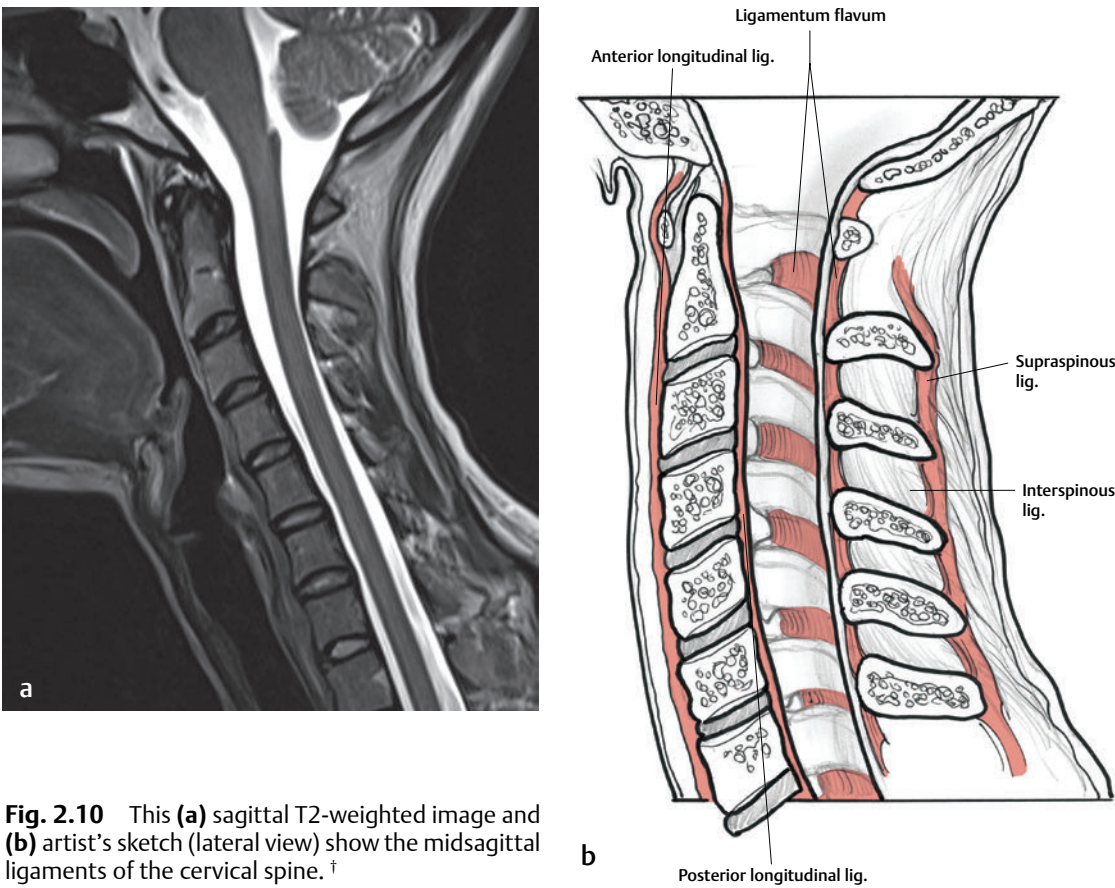


Fig. 2.10 This (a) sagittal T2-weighted image and (b) artist's sketch (lateral view) show the midsagittal ligaments of the cervical spine. †

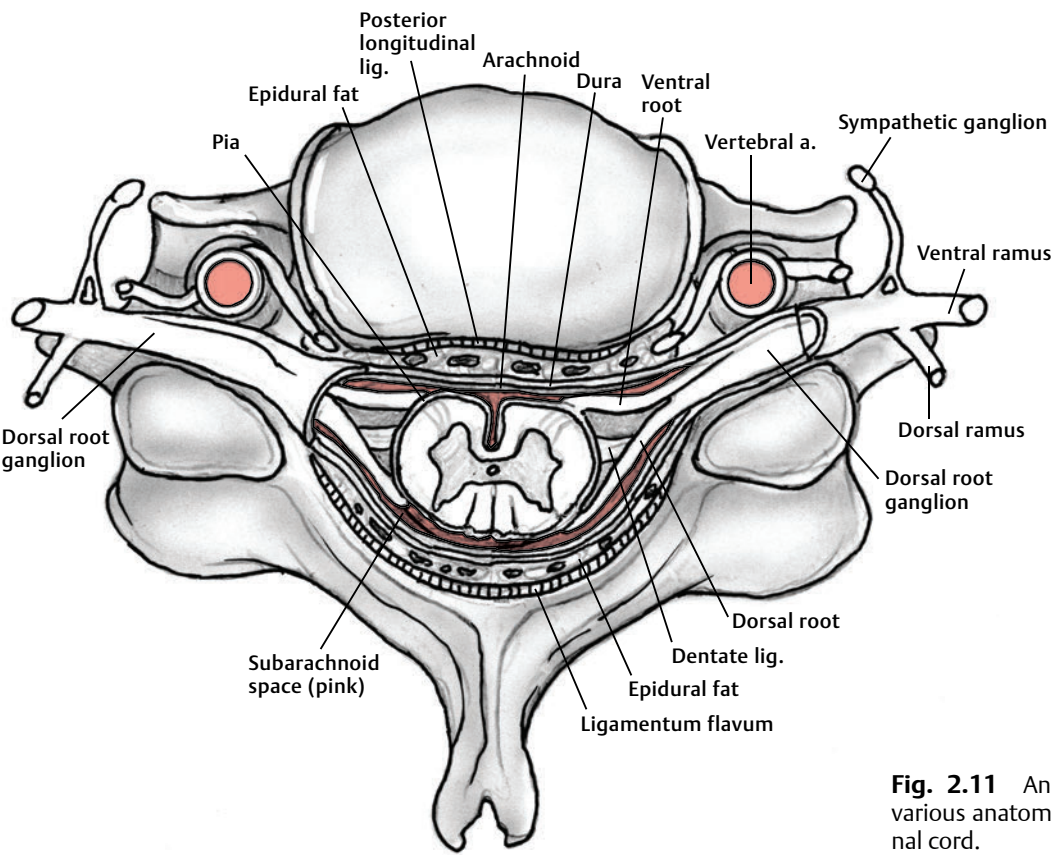


Fig. 2.11 An axial artist's sketch shows various anatomic structures around the spinal cord.

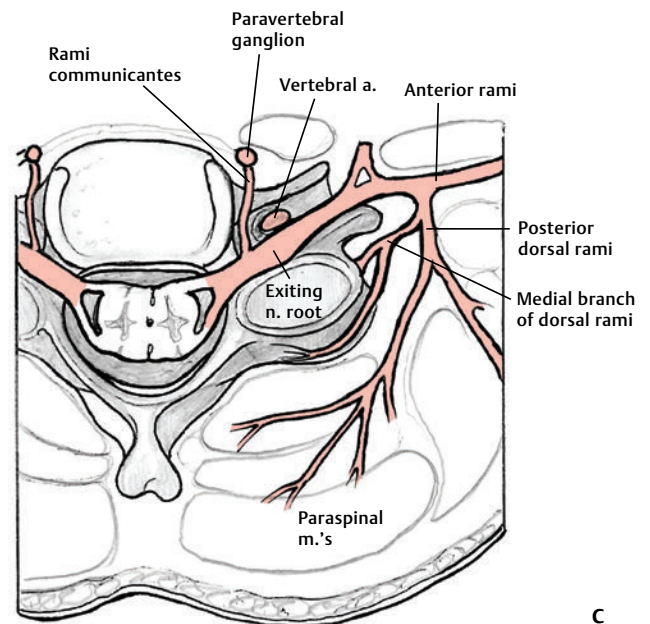
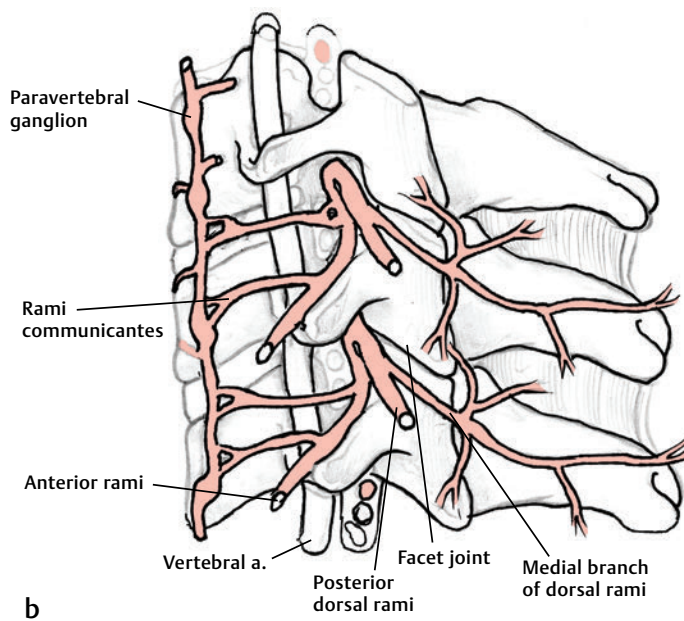
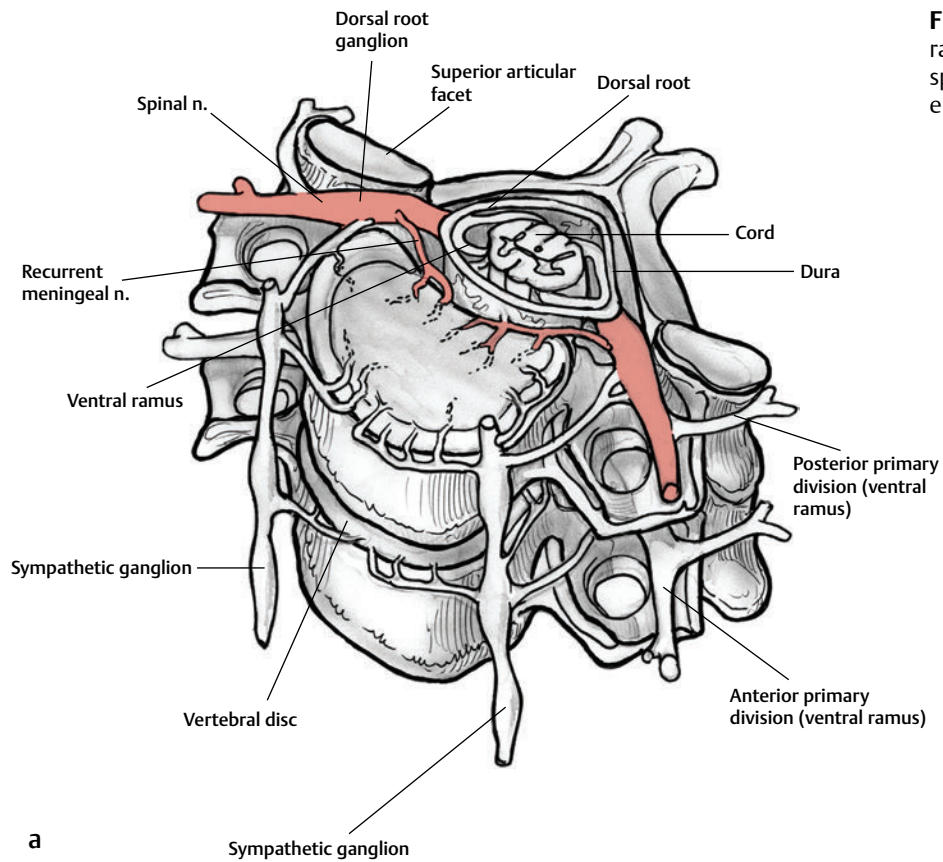


Fig. 2.12 Artist's sketches of the neural structures in and around the cervical spine from the (a) anterosuperior, (b) lateral, and (c) axial perspectives.[†]

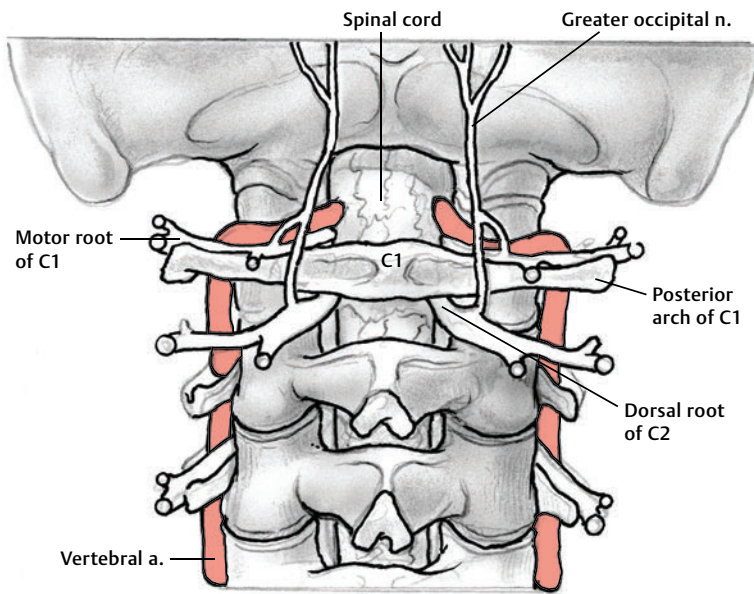


Fig. 2.13 A posterior 3D artist's sketch of the upper cervical spine shows the location of the vertebral artery relative to the posterior arch of C1 and the exit of the C2 nerve root above the pedicle of C2.[†]

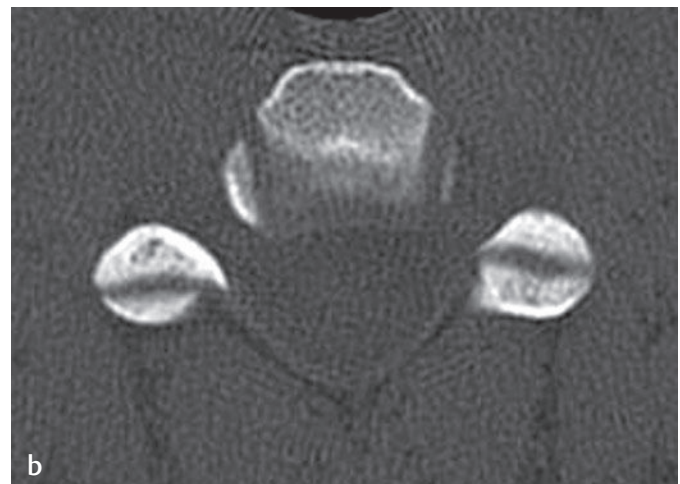


Fig. 2.14 Facet joints in the cervical spine. The facet joint is the articulation of the inferior articular process of the posterior elements of a vertebra with the superior articular process of the posterior elements of the next vertebra. **(a)** Parasagittal T1-weighted MR and **(b)** axial CT images show normal facet joints in the cervical spine.



Fig. 2.15 This 2D time-of-flight sequence shows the normal vascular anatomy of the upper cervical spine.

Spinal radicular arteries supply the vertebrae, meninges, and spinal cord. Radicular arteries arise from the vertebral, deep cervical, posterior intercostal, lumbar, and lateral sacral arteries. Radicular arteries enter through the neuroforamina and divide into anterior and posterior branches (**Fig. 2.16**).

The anterior spinal artery supplies three major regions: the cervicothoracic, the midthoracic, and the thoracolumbar spinal cord (**Figs. 2.5** and **2.17**). There are watershed areas at the margins of each region where adequate collateral flow is not always available. In watershed areas, the spinal cord is vulnerable to infarction in the case of systemic hypotension or compromise of a major radiculomedullary feeding vessel.

There are several major radiculomedullary arteries that merit additional attention. The C3 radiculomedullary artery arises from the vertebral artery. The C6 radiculomedullary artery, or the artery of cervical enlargement, arises from the thyrocervical or costocervical trunk. The T4-T5 radiculomedullary artery arises from the intercostal artery. The T8-conus radiculomedullary artery, also known as the artery of lumbar enlargement or the artery of Adamkiewicz, arises from an intercostal or lumbar artery. The artery of Adamkiewicz has a “hairpin loop” configuration because of the differential growth of the spinal cord. In 85% of cases, the artery of Adamkiewicz arises from the left T9-L2 levels.⁴ In 15% of cases, it arises from T5-T8.⁴

The posterior spinal arteries are smaller and more uniform in caliber than the anterior spinal artery (**Fig. 2.18**). The two posterior spinal arteries are connected by frequent intercommunications across the dorsal surface of the spinal cord. There is infrequent intercommunication along the lateral surfaces of the cord between the posterior spinal arteries and

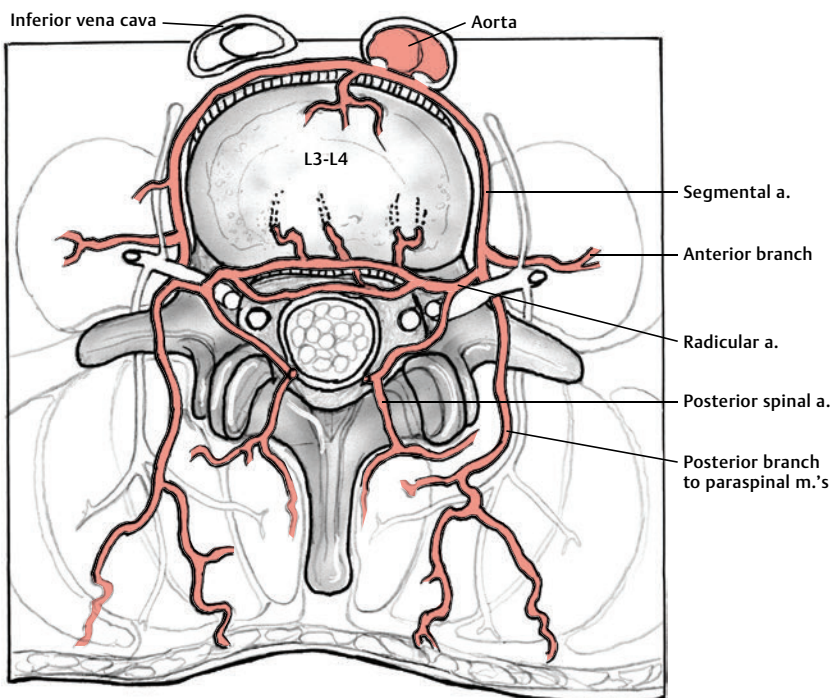


Fig. 2.16 An artist's sketch of the arterial vasculature of the lumbar spine (axial perspective at the L3-L4 level). The spinal radicular arteries supply the vertebrae, meninges, and spinal cord and enter via the neural foramina.

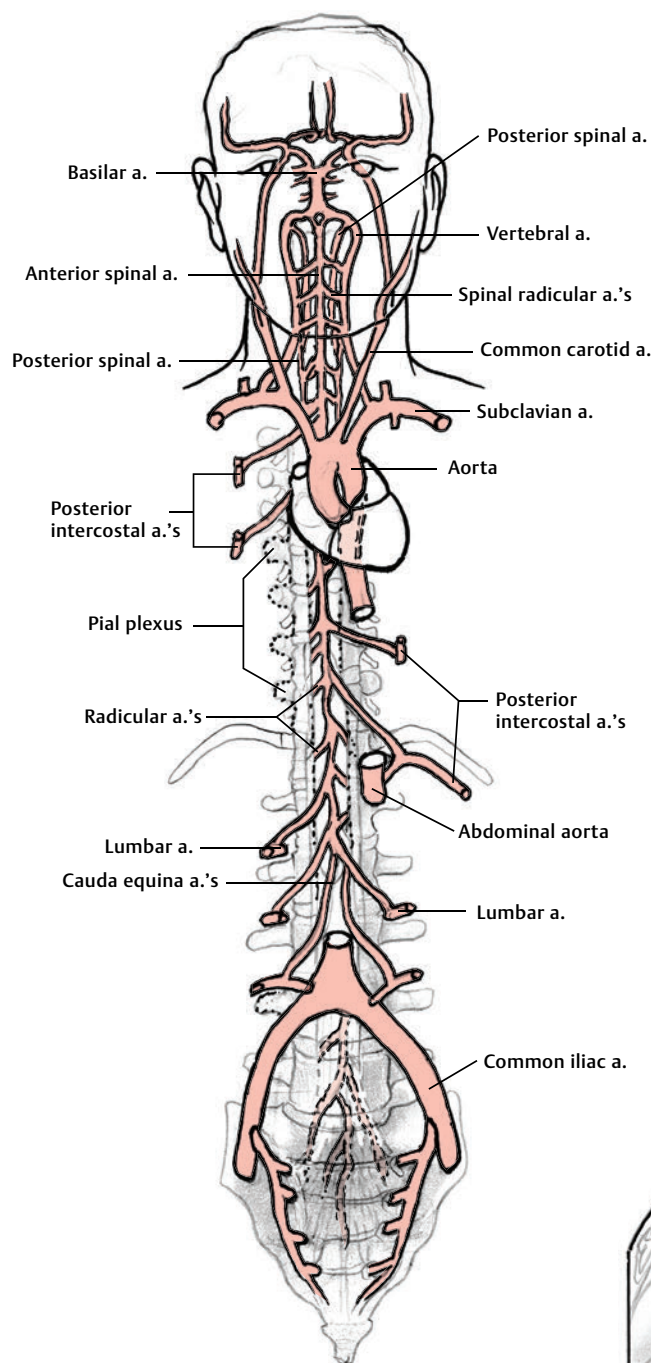


Fig. 2.17 An artist's sketch of the arterial vasculature of the spine from an anterior perspective.

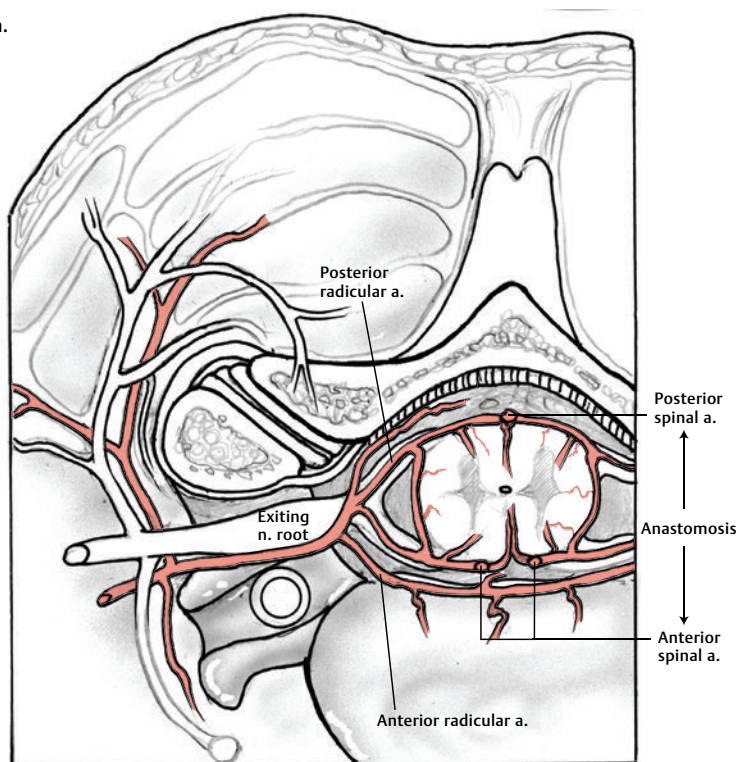


Fig. 2.18 An artist's sketch depicts the anastomoses between the posterior spinal artery and the anterior spinal artery.

the anterior spinal artery through the circumferential pial arterial plexus.

Venous drainage occurs via the external vertebral plexus and subsequently the internal vertebral plexus via basivertebral veins (**Fig. 2.19**). The basi-vertebral plexus has a Y-shaped appearance on axial images. The cord and vertebral plexi drain via radicular and intervertebral veins through neuroforamina into the vertebral vein, ascending lumbar veins, and azygous system (**Fig. 2.20**).

On gadolinium-enhanced MRI, there is normal enhancement of the vessels of the epidural plexus and the basivertebral venous plexus.

Muscles

The paraspinal muscles are the group of superficial and deep muscles that run adjacent to the spine (**Fig. 2.21**). They help support the spine and assist with motion of individual bones and of the core as a whole. The superficial or extrinsic paraspinal muscles include the trapezius, latissimus dorsi, levator scapulae, rhomboid minor, and rhomboid major. The deep muscles of the cervical, thoracic, and lumbar spine include the splenius capitis, splenius cervicis, erector spinae, semispinalis, multifidus, rotatores, interspinalis, and intertransverse. Suboccipital deep muscles include the rectus capitis, oblique capitis superior, and oblique capitis inferior. Prevertebral deep muscles include the rectus capitis, longus colli, longus capitis, scalene, and psoas. The paraspinal



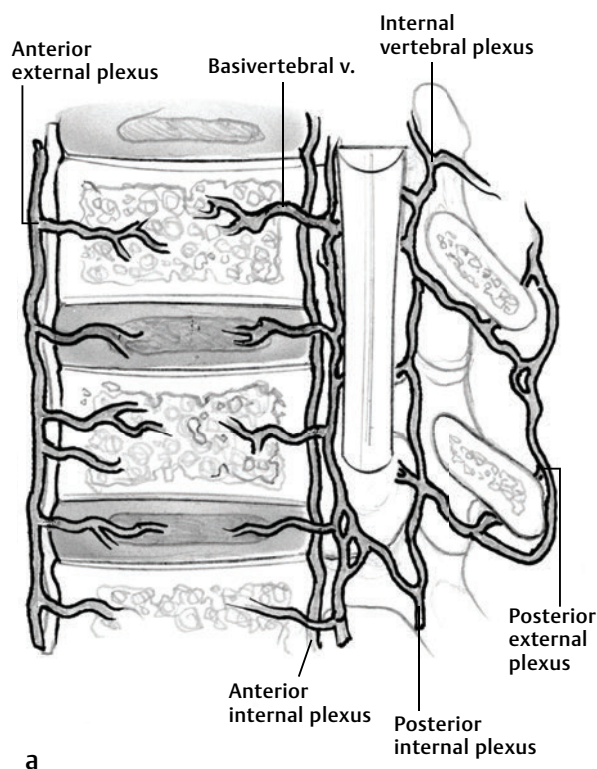
Fig. 2.19 A sagittal fat-suppressed T2-weighted image shows venous drainage in the spine.

muscles should be evaluated by MRI to assess for asymmetry, atrophy, and/or pathology.

■ Cervical Spine

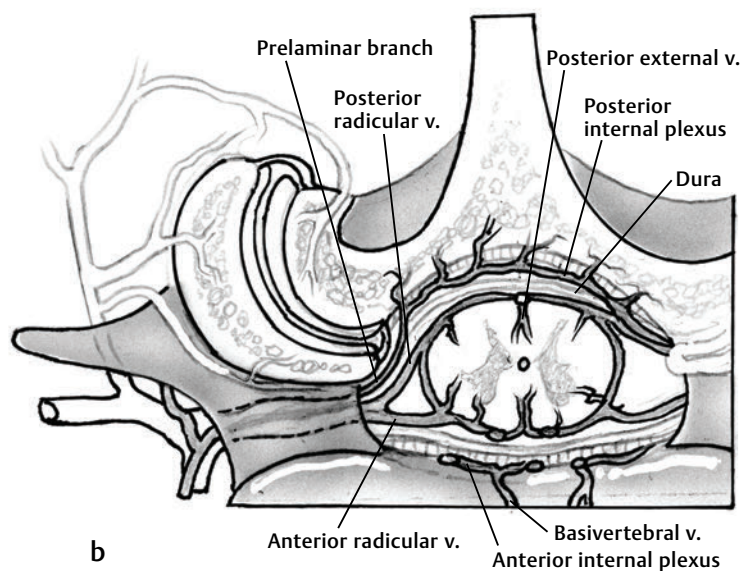
Anatomy

The occiput is labeled as C0. The occipital bone is a broad, flat bone that encircles the cerebellum as it gives rise to the pons and medulla in the posterior fossa. The sphenoid bone also contributes to the anterior aspect of the posterior fossa. The clivus is the portion of the sphenoid bone that meets the occipital bone. The foramen magnum is the opening at the base of the skull. It is defined anteriorly by the basion, posteriorly by the opisthion, and laterally by the occipital condyles. The occipital condyles contain the hypoglossal nerve as it courses anteriorly to exit the hypoglossal foramen. The external occipital protuberance is the attachment site of the ligamentum nuchae and the trapezius muscle. The inion, a term sometimes used as a synonym for the external occipital protuberance, is actually the highest point of the external occipital protuberance. The external occipital protuberance corresponds internally with the confluences of the sinuses. Other important external landmarks include the superior and inferior nuchal lines, which are attachment sites for cervical musculature.



a

Fig. 2.20 Artist's sketches detail the venous drainage of the spine from (a) sagittal and (b) axial perspectives.



b

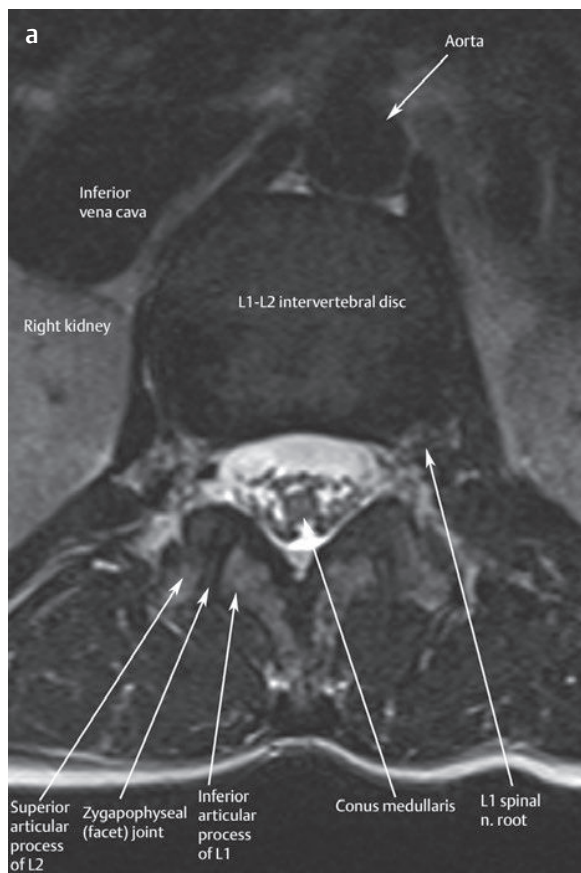


Fig. 2.21 This (a) axial T2-weighted image and (b) artist's sketch of the normal anatomic location of the paraspinal muscles and other neurovascular structures. These views at the level of the L1-L2 intervertebral disc show the conus medullaris and the L1 spinal nerve root, as well as the superior and inferior articular processes of the L1-L2 facet joint.[†]

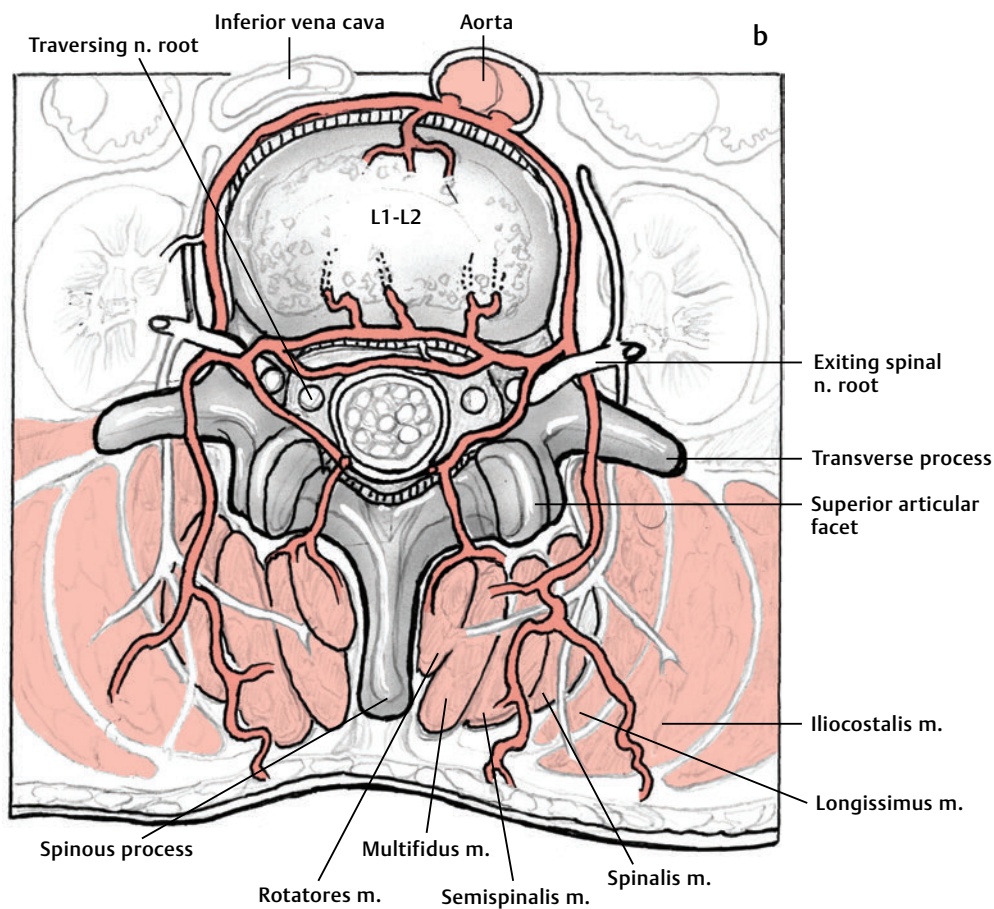




Fig. 2.22 A coronal T1-weighted image shows the normal anatomic articulation of the lateral masses of C1 and C2.

C1, also known as the atlas, is a ring-shaped structure that lacks a vertebral body. It is, instead, composed of two lateral masses, a short anterior arch, a longer posterior arch, and grooves for the vertebral artery. The right and left lateral masses are connected by the anterior and posterior arches. The lateral masses of C1 articulate inferiorly via facet joints with C2 (**Fig. 2.22**). The dens, or odontoid process of C2, articulates with the anterior arch of C1 (**Fig. 2.23**). The C0-C1 articulation is termed the atlantooccipital joint and is a cup-shaped configuration (**Fig. 2.24**). In addition to primary stabilization from the morphology of the joint, ligamentous stabilizing structures are present and include joint capsules, anterior and posterior atlantooccipital membranes, and C0-C2 ligaments. The primary motion of the atlantooccipital joint is flexion-extension by which the occipital condyles glide in the sockets of the atlas. Lateral flexion is constrained by the contralateral alar ligament.

C2 is termed the axis. The dens, or the odontoid process, is a protuberance from the axis. An os odontoideum is a variant in which the dens is separate from the body of the axis (**Fig. 2.25**). The cause of os odontoideum is unknown and may be a congenital failure of fusion secondary to trauma. The C1-C2 articulation is termed the atlantoaxial joint. There are



Fig. 2.23 A sagittal T1-weighted image shows the normal articulation of the anterior arch of C1 and the odontoid process of C2.



Fig. 2.24 A sagittal T1-weighted image shows the cup-shaped configuration of the craniocervical joint; the subaxial facet joints are also well visualized.



Fig. 2.25 A sagittal T1-weighted image shows an os odontoidum, often a normal variant where the dens is separate from the body of the axis.

paired lateral articulations and a midline medial articulation. The lateral atlantoaxial joint is formed between the lateral masses of the atlas and the superior articular surface of the axis. The median atlantoaxial joint is formed between the dens and the anterior arch of the atlas. These joints may communicate in total or in part, as appreciated on T2-weighted and contrast-enhanced MR images. The primary movement of the atlantoaxial joint is axial rotation. Flexion-extension is limited by the transverse ligament and the tectorial membrane. Lateral bending is limited by the contralateral alar ligament.

In addition to the alar ligament, there are several other key ligaments of the craniocervical junction (**Fig. 2.9**). The transverse or horizontal cruciform ligament is the largest and strongest of the craniocervical junction ligaments. It passes posterior to the odontoid process and attaches at the lateral tubercles of the atlas. The apical ligament attaches the tip of the odontoid to the basion and has uncertain biomechanical function. The tectorial membrane is dorsal to the cruciform ligament and is contiguous with the posterior longitudinal ligament inferiorly and the dura of the clivus superiorly. The anterior and posterior atlantooccipital membranes attach the atlas to the foramen magnum. The posterior atlantooccipital membrane plays a role in cervicogenic headaches.

The cervical vertebrae of C3-C7 are small but relatively broad. They contain a large triangular vertebral

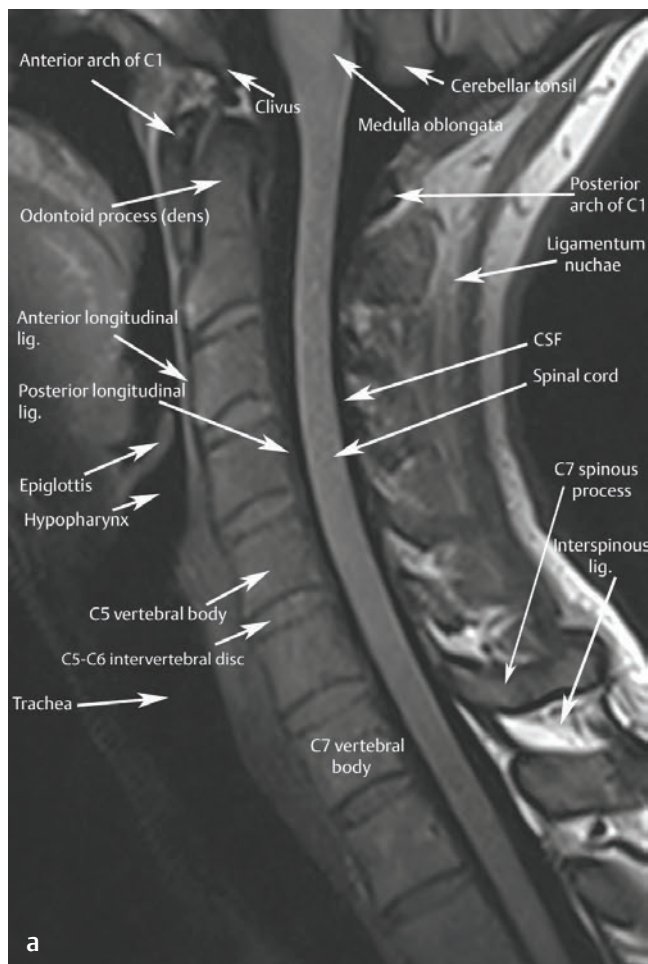


Fig. 2.26 This (a) sagittal T1-weighted midline image and (b) artist's sketch of the cervical spine depict the cervical cord, CSF, and the anterior and posterior longitudinal ligaments, as well as the anterior and posterior elements of the cervical spine and the intervertebral discs.[†]

foramen and short bifid spinous processes. There is a raised lip on the upper surface of the vertebral body. The vertebral arteries ascend in the bilateral foramen transversarium from C1-C6. They pass lateral to the C1-C2 joint and pierce the dura above the C1 arch.

Sagittal MRI

The T1-weighted and T2-weighted sagittal images should be reviewed first to evaluate the spinal anatomy (**Fig. 2.26**). The midsagittal image from the cervicomedullary to cervicothoracic junctions is a good anatomic screen of the cervical vertebral bodies, intervertebral discs, spinal cord, thecal sac, and posterior elements. To find the midsagittal image, the sagittal series should be reviewed for the image that best shows the entire cervical spinal cord and

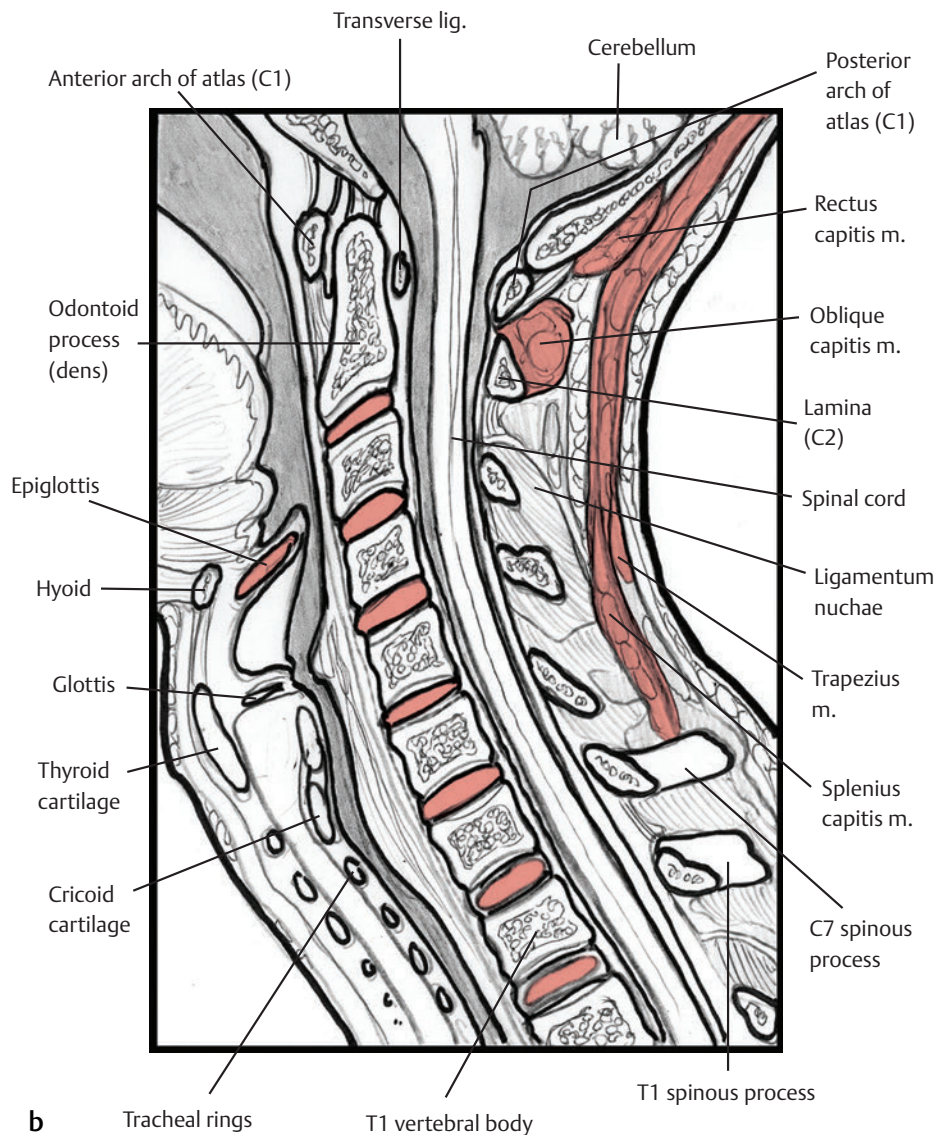


Fig. 2.26 Continued

the odontoid process, basion, opisthion, midbrain, and fourth ventricle.

Sequential evaluation of the sagittal series away from the midsagittal image allows for assessment of facet joints and neural foramina (**Fig. 2.27**). The foramina have an oblique orientation to the sagittal plane, which can cause distortion and lead to artifactual narrowing. T1-weighted images are somewhat limited because they afford poor differentiation of the vertebral body, the annular-posterior longitudinal ligament complex, and the CSF in the adjacent thecal sac.⁵ The posterior longitudinal ligament, a disc herniation, an osseous spur, and CSF all appear as a low-intensity signal on T1-weighted sagittal images.⁵ The CSF-extradural interface is well defined on T2-weighted images, and a myelographic appearance is produced on T2-weighted sagittal im-

ages because of the high signal intensity of CSF. The intervertebral discs show intermediate signal intensity on T1-weighted images and high signal intensity on T2-weighted and gradient-echo images.

The cervical vertebral body has bright signal intensity on T1-weighted images because of the presence of normal fatty bone marrow. Normal cervical spine lordosis should be observed. The AP diameter of the canal tapers from the first to third cervical levels and then is relatively constant. Parasagittal images show the short cervical pedicles. The anterior and posterior longitudinal ligaments are depicted as low-signal-intensity linear structures along the vertebral bodies.^{3,6,7} Often, a small cortical defect is seen in the midportion of the posterior vertebral body; this defect represents a vascular channel and is a normal finding.

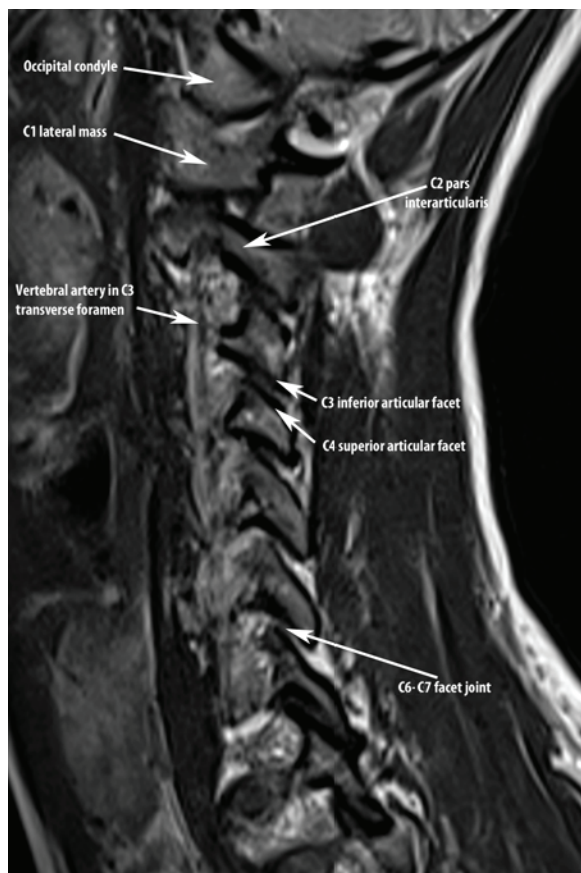


Fig. 2.27 A sagittal T2-weighted paramidline image of the cervical spine shows the vertebral artery in long axis coursing through the transverse foramina of the cervical spine. The facet joints are most easily evaluated in the parasagittal plane, as shown here.[†]

Axial MRI

Evaluation of the cervical spine MR images in the axial plane requires the correct identification of the spinal level, which can be accomplished by using the localizing sagittal images or by evaluating signal-intensity differences between the intervertebral discs and vertebral bodies and sequentially numbering the levels caudal to the odontoid process. Given the potential risk of wrong-level surgery,⁸ special care should be taken to identify the level by using a combination of these two labeling techniques. In addition, most imaging workstations have tools that enable the vertebral bodies to be identified using the numbering techniques just mentioned, which facilitates rapid localization on the midsagittal images while evaluating the associated axial images. In addition, the sagittal and axial images can often be linked on viewing stations and with image-viewing software to enable definitive localization of pathology in the sagittal and axial planes.

Cervical spine anatomy and anatomic pathology are well visualized on axial T1-weighted images; T2-weighted images have good CSF-to-cord contrast (**Fig. 2.8**), which enables evaluation of spinal cord or nerve root compression.^{3,6,7} Knowledge of the location of the various spinal tracts (**Fig. 2.28**) can help a clinician correlate the clinical and radiographic findings in a patient with known or suspected spinal cord injury. Compared with sagittal images, axial T2-weighted images can provide a higher-resolution depiction of the cord (because of the smaller field of view), enabling a more sensitive assessment of its

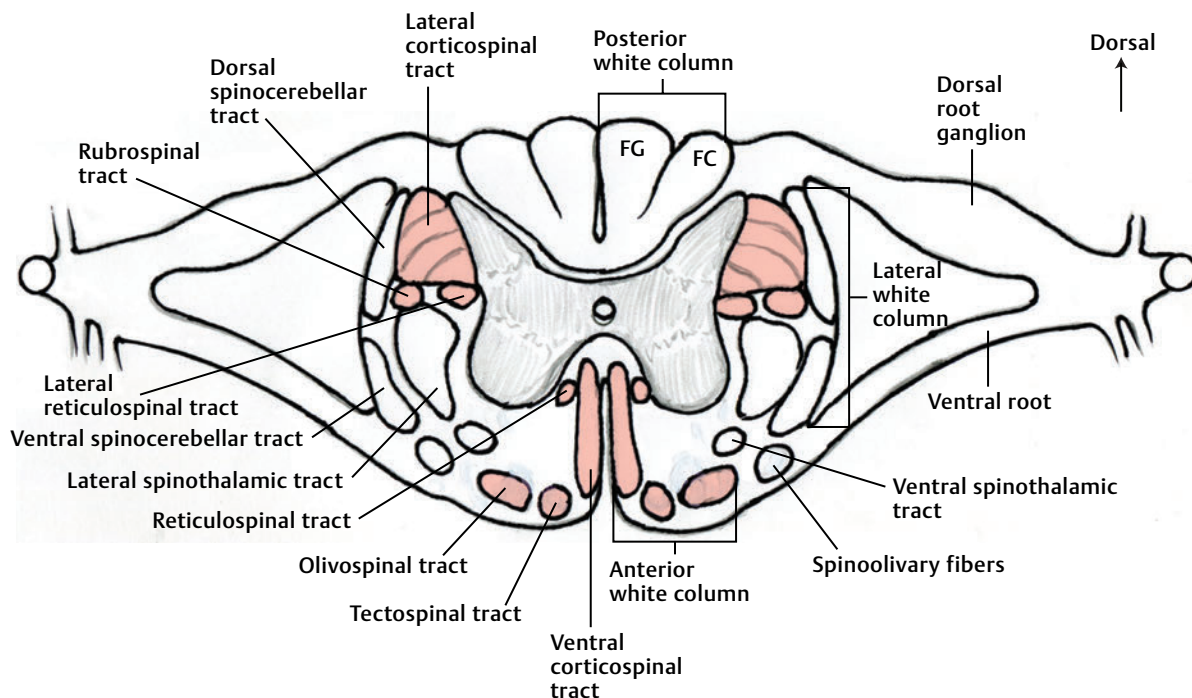


Fig. 2.28 Artist's axial sketch shows spinal cord anatomy, including the various spinal cord tracts.[†] FC, fasciculus cuneatus; FG, fasciculus gracilis.

signal characteristics. Sagittal images are also helpful in evaluating signal abnormalities in the spinal cord because one image can show a long segment of the spinal cord. Neural foramina are best depicted with gradient-echo and T2-weighted images and should be evaluated on axial and parasagittal images. Evaluation of the neural foramina in the axial and sagittal planes improves with experience and training, especially with patients who have scoliosis or poor positioning in the scanner, which can cause each neural foramen to be visualized on different parasagittal or axial images. Care should be taken to evaluate the axial T2-weighted images and to recognize the normal shape and size of the central canal and the neural foramina. Specifically, the degree of contribution of the three primary contributors to cervical spinal stenosis (disc pathology, facet arthropathy, and ligamentum flavum hypertrophy) should be noted, and their combined contribution to the degree of central and foraminal stenosis should be assessed. The anterior border of the neural foramen is the disc, and the posterior border is the facet joint (**Fig. 2.29**). It is important to note the location and course of the vertebral arteries on the axial images. Aberrant vertebral arteries should be identified preoperatively, especially if a cervical corpectomy is being considered. Furthermore, the vertebral arteries should show normal hypointense pulsation signal. As with any radiographic study, in addition to the structures detailed previously, all imaged structures should also be evaluated for potential pathology or incidental findings. For instance, lymph nodes in the neck should be evaluated for size and the presence of a normal fatty hilum. The thyroid should also be evaluated for size and to exclude large nodules.

Coronal MRI

Coronal images show the craniocervical spine articulations, intervertebral discs, uncinat processes, atlantooccipital joints, and lateral atlantoaxial joints.³ Although the sagittal and axial images provide enough information for diagnosis in most cases, coronal images may be especially valuable for evaluating the craniocervical junction or assessing for spinal tumors. Coronal plane MR images, along with conventional radiographs, also facilitate evaluation of the rarely occurring cervical scoliosis because the entire scoliotic spine can be included within a single imaging plane.

■ Thoracic Spine

MRI of the thoracic spine is obtained far less frequently than that of the lumbar and cervical spine. The anatomic structures in the thoracic spine are

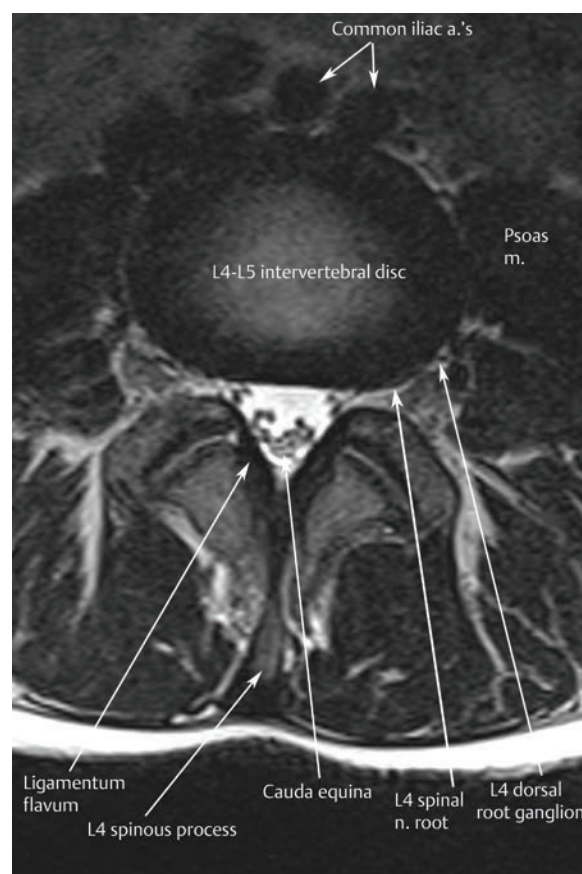


Fig. 2.29 An axial T2-weighted image of the lumbar spine at the L4-L5 level shows the cauda equina, L4 spinal nerve root, and L4 dorsal nerve root ganglion. Normal flow voids are seen within the common iliac arteries, just below the aortic bifurcation.[†]

unique in that the ribs form two additional articulations with the vertebrae: the costocentral joint (between the vertebral body and the rib head) and the costotransverse joint (between the transverse process and proximal rib). The thoracic intervertebral discs are fairly uniform in shape and size. The facet joints are coronally oriented.

■ Lumbar Spine

Anatomy

The lumbar vertebrae have relatively large bodies. The fifth lumbar vertebra should have the largest body. There is a triangular spinal foramen in most cases. The transverse processes are thin and long. The superior articular facets are often concave, whereas the inferior articular facets are often convex.

Sagittal MRI

Sagittal imaging of the lumbar spine is usually obtained with T1-weighted and T2-weighted pulse sequences (**Figs. 2.30** and **2.31**). The T1-weighted images are best used for evaluating the anatomic detail of the lumbar spine. The midsagittal image should be evaluated first. This image shows the full profile of the sacrum and most of the lumbar vertebral bodies, spinal cord, and cauda equina in patients without substantial scoliosis. After evalu-

ating the midsagittal image, the sagittal images are sequentially evaluated toward each side to assess the facet joints and neural foramina. The sagittal images can be concurrently evaluated with the axial sequence to confirm laterality. The bright signal from CSF on T2-weighted images provides a myelographic effect. T1-weighted gradient-echo images assist by providing improved evaluation of end plate and osteophyte anatomy and differentiation of the anterior and posterior longitudinal ligaments from the cortical bone.

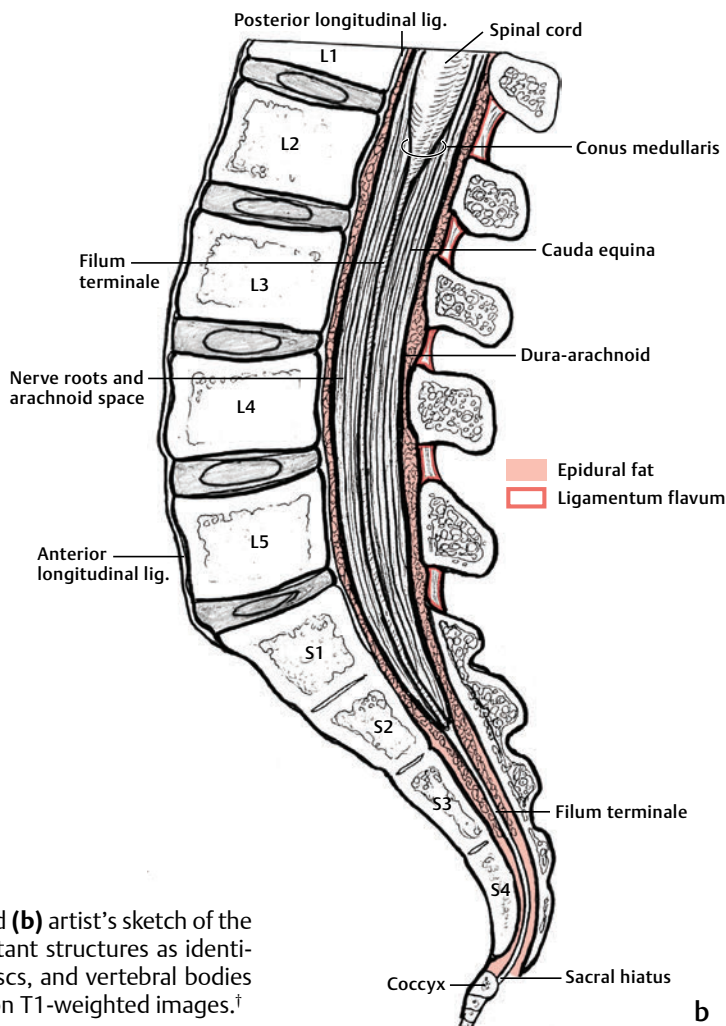
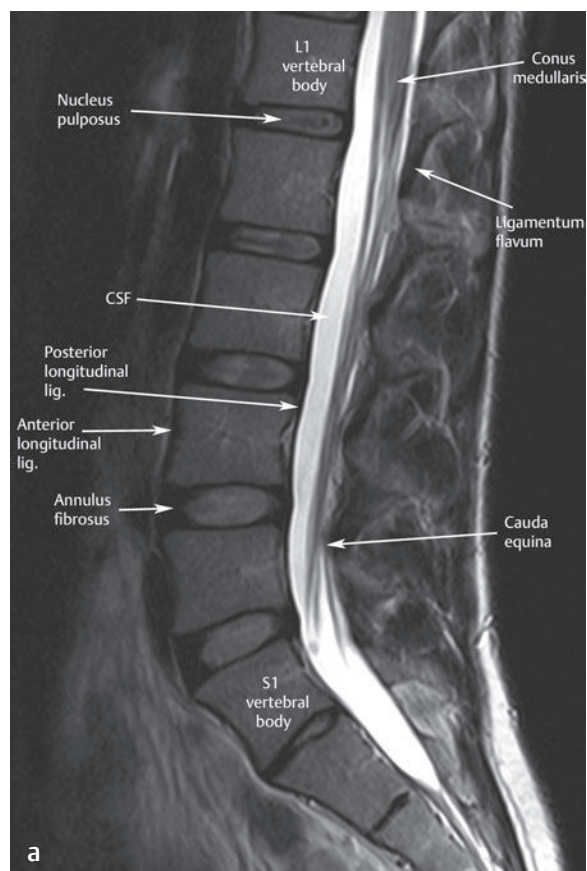


Fig. 2.30 This (a) sagittal T2-weighted midline image and (b) artist's sketch of the lumbar spine show the conus medullaris and other important structures as identified. The posterior longitudinal ligament, intervertebral discs, and vertebral bodies are better differentiated on the T2-weighted images than on T1-weighted images.[†]

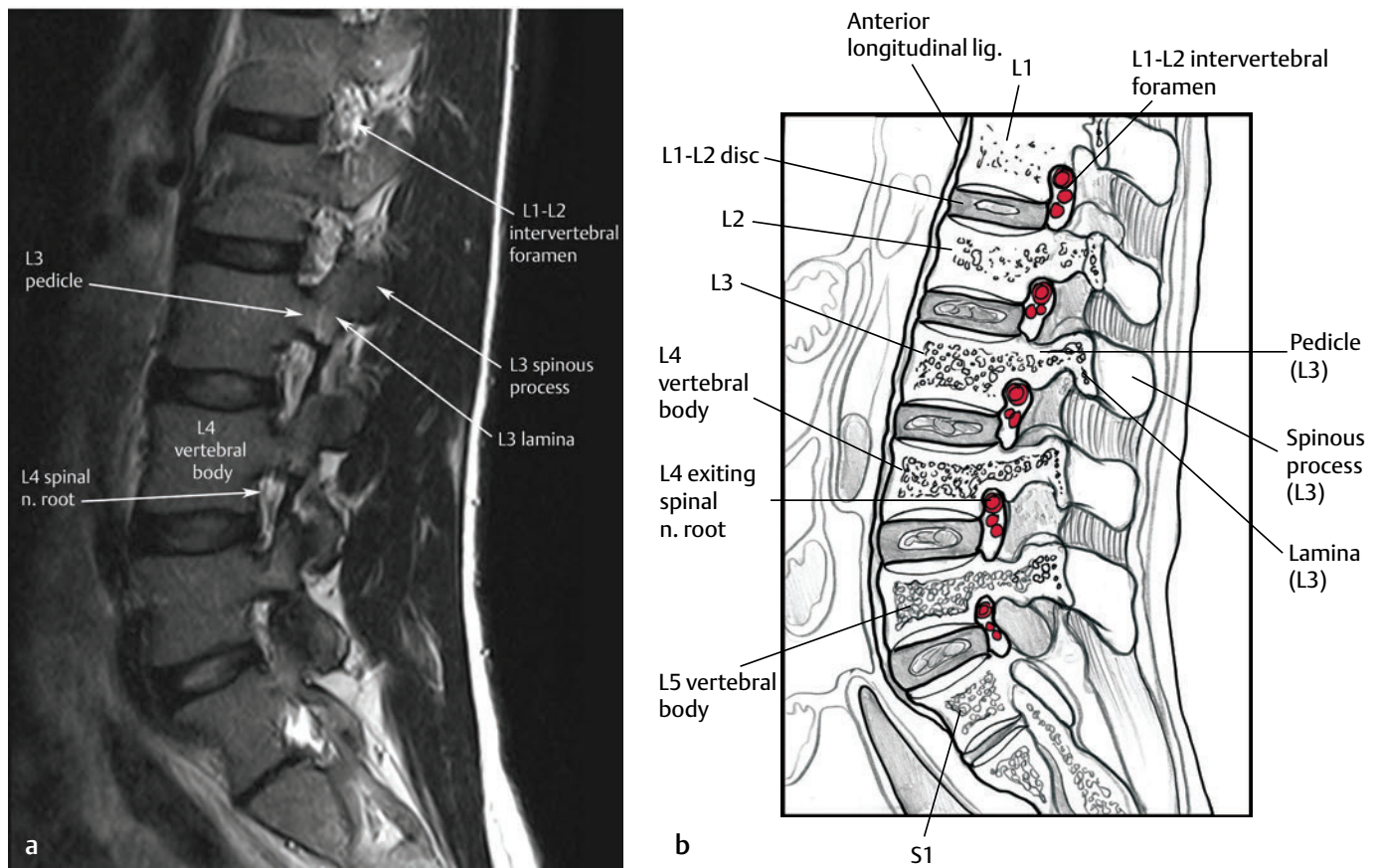


Fig. 2.31 This (a) parasagittal T2-weighted image and (b) artist's sketch of the lumbar spine show the neural foramina and exiting nerve roots at multiple levels.[†]

Axial MRI

When evaluating axial MR images, it is important to accurately identify the level at which the pathology exists, which can be achieved by using the localizing sagittal image. In addition, each level can be identified by starting at the sacrum and numbering each vertebral body from L5-L1. In complex cases where severe pathology is present at multiple levels, it may also be helpful to use the spine-labeling tool discussed previously in the section on the cervical spine. This tool is frequently available on imaging workstations, often with imaging software that includes studies provided on a CD/DVD or via Internet connection. On axial images, the difference in signal intensity be-

tween the intervertebral discs and vertebral bodies allows for the distinction between vertebral levels. Accurate and consistent evaluation of the axial images requires more experience and training than does the evaluation of the sagittal images. Care should be taken to evaluate the axial T2-weighted images and recognize the normal shape and size of the central canal and the neural foramina (**Fig. 2.32**). Specifically, the degree of contribution of the three primary contributors to spinal stenosis (disc pathology, facet arthropathy, and ligamentum flavum hypertrophy) should be noted, and their combined contribution to the degree of central and foraminal stenosis should be carefully assessed (**Fig. 2.33**). The relationship between the superior articular process from the caudal

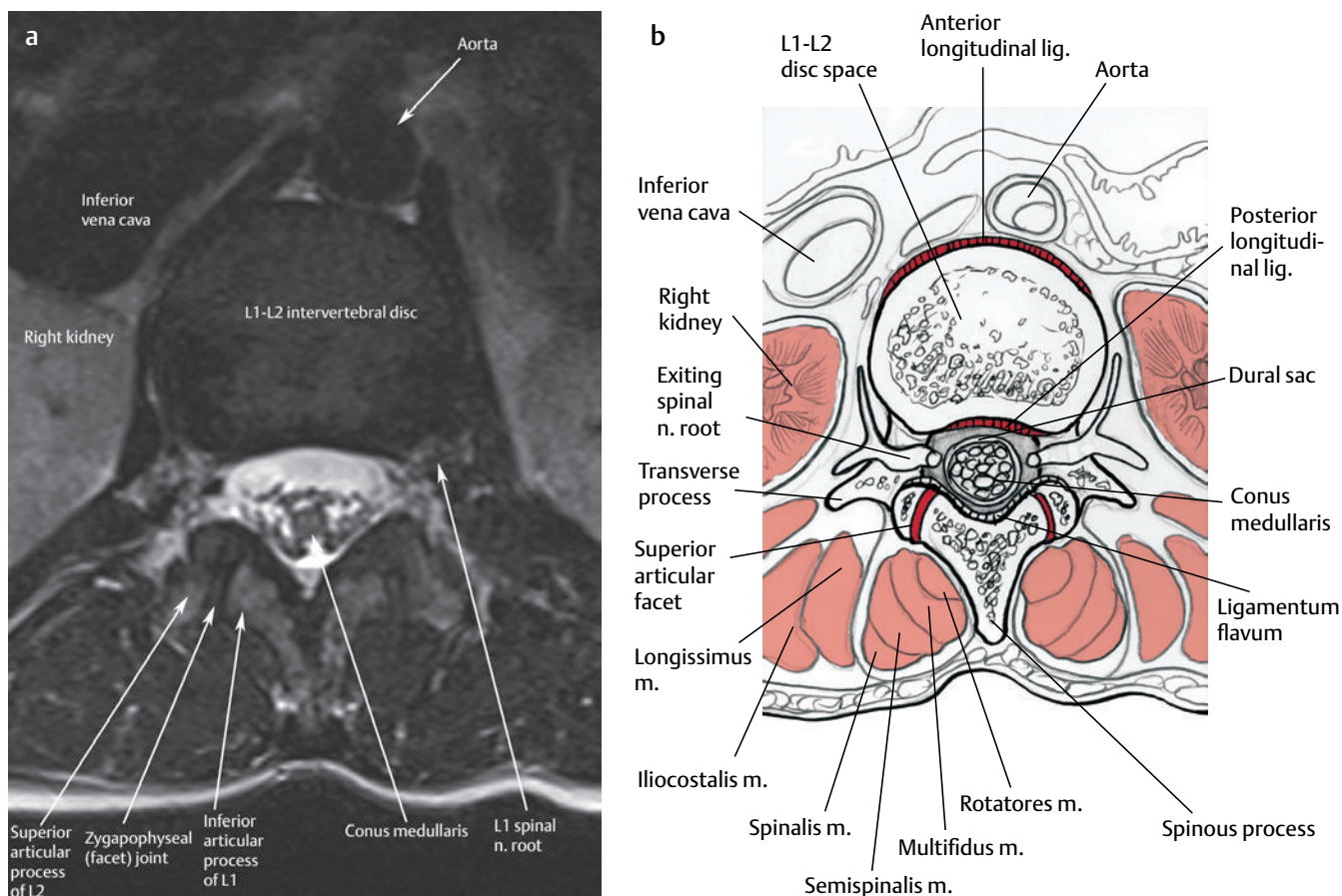


Fig. 2.32 This (a) axial T2-weighted image and (b) artist's sketch of the spine at the level of the L1-L2 intervertebral disc show the conus medullaris and the L1 spinal nerve root, as well as the superior and inferior articular processes of the L1-L2 facet joint.[†]

level and the exiting nerve root should be evaluated because hypertrophy of this structure leads to lateral recess and foraminal stenosis. The extraforaminal zone should also be studied at each level to rule out far-lateral disc pathology. The psoas muscles are seen adjacent to the vertebral bodies in the lumbar spine (**Fig. 2.33**), and the major vessels (including the aorta and vena cava) are seen anterior to the vertebral bodies. Along with the spine, these structures should also be evaluated for pathologic processes such as aneurysm, thrombosis, and infection.

Coronal MRI

Coronal images provide a clear evaluation of the general alignment and anatomy of the lumbar spine, enabling the identification of the vertebrae and intervertebral discs. As with the cervical spine, coro-

nal plane MR images of the lumbar spine, along with conventional radiographs, also facilitate evaluation of lumbar scoliosis. Because lordosis increases toward the caudal aspect of the lumbar spine, it is impossible to obtain one image that visualizes the entire spinal canal and its contents. The coronal plane images can be used to evaluate spinal alignment and transitional anatomy at the lumbosacral junction.

■ Sacrum and Coccyx

The sacrum is a block of bone at the base of the vertebral column that consists of the fusion of S1-S5. It supports the spine and transmits load. The sacrum is normally triangular in shape with broad cephalad tapers. There are anterior and posterior foramina.

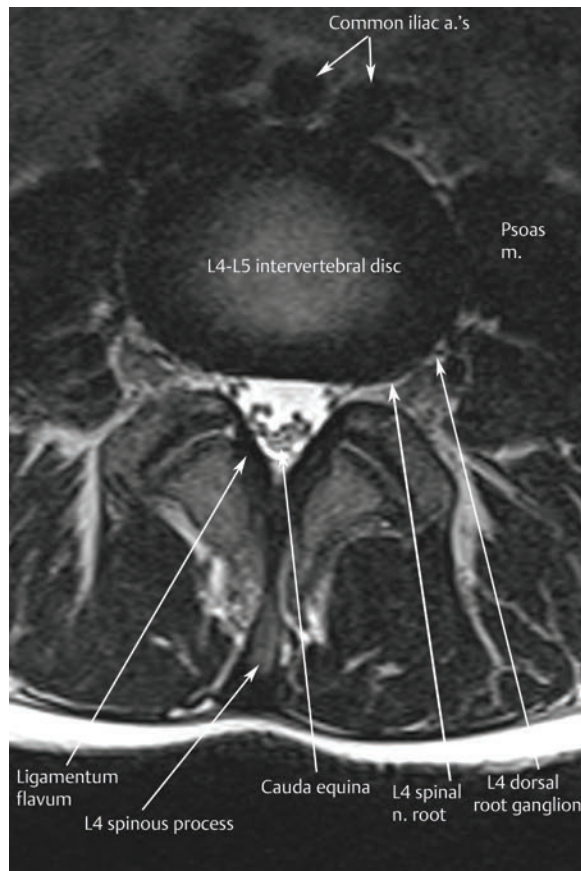


Fig. 2.33 An axial T2-weighted image at the level of the L4-L5 intervertebral disc shows the cauda equina, L4 spinal nerve root, and L4 dorsal root ganglion. Normal flow voids are seen within the common iliac arteries, just below the aortic bifurcation.[†]

The coccyx articulates with the sacrum inferiorly and represents the fusion of four rudimentary vertebrae. The term “sacrum” literally translates to “holy bone.”

The sacroiliac joint has a small range of motion with essentially passive movements (**Fig. 2.34**). There are no associated muscles that execute active movements. The axis of movement passes obliquely across the pelvis. With flexion, the axis passes backward from the pubic symphysis to the sciatic notch. With extension, the axis passes from the pubic symphysis through the pelvis between the ischium and the coccyx.

The sacroiliac joint shows sequential changes with age. In the embryo phase, the sacroiliac joint is a strip of mesenchyme that undergoes cavitation.

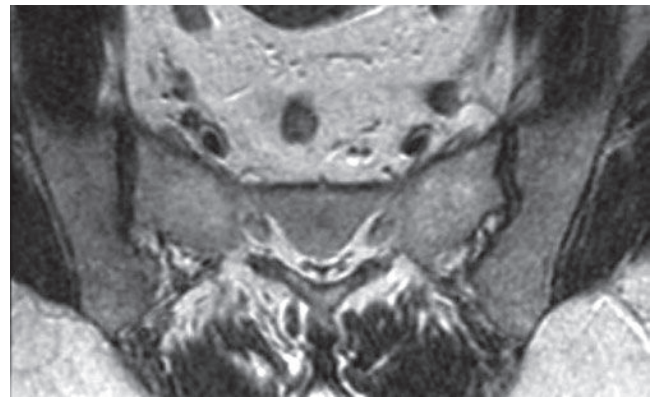


Fig. 2.34 An axial T1-weighted image shows the normal appearance of the sacroiliac joints.

During the first decade of life, the joint enlarges but remains flat. During the second decade, there is corrugation of joint surfaces. Osteophytes develop in the fifth and sixth decades, and large interdigitating osteophytes can develop during the eighth decade.

COMMON CLINICAL QUESTIONS

1. The facet joints are synovial joints between the superior and inferior articular processes. True or false?
2. The spinal column typically comprises 7 cervical vertebrae, 13 thoracic vertebrae, 5 lumbar vertebrae, the sacrum, and the coccyx. True or false?
3. The most common location for a limbus vertebra is the:
 - A. Anterior superior corner
 - B. Anterior inferior corner
 - C. Posterior superior corner
 - D. Posterior inferior corner
4. Normal ligaments are bright on T1-weighted images. True or false?
5. Which pulse sequence provides a “myelographic” view of the spine and best allows for the assessment of spinal stenosis?
 - A. Sagittal T1-weighted images
 - B. Sagittal T2-weighted images
 - C. Sagittal gradient-echo images
 - D. Coronal T1-weighted images
 - E. Sagittal postcontrast T1-weighted images

References

1. Morgan S, Saifuddin A. MRI of the lumbar intervertebral disc. *Clin Radiol* 1999;54(11):703–723 PubMed
2. Mercer S, Bogduk N. The ligaments and annulus fibrosus of human adult cervical intervertebral discs. *Spine (Phila Pa 1976)* 1999;24(7):619–626, discussion 627–628 PubMed
3. White ML. Cervical spine: MR imaging techniques and anatomy. *Magn Reson Imaging Clin N Am* 2000;8(3):453–470 PubMed
4. Lazorthes G, Gouaze A, Zadeh JO, Santini JJ, Lazorthes Y, Burdin P. Arterial vascularization of the spinal cord. Recent studies of the anastomotic substitution pathways. *J Neurosurg* 1971;35(3):253–262 PubMed
5. Kaiser JA, Holland BA. Imaging of the cervical spine. *Spine (Phila Pa 1976)* 1998;23(24):2701–2712 PubMed
6. Boden SD, Lee RR, Herzog RJ. Magnetic resonance imaging of the spine. In: Frymoyer JW, ed. *The Adult Spine: Principles and Practice*. Philadelphia, PA: Lippincott-Raven; 1997:563–629
7. Khanna AJ, Carbone JJ, Kebaish KM, et al. Magnetic resonance imaging of the cervical spine. Current techniques and spectrum of disease. *J Bone Joint Surg Am* 2002;84-A(Suppl 2):70–80 PubMed
8. Palumbo MA, Bianco AJ, Esmende S, Daniels AH. Wrong-site spine surgery. *J Am Acad Orthop Surg* 2013;21(5):312–320 PubMed

ANSWERS TO COMMON CLINICAL QUESTIONS

1. True
Explanation: The facet joint is formed by the articulation between the superior articular process from the caudal vertebral body and the inferior articular process from the cranial vertebral body. It is a synovial joint.
2. False
Explanation: The spinal column typically comprises 7 cervical vertebrae, 12 (not 13) thoracic vertebrae, 5 lumbar vertebrae, the sacrum, and the coccyx.
3. A
Explanation: The most common location for a limbus vertebra is within the anterior superior corner of the vertebral body.
4. False
Explanation: Normal ligaments should have low signal intensity on all pulse sequences.
5. B
Explanation: Sagittal T2-weighted images provide a view of the spine and spinal cord that is similar to that seen with a conventional or CT myelogram in terms of contrast between the spinal cord (low signal) and CSF (high signal). This contrast allows for the optimal detection of spinal stenosis in the sagittal and axial planes.

3

Common Clinical and Correlative Pain Generators of the Cervical and Lumbosacral Spine

Josemaria Paterno, Chad M. Silverberg, A. Jay Khanna, and Aneesh K. Singla

CHAPTER OUTLINE

- I. Biochemical Basis of Radicular and Discogenic Pain
- II. Examination of Neurologic Spinal Levels
- III. Disc Herniation Pathology
- IV. Correlative Anatomy of Cervical Disc Pathology
 - A. C5 Nerve Root
 - B. C6 Nerve Root
 - C. C7 Nerve Root
 - D. C8 Nerve Root
- V. Correlative Anatomy of Lumbar Disc Pathology
 - A. Upper Lumbar Nerve Roots (L1, L2, L3 Radiculopathy)
 - B. Lower Lumbar Nerve Roots (L4, L5, S1 Radiculopathy)
 - 1. L4 Nerve Root
 - 2. L5 Nerve Root
 - 3. S1 Nerve Root
- VI. Nonradicular Axial Back Pain
 - A. Discogenic Axial Back Pain
 - 1. End-Plate Changes
 - 2. High-Intensity Zones and Annular Fissures
 - 3. Disc Herniations
 - B. Posterior Element Axial Back Pain
- VII. Summary

MRI is a highly sensitive imaging modality for the evaluation of spine pathology; however, an understanding of the anatomic basis of disease is essential to interpreting imaging findings correctly. Because a specific anatomic pain generator can be difficult to isolate by history and physical examination alone, imaging has become a useful adjunct to clinical findings in the evaluation of patients with known or suspected spinal pathologies.

It is well known that intervertebral disc pathology is a frequent finding in symptomatic and asymptomatic patients, with an increasing incidence in relative proportion to advancing age.¹⁻⁴ Degenerative changes (**Fig. 3.1**), including disc herniations and discogenic pain, may or may not present symptomatically. Imaging studies involving asymptomatic volunteers have reported the prevalence of disc herniations as ranging from 20% to 36%.^{2,3} Boden et al² noted that of 67 asymptomatic patients older than 60, 79% had annular bulges and 36% showed actual herniated discs on MRI of the lumbar spine. Teresi et al⁴ noted that of 100 asymptomatic patients, 57% had disc protrusion or annular bulge in the cervical spine.

Because symptomatic disease is often present in the midst of asymptomatic findings, interpretation of disc pathology found on MRI should take into account concordant physical examination findings, patient history, and, if available, interval changes from previous imaging studies. By correlating clinical findings with MRI pathology, appropriate therapy can be directed at one or more specific levels by the spine surgeon, interventionalist, or other treating physician. A causal diagnosis requires understanding the presenting nature of each radicular pain syndrome along with the corresponding MRI pathology.

The purpose of this chapter is to provide the reader with correlation among the anatomic, clinical, and MRI findings in patients with spinal pathologies, with a specific focus on MRI findings that have a high degree of correlation with clinical symptoms. This chapter focuses on nerve root compression at the cervical, lumbar, and sacral levels and the associated patterns of radiculopathy. The information in this chapter complements the content in Chapter 2 (Normal Spine MRI Anatomy) and Chapter 4 (A Systematic Approach to the Review of Spine MRI Studies). The foundation provided by this trio of chapters will enable the reader to better understand the material in the region-specific chapters that follow and correlate the imaging findings to their clinical manifestations.

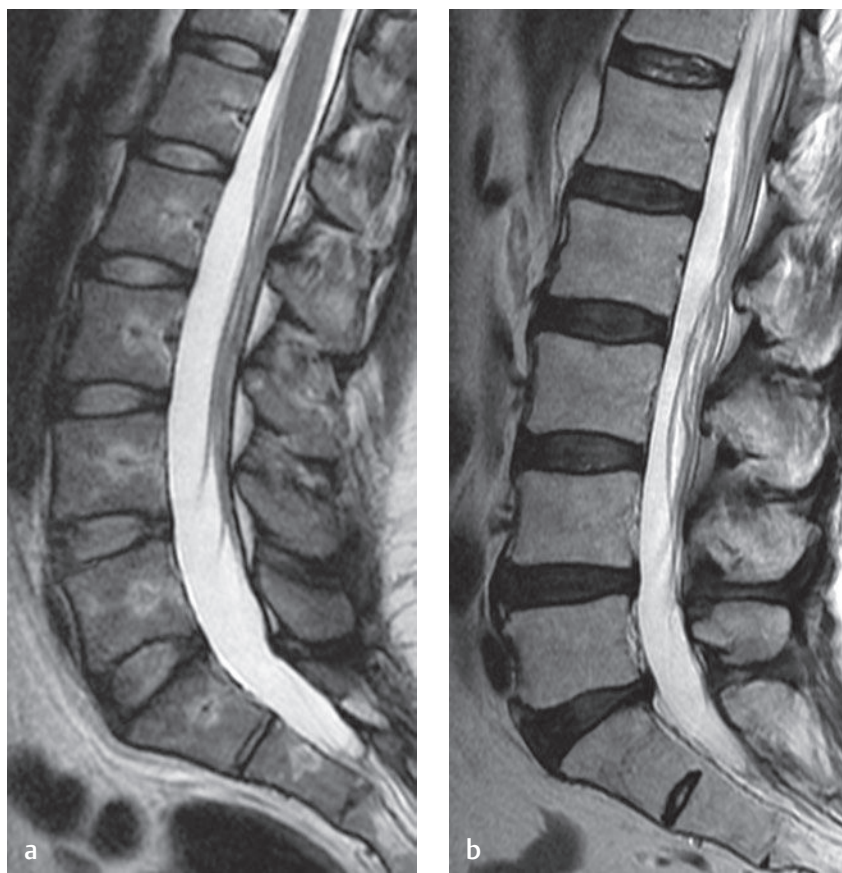


Fig. 3.1 Normal versus desiccated discs. **(a)** A sagittal T2-weighted image shows bright signal within the lumbar disc corresponding to normal disc morphology and hydration at each level in the lumbar spine. **(b)** In another patient, the lack of bright T2-weighted signal within the nucleus pulposus in this sagittal view is compatible with disc desiccation. Disc desiccation can be seen in asymptomatic patients as a component of degenerative disc disease.

■ Biochemical Basis of Radicular and Discogenic Pain

Animal and human studies have suggested that radicular pain requires not just mechanical compression of neural elements but also a concomitant inflammatory response. Kuslich et al⁵ showed that in a population of nonsedated patients undergoing discectomy under local anesthesia, traction on nerves in contact with disc material caused radicular pain; however, traction on nerves not in contact with disc material caused only modest discomfort.

Herniated disc material, specifically the nucleus pulposus, has been shown to initiate a cytokine/inflammatory cascade that transforms an impinged nerve into an acute pain generator.⁶ This model justifies a therapeutic antiinflammatory approach to treating new-onset radicular pain,⁷ such as with transforaminal and interlaminar epidural steroid injections, at the specific symptomatic level.

The annulus fibrosus is innervated by branches of the sinuvertebral nerve, particularly posteriorly. This innervation provides an anatomic path by which pain generators of the posterior disc, such as annular fissures or disc herniations, contribute

to axial back pain symptoms without concomitant radiculopathy.⁸ Discogenic pain can be a potentially confounding factor in attempting to isolate clinical pain symptoms without imaging correlation. Pain symptoms from posterior pain generators, such as the facet joints, and nonradicular discogenic pain can often overlap, creating challenging clinical scenarios. Isolating the primary pain generator often requires a multimodal approach using clinical evaluation, imaging correlation, and diagnostic interventions such as fluoroscopically guided spinal injections and discography.

■ Examination of Neurologic Spinal Levels

Knowledge of the dermatomal and segmental distribution of spinal nerves is necessary to localize pathologic levels. Broad subsets of pathology can affect nerve roots, including but not limited to disc herniation, osteoarthritis, infection, malignancy, trauma, and previously implanted spinal hardware. Before using MRI evaluation to narrow the differential considerations, the clinician must evaluate the

relevant myotome, dermatome, and reflex arc that correlate to the suspected level.

Mechanical pressure on the nerve root can produce a decrease in muscle strength. In grading a muscle, the convention is the Oxford muscle strength test, a 0- to 5-point scale⁹: grade 0, absence of contractility; grade 1, contractile activity but absence of joint motion; grade 2, *assisted* full range of motion against gravity or full range of motion with gravity eliminated (i.e., horizontal plane); grade 3, full range of motion against gravity without assistance; grade 4, full range of motion against limited resistance; and grade 5, full strength.

When evaluating sensation, each dermatome level is tested for light touch and pain perception by a cotton swab and light pinpricks, respectively. Reflex arcs must be compared with those on the other side because baseline individual reflex activity varies from patient to patient. In general, the clinician can note symmetric/normal, decreased/hyporeflexic, or increased/hyperreflexic reflex responses.

■ Disc Herniation Pathology

Most disc herniations occur in the posterolateral direction because of the anatomic protection provided by the posterior longitudinal ligament. On T2-weighted MRI sequences, the nucleus pulposus in nondisciculated discs is of high signal intensity, whereas the annulus fibrosus is of low signal intensity. Normally, the morphology of the disc is ovoid, but disc herniations will change this characteristic shape. With disc protrusions and extrusions, the normal ovoid morphology of the annulus fibrosus becomes abnormal and extends beyond the normal margin of the disc (see Chapter 7, The Thoracic and Lumbar Spine MRI). Disc herniations may contain regions of high T2 signal if there is corresponding nucleus pulposus or acute hemorrhage (**Fig. 3.2**). Most disc herniations show a low-signal-intensity annulus on T2-weighted images, providing a contrast to adjacent epidural fat, which aids in identification. When an acute hemorrhage shows associated T2 hyperintensity, disc herniations may be more difficult to identify because the appearance is similar to that of adjacent epidural fat and, therefore, there is loss of contrast.

■ Correlative Anatomy of Cervical Disc Pathology

In an American population-based study, cervical radiculopathy had an annual incidence of 107/100,000 for males and 65/100,000 for females.¹⁰ Notably, only 22% of cervical radiculopathies were caused by a disc

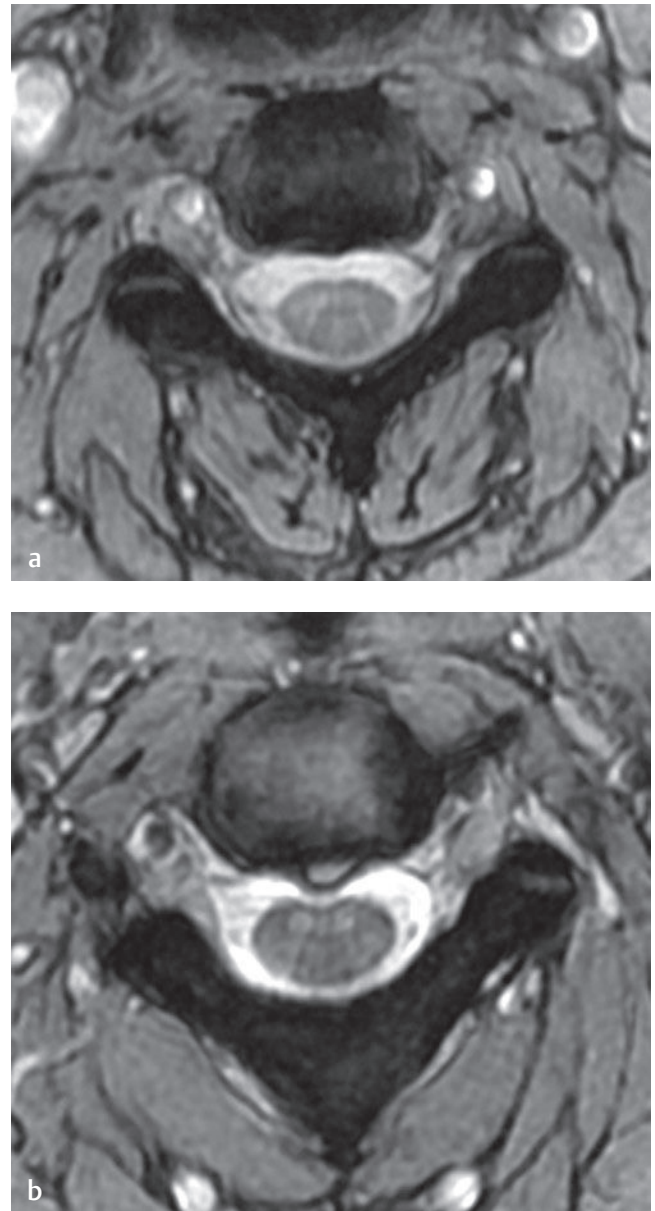


Fig. 3.2 Morphology of disc herniations. **(a)** A normal cervical disc on an axial T2-weighted image conforms to the morphology of the adjacent vertebral bodies. **(b)** In a different patient, an axial view shows a central disc protrusion extending posterior to the margins of the adjacent vertebral bodies and indenting the anterior aspect of the thecal sac. Note the brighter T2-weighted signal, which is secondary to hemorrhage, in the acute disc herniation.

herniation.¹⁰ In the cervical spine, many lesions causing cervical radicular pain are not composed solely of disc material but also have an osseous component, which can be secondary to spondylotic or hypertrophic osteophyte formation involving the end plates, facet joints, or uncovertebral joints (joints of

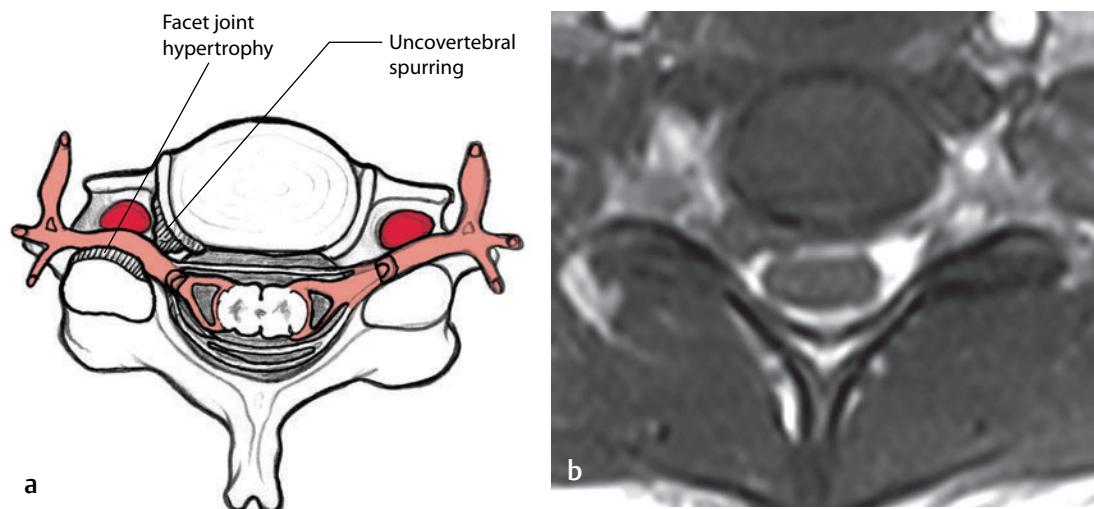


Fig. 3.3 This (a) artist's sketch shows cervical foraminal stenosis and nerve root impingement from facet joint hypertrophy and uncovertebral spurring resulting in cervical nerve root compression.[†] (b) An axial T2-weighted image shows cervical foraminal nerve root compression by a right-side disc herniation.

Luschka) (**Fig. 3.3**). Thus, the most common cause of cervical radiculopathy is a foraminal constriction that may have several different etiologies, including facet arthropathy, uncovertebral joint and end-plate hypertrophy, and loss of disc space height.¹⁰ Therefore, a nerve root compressive lesion in the cervical region is less likely to regress completely than is one in the lumbar region. Cervical disc herniations that undergo spontaneous regression are expected to correlate with an improvement in symptom burden from a resultant compressive neuropathy. The spinal nerves most commonly affected by disc herniations are reported to be C6 and C7.¹⁰

Generally, a cervical disc herniates posterolaterally and impinges on the nerve root at the inferior aspect of the neural foramen (**Fig. 3.4**); however, the herniated disc occasionally is central and can cause myelopathy secondary to mass effect on the cervical cord. Unlike those in the lumbar region, cervical nerves exit in the inferior aspect of the foramen; therefore, the *exiting, not the traversing* nerve is most likely to be impacted by a disc herniation or a disc-osteophyte complex. The cervical nerves exit above the same-numbered pedicle; for example, a C5-C6 herniation will affect the exiting C6 nerve. Patients with cervical radiculopathy often complain of neck pain referred to the medial border of the scapula and radiating down the arm in a concordant distribution with possible numbness and weakness in the same distribution. The C5-C8 cervical neurologic levels are the most vulnerable to disc herniation and a radicular presentation.

C5 Nerve Root

The C5 nerve root innervates the muscles responsible for shoulder abduction and elbow flexion (**Fig. 3.5**). C5 radiculopathy results from pathology at the C4-C5 level and is characterized by weakness in the proximal muscles of the upper extremities. Patients often present with numbness and localized shoulder pain that may be confused with a primary shoulder condition. A rotator cuff tear may present with shoulder pain and weakness of shoulder abduction. However, pain from a pathologic shoulder condition is associated with increased range-of-motion pain and pain on provocative testing, whereas radicular pain is not.

The deltoid is almost entirely innervated by the axillary nerve, which originates predominantly from C5 and C6. The biceps shares innervation from the musculocutaneous nerve, which also originates from C5 and C6. The deltoid muscle is divided into three heads: anterior (flexion), middle (abduction), and posterior (extension) heads. The principal motor deficit of C5 radiculopathy is supraspinatus and deltoid muscle weakness with impaired shoulder abduction. Deltoid weakness is best assessed by shoulder abduction against resistance. The biceps muscle is divided into two heads: the brachii and the brachialis. It is a flexor of the elbow and supinator of the forearm. Classic testing is by flexing the elbow against resistance.

The dermatome of C5 corresponds to the lateral skin overlying the deltoid and the lateral arm from the acromion to the distal elbow. Numbness, paresthesias,

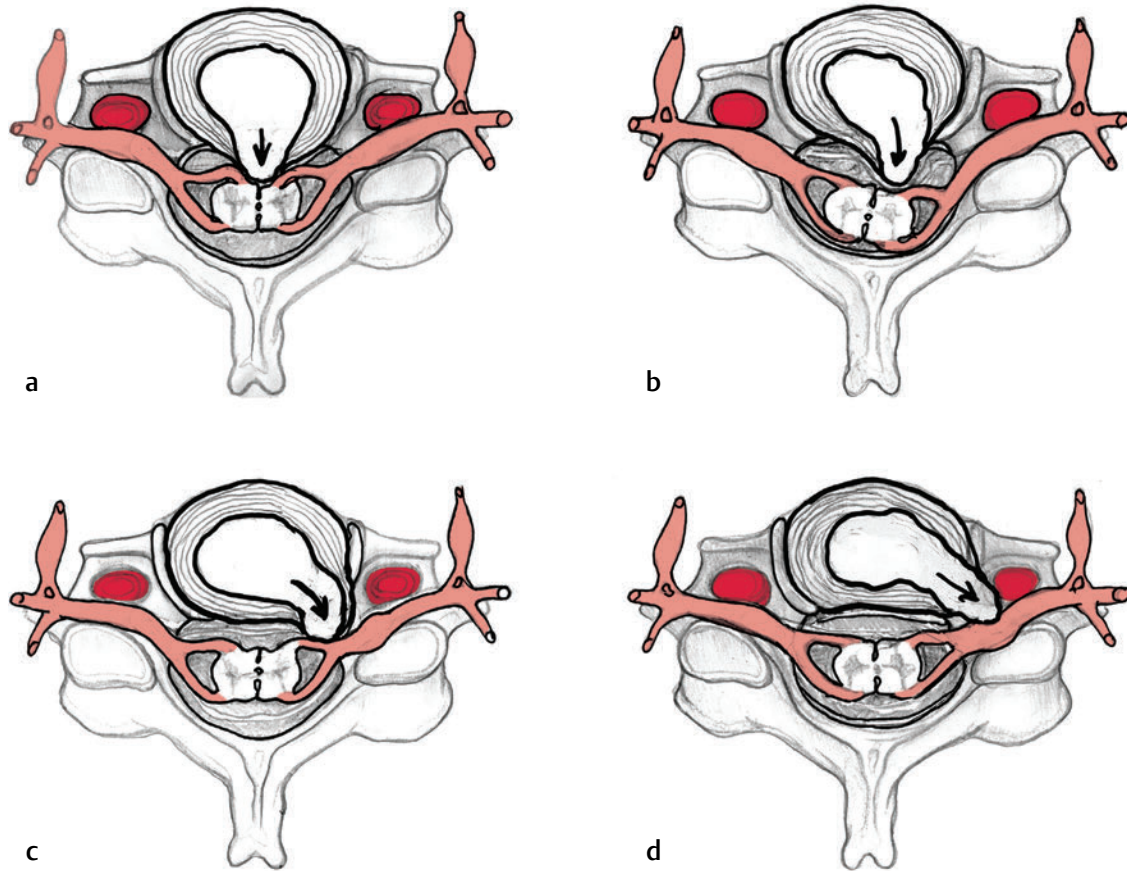


Fig. 3.4 Artist sketches of four types of disc herniations in the cervical spine: (a) central; (b) posterolateral; (c) lateral recess; and (d) foraminal.[†]

or dysesthesias in this region may represent a C5 radicular syndrome. The biceps reflex corresponds to C5 and C6. For the biceps reflex, it is important that the patient's forearm remain in supination to prevent muscle stabilization. Reflex discrepancies between sides could indicate pathology of C5 or C6.

C6 Nerve Root

The C6 nerve root primarily innervates the muscles of wrist extension (**Fig. 3.6**). Compression of the C6 nerve root is the second most common cause of cervical radiculopathy and results from disc herniation or spondylosis at the C5-C6 level (**Fig. 3.7**). Motor deficits in the wrist extensors are the most common. To test wrist extension, the forearm should be stabilized and the wrist extended against resistance. Weakness of the biceps, supinator, and pronator teres may be present because of coinnervation.

The symptoms of C6 radiculopathy may mimic carpal tunnel syndrome, which is caused by me-

dian nerve entrapment at the wrist by the transverse carpal ligament. The unique clinical feature of referred pain with entrapment neuropathies is that pain commonly radiates *proximally* to the site of entrapment.¹¹ Compression of the median nerve at the wrist, for example, may cause referred pain to the arm and even to the neck.¹¹ Unlike cervical radiculopathy, upper limb nerve entrapments such as carpal tunnel syndrome are characterized by pain, paresthesia, and weakness in multiple nerve root distributions (C6-T1) reflective of the median nerve.

Radicular pain from the C6 nerve root dermatome (**Fig. 3.8**) extends from the neck to the lateral aspect of the biceps, the lateral forearm via the musculocutaneous nerve (from C5-C6), and the dorsum of the lateral hand to the tip of the thumb, and it often includes the index finger. Because the biceps reflex also tests the C5 nerve root, C6 integrity is best isolated by the brachioradialis reflex. The brachioradialis tendon is tapped at the distal end of the radius.

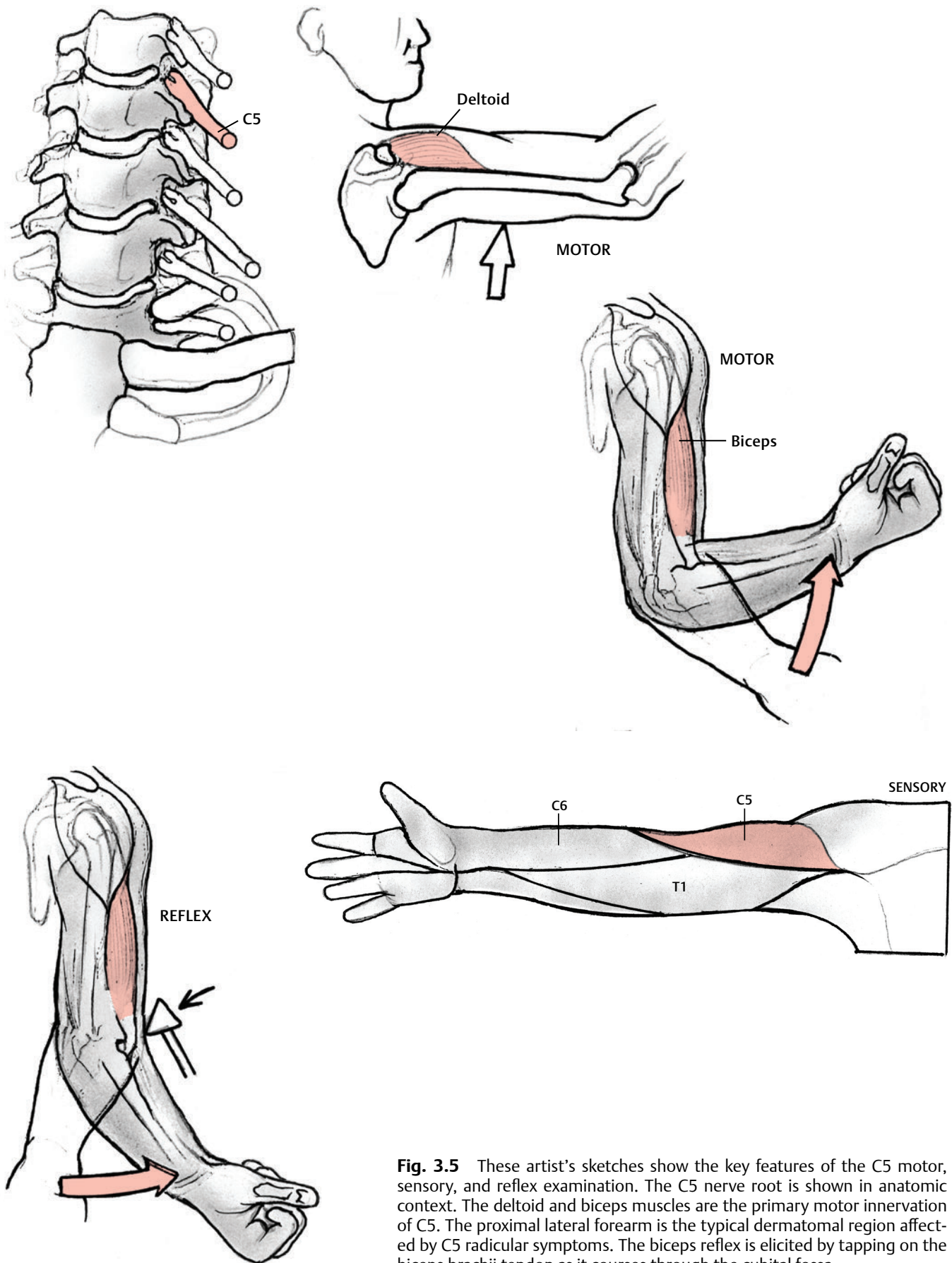


Fig. 3.5 These artist's sketches show the key features of the C5 motor, sensory, and reflex examination. The C5 nerve root is shown in anatomic context. The deltoid and biceps muscles are the primary motor innervation of C5. The proximal lateral forearm is the typical dermatomal region affected by C5 radicular symptoms. The biceps reflex is elicited by tapping on the biceps brachii tendon as it courses through the cubital fossa.

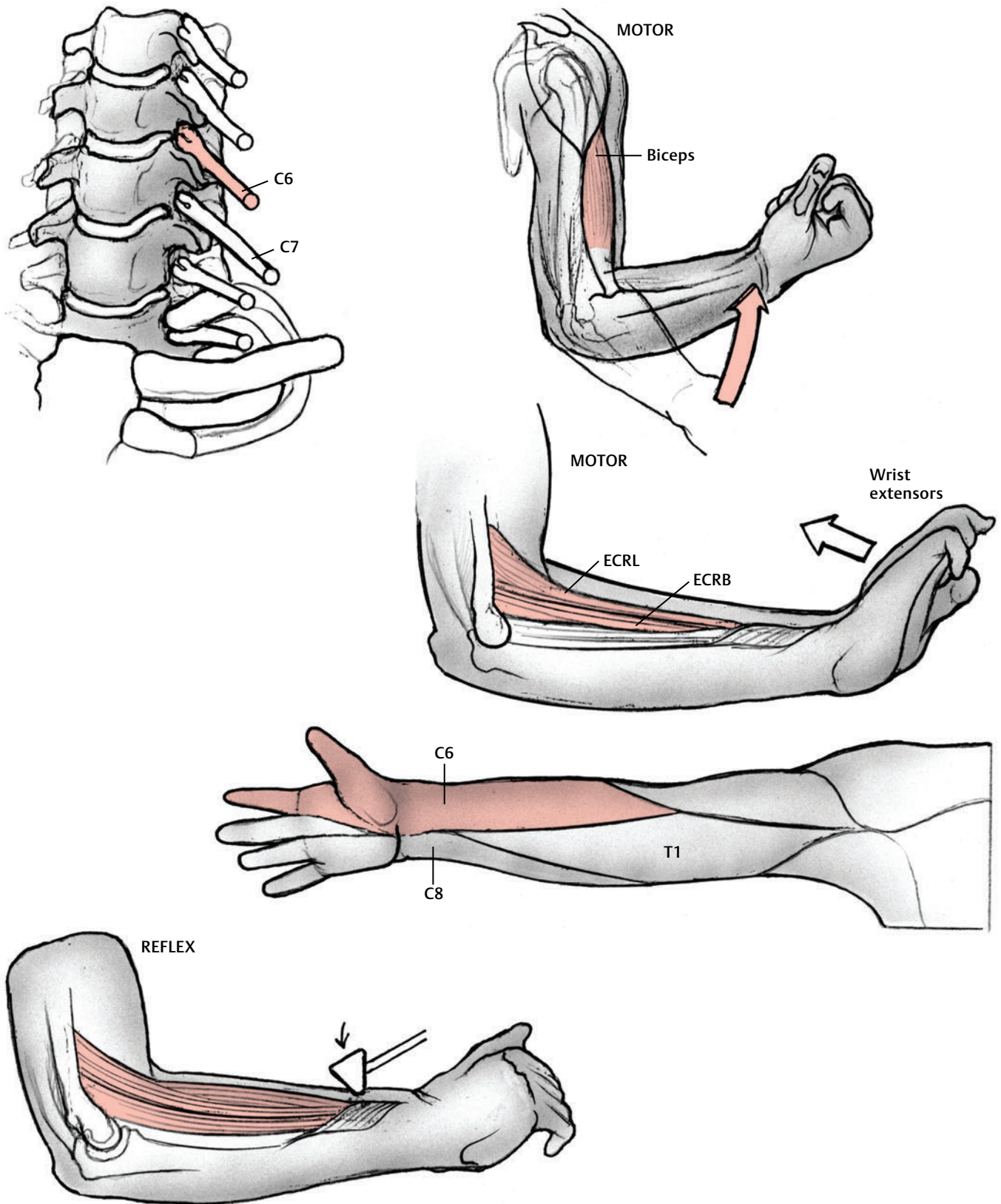


Fig. 3.6 These artist's sketches show the key features of the C6 motor, sensory, and reflex examination. The C6 nerve root is shown in anatomic context. The primary motor innervation of C6 includes the biceps muscle but is isolated by the major functional muscles of wrist extension (extensor carpi radialis longus [ECRL] and extensor carpi radialis brevis [ECRB]). The distal lateral forearm up to the thumb and index finger are the typical dermatomal regions affected by C6 radicular symptoms. The brachioradialis reflex is elicited by tapping on the brachioradialis tendon at the distal radius.

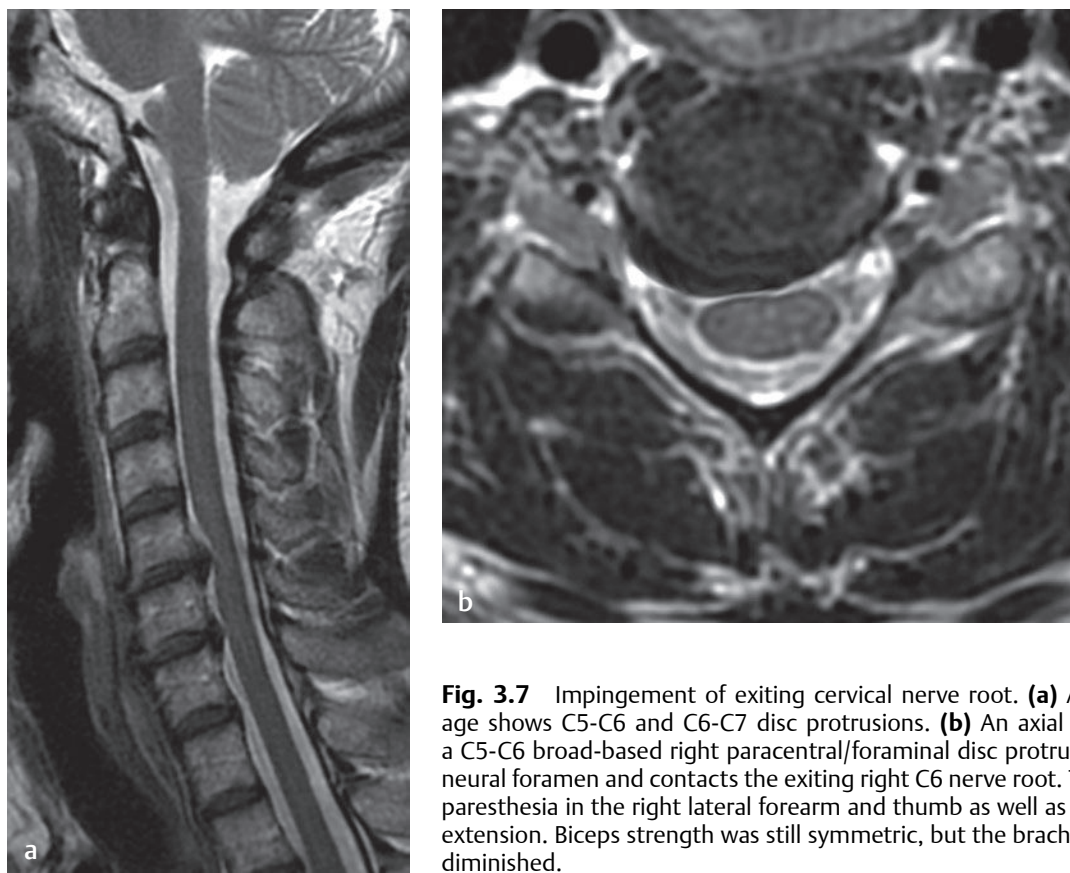


Fig. 3.7 Impingement of exiting cervical nerve root. **(a)** A sagittal T2-weighted image shows C5-C6 and C6-C7 disc protrusions. **(b)** An axial T2-weighted image shows a C5-C6 broad-based right paracentral/foraminal disc protrusion that narrows the right neural foramen and contacts the exiting right C6 nerve root. This patient presented with paresthesia in the right lateral forearm and thumb as well as subtle weakness with wrist extension. Biceps strength was still symmetric, but the brachioradialis reflex was slightly diminished.

C7 Nerve Root

C7 primarily innervates the elbow extensors, wrist flexors, and finger extensors (**Fig. 3.9**). C7 is considered the most frequently involved nerve root in cervical radiculopathy,^{12,13} which is caused by degenerative changes at the C6-C7 level. The C7 nerve root innervates the triceps muscle, the primary elbow extensor. Triceps weakness can be substantial, but it may not be noticed by the patient until it becomes severe because gravity often aids in passive elbow extension. Triceps testing is performed by stabilizing the elbow and asking the patient to extend the forearm against resistance. Wrist flexion is predominantly controlled by the C7 median nerve via the flexor carpi radialis, which can be tested by asking the patient to make a closed fist and flexing the wrist against resistance. The radial nerve also innervates several finger extensor muscles, including the primary extensor group, the extensor digitorum. To test finger extension, the wrist is stabilized in a neutral position and the patient extends the metacarpophalangeal joints against the examiner's hand, which should be placed on the dorsum of the extended proximal phalanges. Simultaneously, the patient is asked to flex the in-

terphalangeal joints to help isolate the long finger extensors and eliminate contribution from the intrinsic hand muscles.

The C7 dermatome varies, but typically the patient may present with pain, dysesthesia, and/or numbness radiating from the posterior aspect of the shoulder, the posterior arm, the dorsolateral aspect of the forearm, and down to the middle finger. Usually, the dorsal and ventral surfaces of the middle finger are within the C7 dermatome, making the long finger most typically representative of C7. Reflex testing of C7 is via the triceps tendon, which is tapped with the reflex hammer where it crosses the olecranon fossa.

C8 also assists the innervation for wrist flexion and finger extension, so even subtle discrepancies in the examination of the wrist and fingers may still be consistent with C7 radiculopathy. Additionally, the motor symptoms of C7 radiculopathy may be confused with entrapment of the posterior interosseous nerve, a continuation of the deep branch of the radial nerve. This entrapment would present with weakness in the finger extensors. Notably, entrapment of the posterior interosseous nerve is a pure motor condition, usually without sensory involvement, and the triceps and wrist flexors are not affected.

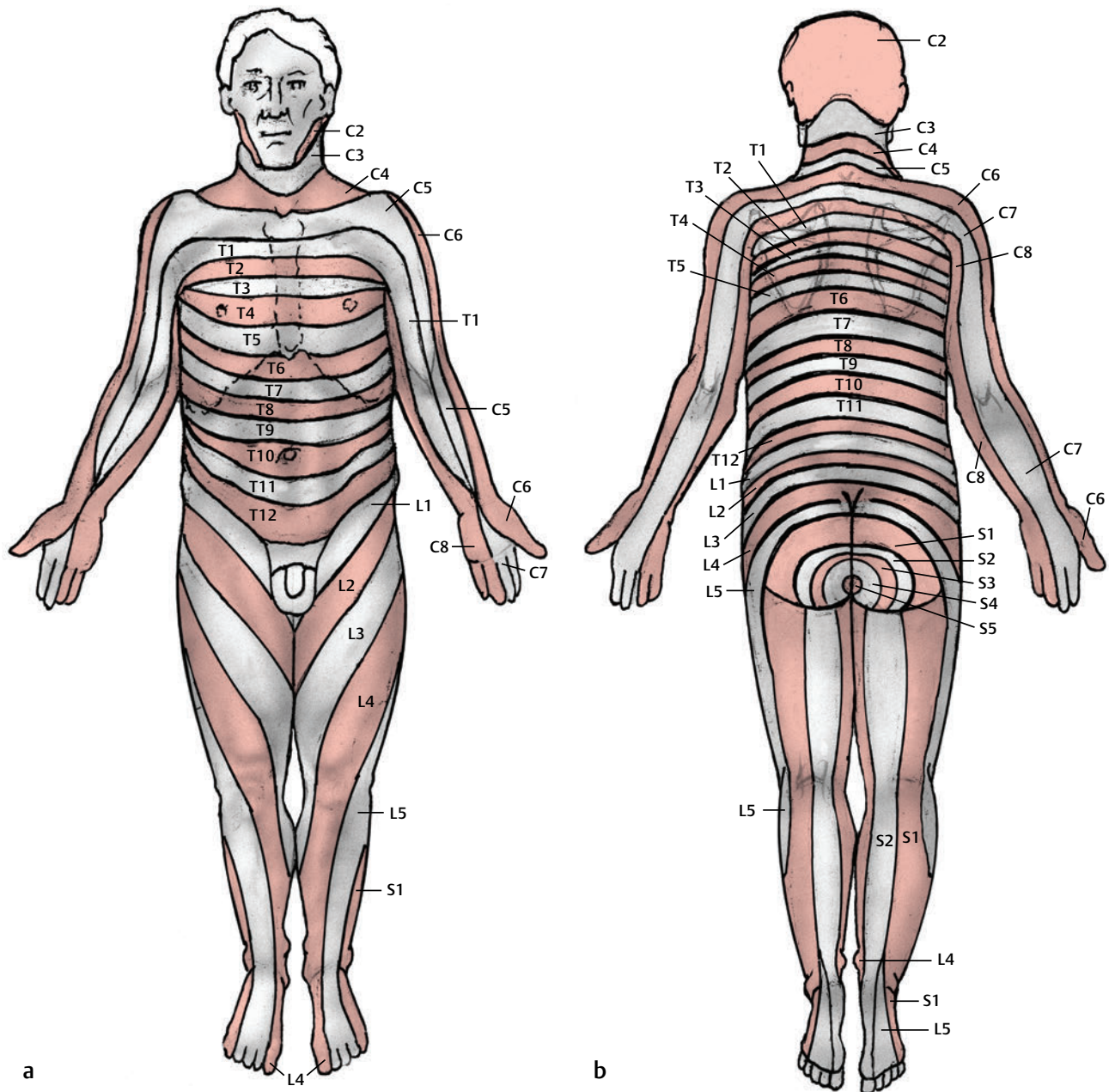


Fig. 3.8 Artist's sketches show (a) AP and (b) PA views of the dermatome map.

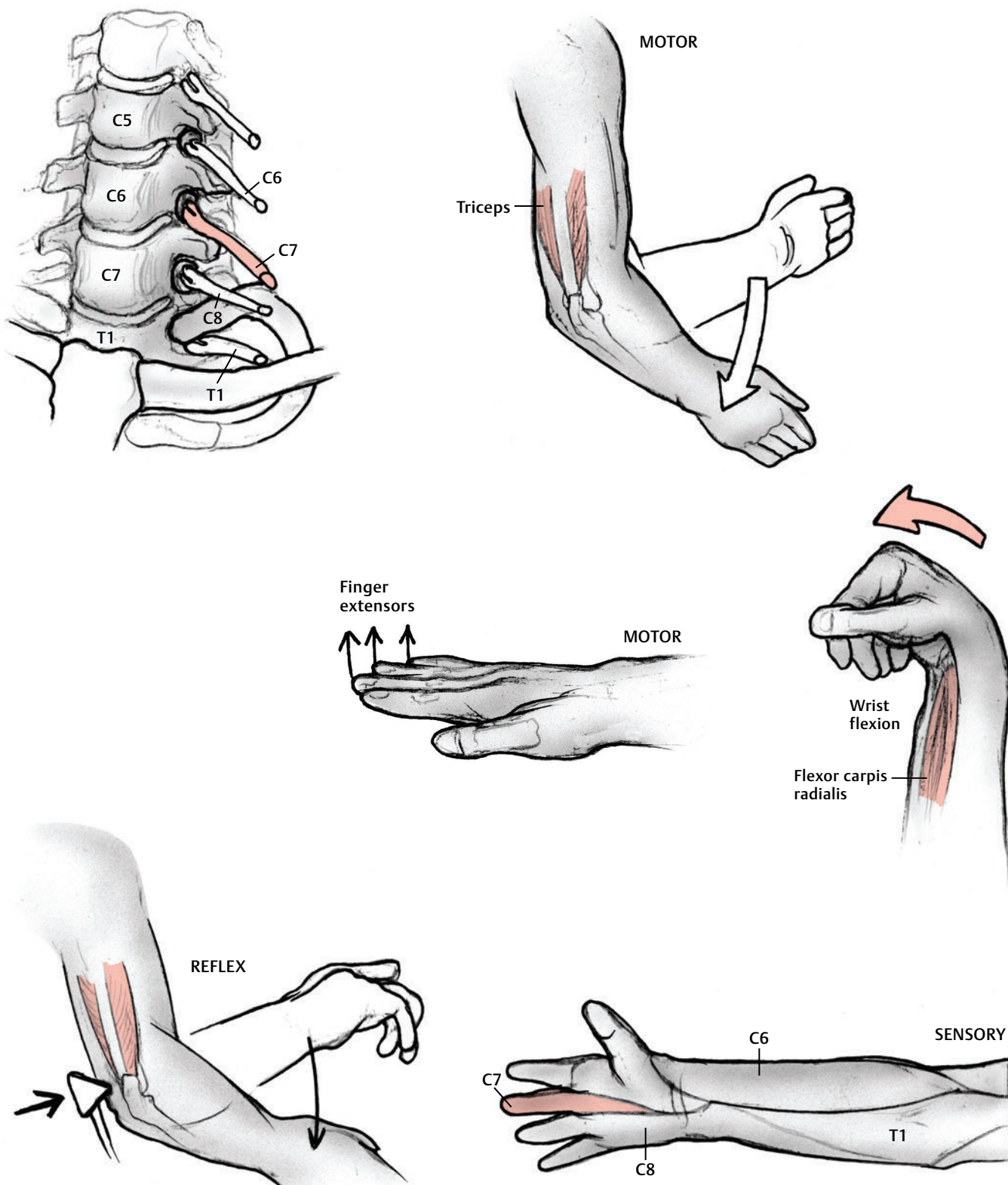


Fig. 3.9 These artist's sketches show the key features of the C7 motor, sensory, and reflex examination. The C7 nerve root is shown in anatomic context. The primary motor innervation of C7 is responsible for several functional movements including elbow extension by the triceps muscle, wrist flexion by the flexor carpi radialis, and finger extension by the extensor digitorum group. The middle of the hand, especially the third finger, is the classic dermatomal region represented in isolation by pure C7 radicular symptoms. The triceps reflex can be elicited by tapping on the triceps tendon as it crosses the olecranon fossa.

C8 Nerve Root

C8 primarily innervates the finger flexor muscles (**Fig. 3.10**). The flexor digitorum profundus flexes the distal interphalangeal joints via the C8 ulnar and median nerves. The flexor digitorum superficialis flexes the proximal interphalangeal joint via the median nerve. To test finger flexion strength, the patient is asked to flex all of the finger joints, including

the metacarpophalangeal, proximal interphalangeal, and distal interphalangeal joints. Then the examiner interlocks fingers with the patient and attempts to straighten the patient's fingers.

The C8 dermatome is classically the skin of the medial distal forearm and ring and small fingers. The ulnar side of the small finger is the most specific location for testing C8 sensation. There is no classic reflex test for C8.

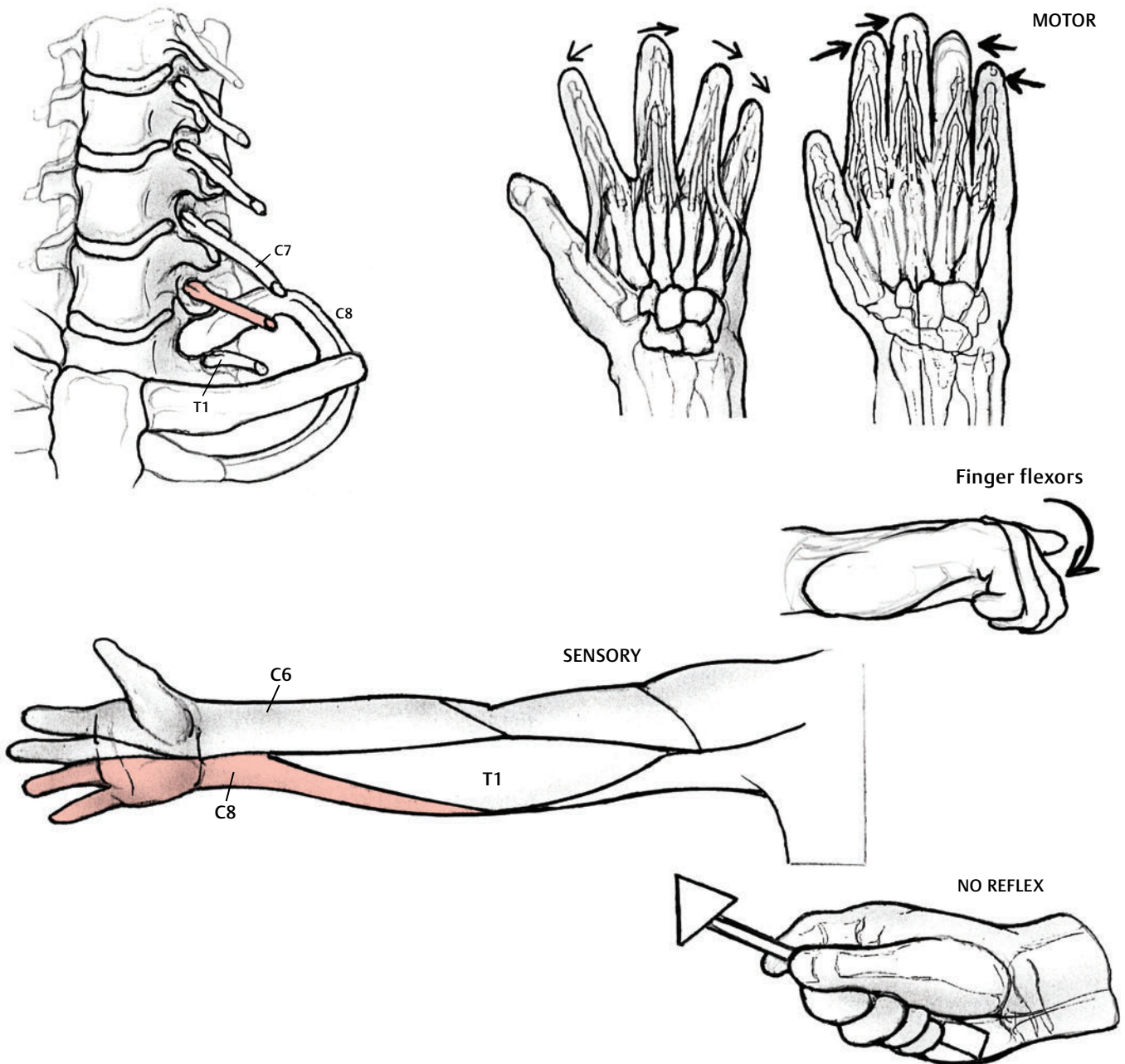


Fig. 3.10 These artist's sketches show the key features of the C8 motor, sensory, and reflex examination. The C8 nerve root is shown in anatomic context. The primary motor innervation of C8 includes the intrinsic muscles of the hand responsible for finger abduction/adduction and finger flexion. The distal medial forearm and hand, including the medial two fingers, constitute the classic dermatomal region affected by C8 radicular symptoms. There is no typical reflex easily elicited for C8 testing.

■ Correlative Anatomy of Lumbar Disc Pathology

In the lumbar spine, the exiting nerve passes immediately inferior to the vertebral pedicle and exits the foramen above the interspace level in the superior region of the foramen (**Fig. 3.11**). Therefore, most lumbar disc herniations do not affect the *exiting* nerve root but rather impinge on the *traversing* nerve root, which exits the foramen under the next lower vertebral pedicle (**Fig. 3.12**). For example, a posterolateral L4-L5 disc herniation results in an L5 radicular pain syndrome or radiculopathy secondary to impingement of the traversing L5 nerve root by the herniated disc as the nerve root travels in an inferior direction to exit from the next lower neural foramen (**Figs. 3.12** and **3.13**).

Disc herniations may also affect the exiting nerve root at the level of disease. For example, a disc her-

niation at the L4-L5 level may affect the L4 nerve root through two possible mechanisms: (1) a posterolateral disc extrusion with *cephalad migration* of disc material in the neural foramen or (2) a *far-lateral* disc protrusion/extrusion that compresses the same-level exiting nerve (**Figs. 3.12** and **3.14**).

A midline disc herniation is rare because of the strength of the posterior longitudinal ligament, but if it does occur, it can involve two nerve roots. For example, a large midline herniation at the L4-L5 disc could compress the L5 and S1 nerve roots in the lateral recesses, resulting in combined L5 and S1 radicular symptoms (**Fig. 3.15**).

The L4-L5 and L5-S1 segments have the greatest motion in the lumbar spine and are thus the most vulnerable to disc herniation injuries. Approximately 90% of lumbar disc herniations occur at these two levels.¹⁴ Of all lumbar disc herniations, 90% are central or paracentral (5% are foraminal and 5% are far lateral).¹⁴

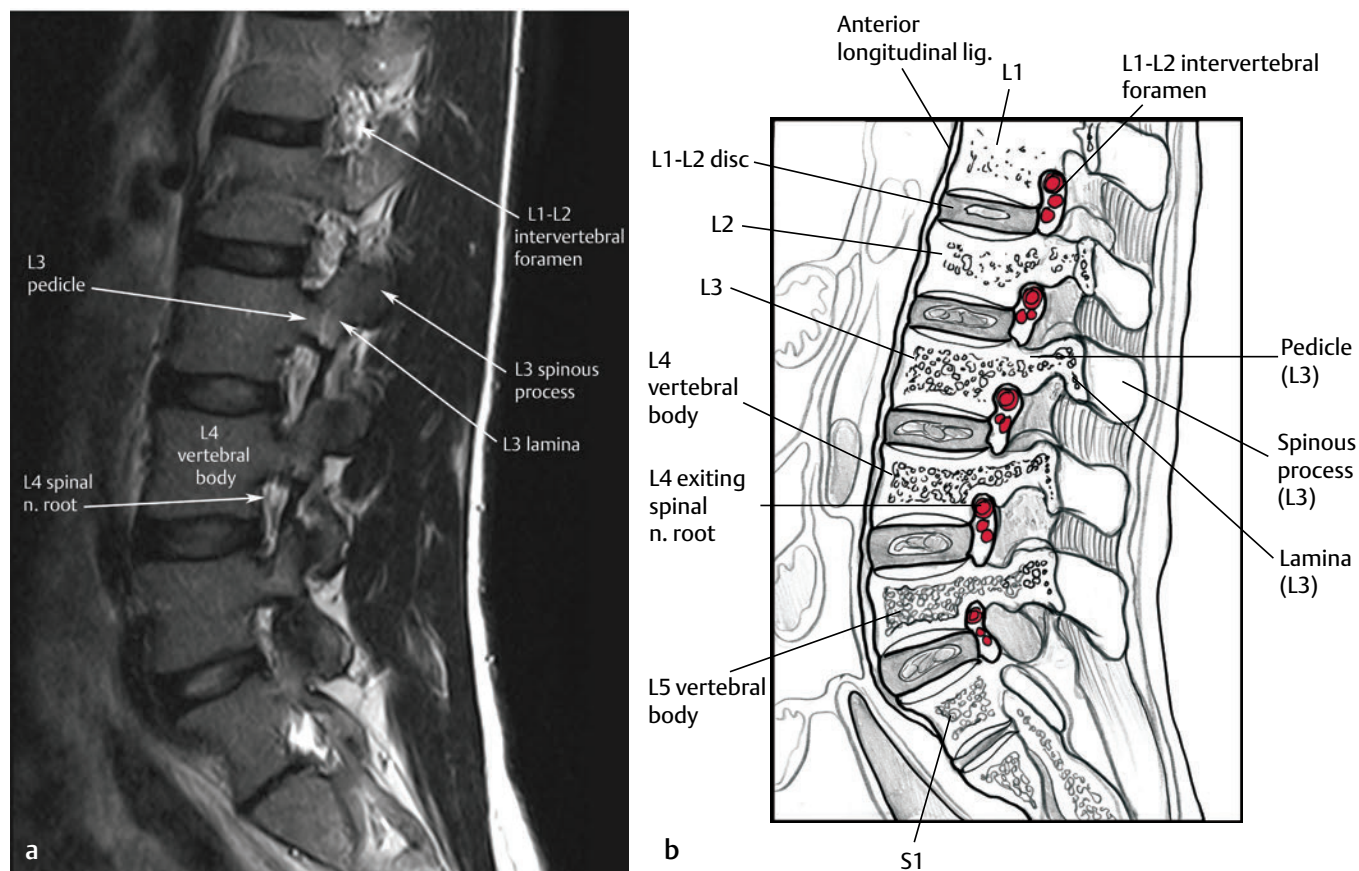


Fig. 3.11 This (a) parasagittal T2-weighted image and (b) artist's sketch of the lumbar spine show the typical neural foramina and exiting nerve roots at multiple levels. Note how the lumbar nerve roots exit in the *superior* foraminal region, inferior to the vertebral pedicle and above the interspace disc.[†]

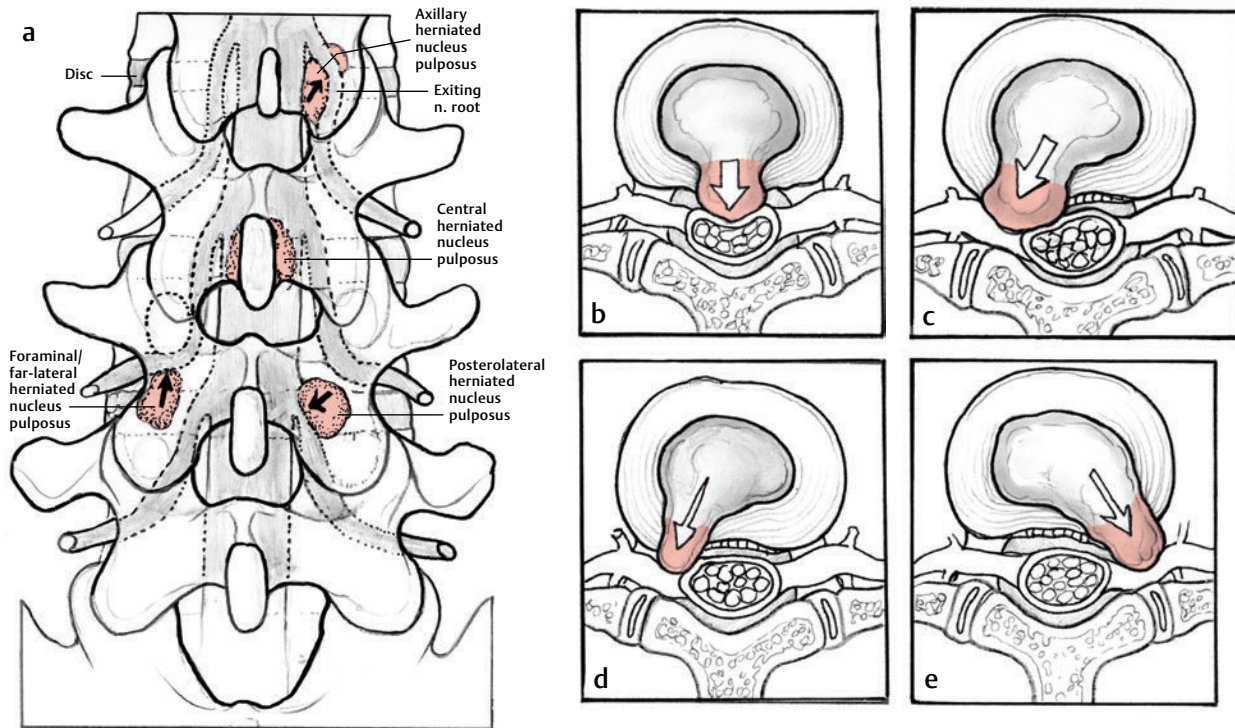


Fig. 3.12 Artist's sketches of types of herniated nucleus pulposus. (a) The posterior view shows their locations at the L2-L5 levels. Note how the far-lateral herniation impinges on the *same-level* nerve root while the posterolateral herniation impinges on the *traversing* nerve root. The corresponding axial views show the (b) central, (c) posterolateral, (d) axillary, and (e) far-lateral disc pathology. Each arrow indicates the direction of herniation. Note how the lumbar nerve roots exit from the superior region of the neural foramen. Before it exits the neural foramen, the nerve root turns at a 45-degree angle *immediately beneath* the vertebral pedicle. Because the pedicle is situated in the upper third of the vertebral body, the nerve root does not cross the disc space below. The result is that a nerve root is commonly involved in herniations of the disc located *above* its point of exit from the neural foramen. (From Phillips, FM, Lauryssen, C. *The Lumbar Intervertebral Disc*. New York, NY: Thieme Publishers, 2009. Reprinted by permission.)

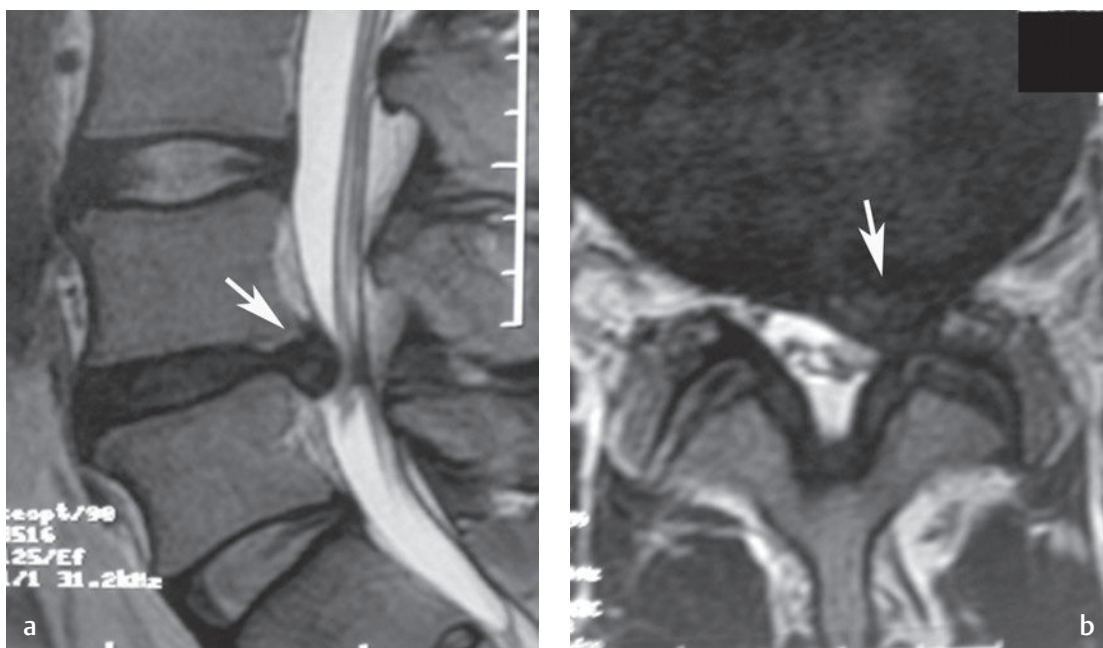


Fig. 3.13 Traversing nerve root impingement. (a) A sagittal T2-weighted image shows L4-L5 disc protrusion (arrow). (b) At the level of the L4-L5 disc, this axial T2-weighted image shows a left central/subarticular disc protrusion (arrow) contacting the traversing left L5 nerve root in the left lateral recess. This patient presented with numbness in the first web spaces of the left foot and diminished strength with hip abduction and great toe extension.[†]

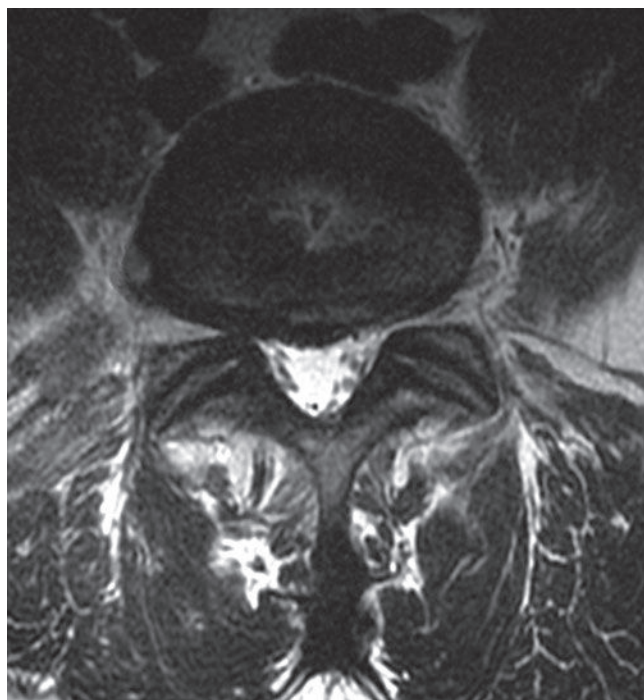


Fig. 3.14 This axial T2-weighted image shows a broad-based disc protrusion at the L4-L5 level with a far-lateral component that contacts the extraforaminal course of the right L4 nerve root. The patient presented with paresthesias in the medial right foot and weakness with dorsiflexion. Functionally, the patient was unable to perform an adequate heel walk.

Upper Lumbar Nerve Roots (L1, L2, L3 Radiculopathy)

The upper lumbar levels function together to innervate large muscle groups responsible for hip flexion (iliopsoas), hip adduction (adductors), and leg extension (quadriceps). Individually, each of these three nerve roots lacks a specific representative muscle and a corresponding reflex. Nevertheless, distinguishing upper versus lower lumbar nerve root pathology is important clinically. The iliopsoas muscle (L1, L2, L3) produces hip flexion. To test hip flexion strength, the patient is seated on the edge of the examining table and actively lifts the thigh off the table against resistance.

The adductor brevis, longus, and magnus muscles are innervated by L2, L3, and L4 via the obturator nerve and are responsible for hip adduction. Hip adduction is tested by having the examiner's hands on the medial sides of both knees and asking the patient to adduct the thighs against resistance.

Nerves from L1, L2, and L3 provide sensation over the anterior groin and thigh (**Fig. 3.8**). The dermatomes resemble spiral bands starting with L1 at the groin and inguinal region, progressing to L2 in the

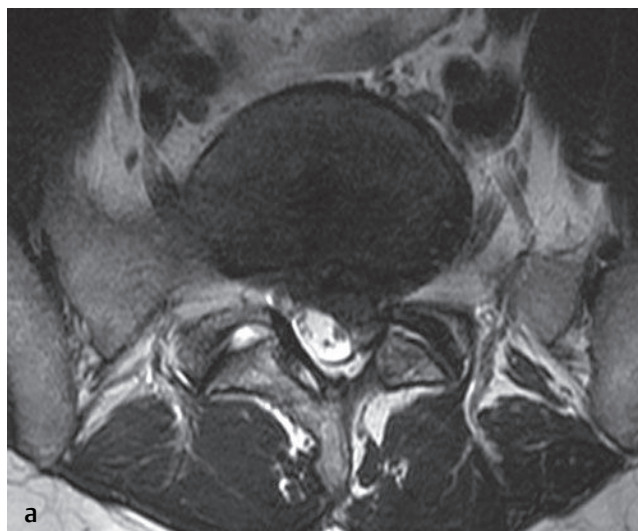


Fig. 3.15 Multiple nerve root contact. **(a)** This axial T2-weighted image shows a moderate-sized left paracentral disc extrusion at the L5-S1 level (with a foraminal component) producing compression of the traversing left S1 nerve root. **(b)** A parasagittal T2-weighted image shows the foraminal component of the L5-S1 disc extrusion contacting the exiting left L5 nerve root. This patient presented with radicular pain along both the L5 and S1 dermatomal distributions.

mid-thigh, and ending in L3 from mid-thigh to immediately above the knee. Nerve root impingement will result in referred pain or paresthesias to the corresponding dermatome. Notably, radicular pain from an L1 lesion is often described by patients as groin pain and, therefore, may be confused with referred pain from intraarticular hip pathology such as a labral tear or osteoarthritis.

Lower Lumbar Nerve Roots (L4, L5, S1 Radiculopathy)

L4 Nerve Root

The L4 nerve root innervates the muscles of knee extension and foot and ankle dorsiflexion/inversion (Fig. 3.16). The quadriceps muscle is less sensitive in

testing for an isolated L4 radiculopathy because of its great strength and bulk and because of its coinervation by L2 and L3. L4 radiculopathy is specifically tested via the tibialis anterior muscle, which is innervated by the deep peroneal nerve and is responsible for dorsiflexion and inversion of the foot. To test functional ability, the patient is asked to walk on his or her heels; in more advanced radiculopathy, a foot drop may be evident. Dorsiflexing the foot against resistance is the classic test for the tibialis anterior muscle. The L4 dermatome includes the medial side of the leg and extends to the medial side of the foot, including the great toe (Fig. 3.8). Although the patellar tendon reflex is supplied by L2, L3, and L4, it primarily reflects L4 integrity. Notably, though, even a subtly diminished patellar reflex on one side may still represent a severely compressed L4 nerve root because of L2 and L3 coinervation.

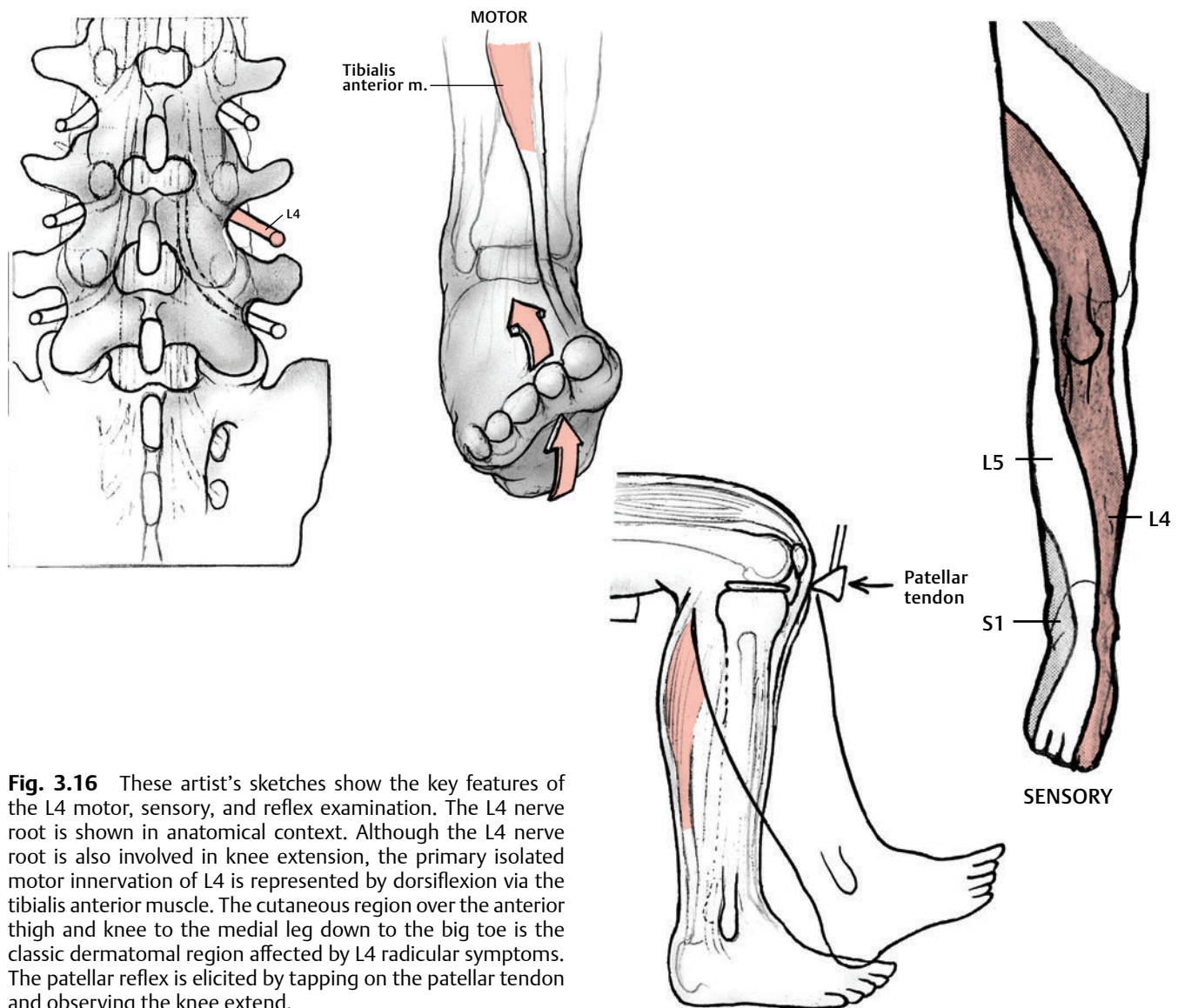


Fig. 3.16 These artist's sketches show the key features of the L4 motor, sensory, and reflex examination. The L4 nerve root is shown in anatomical context. Although the L4 nerve root is also involved in knee extension, the primary isolated motor innervation of L4 is represented by dorsiflexion via the tibialis anterior muscle. The cutaneous region over the anterior thigh and knee to the medial leg down to the big toe is the classic dermatomal region affected by L4 radicular symptoms. The patellar reflex is elicited by tapping on the patellar tendon and observing the knee extend.

L5 Nerve Root

The L5 nerve root innervates the major toe extensors and hip abductors (**Fig. 3.17**). The deep peroneal nerve innervates the extensor hallucis longus and extensor digitorum longus, which extend the great toe and four remaining toes, respectively. To test the toe extensors, the clinician seats the patient and stabilizes the foot with one hand, while the other hand provides resistance against extension of the great toe and lateral four toes. The gluteus medius is innervated by the superior gluteal nerve of L5 and enables hip abduction. To test gluteus medius function, the patient lies on the asymptomatic side while the examiner stabilizes the pelvis and ensures that the hip flexors remain in a neutral position. The patient first fully abducts the lower extremity against gravity and then against resistance with the examiner pushing down on the lateral thigh above the knee.

The L5 dermatome distribution corresponds to the lateral leg and central dorsal area of the foot, although the first web space is the typical site for testing L5 sensory function (**Fig. 3.8**). The palpable crest of the tibia from the knee to the ankle is the general division between the L5 and L4 dermatomes, with skin lateral to the division being innervated by L5. There is no quintessential reflex test for L5. The tibialis posterior muscle can provide an L5 reflex, but it is not easy to elicit routinely.

S1 Nerve Root

The S1 nerve root innervates the muscles of hip extension, ankle plantar flexion, and foot/ankle eversion (**Fig. 3.18**). The inferior gluteal nerve from S1 innervates the gluteus maximus, which extends the hip. Functionally, difficulty with standing from

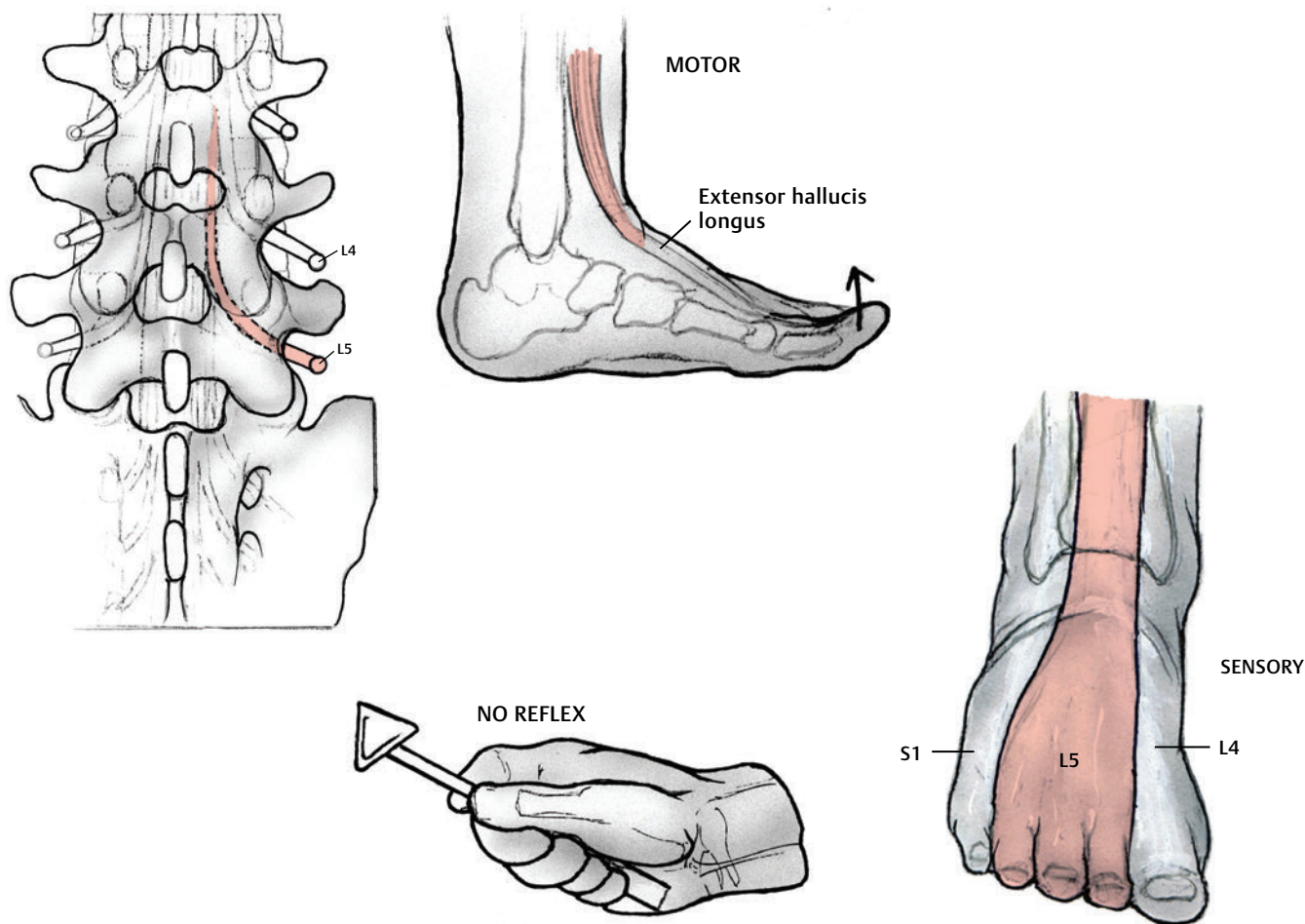


Fig. 3.17 These artist's sketches show the key features of the L5 motor, sensory, and reflex examination. The L5 nerve root is shown in anatomical context. The primary motor innervation of L5 includes extension of the toes, especially the great toe via extensor hallucis longus. The dorsum of the foot, including the web space between the first and second toe, is the classic dermatomal region affected by L5 radicular symptoms. There is no classic reflex that can truly isolate L5 clinically.

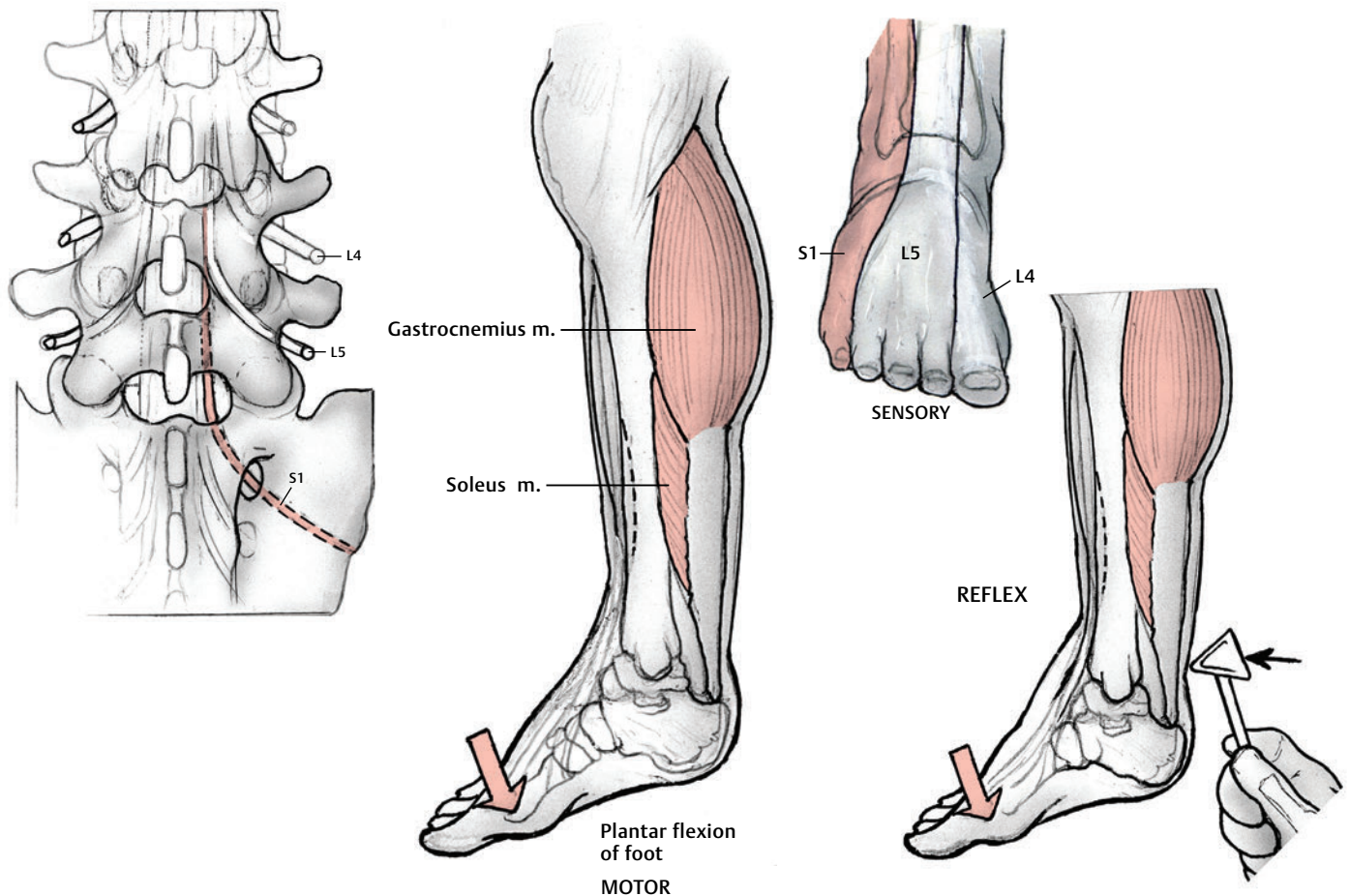


Fig. 3.18 These artist's sketches show the key features of the S1 motor, sensory, and reflex examination. The S1 nerve root is shown in anatomic context. The primary motor innervation of S1 includes plantar flexion of the foot and ankle. The posterior thigh and leg down to the lateral foot including the fifth toe and lateral plantar surface is the classic dermatomal region affected by S1 radicular symptoms. The Achilles reflex is elicited by tapping on the Achilles heel and observing plantar flexion.

a seated position could indicate weakness from S1 radiculopathy.

The gastrocnemius and soleus muscles are innervated by the tibial nerve from S1 and S2. Because these muscles are quite strong, adequate functional testing requires the patient to rise up on his or her toes several times or walk on them across the examination room.

The S1 superficial peroneal nerve innervates the peroneus longus and brevis, which evert the foot and ankle. The examiner should stabilize the ankle with one hand, while holding the lateral aspect of the foot with the other hand, as the patient everts against resistance.

S1 sensation covers a dermatomal band extending from the buttocks down to the posterior thigh and leg to the lateral and plantar foot (**Fig. 3.8**), the region classically vulnerable to the typical shooting radicular pain (sciatica) of a herniated disc impinging on an S1 nerve root. S1 mediates the Achilles tendon reflex. The reflex is elicited by gently dorsiflexing the

foot and striking the Achilles tendon with the reflex hammer to elicit a slight plantar flexion.

■ Nonradicular Axial Back Pain

Discogenic Axial Back Pain

Discogenic back pain, one of the most common causes of axial low back pain,¹⁵ refers to pain that originates from the intervertebral disc, specifically the sinuvertebral nerve and the gray rami communicantes that innervate the outer third of the annulus fibrosis. However, diagnosis of discogenic pain is challenging, because no pathologic or surgical gold standard exists against which to judge provocative discography or MRI diagnosis. Provocative discography has been traditionally used to diagnosis discogenic pain, but it has come under scrutiny because of its invasive nature and potential for harm.¹⁶ Nevertheless, modern

MR imaging can provide a reasonable likelihood of diagnosing discogenic pain. This pain is often described as a deep, achy, midline paraspinous pain that can be exacerbated with axial loading such as lifting heavy objects or prolonged standing or sitting. MRI findings described in the following paragraphs, such as end-plate changes, high-intensity zones/annular fissures, and central disc herniations, are axial spine pain generators of discogenic origin that may not have an associated radicular pain component. Many of these entities can also be present in the asymptomatic patient population and increase with patient age; therefore, a combined imaging and clinical approach is necessary to isolate these entities as primary pain generators, particularly in the aging population.

End-Plate Changes

Degenerative end-plate changes are often associated with intervertebral disc pathology. These degenerative end-plate changes are classified using an MRI characterization originally described by Modic et al^{17,18}: type I, inflammatory/edema-like signal abnormalities; type II, fat-like signal abnormalities; and

type-III, sclerosis-like signal abnormalities (**Fig. 3.19**). Fluid-sensitive sequences such as fat-suppressed T2-weighted or STIR images are ideal for identifying type-I changes; however, a combination of a fluid-sensitive sequence with a T1-weighted pulse sequence is necessary to differentiate Modic types II and III. Images in the sagittal plane provide the highest yield for the evaluation of degenerative end-plate changes because they provide the greatest visualization of end plates. Type-I degenerative end-plate changes have been shown to have the strongest association with pain symptoms because they likely represent an active inflammatory state; type-II and type-III changes are less likely to serve as pain generators.¹⁹

High-Intensity Zones and Annular Fissures

High-intensity zones and annular fissures have a high association with axial back pain symptoms, particularly in studies involving evaluation with discography.^{1,19} High-intensity zones are hyperintense T2 foci within the disc that can extend to the margins of the annulus but without the identified annular deformity seen with disc herniations (**Fig. 3.20**).

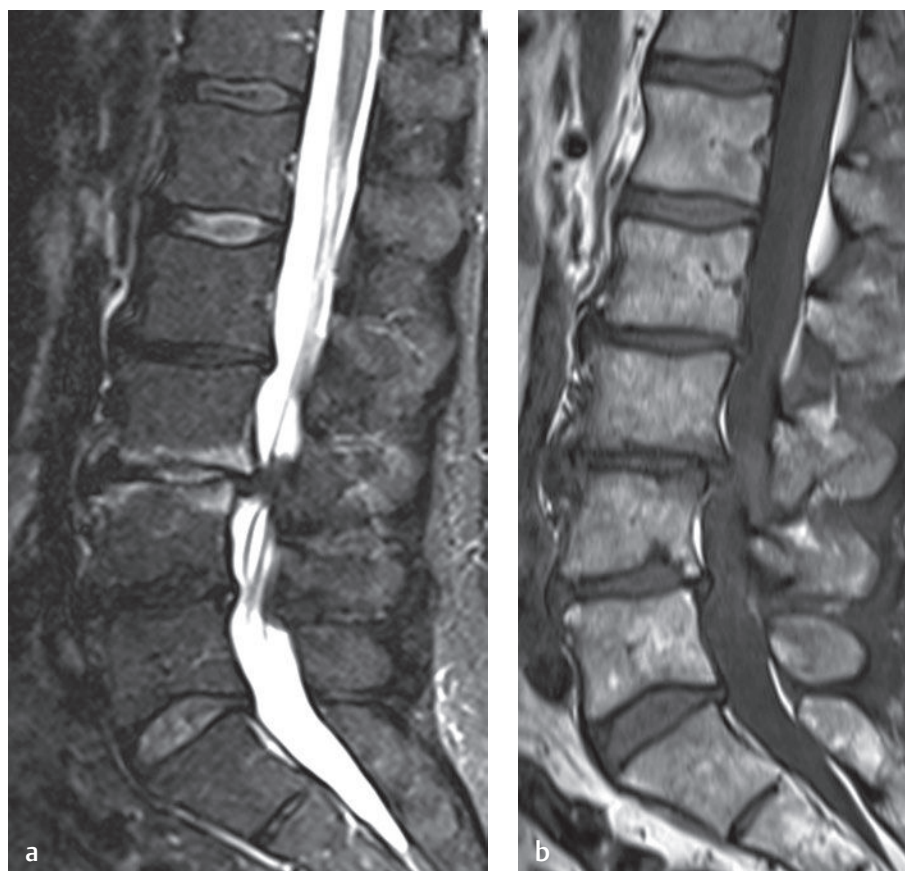


Fig. 3.19 Modic type-I degenerative end-plate changes. **(a)** A sagittal STIR image shows bright signal compatible with edema within the inferior L3 and superior L4 end plates. **(b)** The corresponding sagittal T1-weighted image shows subtle low signal in the same areas.



Fig. 3.20 A sagittal T2-weighted image shows disc desiccation and a bright linear signal abnormality in the L5-S1 disc posteriorly, compatible with an annular fissure. This patient presented with axial discogenic back pain symptoms and prolonged sitting intolerance without radicular pain.

Disc Herniations

The morphology of a disc herniation should be evaluated on axial and sagittal images to categorize the herniation extent (protrusion or extrusion), along with the location of the herniation (central, paracentral, subarticular, foraminal, or extraforaminal), and any contact of adjacent nerve roots should be noted. However, many disc herniations may not contact exiting nerve roots; in isolation, herniations may be associated with radicular or nonradicular discogenic pain symptoms because of the inflammatory biochemical cascade of events involved in the disruption of the annulus fibrosus.

In addition, the inflammatory process associated with *radicular pain* symptoms, but originating from a *nonherniated* disc whose annulus is incompetent, has been described as a chemical radiculitis and can be seen with enhanced studies such as provocative discography, MRI with gadolinium contrast,

or fat-suppressed MR images.^{20,21} The mechanism of pain relates to the incompetent annulus fibrosus, permitting the slow escape of uncontained nucleus pulposus, initiating an inflammatory cascade along adjacent nerve roots.

Interestingly, patients can also present with clinically evident radicular pain or radiculopathy but no evidence of a neural compression lesion on standard recumbent imaging. Such situations may call for imaging technologies that recreate physiologic conditions. Newer MRI systems can provide imaging with the spine under axial load or with physiologic positioning, which can place the compressive element in clearer view (see Chapter 10, Advanced Techniques in Spine MRI). For example, Zamani et al²² showed that 40% of already mildly desiccated discs showed an increase in disc bulging when imaged in an erect extended position compared with a recumbent position. Weishaupt et al²³ also observed more instances of disc-neural contact in images obtained in seated position compared with those obtained in the supine position. Neural foraminal narrowing in the seated erect position was also significantly associated with increased pain.²²

Posterior Element Axial Back Pain

Other causes of generalized low back pain without a radicular or referred pain component can often originate from a posterior spinal column source such as facet arthropathy or synovitis, sacroiliac disease, pedicles, and spinous processes. Although the architectural changes of osteoarthritis (e.g., joint space narrowing, subchondral cysts, osteophyte formation) are common findings in asymptomatic and symptomatic patients, the presence of moderate to high-grade synovitis has a good correlation with pain generation (**Fig. 3.21**).^{24,25} Notably, such axial back pain should not have any neurologic or radicular component. More worrisome causes of such back pain include spinal infection, fracture instability, and malignancy. Posterior-column axial pain can be exacerbated with certain movements such as facet-loading maneuvers (hyperextension and twisting) and with paraspinal palpation on examination. Diagnostic lumbar medial branch blocks followed by RF ablation have been shown to be effective for facet-mediated pain in multiple studies.^{26–28}

In axial cervical neck pain from degenerative disc disease or after whiplash injury, the pain can resemble cervical radicular pain, originating in the neck and radiating to the shoulder and medial border of the scapula. However, weakness and involvement of the distal upper extremity should be absent. As in the lumbar spine, axial cervical pain can have components of myofascial injury and facet arthritic pain or more worrisome causes (mentioned in the

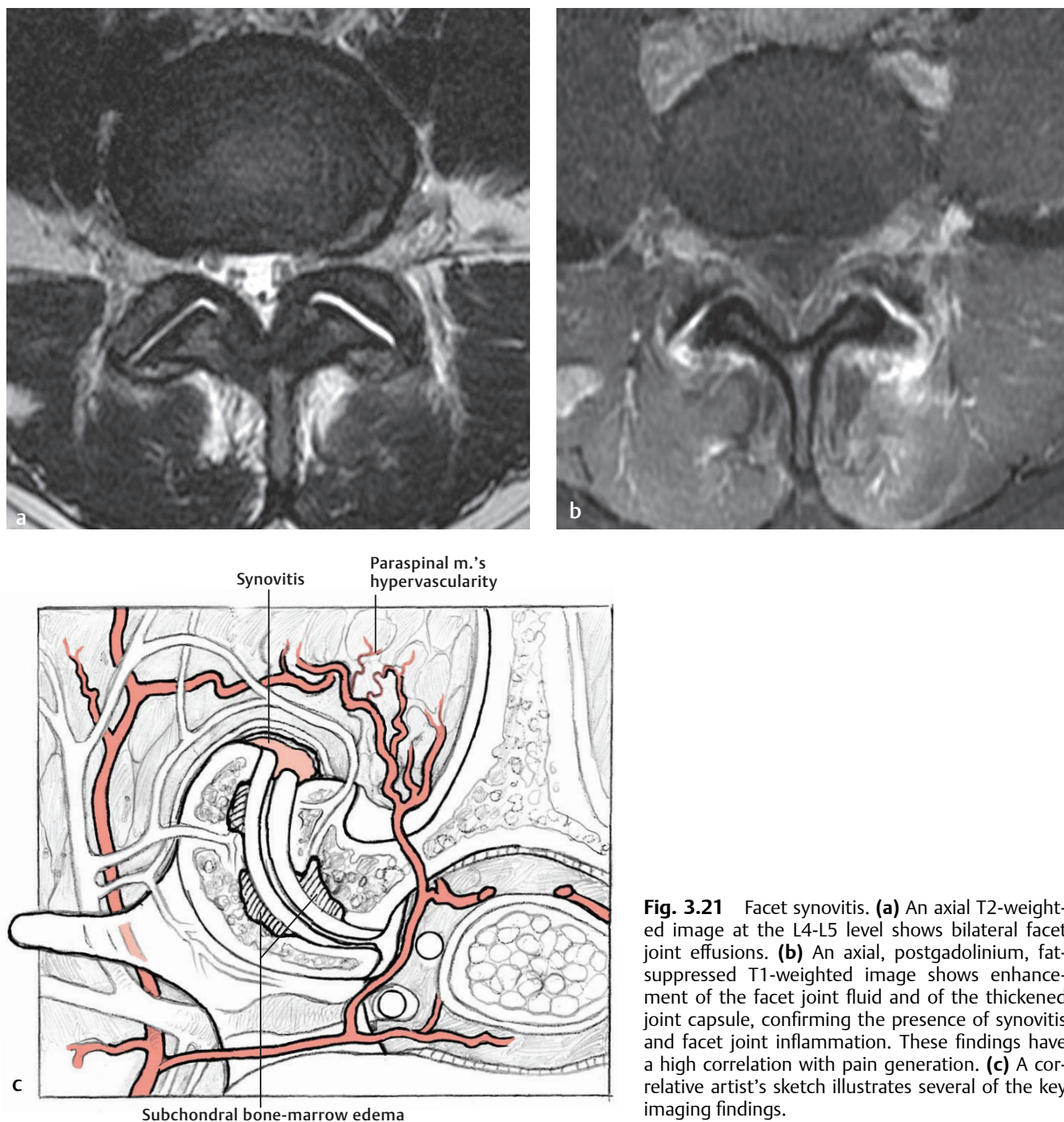


Fig. 3.21 Facet synovitis. **(a)** An axial T2-weighted image at the L4-L5 level shows bilateral facet joint effusions. **(b)** An axial, postgadolinium, fat-suppressed T1-weighted image shows enhancement of the facet joint fluid and of the thickened joint capsule, confirming the presence of synovitis and facet joint inflammation. These findings have a high correlation with pain generation. **(c)** A correlative artist's sketch illustrates several of the key imaging findings.

preceding paragraph). Patients typically have limited neck range of motion, especially with facet-loading maneuvers, and tenderness over the corresponding paraspinal facet regions. As with the lumbar spine, diagnostic cervical medial branch blocks followed by RF ablation have been shown to be effective in several studies and in a randomized controlled trial for cervical facet pain after whiplash injury.^{29–32}

■ Summary

When symptomatic disease is present in the midst of asymptomatic MRI findings, the clinician faces an imperative to correlate imaging pathology with the concordant symptomatology and physical examination (see Fig. 4.20 in Chapter 4, A Systematic Approach

to the Review of Spine MRI Studies). Knowledge of an anatomic basis of clinical pain symptoms is highly applicable to the neurologic levels and their patterns of radicular symptoms because both the imaging and the examination are complementary data points to guide accurate diagnosis and treatment. In the cervical and lumbar spine, several manifestations of nerve root irritation exist, whether by a variety of disc herniations, osseous overgrowth impingement, spinal stenosis, or an incompetent annulus, or any combination thereof. Although many images in this chapter show clear pathologic findings at a single level, many patients present to clinic with combinations of imaging pathology, including Modic changes, disc herniations, and facet arthropathies, often evident

at multiple levels. In these all-too-common cases, knowledge of the correlative history and physical examination works in synergy with radiographic findings to guide nonoperative and interventional treatments. Often, the most salient examination findings correspond to the most prominent imaging findings, but sometimes they do not, and a decision between patient and physician must be made about which levels or anatomic targets to address first in a systematic fashion. Isolating and treating the primary pain generator(s) often requires a multimodal approach through medications, fluoroscopically guided spinal injections, nerve blocks, RF ablation, and surgical intervention to treat the complexities of spinal pain adequately.

COMMON CLINICAL QUESTIONS

1. A C6 disc herniation at the C6-C7 foramen would most likely result in a _____ radiculopathy because, in the cervical spine, the cervical nerves exit in the _____ aspect of the foramen. Therefore, the exiting, not the traversing, nerve is most likely to be affected by a cervical disc herniation.
 - A. C6/superior
 - B. C6/inferior
 - C. C7/superior
 - D. C7/inferior
 - E. C8/inferior
2. A patient comes to the clinic complaining of lower back pain and right lower extremity pain and weakness. Intermittent sharp pain is described along the right lateral leg to the great toe. On examination, the patient demonstrates 4/5 strength with hip abduction and great toe extension. Sensation is diminished along the lateral leg and the dorsum of the foot, and specifically the first web space. The most likely nerve root involved is the _____. The MRI could reasonably show _____ (select all that apply).
 - A. S1 nerve root/posterolateral disc herniation at L5-S1 with caudal migration of disc material
 - B. L5 nerve root/posterolateral disc herniation at L4-L5
 - C. L4 nerve root/posterolateral disc herniation at L4-L5
 - D. L5 nerve root/far-lateral disc herniation at L5-S1
 - E. L5 nerve root/posterolateral disc herniation at L5-S1 with cephalad migration of disc material
3. Select the true statement(s) below:
 - A. Modic type-I changes appear bright on T1-weighted images and dark on T2-weighted images and have the lowest correlation with axial discogenic back pain.
 - B. Modic type-II changes appear bright on both T1-weighted and T2-weighted images and reflect fatty infiltration of sub-end-plate marrow.
 - C. Modic type-II changes appear dark on both T1-weighted and T2-weighted images and reflect fatty infiltration of sub-end-plate marrow.
 - D. Modic type-I changes appear dark on T1-weighted images and bright on T2-weighted images and have the highest correlation with axial discogenic back pain.
 - E. Modic type-III changes appear dark on both T1-weighted and T2-weighted images and represent sclerotic changes to the end-plate region.
4. Cervical nerve roots commonly exit in the _____ aspect of the foramen, whereas lumbar nerve roots exit in the _____ aspect of the foramen.
 - A. Inferior/inferior
 - B. Inferior/superior
 - C. Superior/superior
 - D. Superior/inferior
5. The cervical nerve roots most commonly involved in a disc herniation injury are:
 - A. C3 and C4
 - B. C4 and C5
 - C. C5 and C6
 - D. C6 and C7
 - E. C7 and C8

References

1. Bogduk N. Degenerative joint disease of the spine. *Radiol Clin North Am* 2012;50(4):613–628 PubMed
2. Boden SD, Davis DO, Dina TS, Patronas NJ, Wiesel SW. Abnormal magnetic-resonance scans of the lumbar spine in asymptomatic subjects. A prospective investigation. *J Bone Joint Surg Am* 1990;72(3):403–408 PubMed
3. Borenstein DG, O'Mara JW Jr, Boden SD, et al. The value of magnetic resonance imaging of the lumbar spine to predict low-back pain in asymptomatic subjects : a seven-year follow-up study. *J Bone Joint Surg Am* 2001;83-A(9):1306–1311 PubMed
4. Teresi LM, Lufkin RB, Reicher MA, et al. Asymptomatic degenerative disk disease and spondylosis of the cervical spine: MR imaging. *Radiology* 1987;164(1):83–88 PubMed
5. Kuslich SD, Ulstrom CL, Michael CJ. The tissue origin of low back pain and sciatica: a report of pain response to tissue stimulation during operations on the lumbar spine using local anesthesia. *Orthop Clin North Am* 1991;22(2):181–187 PubMed
6. Mulleman D, Mammou S, Griffoul I, Watier H, Goupille P. Pathophysiology of disk-related low back pain and sciatica. II. Evidence supporting treatment with TNF-alpha antagonists. *Joint Bone Spine* 2006;73(3):270–277 PubMed
7. Cohen SP, Bogduk N, Dragovich A, et al. Randomized, double-blind, placebo-controlled, dose-response, and preclinical safety study of transforaminal epidural etanercept for the treatment of sciatica. *Anesthesiology* 2009;110(5):1116–1126 PubMed
8. Andersson GBJ, Biyani A, Ericksen ST. Lumbar disc disease. In: Herkowitz HN, Garfin SR, Eismont FJ, Bell GR, Balderston RA, eds. *Rothman-Simeone The Spine*. Philadelphia, PA: Saunders; 2011:846–886
9. McDonald CM, Abresch RT, Carter GT, et al. Profiles of neuromuscular diseases. Duchenne muscular dystrophy. *Am J Phys Med Rehabil* 1995;74(5, Suppl):S70–S92 PubMed
10. Radhakrishnan K, Litchy WJ, O'Fallon WM, Kurland LT. Epidemiology of cervical radiculopathy. A population-based study from Rochester, Minnesota, 1976 through 1990. *Brain* 1994;117(Pt 2):325–335 PubMed
11. Abbed KM, Coumans JVCE. Cervical radiculopathy: pathophysiology, presentation, and clinical evaluation. *Neurosurgery* 2007;60(1, Suppl 1):S28–S34 PubMed
12. Heiskari M. Comparative retrospective study of patients operated for cervical disc herniation and spondylosis. *Ann Clin Res* 1986;18(Suppl 47):57–63 PubMed
13. Henderson CM, Hennessy RG, Shuey HM Jr, Shackelford EG. Posterior-lateral foraminotomy as an exclusive operative technique for cervical radiculopathy: a review of 846 consecutively operated cases. *Neurosurgery* 1983;13(5):504–512 PubMed
14. Malfair D, Beall DP. Imaging the degenerative diseases of the lumbar spine. *Magn Reson Imaging Clin N Am* 2007;15(2):221–238, vi PubMed
15. DePalma MJ, Ketchum JM, Saullo T. What is the source of chronic low back pain and does age play a role? *Pain Med* 2011;12(2):224–233 PubMed
16. Carragee EJ, Don AS, Hurwitz EL, Cuellar JM, Carrino JA, Herzog R. 2009 ISSLS Prize Winner: Does discography cause accelerated progression of degeneration changes in the lumbar disc: a ten-year matched cohort study. *Spine (Phila Pa 1976)* 2009;34(21):2338–2345 PubMed
17. Modic MT, Masaryk TJ, Ross JS, Carter JR. Imaging of degenerative disk disease. *Radiology* 1988;168(1):177–186 PubMed
18. Modic MT, Steinberg PM, Ross JS, Masaryk TJ, Carter JR. Degenerative disk disease: assessment of changes in vertebral body marrow with MR imaging. *Radiology* 1988;166(1 Pt 1):193–199 PubMed
19. Maus TP, Aprill CN. Lumbar diskogenic pain, provocation diskography, and imaging correlates. *Radiol Clin North Am* 2012;50(4):681–704 PubMed
20. Marshall LL, Trethewie ER, Curtain CC. Chemical radiculitis. A clinical, physiological and immunological study. *Clin Orthop Relat Res* 1977; (129):61–67 PubMed
21. Peng B, Wu W, Li Z, Guo J, Wang X. Chemical radiculitis. *Pain* 2007;127(1-2):11–16 PubMed
22. Zamani AA, Moriarty T, Hsu L, et al. Functional MRI of the lumbar spine in erect position in a superconducting open-configuration MR system: preliminary results. *J Magn Reson Imaging* 1998;8(6):1329–1333 PubMed
23. Weishaupt D, Schmid MR, Zanetti M, et al. Positional MR imaging of the lumbar spine: does it demonstrate nerve root compromise not visible at conventional MR imaging? *Radiology* 2000;215(1):247–253 PubMed
24. Czervionke LF, Fenton DS. Fat-saturated MR imaging in the detection of inflammatory facet arthropathy (facet synovitis) in the lumbar spine. *Pain Med* 2008;9(4):400–406 PubMed
25. D'Aprile P, Tarantino A, Jinkins JR, Brindicci D. The value of fat saturation sequences and contrast medium administration in MRI of degenerative disease of the posterior/perispinal elements of the lumbosacral spine. *Eur Radiol* 2007;17(2):523–531 PubMed
26. Bogduk N, Dreyfuss P, Govind J. A narrative review of lumbar medial branch neurotomy for the treatment of back pain. *Pain Med* 2009;10(6):1035–1045 PubMed
27. Patel N, Gross A, Brown L, Gekht G. A randomized, placebo-controlled study to assess the efficacy of lateral branch neurotomy for chronic sacroiliac joint pain. *Pain Med* 2012;13(3):383–398 PubMed
28. van Kleef M, Vanelderen P, Cohen SP, Lataster A, Van Zundert J, Mekhail N. 12. Pain originating from the lumbar facet joints. *Pain Pract* 2010;10(5):459–469 PubMed
29. Chua NHL, Vissers KC, Sluijter ME. Pulsed radiofrequency treatment in interventional pain management: mechanisms and potential indications—a review. *Acta Neurochir (Wien)* 2011;153(4):763–771 PubMed
30. Lord SM, Barnsley L, Wallis BJ, Bogduk N. Chronic cervical zygapophysial joint pain after whiplash. A placebo-controlled prevalence study. *Spine (Phila Pa 1976)* 1996;21(15):1737–1744; discussion 1744–1745 PubMed
31. van Eerd M, Patijn J, Lataster A, et al. 5. Cervical facet pain. *Pain Pract* 2010;10(2):113–123 PubMed
32. Nath S, Nath CA, Pettersson K. Percutaneous lumbar zygapophysial (Facet) joint neurotomy using radiofrequency current, in the management of chronic low back pain: a randomized double-blind trial. *Spine (Phila Pa 1976)* 2008;33(12):1291–1297; discussion 1298 PubMed

ANSWERS TO COMMON CLINICAL QUESTIONS

1. D

Explanation: Generally, a cervical disc herniates posterolaterally and impinges upon the nerve root at the inferior aspect of the neural foramen. In contrast to the lumbar region, cervical nerves exit in the inferior aspect of the foramen; therefore, the exiting, not the traversing, nerve is most likely to be impacted by a disc herniation or a disc-osteophyte complex. The cervical nerves exit above the same-numbered pedicle; for this reason, a C6-C7 herniation will affect the exiting C7 nerve.

2. B, D, E

Explanation: In the lumbar spine, the exiting nerve passes immediately inferior to the vertebral pedicle and exits the foramen above the interspace level in the superior region of the foramen. Therefore, because most lumbar disc herniations are posterolateral, they do not affect the exiting nerve root but, rather, impinge on the traversing nerve root, which exits the foramen under the next lower vertebral pedicle. In this case, as in option B, a posterolateral L4-L5 disc herniation results in an L5 radicular pain syndrome or radiculopathy. These symptoms stem from impingement of the traversing L5 nerve root by the herniated disc as the nerve root travels in an inferior direction to exit from the next lower neural foramen. Additionally, a disc herniation may also affect the exiting nerve root at the same level of disease. Classically, as in option D, a far-lateral L5-S1 disc herniation would impinge on the exiting L5 nerve root.

Finally, a disc herniation at the L5-S1 level may cause an L5 radiculopathy if a posterolateral disc herniation extrudes with cephalad migration of disc material into the neural foramen and impinges on the exiting L5 nerve root (option E).

3. B and D

Explanation: Degenerative end-plate changes are classified using an MRI characterization originally described by Modic et al: type I, inflammatory/edema-like signal abnormalities; type II, fat-like signal abnormalities; and type III, sclerosis-like signal. Type-I degenerative end-plate changes have been shown to have the strongest association with pain symptoms because they likely represent an active inflammatory state.

4. B

Explanation: Cervical nerves exit in the inferior aspect of the foramen. The cervical nerves exit above the same-numbered pedicle. Therefore, the exiting, not the traversing, nerve is most likely to be impacted by a disc herniation or a disc-osteophyte complex. In the lumbar spine, the exiting nerve passes immediately inferior to the vertebral pedicle and exits the foramen above the interspace level in the superior region of the foramen. Therefore, most lumbar disc herniations do not affect the *exiting* nerve root but rather impinge on the *traversing* nerve root, which exits the foramen under the next lower vertebral pedicle.

5. D

Explanation: The spinal nerves most commonly affected by disc herniations are reported to be C6 and C7.

4 A Systematic Approach to the Review of Spine MRI Studies

A. Jay Khanna

CHAPTER OUTLINE

- I. Step 1: Determination of Pulse Sequences Available for Review
 - A. T1-Weighted and T2-Weighted Images
 - B. Fat-Suppressed T2-Weighted Images or STIR Images
 - C. Postgadolinium T1-Weighted Images
 - D. MR Angiography Images
- II. Step 2: Evaluation of T2-Weighted Images
 - A. Cervical Spine Example
 - B. Lumbar Spine Example
 - C. Pattern Recognition
- III. Step 3: Evaluation of T1-Weighted Images
- IV. Step 4: Evaluation of Specialized Pulse Sequences
 - A. Fat-Suppressed T2-Weighted or STIR Images
 - B. Postgadolinium T1-Weighted Images
- V. Step 5: Correlation of Imaging Findings with Patient History and Examination Findings to Determine the Most Likely Diagnosis
- VI. Summary

As with any new skill, learning the technique of evaluating an MRI study begins with a systematic approach. Less experienced clinicians may have a tendency to review imaging studies without paying special attention to the type of pulse sequences that are being evaluated or to the plane in which they are being evaluated. When reviewing MRI studies on a computer workstation, they may also tend to review only one pulse sequence or one or two imaging planes. These shortcuts, especially early in a clinician's experience in evaluating MRI studies, may lead to less accurate and less reliable MR study interpretation.

Chapter 1 (Essentials of MRI Physics and Pulse Sequences) provided a summary of the technical foundation that radiologists often use to select the appropriate pulse sequences and imaging techniques for the study of a given region or pathologic process. The purpose of this more clinically oriented chapter is to provide the clinician or radiologist with a method for evaluating MRI studies in an organized and systematic fashion. The adoption of such a system early in a clinician's experience is believed to lead to improved accuracy and reliability in the interpretation of MRI studies. Over time, clinicians may be able to incorporate a more informal method of evaluating MRI studies and rely more on their own experience and personalized method of study evaluation.

The evaluation of an MRI study of the spine can be divided into the following five steps:

1. Determination of which conventional and specialized MRI pulse sequences are available for review
2. Evaluation of T2-weighted images for recognition of areas of increased T2-weighted signal that are not expected or physiologic
3. Evaluation of T1-weighted images for improved detection of anatomic detail and correlation of the alteration in local and regional anatomy on the T1-weighted images with areas of increased signal intensity on the T2-weighted images
4. Evaluation of specialized MRI pulse sequences that may be specific to the region or disease process that is being evaluated
5. Correlation of the imaging information from Steps 1–4 with the patient's history, physical examination, and laboratory study results to identify the most likely differential diagnostic considerations

The use of a general technique of MRI study evaluation described in this chapter, in conjunction with the more region- and concept-specific information

provided in subsequent chapters, will help improve a clinician's ability to interpret MRI studies of the spine accurately.

■ Step 1: Determination of Pulse Sequences Available for Review

The first step in the evaluation of an MRI study is to determine which pulse sequences are available for review. For most cases, such sequences include at least T1-weighted and conventional T2-weighted images, acquired in the sagittal and axial planes. For patients with spinal deformities such as scoliosis, images may also be obtained in the coronal plane.

In addition to conventional T1-weighted and T2-weighted pulse sequences, there are other pulse sequences that are often acquired and that should be recognizable, including the following:

- Fat-suppressed T2-weighted images or STIR images
- Postgadolinium T1-weighted images
- MR angiography images

T1-Weighted and T2-Weighted Images

One should be able to determine whether an image is T1-weighted or T2-weighted using the following techniques:

- Recognition of an area within an image that is known to contain fluid, such as CSF (**Fig. 4.1**). If this fluid is noted to be bright or of high signal intensity, that image is likely T2-weighted. If the region of the fluid is noted to be dark, that image is likely T1-weighted.
- Recognition of the TR and TE values, which are often printed on the film or are visible on the workstation screen. Recognizing these values may enable the clinician to determine whether an image is T1-weighted or T2-weighted. In most institutions and in most cases, images are acquired using an SE technique (for additional details, see Chapter 1, Essentials of MRI Physics and Pulse Sequences). When this technique or similar techniques are used, the TR value is usually 300 to 800 ms for T1-weighted images and 2000 to 5000 ms for T2-weighted images. If the clinician evaluates the image and is unable to use the technique in which fluid recognition allows the differentiation of T1-weighted and T2-weighted images, this technique is a good second option. If the TR



Fig. 4.1 A sagittal T2-weighted image of the cervical spine. Note that the CSF is of high signal intensity.[†]

number is noted to be in the hundreds range, the image likely is T1-weighted. If the TR number is found to be in the thousands range, the image likely is T2-weighted. With newer and more variable pulse sequences, this method may be less reliable.

Fat-Suppressed T2-Weighted Images or STIR Images

Fat-suppressed T2-weighted images are acquired using techniques similar to those for conventional T2-weighted images, and then various computer algorithms and processes are used to “suppress” the signal that is coming from fat. A more “pure” way of achieving this goal is to acquire a STIR image, in which case the signal from fat is not acquired. Because of the suppression of signal from fat in either of these techniques, the images tend to appear quite a bit “darker” than images obtained via other techniques (such as conventional T2-weighted images) and thus help accentuate the increase in T2-weighted signal (relative to the adjacent tissues), which may otherwise be missed (**Fig. 4.2**). Specifically, this technique facilitates the evaluation of bone-marrow edema and edema secondary to other pathologic processes. Fat-suppressed T2-weighted images or STIR images show areas of edema with markedly greater conspicuity

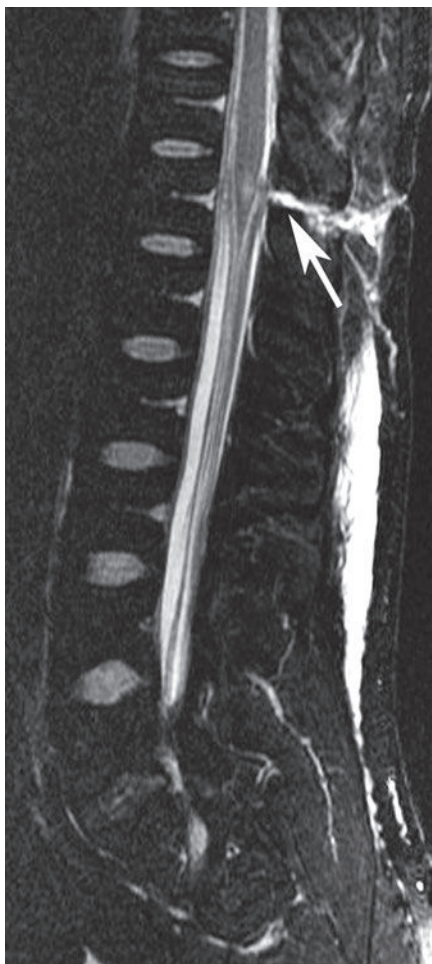


Fig. 4.2 A sagittal STIR image of the thoracolumbar spine accentuates the edema along the track (arrow) of a stab injury to the conus medullaris. Note that, aside from the pathologic fluid, the hydrated discs in this young patient, and the CSF within the spinal canal, this image is quite “dark.”[†]

than that seen on conventional T2-weighted images (see individual chapters for applications of these techniques for region-specific pathology).

As an example, in the evaluation of a patient with back pain secondary to vertebral compression fractures, sagittal T1-weighted or T2-weighted images may not show edema in an acute or subacute vertebral compression fracture, whereas a fat-suppressed T2-weighted image or a STIR image would make such a finding quite obvious (**Fig. 4.3**). These latter images are also useful for determining whether a vertebral compression fracture represents a chronic fracture or an acute or subacute fracture (**Fig. 4.3**).

Postgadolinium T1-Weighted Images

Postgadolinium T1-weighted images and fat-suppressed postgadolinium T1-weighted images are

typically obtained for the evaluation of infection, tumor, postsurgical changes, or scar. These images can sometimes be confused with T2-weighted images because they may show areas of increased signal in the presence of pathology (**Fig. 4.4**); the distinction can be made using the techniques just outlined. Specifically, the clinician should evaluate the areas in which one may expect to find physiologic fluid, such as CSF in the spine. If this fluid is bright, then the images are T2-weighted. If this fluid seems to be dark, and the pathology seems to be bright, then the image is likely a postgadolinium T1-weighted image. In addition, the technique of TR evaluation described previously can also be used to differentiate a postgadolinium T1-weighted image (TR is in the hundreds range) from a T2-weighted image (TR is in the thousands range).

MR Angiography Images

MR angiography images highlight the blood vessels and enable evaluation of the arterial and venous vascular structures (see Chapter 10, Advanced Techniques in Spine MRI) (**Fig. 4.5**). These images are obviously different in appearance from the images acquired using the more conventional pulse sequences and MRI techniques.

■ Step 2: Evaluation of T2-Weighted Images

After the clinician has identified all of the T2-weighted images, they should be systematically evaluated, plane by plane. In almost all instances, the clinician should begin with sagittal T2-weighted images of the cervical or lumbar spine. In rare instances, such as for the patient with a spinal deformity (e.g., degenerative or congenital scoliosis), it may be best to begin with the coronal T2-weighted images.

If the images are being evaluated as films on a light box, they should be viewed in sequential order, starting with all sagittal images, then all axial images, and then all coronal images. The same process should be used when evaluating an imaging study on a computer workstation.

Cervical Spine Example

A description of the evaluation of the cervical spine serves as an illustrative example.

- First, evaluate the sagittal T2-weighted images. Ensure that all of the sagittal T2-weighted images are being visualized in order from one

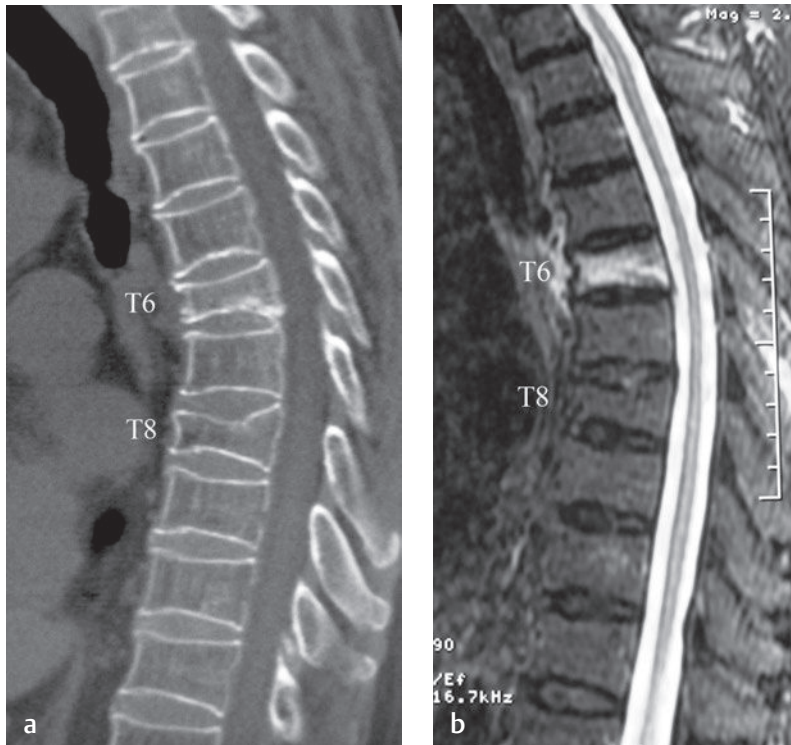


Fig. 4.3 Vertebral compression fracture. **(a)** A sagittal reconstructed CT image shows vertebral compression fractures at the T6 and T8 levels. **(b)** A sagittal STIR image shows that the T6 vertebral compression fracture has increased signal compatible with edema within it, which is representative of an acute or subacute fracture. The T8 vertebral compression fracture shows no increase in signal within it, which is compatible with a chronic vertebral compression fracture.[†]

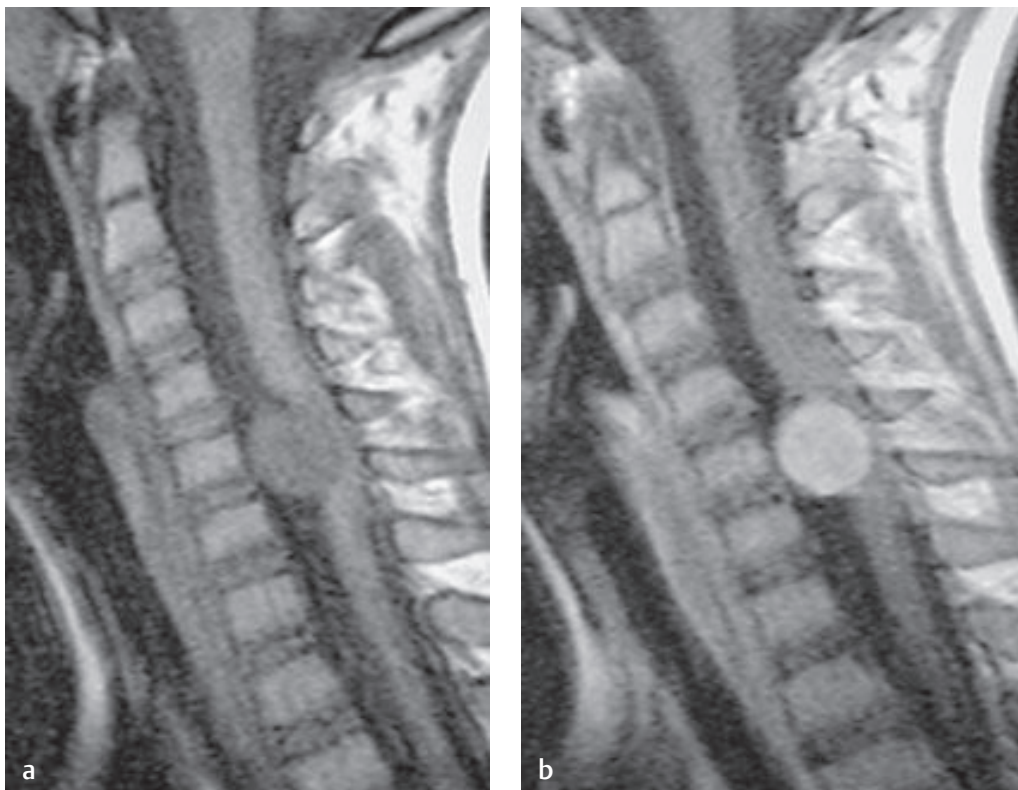


Fig. 4.4 Postgadolinium contrast enhancement. **(a)** A pregadolinium sagittal T1-weighted image shows an intradural-extramedullary mass at the C5-C6 level. **(b)** The associated postgadolinium T1-weighted image shows that the mass has uniform contrast enhancement. This mass was found to be a schwannoma. (From Khanna AJ, Carbone JJ, Kebaish KM, Cohen DB, Riley LH, III, Wasserman BA, Kostuik JP. Magnetic resonance imaging of the cervical spine: current techniques and spectrum of disease. *J Bone Joint Surg Am.* 2002;84(suppl 2, pt 2):70–80. Reprinted by permission.)

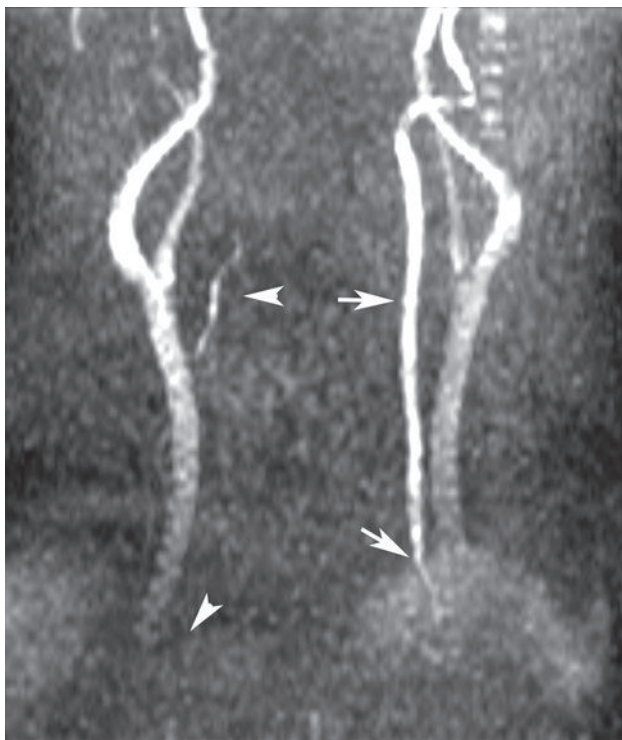


Fig. 4.5 An MR angiogram (anterior view) from a 2D time-of-flight acquisition shows absence of signal intensity in the expected course of the right vertebral artery (arrowheads). Note the normal course of the left vertebral artery (arrows).[†]

side to the other (in this case, from left to right) (Fig. 4.6).

- Next, look for the midline image (Figs. 4.7 and 4.8).
 - For the cervical spine, recognize the midline image by noting that the spinal cord is seen in its entirety (in the patient without scoliosis), extending from the midbrain to the upper thoracic spine.
 - Visualize the CSF anterior and posterior to the cervical spinal cord.
 - Confirm that the midline image is being evaluated by noting the basion and opisthion at the foramen magnum. In addition, the fourth ventricle is visualized, the vertebral bodies are seen as rectangular or square structures, and the odontoid process is seen in profile with its domed tip.
- After evaluating all of the structures in the midline, continue the review to the left or right side to evaluate for foraminal or lateral recess stenosis.
 - Each institution has its own convention as to whether the images for sagittal images are acquired from left to right or right to left.

- The only way to be 100% positive about which side of the cervical spine is being visualized is to evaluate the coronal localizing pulse sequence, which often displays numbers that correspond to the numbers seen on the sagittal images. The other way to determine whether a specific pathologic finding (for example, a disc herniation) is right or left or paracentral is to correlate the sagittal images with the findings seen on the axial images.
- Next, evaluate all of the axial T2-weighted images from the OCJ to the lower cervical spine (Fig. 4.9).
 - The only way to ensure that all of the images are seen in sequence and that none is missed is to look at the image numbers on the printed film or on the workstation screen and to confirm that the image number at the beginning of one sheet of film is, indeed, the next sequential number after that on the previous sheet.
 - Confirm the location at the OCJ by noting that the odontoid process appears different from the remaining cervical vertebral bodies in the subaxial cervical spine.
 - Finally, evaluate all of the images in sequence to view the cervical spinal cord and note that there is CSF (bright signal) around it and adequate space available for the nerve roots at the neural foramina; correlating the axial image number with the sagittal localizing image, which contains lines corresponding with numbers that indicate the level of the axial image, will ensure accurate identification of the spinal level being evaluated. Another option is to “link” the sagittal and axial images with the available image-viewing software so that a line on the sagittal midline image shows the level of the axial image.

Lumbar Spine Example

The same technique just described for the cervical spine can also be used for the lumbar spine.

- First, evaluate the sagittal T2-weighted images. Ensure that all of the sagittal T2-weighted images are being visualized in order from one side to the other.
- Next, look for the midline image (Fig. 4.10).
 - For the lumbar spine, recognize the midline image by noting that the spinal cord is seen in its entirety (in the patient without scoliosis), descending from the thoracolumbar spine to the level of L1-L2

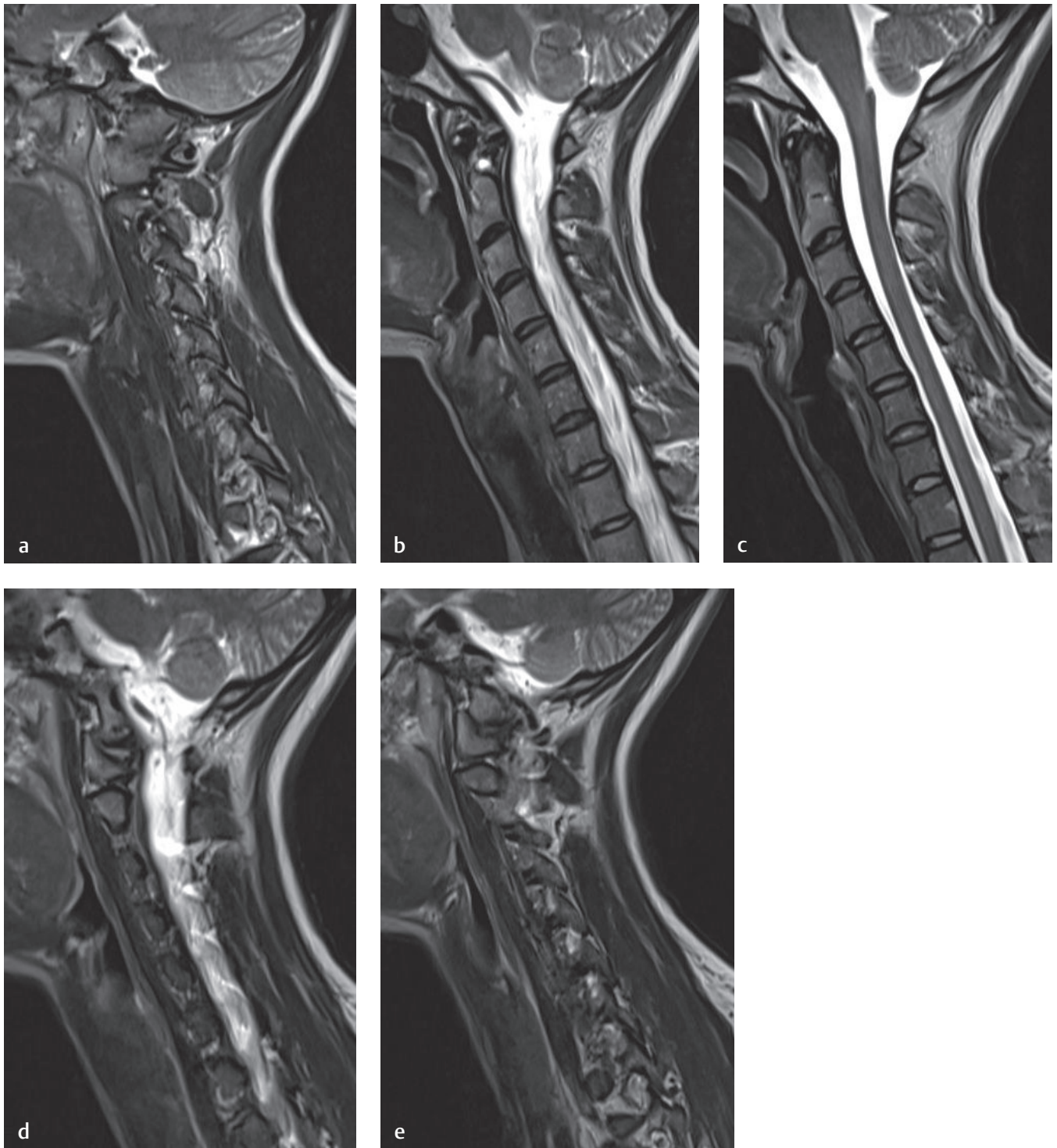


Fig. 4.6 Sequential sagittal imaging of the cervical spine. These T2-weighted images should be viewed in order from (a) left to (e) right. The midline image (c) should be identified.[†]

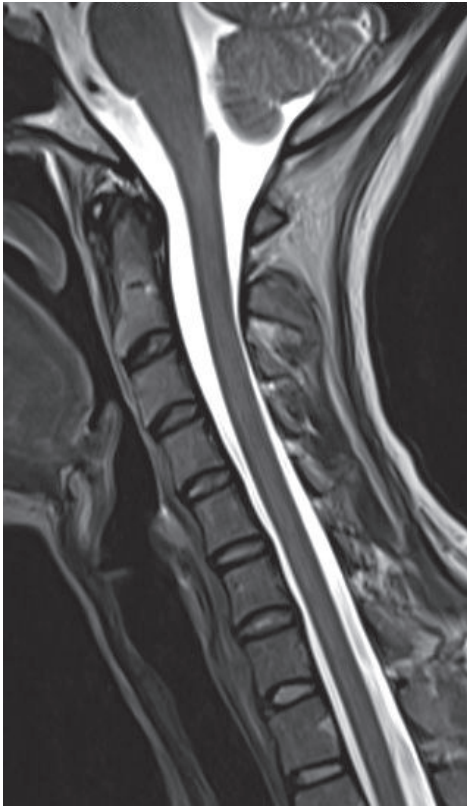


Fig. 4.7 A midline sagittal T2-weighted image of the cervical spine. Note that the spinal cord is seen in its entirety; CSF is seen anterior and posterior to the spinal cord; and the vertebral bodies, odontoid process, and fourth ventricle are seen in profile.

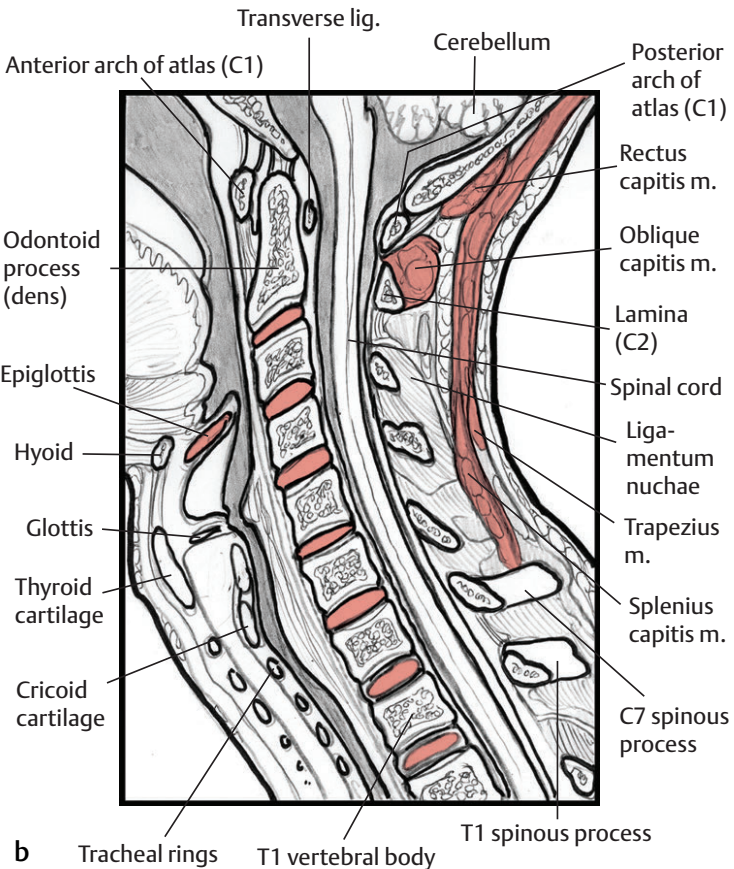
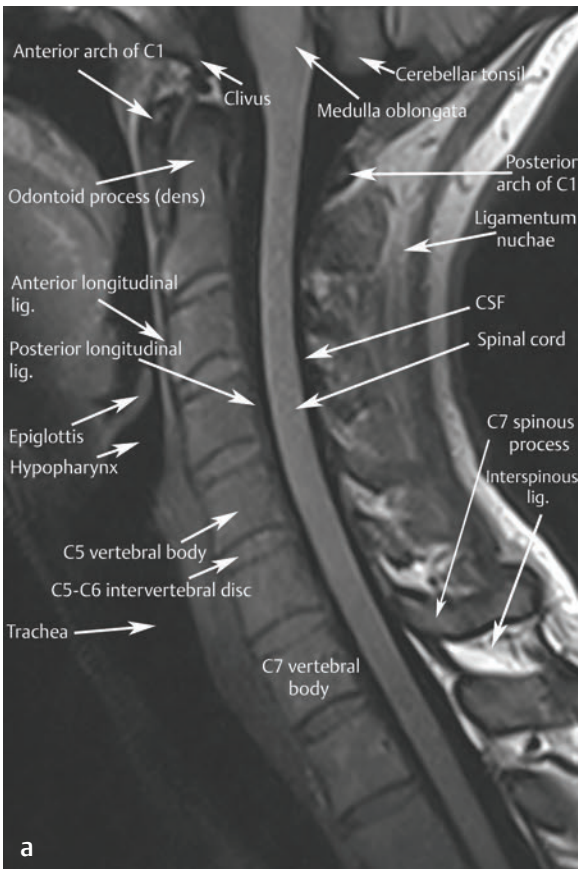


Fig. 4.8 This (a) sagittal T1-weighted midline image and (b) artist's sketch of the cervical spine depict the cervical spinal cord, CSF, and anterior and posterior longitudinal ligaments, as well as the anterior and posterior elements of the cervical spine and the intervertebral discs.[†]

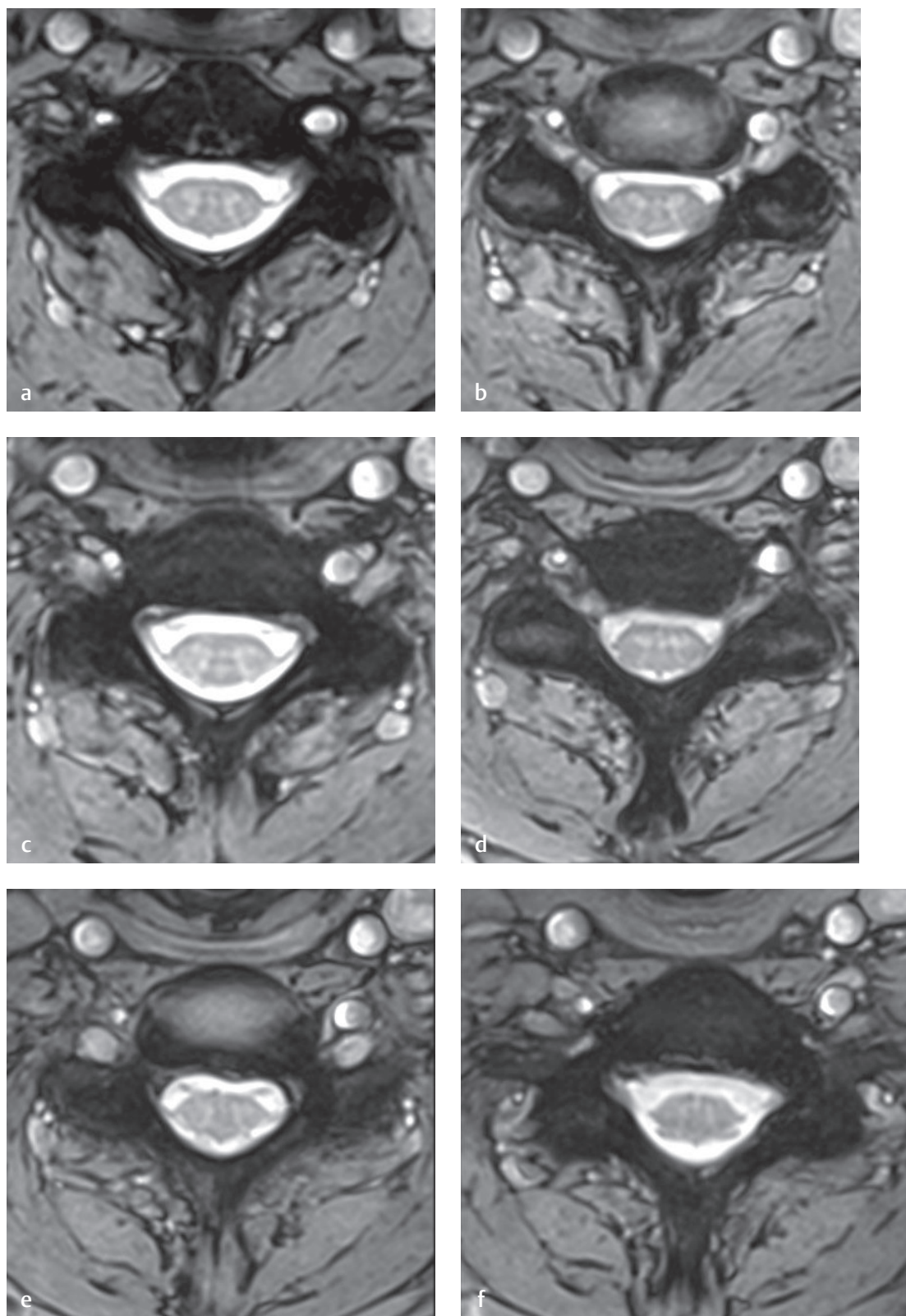


Fig. 4.9 Sequential axial imaging of the cervical spine. These T2-weighted images should be viewed in order from **(a)** C6 to **(f)** T1.[†]

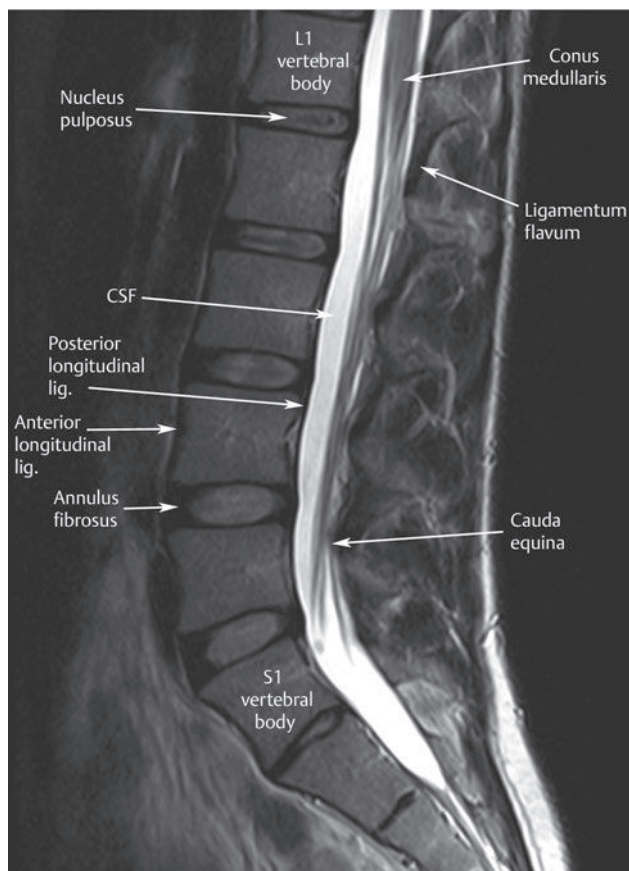


Fig. 4.10 A midline sagittal T2-weighted image of the lumbar spine. Note that the spinal cord is seen in its entirety; CSF is seen anterior and posterior to the spinal cord; and the vertebral bodies and sacrum are seen in profile.[†]

(which is the typical location of the conus medullaris).

- Visualize the CSF anterior and posterior to the spinal cord and around the nerve roots of the cauda equina in the lumbar spine below the conus medullaris.
- Confirm that the midline image is being evaluated by noting the spinal cord and conus medullaris. Additionally, the sacrum should be seen in sagittal cross-section with a normal AP length equal to that of the L5-S1 disc and the other intervertebral discs of the lumbar spine. Lastly, the lumbar vertebral bodies should be seen as square or rectangular structures.
- After evaluating all of the structures in the midline, continue the review to the left or right side to evaluate for foraminal or lateral recess stenosis (**Fig. 4.11**).
 - Each institution has its own convention as to whether the images for sagittal images are acquired from left to right or from right to left.

- As with the cervical spine example just discussed, the only way to be 100% positive about which side of the lumbar spine is being visualized is to evaluate the coronal localizing pulse sequence, which often displays numbers that correspond to the numbers seen on the sagittal images. The other way to see whether a specific pathologic finding (for example, a disc herniation) is right or left or paracentral is to correlate the sagittal images with the findings seen on the axial images.
- Next, evaluate all of the axial T2-weighted images from the lumbosacral junction to L4-L5 (**Fig. 4.12**), to the upper lumbar spine (**Fig. 4.13**).
 - As with the cervical spine example discussed previously, the only way to ensure that all of the images are seen in sequence and that none is missed is to look at the image numbers on the printed film or on the screen and to confirm that the image number at the beginning of one sheet is the next sequential number after that on the previous sheet.
 - Confirm the location at the lumbosacral junction by noting that the sacrum appears different (similar to Napoleon's hat; see **Fig. 4.14**) from the remaining lumbar vertebral bodies in the lumbar spine.
 - Finally, evaluate all of the images in sequence to view the neural structures in the lumbar spine (spinal cord, conus medullaris, and cauda equina) and note whether there is CSF (bright signal) around them and adequate space available for the nerve roots at the neural foramina. Correlating the axial image number with the sagittal localizing image, which contains lines corresponding with numbers that indicate the level of the axial image, will ensure accurate identification of the level being evaluated. Another option is to “link” the sagittal and axial images with the available image-viewing software so that a line on the sagittal midline image shows the level of the axial image.

Pattern Recognition

The next step is to evaluate for any areas of increased T2-weighted signal that should not have increased T2-weighted signal. This evaluation may be relatively easy for a clinician with extensive experience in evaluating MRI studies of a particular region. Most clinicians would agree that in determining these areas of increased T2-weighted signal, they tend to use a gestalt method. However, for the less experienced

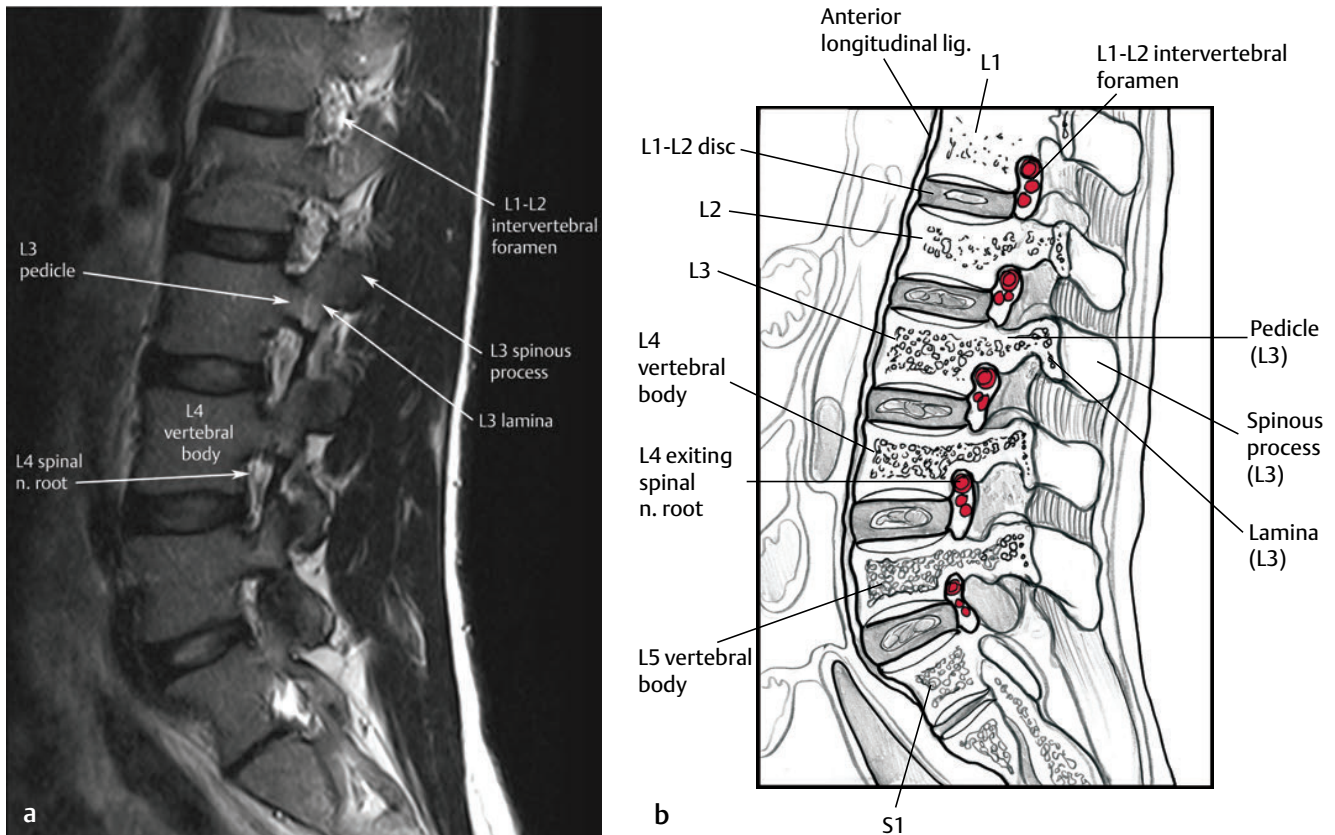


Fig. 4.11 This (a) parasagittal T2-weighted image and (b) artist's sketch of the lumbar spine show the neural foramina and exiting nerve roots at multiple levels.[†]

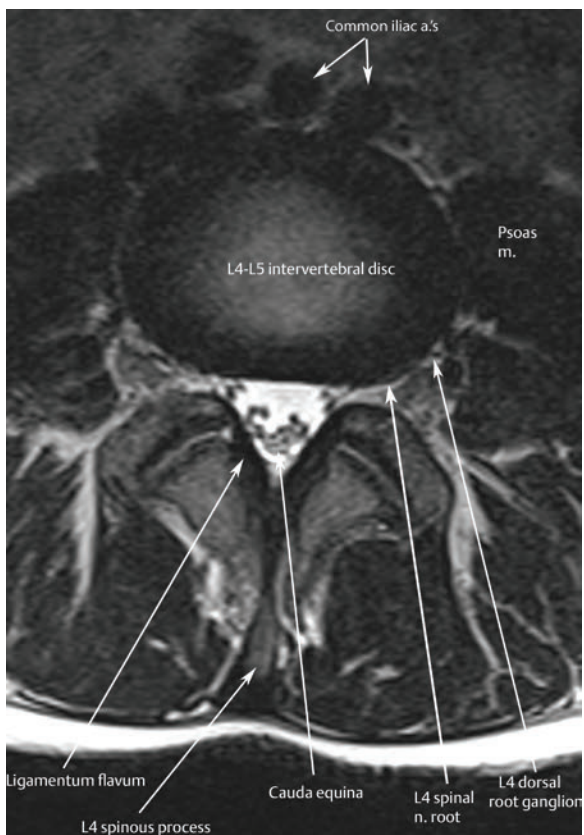


Fig. 4.12 An axial T2-weighted MR image at the level of the L4-L5 intervertebral disc shows the cauda equina, L4 spinal nerve root, and L4 dorsal root ganglion. Normal flow voids are seen within the common iliac arteries, just below the aortic bifurcation.[†]

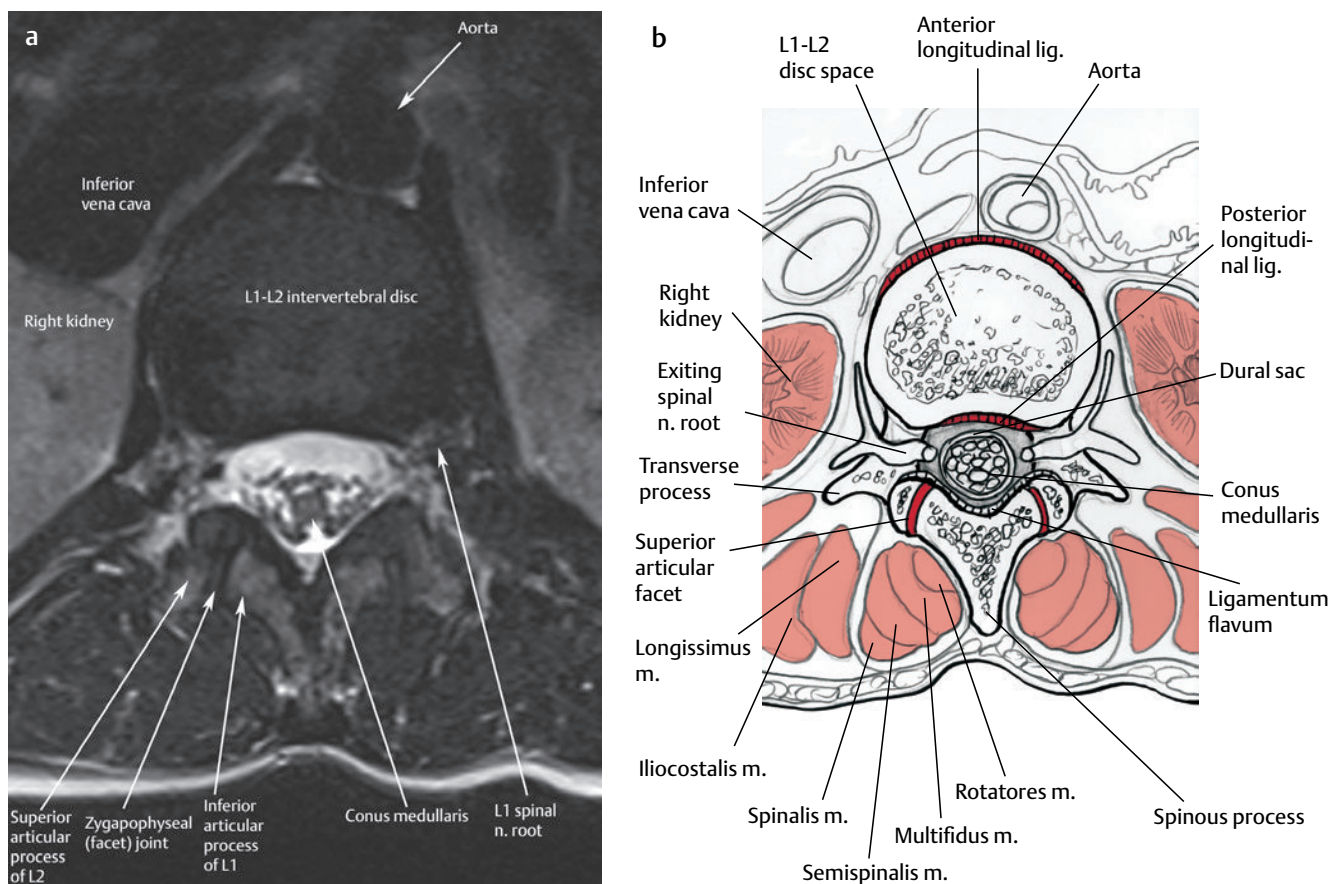


Fig. 4.13 This (a) axial T2-weighted image and (b) artist's sketch of the spine at the level of the L1-L2 intervertebral disc show the conus medullaris and the L1 spinal nerve root, as well as the superior and inferior articular processes of the L1-L2 facet joint.[†]

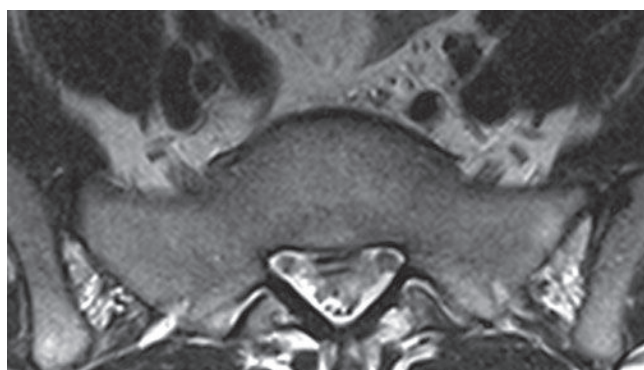


Fig. 4.14 An axial T2-weighted image of the sacrum at the S1 level shows the "Napoleon's hat" configuration of this level.

clinician or the clinician in training, several techniques can be used to determine whether or not an area should show increased T2-weighted signal. These techniques rely on the concepts of pattern recognition and experience:

- Recall the evaluations of the last 20 to 50 MRI studies of the region of interest and attempt to

remember exactly where the increase in T2-weighted signal was seen.

- Increased T2-weighted signal outside of that pattern on the current study may represent an area of pathology.
- This technique of pattern recognition is commonly used by experienced radiologists to read imaging studies. Although clinicians tend to use this technique for in-office patient evaluation, it may or may not be a safe and effective technique.¹
- The other method that one can use to evaluate for areas of abnormal increased T2-weighted signal is to note all areas of increased T2-weighted signal within a given image and then ask oneself whether water does, indeed, "belong" in that area. For example, if the sagittal T2-weighted images of a cervical spine MRI study are being evaluated and a small region of high signal is seen within the spinal cord (an anatomic structure that is obvious to even the least experienced clinician), then one may assume that it represents fluid (or edema) within the spinal cord (Fig. 4.15). The question, then, is whether it is a normal (physiologic) or an excessive (pathologic) amount



Fig. 4.15 A sagittal T2-weighted image shows a large central disc extrusion at the C5-C6 level with associated increased cord signal intensity (*arrow*) compatible with myelomalacia. Note the elevation of the posterior longitudinal ligament (*arrowhead*).[†]

of fluid. The ability to make this determination comes from experience (i.e., the recognition of lack of such a region of increased T2-weighted signal within the spinal cord on many previous studies of other patients) or from a developed fund of knowledge (such as the review of Chapter 6, The Cervical Spine) that would enable the clinician to develop a focused differential diagnosis for this finding.

■ Step 3: Evaluation of T1-Weighted Images

T1-weighted images enable optimal evaluation of anatomic detail. However, with current improvements in MRI techniques and equipment, including dedicated surface and other coils, T2-weighted images also often show excellent anatomic detail. This improvement may be the reason that the author believes the routine use of T1-weighted images by cli-

nicians and radiologists is declining. Nevertheless, the most appropriate way to evaluate an MRI study fully and most effectively is to review all of the images and pulse sequences.

Therefore, after identification of the pulse sequences obtained (Step 1) and evaluation of the T2-weighted images (Step 2), the next step is to review the T1-weighted images for improved evaluation of anatomic detail. This author's routine is to correlate the areas of increased T2-weighted signal seen during the very detailed and systematic evaluation of the T2-weighted images just described with the same region on the T1-weighted images. The improved spatial resolution of the T1-weighted images facilitates the evaluation of regional and local disturbances in anatomic detail. For example, if a sagittal fat-suppressed T2-weighted image of a vertebral compression fracture shows a somewhat indistinct area of increased T2-weighted signal within a vertebral body, the clinician may decide that it represents a vertebral compression fracture, but the clinician may also consider the possibility of other diagnoses such as tumor or infection. However, a relatively sharp and discrete fracture line seen within the sagittal T1-weighted image would likely leave no doubt in the clinician's mind that it represents a fracture and not some other process.

In addition, the T1-weighted images may help the clinician determine the type of tissue that is present in a lesion. Central to this concept is the fact that T1-weighted images tend to show fat as bright signal and fluid as dark signal. Therefore, lesions such as a lipoma are noted to be bright on T1-weighted images and, in fact, follow the signal of subcutaneous fat on all pulse sequences, including fat-suppressed or STIR pulse sequences. As another example, one of the few lesions that is bright on both T2-weighted and T1-weighted images is a hemangioma, which is often seen in the vertebral body (**Fig. 4.16**). Thus, if the lesion is seen to be bright on both of these images and displays the typical pattern of striations, the diagnosis of vertebral body hemangioma can be made with relative certainty.

Like T2-weighted images, T1-weighted images should be evaluated in all planes and in the same sequence as described in Step 2.

■ Step 4: Evaluation of Specialized Pulse Sequences

Fat-Suppressed T2-Weighted or STIR Images

The fat-suppressed T2-weighted or STIR pulse sequences are used to accentuate the increase in signal and edema seen in pathologic processes such as

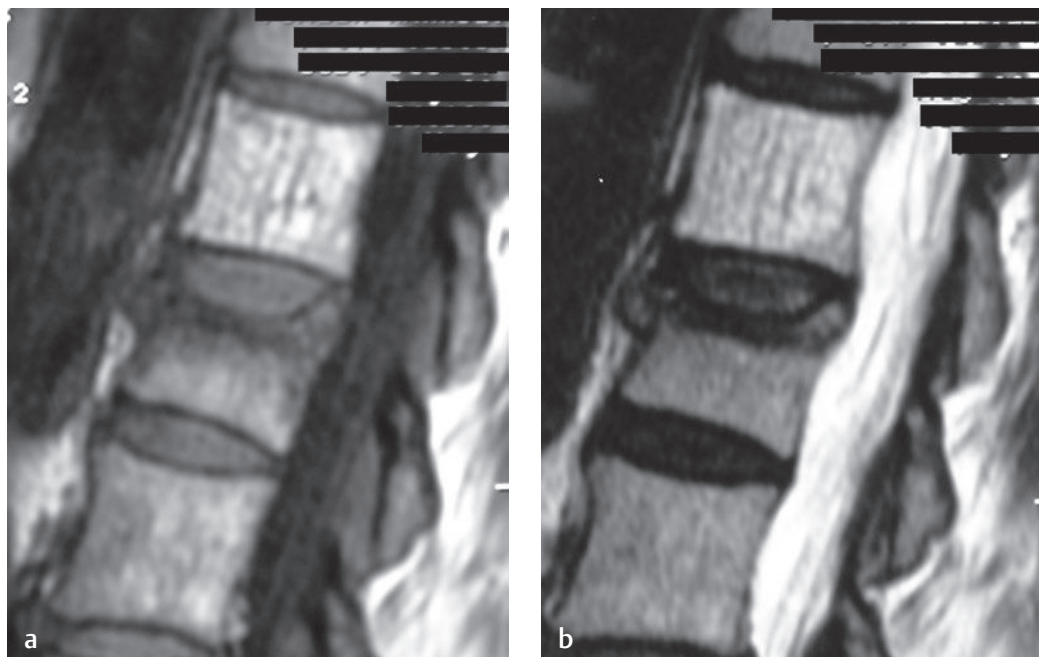


Fig. 4.16 These sagittal (a) T1-weighted and (b) T2-weighted images show a lesion at the T12 level with high signal intensity on both images and with the typical striations compatible with a vertebral body hemangioma. An incidentally noted vertebral compression fracture is seen at the L1 level.[†]

fracture, infection, and tumor. On conventional T2-weighted images, the signal from bone-marrow fat is maintained, and one attempts to recognize edema by noting the presence or absence of a very bright region (marrow pathology or edema) within a bright background (fatty marrow) (**Fig. 4.17a**). On fat-suppressed T2-weighted images, all of the subcutaneous, bone-marrow, and other fat is suppressed, and one can more easily recognize an area of edema as a bright region within a dark background (**Fig. 4.17b**). This author considers fat-suppressed T2-weighted and STIR images to be somewhat like a three-phase nuclear scintigraphy (bone scan) study (see Chapter 11, *Correlation of MRI with Other Imaging Modalities*), which is relatively sensitive to increased bone turnover but not very specific. Similarly, if a region is evaluated with fat-suppressed T2-weighted imaging or STIR imaging and there is no area of increased signal, one can be somewhat reassured that a pathologic process is not present in that region. Conversely, if an area of increased signal is noted, it may represent pathologic change or a normal region of increased signal such as physiologic fluid within a facet joint or CSF. Other pulse sequences, such as T2-weighted and T1-weighted images, provide better anatomic detail for evaluation and help the clinician identify a more specific diagnosis. As discussed previously and in the subsequent region-specific chapters, fat-

suppressed T2-weighted images can be used to evaluate for nondisplaced fractures and to determine the approximate age or chronicity of fractures, including vertebral compression fractures.

Postgadolinium T1-Weighted Images

Postgadolinium T1-weighted images are often acquired to evaluate for the presence or absence of infection and tumor and to assess the postoperative spine. For example, postgadolinium T1-weighted images can help differentiate recurrent disc herniation from epidural fibrosis and scar (**Fig. 4.18**). The recommended method for evaluating these images is to place the postgadolinium T1-weighted images side by side with the pregadolinium T1-weighted images. The region of interest is then compared in the same planes and on matching images. Higher signal intensity in the region or structure of interest on the postgadolinium T1-weighted images is termed *postgadolinium* (or contrast) enhancement. An evaluation can then be made with regard to the degree and pattern of enhancement. For example, peripheral rim enhancement with a central region of nonenhancement in a relatively well-circumscribed lesion is considered, in the appropriate clinical setting, to be a finding suggestive of an abscess.



Fig. 4.17 Vertebral compression fracture. **(a)** A sagittal T2-weighted image of the lumbar spine shows an L1 vertebral body compression fracture of an indeterminate age, given that edema is not definitely seen. **(b)** A sagittal STIR image of the same patient shows edema within the L1 vertebral body, which is compatible with an acute or subacute vertebral compression fracture.

■ Step 5: Correlation of Imaging Findings with Patient History and Examination Findings to Determine the Most Likely Diagnosis

Clinicians and radiologists have distinct advantages and disadvantages relative to one another in terms of evaluating MRI studies of the spine. Radiologists have the advantage of often being trained with a process similar to the one just described and frequently have, and take, the time to evaluate the images in a systematic fashion. However, clinicians have the advantage of knowing the patient's history and physical examination findings, laboratory results, and other parameters.

It is essential that clinicians use this advantage to help maximize the accuracy and reliability of their MRI interpretations. This point is especially true for the evaluation of patients with spinal pathologies because it is well known that many patients with pathology seen on their spine MRI studies are asymptomatic,²⁻⁵ and it is imperative that the clinician treat the patient and not just the MRI findings.

The author believes that an accurate diagnosis, or differential diagnosis, occurs at the “intersection” of a patient's history, physical examination results, radiographic findings, and laboratory study results (**Fig. 4.19**). With an understanding of the clinical scenario, clinicians can arrive at an accurate diagnosis, especially when they are armed with the appropriate techniques for evaluating the MRI studies. One way to leverage the strengths of clinicians and

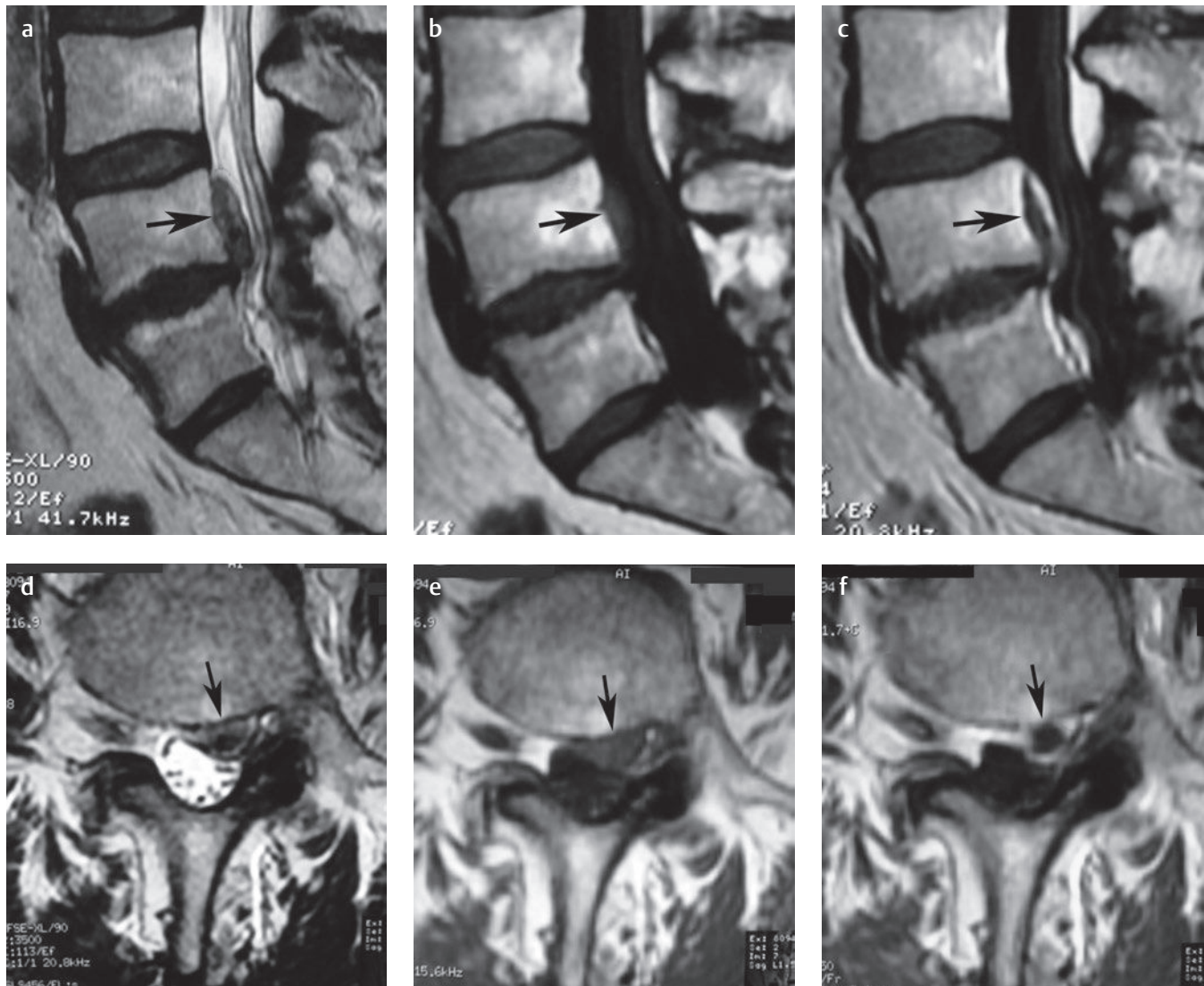


Fig. 4.18 Recurrent lumbar disc extrusion. **(a)** Sagittal T2-weighted, **(b)** T1-weighted, and **(c)** postgadolinium T1-weighted images in a patient with a history of previous L4-L5 discectomy show a large disc extrusion (arrow on each) that has migrated proximally and is located behind the L4 vertebral body. Note that the disc is difficult to see on **(b)** the T1-weighted image and shows peripheral enhancement on **(c)** the postgadolinium T1-weighted image. **(d)** Axial T2-weighted, **(e)** T1-weighted, and **(f)** postgadolinium T1-weighted images at the L4-L5 level show the left paracentral extradural lesion (arrows on each) that appears to be disc material on **(d)** the T2-weighted image and shows peripheral enhancement on **(f)** the postgadolinium T1-weighted image compared with **(e)** the pregadolinium T1-weighted image.[†]

radiologists is to use a collaborative and team approach to the evaluation of patients with complex spinal pathologies.

For example, if a patient presents with low back pain after trauma and is point-tender at the thoracolumbar junction, and the MR image shows a region of increased STIR signal within the T12 vertebral body, the diagnosis of a vertebral compression fracture can be suggested, especially if the region of edema has a linear appearance on the T2-weighted and T1-weighted images. However, if a patient with

similar imaging findings presents with no history of trauma, is elderly, has a history of insidious onset of low back pain (particularly at night), and has a history of a primary malignancy, another diagnosis (e.g., metastatic disease) might be higher on the differential diagnosis. To help determine the correct diagnosis, the clinician would likely obtain a CT scan to evaluate further the osseous anatomy in both patients. The second patient might also benefit from a primary malignancy survey, a three-phase bone scan, and a CT-guided biopsy.

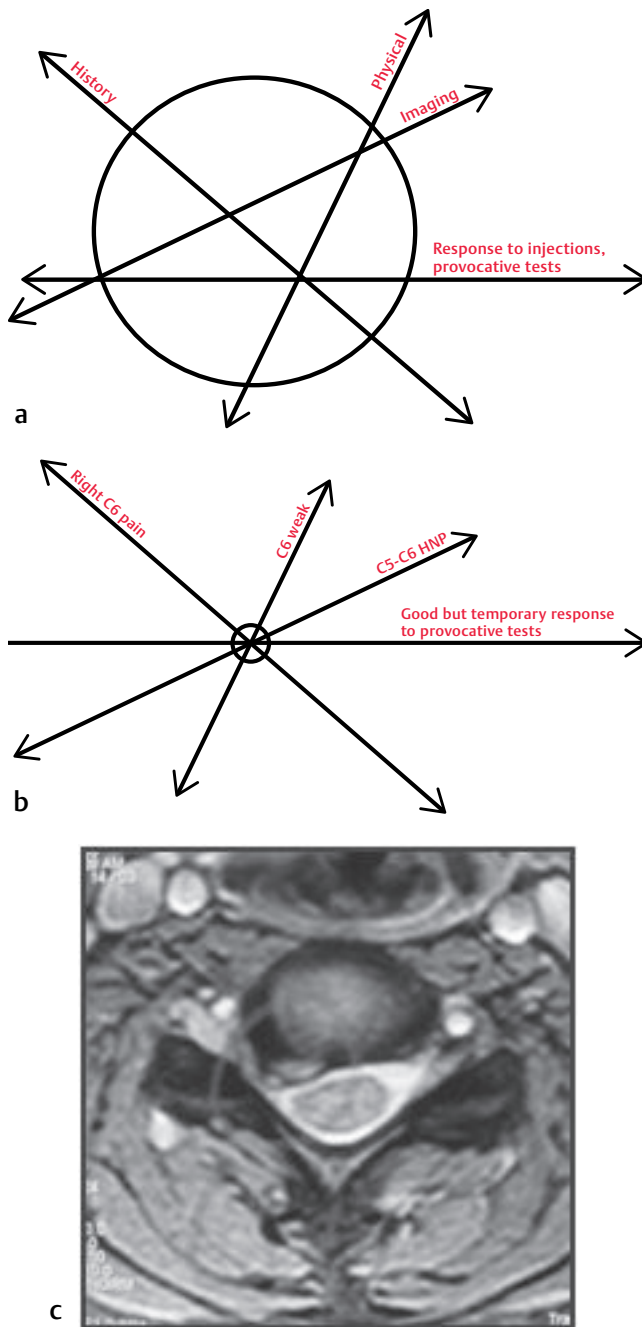


Fig. 4.19 The concept of intersecting lines for diagnosis and surgical decision making. **(a)** In a patient for whom the history, physical examination, imaging findings, and response to provocative tests do not “intersect” within a small circle, it is difficult to identify a diagnosis or to narrow a differential diagnosis. Conversely, for a patient with a smaller region of intersection, such as one with a right C6 radiculopathy **(b)**, one may expect to see a C5-C6 disc protrusion on MRI **(c)**. HNP, herniated nucleus pulposus.

COMMON CLINICAL QUESTIONS

- One should begin the interpretation of an MRI study of the cervical or lumbar spine with which imaging plane and pulse sequence?
 - Sagittal, T1-weighted images
 - Axial, T1-weighted images
 - Sagittal, T2-weighted images
 - Axial, T2-weighted images
 - Coronal, T2-weighted images
- Evaluation of what structure or region will enable one to differentiate T1-weighted and T2-weighted images?
 - Muscle
 - Bone
 - Tendon
 - CSF
 - It is not possible to differentiate these two pulse sequences by viewing an image.
- What is the most common MRI manifestation of almost all pathology such as tumor, fracture, or infection in the spine?
 - Loss of signal on all pulse sequences
 - Increased T2-weighted signal
 - Decreased T2-weighted signal
 - Increased T1-weighted signal
 - Increased signal on all pulse sequences
- What is the primary advantage that clinicians have relative to radiologists when evaluating MRI studies of the spine?
 - Better understanding of spinal anatomy
 - Greater likelihood of having formal training in the evaluation of MRI studies
 - Greater knowledge of the range of the various disease processes that can affect the spine
 - Greater likelihood of being able to correlate the imaging findings with patient's history and physical examination findings to determine the most likely diagnosis
 - B and D
- Aside from “counting” levels up from the sacrum, what is the best way to confirm the spinal level of an axial image in the lumbar spine?
 - Determine the level based on the shape of the vertebral body
 - Determine the level based on the size of the spinal canal
 - Utilize the sagittal localizing pulse sequence and correlate the image number on the axial image with those on the localizing pulse sequence/image.
 - “Link” the sagittal and axial images with the available image-viewing software so that a line on the sagittal midline image demonstrates the level of the axial image.
 - C and D

■ Summary

In summary, the five-step technique described in this chapter will help guide the clinician in systematically evaluating MRI studies of the spine. This author strongly believes that such a systematic technique should be used for the evaluation of all MRI studies and that the tendency to become less meticulous and systematic over time should be avoided. One additional suggestion is to always attempt to read the MRI study using this technique and then to evaluate the “official” radiologist’s reading to determine the degree of correlation between the two readings. Occasionally, the clinician notes findings that were not reported by the radiologist, and vice versa. Over time, this method of checking one’s own evaluation against that of another trained specialist will serve as a method of quality control and assurance and will likely result in a continuously improving ability to evaluate MRI studies accurately.

References

1. Groopman J. *How Doctors Think*. Boston: Houghton Mifflin; 2007
2. Boden SD, Davis DO, Dina TS, Patronas NJ, Wiesel SW. Abnormal magnetic-resonance scans of the lumbar spine in asymptomatic subjects. A prospective investigation. *J Bone Joint Surg Am* 1990;72(3):403–408 PubMed
3. Bogduk N. Degenerative joint disease of the spine. *Radiol Clin North Am* 2012;50(4):613–628 PubMed
4. Borenstein DG, O'Mara JW Jr, Boden SD, et al. The value of magnetic resonance imaging of the lumbar spine to predict low-back pain in asymptomatic subjects: a seven-year follow-up study. *J Bone Joint Surg Am* 2001;83-A(9):1306–1311 PubMed
5. Teresi LM, Lufkin RB, Reicher MA, et al. Asymptomatic degenerative disk disease and spondylosis of the cervical spine: MR imaging. *Radiology* 1987;164(1):83–88 PubMed

ANSWERS TO COMMON CLINICAL QUESTIONS

1. C
Explanation: In almost all instances, the clinician should begin with the midline sagittal T2-weighted images of the cervical or lumbar spine because the high contrast between the CSF and the neural elements provides a myelographic view of the spine, which provides a good “overview” of the condition of the spine. In rare instances, such as for the patient with a spinal deformity (e.g., degenerative or congenital scoliosis), it may be best to begin with the coronal T2-weighted images.
2. D
Explanation: Recognition of an area within an image that is known to contain fluid, such as CSF, will allow one to differentiate T1-weighted and T2-weighted images. If this fluid is noted to be bright or of high signal intensity, that image is likely T2-weighted. If the region of the fluid is noted to be dark, that image is likely T1-weighted.
3. B
Explanation: The most common MRI manifestation of almost all pathology such as tumor, fracture, or infection in the spine (or any other structure in the musculoskeletal system) is increased T2-weighted signal because it represents the edema (free extracellular fluid) that is common to most pathologic processes.
4. D
Explanation: Clinicians and radiologists have distinct advantages and disadvantages relative to one another in terms of evaluating MRI studies of the spine. Radiologists have the advantage of often being trained, and frequently have, and take, the time to evaluate the images in a systematic fashion. However, clinicians have the advantage of knowing the patient’s history and physical examination findings, laboratory results, and other parameters. It is essential that clinicians use this advantage to help maximize the accuracy and reliability of their MRI interpretations.
5. E
Explanation: Aside from “counting” levels up from the sacrum, the best way to confirm the spinal level of an axial image in the lumbar (or cervical) spine is to use the localizing sagittal pulse sequence. One can correlate the image number on the axial image with that on the localizing pulse sequence/image or “link” the sagittal and axial images with the available image-viewing software so that a line on the sagittal midline image shows the level of the axial image. The size, shape, and configuration of the vertebral body or spinal canal are not reliable methods of determining a spinal level.

|| Spine

5 The Occipitocervical Junction

Colin M. Haines, A. Jay Khanna, John A. Carrino, Shih-Chun David Lin,
and Joseph R. O'Brien

CHAPTER OUTLINE

- I. Occipitocervical Craniometry
- II. MRI Anatomy and Imaging Protocols
- III. Pathology of the OCJ
 - A. Primary/Congenital Conditions
 - 1. Congenital Anomalies of the Occiput
 - 2. Congenital Anomalies of the Atlas
 - 3. Congenital Anomalies of the Axis
 - 4. Chiari Malformations
 - 5. Klippel-Feil Syndrome
 - B. Acquired Conditions
 - 1. Basilar Impression
 - 2. RA/Cranial Settling
 - C. Neoplasms
 - 1. Primary Osseous/Extradural Tumors
 - 2. Intradural-Extramedullary Tumors
 - 3. Intramedullary Tumors
- IV. Miscellaneous
 - A. Down Syndrome
 - B. Trauma to the OCJ
 - 1. Occipitocervical Trauma
 - 2. Trauma to the Atlas
 - 3. Trauma to the Axis
 - 4. Traumatic Spondylolisthesis of the Axis
- V. Summary

The OCJ, also termed the craniovertebral junction in the literature, refers to the articulations among the occiput (C0), atlas (C1), and axis (C2). The OCJ is highly mobile, with ~50% of cervical flexion–extension and rotation coming from the C0–C1 and C1–C2 articulations, respectively.¹ This region's strong capsuloliga-

mentous attachments, rather than its intervertebral discs, are the basis of its stability.^{2,3} An understanding of occipitocervical craniometry adds value in the diagnosis of pathology at the OCJ. The treatment of pathologic conditions involving the OCJ requires a thorough understanding of osseous, ligamentous, and neurovascular anatomy (see Chapter 2, Normal Spine MRI Anatomy). Most orthopedic surgeons without advanced training in spine surgery do not have a great deal of experience in evaluating and treating pathology in this area. However, the ability to recognize the most common abnormalities in this region is important so that the patient can be referred appropriately for treatment, if needed.

■ Occipitocervical Craniometry

The OCJ may be imaged with conventional radiography, MRI, and CT to evaluate pathologic conditions.^{4–8} Although normal relationships were originally defined with radiographs,^{7,9–11} many of these relationships and lines are also used with MRI (**Table 5.1** and **Fig. 5.1**), which offers more clarity and accuracy.⁸

Wackenheim's clivus baseline aids in diagnosing superior migration of the odontoid. The line is formed by creating a line along the rostral surface of the clivus¹¹; protrusion of the odontoid tip above or posterior to this line is considered abnormal. The *clivus canal angle* is formed by intersecting Wackenheim's line and a line connecting the posterior vertebral bodies. In extension, 180 degrees is normal; in flexion, 150 degrees is normal. *Chamberlain's line* is drawn between the hard palate and the opisthion (posterior lip of the foramen magnum), with >3 mm of dens protrusion indicating abnormality.⁹ Use of this line may be limited by the difficulty in identifying the hard palate and the margin of the opisthion on the lateral radiograph. *McGregor's line* is drawn from the hard palate to the most inferior point on

Table 5.1 Anatomic relationships and lines for use with MRI, CT, and conventional radiography[†]

Eponym	Parameters	Abnormality
Wackenheim's clivus baseline	Tangent drawn along the superior surface of the clivus	Dens should be below line.
Clivus canal angle	Angle formed between Wackenheim's line and the posterior vertebral body line	Normal ranges are 180 degrees in extension to 150 degrees in flexion. An angle of <150 degrees is considered abnormal.
Chamberlain's line	Between the hard palate and opisthion	Protrusion of the dens >3 mm above this line is considered abnormal.
McRae's line	From the basion to the opisthion	Protrusion of the dens above this line is considered abnormal.
McGregor's line	From the hard palate to the most caudal point on the midline occipital curve	Odontoid process rising >4.5 mm above this line is considered abnormal.
Ranawat's criterion	Distance between the center of the pedicle of C2 and the transverse axis of C1	Measurement of <15 mm in males and <13 mm in females is abnormal.
Welcher's basal angle	Tangent to the clivus as it intersects a tangent to the sphenoid bone	The normal range is 125 to 143 degrees. Platybasia exists when the basal angle is >143 degrees.

the midline occipital curve.¹⁰ If the odontoid process rises >4.5 mm above this line, it is considered pathologic.¹⁰ Difficulty in identifying the hard palate can limit the use of this line, but use of the occiput can be easier than use of the opisthion. *McRae's line* is drawn from the opisthion to the basion (anterior lip of the foramen magnum), and any rostral odontoid elevation above this line is pathologic.^{12,13} Again, identification of the opisthion may be difficult on the lateral radiograph. The *Ranawat's criterion* is calculated by measuring the distance between the center of the pedicle of C2 and the C1 transverse axis.¹⁴ In men, <15 mm is abnormal; in women, <13 mm is abnormal.¹⁴

Platybasia is measured by drawing *Welcher's basal angle*¹⁵ (**Fig. 5.2**). This condition, originally described by Virchow¹⁶ to denote flattening of the skull base, is associated with basilar invagination or occipitalization of the atlas. Welcher's basal angle is created from a line parallel to the clivus as it intersects a line along the surface of the sphenoid. The normal range is 125 to 143 degrees, and platybasia exists when the basal angle is >143 degrees.

It is important to note that the previously mentioned radiographic parameter has a sensitivity or negative predictive value of >90% on conventional radiographs alone.⁸ Therefore, it is recommended that any suggestion of cranial settling on conventional radiographs be investigated with MRI or CT.⁸

■ MR Anatomy and Imaging Protocols

MRI has enabled the detailed study of the normal anatomy¹⁷ and the pathology^{8,18,19} of the OCJ. The widespread use of MRI for studying this area has resulted in part from its ability to image directly in the sagittal and coronal planes.²⁰ Previously, detailed study of the OCJ required the use of polytomography or thin-section CT with coronal and sagittal reconstructions rather than images obtained directly in the coronal or sagittal planes.²¹ In general, MRI produces images in which cortical bone has a low signal on T1-weighted and T2-weighted images. However, low signal intensity does not limit the usefulness of MRI in studying the OCJ. Specialized pulse sequences may be used to evaluate fully the particular details of the OCJ anatomy.^{17,22}

Many authors have reported difficulty in visualizing the alar ligaments with standard MRI protocols,^{23–26} and others have reported abnormal signals in healthy volunteers.^{27,28} Krakenes et al¹⁷ developed an MRI protocol with which to address the need for accurate visualization of the craniovertebral ligaments: intermediate-weighted sequences with 2-mm sections obtained with a standard 1.5-T coil with the patient's head in the neutral position. Their protocol has been validated by recent studies^{22,29} that visualize the normal ligaments of the OCJ (**Fig. 5.3**).

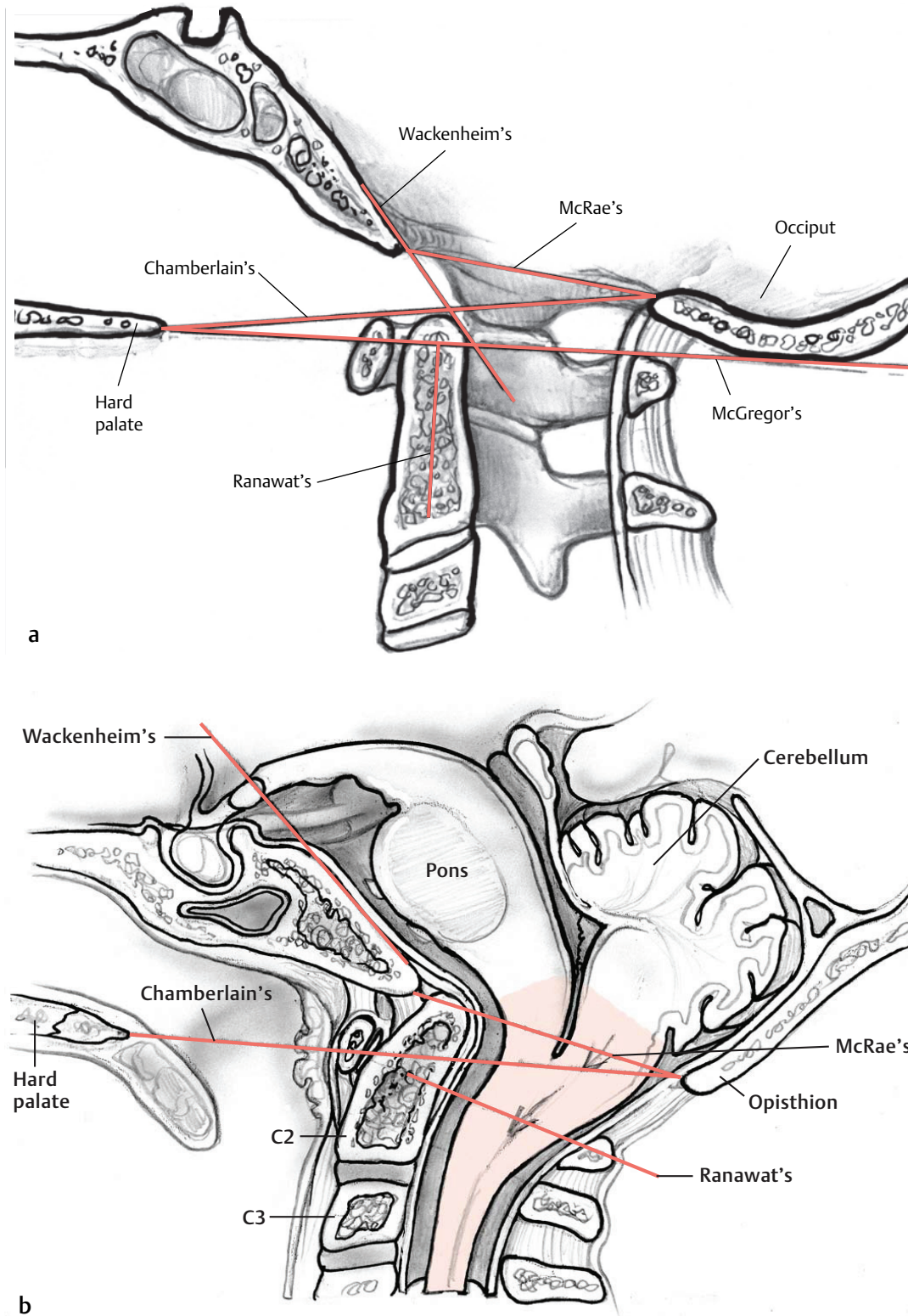
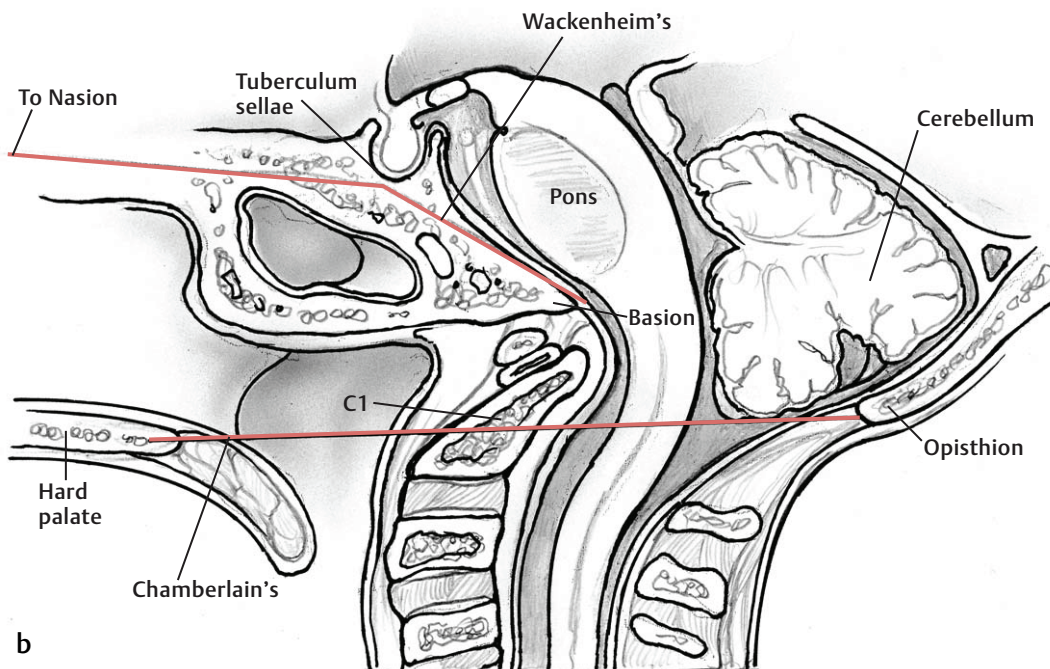


Fig. 5.1 Lines and measurements for the evaluation of basilar invagination. **(a)** Artist's sketch of a case of normal relationships at the OCJ.[†] **(b)** An artist's sketch of a case with basilar invagination and Chiari type-II malformation.



Fig. 5.2 This (a) sagittal T1-weighted image (*dotted line*, Wackenheim's clivus baseline) and (b) artist's sketch of platybasia. Welcher's angle measures 160 degrees in this case; the normal measurement is 125 to 143 degrees. (a, from Smoker WRK. MR imaging of the craniocervical junction. *Magn Reson Imaging Clin N Am* 2000;8(3):635–650. Reprinted by permission.)



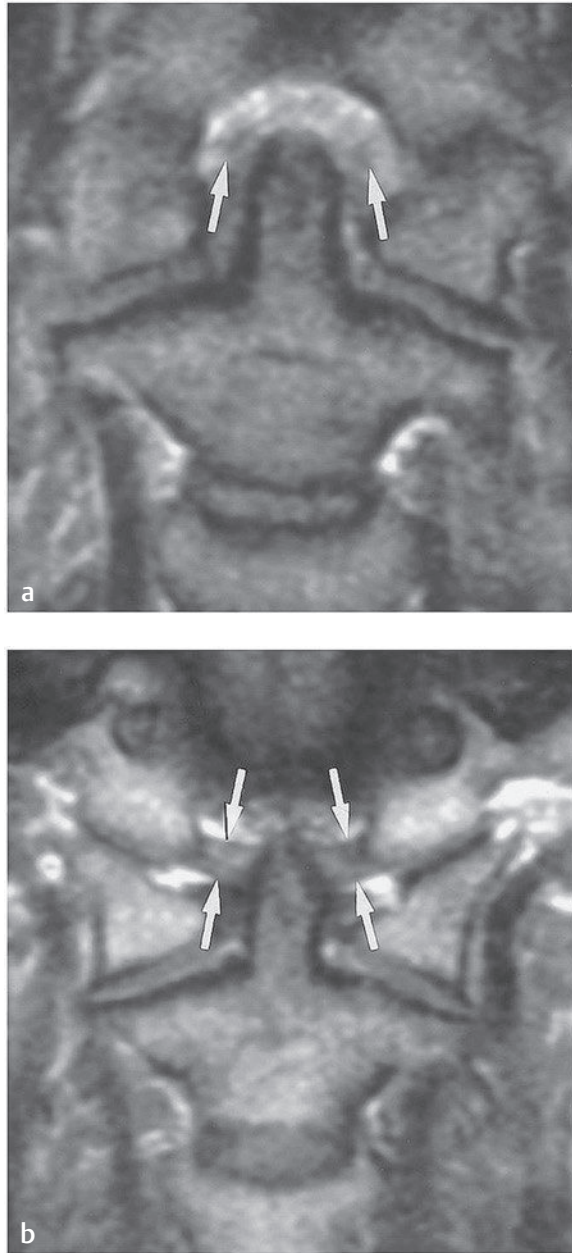


Fig. 5.3 The intact alar ligaments (*arrows*) in a normal spine are very difficult to identify on **(a)** a coronal T2-weighted image but are more easily visualized on **(b)** a specialized intermediate-weighted image.

The gross anatomy of the OCJ is precisely displayed on high-signal-to-noise T1-weighted images.³⁰ Gated T2-weighted images produce high signal from CSF, edema from abnormalities, and other parenchymal lesions while minimizing CSF pulsation artifact.³⁰ For instance, myelomalacia from spinal cord compression is best visualized on T2-weighted images.

Sagittal images are ideally suited for evaluation of the brainstem, fourth ventricle, and upper cervical spine.³⁰ Sagittal and parasagittal sections are taken

from one occipital condyle to the other.¹⁷ As detailed above, craniometry measurements may be made from sagittal MRIs.⁸ For instance, midsagittal MRIs can be used to measure the atlanto-axial interval, the posterior space available for the cord, or basilar impression using Wackenheim's line. The presence or absence of pannus at the C1-C2 articulation also may be delineated on the sagittal images (**Figs. 5.4** and **5.5**). Parasagittal images may detail the C0-C1 and C1-C2 articulations. The sagittal and parasagittal images are also useful for mapping the vertebral artery anatomy, which is essential for planning before surgical procedures at the C1 and C2 levels.

Coronal images are useful for evaluating the cerebellar tonsils and the C0-C1 and C1-C2 articulations. Coronal sections are taken from the anterior arch of the atlas to its posterior arch.¹⁷ Coronal images show the lateral masses of C1 and the apical and alar ligaments.

Axial sections, typically obtained from the foramen magnum to the base of the dens,¹⁷ provide detailed information on the cross-sectional anatomy of the OCJ. In particular, they are useful for characterizing the space available for the cord, atlantoaxial subluxation, and vertebral artery anatomy within C1 and C2. Correlation of axial images with the sagittal or coronal localizing images is vital when evaluating the OCJ to confirm the level (occiput versus C1 versus C2) that is being evaluated.

■ Pathology of the OCJ

OCJ pathology can result in compression of neural elements and odontoid elevation. Conditions affecting the OCJ can be classified as primary/congenital or acquired.

Primary/Congenital Conditions

When congenital conditions result in brain stem compression, use of the term *basilar invagination* is appropriate.^{21,30}

Congenital Anomalies of the Occiput

Anomalies of the occiput may be the results of failure of formation (often referred to as hypoplasias) or of segmentation.^{12,31–33} Failures of formation include both basioccipital and occipital condyle hypoplasia.^{21,33} Basioccipital hypoplasia results in a shortened clivus from poor development of the sclerotomes (**Fig. 5.6**).^{33,34} This condition has a wide range of clinical severity, although it often results in basilar invagination, which may be best seen with Chamberlain's line.²¹ In occipital condyle hypoplasia, the deformity

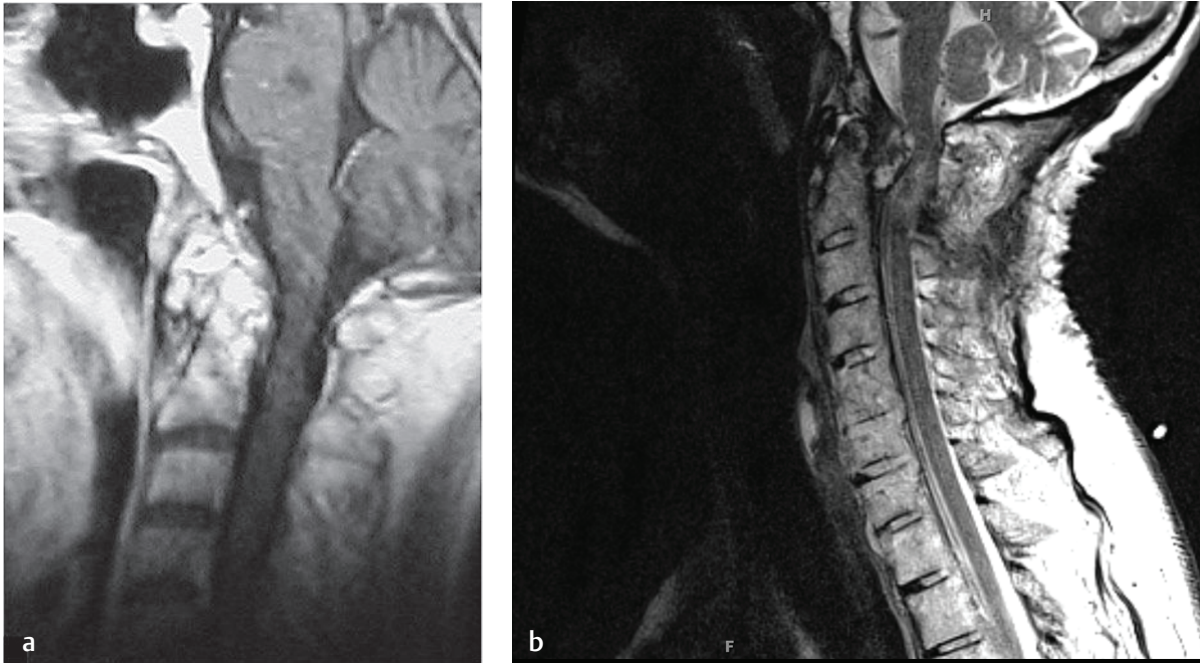


Fig. 5.4 C1-C2 pannus formation. **(a)** A sagittal T1-weighted image shows a large pannus in the atlanto–dens interval in a patient with RA and cranial settling. **(b)** A sagittal T2-weighted image of a patient with a large pannus posterior to the odontoid shows it is causing cord compression.

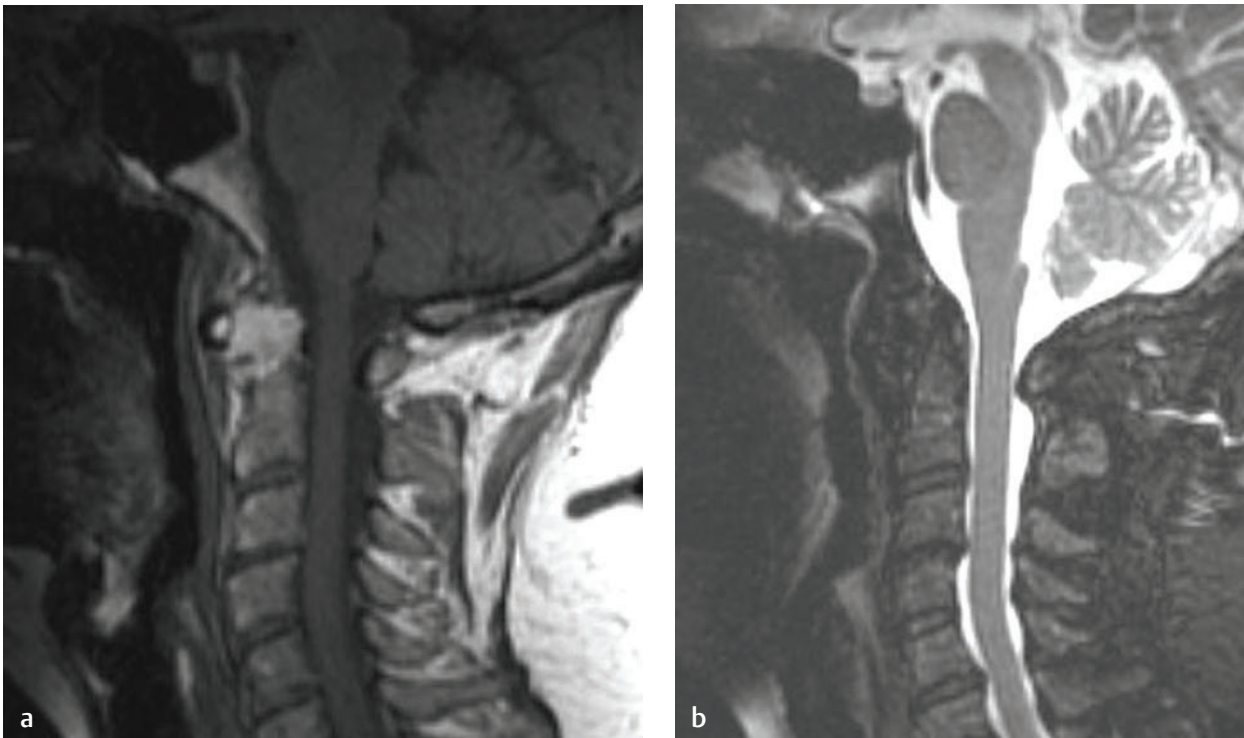


Fig. 5.5 These sagittal **(a)** T1-weighted and **(b)** STIR images of another patient with RA and large pannus formation that, in this case, the pannus has caused substantial osseous erosion.

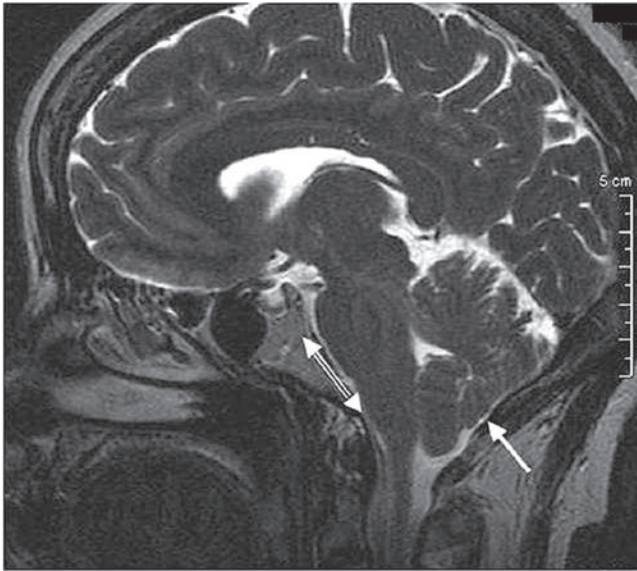


Fig. 5.6 A sagittal T2-weighted image shows basiocapital hypoplasia with Chiari type-I malformation (*single arrow*) and a shortened clivus (*double arrow*). (From Noudel R, Jovenin N, Eap C, Scherpereel B, Pierot L, Rousseaux P. Incidence of basiocapital hypoplasia in Chiari malformation type I: comparative morphometric study of the posterior cranial fossa. *J Neurosurg* 2009;111:1046–1052. Reprinted by permission.)

is usually bilateral; however, unilateral cases have also been reported.^{21,35} Shortened, flat condyles result in basilar invagination, and notably, the atlantooccipital joint axis angle seen on coronal MRI is widened. Clinically, this condition may result in limited atlantooccipital joint motion.

Failure of segmentation at the OCJ may result in atlantooccipital assimilation (**Fig. 5.7**), which may be partial or complete.^{21,36} The incidence in the general population has been reported to be 0.08% to 2.76%,³⁶ and sagittal MRI scans often reveal a comma-shaped basion.²¹ This finding is often incidentally discovered on imaging after patients present with neck pain after minor trauma.^{12,13,36} Approximately half of patients with C0-C1 assimilation progress to subsequent atlantoaxial instability and early-onset myelopathy.^{12,13,33,37–39} Families of children with atlantooccipital assimilation should be educated on the natural history of the disease and the warning signs of myelopathy.³⁶

Congenital Anomalies of the Atlas

Rachischisis is the developmental failure of the atlas.²¹ In normal development, the posterior arch fuses with the lateral masses at 3 to 4 years of age, and the anterior arch fuses with the lateral masses at 6



Fig. 5.7 A sagittal T2-weighted image shows atlantooccipital assimilation. The basion is more curved than normal, and there is superior migration of the odontoid process.

to 8 years of age. In contrast to failure of segmentation, failure of formation of the atlas is only rarely associated with basilar invagination.^{21,40} Posterior atlas arch clefts are the most common pattern seen, with an incidence of 4% in autopsy specimens.^{41,42} Most of these clefts are midline; only 3% are at the sulcus for the vertebral artery.^{41,42} Anterior arch clefts are more rare, with an incidence of 0.1% of autopsy specimens^{41,42}; they may be associated with posterior clefts and may mimic a Jefferson fracture.⁴² Well-corticated margins and the lack of a posterior tubercle suggest an arch defect.^{21,41–43} In contrast, a defect with increased MRI signal intensity on fluid-sensitive sequences is more indicative of a Jefferson fracture. It is important to note that the midline physis closes at 4 years of age.^{39,44} Overall, axial MRI views best illustrate any C1 defects.

Congenital Anomalies of the Axis

Congenital anomalies of the axis usually are confined to the odontoid process and are rarely associated with basilar invagination²¹ but may result in atlantoaxial

instability.⁴⁵ To clarify the formation anomalies, a review of the physiologic axis development is detailed.⁴⁶

Failure of fusion of the terminal ossicle results in a Bergman ossicle,²¹ which may be confused with a type-I odontoid fracture⁴⁷ and is of little clinical significance. Fusion of the dentocentral synchondrosis normally occurs at 6 years of age.⁴⁸ Failure of fusion or fracture of the dentocentral synchondrosis results in an os odontoideum (**Fig. 5.8**). This term refers to an ossicle that is above the body of C2. The anterior arch of C2 is rounded and hypertrophic, and the body of C2 has a well-corticated, convex upper margin.²¹ Atlantoaxial instability is a hallmark of this disorder.^{21,45} It is associated with congenital diseases involving abnormalities of connective tissue such as Down syndrome, spondyloepiphyseal dysplasia, and Morquio syndrome.⁴⁹ Odontoid aplasia is extremely rare and is associated with atlantoaxial instability.^{21,45}

Although diagnosis of fusion failures of C2 may be made on radiography, MRI provides more detailed information.⁵⁰ To differentiate fusion failures from acute fractures, coronal and sagittal cuts are most valuable. Fractures lack cortication on T1-weighted images and show edema on T2-weighted and fat-suppressed T2-weighted images.

Chiari Malformations

A type-I Chiari malformation^{51,52} is defined as a defect in the cerebellum with a downward displacement of the tonsils >5 mm below the plane of the foramen magnum; however, some authors have referred to downward displacement from 3 to 5 mm as a borderline diagnosis based on clinical parameters (**Figs. 5.9** and **5.10**).^{53,54} Associated conditions include basilar invagination in 50%, atlantooccipital assimilation in 10%, and Klippel-Feil syndrome in 5%.^{53,54} Midsagittal images most consistently show the downward tonsil displacement and decreased CSF content in the retrocerebellar space.⁵⁵

A type-II Chiari malformation, or the Arnold-Chiari malformation, results from dysgenesis of the hindbrain.²¹ It is almost always associated with myelomeningocele and can present with multiple anatomic anomalies, including hydrocephalus, hypoplasia of intracranial structures (falx cerebri, corpus callosum), and downward displacement of posterior fossa content (inferior cerebellar vermis, fourth ventricle, and medulla).⁴¹ It is not generally associated with atlantooccipital assimilation or basilar invagination.²¹



Fig. 5.8 Os odontoideum versus chronic odontoid fracture. **(a)** A sagittal T2-weighted image of an os odontoideum. An os is often round and does not preserve the shape of the dens, but a chronic odontoid fracture, as seen on **(b)** a sagittal T2-weighted image, typically retains the typical anatomic architecture of the odontoid.

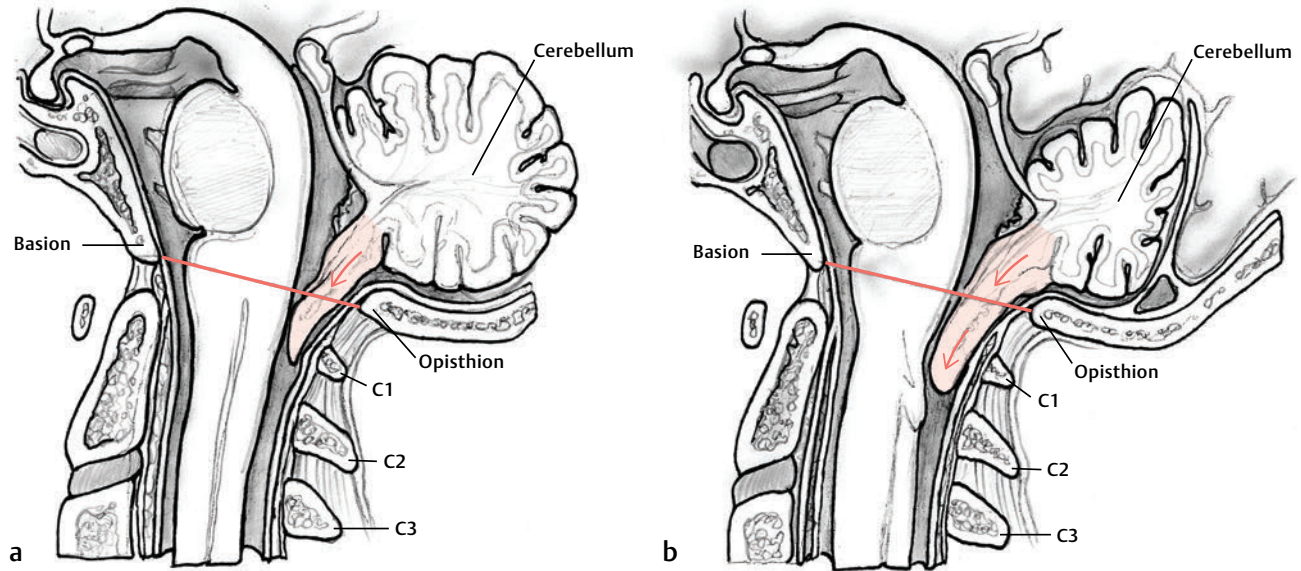


Fig. 5.9 Artist's sketches show the typical features of (a) type-I and (b) type-II Chiari malformations.

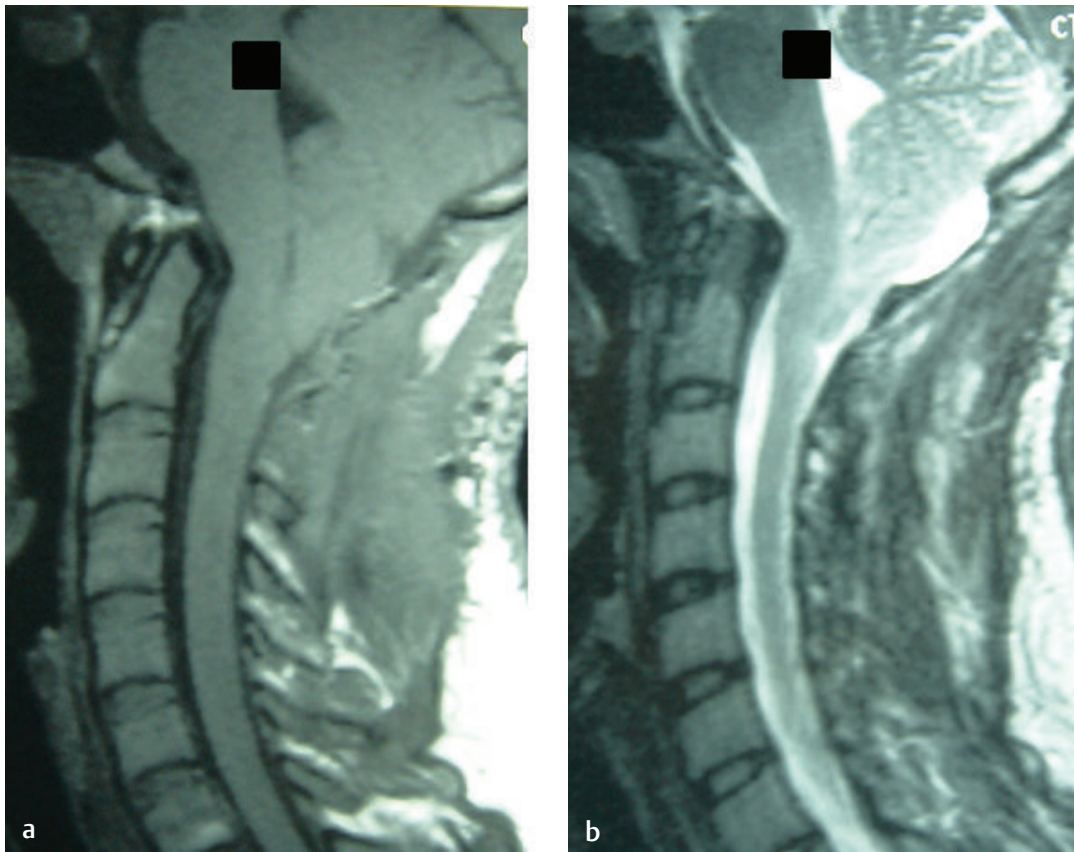


Fig. 5.10 These sagittal (a) T1-weighted and (b) T2-weighted images of a patient with a type-I Chiari malformation who has undergone a suboccipital decompression procedure.

A type-III Chiari malformation, which is a herniation of the hindbrain into a high cervical encephalocele, occurs rarely.^{21,56}

A type-IV Chiari malformation involves cerebellar hypoplasia without cerebellar herniation.

Klippel-Feil Syndrome

Klippel-Feil syndrome is classically described as a triad of a low posterior hair line, short neck, and limited neck mobility in association with congenital cervical fusions.⁵⁷ For the diagnosis to be made, there must be failure of segmentation of at least two cervical vertebrae.⁵⁸ Accelerated degeneration of adjacent levels and increased susceptibility to cord injury after minor trauma have been reported.^{58,59} Coronal and sagittal images are most useful in diagnosing the lack of segmentation.

Acquired Conditions

Acquired conditions cause pathology by softening the skull base, thereby potentiating odontoid elevation. Many disease processes may cause such elevation of the odontoid process, including osteogenesis imperfecta, Paget disease, rickets, osteomalacia, RA, and ankylosing spondylitis. *Basilar impression* is the term used to denote the odontoid's superior migration in the setting of acquired skull base softening.^{21,30}

Basilar Impression

It is useful to review certain terms related to craniocervical instability. Cranial settling differs from basilar invagination and basilar impression. Cranial settling is vertical subluxation of the odontoid caused by a loss of supporting ligamentous structures.²⁰ This condition may occur with RA or psoriatic arthritis. Basilar invagination results from a loss of skull height secondary to congenital abnormalities.²⁰ Basilar impression results from skull base softening secondary to an acquired condition such as Paget disease.

RA/Cranial Settling

RA is a systemic disease that causes inflammation of synovial joints. The synovial joints develop a pannus that generates enzymatic erosion of supporting ligamentous structures.^{60,61} In the cervical spine, this condition may affect both the craniocervical junction and the subaxial cervical spine.⁶⁰⁻⁶³ Most commonly, atlantoaxial instability develops secondary to erosion of the ligaments at the OCJ.^{60,61} As the disease progresses, erosion of the lateral masses of C1, the occipital condyles, and facets of C2 occurs, resulting in cranial settling (**Fig. 5.11**).^{21,60,61} Once the odontoid begins to occupy a relatively more rostral position, it compresses the brain stem and vertebrobasilar system. This pathologic process is postulated by some as the cause of sudden death in those with advanced RA.^{21,60,61,64} It is important to note that, in contrast to other disorders, the C1 arch

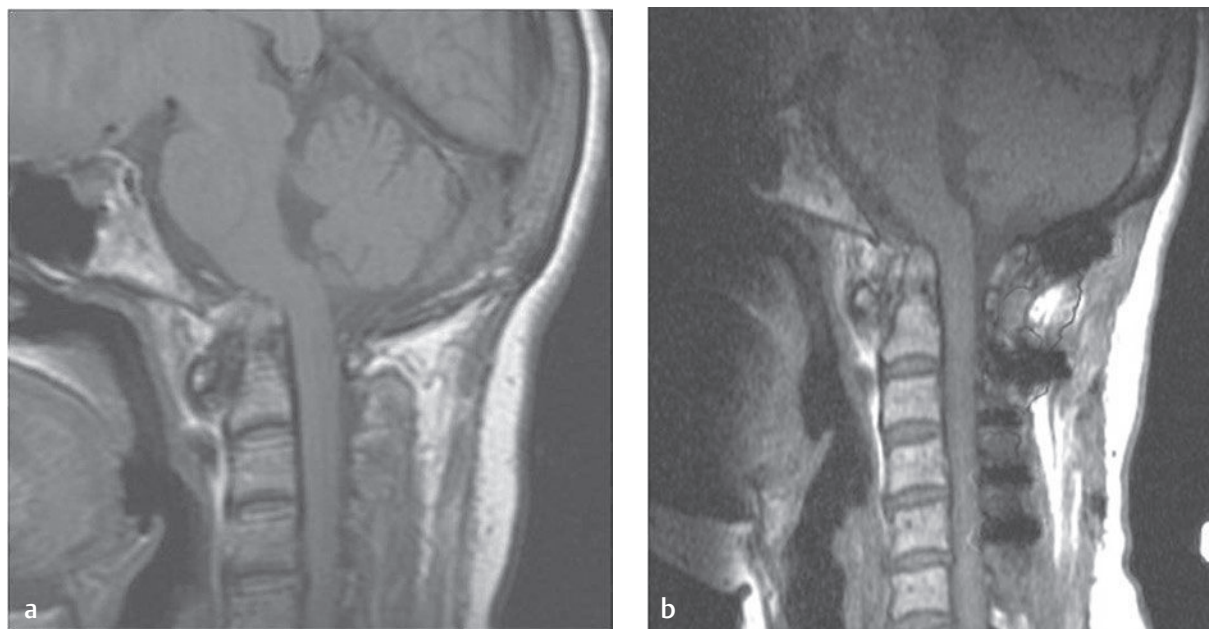


Fig. 5.11 Cranial settling. **(a)** A sagittal T1-weighted image shows cranial settling in a patient with RA. **(b)** A sagittal T1-weighted image with metal suppression after instrumented reduction from the occiput to C5, which resulted in decreased brainstem compression.

migrates with the skull base to lie in a more caudal position.²¹ In some cases, it has been reported to be as inferior as the C2-C3 disc space.^{5,58,59,65} Because of the erosion of the osseous structures that takes place, the method of Redlund-Johnell and Pettersson⁷ may be used to gauge settling. This technique uses the vertical distance from McRae's line to the C2-C3 disc space to gauge cranial settling. Boden and colleagues^{60,61} reported on the use of MRI to measure the space available for the cord as a technique for predicting recovery after cervical stabilization for patients with RA and atlantoaxial instability. A cord space, or space available for the cord, of >14 mm on MRI was associated with better clinical outcomes than was a space of <10 mm, which was associated with a poor prognosis.^{60,61}

Neoplasms

The neoplastic abnormalities that can affect the craniocervical junction are similar to neoplasms that affect the rest of the spine (see Chapter 8, Tumors of the Spine). As with the rest of the spine, tumors of the OCJ can be located within one of three compartments:

- Extradural
- Intradural-extramedullary
- Intramedullary

Osseous neoplastic lesions within this region can be divided into primary and metastatic lesions, a distinction that becomes critical when applying a treatment paradigm. Imaging of this region is best performed with a combination of conventional radiography, CT, and MRI. Although the imaging modalities can help narrow the differential diagnosis, biopsy is the only method for definitive diagnosis.

Primary Osseous/Extradural Tumors

The primary osseous tumors in this region are:

- Hemangioma
- Chondroblastoma
- Osteoid osteoma
- Osteoblastoma
- Chordoid rest
- Aneurysmal bone cyst
- Giant cell tumor
- Chordoma
- Various sarcomas

The differential diagnosis of these primary bone tumors can be narrowed based on the tumor's location (**Fig. 5.12**) and imaging characteristics. Most primary tumors of the spine originate within the posterior elements (pedicles, facets, pars, lamina, and spinous processes). Hemangiomas, chordoid rests, chordomas, and giant cell tumors are more likely to be located an-

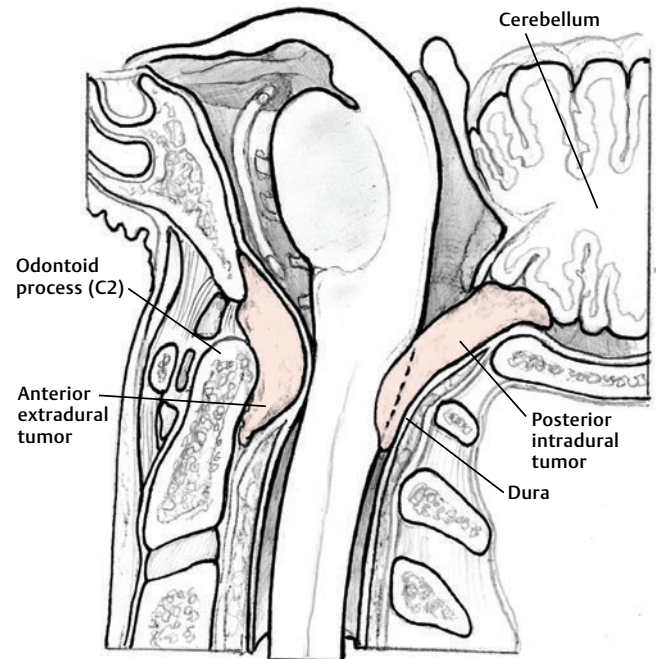


Fig. 5.12 An artist's sketch shows anterior extradural and posterior intradural tumors at the OCJ.

teriorly and to arise from the midline. Chondroblastomas, osteoid osteomas, and osteoblastomas tend to arise from the posterior elements of the spine.

Hemangiomas, chordoid rests, and chordomas are most frequently slow-growing tumors, and the bone tends to show evidence of remodeling. Chordoid rests and chordomas tend to have a bright "bubbly" appearance on T2-weighted MRI sequences, and in most cases they arise within the vertebral body.⁶⁶ The distinction between a chordoid rest and a chordoma largely depends on the lesion's size and clinical history. Hemangiomas also tend to be anteriorly located. They have a spiculated, "wagon-wheel" appearance, with clearly defined margins. Aggressive or atypical hemangiomas can lose this characteristic appearance if they grow to considerable size.^{67,68}

In contrast, more aggressive tumors typically exhibit varying degrees of osseous erosion. Giant cell tumors are often hypodense on T1-weighted and T2-weighted images and frequently enhance on T1-weighted images with contrast administration. MR images of giant cell tumors typically show lytic lesions.⁶⁹ Sarcomas usually have an invasive appearance on MRI, as evidenced by cortical destruction and infiltration of the surrounding tissues. They tend to be anteriorly located and have a varying degree of soft-tissue component.

Osteoid osteomas and osteoblastomas appear similar on imaging studies, but they are distinguished based on size: lesions <1.5 cm are termed osteoid osteomas; larger lesions are called osteoblastomas. Both lesions have areas of blastic and clastic activity,

giving a characteristic target appearance on CT imaging, or a central sclerotic area, surrounded by a hypodense area, contained within a calcified margin.⁷⁰ If MR angiography is performed, it may show hypervascularity in the surrounding musculature that may suggest a more aggressive appearance of the lesion (e.g., osteosarcoma), but in reality, the hypervascularity is a reactive phenomenon and still compatible with the benign diagnosis of osteoid osteoma.⁷¹

Aneurysmal bone cysts are characterized by a slowly growing lesion with sclerotic boundaries on conventional radiographs or CT. On MRI, a thin expansile rim and fluid-fluid levels on T2-weighted imaging, representing areas of hemorrhage in different stages of evolution, can help confirm the diagnosis of aneurysmal bone cyst.⁷² Multiple septate and small lobulations are usually present on T2-weighted images but may be imperceptible on T1 sequences.⁷³

Lesions that metastasize to the osseous spine often appear aggressive on imaging studies. They are often anteriorly located and show substantial osseous destruction. Compared with metastasis to other levels of the spine, epidural extension of the tumor at the level of the OCJ is unusual. Spinal cord compression seen with these lesions usually is the result of overt instability and osseous compression rather than epidural extension of the tumor. The apical, transverse, posterior longitudinal, and nuchal ligaments are very thick in this region, which prevents direct compression from epidural extension.⁷⁴

Intradural-Extramedullary Tumors

Intradural-extramedullary abnormality in this region is also similar to that of all other levels of the spine. These lesions are best characterized using MRI (T1-weighted, T2-weighted, and postcontrast T1-weighted sequences). Tumors seen in this region are:

- Meningioma
- Hemangiopericytoma
- Schwannoma
- Neurofibroma
- Metastatic disease (less commonly)

Meningiomas and hemangiopericytomas tend to be hypointense to isointense on T1-weighted and T2-weighted MRI, and they strongly enhance with contrast administration. These tumors typically produce a “dural tail,” which appears as an epidural extension of the tumor, beyond the main bulk of the tumor, in the subdural space along the dura.^{75–77} Although this finding may be seen with schwannomas and neurofibromas, its presence suggests a meningioma or hemangiopericytoma. These lesions also tend to display substantial vascularity on angiography (hemangiopericytomas are very vascular lesions). Schwannomas (**Fig. 5.13**) and neurofibromas usually have a less midline location and usually extend toward (and sometimes through) the neural foramen.^{66,78,79} They originate from the nerve

root, which explains the eccentric nature. The imaging of these lesions can be varied, but it often resembles that of meningiomas, without a dural tail. A spinal fluid space between the tumor and the spinal cord at either end of the tumor can suggest a nerve sheath tumor over a meningioma in the differential diagnosis.

Intramedullary Tumors

The intramedullary abnormalities that can be found at the OCJ are:

- Ependymoma
- Hemangioblastoma
- Glial tumors
- Vascular lesions (i.e., cavernous malformation or arteriovenous malformation)

Ependymomas arise from the ependymal layer of the central canal and are slow-growing lesions. They are usually centrally located, grow rostrally and caudally, and frequently have an associated syrinx. They are most often hypointense on T1-weighted and T2-weighted MRI sequences, and they homogeneously enhance with contrast administration (**Fig. 5.14**).^{80,81} Hemangioblastomas are also commonly hypointense on T1-weighted and T2-weighted MRI sequences and enhance with contrast administration. They are usually seen to be eccentric in location within the spinal cord and often have a large syrinx associated with them. Areas of hemorrhage of different ages may be seen surrounding the tumor and can markedly vary the appearance of these tumors on MRI.⁸²

Angiography can be useful in showing the vascularity of the tumor and the location of the arterial feeders and draining veins.⁸³ Glial tumors can arise anywhere within the spinal cord substance. Unlike ependymomas, glial tumors usually do not have an associated syrinx or distinct margins on imaging studies. The cord has a swollen appearance (increased diameter) in the region of the tumor. These tumors are visualized best on T2-weighted imaging, and the degree of contrast enhancement usually correlates with the grade of the tumor. Given the imaging characteristics of a glial tumor, these lesions can be difficult to distinguish from transverse myelitis and spinal cord signal change secondary to myelopathy and ischemia.⁷⁰

The MRI characteristics of the multitude of tumors just described that can be seen at the OCJ can be used to generate and then narrow a differential diagnosis. Subsequently, a definitive diagnosis is made with an open or percutaneous (usually image-guided) biopsy. The tissue diagnosis, along with the location of the tumor, alteration in regional anatomy, degree of stenosis, presence or absence of instability, and degree of neural compromise, can all help to guide the surgical or nonsurgical treatment. For patients treated surgically, MRI characteristics can help select the approach and assist with preoperative planning and postoperative follow-up.

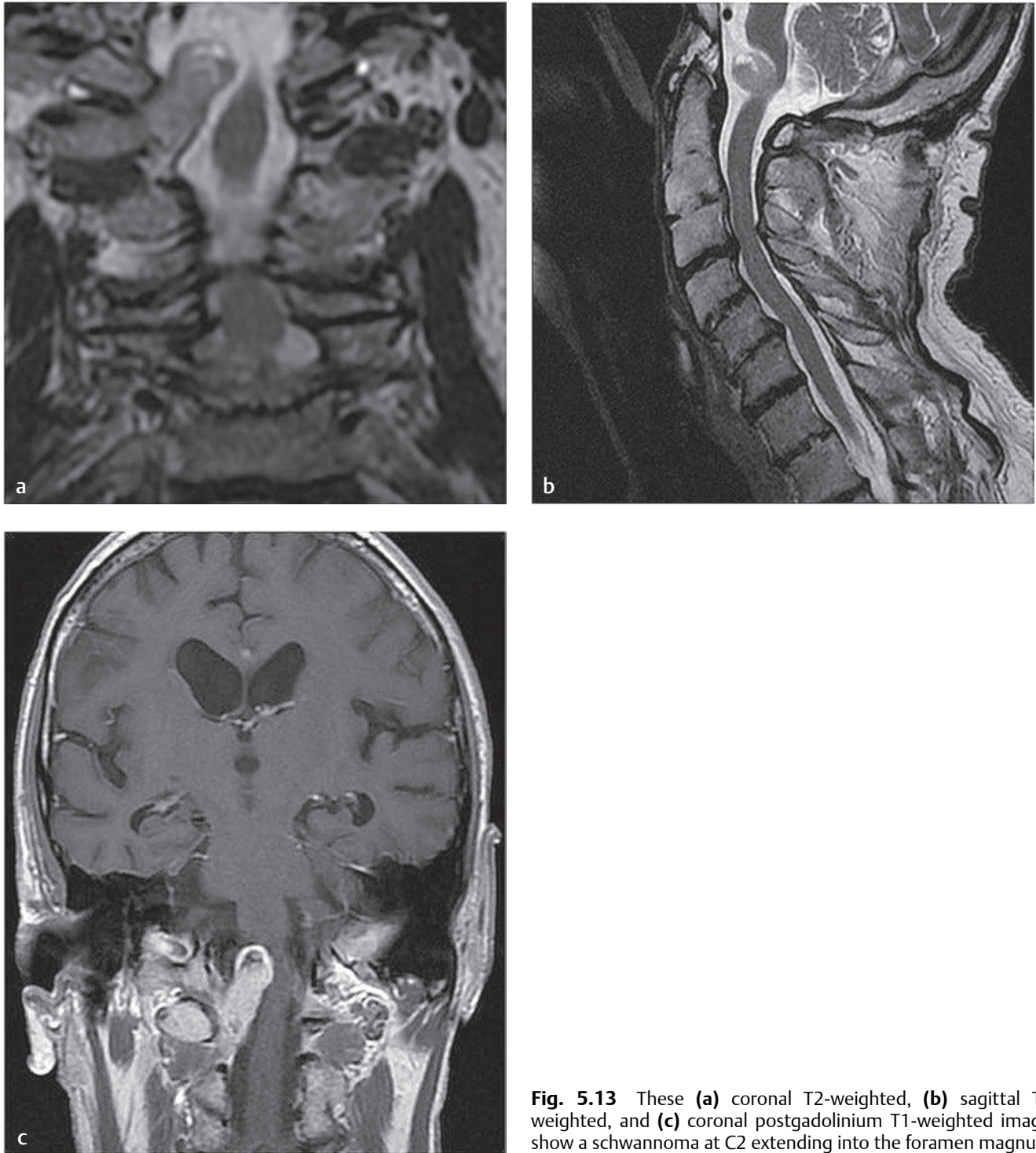


Fig. 5.13 These (a) coronal T2-weighted, (b) sagittal T2-weighted, and (c) coronal postgadolinium T1-weighted images show a schwannoma at C2 extending into the foramen magnum.

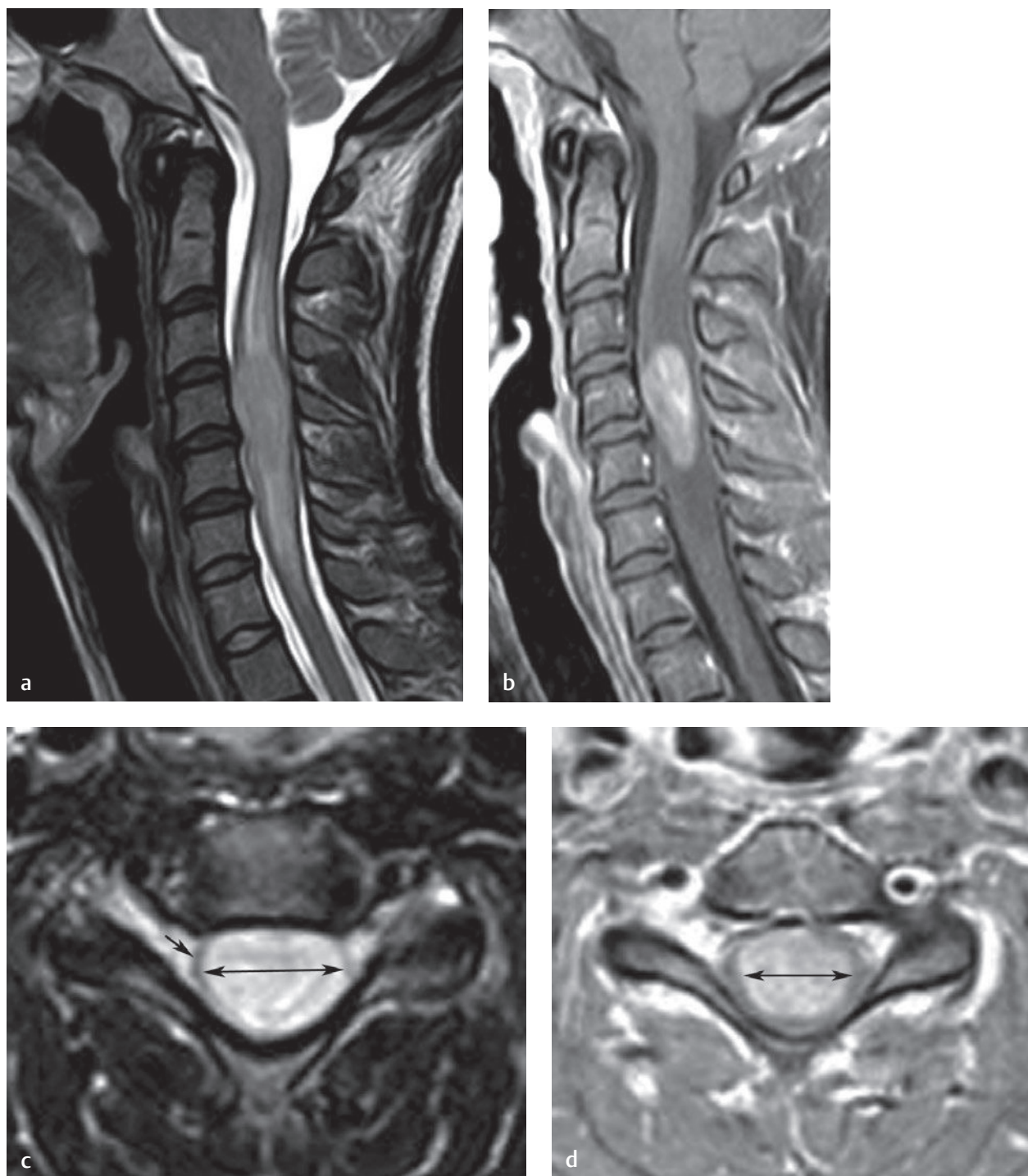


Fig. 5.14 Cervical ependymoma. **(a)** A sagittal T2-weighted image shows a large cervical ependymoma centered at C4-C5 but with cord signal change extending from C2 to C7. **(b)** A sagittal postgadolinium T1-weighted image shows that the tumor is located at C4-C5 and that the signal change extended from C2 to C7 shown in **(a)** represents edema proximal and distal to the lesion. **(c)** An axial T2-weighted image shows that the lesion (between *arrowheads*) is located within the spinal cord, which is seen as a thin sliver of low signal intensity surrounding the lesion (*arrow*). **(d)** An axial postgadolinium T1-weighted image shows similar findings with enhancement of the tumor.[†]

■ Miscellaneous

Down Syndrome

Down syndrome is caused by trisomy 21. Among the disorders associated with Down syndrome, ligamentous laxity figures prominently. Atlantoaxial and atlantooccipital instability have also been described.^{84–91} Although flexion-extension conventional radiographs can be used to detect atlantoaxial instability⁹² in children with Down syndrome and are used widely as screening tools,^{93,94} surgical decision making should be based on neural impingement seen on MRI.⁹¹ Flexion-extension MRI can also be used to evaluate for stenosis in patients with Down syndrome, as it is in patients with known or suspected instability secondary to more conventional degenerative stenosis (**Fig. 5.15**). It is important to note that patients with Down syndrome have higher incidences of os odontoideum and hypoplasia of the arch of the atlas than does the general population.^{21,30,95}

Trauma to the OCJ

In a study of 34,069 patients with blunt trauma, 2.4% had trauma to the cervical spine.⁹³ Of those patients with cervical fracture, 34% had an injury to the OCJ.⁹³ Recognition of OCJ trauma is crucial because of the devastating effects of injury to this anatomic area.^{96–98}

In 2007, the Spine Trauma Study Group provided a consensus statement on measurement techniques for upper cervical spine injuries.⁹⁹ Many of the techniques reviewed were developed for studying patients with cranial settling associated with RA.^{12,13} Different measurement techniques are recommended in the setting of OCJ trauma.⁹⁹

Occipitocervical Trauma

Occipitocervical dislocation (**Fig. 5.16**) can be a devastating injury.^{96–98} Postmortem studies show that approximately one third of individuals who die as a result of traffic accidents have this injury.^{96,97,100} Delays in diagnosis averaging 2 days after the injury, correlating with worse neurologic outcomes, have been reported.¹⁰¹ In addition, even without frank dislocation, the C0–C1 junction may be injured, as indicated by postmortem studies.^{96,97,102} Therefore, familiarity with the advanced imaging appearance of the ligaments is vital for the practicing spine surgeon.^{17,22,103,104}

Atlantoaxial dissociation (**Fig. 5.17**) may also be the result of a traumatic event.¹⁰⁵ It is associated with odontoid fractures or osseous displacement in the sagittal plane. T2-weighted sequences are most useful in identifying a transverse ligament injury or

osseous edema, which often accompanies the dissociation. Adjuvant dynamic MRI may also be helpful in illustrating the transverse ligament injury.

The Harris technique (**Fig. 5.18**) is useful in the radiographic diagnosis of atlantooccipital dislocation. To use this tool, the basion–dental interval and the basion–posterior axial line interval are calculated on midsagittal MRI sequences.⁸⁹ Measurements >12 mm for the basion–dental interval and basion–posterior axial line interval are abnormal and suggestive of a dislocation. The Powers ratio¹⁰⁶ (**Fig. 5.19**) has also been used to calculate injury. The distance from the basion to the posterior arch is divided by the distance from the anterior arch to the opisthion. A value of 1 is considered normal. If the value is >1, an anterior dislocation must be suspected, and if it is <1, the potential for posterior dislocation exists.¹⁰⁶ However, the Harris technique has been shown to be better than the Powers ratio for diagnosing dislocation.⁹⁹

Occipital condyle injuries have been classified on the basis of osseous versus ligamentous involvement.¹⁰⁷ Large osseous fragments have been noted to be more stable and have a greater chance at healing with nonoperative immobilization.^{108,109} Although characterization of occipital condyle fractures is best performed with parasagittal and coronal CT images,¹⁰⁷ MRI will highlight the fracture and also the associated ligamentous injuries.

Trauma to the Atlas

An axial load to the OCJ at the atlas may result in burst fractures, which were originally described by Sir Geoffrey Jefferson.¹¹⁰ The injury is typically visualized on open-mouth odontoid radiographs or coronal CT images.^{99,111,112} On open-mouth radiography, the rule of Spence¹¹⁰ indirectly measures the integrity of the transverse ligament, which is paramount for stability. However, axial T2-weighted images can directly assess transverse ligament injury, including avulsion injuries (**Fig. 5.20**).

Trauma to the Axis

C2 is the most commonly fractured cervical spine level.^{93,113,114} Of cervical fractures secondary to blunt trauma, 24% involve C2 and one third are odontoid fractures.⁹³ Fractures occur in a bimodal incidence: one spike in the young and one in the elderly.¹¹⁴ Elderly patients tend to have odontoid fractures that are posteriorly displaced. Fracture morphology, important in determining the healing potential, can be best illustrated on lateral cervical radiography or CT,⁹⁹ whereas MRI can assess neural compression and also provide insight regarding the age of the fracture (**Fig. 5.21**).

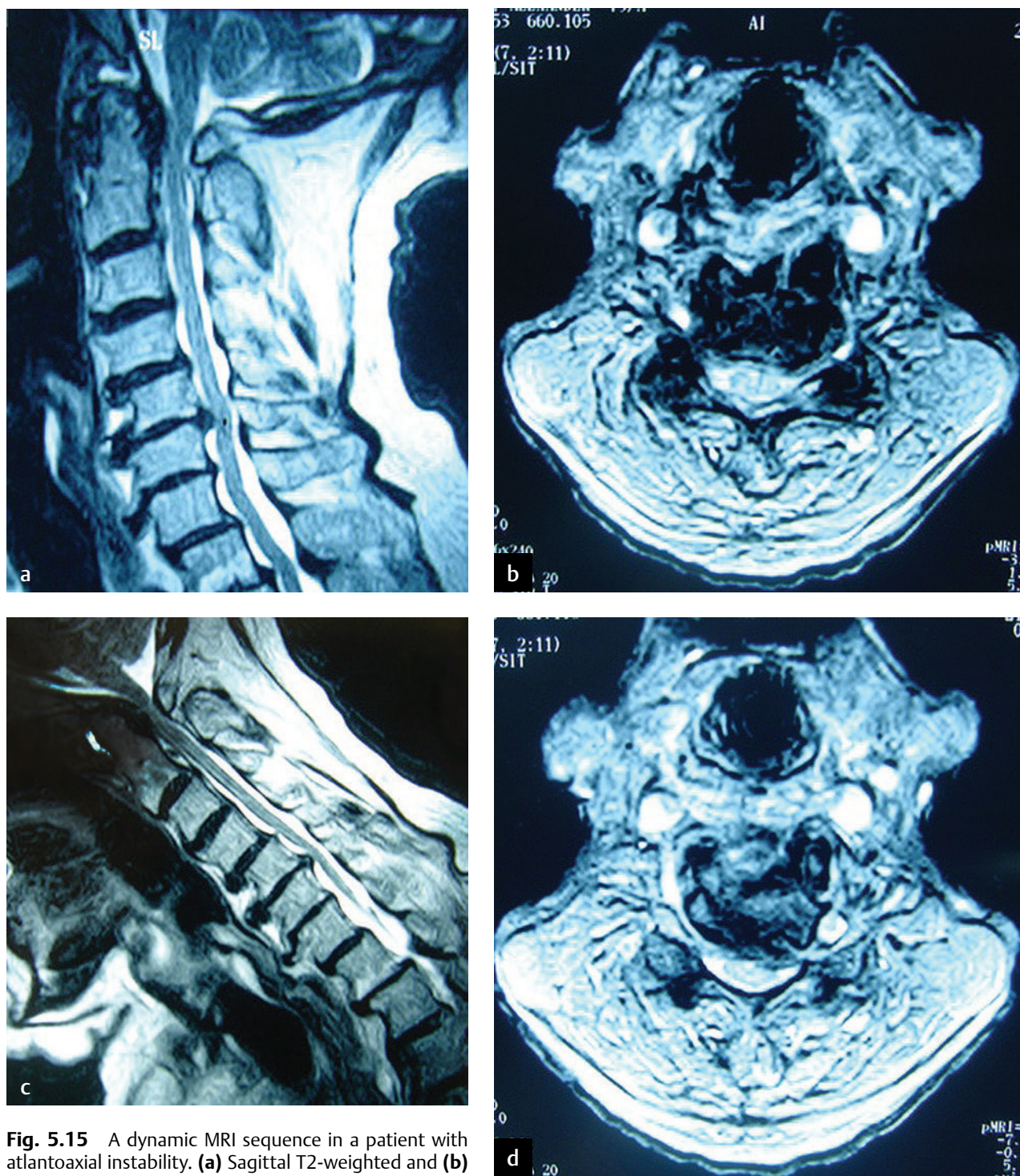


Fig. 5.15 A dynamic MRI sequence in a patient with atlantoaxial instability. **(a)** Sagittal T2-weighted and **(b)** axial T2-weighted images in extension show only mild cord compression, whereas **(c)** sagittal T2-weighted and **(d)** axial T2-weighted images in flexion show severe cord compression and widening of the anterior atlanto-dens interval.

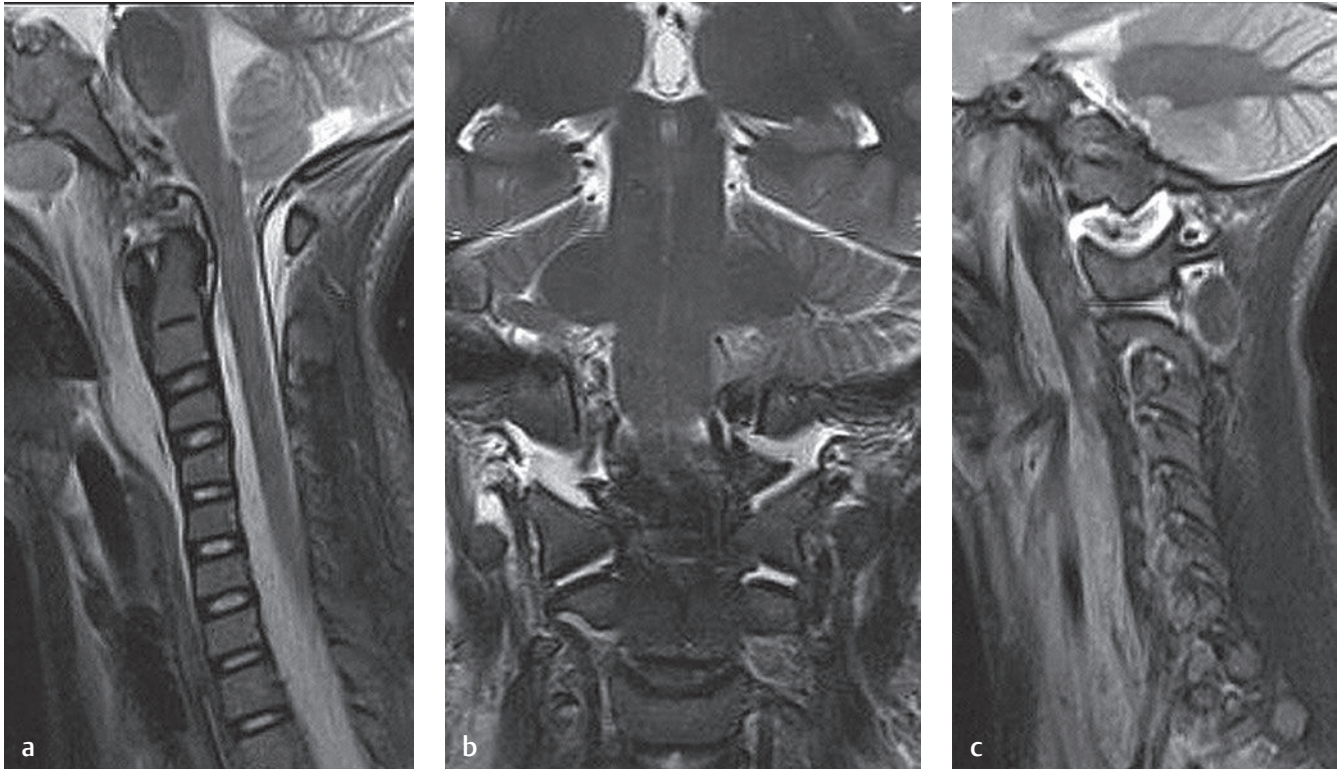


Fig. 5.16 These (a) midsagittal, (b) coronal, and (c) parasagittal T2-weighted images show atlantooccipital dissociation. The midsagittal image shows an increased distance between the basion and tip of the odontoid, whereas the coronal and parasagittal images show edema in the C0-C1 joint.

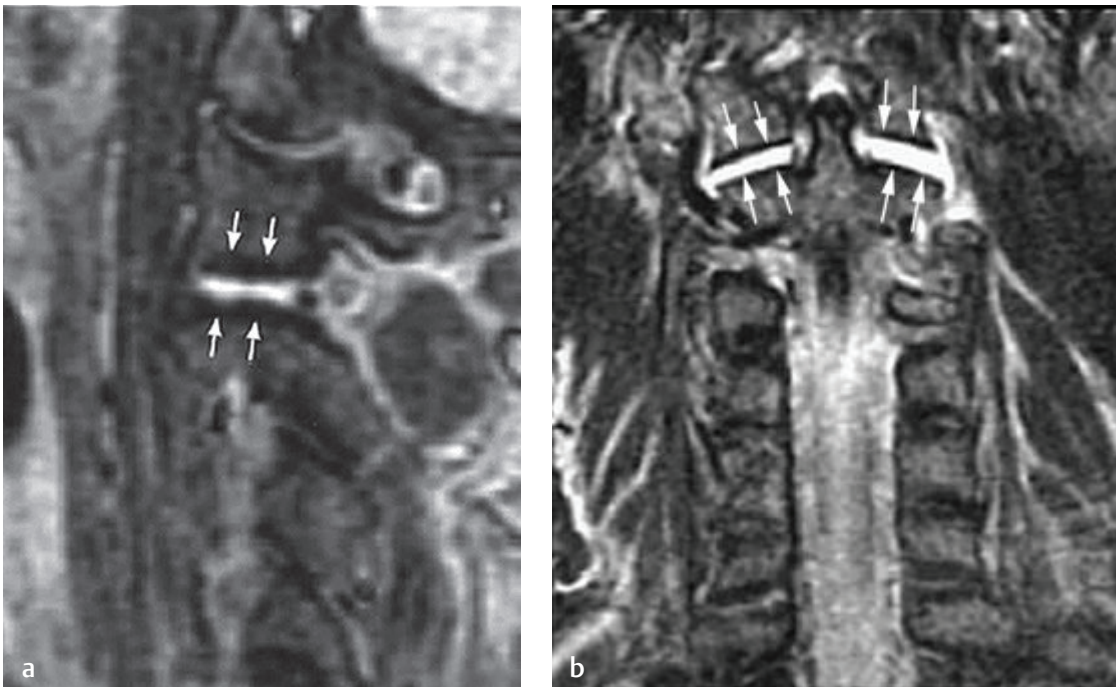


Fig. 5.17 These (a) sagittal T2-weighted and (b) coronal T2-weighted images of atlantoaxial dissociation show edema and distraction (arrows on each) through the C1-C2 joint.

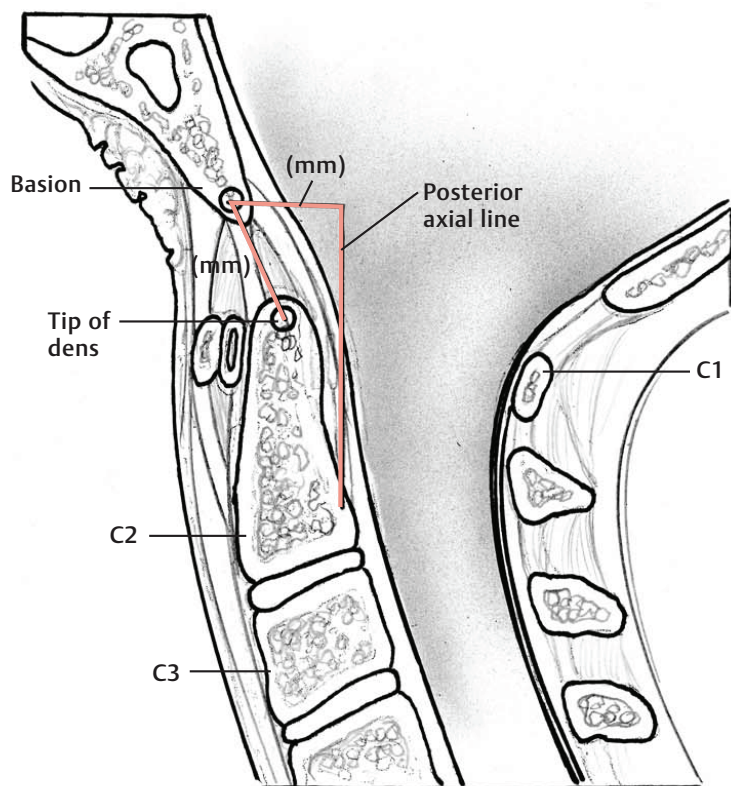


Fig. 5.18 An artist's sketch depicts the Harris technique, which is used to evaluate the relationship between the occiput and cervical spine in cases of known or suspected atlantooccipital dissociation.

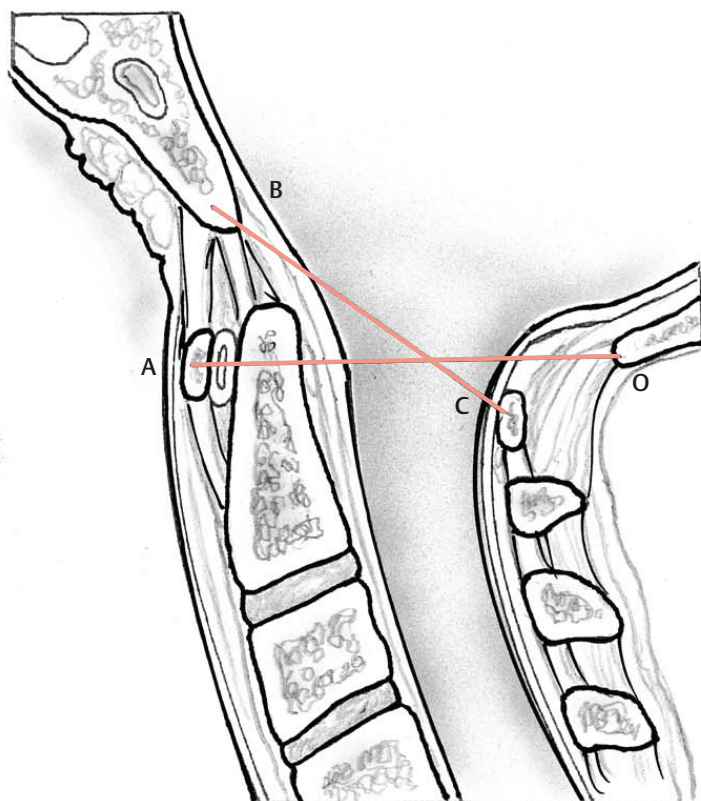


Fig. 5.19 An artist's sketch depicts the Powers ratio, which, like the Harris technique, is used to evaluate the relationship between the occiput and cervical spine in cases of known or suspected atlantooccipital dissociation. A, anterior arch of C1; B, basion; C, posterior arch of C1; O, opisthion.

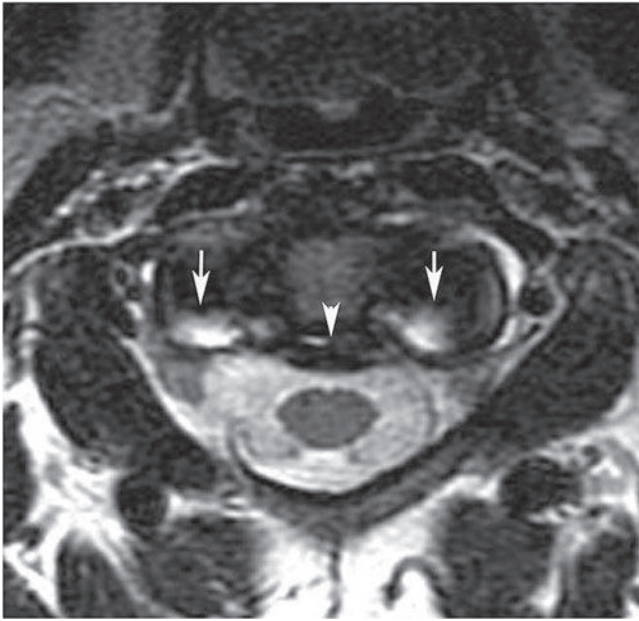


Fig. 5.20 An axial T2-weighted image shows prominence and edema at the insertion site of the transverse ligament (*arrowhead*) on the lateral masses of C1 (*arrows*).

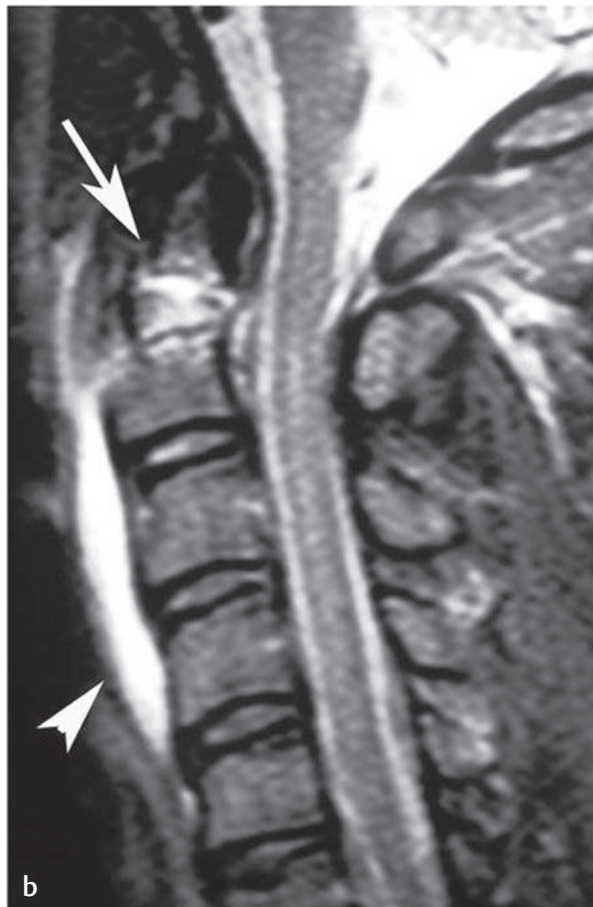


Fig. 5.21 These sagittal (a) T1-weighted and (b) T2-weighted images of a type-II odontoid fracture (*arrow*). Note the osseous and paravertebral edema or hematoma (*arrowhead*), which indicates an acute or subacute fracture.

Traumatic Spondylolisthesis of the Axis

Levine and Edwards¹¹⁵ were the first to describe thoroughly the clinical and radiographic findings of traumatic spondylolisthesis of the axis. Treatment is guided by the fracture displacement and angulation, typically best viewed on CT but also evident on MRI.^{99,115} MRI is obtained to evaluate for cord or nerve compression.

■ Summary

MRI enables excellent imaging and assessment of the OCJ. T1-weighted sequences show normal anatomy well, whereas T2-weighted sequences highlight CSF and edema. Although many measurements and identification lines were originally created for use with conventional radiographs, they are now used on MR images with increased accuracy. Using midsagittal sequences, Wackenheim's clivus baseline, McRae's line, McGregor's line, and Ranawat's criteria are useful in assessing for superior migration of C2. Similarly, midsagittal MRI sequences most clearly show malformations of the hindbrain, occipital condyles, and the odontoid process. Axial MRI sequences are also invaluable in identifying many OCJ malformations, including ring defects of C1 or C2. Coronal images best illustrate the cerebellar tonsils, the alar and apical ligaments, the atlantooccipital joint, and the atlantoaxial joint.

Tumors, which may be well assessed with MR images, are classified as extradural, intradural-extramedullary, or intramedullary. In general, posteriorly based lesions are primary, whereas anterior masses usually represent metastases. Aggressive lesions, such as sarcomas or metastases, typically show bony erosions, soft-tissue masses, and hypervascularity, whereas benign or slow-growing tumors appear less destructive and cause less soft-tissue mass effect. A tumor's vascularity is most readily apparent on MR angiography but is often evident on both T1-weighted and T2-weighted sequences.

Trauma is well assessed by MRI. On T2-weighted sequences, edema is apparent with bony or ligamentous disruption. Vertebral artery injury may be seen on both MRI and MR angiography. These modalities enable localizing the vertebral artery when planning for surgery at the OCJ.

Many special measurements can aid in traumatic diagnoses. Midsagittal images may be used to calculate the Powers ratio and Harris technique for atlantooccipital dissociation or the atlanto-axial interval for C1-C2 instability. Coronal images are useful in diagnosing transverse ligament disruption by calculating the rule of Spence. Both axial and sagittal images are useful for correlating neurologic compression in the traumatic or nontraumatic setting.

COMMON CLINICAL QUESTIONS

1. All of the following are radiographic measurements useful for detecting cranial settling *except*:
 - A. Wackenheim's clivus line
 - B. Chamberlain's line
 - C. Welcher's basal angle
 - D. Ranawat's criteria
 - E. McGregor's line
2. Which of the following defines cranial settling?
 - A. Acquired loss of ligamentous support resulting in upward migration of the odontoid
 - B. Acquired skull softening resulting in upward migration of the odontoid
 - C. Congenital loss of skull height resulting in an elevated odontoid
3. Which of the following is true of a type-II Chiari malformation?
 - A. It most commonly results in death.
 - B. It occurs when the hindbrain herniates into an encephalocele.
 - C. It is the inferior herniation of the cerebellar vermis, fourth ventricle, and medulla.
 - D. It is the downward herniation of the cerebellar tonsils only.
 - E. It is associated with basilar invagination.
4. All of the following are true about atlantooccipital dissociation *except*:
 - A. This injury is associated with high mortality.
 - B. Diagnosis is typically delayed.
 - C. The Harris technique is useful in diagnosis.
 - D. The rule of Spence is useful in diagnosis.
 - E. The Powers ratio is useful in diagnosis.
5. From the following list, which is seen earliest on MR imaging in a rheumatoid spine?
 - A. Pannus formation in the subaxial spine
 - B. Pannus formation between C1 and C2
 - C. Cranial settling
 - D. Posterior ligamentous complex laxity
 - E. Occipital condyle erosion

References

- White AA III, Panjabi MM. The clinical biomechanics of the occipitoatlantoaxial complex. *Orthop Clin North Am* 1978;9(4):867–878 PubMed
- McMinn RMH. Head and neck. In: McMinn RMH, ed. *Last's Anatomy Regional and Applied*. New York, NY: Churchill Livingstone; 1990:421–578
- White AA III, Panjabi MM. *Clinical Biomechanics of the Spine*. Philadelphia, PA: Lippincott Williams & Wilkins; 1990
- Benke M, Yu WD, Peden SC, O'Brien JR. Occipitocervical junction: imaging, pathology, instrumentation. *Am J Orthop* 2011;40(10):E205–E215 PubMed
- Kauppi M, Sakaguchi M, Kontinen YT, Hämäläinen M. A new method of screening for vertical atlantoaxial dislocation. *J Rheumatol* 1990;17(2):167–172 PubMed
- Pellicci PM, Ranawat CS, Tsairis P, Bryan WJ. A prospective study of the progression of rheumatoid arthritis of the cervical spine. *J Bone Joint Surg Am* 1981;63(3):342–350 PubMed
- Redlund-Johnell I, Pettersson H. Radiographic measurements of the cranio-vertebral region. Designed for evaluation of abnormalities in rheumatoid arthritis. *Acta Radiol Diagn (Stockh)* 1984;25(1):23–28 PubMed
- Riew KD, Hilibrand AS, Palumbo MA, Sethi N, Bohlman HH. Diagnosing basilar invagination in the rheumatoid patient. The reliability of radiographic criteria. *J Bone Joint Surg Am* 2001;83-A(2):194–200 PubMed
- Chamberlain WE. Basilar impression (platybasia). A bizarre developmental anomaly of the occipital bone and upper cervical spine with striking and misleading neurologic manifestations. *Yale J Biol Med* 1939;11(5):487–496 PubMed
- McGregor M. The significance of certain measurements of the skull in the diagnosis of basilar impression. *Br J Radiol* 1948;21(244):171–181 PubMed
- Wackenheim A. *Roentgen Diagnosis of the Craniovertebral Region*. New York, NY: Springer-Verlag; 1974
- McRae DL. Bony abnormalities in the region of the foramen magnum: correlation of the anatomic and neurologic findings. *Acta Radiol* 1953;40(2-3):335–354 PubMed
- McRae DL, Barnum AS. Occipitalization of the atlas. *Am J Roentgenol Radium Ther Nucl Med* 1953;70(1):23–46 PubMed
- Ranawat CS, O'Leary P, Pellicci P, Tsairis P, Marchisello P, Dorr L. Cervical spine fusion in rheumatoid arthritis. *J Bone Joint Surg Am* 1979;61(7):1003–1010 PubMed
- Taveras M, Wood EH. Congenital anomalies. Part I: The skull. In: *Diagnostic Neuroradiology*. Baltimore, MD: Williams & Wilkins; 1976:45–65
- Virchow R. Erklärung der Abbildungen. In: *Untersuchungen über die Entwicklung des Schädelgrundes*. Berlin, Germany: Druck und Verlag von Georg Reimer; 1857:123–128
- Krakenes J, Kaale BR, Rorvik J, Gilhus NE. MRI assessment of normal ligamentous structures in the craniovertebral junction. *Neuroradiology* 2001;43(12):1089–1097 PubMed
- Dominguez R, Talmachoff P, Rodriguez A. Radiological evaluation of the craniocervical junction in bone dysplasias and other related syndromes. *Clin Imaging* 1995;19(2):77–84 PubMed
- Tassanawipas A, Mookhavesa S, Chatchavong S, Worawitayawong P. Magnetic resonance imaging study of the craniocervical junction. *J Orthop Surg (Hong Kong)* 2005;13(3):228–231 PubMed
- Lee BCP, Kneeland JB, Deck MDF, Cahill PT. Posterior fossa lesions: magnetic resonance imaging. *Radiology* 1984;153(1):137–143 PubMed
- Smoker WRK. MR imaging of the craniovertebral junction. *Magn Reson Imaging Clin N Am* 2000;8(3):635–650 PubMed
- Krakenes J, Kaale BR. Magnetic resonance imaging assessment of craniovertebral ligaments and membranes after whiplash trauma. *Spine* 2006;31(24):2820–2826 PubMed
- Barnsley L, Lord SM, Wallis BJ, Bogduk N. The prevalence of chronic cervical zygapophysial joint pain after whiplash. *Spine* 1995;20(1):20–25 PubMed
- Schmidt P, Mayer TE, Drescher R. Delineation of alar ligament morphology: comparison of magnetic resonance imaging at 1.5 and 3 Tesla. *Orthopedics* 2012;35(11):e1635–e1639 PubMed
- Willauschus WG, Kladny B, Beyer WF, Glückert K, Arnold H, Scheithauer R. Lesions of the alar ligaments. In vivo and in vitro studies with magnetic resonance imaging. *Spine* 1995;20(23):2493–2498 PubMed
- Wilmink JT, Patijn J. MR imaging of alar ligament in whiplash-associated disorders: an observer study. *Neuroradiology* 2001;43(10):859–863 PubMed
- Pfirsrmann CW, Binkert CA, Zanetti M, Boos N, Hodler J. MR morphology of alar ligaments and occipitoatlantoaxial joints: study in 50 asymptomatic subjects. *Radiology* 2001;218(1):133–137 PubMed
- Roy S, Hol PK, Laerum LT, Tillung T. Pitfalls of magnetic resonance imaging of alar ligament. *Neuroradiology* 2004;46(5):392–398 PubMed
- Kaale BR, Krakenes J, Albrektsen G, Wester K. Head position and impact direction in whiplash injuries: associations with MRI-verified lesions of ligaments and membranes in the upper cervical spine. *J Neurotrauma* 2005;22(11):1294–1302 PubMed
- Ross JS. Cervicomedullary and craniovertebral junctions. In: Modic MT, Masaryk TJ, Ross JS, eds. *Magnetic Resonance Imaging of the Spine*. St. Louis, MO: Mosby-Year Book; 1994:191–215
- Garber JN. Abnormalities of the atlas and axis vertebrae—congenital and traumatic. *J Bone Joint Surg Am* 1964;46:1782–1791 PubMed
- Macalister A. Notes on the development and variations of the atlas. *J Anat Physiol* 1893;27(Pt 4):519–542 PubMed
- VanGilder JC, Menezes AH, Dolan KD. *The Craniovertebral Junction and Its Abnormalities*. Mount Kisco, NY: Futura Publishing; 1987
- Nager GT. Cephaloceles. *Laryngoscope* 1987;97(1):77–84 PubMed
- Kunicki J, Ciszek B. The clinical anatomy and the occipital condyle variants. (letter) *Clin Anat* 2005;18(8):646–647, author reply 648 PubMed
- Gholive PA, Hosalkar HS, Ricchetti ET, Pollock AN, Dormans JP, Drummond DS. Occipitalization of the atlas in children. Morphologic classification, associations, and clinical relevance. *J Bone Joint Surg Am* 2007;89(3):571–578 PubMed
- Guille JT, Sherk HH. Congenital osseous anomalies of the upper and lower cervical spine in children. *J Bone Joint Surg Am* 2002;84-A(2):277–288 PubMed
- Sherk HH. Lesions of the atlas and axis. *Clin Orthop Relat Res* 1975;109(109):33–41 PubMed
- Von Torklus D, Gehl W. *The Upper Cervical Spine. Regional Anatomy, Pathology and Traumatology. A Systematic Ra-*

- diologic Atlas and Textbook. New York, NY: Grune & Stratton; 1972
40. Nishikawa K, Ludwig SC, Colón RJ, Fujimoto Y, Heller JG. Cervical myelopathy and congenital stenosis from hypoplasia of the atlas: report of three cases and literature review. *Spine* 2001;26(5):E80–E86 PubMed
 41. Chambers AA, Gaskill MF. Midline anterior atlas clefts: CT findings. *J Comput Assist Tomogr* 1992;16(6):868–870 PubMed
 42. Gehweiler JA Jr, Daffner RH, Roberts L Jr. Malformations of the atlas vertebra simulating the Jefferson fracture. *AJR Am J Roentgenol* 1983;140(6):1083–1086 PubMed
 43. de Zoete A, Langeveld UA. A congenital anomaly of the atlas as a diagnostic dilemma: a case report. *J Manipulative Physiol Ther* 2007;30(1):62–64 PubMed
 44. Hosalkar HS, Gerardi JA, Shaw BA. Combined asymptomatic congenital anterior and posterior deficiency of the atlas. *Pediatr Radiol* 2001;31(11):810–813 PubMed
 45. Hensinger RN, Fielding JW. The cervical spine. In: Morrissy RT, ed. *Lovell and Winter's Pediatric Orthopaedics*. Philadelphia, PA: JB Lippincott; 1990:703–739
 46. Copley LA, Dormans JP. Cervical spine disorders in infants and children. *J Am Acad Orthop Surg* 1998;6(4):204–214 PubMed
 47. Anderson LD, D'Alonzo RT. Fractures of the odontoid process of the axis. *J Bone Joint Surg Am* 1974;56(8):1663–1674 PubMed
 48. Cokluk C, Aydin K, Rakunt C, Iyigun O, Onder A. The borders of the odontoid process of C2 in adults and in children including the estimation of odontoid/body ratio. *Eur Spine J* 2006;15(3):278–282 PubMed
 49. David KM, McLachlan JC, Aiton JF, et al. Cartilaginous development of the human craniovertebral junction as visualised by a new three-dimensional computer reconstruction technique. *J Anat* 1998;192(Pt 2):269–277 PubMed
 50. Arvin B, Fournier-Gosselin MP, Fehlings MG. Os odontoid: etiology and surgical management. *Neurosurgery* 2010;66(3, Suppl):22–31 PubMed
 51. Batzdorf U. Pathogenesis and development theories. In: Anson JA, Benzel EC, Awad IA, eds. *Syringomyelia and the Chiari Malformations*. Park Ridge, IL: American Association of Neurological Surgeons; 1997:35–40
 52. Schenk M, Ruggieri PM. Imaging of syringomyelia and the Chiari malformations. In: Anson JA, Benzel EC, Awad IA, eds. *Syringomyelia and the Chiari Malformations*. Park Ridge, IL: American Association of Neurological Surgeons; 1997:41–56
 53. Aboulezz AO, Sartor K, Geyer CA, Gado MH. Position of cerebellar tonsils in the normal population and in patients with Chiari malformation: a quantitative approach with MR imaging. *J Comput Assist Tomogr* 1985;9(6):1033–1036 PubMed
 54. Barkovich AJ, Wippold FJ, Sherman JL, Citrin CM. Significance of cerebellar tonsillar position on MR. *AJNR Am J Neuroradiol* 1986;7(5):795–799 PubMed
 55. Milhorat TH, Chou MW, Trinidad EM, et al. Chiari I malformation redefined: clinical and radiographic findings for 364 symptomatic patients. *Neurosurgery* 1999;44(5):1005–1017 PubMed
 56. Castillo M, Quencer RM, Dominguez R. Chiari III malformation: imaging features. *AJNR Am J Neuroradiol* 1992;13(1):107–113 PubMed
 57. Pang D, Pollack IF. Spinal cord injury without radiographic abnormality in children—the SCIWORA syndrome. *J Trauma* 1989;29(5):654–664 PubMed
 58. Ulmer JL, Elster AD, Ginsberg LE, Williams DW III. Klippel-Feil syndrome: CT and MR of acquired and congenital abnormalities of cervical spine and cord. *J Comput Assist Tomogr* 1993;17(2):215–224 PubMed
 59. Nagib MG, Maxwell RE, Chou SN. Identification and management of high-risk patients with Klippel-Feil syndrome. *J Neurosurg* 1984;61(3):523–530 PubMed
 60. Boden SD. Rheumatoid arthritis of the cervical spine. Surgical decision making based on predictors of paralysis and recovery. *Spine* 1994;19(20):2275–2280 PubMed
 61. Boden SD, Dodge LD, Bohlman HH, Rechtine GR. Rheumatoid arthritis of the cervical spine. A long-term analysis with predictors of paralysis and recovery. *J Bone Joint Surg Am* 1993;75(9):1282–1297 PubMed
 62. Dreyer SJ, Boden SD. Natural history of rheumatoid arthritis of the cervical spine. *Clin Orthop Relat Res* 1999;366(366):98–106 PubMed
 63. Reiter MF, Boden SD. Inflammatory disorders of the cervical spine. *Spine* 1998;23(24):2755–2766 PubMed
 64. Oda T, Fujiwara K, Yonenobu K, Azuma B, Ochi T. Natural course of cervical spine lesions in rheumatoid arthritis. *Spine* 1995;20(10):1128–1135 PubMed
 65. Goel A. Treatment of basilar invagination by atlantoaxial joint distraction and direct lateral mass fixation. *J Neurosurg Spine* 2004;1(3):281–286 PubMed
 66. Ross JS, Brant-Zawadzki M, Moore KR, Crim J, Chen MZ, Katzman GL. Part IV: Neoplasms, cysts, and other masses. In: Ross JS, Brant-Zawadzki M, Moore KR, et al, eds. *Diagnostic Imaging: Spine*. Salt Lake City, UT: Amirsys; 2004:IV-1–2-IV-2–32
 67. Baudrez V, Galant C, Vande Berg BC. Benign vertebral hemangioma: MR-histological correlation. *Skeletal Radiol* 2001;30(8):442–446 PubMed
 68. Yochum TR, Lile RL, Schultz GD, Mick TJ, Brown CW. Acquired spinal stenosis secondary to an expanding thoracic vertebral hemangioma. *Spine* 1993;18(2):299–305 PubMed
 69. Murphey MD, Nomikos GC, Flemming DJ, Gannon FH, Temple HT, Kransdorf MJ. From the archives of AFIP. Imaging of giant cell tumor and giant cell reparative granuloma of bone: radiologic-pathologic correlation. *Radiographics* 2001;21(5):1283–1309 PubMed
 70. Osborn AG. Cysts, tumors, and tumorlike lesions of the spine and spinal cord. In: Osborn AG, ed. *Diagnostic Neuroradiology*. St. Louis, MO: Mosby; 1994:876–918
 71. Liu PT, Chivers FS, Roberts CC, Schultz CJ, Beauchamp CP. Imaging of osteoid osteoma with dynamic gadolinium-enhanced MR imaging. *Radiology* 2003;227(3):691–700 PubMed
 72. Boriani S, De Iure F, Campanacci L, et al. Aneurysmal bone cyst of the mobile spine: report on 41 cases. *Spine* 2001;26(1):27–35 PubMed
 73. Munk PL, Helms CA, Holt RG, Johnston J, Steinbach L, Neumann C. MR imaging of aneurysmal bone cysts. *AJR Am J Roentgenol* 1989;153(1):99–101 PubMed
 74. Fourny DR, York JE, Cohen ZR, Suki D, Rhines LD, Gokaslan ZL. Management of atlantoaxial metastases with posterior occipitocervical stabilization. *J Neurosurg* 2003;98(2, Suppl):165–170 PubMed
 75. Akhaddar A, Chakir N, Amarti A, et al. Thoracic epidural hemangiopericytoma. Case report. *J Neurosurg Sci* 2002;46(2):89–92 PubMed

76. Cohen-Gadol AA, Zikel OM, Koch CA, Scheithauer BW, Krauss WE. Spinal meningiomas in patients younger than 50 years of age: a 21-year experience. *J Neurosurg* 2003; 98(3, Suppl):258–263 PubMed
77. Naderi S. Spinal meningiomas. *Surg Neurol* 2000;54(1): 95 PubMed
78. Conti P, Pansini G, Mouchaty H, Capuano C, Conti R. Spinal neurinomas: retrospective analysis and long-term outcome of 179 consecutively operated cases and review of the literature. *Surg Neurol* 2004;61(1):34–43 PubMed
79. Murphey MD, Smith WS, Smith SE, Kransdorf MJ, Temple HT. From the archives of the AFIP. Imaging of musculoskeletal neurogenic tumors: radiologic-pathologic correlation. *Radiographics* 1999;19(5):1253–1280 PubMed
80. Lowe GM. Magnetic resonance imaging of intramedullary spinal cord tumors. *J Neurooncol* 2000;47(3): 195–210 PubMed
81. Sun B, Wang C, Wang J, Liu A. MRI features of intramedullary spinal cord ependymomas. *J Neuroimaging* 2003; 13(4):346–351 PubMed
82. Murota T, Symon L. Surgical management of hemangioblastoma of the spinal cord: a report of 18 cases. *Neurosurgery* 1989;25(5):699–707 PubMed
83. Sciubba DM, Mavinkurve GG, Gailloud P, et al. Preoperative imaging of cervical spine hemangioblastomas using three-dimensional fusion digital subtraction angiography. Report of two cases. *J Neurosurg Spine* 2006;5(1): 96–100 PubMed
84. Brooke DC, Burkus JK, Benson DR. Asymptomatic occipito-atlantal instability in Down syndrome (trisomy 21). Report of two cases in children. *J Bone Joint Surg Am* 1987; 69(2):293–295 PubMed
85. El-Khoury GY, Clark CR, Dietz FR, Harre RG, Tozzi JE, Kathol MH. Posterior atlantooccipital subluxation in Down syndrome. *Radiology* 1986;159(2):507–509 PubMed
86. French HG, Burke SW, Roberts JM, Johnston CE II, Whitecloud T, Edmunds JO. Upper cervical ossicles in Down syndrome. *J Pediatr Orthop* 1987;7(1):69–71 PubMed
87. Gabriel KR, Mason DE, Carango P. Occipito-atlantal translation in Down's syndrome. *Spine* 1990;15(10): 997–1002 PubMed
88. Georgopoulos G, Pizzutillo PD, Lee MS. Occipito-atlantal instability in children. A report of five cases and review of the literature. *J Bone Joint Surg Am* 1987;69(3): 429–436 PubMed
89. Harris JH Jr, Carson GC, Wagner LK. Radiologic diagnosis of traumatic occipitovertebral dissociation: 1. Normal occipitovertebral relationships on lateral radiographs of supine subjects. *AJR Am J Roentgenol* 1994;162(4): 881–886 PubMed
90. Hungerford GD, Akkaraju V, Rawe SE, Young GF. Atlanto-occipital and atlanto-axial dislocations with spinal cord compression in Down's syndrome: a case report and review of the literature. *Br J Radiol* 1981;54(645): 758–761 PubMed
91. Karol LA, Sheffield EG, Crawford K, Moody MK, Browne RH. Reproducibility in the measurement of atlanto-occipital instability in children with Down syndrome. *Spine* 1996;21(21):2463–2467 PubMed
92. Bernini FP, Elefante R, Smaltino F, Tedeschi G. Angiographic study on the vertebral artery in cases of deformities of the occipitocervical joint. *Am J Roentgenol Radium Ther Nucl Med* 1969;107(3):526–529 PubMed
93. Goldberg W, Mueller C, Panacek E, Tigges S, Hoffman JR, Mower WR; NEXUS Group. Distribution and patterns of blunt traumatic cervical spine injury. *Ann Emerg Med* 2001; 38(1):17–21 PubMed
94. Wiesel SW, Rothman RH. Occipitoatlantal hypermobility. *Spine* 1979;4(3):187–191 PubMed
95. Browd S, Healy LJ, Dobie G, et al. Morphometric and qualitative analysis of congenital occipitocervical instability in children: implications for patients with Down syndrome. *J Neurosurg* 2006;105(1, Suppl):50–54 PubMed
96. Adams VI. Neck injuries: I. Occipitoatlantal dislocation—a pathologic study of twelve traffic fatalities. *J Forensic Sci* 1992;37(2):556–564 PubMed
97. Adams VI. Neck injuries: III. Ligamentous injuries of the craniocervical articulation without occipito-atlantal or atlanto-axial facet dislocation. A pathologic study of 21 traffic fatalities. *J Forensic Sci* 1993;38(5):1097–1104 PubMed
98. Ahuja A, Glasauer FE, Alker GJ Jr, Klein DM. Radiology in survivors of traumatic atlanto-occipital dislocation. *Surg Neurol* 1994;41(2):112–118 PubMed
99. Bono CM, Vaccaro AR, Fehlings M, et al; Spine Trauma Study Group. Measurement techniques for upper cervical spine injuries: consensus statement of the Spine Trauma Study Group. *Spine* 2007;32(5):593–600 PubMed
100. Alker GJ Jr, Oh YS, Leslie EV. High cervical spine and craniocervical junction injuries in fatal traffic accidents: a radiological study. *Orthop Clin North Am* 1978; 9(4):1003–1010 PubMed
101. Bellabarba C, Mirza SK, West GA, et al. Diagnosis and treatment of craniocervical dislocation in a series of 17 consecutive survivors during an 8-year period. *J Neurosurg Spine* 2006;4(6):429–440 PubMed
102. Saternus KS, Thrun C. [Traumatology of the alar ligaments]. [in German] *Aktuelle Traumatol* 1987;17(5): 214–218 PubMed
103. Chaput CD, Walgama J, Torres E, et al. Defining and detecting missed ligamentous injuries of the occipitocervical complex. *Spine* 2011;36(9):709–714 PubMed
104. Radcliff K, Kepler C, Reitman C, Harrop J, Vaccaro A. CT and MRI-based diagnosis of craniocervical dislocations: the role of the occipitoatlantal ligament. *Clin Orthop Relat Res* 2012;470(6):1602–1613 PubMed
105. Pisonnier ML, Lazennec JY, Renoux J, Rousseau MA. Trauma of the upper cervical spine: focus on vertical atlantoaxial dislocation. *Eur Spine J* 2013;22(10):2167–2175 10.1007/s00586-013-2841-2 PubMed
106. Powers B, Miller MD, Kramer RS, Martinez S, Gehweiler JA Jr. Traumatic anterior atlanto-occipital dislocation. *Neurosurgery* 1979;4(1):12–17 PubMed
107. Anderson PA, Montesano PX. Morphology and treatment of occipital condyle fractures. *Spine* 1988;13(7): 731–736 PubMed
108. Hanson JA, Deliganis AV, Baxter AB, et al. Radiologic and clinical spectrum of occipital condyle fractures: retrospective review of 107 consecutive fractures in 95 patients. *AJR Am J Roentgenol* 2002;178(5):1261–1268 PubMed
109. Young WF, Rosenwasser RH, Getch C, Jallo J. Diagnosis and management of occipital condyle fractures. *Neurosurgery* 1994;34(2):257–260, discussion 260–261 PubMed

110. Jefferson G. Fractures of the atlas vertebra. Report of four cases, and a review of those previously recorded. *Br J Surg* 1920;7:407–422
111. Lee C, Woodring JH. Unstable Jefferson variant atlas fractures: an unrecognized cervical injury. *AJNR Am J Neuroradiol* 1991;12(6):1105–1110 PubMed
112. Lee TT, Green BA, Petrin DR. Treatment of stable burst fracture of the atlas (Jefferson fracture) with rigid cervical collar. *Spine* 1998;23(18):1963–1967 PubMed
113. Horlyck E, Rahbek M. Cervical spine injuries. *Acta Orthop Scand* 1974;45(6):845–853 PubMed
114. Ryan MD, Henderson JJ. The epidemiology of fractures and fracture-dislocations of the cervical spine. *Injury* 1992;23(1):38–40 PubMed
115. Levine AM, Edwards CC. The management of traumatic spondylolisthesis of the axis. *J Bone Joint Surg Am* 1985; 67(2):217–226 PubMed

ANSWERS TO COMMON CLINICAL QUESTIONS

1. C
Explanation: Wackenheim's clivus line, Chamberlain's line, Ranawat's criteria, and McGregor's line can all be used to evaluate for cranial settling (see **Fig. 5.1**). Welcher's basal angle is a measurement that is useful for the detection of platybasia.
2. A
Explanation: Cranial settling differs from basilar invagination and basilar impression. Cranial settling is vertical subluxation of the odontoid caused by a loss of supporting ligamentous structures. This condition may occur with RA or psoriatic arthritis. Basilar impression results from skull base softening secondary to an acquired condition such as Paget disease. Basilar invagination results from a loss of skull height secondary to congenital abnormalities.
3. C
Explanation: A type-II Chiari malformation, or the Arnold-Chiari malformation, results from dysgenesis of the hindbrain. It involves herniation of the inferior cerebellar vermis, fourth ventricle, and medulla and is associated with myelomeningocele. It is not generally associated with atlantooccipital assimilation or basilar invagination.
4. D
Explanation: The rule of Spence is used to evaluate integrity of the transverse ligament—typically with Jefferson burst fractures. Atlantooccipital dissociation is associated with high mortality, and diagnosis is typically delayed. Both the Harris technique and the Powers ratio can be used to diagnose atlantooccipital dissociation.
5. B
Explanation: Pannus formation between C1 and C2 is an early finding of RA that can be seen on MRI of the cervical spine. The other findings tend to occur in patients with more advanced RA.

6 The Cervical Spine

Lukas P. Zebala, Jacob M. Buchowski, Aditya Daftary, Joseph R. O'Brien, John A. Carrino, and A. Jay Khanna

CHAPTER OUTLINE

- I. Specialized Pulse Sequences and Protocols
- II. Traumatic Conditions
 - A. Classification of Cervical Spine Trauma
 - 1. Hyperflexion Injuries
 - 2. Hyperextension Injuries
 - 3. Axial Load Injuries
 - B. OCJ Injuries
 - 1. Atlantooccipital Dissociation
 - 2. Trauma to the Atlas
 - 3. Trauma to the Axis
 - 4. Atlantoaxial Dissociation
 - C. Vertebral Artery Injury
 - D. Penetrating Trauma
 - E. Characterization of Spinal Cord Injury
 - F. Characterization of Cervical Spine Instability
- III. Degenerative Conditions
 - A. Degenerative Disc Disease
 - B. Disc Displacement
 - C. Spinal Stenosis
 - D. RA
- IV. Infectious Conditions
 - A. Cervical Vertebral Osteomyelitis and Discitis
 - B. Epidural Abscess
 - C. Intradural Infections
- V. Other Pathologic Conditions
 - A. Tumors
 - B. Intrinsic Inflammatory Myelopathies
 - 1. Multiple Sclerosis
 - 2. Acute Transverse Myelopathy
 - 3. Subacute Necrotizing Myelopathy
 - 4. Acquired Immune Deficiency Syndrome

- 5. Viral Diseases
- 6. Bacterial, Parasitic, and Granulomatous Diseases
- 7. Metabolic or Toxic Diseases
- C. Arthritides
 - 1. RA
 - 2. Juvenile RA
 - 3. Ankylosing Spondylitis
 - 4. Psoriatic Arthritis
 - 5. Amyloidosis
 - 6. Gout
 - 7. Calcium Pyrophosphate Dihydrate Deposition Disease
- VI. Summary

■ Specialized Pulse Sequences and Protocols

Although imaging protocols of the cervical spine for specific indications can vary among institutions, standard MRI of the cervical spine for degenerative pathologies usually includes the following pulse sequences:

- Sagittal T1-weighted SE
- Sagittal T2-weighted FSE
- Axial gradient-echo
- Axial T2-weighted FSE

A detailed discussion of all the imaging sequences used in the cervical spine is beyond the scope of this chapter; however, salient features of commonly used sequences are discussed in the following paragraphs.

T1-weighted images are useful in identifying fracture lines. Because they are sensitive to the presence of gadolinium contrast, they are also used for contrast-enhanced imaging, which is helpful in assessing neoplasms, infections, and the postoperative spine.

Typically, fat-suppressed postgadolinium T1-weighted images are used to make lesions more conspicuous. T2-weighted images are sensitive to water (and thus edema) and are useful in identifying areas of potential pathology. However, care must be taken with regard to interpreting bone-marrow edema because it may be seen with a variety of conditions, including infection, inflammation, trauma, and degeneration. Although edema may focus attention toward an abnormality, many of these conditions can coexist, so additional analysis is required before finalizing a conclusion. FSE is now routinely used to acquire T2-weighted images at speeds up to 64 times faster than conventional SE T2-weighted images. Sometimes the differentiation of fat, water, and lesions can be difficult, especially on T2-weighted FSE images, and therefore fat suppression is used to make these areas more conspicuous. This sequence can be obtained by applying a fat-suppression pulse to produce fat-suppressed T2-weighted images or by obtaining a STIR sequence. Visualizing edema is helpful in identifying ligamentous injuries, and such visualization is best achieved with STIR or fat-suppressed T2-weighted images.¹ T2-weighted images are also most sensitive for evaluating the cord parenchyma for lesions and edema, which are seen as abnormally bright signal, although the sagittal orientation is subject to linear bright artifact within the cord (Gibbs phenomenon). For this reason, axial T2-weighted images serve as a useful tool for detecting cord abnormalities and confirming lesions suspected on sagittal T2-weighted images.

Gradient-echo images are very susceptible to magnetic artifacts; this important characteristic makes them useful for detecting small areas of hemorrhage, such as with cervical spine trauma and vascular malformations. However, these images can also overestimate the degree of canal and foraminal stenosis secondary to artifact from the adjacent bone. Because of the rapidity with which gradient-echo images are acquired, studies can be obtained with higher resolution than that required for other pulse sequences and even as a 3D volume set, which provides isotropic voxels and enables reformations in multiple planes. This volume set can then enable one to characterize the cervical foramina in the appropriate oblique plane.

For the evaluation of vascular structures in the neck, MR angiography can be obtained without contrast, using 2D or 3D time-of-flight or phase-contrast imaging. These sequences create contrast between flowing and stationary structures. Phase-contrast imaging may also provide flow-velocity information. As a result of the technique, time-of-flight imaging shows fat or subacute thrombus as bright signal and may be useful in detecting small, subtle thrombi. The 3D techniques require more time and are slightly less sensitive to slow flow states. Gadolinium-enhanced MR angiography may also be obtained and is extremely accurate.

■ Traumatic Conditions

Although the cervical spine is injured in only 2% to 3% of blunt-trauma accidents,² the potential for instability and critical neurologic injury makes prompt identification and management of cervical spine injuries important. Patients with suspected cervical spine injury should be evaluated initially with conventional radiographs (AP, lateral, and open-mouth odontoid views). CT imaging offers greater osseous detail than conventional radiography does and may reveal fractures or details that are not detected with radiography. CT is especially helpful in assessing fractures of the occipital condyles and cervicothoracic junction, where osseous overlap on conventional radiographs makes fracture detection difficult. MRI provides soft-tissue visualization superior to that of conventional radiography or CT and is useful for the assessment of spinal cord injury, ligamentous injury, degree of spinal stenosis, and additional fracture evaluation. Occult fractures not visible on conventional radiographs or CT images may be detected by the presence of vertebral body edema on MR images. Although MRI is extremely sensitive in identifying cervical spine fractures, their characteristics and the exact appearance of the osseous components can be challenging; CT may be a better choice for assessing such details. In addition, MRI is useful for the evaluation of obtunded patients or those with cervical spine injury, neurologic deficits, or an unreliable physical examination.³⁻⁸

MRI is indicated specifically when neurologic deficit, vascular injury, or soft-tissue injury is suspected in the setting of trauma. It is also useful in assessing posttraumatic sequelae.⁹ Use of MRI in imaging spinal gunshot injuries is controversial. Theoretically, a ferrous gunshot fragment may become mobile, but most bullets are nonferrous, and therefore such patients can usually be imaged without consequences. Unfortunately, the exact composition of a gunshot fragment is seldom known, and therefore MRI remains controversial and dependent on the clinical need.^{10,11}

It should be noted that there are obstacles to obtaining MRI studies in the trauma setting, especially with regard to cervical spine trauma, because patients may have clinically significant neurologic deficits. These obstacles include the following:

- Lack of availability of MRI capabilities on an urgent basis
- MR incompatibility of some ventilators, traction devices, and other equipment
- Lack of clinical access to patients during the imaging study

MRI protocols vary by institution, but commonly used sequences in trauma evaluation include the following¹²:

- Sagittal T1-weighted images to assess the alignment of the cervical spine, vertebral body integrity, fractures, and spinal cord caliber
- Sagittal T2-weighted images to assess for the presence of cord edema, compression, and spondylotic changes
- Sagittal STIR images to assess for the presence of paraspinal ligamentous injury and bone-marrow edema
- Axial T1-weighted and T2-weighted images to assess for the presence of posterior element fractures, to evaluate for spinal stenosis, to define disc pathology better, and to confirm the precise location of abnormalities detected on sagittal images
- Sagittal T2-weighted gradient-echo images (in some institutions) to assess for the presence of acute spinal cord hemorrhage and disc herniation (high signal in the disc even with severe osseous degeneration, which enables the distinction between bone fragments and a disc herniation)

Regardless of the specific institutional MRI protocol, a systematic approach (see Chapter 4, A Systematic Approach to the Review of Spine MRI Studies) for the evaluation of cervical spine MRI should be used to avoid missing pathologic conditions (see **Table 6.1** for important cervical spine structures to evaluate). In addition, it is essential that the MRI findings be interpreted in conjunction with the other available imaging modalities, including conventional radiographs (with flexion and extension views if clinically indicated) and CT (see Chapter 11, Correlation of MRI with Other Imaging Studies).

Classification of Cervical Spine Trauma

Cervical spine injuries can be classified based on the mechanism of injury. Although the Allen-Ferguson classification system originally described six categories of fractures based on the suspected position of the spine at the time of injury and the dominant mechanism of spinal failure (vertical compression, compressive flexion, distractive flexion, lateral flexion, compressive extension, and distractive extension¹³) (**Fig. 6.1**), the classification scheme is simplified here into three broad categories:

- Hyperflexion
- Hyperextension
- Axial loading

Table 6.1 Evaluation of cervical spine trauma

Anatomy	Evaluation
Spinal column/ vertebral bodies	Alignment Vertebral body fracture Posterior element fracture Edema Degenerative change
Ligaments	Anterior longitudinal ligament Posterior longitudinal ligament Interspinous and supraspinous ligaments Ligamentum flavum Evaluation for edema/rupture
Spinal cord	Edema Hemorrhage Compression Syrinx
Epidural space	Hematoma Disc herniation Osseous fragment
Vascular	Vertebral artery

Source: Takhtani D, Melhelm ER. MR imaging in cervical spine trauma. *Magn Reson Imaging Clin N Am* 2000;8:615–634. Modified with permission.

In many instances, the mechanism of injury can be difficult to determine from an analysis of the clinical situation (in the absence of imaging findings), and therefore clinicians may choose to broadly classify cervical spine injuries as follows:

- Secondary to blunt trauma
- Secondary to penetrating trauma

In addition, cervical spine injuries can be subdivided based on the region of injury within the occipitocervical spine:

- OCJ
- Suboccipital cervical spine (C1–C2)
- Subaxial cervical spine (C3–C7)¹⁴

More recently, the Subaxial Injury Classification system (also known as the SLIC system) has been developed to evaluate injuries based on fracture morphology, neurologic injury, and the integrity of the discoligamentous complex (**Table 6.2**).^{15,16} A systematic evaluation of these three components can be used to guide the treatment of patients with cervical spine fractures.

Hyperflexion Injuries

Flexion-compression injuries range from the minor anterior compression of the anterosuperior end plate (**Fig. 6.2**) to a severe teardrop or quadrangular

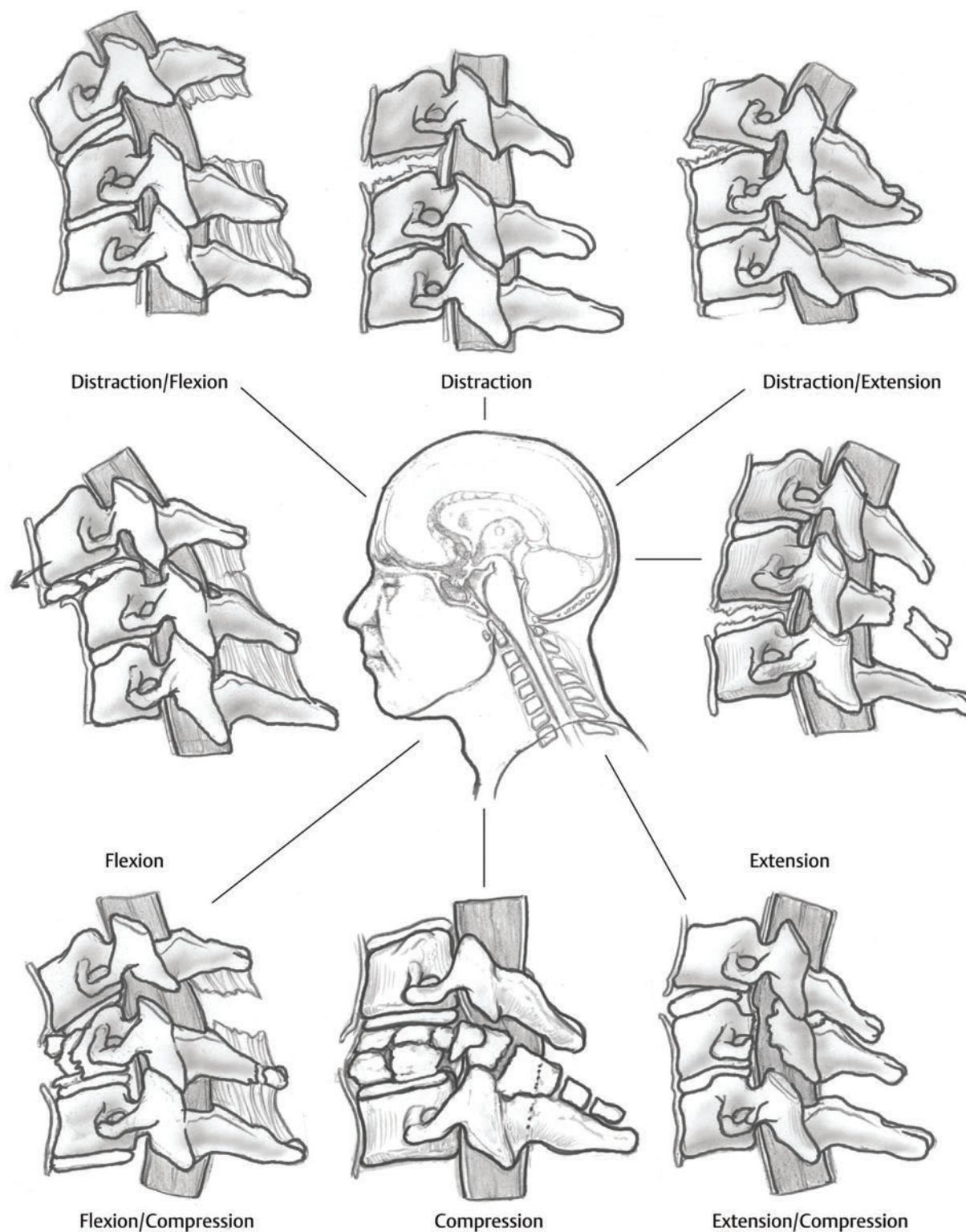


Fig. 6.1 An artist's representation of the Allen-Ferguson mechanistic classification system for subaxial cervical spine fractures. (From Chapman JR, Anderson PA. Cervical spine trauma. In: Frymoyer J, Ducker TB, Hadler NM et al, eds. *The Adult Spine: Principles and Practice*. 2nd ed. Philadelphia, PA: Lippincott-Raven; 1997:1245–1295. Reprinted by permission.)

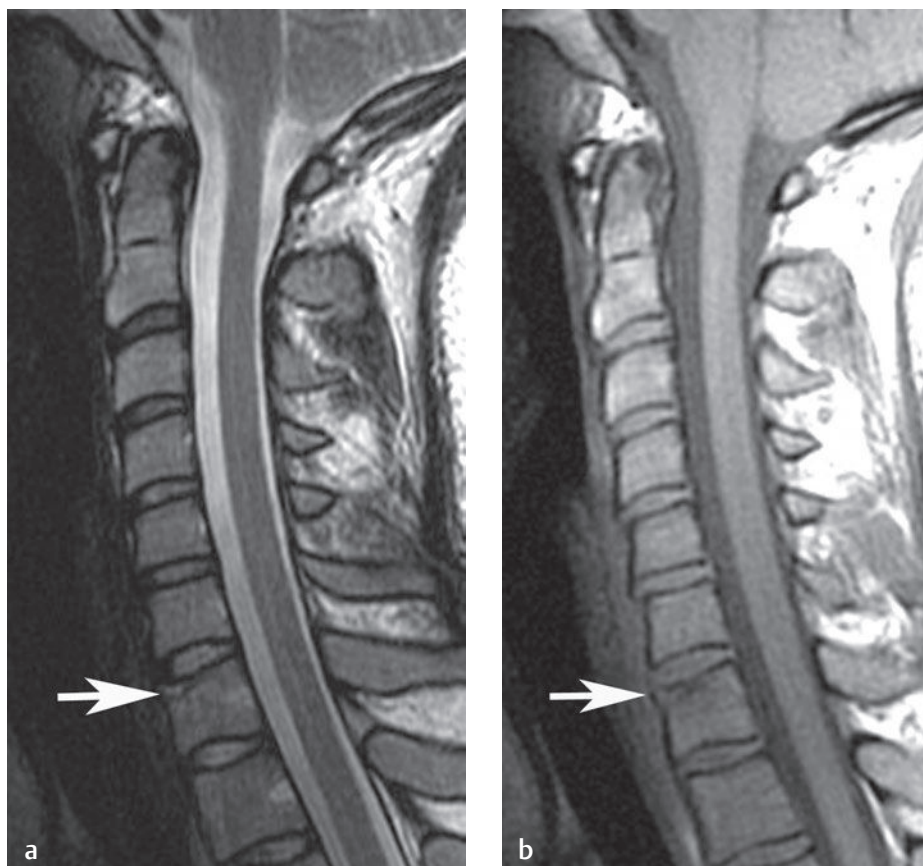


Fig. 6.2 C7 vertebral compression fracture. Sagittal (a) T2-weighted and (b) T1-weighted images show the fracture (arrow on each) with minimal loss of height.[†]

Table 6.2 Subaxial Cervical Spine Injury Classification System Scale

Morphology	Points
No abnormality	0
Compression	1
Burst	+1 = 2
Distraction (e.g., facet perch, hyperextension)	3
Rotation/translation (e.g., facet dislocation, unstable teardrop, or advanced-stage flexion-compression injury)	4
Discoligamentous complex	
Intact	0
Indeterminate (e.g., isolated interspinous widening, MRI signal change only)	1
Disrupted (e.g., widening of disc space, facet perch, or dislocation)	2
Neurologic status	
Intact	0
Root injury	1
Complete cord injury	2
Incomplete cord injury	3
Continuous cord compression in setting of neuro deficit (neuro modifier)	+1

Source: Vaccaro AR, Hulbert RJ, Patel AA, et al; Spine Trauma Study Group. The subaxial cervical spine injury classification system. A novel approach to recognize the importance of morphology, neurology, and integrity of the disco-ligamentous complex. *Spine* 2007;32:2365–2374. Reprinted by permission.



Fig. 6.3 Quadranular fracture. **(a)** A lateral radiograph, **(b)** sagittal reconstructed CT image, and **(c)** axial CT image show a flexion-compression injury (quadranular fracture) at C5. Retrolisthesis of the C5 vertebral body can be seen in **a** and **b**; the sagittal plane fracture can be seen in **c**. **(d)** A sagittal T2-weighted image shows similar features as well as spinal cord compression and prevertebral edema. (From Khanna AJ, Kwon BK. Subaxial cervical spine injuries. In: Rao RD, Smuck M, eds. *Orthopaedic Knowledge Update: Spine 4*. 4th ed. Rosemont, IL: American Academy of Orthopaedic Surgeons, 2012:221–233. Reprinted by permission.)

fracture (**Fig. 6.3**). These injuries are associated with retrolisthesis, kyphosis, and circumferential soft-tissue disruption. The radiographic evaluation of flexion-compression injuries includes inspection for the following:

- Anterior and middle column compromise
- Vertebral body-height loss
- Translation
- Angulation
- Posterior element competence

Although conventional radiographs and CT scans can evaluate fracture pattern, alignment, angulation, and translation, MRI provides additional diagnostic value and can assist with the determination of treatment options for such patients because it facilitates the assessment of spinal cord compression and posterior element compromise.

Flexion-distraction forces can lead to facet subluxations, dislocations, or fracture-dislocations. These

injuries represent a spectrum of osteoligamentous pathology, ranging from the purely ligamentous dislocation to fracture of the facet and lateral mass. MRI helps assess the compromise of posterior musculature, interspinous ligaments, ligamentum flavum, and facet capsules that is often seen with flexion-distraction injuries.¹⁷ The role of MRI in the treatment algorithm of patients who present with bilateral cervical facet dislocations (**Fig. 6.4**) without neurologic compromise is the subject of substantial debate in the literature and among spine surgeons.¹⁷⁻¹⁹ The treatment options include MRI before attempting closed reduction or surgical intervention; closed reduction with traction while monitoring the patient's neurologic examination; and surgical intervention via anterior, posterior, or combined approaches.¹⁷⁻¹⁹ One of the purposes of obtaining an MRI study before the reduction of bilateral facet dislocations is to rule out the possibility of an extruded disc fragment, which may displace into the spinal canal during a closed reduction (**Fig. 6.5**).

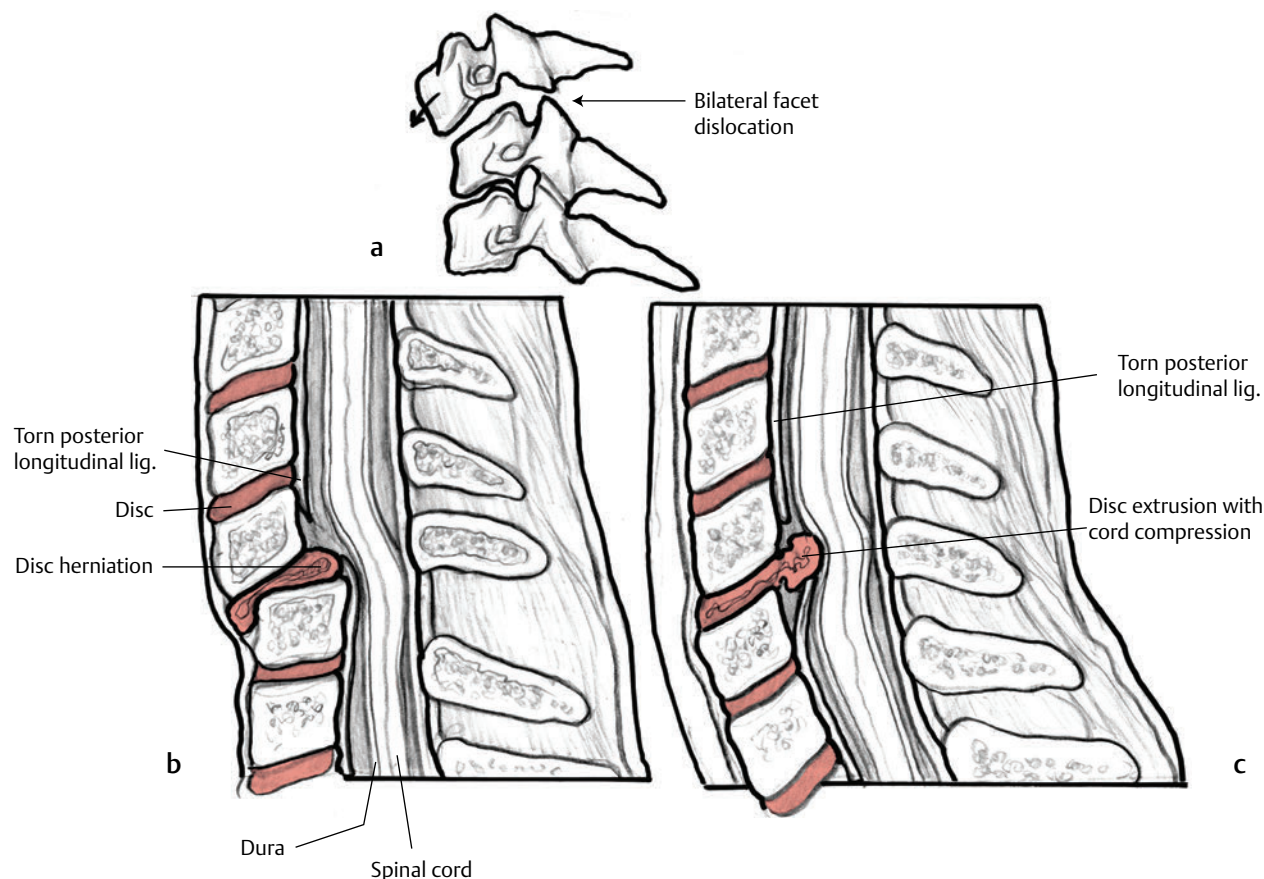


Fig. 6.4 Artist's sketches illustrating the pathology in bilateral facet dislocation. **(a)** A lateral view of osseous structures shows that the facets are perched and that additional translation will lead to complete dislocation. **(b)** A lateral view before reduction shows ~50% translation of the superior vertebral body relative to the inferior one and displacement of the intervertebral disc. **(c)** A lateral view after reduction shows that the intervertebral disc has displaced into the spinal canal and compressed the spinal cord during the reduction maneuver.[†]

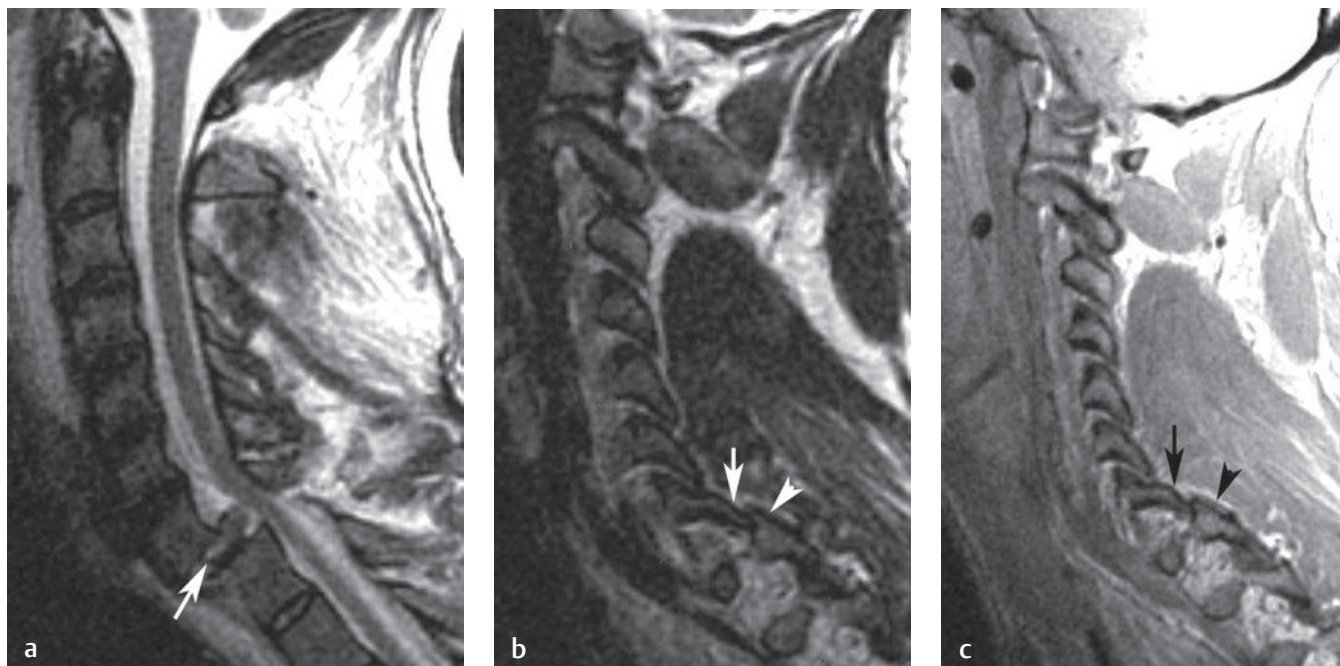


Fig. 6.5 Bilateral cervical facet dislocation. **(a)** A sagittal T2-weighted image shows anterior translation of C7 over T1 with an associated disc extrusion (arrow) and cord compression. **(b)** Parasagittal T2-weighted and **(c)** gradient-echo images show the inferior articular process of C7 (arrow on each) displaced anterior to the superior articular process of T1 (arrowhead on each).[†]

Most flexion injuries are well visualized on MRI, and MRI is particularly effective for the assessment of the following¹²:

- Alignment
- Fractures
- Ligamentous injury
- Cord abnormalities
- Acute disc herniations
- The cause of anterior subluxation, either chronic degenerative changes or hyperflexion sprain

Facet joint injuries may be seen on parasagittal or axial images, which show increased signal on T2-weighted images secondary to edema from facet capsule tears.^{12,20–22} Injury to posterior ligaments may be seen as areas of hyperintensity on T2-weighted images, especially fat-suppressed T2-weighted or STIR images (**Figs. 6.6** and **6.7**).

Hyperextension Injuries

Cervical spine extension injury results in the posterior translation or rotation of a vertebral body in the sagittal plane.^{5,12,23} Hyperextension injuries often are produced by rear-impact motor vehicle collisions or direct facial trauma.

In cervical spine hyperextension injuries, potential findings include the following^{5,12,20,22,23}:

- Tear(s) of the anterior longitudinal ligament
- Avulsion of the intervertebral disc from an adjacent vertebral body
- Horizontal intervertebral disc rupture (**Fig. 6.8**)

More severe and potentially unstable hyperextension injuries may be associated with the following⁵:

- Prevertebral hematoma (**Fig. 6.9**)
- Widening of the disc space
- Posterior ligament complex edema
- Herniated disc

Elderly patients with spondylosis and kyphosis of the cervical spine may suffer spinal cord injury without fracture or ligamentous injury because of posterior infolding of the ligamentum flavum upon a spinal canal already narrowed by posterior vertebral osteophytes.⁵

Whiplash injuries often have no associated osseous injury on standard radiographs or CT images, and flexion-extension radiographs may be nondiagnostic because of poor excursion secondary to pain. However, MRI is of limited value for the assessment of whiplash; several studies have failed to show positive MRI findings in the absence of neurologic

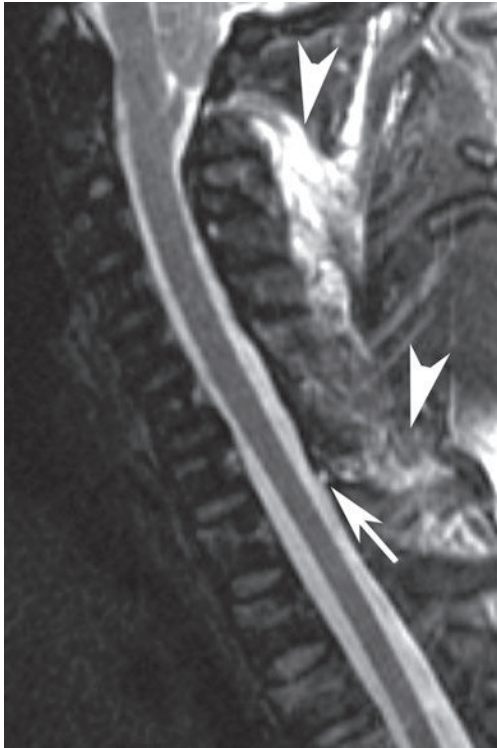


Fig. 6.6 A sagittal STIR image shows edema in the supraspinous ligament region (*arrowheads*) and interspinous region at C6-C7 and C7-T1, with a small, focal region of increased T2-weighted signal in the ligamentum flavum at the C7-T1 level (*arrow*) compatible with a partial tear.[†]

symptoms.^{21,24,25} In contrast, patients with a fused cervical spine secondary to ankylosing spondylitis or diffuse idiopathic skeletal hyperostosis may benefit from an MRI examination to assess for acute fracture, instability, or neurologic compromise. In such patients, the fused cervical spine acts like a long-bone fracture, and even minimally displaced fractures may be unstable (**Fig. 6.10**).²⁶

Finally, MRI can assess intervertebral disc injury and subtle fractures caused by any of the aforementioned mechanisms.^{12,20–22,27} Intervertebral disc injury may range from tear(s) of the outer annulus fibrosus (seen as increased T2-weighted signal in the outer annular fibers) to frank intervertebral disc herniation. The identification of an annular tear on MRI does not indicate acute traumatic injury and can be seen in asymptomatic individuals.^{28,29} Intervertebral disc separation from the adjacent vertebral body may be seen as a horizontal hyperintense T2-weighted signal.^{12,20,22} Subtle fractures, such as vertebral end-plate fractures, may be best visualized with MRI because it can detect osseous edema and hemorrhage not seen on conventional radiographs or CT images.^{12,20,22}

Axial Load Injuries

Axial load injuries are caused by the axial transmission of force through the skull, through the occipital condyles, and into the spine. This force transmission

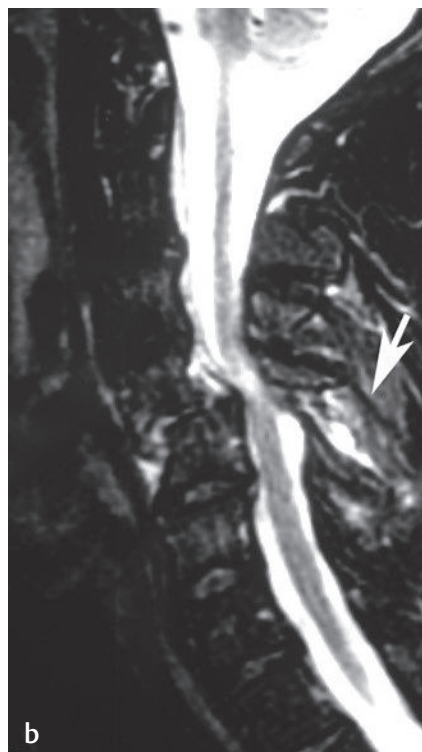


Fig. 6.7 A discoligamentous complex injury. **(a)** A lateral radiograph shows bilateral facet subluxation at C4-C5, with widening of the interspinous process space (between *arrowheads*). **(b)** A sagittal STIR image shows edema in the region of the interspinous and supraspinous ligaments between C4 and C5 (*arrow*), which is compatible with injury to the discoligamentous complex. (From Khanna AJ, Kwon BK. Subaxial cervical spine injuries. In: Rao RD, Smuck M (eds). Orthopaedic Knowledge Update: Spine 4. Ed 4. Rosemont (IL): American Academy of Orthopaedic Surgeons, 2012:221–233. Reprinted by permission.)

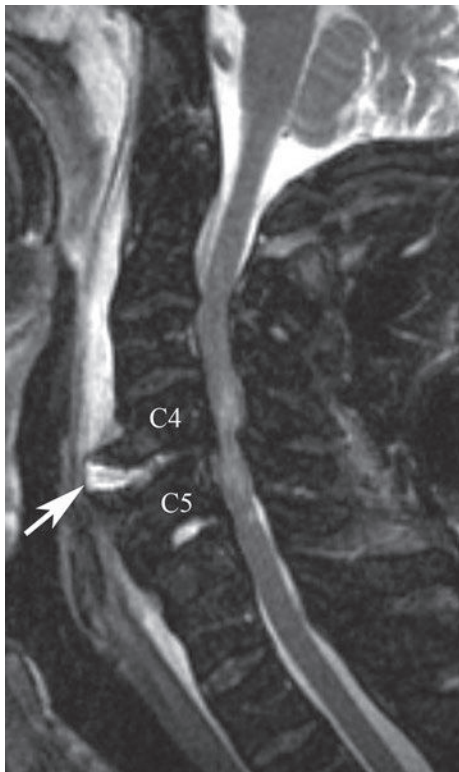


Fig. 6.8 A sagittal STIR image shows an intervertebral disc rupture at C4-C5 (*arrow*) in a patient who sustained a hyperextension injury to the cervical spine. Note the associated prevertebral hematoma and the severe multilevel degenerative stenosis with associated cord signal change.[†]

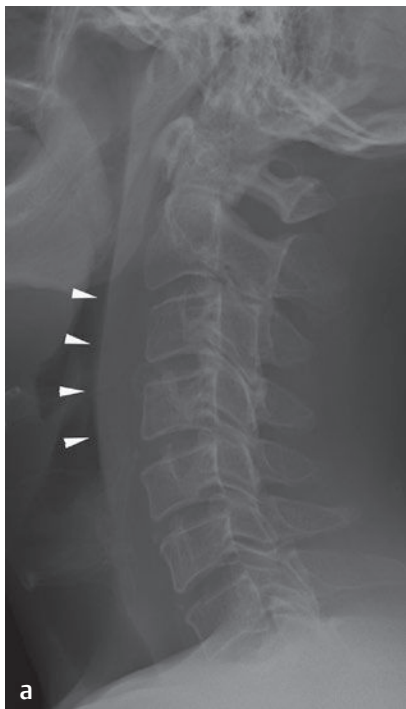


Fig. 6.9 Extension-distraction injury with incomplete spinal cord injury in a 35-year-old man who was injured in a fall from a scaffold, with forcible extension of the neck. **(a)** A lateral radiograph shows substantial edema in the anterior soft tissues (*arrowheads*). **(b)** A sagittal reconstructed CT scan shows avulsion from the C4 inferior end plate (*arrow*). **(c)** A sagittal T2-weighted image shows the acute tensile failure of the C4-C5 disc, with bright signal within the disc (*arrow*); anterior soft-tissue edema also is visible (*arrowheads*). The patient was treated nonsurgically because of the absence of severe instability or cord compression. (From Khanna AJ, Kwon BK. Subaxial cervical spine injuries. In: Rao RD, Smuck M, eds. Orthopaedic Knowledge Update: Spine 4. 4th ed. Rosemont, IL: American Academy of Orthopaedic Surgeons, 2012:221–233. Reprinted by permission.)

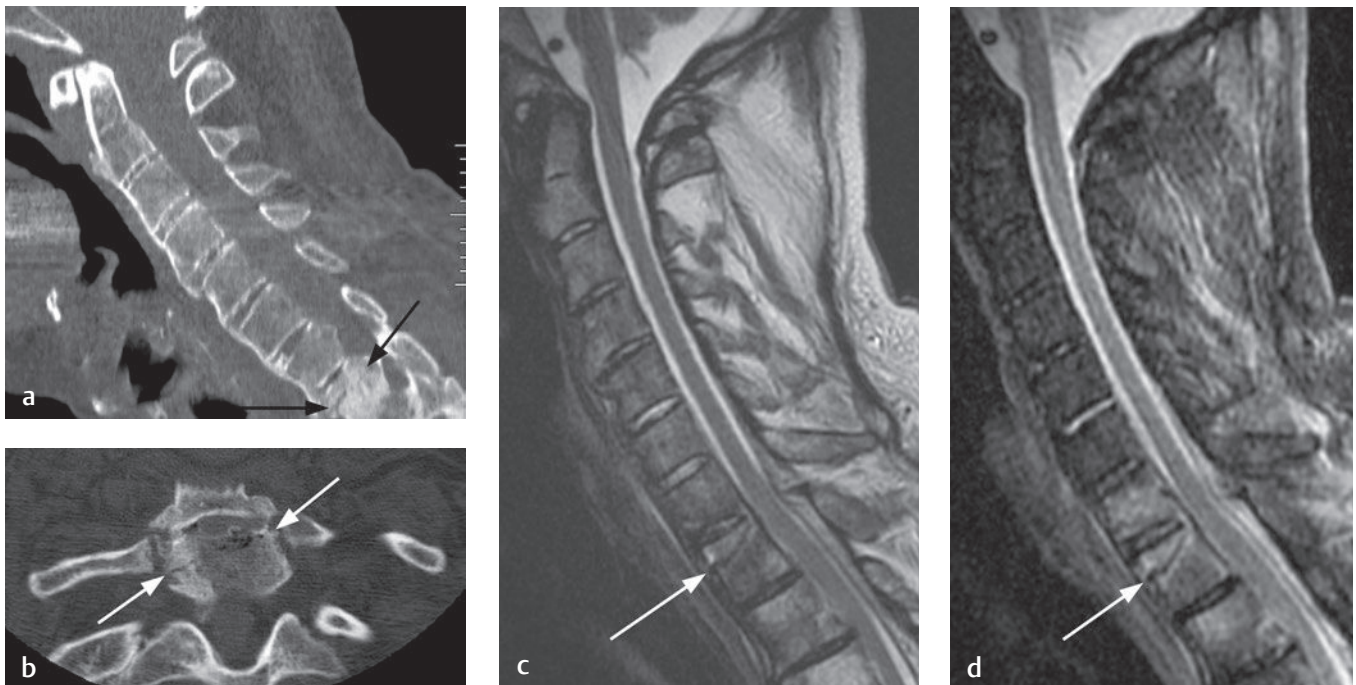


Fig. 6.10 Ankylosing spondylitis. **(a)** Sagittal and **(b)** axial CT images of the cervical spine in a patient with ankylosing spondylitis show a nondisplaced fracture at the T1 level (arrows on each), which could easily be missed. **(c)** Sagittal T2-weighted and **(d)** STIR images show the same fracture (arrows on each). In **(d)**, edema at the fracture site indicates a relatively acute injury. (From Khanna AJ, Kwon BK. Subaxial cervical spine injuries. In: Rao RD, Smuck M, eds. *Orthopaedic Knowledge Update: Spine 4*. 4th ed. Rosemont, IL: American Academy of Orthopaedic Surgeons, 2012:221–233. Reprinted by permission.)

can cause a Jefferson burst fracture or burst fractures of the subaxial cervical spine. MRI is useful for the assessment of C1 compression fractures and associated pathologies such as lateral mass displacement on coronal images, atlanto-dental interval increase on sagittal images, and transverse ligament disruption on axial images.¹² For burst fractures, MRI is useful for diagnosing associated spinal cord injury caused by an acute herniated disc or retropulsion of osseous fragments (**Fig. 6.11**). Because a purely axial force subjects the posterior capsuloligamentous structures to compression only, these posterior structures should remain intact.^{12,23} However, during the traumatic event, there often is some degree of spine flexion that may cause injury to the posterior spinal elements, which can be detected by MRI.²³ It is important to scrutinize the fat-suppressed T2-weighted and other images carefully for evidence of injury to the posterior ligamentous and osseous structures because such injury will lead to consideration of posterior fusion in addition to the anterior decompression and fusion that is often performed for patients with cervical burst fractures.

OCJ Injuries

Although injury to the OCJ occurs in a small percentage of blunt-trauma victims (0.8% in one study³⁰), recognition of such injuries is crucial because of their devastating effects^{31–34} (see Chapter 5, The Occipitocervical Junction, for a detailed discussion of occipitocervical craniotomy and the various measurement techniques for evaluation of occipitocervical pathology). It is important to keep in mind that MRI studies of the OCJ should be reviewed in conjunction with conventional radiographic and CT imaging.

Atlantooccipital Dissociation

Atlantooccipital dissociation is any separation of the atlantooccipital articulation. The skull may displace anteriorly, posteriorly, or superiorly, and the displacement may be complete (dislocation) or partial (subluxation). Atlantooccipital dissociation can be a devastating injury.^{31–34} The primary injury is to the ligaments that provide structural support to the

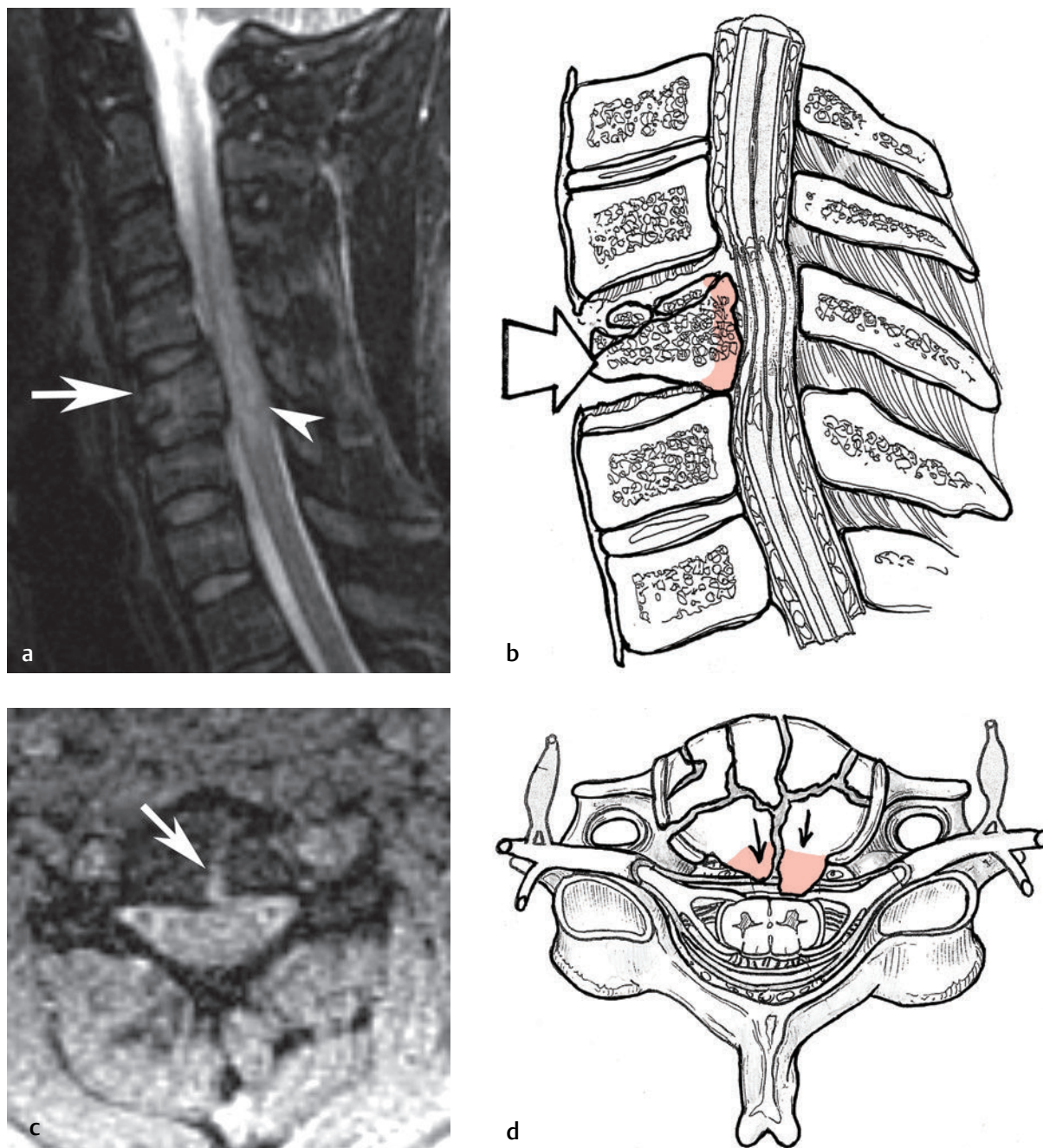


Fig. 6.11 Cervical burst fracture. **(a)** A sagittal fat-suppressed T2-weighted image and **(b)** corresponding artist's sketch show a C5 burst fracture (*arrow* on each) with moderate loss of height, retropulsion, and spinal cord contusion (*arrowhead* on **a**). **(c)** An axial T2-weighted gradient-echo image and **(d)** corresponding artist's sketch show the sagittal split component of the fracture (*arrow[s]* on each).[†]

cervicocranial junction. In addition, even without frank dislocation, the occiput–C1 junction may be injured, as indicated by postmortem studies.^{31,32} Although this injury may be fatal, improvement in resuscitative and medical treatment has increased survival rates. CT imaging may be used to assess associated fractures or relationships among the basion, dens, occipital condyles, and atlas in conjunction with atlantooccipital dissociation, whereas MRI is better at detecting injury to the cervicocranial ligaments (e.g., transverse, apical, cruciate, atlantooccipital membrane and capsular ligaments, tectorial membrane), brainstem, or spinal cord.^{12,22,35}

Trauma to the Atlas

Axial load to the OCJ at the atlas may result in a burst fracture of the atlas. The injury is visualized on open-mouth odontoid radiographs or coronal CT images.^{36,37} As indicated by the cadaver study of Spence et al,³⁸ combined overhang of the lateral masses of C1 over C2 of ≥ 6.9 mm is associated with transverse ligament rupture and indicates a relatively unstable Jefferson burst fracture. The axial T2-weighted images can be critically evaluated to rule in or rule out injury

to the transverse ligament. These images should be carefully scrutinized for increased T2-weighted signal in or along the course of the transverse ligament. The ligament should also be evaluated for regions of discontinuity.

Trauma to the Axis

C2 is the most commonly fractured cervical spine level.³⁰ In the elderly, odontoid fractures tend to be posteriorly displaced. Fracture location, displacement, and angulation are important factors that assist with clinical decision making. Lateral cervical radiographs and CT scans can be used to characterize such fractures and better evaluate the osseous detail. MRI can assist in the evaluation of these fractures by providing assessment of the degree of edema at the fracture site (**Fig. 6.12**). This information provides insight into the age of the fracture (acute versus subacute versus chronic), which can be used to guide treatment. The sagittal and axial T2-weighted images should also be carefully evaluated to determine the degree of neural compression from either a displaced fracture or underlying degenerative changes.

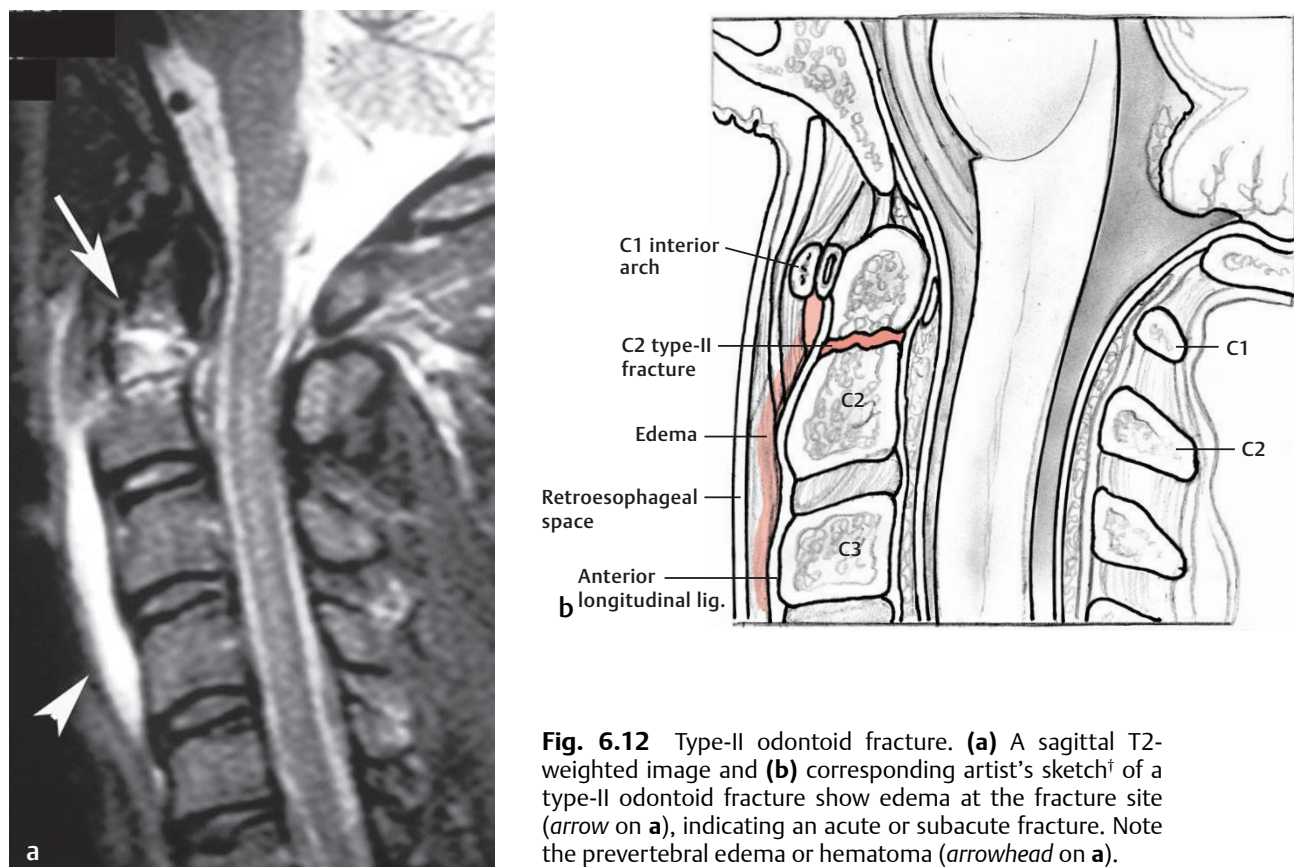


Fig. 6.12 Type-II odontoid fracture. **(a)** A sagittal T2-weighted image and **(b)** corresponding artist's sketch† of a type-II odontoid fracture show edema at the fracture site (arrow on **a**), indicating an acute or subacute fracture. Note the prevertebral edema or hematoma (arrowhead on **a**).

Atlantoaxial Dissociation

Atlantoaxial dissociation may be caused by distraction with superior migration of the atlas away from the axis or by odontoid fractures with anterior or posterior displacement of C1 relative to C2. MRI clearly depicts the associated pathology seen with atlantoaxial dissociation.¹² As noted above, MRI is very useful for detecting ligamentous and spinal cord injury. The relationship of the atlas to the axis is clearly visible with MRI. Specifically, the integrity of the transverse ligament should be evaluated along with the approximate size of the anterior atlantodens interval. This measurement is more frequently evaluated on flexion and extension lateral cervical spine radiographs (**Fig. 6.13**).

Vertebral Artery Injury

Vertebral artery injury is associated with blunt cervical trauma, with an incidence as high as 11%.³⁹ This potentially devastating injury may occur with cervical spine fractures extending into the transverse foramen, but it is associated most often with unilateral or bilateral facet dislocations.^{22,40,41} MR angiography may be used to assess vertebral artery patency, especially with such fractures.²² MR angiography may show areas of vascular stenosis or occlusion. Flowing blood creates a signal void on axial SE images and is seen as a bright signal on gradient-echo images; merging the data from these two modalities can help determine the status of blood flow in the vertebral arteries^{22,42} (**Fig. 6.14**).

The types of vertebral artery injuries are thrombosis, dissection,⁴³ and transection (rare). MR angiography shows vertebral artery thrombosis as the absence of flow-related enhancement on images in the expected course of the vertebral artery and as an acute thrombus in the foramen transversarium, dissection as a tapering of the vessel, and transection as a focal discontinuity of the vessel. Major clues to vascular injury include changes in vessel caliber, loss of the normal rounded shape, increase in caliber from proximal to distal (except at the carotid bulb), or the presence of an extraluminal thrombus or a slit or dark band through the lumen.

Penetrating Trauma

Penetrating injury to the cervical spine can be caused by projectiles (e.g., bullets) or puncture mechanisms. Missiles can cause spinal cord injury by direct penetration; displacement of bone fragments into the spinal canal, compressing the spinal cord; or a blast effect. The osseous architecture of the spine often protects the spinal cord from direct injury from a stabbing mechanism because the lamina and spinous

processes can deflect the penetrating object into the paraspinal soft tissues. MRI is useful for assessing the specific location, extent, and type of cord injury from penetrating trauma.

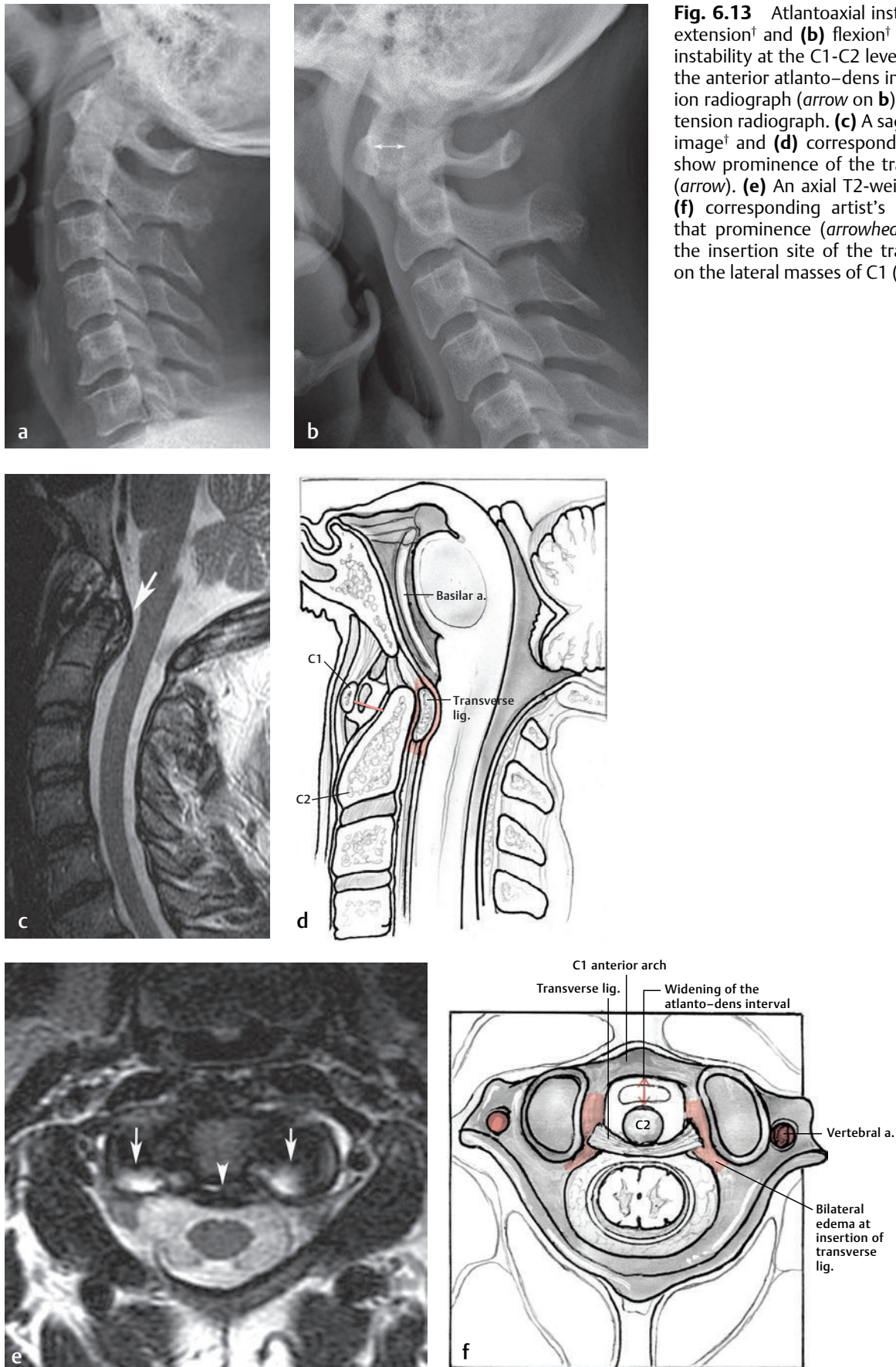
Characterization of Spinal Cord Injury

The severity of spinal cord injury depends on the characteristics of the traumatic event (including the amount, duration, and location of the applied force) and the underlying health of the spinal cord. Spinal cord insult may range from a concussive injury (purely functional and reversible) to complete transection (irreversible). Spinal cord concussive injury often has no MRI evidence of edema (increased T2-weighted signal), or the edema is transient and resolves with time.¹² Spinal cord contusion is a more severe injury and may be caused by transient compression or stretching of the spinal cord. Spinal cord compression may show injury characteristics similar to those of spinal contusion, but it can be associated with a specific compressive lesion such as disc herniation (**Fig. 6.15**) or an osseous fragment.

An injured spinal cord segment may have an increase in cord diameter because of swelling, edema, or hemorrhage. MRI characteristics of an injured spinal cord segment are based on the degree of swelling, edema, or hemorrhage, each of which may have a different pattern of signal changes on various pulse sequences.^{6,44} On T2-weighted images, edema and acute hemorrhage are seen as bright signal, whereas chronic hemorrhage is seen as darker signal. Gradient-echo images show dark areas that are larger than the abnormality on the T2-weighted images. This enlargement, or “blooming,” is the result of the magnetic susceptibility artifact from methemoglobin.⁶ The anatomic location, morphology, and length of the spinal cord lesion are important factors in determining the degree of neurologic loss. Initial neurologic deficit and potential for recovery are related directly to the extent of spinal cord damage by hemorrhage or edema.⁶ Evidence of parenchymal hemorrhage on MRI may predict worse functional outcomes or neurologic recovery than is associated with a spinal cord injury with predominantly edematous changes.⁶

Highly T2-weighted images offer a myelographic effect for the assessment of spinal cord compression. These images should be carefully evaluated in the sagittal and axial planes for regions of effacement of the ventral or dorsal CSF spaces, which indicate spinal stenosis and cord compression. Trauma patients who have underlying degenerative or congenital stenosis are at increased risk for spinal cord injury because of the decrease in the cross-sectional area available for the spinal cord.

Clinical and experimental evidence has shown that surgical decompression of stenotic areas has a beneficial effect on neurologic recovery, which



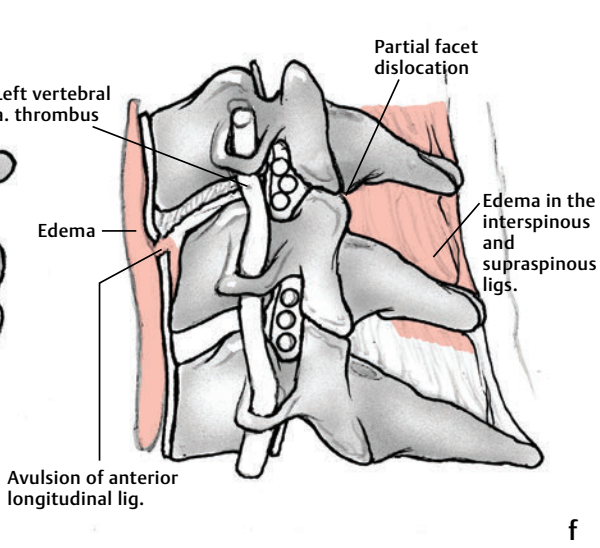
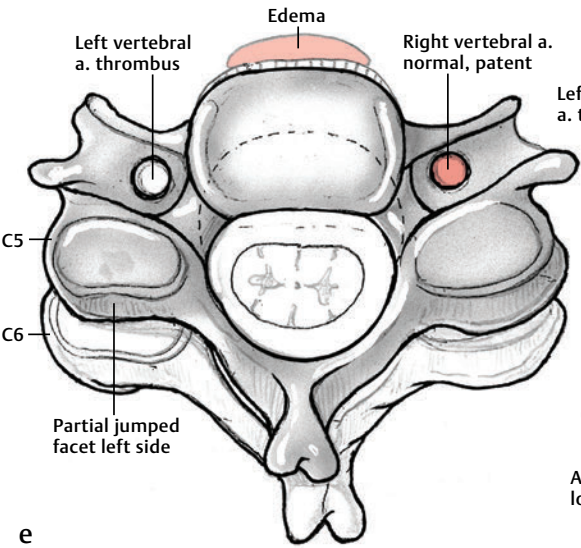
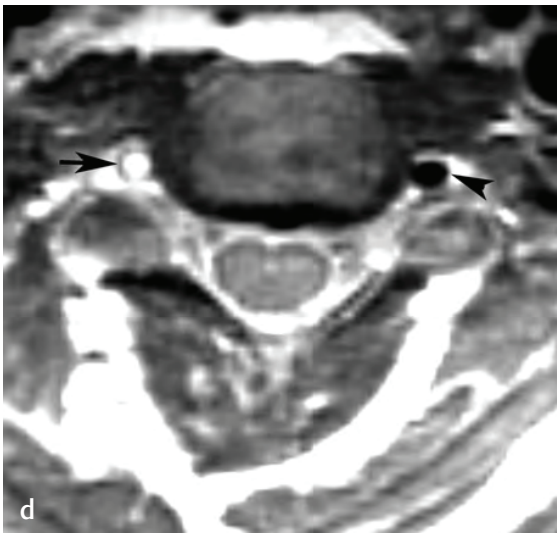
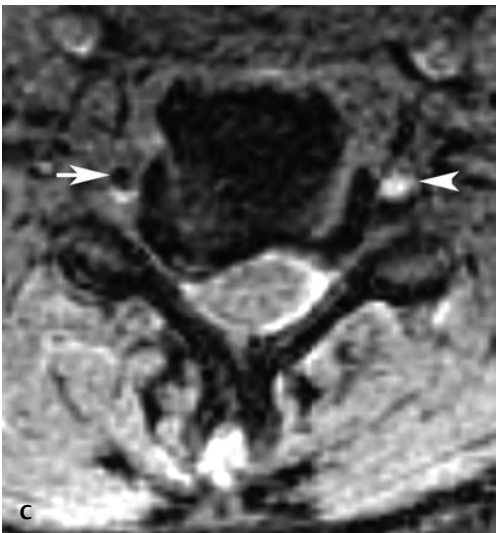
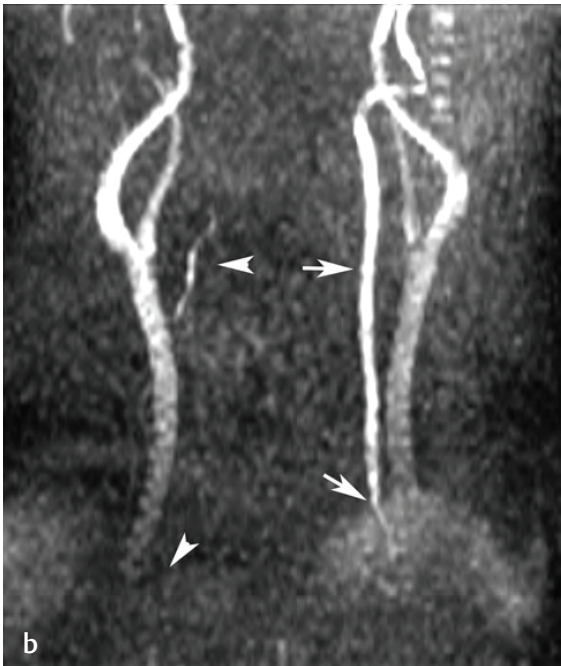




Fig. 6.15 A sagittal T2-weighted image shows a large central disc extrusion at the C5-C6 level with associated increased cord signal intensity (*arrow*) compatible with myelomalacia. Note the elevation of the posterior longitudinal ligament (*arrowhead*).[†]

makes prompt identification of stenotic areas and distinguishing these areas from simple contusions important.¹² In addition, MRI assessment of cervical spine fractures in obtunded or uncooperative patients may identify disc herniations that may cause spinal cord compression and iatrogenic or progressive neurologic injury during fracture reduction.^{23,45,46}

Characterization of Cervical Spine Instability

White et al⁴⁷ defined cervical spine instability as the inability to maintain a normal association between vertebral segments while under a physiologic load. Cervical spine instability may be caused by damage to the osseous and/or ligamentous structures. Conventional radiographs and CT scans often provide the best assessment of osseous injuries. Ligamentous injury contributing to cervical spine instability may be assessed with flexion and extension lateral cervical spine radiographs and by physical examination. MRI can also be used to evaluate for ligamentous injury; the sensitivity for detection of such injuries is greatest within 24 to 72 hours postinjury.^{8,20,22,48} Important ligaments to assess include the following²³:

- Anterior longitudinal ligament
- Posterior longitudinal ligament
- Posterior column ligament complex (supraspinous ligament, interspinous ligament, and ligamentum flavum), which has been recognized as an important restraint to spinal instability (especially kyphosis)^{25,49}
- Transverse ligament

Fig. 6.14 Vertebral artery injury after unilateral facet dislocation at C5-C6 without spinal cord injury. **(a)** A sagittal T2-weighted image shows an injured disc at C5-C6 with increased signal intensity in the disc and probable avulsion of the anterior longitudinal ligament (*arrow*). Prevertebral edema (*small arrowheads*) and edema in the posterior paraspinal musculature (*large arrowhead*) are present. **(b)** An MR angiogram (anterior view) from a 2D time-of-flight acquisition shows absence of signal intensity in the expected course of the right vertebral artery (*arrowheads*). Note the normal course of the left vertebral artery (*arrows*). **(c)** An axial image from a 3D gradient-echo acquisition shows an oval area of low signal intensity in the right foramen transversarium (*arrow*), corresponding to a thrombus in the right vertebral artery. Note the normal flow-related enhancement in the left foramen transversarium (*arrowhead*). **(d)** An axial FSE image obtained at a similar level to that in **(c)** shows a high-signal-intensity thrombus (*arrow*) in the right foramen transversarium, indicative of a thrombosed vertebral artery. Note the normal flow void of the left vertebral artery in the left foramen transversarium (*arrowhead*). Artist's sketches in the **(e)** sagittal and **(f)** axial planes show the displacement that leads to vertebral artery injury in this scenario. (**a–d** from Torina PJ, Flanders AE, Carrino JA, et al. Incidence of vertebral artery thrombosis in cervical spine trauma: correlation with severity of spinal cord injury. *AJNR Am J Neuroradiol* 2005;26:2645–2651. Reprinted by permission.)



Fig. 6.16 A sagittal STIR image of a patient who sustained a hyperflexion injury to the cervical spine shows increased signal intensity within the region of the supraspinous and interspinous ligaments between C3 and C6 (arrow). These findings are compatible with injury to the posterior ligamentous structures.[†]

MRI characteristics of ligamentous injury include increased T2-weighted signal (from edema) within the ligamentous and other posterior structures (**Fig. 6.16**) or loss of ligament continuity (normally a low-intensity continuous signal). Ligamentous injury is best assessed on STIR or fat-suppressed T2-weighted images.²³ A ligament strain, without complete disruption, may be seen as an elongated or redundant ligament on sagittal MR images. Despite the capability of MRI to detect ligamentous injury, not all MRI-detected ligamentous injuries result in spinal instability or warrant treatment.^{23,24} For example, minor motor vehicle accidents that result in acute whiplash injury of the cervical spine without fracture do not need emergent MRI evaluation for ligamentous injury and may be treated symptomatically only.²⁴

With the increasing availability of flexion-extension (kinematic) cervical spine MRI, a dynamic assessment of cervical spinal instability and associated stenosis can be obtained.⁵⁰ Although such information provides insight into the degree of spinal instability, it tends to be most useful for the evaluation of patients with degenerative disorders of the cervical and lumbar spine (**Fig. 6.17**).^{51,52} Patients who have sustained severe trauma to the cervical spine are likely to be immobilized. After a period of immobilization, and after frank instability of the cervi-

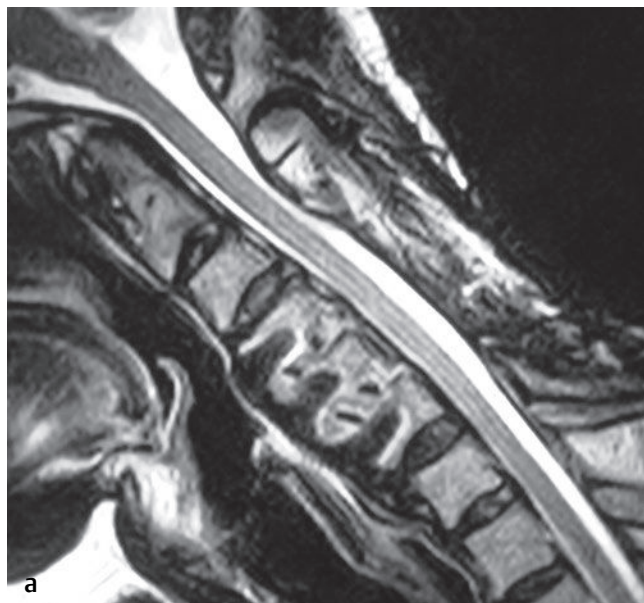


Fig. 6.17 Sagittal T2-weighted images of a patient after C4-C6 anterior cervical decompression and fusion with allograft and plate. (a) Image obtained in flexion on an open, upright MR system shows no substantial stenosis. (b) Image obtained in extension shows moderate stenosis at the C6-C7 level secondary to buckling of the ligamentum flavum (arrow) and disc bulge.[†]

cal spine has been ruled out with patient-controlled flexion-extension cervical spine radiographs, a kinematic cervical spine MRI study can be considered. The information obtained from such kinematic studies can be used to guide surgical treatment and may enable the surgeon to decide among anterior, posterior, or combined surgical approaches.

■ Degenerative Conditions

Degenerative changes of the cervical spine are common after the fourth decade of life.⁵³ Cervical spine degeneration may be asymptomatic or have acute or insidious onset of symptoms; it may result in pain, stiffness, radiculopathy, myelopathy, and even permanent disability. Degenerative pathology may affect multiple areas in the cervical spine, including the following:

- Intervertebral discs
- Facet joints
- Uncovertebral joints of Luschka
- Ligaments
- Paravertebral musculature

Because these elements are biomechanically linked, a single cervical spine level may have multiple degenerative pathologies and cause adjacent-level degenerative changes. Conventional radiographs are often the initial screening studies for evaluating cervical spine degeneration and may guide the selection of more advanced imaging techniques.⁵⁴ MRI is usually considered the preferred initial advanced imaging modality for the evaluation of symptomatic cervical spine degeneration; it has a reported sensitivity and specificity of 91% for the detection of cervical degenerative changes.^{54,55} Despite this high sensitivity and specificity, it is important to understand that radiographic and MRI abnormalities do not always correlate with a symptomatic degenerative lesion.⁵⁶ Boden et al⁵³ reported that almost 60% of their asymptomatic patients >40 years old had cervical spine degenerative disc disease on MRI.

Although one should always correlate the patient's history and physical examination with the imaging findings (see Chapter 4, A Systematic Approach to the Review of Spine MRI Studies), this practice is especially important when evaluating the MRI studies of a patient with a suspected cervical or lumbar spine degenerative disorder. Specifically, one should know whether a patient is presenting with neck pain, radiculopathy, myelopathy, or a more focal neurologic deficit. The laterality and level of the symptoms should also be assessed, and this information should be taken into consideration, along with the imaging findings, when making a choice among the various nonoperative and surgical treatment options.

Degenerative Disc Disease

An intervertebral disc is composed of an outer annulus fibrosus, an inner nucleus pulposus, and superior and inferior cartilaginous end plates. The structural composition of the intervertebral disc changes with age: the water content of the nucleus pulposus and annulus fibrosus decreases from ~90% in the first year of life to 70% to 75% in the eighth decade.^{20,57,58} The remainder of the nucleus pulposus consists of proteoglycans and collagen that attract water, which creates pressure that enables the nucleus pulposus to resist axial loading. The collagen fibers in the annulus are abundant anteriorly but deficient posterolaterally, creating a potential weak area at risk for degenerative tears and disc herniation.⁵⁸ The posterior longitudinal ligament reinforces this deficient area.⁵⁸

With advancing age, the proteoglycan composition of the intervertebral disc changes and water is lost, diminishing the disc's ability to support load. The nucleus pulposus is replaced with more fibrous structures and blends with the adjacent annulus fibrosus into amorphous fibrocartilaginous tissue.⁵⁵ Disc desiccation leads to bulging of the annulus fibrosus and loss of disc height, causing increased stress transfer to adjacent facet and uncovertebral joints.⁵⁵ This increased stress on facet and uncovertebral joints propagates osteocartilaginous hypertrophy and osteophyte formation. In addition, the loss of intervertebral disc elasticity exposes these small vertebral joints to increased motion and instability, furthering their degeneration. Nerve root compression may occur secondary to the decreased width and height of the adjacent neural foramina caused by disc height loss, annulus bulging, and uncinate process and facet hypertrophy. On MRI, a normal intervertebral disc has intermediate signal intensity on T1-weighted images and high signal intensity on T2-weighted sequences, whereas disc desiccation shows as low signal intensity on T1-weighted and T2-weighted images (**Fig. 6.18**).^{54,55}

As the disc degenerates and desiccates, degenerative changes also affect the annulus fibrosus and result in deamination of and change in the architecture of the concentric annular fibers.²⁰ These changes may lead to annular tears. Discogenic pain may be associated with transverse, radial, or complete tears.⁵⁵ On T2-weighted images, tears are seen as areas of high signal intensity within the annulus (**Fig. 6.19**).^{54,55} A weakened annulus fibrosus may lead to a spectrum of intervertebral disc pathology based on the extent of annulus bulging and disc herniation (**Table 6.3**). The findings of degenerative disc disease seen on MRI should also be correlated with the degenerative changes seen on cervical spine radiographs. Specifically, the degree of vertebral body end-plate sclerosis can be best evaluated on radiographs, and oblique radiographs will best show foraminal stenosis secondary to osteophyte formation.



Fig. 6.18 Multilevel degenerative disc disease. **(a)** A sagittal T2-weighted image shows multilevel degenerative disc disease as evidenced by the loss of the normal high signal intensity within the discs. Note the degenerative spondylolisthesis at C2-C3, C3-C4 (subtle), and C7-T1, and the multilevel anterior osteophyte formation (*arrowheads*). There is also a loss of the normal cervical lordosis. **(b)** An axial T2-weighted image at the C3-C4 level shows a right paracentral disc bulge (*arrowhead*), resulting in moderate stenosis with asymmetric cord compression. **(c)** An axial T2-weighted image at the C5-C6 level shows moderate central stenosis. **(d)** A sagittal reconstructed CT image also shows multilevel degenerative disc disease and provides improved osseous detail that complements the information seen on the MR images. Note the gas-containing subchondral cyst at the inferior end plate of C6 (*arrowhead*) and the multilevel anterior osteophyte formation.[†]

Table 6.3 Intervertebral disc pathology

Disc Pathology	MRI Findings
Bulge	Symmetric extension of annulus beyond confines of adjacent end plates
Protrusion	Focal area of disc material that extends beyond vertebral margin, but remains contained within the outer annular fibers
Extrusion	Herniation of nucleus pulposus beyond confines of annulus with disc attached to remainder of nucleus pulposus by a narrow pedicle
Sequestration	Portion of disc fragment entirely separated from parent disc

Source: Khanna AJ, Carbone JJ, Kebaish KM, et al. Magnetic resonance imaging of the cervical spine. *J Bone Joint Surg Am.* 2002;84:70–80. Modified with permission.

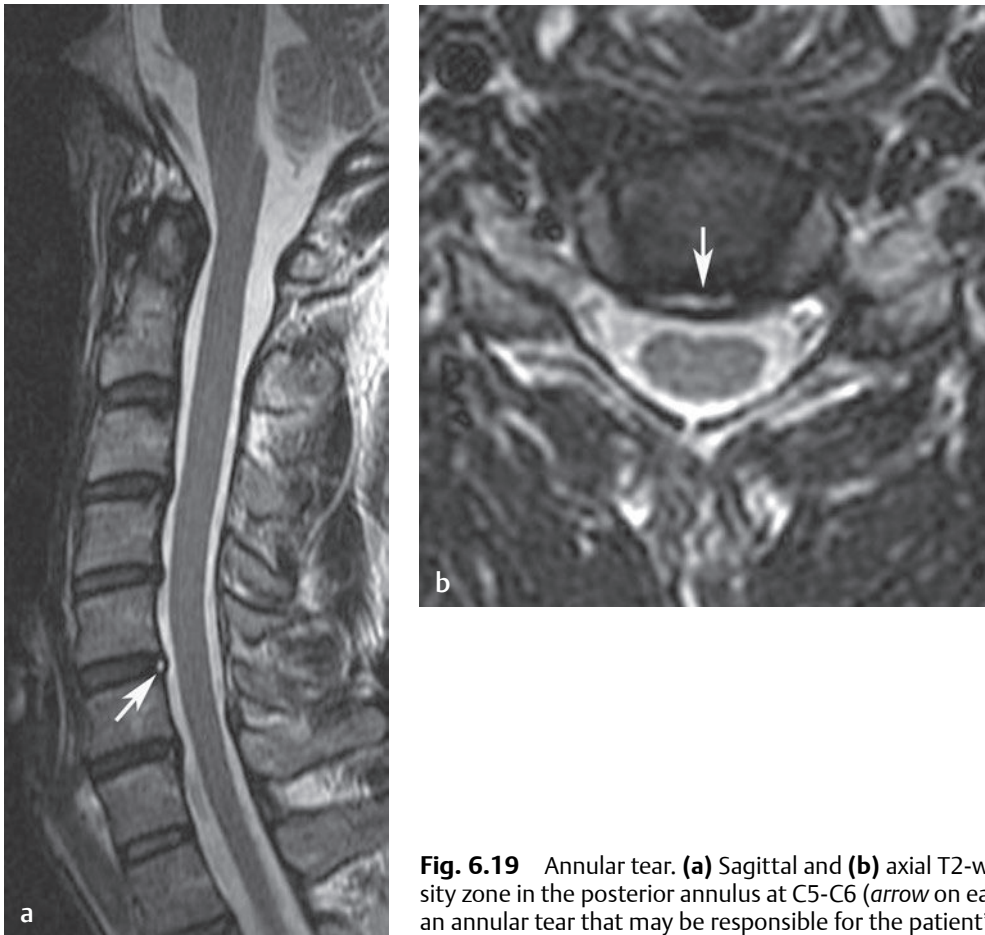


Fig. 6.19 Annular tear. **(a)** Sagittal and **(b)** axial T2-weighted images show a high-intensity zone in the posterior annulus at C5-C6 (arrow on each). This finding is compatible with an annular tear that may be responsible for the patient's discogenic neck pain.[†]

Disc Displacement

Along with the degenerative disc disease and the normal aging process described in the preceding paragraphs, elevated pressures within the nucleus pulposus and compromise of the structural integrity of the annulus fibrosus can lead to migration of disc material toward the neural elements and produce the clinical findings of radiculopathy or myelopathy. Patients with large central disc herniations tend to present with symptoms of myelopathy, whereas those with posterolateral disc herniations tend to present with radiculopathy.

Disc herniations most commonly occur at the levels with greatest motion (C5-C6 and C6-C7) and may be generally classified as the following:

- Central (compression of the medial portion of the spinal cord) (**Fig. 6.20**)
- Posterolateral (compression of the lateral portion of spinal cord and nerve root) (**Fig. 6.21**)
- Lateral (compression of the nerve root only) (**Fig. 6.22**)

The nomenclature used to describe cervical disc displacements varies widely among radiologists and

clinicians. Although a task force has provided formal guidelines for the description of lumbar disc pathology⁵⁹ (see Chapter 7, The Thoracic and Lumbar Spine), similar guidelines have not been widely adopted for the cervical spine. The terms *bulge*, *protrusion*, *extrusion*, and *sequestration* are commonly used to describe cervical disc pathology (**Table 6.3**). It should be noted that the anatomy of the cervical facet joints (which are located more laterally than those in the lumbar spine) essentially makes them the posterior wall of the intervertebral nerve root canals, and there is no subarticular recess in the cervical spine. Thus, disc herniation positions in the cervical spine are described as central, paracentral (left or right), foraminal, and far lateral.

With regard to the size of the disc abnormality, it may be more important to note the degree of mass effect on neural structures than the size of the abnormality itself. For example, a small protrusion in a person with developmental spinal stenosis will be more likely to produce symptoms than a similar protrusion in a patient with a capacious spinal canal.

In addition to an evaluation of the level, direction, and configuration of disc displacement, the MRI study should also be scrutinized for the presence or

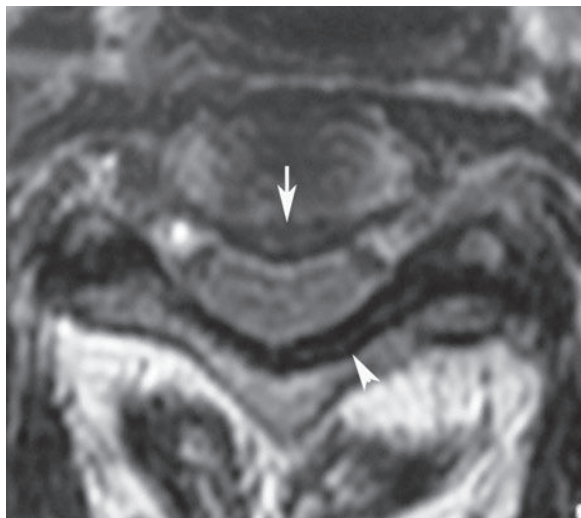


Fig. 6.20 An axial T2-weighted image at the C5-C6 level shows a central disc bulge (*arrow*) with moderate stenosis. The disc bulge and ligamentum flavum hypertrophy (*arrowhead*) act to produce effacement of the ventral and dorsal CSF spaces and deformity of the spinal cord.[†]

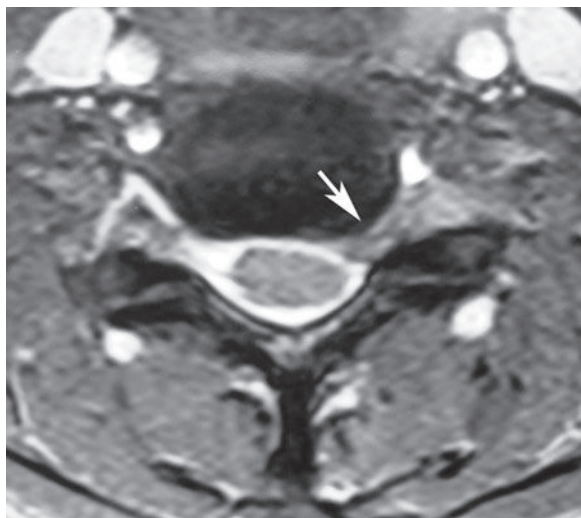


Fig. 6.22 An axial T2-weighted image at the C5-C6 level shows a lateral or foraminal disc protrusion (*arrow*) on the left side, which produces severe foraminal stenosis and compresses the nerve root. Note that the signal is different from that of the bone.[†]

absence of areas of calcium deposition, anterior or posterior osteophyte formation, and vertebral endplate changes.^{54,55,60,61} These findings should be correlated with the findings seen on lateral and oblique cervical spine radiographs.

Additional scrutiny of the imaging findings also enables the surgeon to determine whether a cervical disc protrusion can be classified as a “soft” (rela-

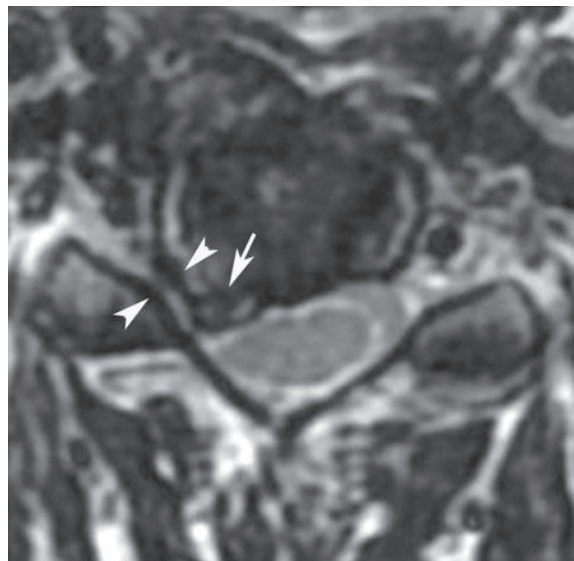


Fig. 6.21 An axial T2-weighted image at the C5-C6 level shows a right posterolateral disc protrusion with associated uncovertebral joint hypertrophy (*arrow*), which produces mild deformity of the right side of the spinal cord and severe foraminal stenosis (between *arrowheads*). Note the normal size of the neural foramen on the left side.[†]

tively well-hydrated) or “hard” (poorly hydrated) disc (**Fig. 6.23**). This information may help in determining whether an anterior or posterior approach is chosen for the treatment of a patient with unilateral cervical radiculopathy. Such a determination can be made by reviewing the images for increased T2-weighted signal within the displaced disc, which would be expected in a patient with a soft disc herniation. Conversely, a hard disc herniation shows low signal on T2-weighted images and may also show associated osteophytes on gradient-echo and other pulse sequences. This combination of hard disc disease and associated osteophyte is often referred to as a *disc-ridge complex* and may preclude the performance of a posterior keyhole foraminotomy and discectomy for the treatment of a patient with unilateral radiculopathy.

The findings on MR images should be used to differentiate cervical disc disease and protrusions from ossification of the posterior longitudinal ligament. On most MR images showing cervical stenosis secondary to disc displacement (for example, **Figs. 6.15** and **6.18**), the pathology and stenosis is based at the level of the disc, and stenosis is seen only behind the vertebral body in cases of disc extrusion and migration (**Fig. 6.24**). Conversely, MRI in patients with ossification of the posterior longitudinal ligament shows stenosis at the level of the disc and also along the course of the posterior longitudinal ligament, which runs along the posterior aspect of the vertebral bodies (**Fig. 6.25**).⁶²

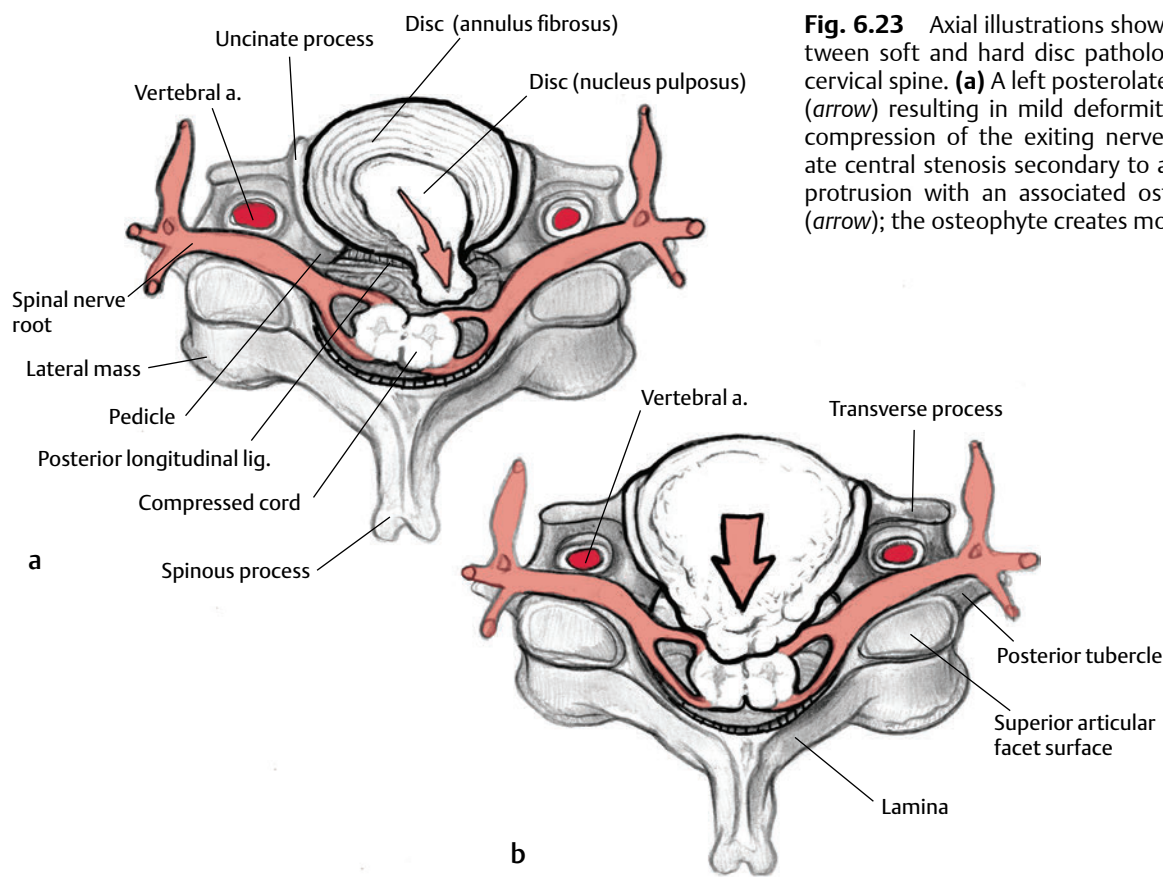


Fig. 6.23 Axial illustrations show the difference between soft and hard disc pathology in the subaxial cervical spine. **(a)** A left posterolateral disc protrusion (arrow) resulting in mild deformity of the cord and compression of the exiting nerve root. **(b)** Moderate central stenosis secondary to a large central disc protrusion with an associated osteophyte complex (arrow); the osteophyte creates most of the stenosis.[†]

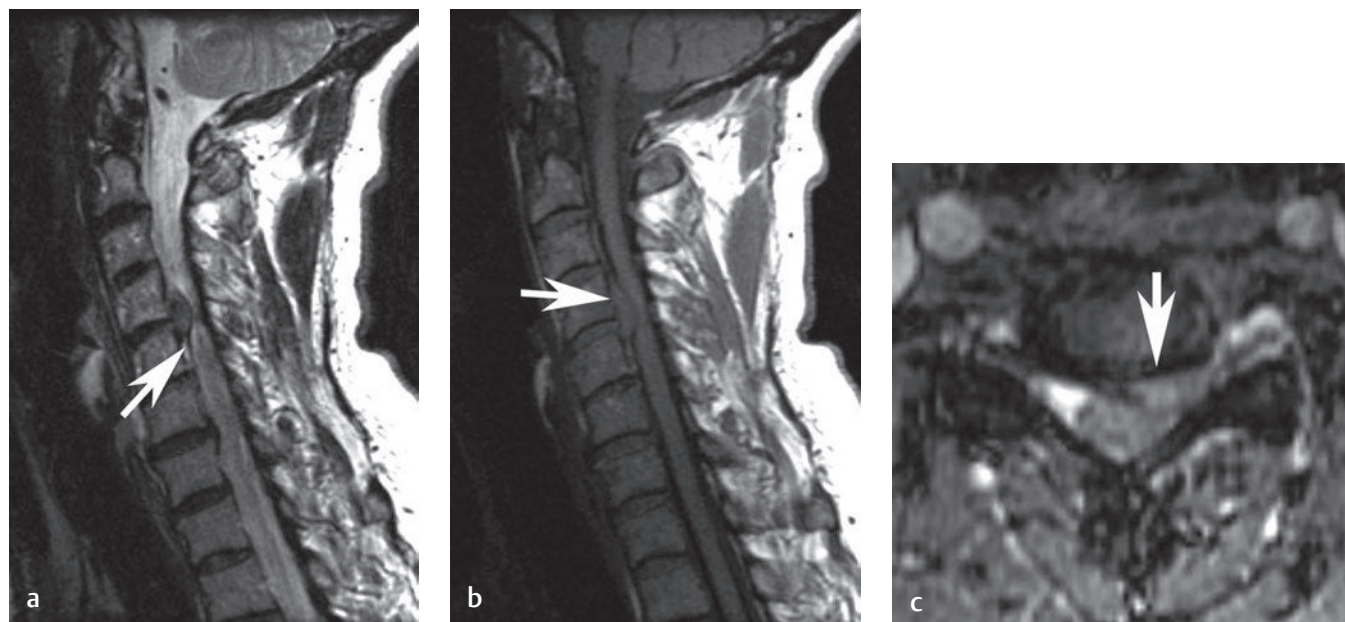


Fig. 6.24 Cervical disc extrusion. **(a)** A sagittal T2-weighted image shows a large disc extrusion at the C4-C5 level (arrow) that has migrated proximally, tenting the posterior longitudinal ligament. **(b)** A sagittal T1-weighted image shows the disc extrusion at the C4-C5 level (arrow) that is isointense to the intervertebral disc. **(c)** An axial T2-weighted image shows a left paracentral disc extrusion (arrow), which produces severe foraminal stenosis and deformity on the left side of the cord.[†]

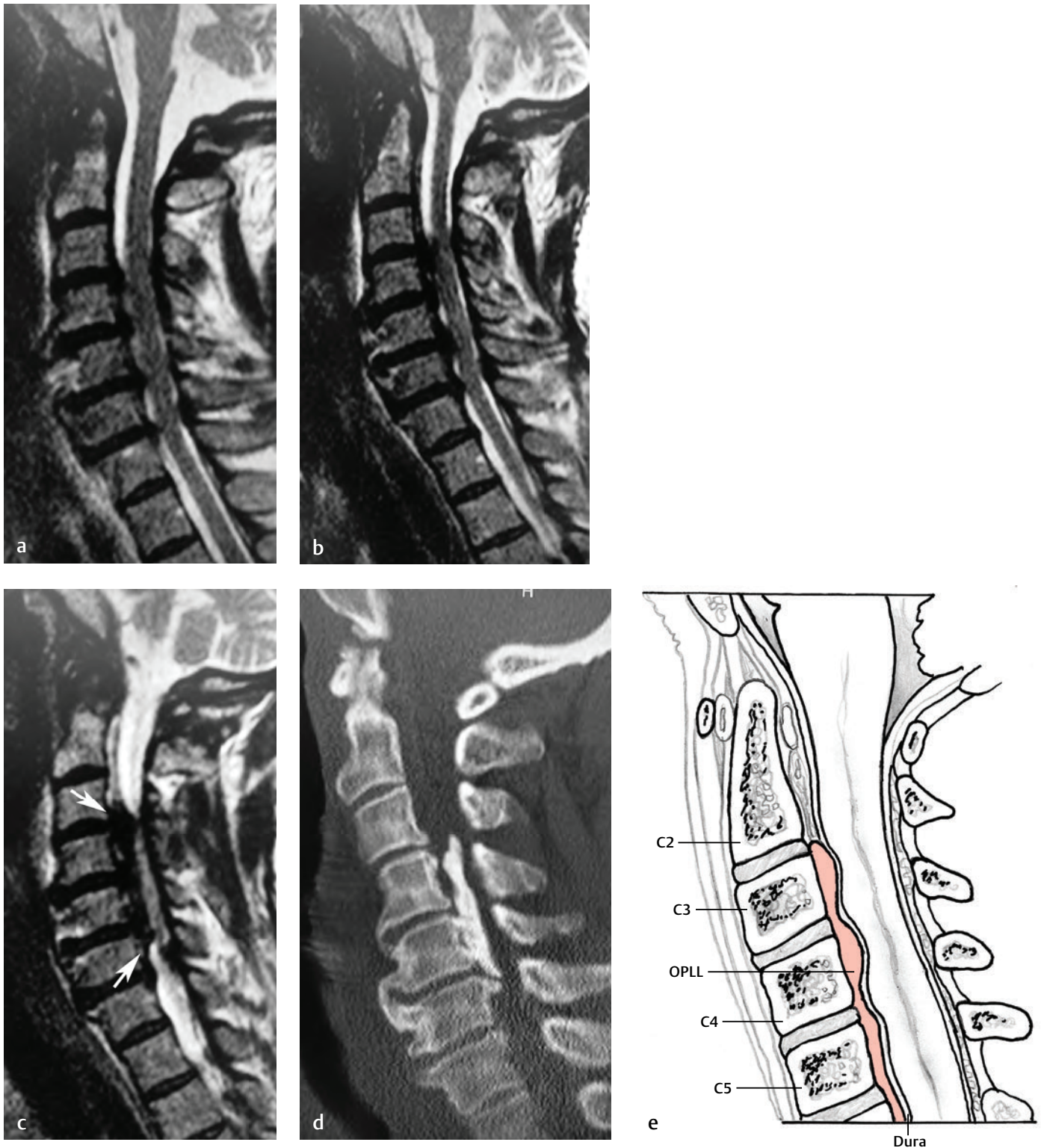


Fig. 6.25 Ossification of the posterior longitudinal ligament (OPLL). **(a)** A midline sagittal T2-weighted image shows multilevel degenerative disc disease and moderate stenosis from C3-C4 to C6-C7. The stenosis appears to be centered at the level of the disc spaces on this midline image.[†] **(b)** A parasagittal T2-weighted image, obtained a few millimeters lateral to the midline, suggests that the posterior longitudinal ligament is thickened and that the stenosis is present at the level of the vertebral bodies and discs from C3 to C7.[†] **(c)** A parasagittal T2-weighted image, obtained farther from the midline, shows that the posterior longitudinal ligament is markedly hypertrophied and nearly fills the spinal canal (*between arrows*).[†] **(d)** A parasagittal reconstructed CT image, obtained at the same level as **(c)**,[†] and **(e)**, corresponding artist's sketch, show ossification of the posterior longitudinal ligament extending from C3-C4 to C5-C6.

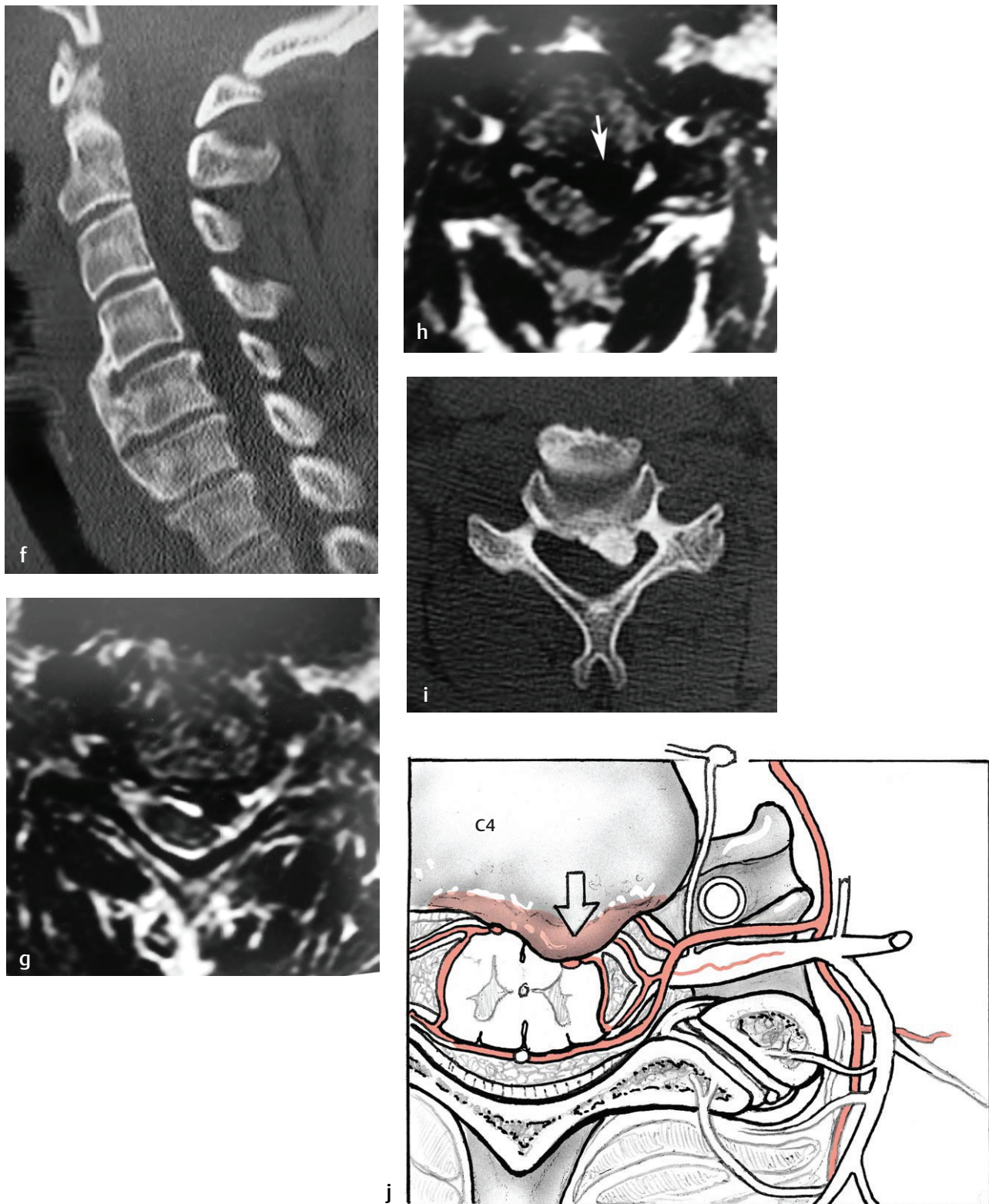


Fig. 6.25 (Continued) (f) A midline sagittal reconstructed CT image shows anterior osteophyte formation but no substantial canal stenosis.[†] (g) An axial T2-weighted image at the level of the C4-C5 disc shows similar findings.[†] (h) An axial T2-weighted image shows severe left paracentral stenosis secondary to what appears to be a disc protrusion (arrow) but is actually a focal region of ossification of the posterior longitudinal ligament at the level of the C4 vertebral body.[†] (i) An axial CT image, obtained at the same level as (h),[†] and (j), corresponding artist's sketch, shows that what appears to be a disc protrusion on MRI is actually a focal region of ossification.

In patients with suspected ossification of the posterior longitudinal ligament, CT imaging can be obtained to rule in or rule out this diagnosis, given that it provides optimal visualization of calcification and osseous detail. The importance of this differentiation lies in the fact that anterior decompression for patients with ossification of the posterior longitudinal ligament tends to be difficult and is associated with higher rates of durotomy and bleeding, and therefore surgeons may prefer to proceed with posterior decompression even though the primary compression is located ventral to the spinal cord.

Spinal Stenosis

The term *spinal stenosis* describes the compression of the neural elements in the spinal canal, lateral recesses, or neural foramina (**Fig. 6.26**). Spinal stenosis can develop from congenital or acquired causes (**Table 6.4**); patients can also develop degenerative stenosis superimposed on preexisting congenital stenosis (**Fig. 6.27**).

Foraminal stenosis may be caused by a disc herniation or uncovertebral or facet joint hypertrophy. Central canal stenosis is most often caused by a combination of two or more of the following (**Fig. 6.28**):

- Disc bulge or herniation
- Uncovertebral joint osteophyte formation
- Ligamentum flavum hypertrophy
- Facet arthrosis
- Thickening, calcification, or ossification of the posterior longitudinal ligament or other structures

On MRI, central canal stenosis is characterized by compression of the thecal sac, best seen on the sagittal and axial T2-weighted images. Such images provide a “myelographic effect,” in which the CSF is seen as bright signal anterior and posterior to the spinal cord on sagittal images and circumferentially around the spinal cord on axial images. Effacement, discontinuity, or displacement of this CSF space is seen in patients with focal and concentric spinal stenosis.

The degree of central canal stenosis can range from mild encroachment on the ventral subarachnoid space

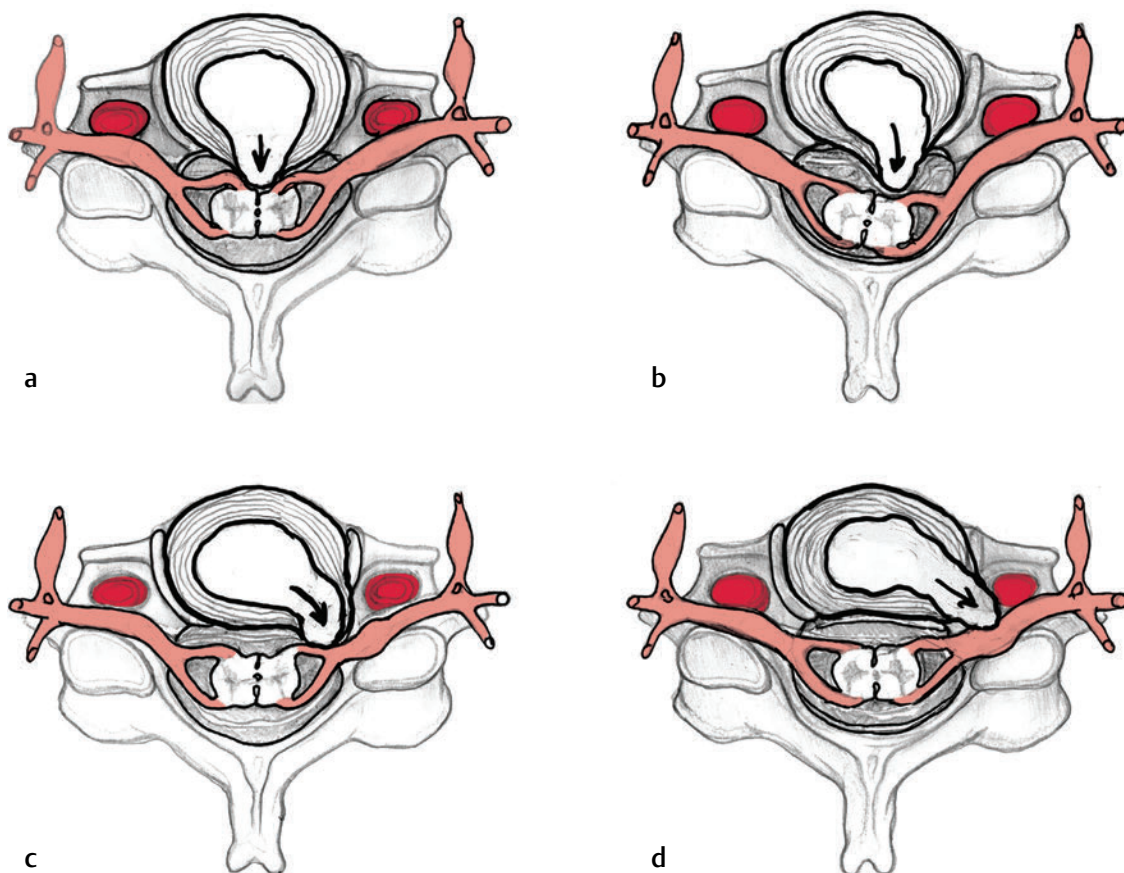


Fig. 6.26 Artist's sketches show four types of disc herniations in the cervical spine: (a) central, (b) posterolateral, (c) lateral recess, and (d) foraminal.[†]

Table 6.4 Acquired and congenital factors associated with spinal stenosis

Type	Factor
Acquired	Intervertebral disc pathology
	Uncovertebral joint hypertrophy
	Facet joint hypertrophy
	Ligamentous origin (ligamentum flavum hypertrophy/ossification, ossification of the posterior longitudinal ligament, diffuse idiopathic skeletal hyperostosis)
	Spondylosis
	Metabolic causes
	Postinflammatory pathology
	Spondylolisthesis
	Postoperative pathology
	Neoplasm
Congenital	Idiopathic stenosis with short pedicles
	Skeletal growth disorders
	Down syndrome
	Achondroplasia
	Mucopolysaccharidosis
	Scoliosis

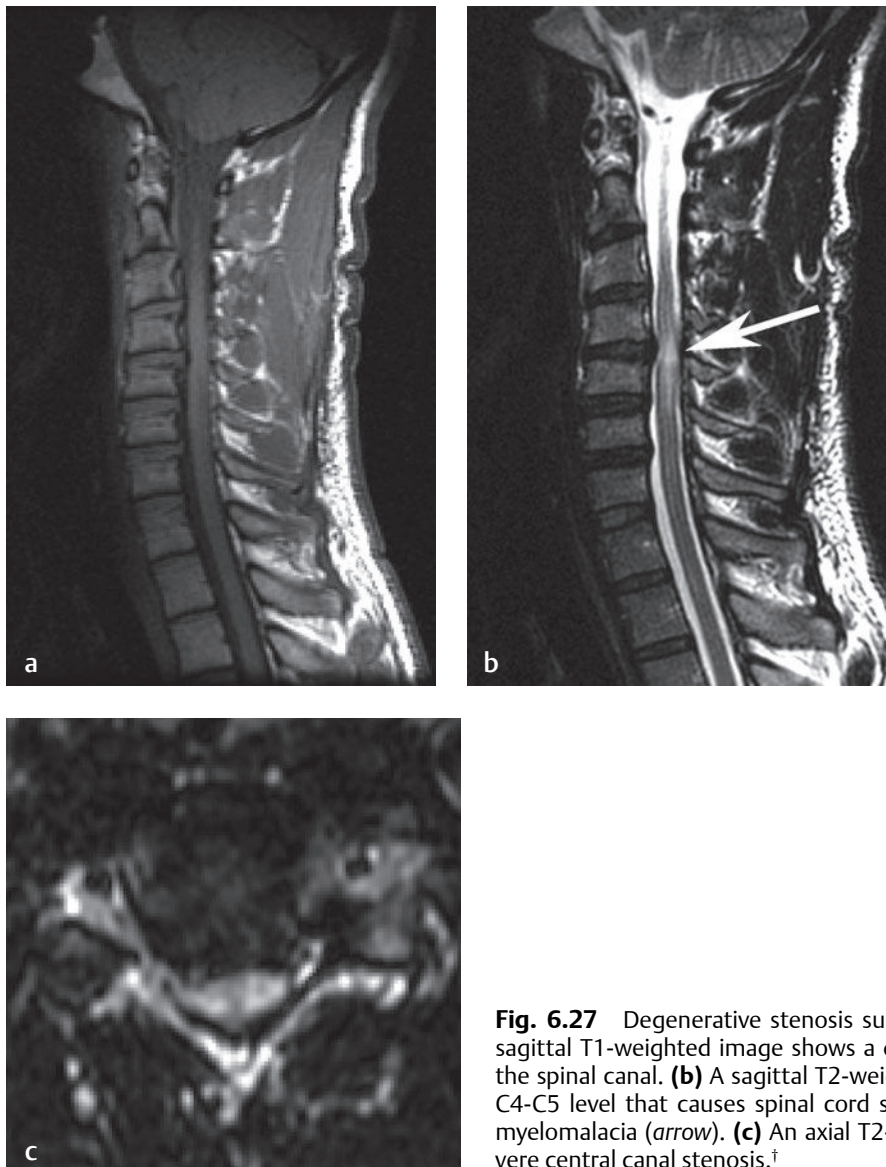


Fig. 6.27 Degenerative stenosis superimposed upon congenital stenosis. **(a)** A sagittal T1-weighted image shows a developmentally shortened AP dimension of the spinal canal. **(b)** A sagittal T2-weighted image shows a small disc bulge at the C4-C5 level that causes spinal cord signal abnormality, representing spondylotic myelomalacia (arrow). **(c)** An axial T2-weighted image shows the moderate to severe central canal stenosis.[†]

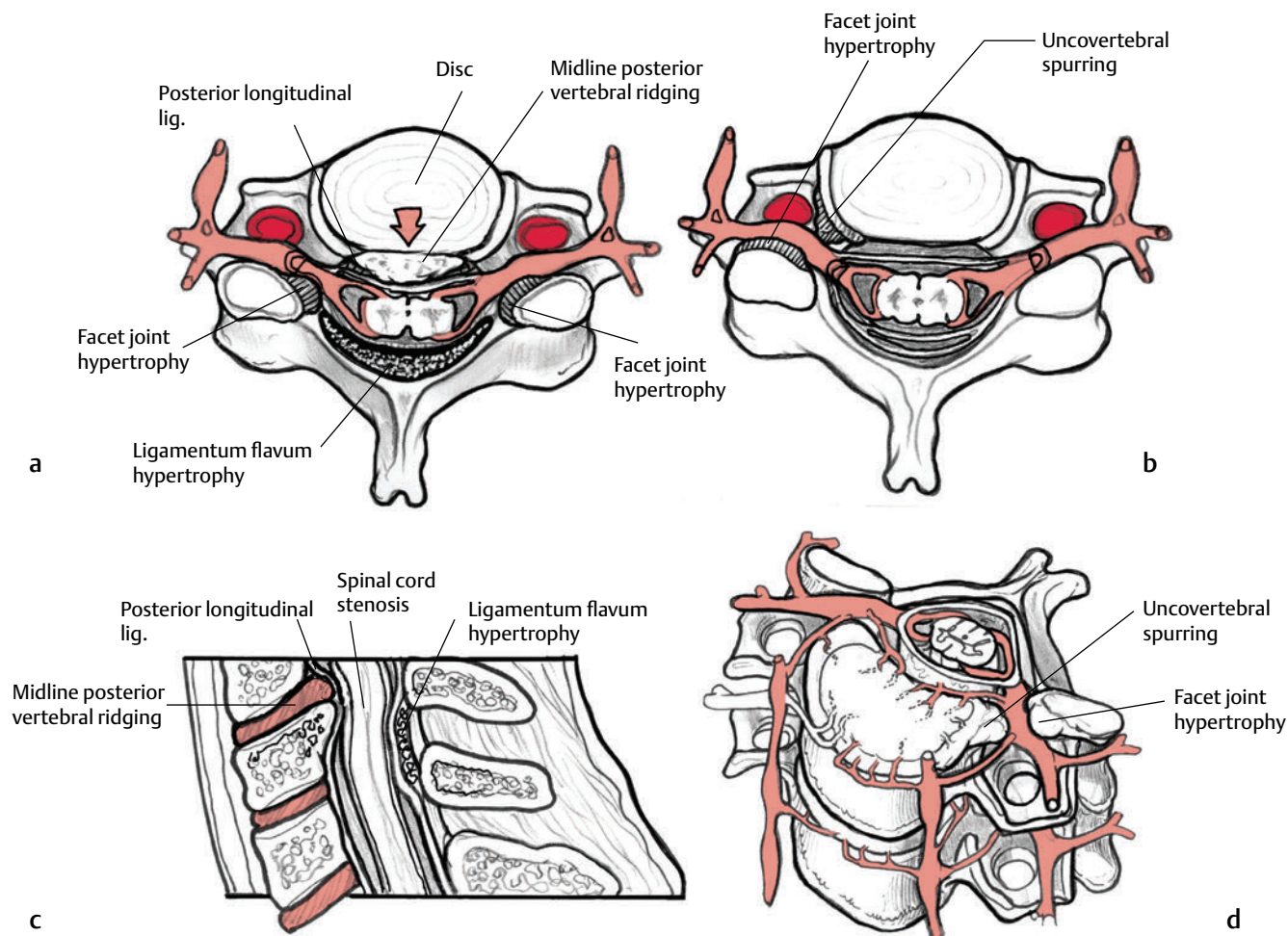


Fig. 6.28 Artist's sketches show various potential contributors to cervical spinal stenosis: central disc bulge, facet joint hypertrophy, and ligamentum flavum hypertrophy. **(a)** An axial view shows central stenosis. **(b)** An axial view shows foraminal stenosis. **(c)** A lateral view shows central stenosis with cord compression. **(d)** A 3D superolateral view shows foraminal stenosis.[†]

to severe compression and flattening of the spinal cord with myelomalacia. MRI findings may correspond to the severity and duration of the compression.⁵⁴ Early changes of spinal cord compression can be seen as cord edema (high signal areas on T2-weighted images); progressive compression may cause spinal cord necrosis and atrophy (**Fig. 6.29**), cystic degeneration, and syrinx formation (low signal on T1-weighted and high signal on T2-weighted images).⁵⁴

Given that the great majority of cervical spine MRI studies are obtained to evaluate for the presence, location, and degree of degenerative cervical spinal stenosis, one should have a systematic approach to the evaluation of these studies. The authors' suggested approach for the evaluation of a cervical spine MRI study (see Chapter 4, A Systematic Approach to the Review of Spine MRI Studies) includes a critical evaluation of the degree of spinal cord and nerve root compression on the sagittal, parasagittal, and axial T2-weighted images. The midline sagittal T2-

weighted images provide a global view of the levels and degree of effacement of the CSF column and spinal cord compression, whereas the parasagittal images enable visualization of lateral recess and foraminal stenosis (**Fig. 6.30**). The information from these images should be correlated with that from the axial images, which show the same pathology in an orthogonal plane.

There are several objective measures of cervical spinal stenosis. Relative stenosis is defined as an AP canal diameter of <13 mm, and absolute stenosis is defined as an AP canal diameter of <10 mm. The Torg or Pavlov ratio is calculated by dividing the AP canal diameter by the AP vertebral body diameter, with a ratio <0.8 defined as stenotic.⁶³ This ratio is often used to evaluate for congenital stenosis in athletes. Although such definitions are well known, most clinicians and radiologists tend to grade the degree of spinal stenosis using the terms *mild*, *moderate*, and *severe*, and gradations such as *moderate-severe*. The

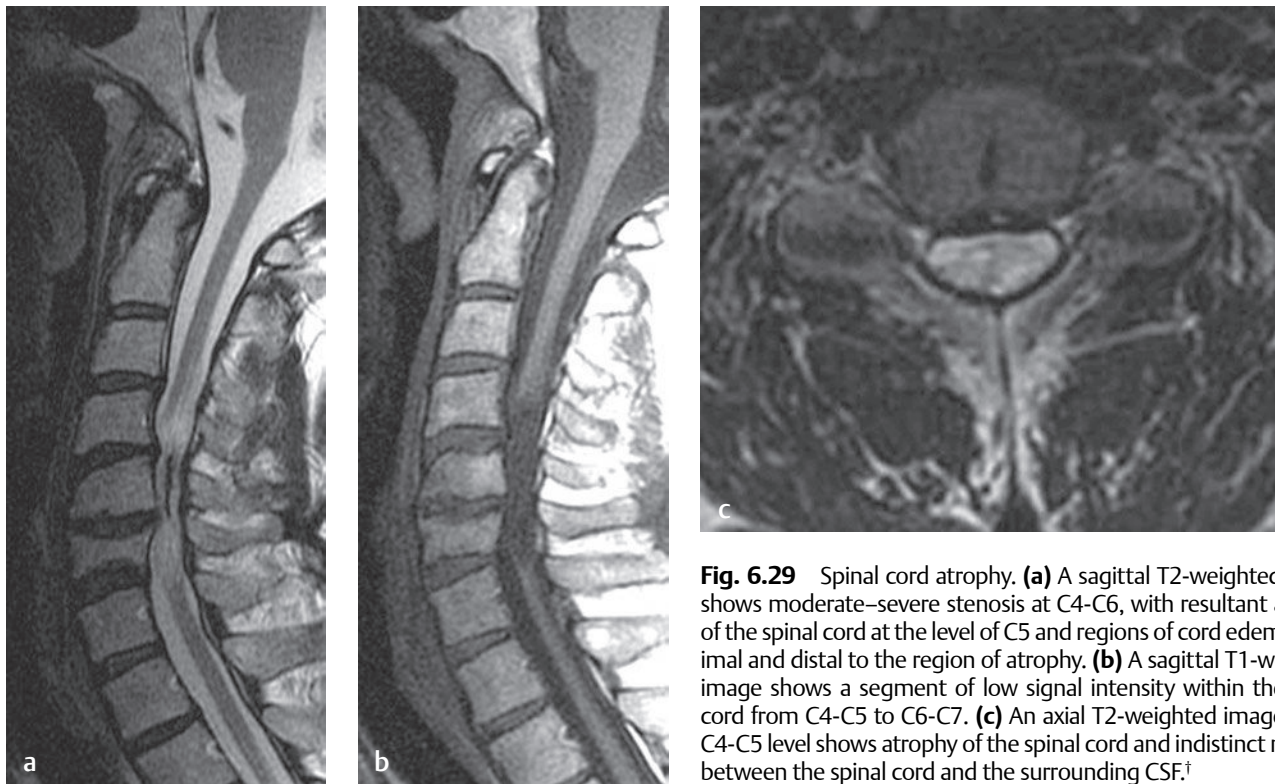


Fig. 6.29 Spinal cord atrophy. **(a)** A sagittal T2-weighted image shows moderate-severe stenosis at C4-C6, with resultant atrophy of the spinal cord at the level of C5 and regions of cord edema proximal and distal to the region of atrophy. **(b)** A sagittal T1-weighted image shows a segment of low signal intensity within the spinal cord from C4-C5 to C6-C7. **(c)** An axial T2-weighted image at the C4-C5 level shows atrophy of the spinal cord and indistinct margins between the spinal cord and the surrounding CSF.[†]

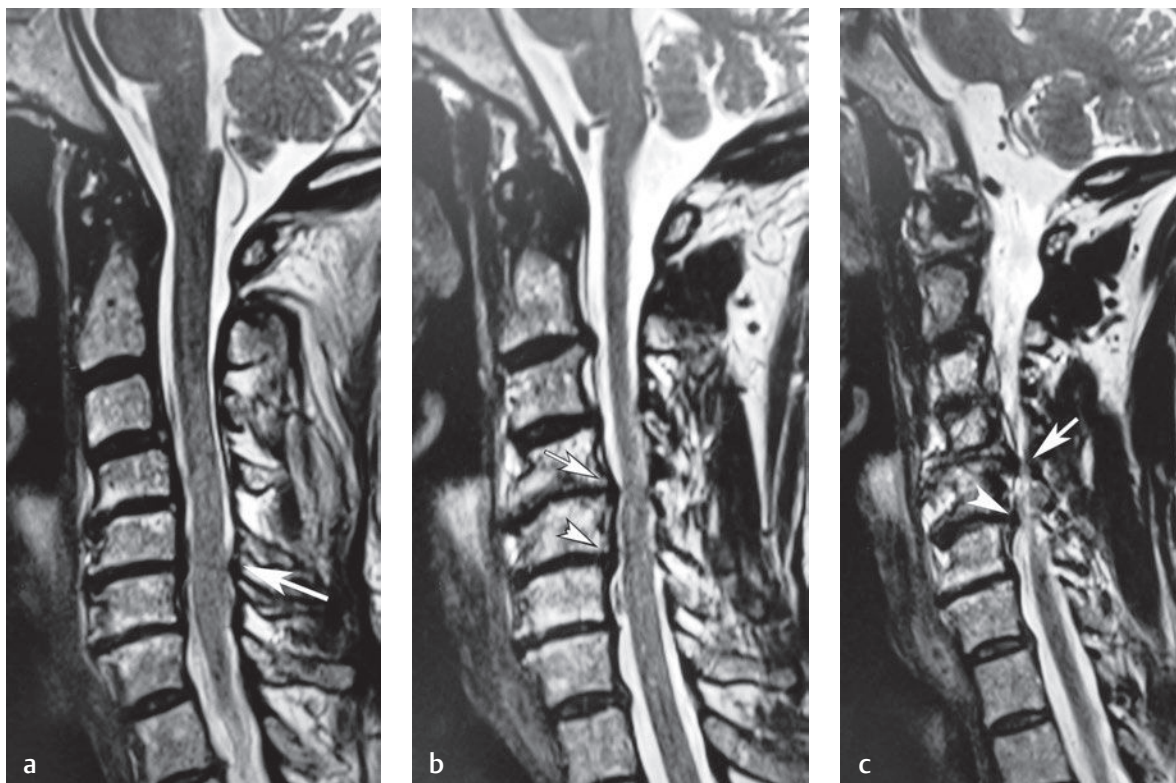


Fig. 6.30 Cervical stenosis. **(a)** A midline sagittal T2-weighted image shows multilevel degenerative disc disease with mild spondylolisthesis at C3-C4 and thickening of the posterior longitudinal ligament at multiple levels. There is focal thickening of the ligamentum flavum at the C5-C6 level (*arrow*). **(b)** A parasagittal T2-weighted image obtained several millimeters lateral to the midline shows effacement of the ventral CSF space and moderate stenosis at the C4-C5 level (*arrow*) due to osteophyte formation and thickening of the posterior longitudinal ligament. Similar, but less severe, changes are seen at the C5-C6 level (*arrowhead*). **(c)** A parasagittal T2-weighted image obtained farther laterally in the plane of the neuroforamina shows severe foraminal stenosis at the C4-C5 level (*arrow*) and moderate foraminal stenosis at the C5-C6 level (*arrowhead*).[†]

authors tend to use the following terms and definitions (**Figs. 6.31** and **6.32**):

- Mild—stenosis occupying less than one third of normal canal dimension, in which the ventral and dorsal CSF spaces are partially effaced by disc bulging, ligamentum flavum hypertrophy, and facet arthropathy; no mass effect on the cord
- Moderate—stenosis occupying between one third and two thirds of normal canal dimension; findings similar to those of mild stenosis but with compression and minimal flattening and deformity of the spinal cord
- Severe—stenosis occupying more than two thirds of normal canal dimension, with very pronounced flattening and deformity of the spinal cord that is obvious on both sagittal and axial T2-weighted images

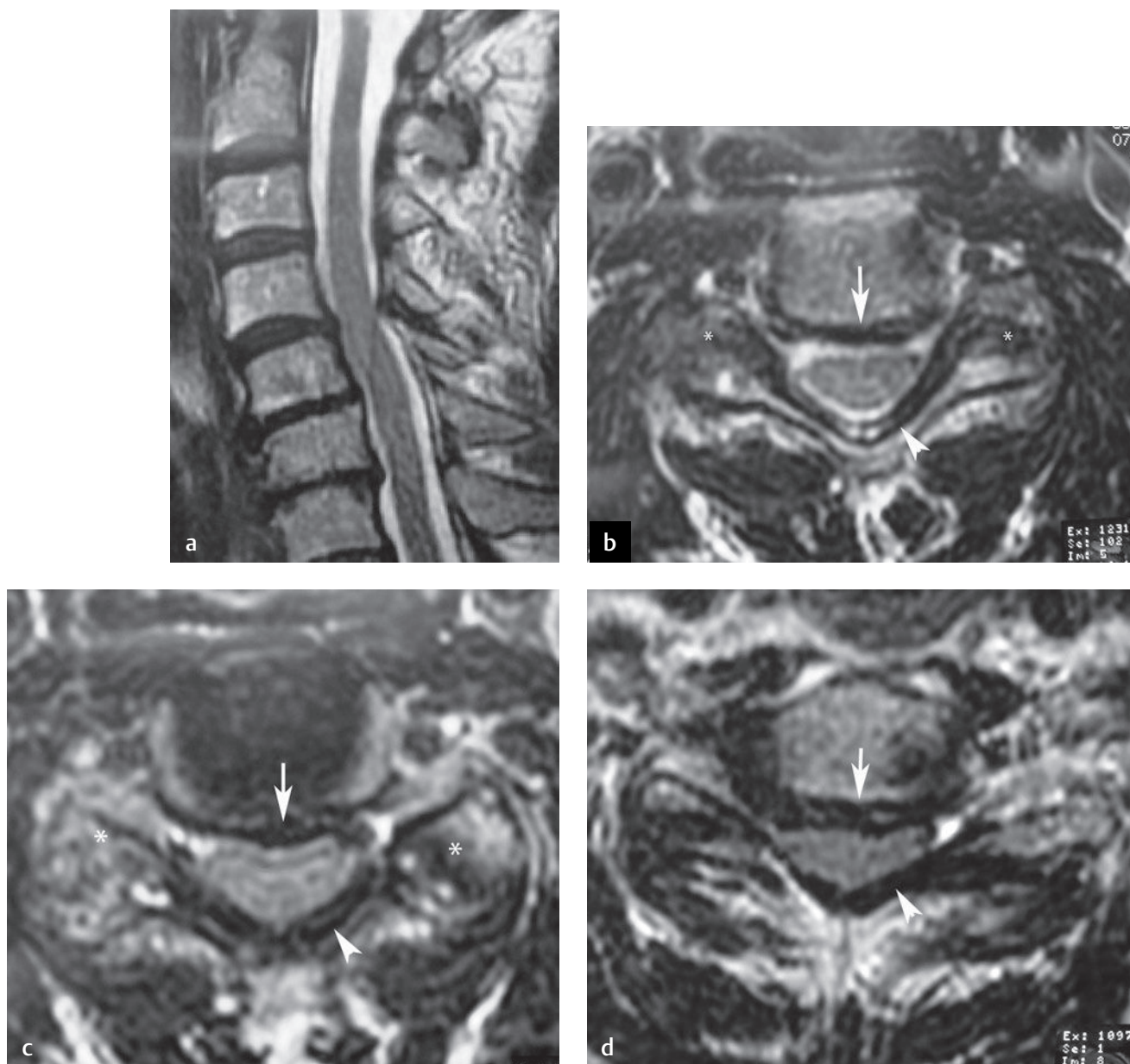


Fig. 6.31 Grading of cervical stenosis: mild to moderate-severe. **(a)** A sagittal T2-weighted image shows minimal spondylolisthesis at C4-C5 with **moderate** stenosis at this level. **(b)** An axial T2-weighted image at the C5-C6 level shows **mild** stenosis secondary to a central disc bulge (*arrow*), ligamentum flavum hypertrophy (*arrowhead*), and facet arthropathy (*asterisk*). **(c)** An axial T2-weighted image at the C4-C5 level shows **moderate** stenosis secondary to more substantial central disc bulge (*arrow*), ligamentum flavum hypertrophy (*arrowhead*), and facet arthropathy (*asterisk*). **(d)** An axial T2-weighted image (different patient) shows **moderate-severe** stenosis at the C5-C6 level as a result of even greater central disc bulge (*arrow*) and ligamentum flavum hypertrophy (*arrowhead*).[†]

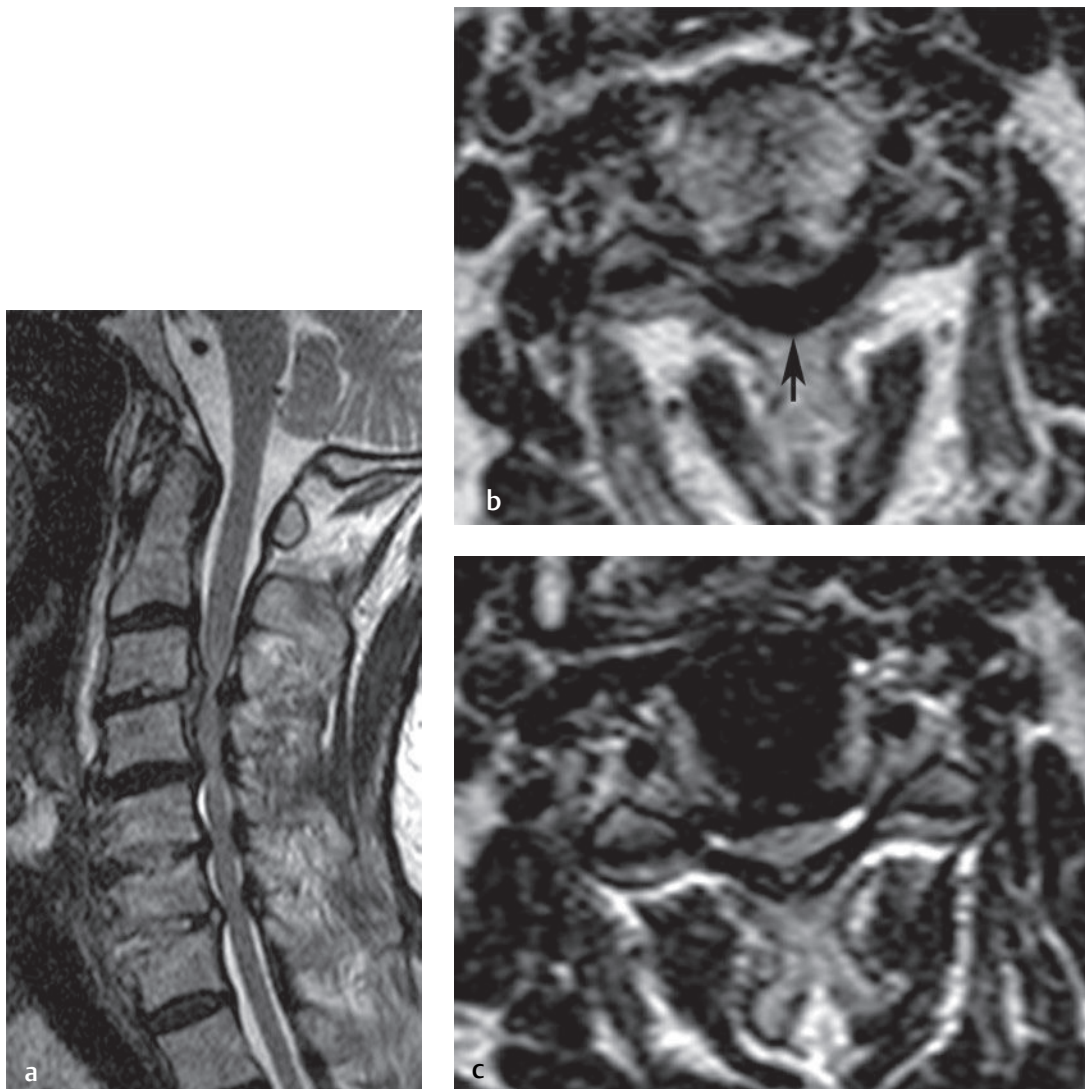


Fig. 6.32 Grading of cervical stenosis: severe. **(a)** A sagittal T2-weighted image shows **severe** stenosis at the C3-C4 level and **moderate to moderate-severe** stenosis at the C4-C5, C5-C6, and C6-C7 levels. **(b)** An axial image at the C3-C4 level shows **very severe** stenosis with complete obliteration of the CSF space and compression of the spinal cord to an AP diameter of 2 mm secondary to a central disc bulge and severe ligamentum flavum hypertrophy (*arrow*). **(c)** An axial T2-weighted image at the C4-C5 level shows **severe**, but less severe than in **(b)**, stenosis with compression and deformity of the spinal cord with minimal CSF seen in the lateral recesses bilaterally. (Images courtesy of Mesfin A. Lemma, MD.)[†]

RA

RA is a systemic disease that causes inflammation of synovial joints. The synovial joints develop pannus secondary to erosion of supporting ligamentous structures and the associated instability.⁶⁴⁻⁶⁶ In the cervical spine, this condition may affect the craniocervical junction as well as the subaxial cervical spine, as described subsequently.⁶⁴⁻⁶⁸ Most commonly, atlantoaxial instability develops secondary to erosion of the ligaments at the OCJ.^{64,65} As the disease progresses, erosion of the lateral masses of C1, the occipital condyles, and facets of C2 occurs, resulting in cranial settling.⁶⁴⁻⁶⁶ As the odontoid process be-

gins to occupy a relatively more rostral position, it compresses the brainstem and verteobasilar system. This pathologic process is postulated by some as the etiology of sudden death in those with advanced RA.^{64-66,69} It is important to note that in contrast to other disorders, the C1 arch migrates with the skull base to lie in a more caudal position.⁶⁶ In some cases, it has been reported to be as inferior as the C2-C3 disc space.^{64-66,70} Two studies reported on the use of MRI to measure the space available for the cord as a technique for predicting recovery after cervical stabilization for patients with RA and atlantoaxial instability.^{64,65} A cord space, or space available for the cord, of >14 mm on MRI was associated with

better clinical outcomes than was a space of <10 mm, which was associated with a poor prognosis.^{64,65} Flexion-extension MRI is particularly useful for evaluating patients with RA and specifically those with instability at the OCJ and suboccipital cervical spine (**Fig. 6.33**), especially because supine extension MRI does not account for the commonly occurring subluxations in such patients that are exaggerated with movement. Similar information can be obtained by combining the information obtained from a static (conventional) MRI study and flexion-extension cervical spine radiographs (**Fig. 6.13**).

MRI can detect pannus formation in the cervical spine well before conventional radiographic signs become evident. In addition, involvement of the facet joints (inflammation, edema, and fusion)

may be detected on MRI. Patients with RA may also present with a rheumatoid discitis that manifests as increased T2-weighted and decreased T1-weighted signal in the disc. The substantial differences between imaging and clinical features of RA in the spine have been documented and are well known.^{71,72}

■ Infectious Conditions

The treatment of spinal infections continues to be a challenge despite advances in imaging, diagnostic testing, and antimicrobial therapy. A delay in diagnosis is common because spinal infections often have an early indolent course and early symptoms may be

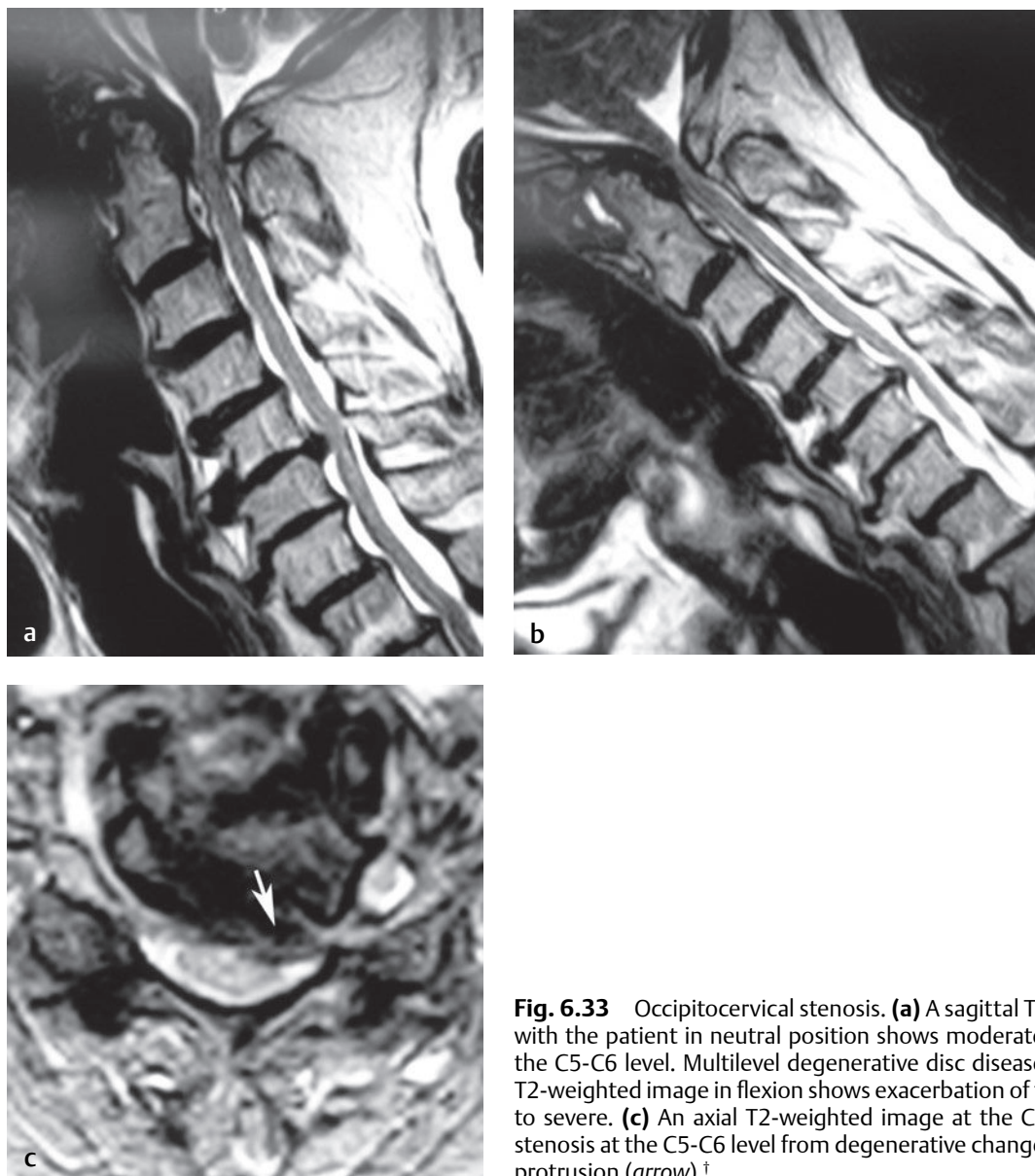


Fig. 6.33 Occipitocervical stenosis. **(a)** A sagittal T2-weighted image obtained with the patient in neutral position shows moderate stenosis at the OCJ and at the C5-C6 level. Multilevel degenerative disc disease is also seen. **(b)** A sagittal T2-weighted image in flexion shows exacerbation of the occipitocervical stenosis to severe. **(c)** An axial T2-weighted image at the C5-C6 level shows moderate stenosis at the C5-C6 level from degenerative changes and a left paracentral disc protrusion (arrow).[†]

nonspecific (e.g., neck pain, muscle spasm), leading to a misdiagnosis of more common spinal ailments (e.g., muscle strain, degenerative disease). Spine infections may involve the vertebral body, posterior elements, intervertebral discs, epidural space, subdural space, subarachnoid space, or the spinal cord.

Cervical Vertebral Osteomyelitis and Discitis

Infections of the cervical spine account for ~10% of spine infections and are less common than thoracic (~40%) or lumbar (~50%) spine infections.⁷³ Anatomic differences between the cervical and thoracolumbar spine (smaller canal diameter relative to the size of the spinal cord, intervertebral discs, and epidural space, and a vast venous plexus) may allow cervical spine infections to have a more aggressive and rapid progression that requires expedited treatment.⁷⁴ In general, the clinical presentation of vertebral osteomyelitis and discitis has variable signs and symptoms, including fever (~50% of the time), weight loss, and neck or back pain, that do not vary with activity level. Neurologic symptoms may vary based on the level of spinal involvement, spinal cord compression, spinal instability, or deformity.^{20,21,73–76} Neurologic deficits secondary to spinal infection are more common in patients >50 years old and in those with comorbidities such as diabetes, RA, and immunodeficiency.^{20,73}

Bacterial inoculation of the spine may occur through hematogenous seeding, direct inoculation, or contiguous spread from local infection. *Staphylococcus aureus* is the most commonly cultured organism causing cervical osteomyelitis and discitis.^{73,74} It is found in 50% to 65% of culture-positive cases and accounts for >80% of pediatric spinal infections.⁷⁷ Gram-negative infections (*Escherichia coli*, *Pseudomonas*, *Proteus*) may occur after genitourinary infections. Immunocompromised patients are susceptible to infections with atypical pathogens such as *Aspergillus*, *Candida*, *Nocardia asteroides*, and *Mycobacterium*. *Pseudomonas* infections may occur in intravenous drug abusers. Children with sickle cell disease may develop spine infections secondary to *Salmonella*.

Isolated discitis is common in the pediatric population because vascularity extends through the cartilaginous growth plate into the nucleus pulposus, allowing direct deposition of bacteria into the disc center. In adults, blood vessels reach only the annulus fibrosus, limiting bacterial deposition to the vertebral body metaphysis and end plate. In adult infections, intervertebral disc destruction may occur through bacterial proteolytic enzyme infiltration.

MRI is the imaging modality of choice for the diagnosis and evaluation of spinal infections and for

monitoring the response to treatment.⁷⁴ High sensitivity (96%), specificity (93%), and accuracy (94%) have been reported for the MRI diagnosis of vertebral osteomyelitis.⁶⁰ MRI is more sensitive than conventional radiographs or CT and more specific than nuclear scintigraphy in identifying vertebral osteomyelitis.⁷⁴ Infectious spondylitis may present with findings such as low T1-weighted signal with or without high T2-weighted signal (high signal is often more evident on fat-suppressed T2-weighted or STIR images); increased T2-weighted signal within the intervertebral disc; contrast enhancement in the disc, subchondral marrow, and epidural space; erosion of end plates; epidural fluid collections; paraspinal soft-tissue abnormalities; and posterior element involvement^{20,74,76,78} (Fig. 6.34). Unfortunately, these imaging characteristics are the same as those of many spine pathologies, including neoplastic disease. One can differentiate infection from other processes affecting the vertebral body bone marrow by noting that the epicenter of the former pathology tends to be at the intervertebral disc. Conversely, neoplastic processes tend to have their epicenters within the vertebral body, and the edema tends not to cross the intervertebral disc. In addition, the vertebral end plate may have an irregular appearance because of infectious destruction, and disc height loss or collapse may occur with progressive infection. On gadolinium-enhanced images, disc enhancement is an essential factor for the diagnosis of discitis, and enhancement of the vertebral subchondral bone may indicate a well-established and chronic infection.^{20,74,76}

In comparison with other bacterial infections, *Mycobacterium tuberculosis* infection of the spine has some distinct differences:

- Intervertebral discs are damaged less or completely spared and may not show signal enhancement on T2-weighted images.⁷⁴
- Tuberculous spondylodiscitis is a slow-growing process that often results in marked collapse of the vertebral bodies.
- Subligamentous spread of infection is often observed.
- Telescoping of one vertebral body disc into an adjacent level may be seen.

Gadolinium-enhanced MRI also is essential for monitoring the efficacy of treatment of vertebral infection.⁷⁹ With appropriate treatment of the infection, a regression of the T2-weighted signal hyperintensity is observed.⁷⁶ Scar formation within the intervertebral disc is seen as a region of low signal intensity. A region of mottled signal intensity may also develop within the area of previous infection with associated contrast enhancement. Over time, osteophytic bridging may occur, followed by segmental

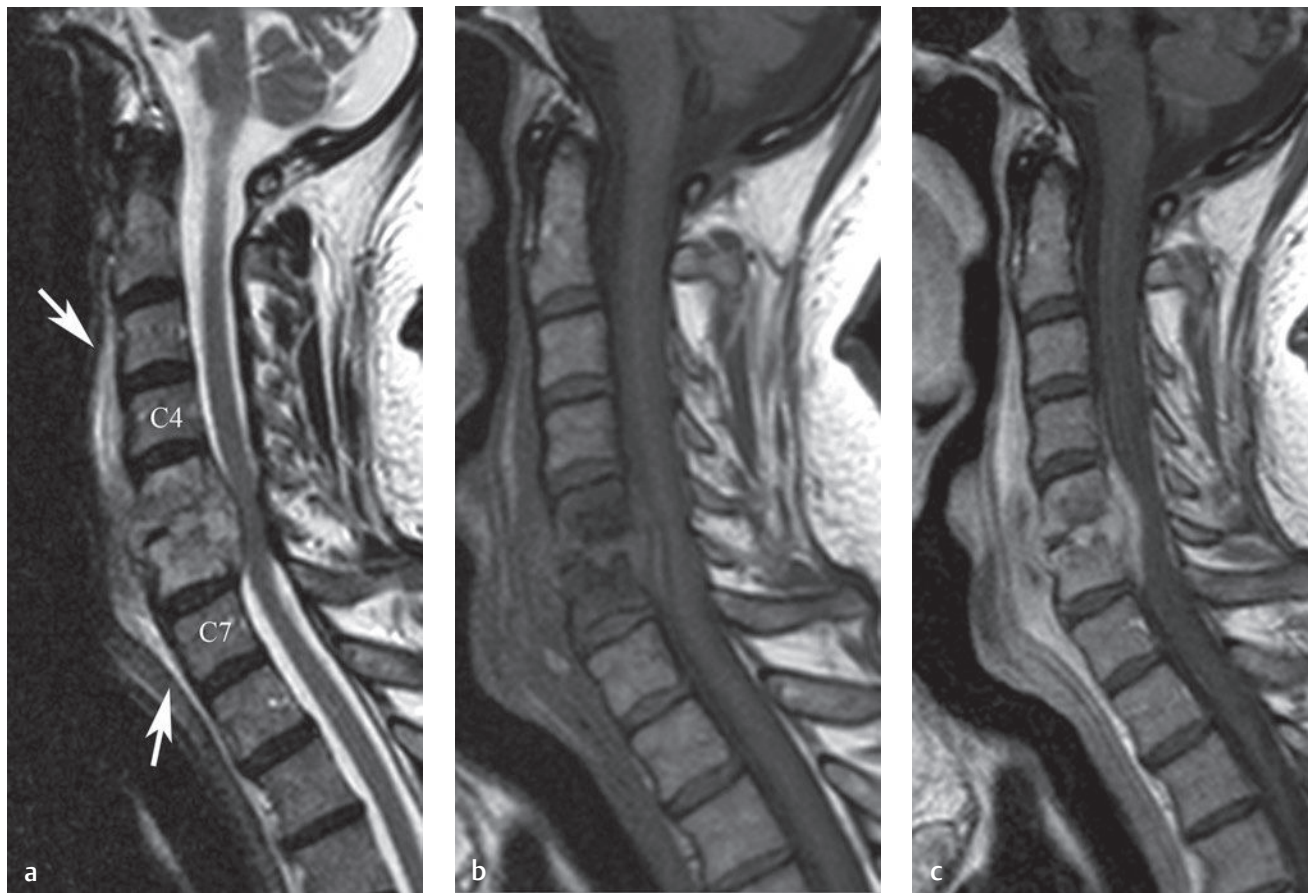


Fig. 6.34 Cervical spine discitis and osteomyelitis. **(a)** A sagittal T2-weighted image shows obliteration of the C5-C6 disc space with associated edema in the C5-C6 vertebral bodies and an associated epidural component, which produces moderate spinal stenosis in a patient with infectious symptoms and findings. Note the prevertebral edema and soft-tissue fullness (between *arrows*). **(b)** Pregadolinium and **(c)** postgadolinium T1-weighted images show enhancement at the disc space, in the vertebral body's epidural component, and in the prevertebral space.[†]

fusion.⁷⁶ It should be noted, however, that a lack of improvement on MRI and even deterioration of MRI features in the setting of clinical improvement do not necessarily indicate failure of treatment.^{80,81}

In the postoperative patient, evaluation for cervical spine infection may be complicated by the normal enhancement of the uninfected disc. MRI findings of infection in a postoperative patient include contrast enhancement of the subchondral bone and marrow adjacent to the infected disc.⁷⁴ Graft material and native vertebrae should not enhance within the first few days after spinal surgery. After several months, graft enhancement occurs, but it is often less intense and less uniform than that caused by infection. Bone graft usually has high signal intensity on T2-weighted images during the first postoperative year, and the signal gradually decreases with time as the bone graft is vascularized and fused.⁷⁴ An enhancing mass

adjacent to the graft or a graft dislodgment is a sign of potential infection.⁷⁴

Epidural Abscess

A spinal epidural abscess is a collection of purulent material outside the dura mater. An epidural abscess is usually associated with vertebral osteomyelitis, and direct extension from an adjacent infected vertebral body is the most common source for an epidural abscess.⁷⁴ Epidural abscesses are less common in the cervical spine than in the thoracic or lumbar spine and may be located anterior or posterior to the spinal cord.⁷⁴ Multiple spinal segments are usually involved (most commonly, C4-C7).⁷⁴

Along with the increase in the number of patients with risk factors for spinal infections, the number

of patients with cervical epidural abscess is also increasing. The risk factors associated with vertebral osteomyelitis include the following:

- Age >50 years
- Alcoholism
- Diabetes
- Immunodeficiency (e.g., from medications, human immunodeficiency virus)
- Intravenous drug abuse
- Male gender
- Malignancy
- Malnutrition
- Obesity
- Previous spinal procedure
- Recent systemic illness
- Tobacco use
- Trauma

These factors also increase the risk for developing an epidural abscess. The clinical presentation for an epidural abscess may be similar to that of vertebral osteomyelitis. Mass effect from the abscess compressing the spinal cord or nerve roots may present as radiculopathy, myelopathy, or paralysis.

As it is for vertebral osteomyelitis, MRI is the diagnostic study of choice for the evaluation of an epidural abscess.^{20,74,76} Gadolinium-enhanced, fat-suppressed, T1-weighted images provide anatomic detail of the location and extension of the abscess and any associated vertebral infections.⁷⁴ T2-weighted and fat-suppressed T2-weighted images also show the boundaries of the epidural abscess and allow for the assessment of the degree of spinal cord compression. Gadolinium enhancement patterns may vary from a thin, peripheral pattern (which may represent a collection of liquefied pus with a surrounding rim) to a homogeneous pattern seen with a phlegmon. The spinal cord may be evaluated for the level and amount of compression, as described previously.

Intradural Infections

Intradural infections may be categorized as subdural abscess, leptomeningitis, or myelitis. A subdural abscess, which is clinically indistinguishable from an epidural abscess, is caused by direct extension from an epidural abscess, hematogenous spread, or iatrogenic contamination. Gadolinium-enhanced MRI shows the enhancing intradural-extramedullary abscess next to a compressed spinal cord. T2-weighted images show an associated signal intensity change within the spinal cord secondary to compression, ischemia, or myelitis.

Spinal leptomeningeal infections can be caused by many organisms, including *Neisseria meningitidis*, *Coccidioides immitis*, *Cryptococcus* sp., *Treponema*

pallidum, and viral organisms. Gadolinium-enhanced MRI shows abnormal meningeal enhancement along the surface of the cord or nerve roots.⁸² Meningeal enhancement can be seen incidentally over the brain, but meningeal enhancement of the spinal cord is abnormal.

Spinal cord infections and abscesses are uncommon but are associated with a high mortality rate.^{74,76} Hematogenous seeding of bacteria is the most common etiology. Early cord infection shows increased T2-weighted signal and poorly defined enhancement with gadolinium.^{74,76} Progressive infection may cause spinal cord cavitation, depicted as areas of low signal intensity on T1-weighted images and high signal intensity on T2-weighted images. In addition, the spinal cord may become edematous and enlarged from the infection, with MRI characteristics as described previously.

Other Pathologic Conditions

Tumors

Spine tumors are categorized by their anatomic location (see Chapter 8, Tumors of the Spine) as follows⁷⁵:

- Extradural
- Intradural-extramedullary
- Intramedullary

A reasonable differential diagnosis may be established by incorporating a clinical history, physical examination, a basic understanding of possible tumor location, and the MRI examination findings.⁷⁵ A definitive diagnosis often requires a biopsy of the lesion.

MRI is an effective technique for imaging spine tumors because it:

- Provides unparalleled soft-tissue detail
- Evaluates the neural elements
- Reveals important tissue characteristics of the tumor (e.g., vascularity, density, vascular perfusion, extent of marrow involvement)
- Assesses the extent of spinal cord compression

The entire spine needs to be evaluated because of possible skip lesions from intrathecal seeding, multiple primary sites, or a syrinx. The spinal cord can be screened with sagittal T1-weighted SE images and sagittal T2-weighted FSE images to obtain a myelogram-like examination of the spinal cord. Axial images may be helpful for specific areas of interest. Contrast enhancement is beneficial for increasing the detection of most intramedullary and intradural-extramedullary tumors.⁷⁵ However, gadolinium enhancement may obscure the contrast

between metastatic lesions and normal bone marrow if fat suppression is not applied.⁸³ Gradient-echo images usually are not helpful in imaging spinal cord tumors because of the limited ability to distinguish between soft tissue or tumor and CSF. For osseous tumors, gradient-echo imaging may reveal areas of calcification or hemorrhage within the tumor (see Chapter 8, Tumors of the Spine, for a more detailed discussion).⁸³

Intrinsic Inflammatory Myelopathies

The most common cause of myelopathy is extrinsic compression, as noted above. Although orthopaedic surgeons typically do not treat intrinsic inflammatory myelopathies, they should realize that they exist and can be differentiated from myelopathy secondary to extrinsic compression.⁸⁴ A basic understanding of these processes is important, specifically so that surgery is not considered for the treatment of a patient who presents with an intrinsic inflammatory myelopathy in the presence of incidentally noted or minimal stenosis. Briefly described in the following paragraphs are the most common inflammatory myelopathies affecting the cervical spinal cord and their MRI findings.⁷⁵

Multiple Sclerosis

Approximately 60% to 75% of multiple sclerosis plaques outside of the brain occur in the cervical spinal cord, and 90% of patients with cord plaques also have brain plaques.^{85,86} Most plaques span two or fewer vertebral levels, occupy less than half the spinal cord diameter, and are located peripherally in the spinal cord.⁸⁶ MRI findings may include increased signal on T2-weighted sequences, decreased signal on T1-weighted images, patchy cord enhancement with gadolinium administration, and cord swelling or atrophy with larger plaques (**Fig. 6.35**).⁸⁷

Acute Transverse Myelopathy

Acute transverse myelitis is a monophasic, acute inflammatory condition of the entire spinal cord that produces motor, sensory, and sphincter impairment. There are multiple causes, including inflammatory processes, viral infections, vascular disorders, collagen vascular disease, postinfectious states, and idiopathic processes.⁸⁵ MRI findings vary, with T2-weighted pulse sequences showing areas of hyperintensity of various length and width, often involving more than three or four spinal segments.⁸⁸ Enlarge-

ment of the spinal cord and gadolinium enhancement also vary.⁸⁹

Subacute Necrotizing Myelopathy

Subacute necrotizing myelopathy is a rare, progressive myelopathy that occurs most often in elderly persons and often is attributed to spinal dural arteriovenous fistula, causing venous congestion, ischemia, and infarction of the spinal cord. Symptoms range from spastic to flaccid paraparesis, sensory abnormalities, and bowel and bladder dysfunction. MRI typically reveals a long segment of fusiform cord swelling and edema with peripheral contrast enhancement.⁸⁵

Acquired Immune Deficiency Syndrome

Spinal cord disease in patients with acquired immune deficiency syndrome is common and includes human immunodeficiency virus myelitis and vacuolar myelopathy. Human immunodeficiency virus myelitis may be caused by direct human immunodeficiency virus infection, lymphoma, opportunistic infections, or metabolic and vascular disorders. Vacuolar myelopathy, a spongy degeneration primarily involving the posterior and lateral spinal columns causing progressive ataxia and paraparesis,⁸⁵ is the most common spinal cord disease associated with acquired immune deficiency syndrome.⁹⁰ T2-weighted MR images reveal cord atrophy and symmetric hyperintense focal lesions in the dorsal and lateral columns.⁹¹ There is no cord swelling or gadolinium enhancement.

Viral Diseases

Viral infections of the spinal cord may be caused by multiple viruses affecting immunocompetent and immunocompromised patients. MRI characteristics of viral infection vary according to which virus is causing the infection and may include hyperintense areas on T2-weighted images, nerve root thickening, clumping and enhancement, and diffuse atrophy.⁸⁵ Gadolinium enhancement varies by spinal cord area and characteristic, depending on which virus is the underlying cause of the infection.

Bacterial, Parasitic, and Granulomatous Diseases

Clinical symptoms of myelitis, meningitis, and radiculitis can result from spinal cord invasion by bacterial, parasitic, or granulomatous infection. MRI findings

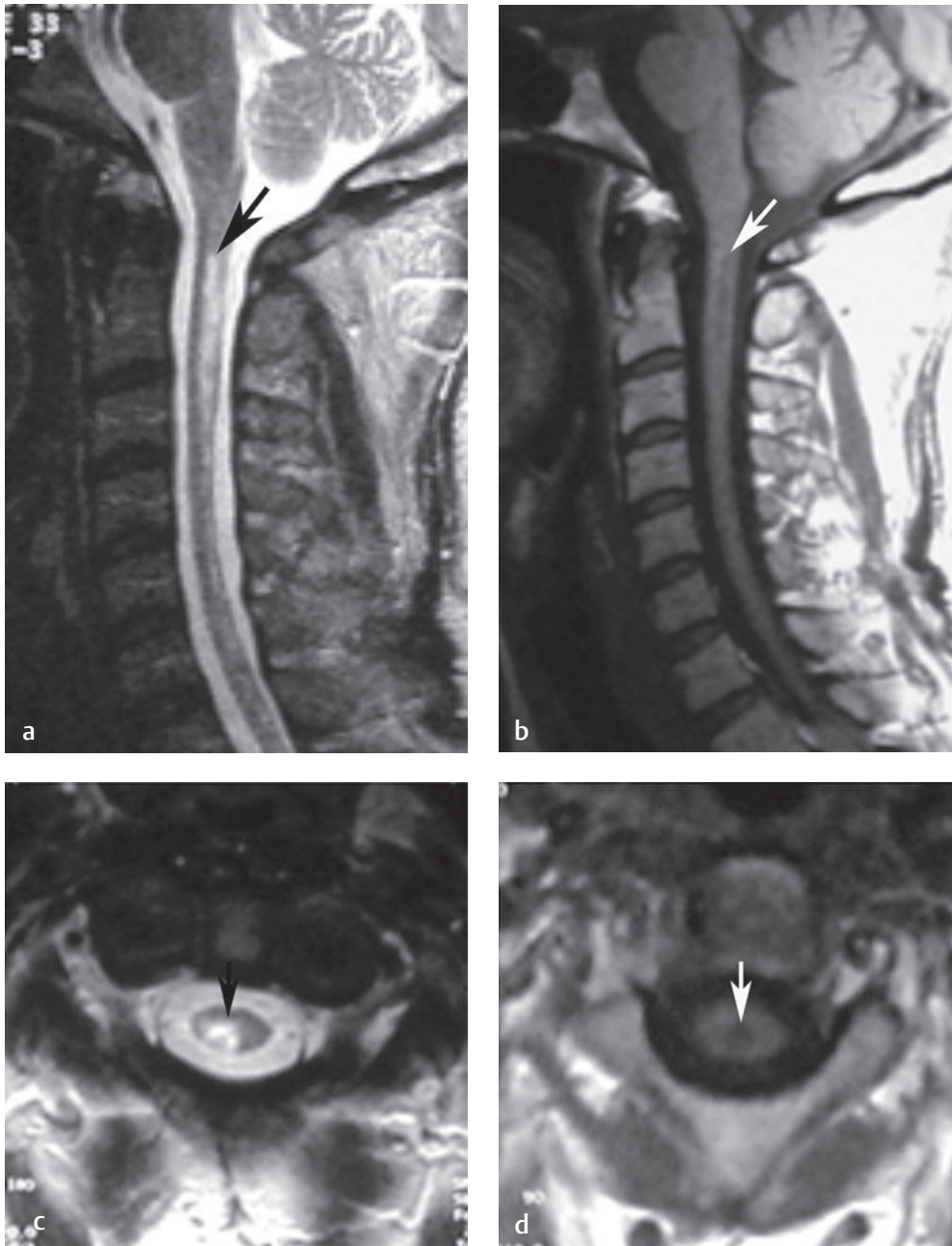


Fig. 6.35 Multiple sclerosis. **(a)** Sagittal T2-weighted, **(b)** sagittal T1-weighted, **(c)** axial T2-weighted, and **(d)** axial T1-weighted images show a focal region of increased **(a, c)** and decreased **(b, d)** signal within the spinal cord (*arrow* on each). In the appropriate clinical setting, these findings are compatible with multiple sclerosis; the diagnosis can be confirmed with lumbar puncture and CSF analysis.[†]

vary and may include cord swelling, cord edema, rim-enhancing lesions, and nerve enhancement.⁸⁵

Metabolic or Toxic Diseases

Subacute combined degeneration is a complication of vitamin B₁₂ deficiency or nitrous oxide poisoning. The dorsal and lateral spinal columns show demyelination, axonal loss, and gliosis. MRI may show increased signal in the dorsal and lateral columns on T2-weighted images.⁸⁵ Radiation myelopathy is a progressive myelopathy most often seen in patients treated with radiation therapy for head and neck cancer. MRI may reveal cord swelling, edema, and contrast enhancement corresponding to cord necrosis, demyelination, and gliosis.⁹²

Arthritides

Common arthritic conditions that affect the cervical spine and characteristic MRI findings are described in the following paragraphs. Imaging evaluation of these conditions often begins with conventional radiographs to assess the pattern and

extent of osseous involvement. MRI is the preferred modality for the assessment of the spinal cord and neural elements.

RA

RA is the most common inflammatory arthropathy, and the cervical spine is the most common area of spinal involvement.⁹³ The destructive process is through an inflammatory synovitis, leading to bone, cartilage, ligament, and periarticular destruction. Clinical symptoms include pain, deformity, loss of mobility, paresthesias, myelopathy, radiculopathy, paralysis, and sudden death. MRI is useful for the evaluation of the craniocervical junction and for the assessment of atlantoaxial and subaxial subluxation, basilar invagination, and spinal cord compression (**Fig. 6.36**).⁹³ In addition, MRI depicts the extent of periodontoid pannus formation, associated dens fractures, nodular fibrosis, and perivertebral erosions.⁹³ Patients with RA who are undergoing elective surgery for another musculoskeletal condition, such as major joint replacement, should be evaluated with cervical spine radiographs with flexion and extension views. If evidence of instability is noted on conventional

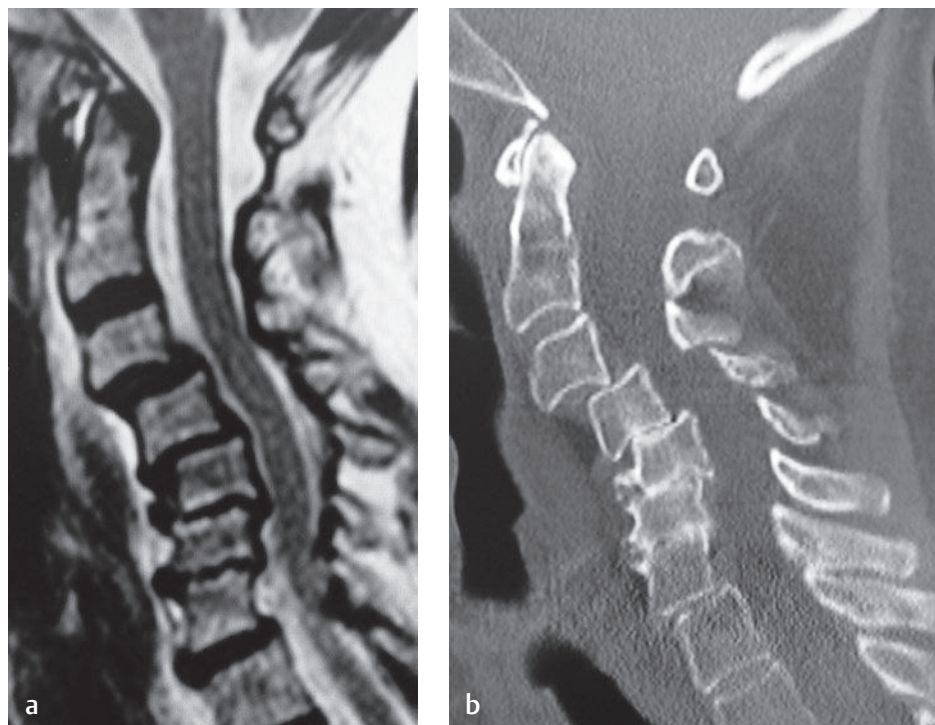


Fig. 6.36 Subaxial subluxation in RA. **(a)** Sagittal T2-weighted and **(b)** sagittal reconstructed CT images show multilevel subaxial subluxation and degenerative disc disease. Specifically, there is spondylolisthesis at C3-C4 and C4-C5 and retrolisthesis at C5-C6. Note the improved osseous detail provided by the CT image compared with the MR image.[†]

radiographs, MRI should be considered to evaluate further, especially for atlantoaxial instability.

Juvenile RA

Juvenile RA is the most common connective tissue disorder in children and may present as one of three types: oligoarthritis (60%), polyarthritis (30%), or systemic disease (10%).⁹³ As it is for the adult form, MRI is excellent for identifying synovial hypertrophy, cartilage and bone destruction, and joint effusion in the juvenile form.⁹³

Ankylosing Spondylitis

Ankylosing spondylitis, a seronegative spondyloarthropathy, is a chronic inflammatory arthropathy of unknown origin that affects ~1% of the general population⁹³ and predominantly involves the axial skeleton. Males are affected more often than are females, and symptoms appear in late adolescence and early adulthood. The disease begins in the thoracolumbar and lumbosacral junctions and ascends to involve the thoracic and cervical spine.⁹³ MRI is useful for the evaluation of early development of ankylosing spondylitis,⁹⁴ acute fractures, advanced degenerative changes, vertebral body subluxations, epidural hematoma, cord compression, and deformity.⁹³ MRI findings often provide guidance for medical and surgical treatment.⁹⁵

A common clinical scenario is one in which a patient with known or previously unknown ankylosing spondylitis presents with a complaint of neck pain after minor trauma. Conventional radiographs may show ankylosis of the cervical (or lumbar) spine but no evidence of fracture or displacement. It is important to note that such patients may have an unrecognized nondisplaced fracture. MRI can be obtained to rule out the presence of a nondisplaced fracture through the ankylosed spine. Such fractures are best seen on fat-suppressed T2-weighted images (Fig. 6.10).

Psoriatic Arthritis

Psoriatic arthritis may present before skin lesions. Axial skeleton radiographic findings are similar to those seen with RA.⁹³ MRI may reveal disc space narrowing and erosions of the apophyseal joints, vertebral end plates, and spinous process. On MRI, the atlantoaxial damage in patients with psoriatic arthritis is indistinguishable from that of patients with RA.⁹³

Amyloidosis

Amyloidosis is characterized by extracellular deposition of insoluble fibrillar proteins throughout the body.⁹³ In addition, amyloidosis displays primary, secondary, familial, and dialysis-associated patterns. The dialysis-associated form, β_2 -microglobulin, has a particular affinity for the musculoskeletal system and mimics inflammatory arthritis in its destructive nature.⁹³ Although the classic triad of β_2 -microglobulin deposition includes shoulder pain, carpal tunnel syndrome, and scapulohumeral arthritis, it is also associated with destructive spondyloarthropathy of the cervical spine.⁹⁶ Amyloid deposits are found in the intervertebral discs, ligaments, and synovial tissue; the deposits have affinity for the atlantoaxial region.^{93,96} Amyloid arthritis findings may mimic those of degenerative change, infectious destruction, inflammatory arthritides, or tumor. MRI is useful for distinguishing amyloid deposition destruction from others in the differential diagnosis. Amyloid deposits exhibit low signal intensity on MRI sequences and have variable enhancement patterns on contrast-supplemented sequences.⁹³

Gout

Gout, which is caused by an imbalance in uric acid metabolism, is characterized by polyarticular inflammation, soft-tissue tophi, gouty nephritis, and renal stones. The classic presentation is monoarticular inflammation involving the first metatarsophalangeal joint. Gouty involvement of the spine, especially cervical and lumbar regions, is rare and is seen in patients with long-standing peripheral articular manifestations.⁹³ MRI characteristics of gouty tophi include intermediate signal intensity on T1-weighted images, variable signal intensity on T2-weighted sequences, and variable contrast enhancement patterns.⁹⁷

Calcium Pyrophosphate Dihydrate Deposition Disease

This common crystal-induced arthritis affects peripheral joints and occasionally the spine. Spinal involvement may include calcium deposition in the intervertebral discs or ligaments. Areas affected with calcium pyrophosphate dihydrate deposition appear as isointense or hypointense signal on T1-weighted images relative to brain tissue, mixed signal intensity on T2-weighted images, and marked peripheral enhancement with gadolinium.⁹³ Sometimes, calcification may surround the dens, producing a characteristic “crowned dens” sign.

■ Summary

The typical MRI protocol of the cervical spine for the evaluation of degenerative pathologies includes T2-weighted and T1-weighted images in both sagittal and axial planes. However, imaging protocols of the cervical spine for specific indications can vary among institutions and should be modified when specific diagnoses, such as infection or tumor, are being considered.

The initial evaluation of patients with known or suspected cervical spine injury begins with conventional radiographs and/or CT imaging, which provide greater osseous detail and may reveal fractures or details that are not detected with conventional radiography. MRI provides soft-tissue visualization that is superior to that of conventional radiography or CT and is useful for the assessment of spinal cord injury, ligamentous injury, degree of spinal stenosis, and additional fracture evaluation. In addition, MRI is useful for the evaluation of obtunded patients or those with cervical spine injury, neurologic deficits, or an unreliable physical examination.

MRI is the preferred initial advanced imaging modality for the evaluation of symptomatic cervical spine degeneration and is highly sensitive and specific for the detection of cervical degenerative changes. Despite this high sensitivity and specificity, it is important to understand that radiographic and MRI abnormalities do not always correlate with a symptomatic degenerative lesion and, thus, it is very important that the spine surgeon or specialist correlate the findings on MRI with the patient's history and physical examination, as discussed in Chapter 4, A Systematic Approach to the Review of Spine MRI Studies, and in Chapter 3, Common Clinical and Correlative Pain Generators of the Cervical and Lumbosacral Spine. Degenerative conditions that can be evaluated on cervical spine MRI include disc displacement, disc degeneration, and spinal stenosis.


Although the most common indication for MRI of the cervical spine is the evaluation of degenerative conditions, this modality is also frequently and effectively used for the evaluation of patients with nondegenerative conditions such as Chiari malformations, infectious conditions, spinal tumors, inflammatory processes involving the spinal cord, and various arthritides.

COMMON CLINICAL QUESTIONS

- Which MRI pulse sequence is the best for evaluating the integrity of the posterior ligamentous complex in patients with known or suspected cervical spine trauma?
 - Axial T1-weighted images
 - Axial T2-weighted images
 - Sagittal T1-weighted images
 - Sagittal T2-weighted images
 - Sagittal STIR images
- What percentage of asymptomatic patients >40 years old have evidence of degenerative disease on their cervical spine MRI?

A. 20%	C. 40%	E. 90%
B. 30%	D. 60%	
- What diagnosis should be considered in a patient with clinical evidence of cervical radiculopathy and myelopathy and the single sagittal T2-weighted image shown here, and what imaging study can be obtained to confirm this diagnosis?

- Multilevel disc protrusions; conventional radiographs
 - Multilevel disc herniations; conventional radiographs
 - Spinal tumor; MRI with and without gadolinium contrast enhancement
 - Ossification of the posterior longitudinal ligament; CT
 - Epidural abscess; MRI with and without gadolinium contrast enhancement


- What is the definition of absolute stenosis?
 - AP canal diameter <10 mm
 - AP canal diameter <13 mm
 - Canal cross-sectional area <100 mm²
 - Torg ratio >0.8
 - Torg ratio <1.0
- What imaging study should be obtained to evaluate a patient with ankylosing spondylitis of the spine who presents with neck pain after a fall?
 - Conventional radiographs only
 - Conventional radiographs and CT
 - Conventional radiographs and MRI
 - Single proton emission CT scan
 - Three-phase bone scan

References

- Henry M, Scarlata K, Riesenburger RI, et al. Utility of STIR MRI in pediatric cervical spine clearance after trauma. *J Neurosurg Pediatr* 2013;12(1):30–36 PubMed
- Lowery DW, Wald MM, Browne BJ, Tigges S, Hoffman JR, Mower WR; NEXUS Group. Epidemiology of cervical spine injury victims. *Ann Emerg Med* 2001;38(1):12–16 PubMed
- Ackland HM, Cooper DJ, Malham GM, Stuckey SL. Magnetic resonance imaging for clearing the cervical spine in unconscious intensive care trauma patients. *J Trauma* 2006;60(3):668–673 PubMed
- Carrino JA, Manton GL, Morrison WB, Vaccaro AR, Schweitzer ME, Flanders AE. Posterior longitudinal ligament status in cervical spine bilateral facet dislocations. *Skeletal Radiol* 2006;35(7):510–514 PubMed
- Davis SJ, Teresi LM, Bradley WG Jr, Ziemba MA, Bloze AE. Cervical spine hyperextension injuries: MR findings. *Radiology* 1991;180(1):245–251 PubMed
- Flanders AE, Spettell CM, Tartaglino LM, Friedman DP, Herbison GJ. Forecasting motor recovery after cervical spinal cord injury: value of MR imaging. *Radiology* 1996;201(3):649–655 PubMed
- Rizzolo SJ, Vaccaro AR, Cotler JM. Cervical spine trauma. *Spine (Phila Pa 1976)* 1994;19(20):2288–2298 PubMed
- Stassen NA, Williams VA, Gestring ML, Cheng JD, Bankey PE. Magnetic resonance imaging in combination with helical computed tomography provides a safe and efficient method of cervical spine clearance in the obtunded trauma patient. *J Trauma* 2006;60(1):171–177 PubMed
- Silberstein M, Tress BM, Hennessy O. Delayed neurologic deterioration in the patient with spinal trauma: role of MR imaging. *AJNR Am J Neuroradiol* 1992;13(5):1373–1381 PubMed
- Smith AS, Hurst GC, Duerk JL, Diaz PJ. MR of ballistic materials: imaging artifacts and potential hazards. *AJNR Am J Neuroradiol* 1991;12(3):567–572 PubMed
- Teitelbaum GP, Yee CA, Van Horn DD, Kim HS, Colletti PM. Metallic ballistic fragments: MR imaging safety and artifacts. *Radiology* 1990;175(3):855–859 PubMed
- Takhtani D, Melhem ER. MR imaging in cervical spine trauma. *Magn Reson Imaging Clin N Am* 2000;8(3):615–634 PubMed
- Allen BL Jr, Ferguson RL, Lehmann TR, O'Brien RP. A mechanistic classification of closed, indirect fractures and dislocations of the lower cervical spine. *Spine (Phila Pa 1976)* 1982;7(1):1–27 PubMed
- Khanna AJ, Kwon BK. Subaxial cervical spine injuries. In: Rao RD, Smuck M, eds. *Orthopaedic Knowledge Update: Spine 4*. Rosemont, IL: American Academy of Orthopaedic Surgeons; 2012:221–233
- Bono CM, Schoenfeld A, Gupta G, et al. Reliability and reproducibility of subaxial cervical injury description system: a standardized nomenclature schema. *Spine (Phila Pa 1976)* 2011;36(17):E1140–E1144 PubMed
- Vaccaro AR, Hulbert RJ, Patel AA, et al; Spine Trauma Study Group. The subaxial cervical spine injury classification system: a novel approach to recognize the importance of morphology, neurology, and integrity of the disco-ligamentous complex. *Spine (Phila Pa 1976)* 2007;32(21):2365–2374 PubMed
- Vaccaro AR, Madigan L, Schweitzer ME, Flanders AE, Hilibrand AS, Albert TJ. Magnetic resonance imaging analysis of soft tissue disruption after flexion-distraction injuries of the subaxial cervical spine. *Spine (Phila Pa 1976)* 2001;26(17):1866–1872 PubMed
- Hart RA. Cervical facet dislocation: when is magnetic resonance imaging indicated? *Spine (Phila Pa 1976)* 2002;27(1):116–117 PubMed
- Lee JY, Nassr A, Eck JC, Vaccaro AR. Controversies in the treatment of cervical spine dislocations. *Spine J* 2009;9(5):418–423 PubMed
- Boden SD, Lee RR, Herzog RJ. Magnetic resonance imaging of the spine. In: Frymoyer JW, Ducker TB, Hadler NM et al, eds. *The Adult Spine: Principles and Practice*. 2nd ed. Philadelphia, PA: Lippincott-Raven; 1997:563–629
- Kaiser JA, Holland BA. Imaging of the cervical spine. *Spine (Phila Pa 1976)* 1998;23(24):2701–2712 PubMed
- Mirvis SE. Use of MRI in acute spinal trauma. In: Uhlenbrock D, ed. *MR Imaging of the Spine and Spinal Cord*. New York, NY: Thieme; 2004:437–465
- Kwon BK, Vaccaro AR, Grauer JN, Fisher CG, Dvorak MF. Subaxial cervical spine trauma. *J Am Acad Orthop Surg* 2006;14(2):78–89 PubMed
- Ronnen HR, de Korte PJ, Brink PRG, van der Bijl HJ, Tonino AJ, Franke CL. Acute whiplash injury: is there a role for MR imaging?—a prospective study of 100 patients. *Radiology* 1996;201(1):93–96 PubMed
- Li Q, Shen H, Li M. Magnetic resonance imaging signal changes of alar and transverse ligaments not correlated with whiplash-associated disorders: a meta-analysis of case-control studies. *Eur Spine J* 2013;22(1):14–20 PubMed
- Kwon BK, Hilibrand AS. Management of cervical fractures in patients with diffuse idiopathic skeletal hyperostosis. *Curr Opin Orthop* 2003;14:187–192
- White ML. Cervical spine: MR imaging techniques and anatomy. *Magn Reson Imaging Clin N Am* 2000;8(3):453–470 PubMed
- Quencer RM. The abnormal annulus fibrosus: can we infer the acuteness of an annular injury? *AJNR Am J Neuroradiol* 2002;23(7):1069 PubMed
- Stadnik TW, Lee RR, Coen HL, Neirynck EC, Buisseret TS, Osteaux MJC. Annular tears and disk herniation: prevalence and contrast enhancement on MR images in the absence of low back pain or sciatica. *Radiology* 1998;206(1):49–55 PubMed
- Goldberg W, Mueller C, Panacek E, Tigges S, Hoffman JR, Mower WR; NEXUS Group. Distribution and patterns of blunt traumatic cervical spine injury. *Ann Emerg Med* 2001;38(1):17–21 PubMed
- Adams VI. Neck injuries: I. Occipitoatlantal dislocation—a pathologic study of twelve traffic fatalities. *J Forensic Sci* 1992;37(2):556–564 PubMed
- Adams VI. Neck injuries: III. Ligamentous injuries of the craniocervical articulation without occipito-atlantal or atlanto-axial facet dislocation. A pathologic study of 21 traffic fatalities. *J Forensic Sci* 1993;38(5):1097–1104 PubMed
- Ahuja A, Glasauer FE, Alker GJ Jr, Klein DM. Radiology in survivors of traumatic atlanto-occipital dislocation. *Surg Neurol* 1994;41(2):112–118 PubMed
- Alker GJ Jr, Oh YS, Leslie EV. High cervical spine and craniocervical junction injuries in fatal traffic accidents: a radiological study. *Orthop Clin North Am* 1978;9(4):1003–1010 PubMed
- Goldberg AL, Baron B, Daffner RH. Atlantooccipital dislocation: MR demonstration of cord damage. *J Comput Assist Tomogr* 1991;15(1):174–175 PubMed
- Bono CM, Vaccaro AR, Fehlings M, et al; Spine Trauma Study Group. Measurement techniques for upper cervical spine injuries: consensus statement of the Spine Trauma Study Group. *Spine (Phila Pa 1976)* 2007;32(5):593–600 PubMed

37. Lee C, Woodring JH. Unstable Jefferson variant atlas fractures: an unrecognized cervical injury. *AJNR Am J Neuro-radiol* 1991;12(6):1105–1110 PubMed
38. Spence KF Jr, Decker S, Sell KW. Bursting atlantal fracture associated with rupture of the transverse ligament. *J Bone Joint Surg Am* 1970;52(3):543–549 PubMed
39. Hadley MN. Management of vertebral artery injuries after nonpenetrating cervical trauma. *Neurosurgery* 2002;50(3, Suppl):S173–S178 PubMed
40. Even J, McCullough K, Braly B, et al. Clinical indications for arterial imaging in cervical trauma. *Spine (Phila Pa 1976)* 2012;37(4):286–291 PubMed
41. Kathol MH. Cervical spine trauma. What is new? *Radiol Clin North Am* 1997;35(3):507–532 PubMed
42. Bowen BC, Pattany PM. Contrast-enhanced MR angiography of spinal vessels. *Magn Reson Imaging Clin N Am* 2000;8(3):597–614 PubMed
43. Hunter MA, Santosh C, Teasdale E, Forbes KP. High-resolution double inversion recovery black-blood imaging of cervical artery dissection using 3T MR imaging. *AJNR Am J Neuroradiol* 2012;33(11):E133–E137 PubMed
44. Bozzo A, Marcoux J, Radhakrishna M, Pelletier J, Goulet B. The role of magnetic resonance imaging in the management of acute spinal cord injury. *J Neurotrauma* 2011;28(8):1401–1411 PubMed
45. Eismont FJ, Arena MJ, Green BA. Extrusion of an intervertebral disc associated with traumatic subluxation or dislocation of cervical facets. Case report. *J Bone Joint Surg Am* 1991;73(10):1555–1560 PubMed
46. Robertson PA, Ryan MD. Neurological deterioration after reduction of cervical subluxation. Mechanical compression by disc tissue. *J Bone Joint Surg Br* 1992;74(2):224–227 PubMed
47. White AA, Southwick WO, Panjabi MM. Clinical instability in the lower cervical spine. A review of past and current concepts. *Spine (Phila Pa 1976)* 1976;1:15–27
48. D'Alise MD, Benzel EC, Hart BL. Magnetic resonance imaging evaluation of the cervical spine in the comatose or obtunded trauma patient. *J Neurosurg* 1999;91(1, Suppl):54–59 PubMed
49. Patel AA, Hurlbert RJ, Bono CM, Bessey JT, Yang N, Vaccaro AR. Classification and surgical decision making in acute subaxial cervical spine trauma. *Spine (Phila Pa 1976)* 2010;35(21, Suppl):S228–S234 PubMed
50. Miyazaki M, Hymanson HJ, Morishita Y, et al. Kinematic analysis of the relationship between sagittal alignment and disc degeneration in the cervical spine. *Spine (Phila Pa 1976)* 2008;33(23):E870–E876 PubMed
51. Miura J, Doita M, Miyata K, et al. Dynamic evaluation of the spinal cord in patients with cervical spondylotic myelopathy using a kinematic magnetic resonance imaging technique. *J Spinal Disord Tech* 2009;22(1):8–13 PubMed
52. Zhang L, Zeitoun D, Rangel A, Lazennec JY, Catonné Y, Pascal-Mousellard H. Preoperative evaluation of the cervical spondylotic myelopathy with flexion-extension magnetic resonance imaging: about a prospective study of fifty patients. *Spine (Phila Pa 1976)* 2011;36(17):E1134–E1139 PubMed
53. Boden SD, McCowin PR, Davis DO, Dina TS, Mark AS, Wiesel S. Abnormal magnetic-resonance scans of the cervical spine in asymptomatic subjects. A prospective investigation. *J Bone Joint Surg Am* 1990;72(8):1178–1184 PubMed
54. Boutin RD, Steinbach LS, Finnesey K. MR imaging of degenerative diseases in the cervical spine. *Magn Reson Imaging Clin N Am* 2000;8(3):471–490 PubMed
55. Uhlenbrock D. Degenerative disorders of the spine. In: Uhlenbrock D, ed. *MR Imaging of the Spine and Spinal Cord*. New York, NY: Thieme; 2004:159–268
56. Matsumoto M, Fujimura Y, Suzuki N, et al. MRI of cervical intervertebral discs in asymptomatic subjects. *J Bone Joint Surg Br* 1998;80(1):19–24 PubMed
57. Boos N, Weissbach S, Rohrbach H, Weiler C, Spratt KF, Nerlich AG. Classification of age-related changes in lumbar intervertebral discs: 2002 Volvo Award in basic science. *Spine* 2002;27(23):2631–2644 PubMed
58. Mercer S, Bogduk N. The ligaments and annulus fibrosus of human adult cervical intervertebral discs. *Spine (Phila Pa 1976)* 1999;24(7):619–626, discussion 627–628 PubMed
59. Fardon DF, Milette PC; Combined Task Forces of the North American Spine Society, American Society of Spine Radiology, and American Society of Neuroradiology. Nomenclature and classification of lumbar disc pathology. Recommendations of the Combined task Forces of the North American Spine Society, American Society of Spine Radiology, and American Society of Neuroradiology. *Spine (Phila Pa 1976)* 2001;26(5):E93–E113 PubMed
60. Modic MT, Feiglin DH, Piraino DW, et al. Vertebral osteomyelitis: assessment using MR. *Radiology* 1985;157(1):157–166 PubMed
61. Modic MT, Steinberg PM, Ross JS, Masaryk TJ, Carter JR. Degenerative disk disease: assessment of changes in vertebral body marrow with MR imaging. *Radiology* 1988;166(1 Pt 1):193–199 PubMed
62. Matsunaga S, Sakou T. Ossification of the posterior longitudinal ligament of the cervical spine: etiology and natural history. *Spine (Phila Pa 1976)* 2012;37(5):E309–E314 PubMed
63. Pavlov H, Torg JS, Robie B, Jahre C. Cervical spinal stenosis: determination with vertebral body ratio method. *Radiology* 1987;164(3):771–775 PubMed
64. Boden SD. Rheumatoid arthritis of the cervical spine. Surgical decision making based on predictors of paralysis and recovery. *Spine (Phila Pa 1976)* 1994;19(20):2275–2280 PubMed
65. Boden SD, Dodge LD, Bohlman HH, Rechtine GR. Rheumatoid arthritis of the cervical spine. A long-term analysis with predictors of paralysis and recovery. *J Bone Joint Surg Am* 1993;75(9):1282–1297 PubMed
66. Smoker WRK. MR imaging of the craniovertebral junction. *Magn Reson Imaging Clin N Am* 2000;8(3):635–650 PubMed
67. Dreyer SJ, Boden SD. Natural history of rheumatoid arthritis of the cervical spine. *Clin Orthop Relat Res* 1999;366(366):98–106 PubMed
68. Reiter MF, Boden SD. Inflammatory disorders of the cervical spine. *Spine (Phila Pa 1976)* 1998;23(24):2755–2766 PubMed
69. Oda T, Fujiwara K, Yonenobu K, Azuma B, Ochi T. Natural course of cervical spine lesions in rheumatoid arthritis. *Spine (Phila Pa 1976)* 1995;20(10):1128–1135 PubMed
70. Ross JS. Cervicomedullary and craniovertebral junctions. In: Modic MT, Masaryk TJ, Ross JS, eds. *Magnetic Resonance Imaging of the Spine*. St. Louis, MO: Mosby-Year Book; 1994:191–215
71. Bundschuh C, Modic MT, Kearney F, Morris R, Deal C. Rheumatoid arthritis of the cervical spine: surface-coil MR imaging. *AJR Am J Roentgenol* 1988;151(1):181–187 PubMed

72. Oostveen JCM, Roozeboom AR, van de Laar MAFJ, Heeres J, den Boer JA, Lindeboom SF. Functional turbo spin echo magnetic resonance imaging versus tomography for evaluating cervical spine involvement in rheumatoid arthritis. *Spine (Phila Pa 1976)* 1998;23(11):1237–1244 PubMed
73. Tay BKB, Deckey J, Hu SS. Spinal infections. *J Am Acad Orthop Surg* 2002;10(3):188–197 PubMed
74. Ruiz A, Post MJ, Sklar EM, Holz A. MR imaging of infections of the cervical spine. *Magn Reson Imaging Clin N Am* 2000;8(3):561–580 PubMed
75. Khanna AJ, Carbone JJ, Kebaish KM, et al. Magnetic resonance imaging of the cervical spine. Current techniques and spectrum of disease. *J Bone Joint Surg Am* 2002;84-A(Suppl 2):70–80 PubMed
76. Uhlenbrock D, Henkes H, Weber W, Felber S, Kuehne D. Inflammatory disorders of the spine and spinal canal. In: Uhlenbrock D, ed. *MR Imaging of the Spine and Spinal Cord*. New York, NY: Thieme; 2004:357–435
77. Harris LF, Haws FP. Disc space infection. *Ala Med* 1994;63(7):12–14 PubMed
78. Renfrew DL. Infectious spondylitis. In: Renfrew DL, ed. *Atlas of Spine Imaging*. Philadelphia, PA: Saunders; 2003:259–280
79. Bierry G, Jehl F, Prevost G, Mohr M, Meyer N, Dietemann JL, Kremer S. Percutaneous inoculated rabbit model of intervertebral disc space infection: magnetic resonance imaging features with pathological correlation. *Joint Bone Spine (Phila Pa 1976)* 2008;75(4):465–470
80. Carragee EJ. The clinical use of magnetic resonance imaging in pyogenic vertebral osteomyelitis. *Spine (Phila Pa 1976)* 1997;22(7):780–785 PubMed
81. Gillams AR, Chaddha B, Carter AP. MR appearances of the temporal evolution and resolution of infectious spondylitis. *AJR Am J Roentgenol* 1996;166(4):903–907 PubMed
82. Murphy KJ, Brunberg JA, Quint DJ, Kazanjian PH. Spinal cord infection: myelitis and abscess formation. *AJNR Am J Neuroradiol* 1998;19(2):341–348 PubMed
83. Keogh C, Bergin D, Brennan D, Eustace S. MR imaging of bone tumors of the cervical spine. *Magn Reson Imaging Clin N Am* 2000;8(3):513–528 PubMed
84. DeSanto J, Ross JS. Spine infection/inflammation. *Radiol Clin North Am* 2011;49(1):105–127 PubMed
85. Finelli DA, Ross JS. MR imaging of intrinsic inflammatory myelopathies. *Magn Reson Imaging Clin N Am* 2000;8(3):541–560 PubMed
86. Tartaglino LM, Friedman DP, Flanders AE, Lublin FD, Knobler RL, Liem M. Multiple sclerosis in the spinal cord: MR appearance and correlation with clinical parameters. *Radiology* 1995;195(3):725–732 PubMed
87. Wiebe S, Lee DH, Karlik SJ, et al. Serial cranial and spinal cord magnetic resonance imaging in multiple sclerosis. *Ann Neurol* 1992;32(5):643–650 PubMed
88. Choi KH, Lee KS, Chung SO, et al. Idiopathic transverse myelitis: MR characteristics. *AJNR Am J Neuroradiol* 1996;17(6):1151–1160 PubMed
89. Pardatscher K, Fiore DL, Lavano A. MR imaging of transverse myelitis using Gd-DTPA. [in French and English] *J Neuroradiol* 1992;19(1):63–67 PubMed
90. Budka H. Neuropathology of myelitis, myelopathy, and spinal infections in AIDS. *Neuroimaging Clin N Am* 1997;7(3):639–650 PubMed
91. Chong J, Di Rocco A, Tagliati M, Danisi F, Simpson DM, Atlas SW. MR findings in AIDS-associated myelopathy. *AJNR Am J Neuroradiol* 1999;20(8):1412–1416 PubMed
92. Wang PY, Shen WC, Jan JS. Serial MRI changes in radiation myelopathy. *Neuroradiology* 1995;37(5):374–377 PubMed
93. Janssen H, Weissman BN, Aliabadi P, Zamani AA. MR imaging of arthritides of the cervical spine. *Magn Reson Imaging Clin N Am* 2000;8(3):491–512 PubMed
94. Amrami KK. Imaging of the seronegative spondyloarthropathies. *Radiol Clin North Am* 2012;50(4):841–854 PubMed
95. Konca S, Keskin D, Ciliz D, Bodur H, Sakman B. Spinal inflammation by magnetic resonance imaging in patients with ankylosing spondylitis: association with disease activity and outcome parameters. *Rheumatol Int* 2012;32(12):3765–3770 PubMed
96. Brzeski M, Fox JG, Boulton-Jones JM, Capell HA. Vertebral body collapse due to primary amyloidosis. *J Rheumatol* 1990;17(12):1701–1703 PubMed
97. Yu JS, Chung C, Recht M, Dailiana T, Jurdi R. MR imaging of tophaceous gout. *AJR Am J Roentgenol* 1997;168(2):523–527 PubMed

ANSWERS TO COMMON CLINICAL QUESTIONS

1. E

Explanation: Injury to posterior ligaments may be seen as areas of hyperintensity on T2-weighted images, especially fat-suppressed T2-weighted or STIR images. Sagittal STIR or fat-suppressed T2-weighted images are superior to T2-weighted images in that they are more “fluid sensitive” and, thus, accentuate the edema seen with ligamentous injury.

2. D

Explanation: Boden et al⁵³ reported that almost 60% of their asymptomatic patients >40 years old had cervical spine degenerative disc disease on MRI. This fact is important in that the finding of degenerative changes, alone, on MRI is not an indication for surgical or other intervention. The patient should have clinical findings that correlate, are clinically significant, and/or are not amenable to or have not responded to nonoperative management.

3. D

Explanation: Although it is difficult to make a diagnosis with a single image in a single plane from an MRI study, this image suggests the diagnosis of ossification of the posterior longitudinal ligament. The findings on MRI should be used to differentiate cervical disc disease and protrusions from ossification of the posterior longitudinal ligament. On most MR images showing cervical stenosis secondary to disc displacement, the pathology and stenosis is based at the level of the disc, and stenosis is seen only behind the vertebral body in cases of disc extrusion and migration. Conversely, MRI in patients with ossification of the posterior longitudinal ligament shows stenosis at the level of the disc and also along the course of the posterior longitudinal ligament,

which runs along the posterior aspect of the vertebral bodies. In patients with suspected ossification of the posterior longitudinal ligament, CT imaging can be obtained to rule in or rule out this diagnosis, given that it provides optimal visualization of calcification and osseous detail.

4. A

Explanation: There are several objective measures of cervical spinal stenosis. Relative stenosis is defined as an AP canal diameter of <13 mm, and absolute stenosis is defined as an AP canal diameter of <10 mm. The Torg or Pavlov ratio is calculated by dividing the AP canal diameter by the AP vertebral body diameter, with a ratio <0.8 defined as stenotic. This ratio is often used to evaluate for congenital stenosis in athletes.

5. C

Explanation: A common clinical scenario is one in which a patient with known or previously unknown ankylosing spondylitis presents with a complaint of neck pain after minor trauma. Conventional radiographs may show ankylosis of the cervical (or lumbar) spine but no evidence of fracture or displacement. It is important to note that such patients may have an unrecognized nondisplaced fracture. MRI can be obtained to rule out the presence of a nondisplaced fracture through the ankylosed spine. Such fractures are best seen on fat-suppressed T2-weighted images. CT imaging may not demonstrate a nondisplaced fracture. Single proton emission CT imaging is best for the evaluation of isthmic spondylolisthesis. A three-phase bone scan may show increased radiotracer activity at the fracture site, but such activity may not be seen in the early postinjury time period, and the demonstration of osseous detail and fracture pattern will be superior with MRI.

7

The Lumbar and Thoracic Spine

Gbolahan O. Okubadejo, Aditya Daftary, Jacob M. Buchowski, John A. Carrino, and A. Jay Khanna

CHAPTER OUTLINE

- I. Specialized Pulse Sequences and Imaging Protocols
- II. Traumatic Conditions
 - A. Classification of Thoracolumbar Spine Trauma
 - B. Role of MRI in Thoracolumbar Spine Trauma
 1. Evaluation of Fracture Morphology
 2. Assessment of Stability
 - a. Three-Column Concept
 - b. Posterior Ligamentous Complex
 3. Assessment of Neural Compromise
 - a. Burst Fracture
 - b. Disc Pathology
 - c. Epidural Hematomas
 - d. Vertebral Translation or Dislocation
- III. Nomenclature and Classification of Lumbar Disc Pathology
- IV. Degenerative Conditions
 - A. Discs and End Plates
 1. Degenerative Disc Disease
 2. Annular Tears
 3. Lumbar Herniated Nucleus Pulposus
 4. Thoracic Disc Herniation
 5. Schmorl Nodes
 - B. Facets
 1. Facet Arthropathy
 2. Synovial Cyst
 - C. Lumbar Spinal Stenosis
 - D. Cauda Equina Syndrome
 - E. Spondylolisthesis
 - F. Scoliosis
 - G. Epidural Lipomatosis

- V. Infectious Conditions
 - A. Vertebral Osteomyelitis
 - B. Discitis
 - C. Epidural Abscess
 - D. Tuberculosis
- VI. Postoperative MRI Findings
 - A. After Decompression without Instrumentation/Fusion
 - B. After Instrumentation/Fusion
 - C. Hematoma
 - D. Pseudomeningocele
 - E. Arachnoiditis
- VII. Summary

■ Specialized Pulse Sequences and Imaging Protocols

Although imaging protocols of the lumbar spine for specific indications can vary among institutions, standard MRI studies of the lumbar spine for degenerative pathologies usually include the following sequences:

- Sagittal T1-weighted SE
- Sagittal T2-weighted FSE
- Sagittal T2-weighted with fat suppression or sagittal STIR
- Axial T2-weighted FSE
- Axial T1-weighted SE or axial gradient echo

T1-weighted images are good for identifying anatomy and assessing the quantity of fat in neural foramina and the epidural spaces. They also help identify the presence of fracture lines. However, edema has low signal on T1-weighted images and may be difficult to identify. Signal on T1-weighted images increases in the presence of gadolinium contrast, so

these images are used to assess for contrast enhancement. Contrast enhancement is particularly useful in differentiating recurrent disc pathology from scar tissue and in assessing infection, neoplasms, and vascular malformations. Contrast enhancement may be made more conspicuous by obtaining postgadolinium fat-suppressed images.

T2-weighted images are sensitive to edema, which is usually one of the early signs of pathology. Distinction between fat and fluid (edema) may be difficult on T2-weighted images. For this reason, fat suppression via a fat-suppressed T2-weighted or STIR image may be obtained to make edema more conspicuous. STIR images are preferred over fat-suppressed T2-weighted images for patients with spinal instrumentation because STIR images are less prone to magnetic susceptibility artifacts. T2-weighted and fat-suppressed T2-weighted or STIR images are extremely helpful in identifying ligamentous injury, subtle fractures, neoplasms, infection, and fluid collections, including joint effusions.

Highly T2-weighted images produce an “MR myelogram” that provides a nice perspective, which is similar to that of images obtained with conventional myelography and CT myelography. As with other myelographic images, these MR images can be used to evaluate for spinal stenosis. However, such images should always be interpreted in conjunction with other MR pulse sequences because they may be prone to artifacts that exaggerate or underestimate abnormalities, including the degree of stenosis.

By decreasing the degree to which protons are “flipped” during image acquisition (compared with T1-weighted and T2-weighted images, in which they are flipped by 90 to 180 degrees), gradient-echo images can be acquired much more quickly. Adjustments in the “flip angle,” TR, and TE can create T1 and T2 weighting in these images. Gradient-echo images are very susceptible to magnetic susceptibility artifacts, which makes them quite useful for the detection of small areas of hemorrhage, such as those that occur with trauma and vascular malformations. On the other hand, this susceptibility also causes gradient-echo images to overestimate canal and foraminal stenosis because of artifact from the adjacent bone. Advances in MRI techniques are decreasing the latter problem.¹ Because of the rapidity with which images are acquired, they can be obtained with higher resolution and even as a 3D volume, which makes isotropic voxels and reformations in multiple planes possible.

■ Traumatic Conditions

Patients with suspected lumbar spine injuries should be evaluated initially with conventional radiographs. CT imaging offers greater osseous detail than do con-

ventional radiographs and may reveal fractures or details that are not detected with radiography. MRI provides superior visualization of soft tissues compared with conventional radiographs or CT images and is useful for the assessment of ligamentous injury, degree of spinal stenosis, additional fracture evaluation, and associated findings such as epidural hematomas. Occult fractures not visible on conventional radiographs or CT images may be detected by the presence of vertebral body edema on MR images. Although MRI is extremely sensitive in identifying thoracolumbar spine fractures, their characteristics and the exact appearance of the osseous components can be challenging; CT may be a better choice for assessing these aspects of the fractures. MRI is indicated when neurologic deficit, vascular injury, or soft-tissue injury is suspected in the setting of trauma. It is also useful for the assessment of post-traumatic sequelae.

A systematic approach (see Chapter 4, A Systematic Approach to the Review of Spine MRI Studies) for the evaluation of lumbar spine MRI should be used to avoid missing pathologic conditions (see **Table 7.1** for important lumbar spine structures to evaluate). In addition, it is essential that the MRI findings be interpreted in conjunction with other available imaging modalities, including conventional radiographs (with flexion and extension views if clinically indicated) and CT (see Chapter 11, Correlation of MRI with Other Imaging Studies).

Table 7.1 Evaluation of lumbar and thoracic spine trauma

Anatomy	Evaluation
Spinal column/ vertebral bodies	Alignment Vertebral body fracture Posterior element fracture Edema Degenerative change
Ligaments	Anterior longitudinal ligament Posterior longitudinal ligament Interspinous ligament Edema/rupture
Spinal cord	Edema Hemorrhage Compression Syrinx
Epidural space	Hematoma Disc herniation Osseous fragment

Source: Takhtani D, Melhem ER. MR imaging in cervical spine trauma. *Magn Reson Imaging Clin N Am* 2000;8:615–634. Modified with permission.

Classification of Thoracolumbar Spine Trauma

Thoracolumbar spine trauma is a common and complex condition. There are many classification systems, all of which are based on a variety of factors such as mechanism of injury; morphology of fracture; involvement of columns; and presence, absence, or degree of neural compromise.²⁻⁴ Like many classification systems, those for the evaluation of thoracolumbar spine trauma have not been universally accepted. This lack of acceptance may be the result of their complexity, lack of reproducibility, poor validity, or any combination thereof.

The Thoracolumbar Injury Classification and Severity Score recognizes the importance of the following three factors⁵:

- Fracture morphology (**Fig. 7.1**)
- Integrity of the posterior ligamentous complex (stability or potential for neurologic compromise)
- Neurologic status of the patient

Although a detailed review of this classification system is outside the scope of this chapter, these three components are used here to review and highlight the role of MRI in the evaluation of patients with thoracolumbar spine trauma. In addition, a systematic evaluation of these three components and calculation of an injury severity score⁵ can be used to guide the treatment of patients with thoracolumbar spine fractures.⁶ The Thoracolumbar Injury Classification and Severity Score (**Table 7.2**) provides prognostic information and has been found to be helpful in medical decision making.^{6,7} Studies have shown that it has excellent reliability and validity.^{8,9}

Role of MRI in Thoracolumbar Spine Trauma

Evaluation of Fracture Morphology

The first element in the MRI evaluation of a thoracolumbar injury is the assessment of fracture morphology. The morphology description includes the type of fracture (compression, burst, etc.) and the position of various osseous fragments relative to their anatomic origin and to the spinal canal. As discussed above, for the assessment of the osseous components of a fracture, CT is superior to conventional radiography and MRI because of the excellent spatial resolution and osseous detail it provides (**Fig. 7.2**). MRI may help provide additional information regarding the morphology of a fracture in a limited number of situations.

For example, subtle fractures may be difficult to identify on CT or conventional radiographs, especially in patients with degenerative disc disease, where end-plate anatomy and vertebral morphology are affected by the degenerative changes. Furthermore, patients with osteoporosis or osteopenia may show less osseous reactive change, which typically enables the detection of subtle or subacute fractures on conventional radiographs. Fluid-sensitive pulse sequences such as fat-suppressed T2-weighted or STIR images are excellent for identifying areas of subtle bone-marrow edema and focusing attention on an area of potential osseous injury. This bone-marrow edema often appears almost immediately after injury and can persist for several months or even a year thereafter.^{10,11} It should be noted, however, that the differential considerations for bone-marrow edema in a vertebral

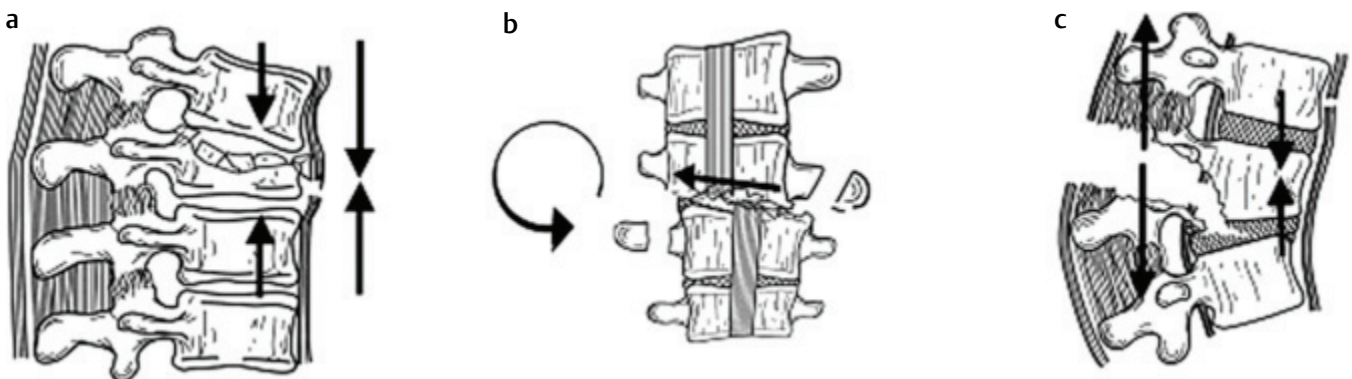


Fig. 7.1 Artist's sketches of the three major morphologic descriptors in the Thoracolumbar Injury Classification and Severity Score (compression, translation/rotation, and distraction). These descriptors are determined from a combination of conventional radiographs, CT images, and MRI sequences. **(a)** In compression, the vertebral body buckles under load to produce a compression or burst fracture. **(b)** In translation/rotation, the vertebral column is subjected to shear or torsional forces that cause the rostral part of the spinal column to translate or rotate with respect to the caudal part. **(c)** In distraction, the rostral spinal column becomes separated from the caudal segment because of distractive forces. Combinations of these morphologic patterns may occur. (From Vaccaro AR, Lehman RA Jr, Hurlbert RJ, et al. A new classification of thoracolumbar injuries. The importance of injury morphology, the integrity of the posterior ligamentous complex, and neurologic status. *Spine* 2005;30:2325–2333. Reprinted by permission.)

Table 7.2 Thoracolumbar Injury Classification and Severity Score

Injury Characteristic	Qualifier	Points
<i>Injury morphology</i>		
Compression	—	1
	Burst	+1
Rotation/translation	—	3
Distraction	—	4
<i>Neurologic status</i>		
Intact	—	0
Nerve root	—	2
Spinal cord, conus medullaris	Incomplete	3
	Complete	2
Cauda equina	—	3
<i>Posterior ligamentous complex integrity</i>		
Intact	—	0
Suspected/indeterminate	—	2
Disrupted	—	3

+ = 1 additional point given to the morphology

Source: Patel AA, Vaccaro AR. Thoracolumbar spine trauma classification. J Am Acad Orthop Surg. 2010;18(2):63–71.

body are varied and include other entities such as tumors, end-plate degeneration, and infection. For this reason, correlation with other imaging findings, imaging techniques, and clinical information is important for making a definitive diagnosis.

For patients in whom vertebral compression fractures are associated with pain, vertebral augmentation procedures such as vertebroplasty or kyphoplasty may be considered as a treatment option. In a study of patients with chronic (1 year) vertebral compression fractures treated with vertebroplasty, Brown et al¹¹ found that clinical improvement was definitively correlated with the presence of preprocedural bone-marrow edema. Therefore, it is essential that the MR images be reviewed for the absence, presence, and degree of bone-marrow edema for each fracture (**Fig. 7.2**).

Differentiating posttraumatic and osteoporotic fractures from neoplastic or pathologic fractures can be challenging (**Figs. 7.2** and **7.3**), especially in elderly patients. Neoplastic processes tend to fracture when most of the vertebral body is infiltrated with tumor (**Fig. 7.3**). Key MRI features that suggest the presence of a malignant fracture include the following¹²:

- Convex posterior margin of the vertebral body (from tumor infiltration) (**Fig. 7.4**)
- Abnormal signal in the posterior elements
- Epidural mass and neural encasement by the same focal paraspinal mass
- Presence of other osseous lesions

In the search for other lesions, care should be taken not to mistake additional osteoporotic vertebral fractures for metastatic lesions. A horizontal linear bright fracture line on T2-weighted images is considered the most reliable sign of a nonmalignant fracture (**Fig. 7.2**). Other signs that decrease the likelihood of underlying tumor include a retropulsed fragment off of the posterior aspect of the vertebral body, multiple fractures, and normal bone-marrow signal.^{12,13} Because contrast enhancement is often seen with acute benign fractures, it is no longer considered diagnostic for an underlying lesion or malignancy.^{12,14}

Assessment of Stability

The term *spinal stability* refers to the ability of the spine to limit neurologic compromise under physiologic loads. Panjabi et al¹⁵ have defined spinal stability as the degree of motion that prevents pain, neurologic deficit, and abnormal angulation. The definition can also be extended to include the ability of the spine to avoid the development of spinal deformity. Two key concepts in the MRI determination of spinal stability are the three-column concept and the assessment of the posterior ligamentous complex.

Three-Column Concept

More than 25 years ago, Denis² introduced the concept of the three-column spine and its clinical significance

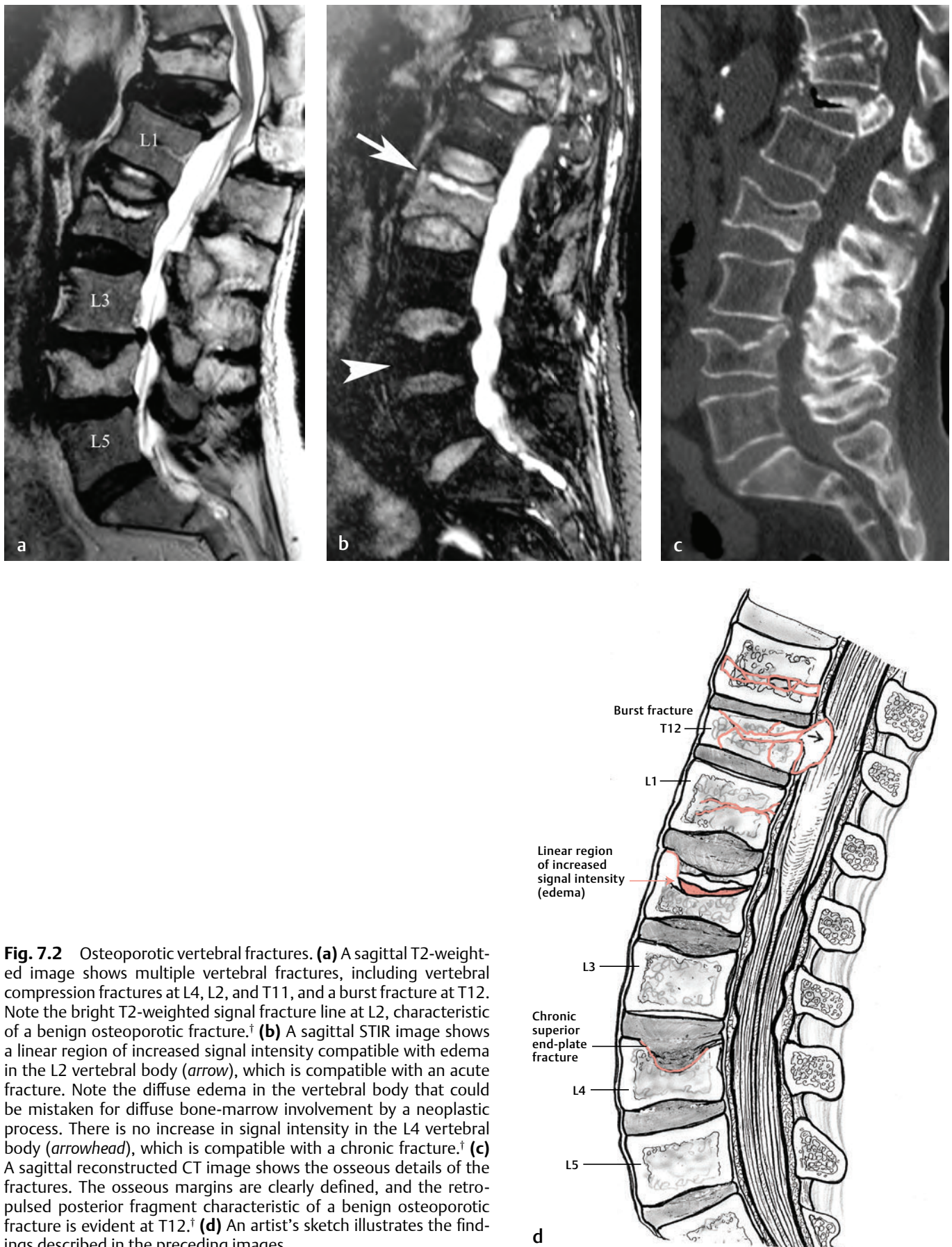


Fig. 7.2 Osteoporotic vertebral fractures. **(a)** A sagittal T2-weighted image shows multiple vertebral fractures, including vertebral compression fractures at L4, L2, and T11, and a burst fracture at T12. Note the bright T2-weighted signal fracture line at L2, characteristic of a benign osteoporotic fracture.[†] **(b)** A sagittal STIR image shows a linear region of increased signal intensity compatible with edema in the L2 vertebral body (arrow), which is compatible with an acute fracture. Note the diffuse edema in the vertebral body that could be mistaken for diffuse bone-marrow involvement by a neoplastic process. There is no increase in signal intensity in the L4 vertebral body (arrowhead), which is compatible with a chronic fracture.[†] **(c)** A sagittal reconstructed CT image shows the osseous details of the fractures. The osseous margins are clearly defined, and the retro-pulsed posterior fragment characteristic of a benign osteoporotic fracture is evident at T12.[†] **(d)** An artist's sketch illustrates the findings described in the preceding images.

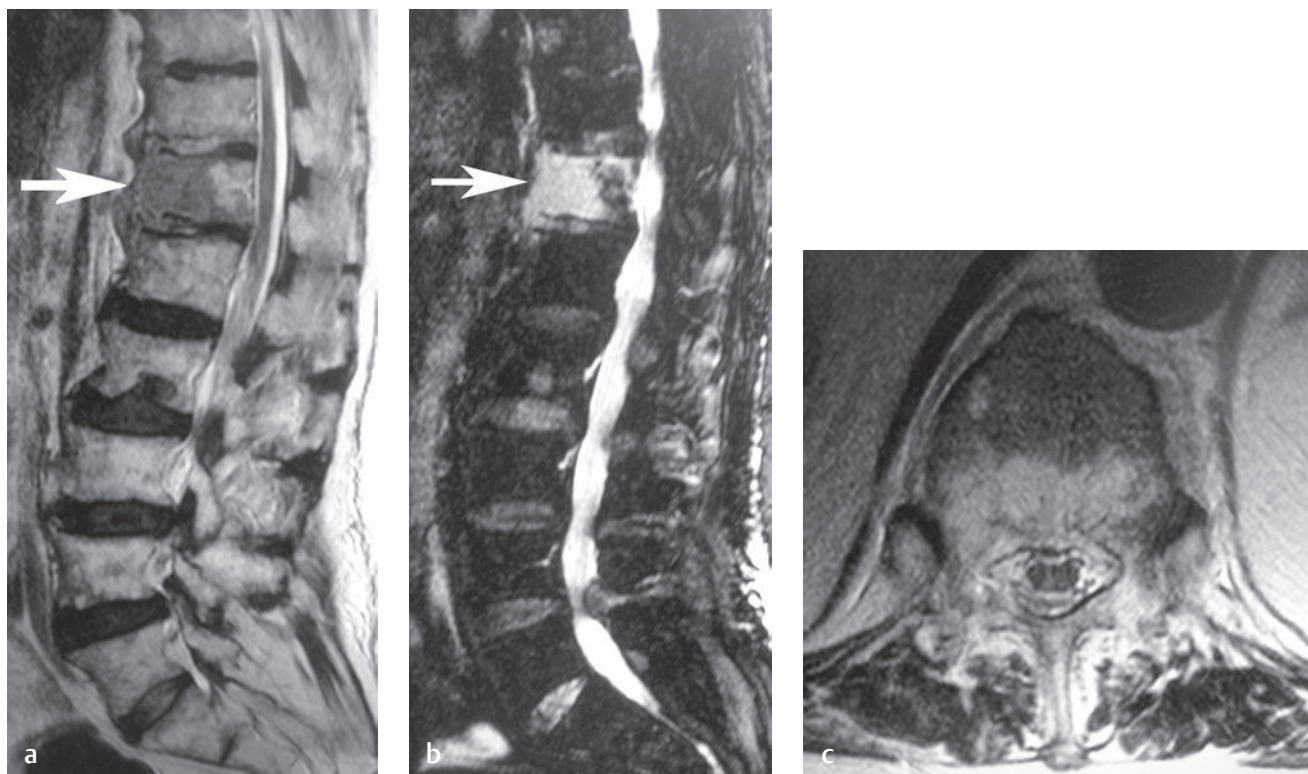


Fig. 7.3 Vertebral body metastasis in a patient with lung cancer. **(a)** A sagittal T2-weighted image shows heterogeneous bone-marrow signal intensity in multiple vertebral bodies (which can be seen with osteoporosis) but most prominently within the anterior half of the T12 vertebral body (*arrow*). Note that the anterior aspect of the vertebral body appears expanded as it is infiltrated with tumor. **(b)** A sagittal STIR image shows markedly increased signal intensity in the same region (*arrow*). **(c)** An axial T2-weighted image shows heterogeneous signal intensity within the vertebral body. A percutaneous biopsy confirmed evidence of metastatic lung cancer.[†]



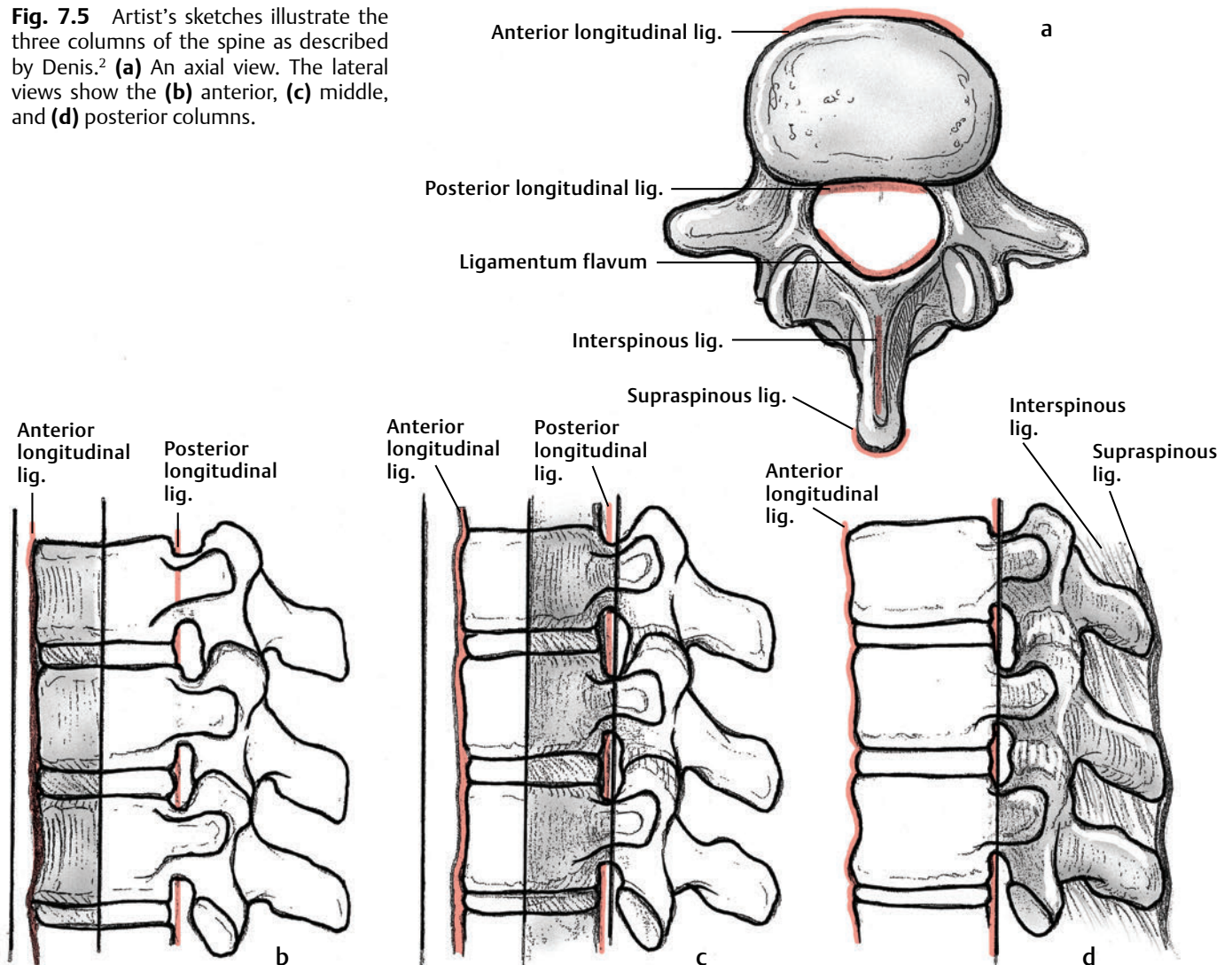
Fig. 7.4 A sagittal STIR image shows a pathologic burst fracture of the L3 vertebral body in a patient with metastatic lung cancer. Note the diffusely increased signal within the vertebral body and the convex posterior margin of the vertebral body.[†]

in the evaluation of spinal stability in patients with acute thoracolumbar injuries. Although the reliability and validity of the Denis system have been questioned,^{9,16} it is still used frequently to help evaluate the degree of spinal instability. Spinal instability may be assessed based on the number of columns involved in an injury. The three columns are defined as follows (**Fig. 7.5**):

- *Anterior*: anterior longitudinal ligament and the anterior portion of the vertebral body and annulus
- *Middle*: posterior vertebral body and annulus, and the posterior longitudinal ligament
- *Posterior*: facet joints, posterior elements, and posterior ligaments (supraspinous and interspinous ligaments and ligamentum flavum)

If one column is involved, the spine is generally considered stable; with two-column involvement, the spine is variably stable, depending on the degree of involvement; and the involvement of all three columns leads to a highly unstable spine.

Fig. 7.5 Artist's sketches illustrate the three columns of the spine as described by Denis.² (a) An axial view. The lateral views show the (b) anterior, (c) middle, and (d) posterior columns.



Posterior Ligamentous Complex

The posterior column and posterior ligamentous complex is an area of increasing concern in spinal stability (**Fig. 7.1c**).^{5,17–19} The components of the posterior ligamentous complex include the supraspinous ligament, interspinous ligament, ligamentum flavum, and the facet joint capsules.⁵ The three ligaments that constitute the posterior ligamentous complex normally appear as dark and continuous bands on T1-weighted and T2-weighted images. When traumatized, they may show increased signal on fluid-sensitive pulse sequences (T2-weighted fat-suppressed and STIR) (**Fig. 7.6**). Discontinuity of the dark signal of the fibers is also seen on MRI. It has been suggested that the MR images be reviewed with the intent of describing these ligaments to be intact, indeterminate, or disrupted.⁵

Subtle fractures and dislocations of the facet joints and posterior elements are detected well on CT, but

in some instances, the edema identified on MRI may be helpful in combination with close scrutiny of the CT images to identify subtle fractures. However, the true role of MRI in these instances is in identifying ligamentous injuries and hematomas; 28% to 47% of patients with thoracolumbar burst fractures are estimated to have disruption of the posterior ligamentous complex.²⁰

Assessment of Neural Compromise

MRI plays its most vital role in the assessment of neural compromise and is excellent in its ability to determine the cause of compression. Neural compromise can be graded on MRI as mild, moderate, or severe (see the subsequent discussion of lumbar spinal stenosis). In addition to an evaluation of the degree of stenosis, the type of stenosis should also be described (central, lateral recess, or foraminal). In



Fig. 7.6 A sagittal STIR image shows a T11 flexion-distraction injury with compression fracture of T11 and an associated injury of the interspinous and supraspinous ligaments, as evidenced by increased signal intensity in the interspinous and supraspinous region between T10 and T11 (arrow).[†]

addition, one should note whether there is compression of specific neurologic structures, such as the spinal cord or a specific nerve root. Common causes of neural compromise in patients after thoracolumbar spine trauma include the following:

- Burst fractures
- Disc pathology
- Epidural hematoma
- Vertebral translation or dislocation
- Penetrating trauma (**Fig. 7.7**)

Burst Fracture

Although CT is excellent in assessing the osseous component of a burst fracture, the associated neural compression and hematoma may be difficult to assess on CT, and MRI is far more accurate. It is important to differentiate a burst fracture (**Fig. 7.8**) from a

compression fracture (**Fig. 7.2**). The former involves injury to the anterior and middle columns, whereas the latter involves injury to the anterior column only. The MR images should be carefully evaluated for the absence or presence and degree of stenosis, which can be secondary to the fracture alone or to preexisting degenerative changes, or to any combination thereof. Specifically, the sagittal T2-weighted images should be evaluated in the midline for the degree of posterior vertebral body wall encroachment on the spinal canal, CSF column, spinal cord, or cauda equina. Next, the parasagittal images should be evaluated for the same. Finally, the axial T2-weighted images can be reviewed to determine the location and degree of neural compromise in an orthogonal plane.

Disc Pathology

Traumatic compressive forces on the disc may lead to annular tears (also known as annular fissures), disc protrusions, extrusions, and sequestrations. Rupture of a few annular fibers leads to a small amount of fluid tracking from the nucleus pulposus to between the annular fibers, leading to a focus of high intensity on T2-weighted images. This finding of focal high intensity in the annulus is referred to as a *high-intensity zone* (**Fig. 7.9**) and is suggestive of an annular tear. Although this finding may be seen in association with trauma, its level of importance is controversial because it is also seen as a natural process of disc degeneration and may or may not be associated with acute pain.^{21–23} MRI is the modality of choice for assessing such abnormalities and associated areas for potential neurologic compromise (see the subsequent discussion of degenerative disc disease). The sagittal and axial T2-weighted images should be carefully evaluated for the presence of disc pathology such as protrusion, extrusions, and sequestrations. If present, the degree of neural compromise should be noted (see the subsequent sections).

Epidural Hematomas

Hematomas may occasionally be seen in association with thoracolumbar spine trauma, and they can be difficult to differentiate from disc protrusions and extrusions. Hematomas often resolve spontaneously and may provide an explanation for patients who show a rapid and spontaneous resolution of apparent disc herniations.^{24–26} Key differentiating features between a disc extrusion and a hematoma or fluid collection are the hematoma's larger size, different signal, obtuse margin along the posterior aspect of the vertebral body with maximum dimension at the midvertebral body level, and possible containment by the central septum (which attaches the posterior longitudinal ligament to the vertebral body).^{27,28}

The signal pattern associated with epidural hemorrhage is related directly to the state of the

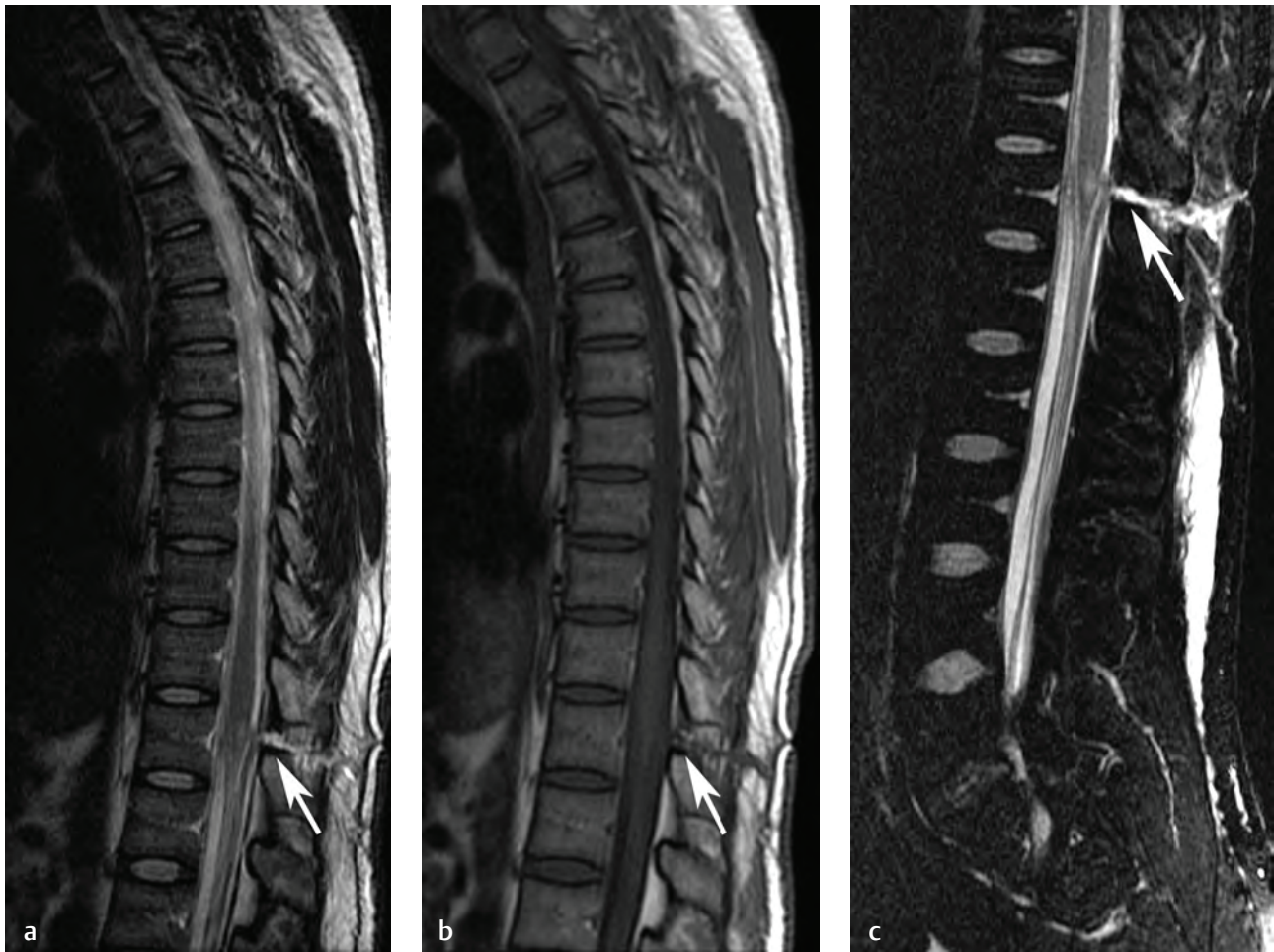


Fig. 7.7 Cord injury from a stab injury to the conus medullaris. **(a)** A sagittal T2-weighted image of the thoracic spine shows a linear track (*arrow*) from the skin to the conus medullaris with an associated region of increased signal within the conus medullaris, compatible with edema. **(b)** A sagittal T1-weighted image of the thoracic spine also shows the track (*arrow*) but does not show the edema within the conus medullaris. **(c)** A sagittal STIR image of the lumbar spine accentuates the edema along the track (*arrow*) and also that within the conus medullaris.[†]

oxygenation of the blood that pools in the regions of interest adjacent to the cord. In the acute phase, T1-weighted images show signal that is isointense compared with that of the adjacent spinal cord, and T2-weighted images show heterogeneous areas of increased and decreased signal intensity. During the acute phase, deoxyhemoglobin is the main component of the hematoma. Deoxyhemoglobin appears isointense or slightly low in signal intensity compared with that of the normal spinal cord on T1-weighted images and as a hypointense signal on T2-weighted images. Within 2 to 4 days after injury, T1-weighted and T2-weighted images may show increased signal intensity.²⁰ By 8 to 10 days, the primary component of the hemorrhage is methemoglobin, which is hyperintense on T1-weighted images.²⁹

Vertebral Translation or Dislocation

The posttraumatic translation of vertebral bodies may produce canal or foraminal narrowing with associated neural compression. Dislocation of the spine indicates an alteration of spinal alignment in all three planes and the displacement of one vertebral body relative to an adjacent one. Typical MRI signs of dislocations include the following:

- Altered facet joint anatomy with increased T2-weighted signal (or fluid) in the facet joints: the osseous anatomy is often better seen on CT, but as mentioned previously, edema and fluid on MRI help focus the search for a subtle injury.

Fig. 7.8 (a) A sagittal T2-weighted imageⁱ and artist's sketches in the (b) axial plane and (c) posterolateral perspective show an L1 burst fracture. Note that the posterior-superior margin of the vertebral body has displaced and rotated into the spinal canal. This displaced and rotated fragment (arrow on each) has been termed the *sentinel* or *culprit* fragment.

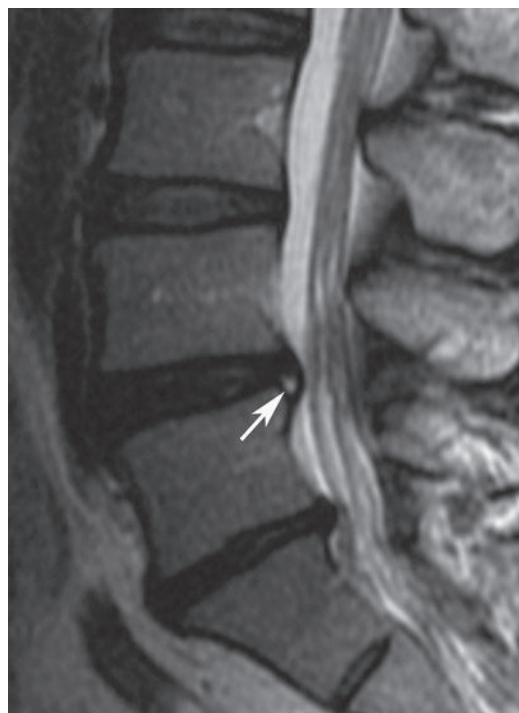
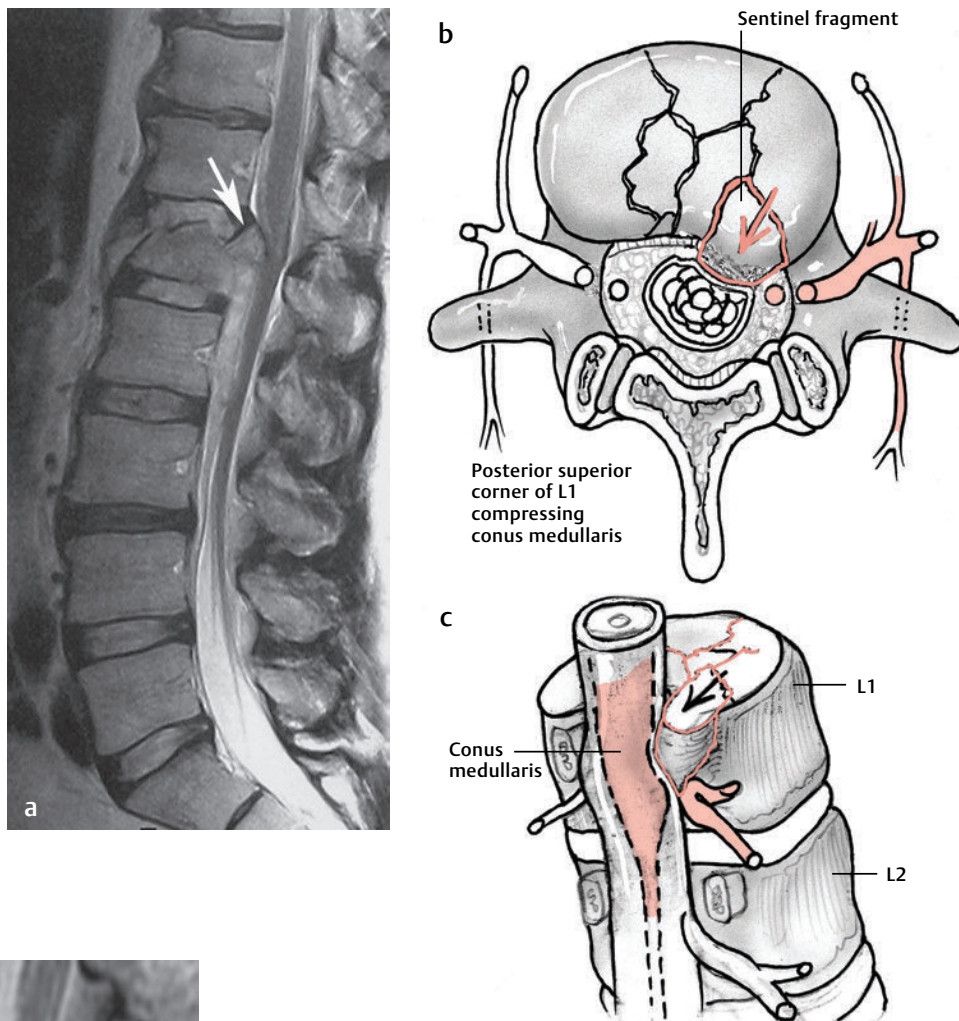


Fig. 7.9 A sagittal T2-weighted image shows a high-intensity zone at the posterior annulus of L4-L5 (arrow). Also noted is degenerative disc disease at L5-S1 with moderate loss of disc height. The L3-L4 disc is normal.ⁱ

- Disc herniation or pseudoherniation: with translation of one vertebral body in relation to the adjacent one, there may be uncovering of the disc, which gives the appearance of a herniation (pseudoherniation).
- Vertebral body translation: sagittal and coronal images are excellent in determining translation of vertebral bodies (**Fig. 7.10**). Care should be taken in determining whether translations are the result of facet degeneration, osseous injury, facet joint displacement, or pars defects.

■ Nomenclature and Classification of Lumbar Disc Pathology

The nomenclature used for describing lumbar disc pathology should be consistent and uniformly applied. Fardon and Milette³⁰ have provided a

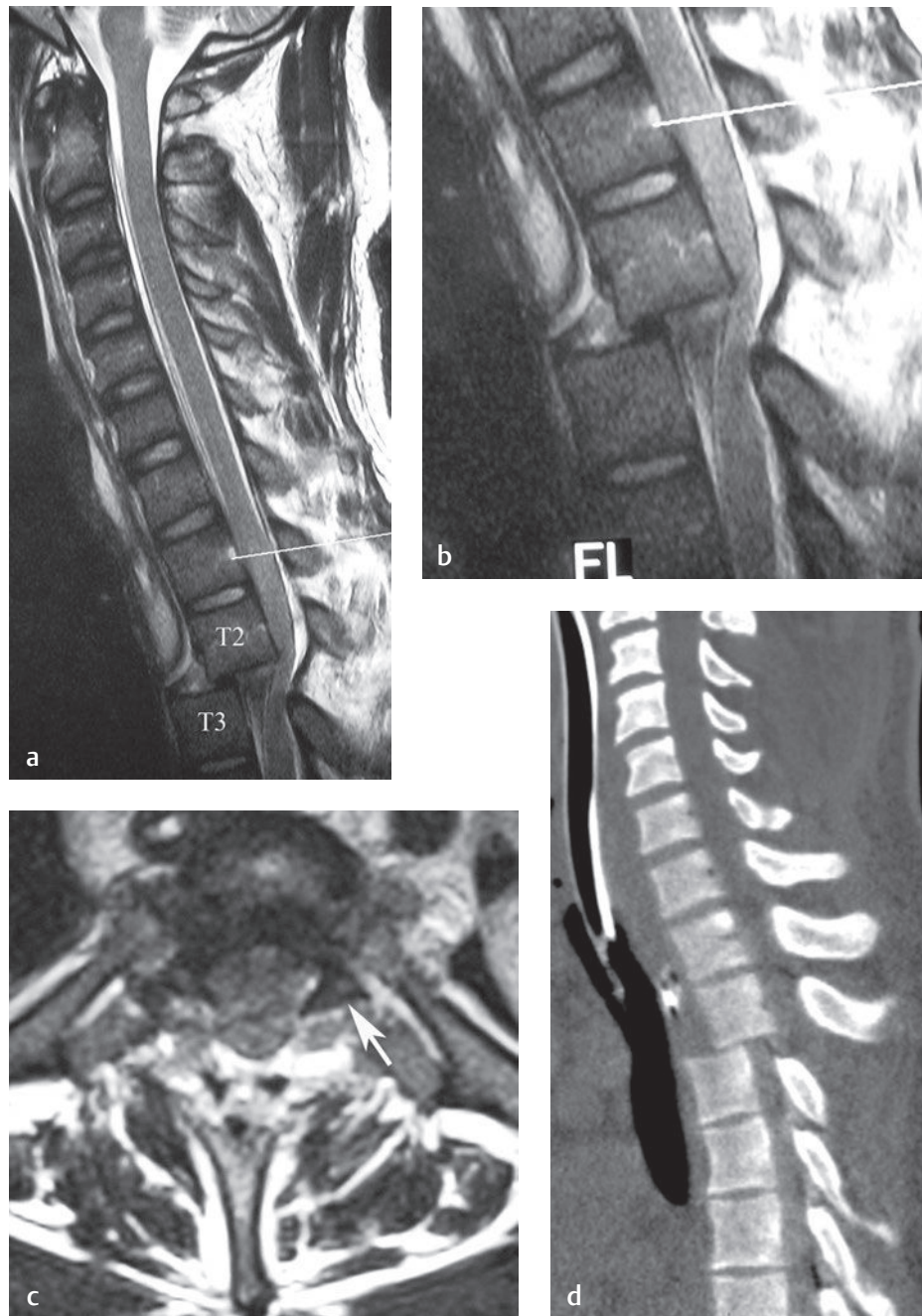


Fig. 7.10 T2-T3 dislocation. This (a) sagittal T2-weighted image and (b) zoom-in show anterior dislocation of T3 relative to T2 without fracture, with resultant severe cord compression, deformity, and acute signal change within the cord; the *line* on each points to the T1 vertebral body. (c) An axial T2-weighted image shows that the facets are “naked” or dissociated, a finding better seen on the left side (*arrow*). (d) A sagittal reconstructed CT image also shows the dislocation and confirms the absence of a fracture.[†]

comprehensive review of the nomenclature and classification of lumbar disc pathology. This nomenclature and classification scheme represents the recommendations of the combined task forces of the North American Spine Society, the American Society of Spine Radiology, and the American Society of Neuroradiology. Several other societies,

including the American Academy of Orthopaedic Surgery, support and recommend the use of the nomenclature described here. Surgeons and radiologists involved in the care of patients with known or suspected lumbar disc pathology and the evaluation of their MR images should consider reviewing this publication³⁰ for additional details.

With this system, disc lesions are classified as follows:

- **Normal:** a young disc that is morphologically normal (no lesion)
- **Congenital/developmental variant:** discs that are congenitally abnormal or that have undergone changes in morphology secondary to abnormal growth of the spine
- **Degenerative/traumatic lesion:** annular tear, degeneration, herniation
- **Inflammation/infection:** inflammatory spondylitis of subchondral end plate and bone marrow manifested as Modic type-1 MRI changes^{31–34}
- **Neoplasia:** all pathologic entities that may be primary or metastatic
- **Morphologic variant of unknown importance**

In the degenerative category, annular tears (also called annular fissures) are separations between annular fibers, avulsion of fibers from their vertebral body insertions, or other injuries of the fibers that involve one or multiple layers of the annular lamellae (**Fig. 7.11**).

The degenerative process includes desiccation, fibrosis, narrowing of the disc space, diffuse bulging of the annulus beyond the disc space, extensive fissuring, mucinous degeneration of the annulus, defects and sclerosis of the end plates, and osteophytes at the vertebral apophyses. Degenerative changes can also be subcategorized as spondylosis deformans (changes in the disc associated with a normal aging process) and intervertebral osteochondrosis (consequences of a more clearly pathologic process) (**Fig. 7.12**).

Herniation is defined as a localized displacement of disc contents beyond the borders of the intervertebral disc space (**Fig. 7.13a**). The disc material may include nucleus, cartilage, fragmented apophyseal bone, annular tissue, or a combination of those materials. Most clinicians tend to describe disc pathology using the terms *bulge*, *herniation*, *extrusion*, and *sequestration*. Although the last two terms are often used correctly, there seems to be a high degree of interobserver variability in the use of the first two terms.

The currently accepted nomenclature is as follows: A herniation is considered “localized” if it involves $\leq 50\%$ of the disc circumference and

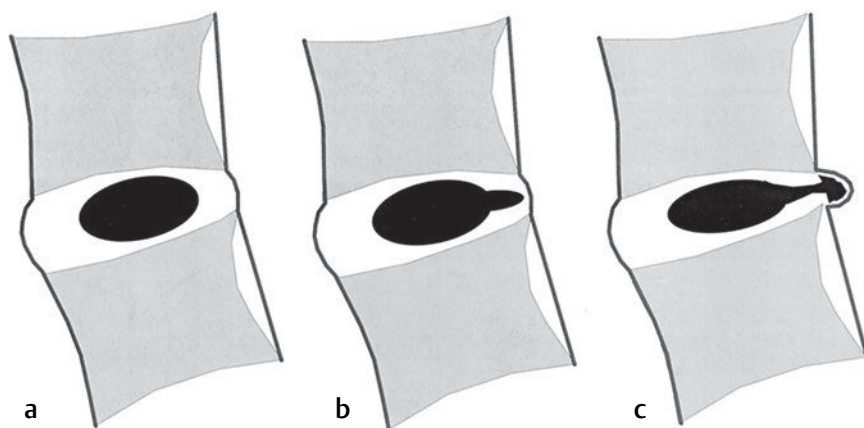
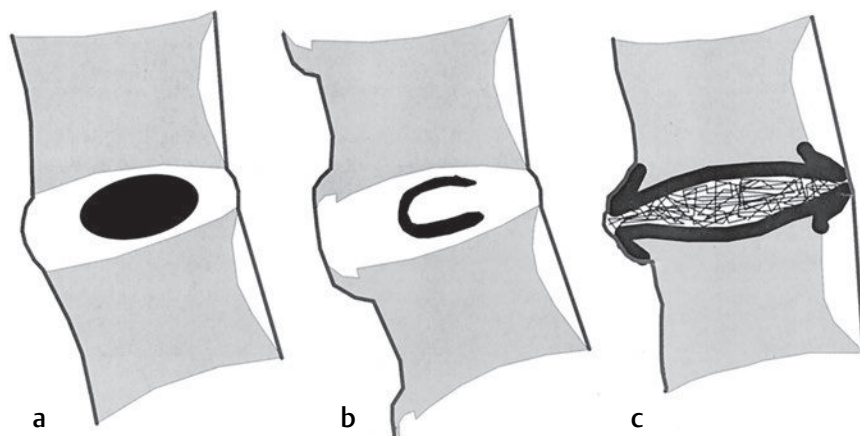


Fig. 7.11 Schematic sagittal drawings show differentiating MRI features of disc pathology. **(a)** A normal disc. **(b)** An annular tear (radial tear, in this case). **(c)** A disc herniation. The term *tear* is used to refer to a localized radial, concentric, or horizontal disruption of the annulus without associated displacement of disc material beyond the limits of the intervertebral disc space. Nuclear material is shown in black, and the annulus (internal and external) corresponds to the white portion of the intervertebral space. (From Milette PC. The proper terminology for reporting lumbar intervertebral disc disorders. *AJNR Am J Neuroradiol* 1997;18:1859–1866. Reprinted by permission.)

Fig. 7.12 Schematic sagittal drawings show differentiating disc MRI characteristics. **(a)** Normal disc. **(b)** Spondylosis deformans. **(c)** Intervertebral osteochondrosis. The distinction between these three entities is usually possible on all imaging modalities, including conventional radiographs. (From Milette PC. The proper terminology for reporting lumbar intervertebral disc disorders. *AJNR Am J Neuroradiol* 1997;18:1859–1866. Reprinted by permission.)



“generalized” if it involves >50%. A localized displacement is considered “focal” if <25% of the disc circumference is involved (**Fig. 7.13b**) and “broad-based” if the herniating disc content is between 25% and 50% (**Fig. 7.13c**). Disc tissue noted circumferentially, between 50% and 100%, and beyond the edges of the ring apophyses is termed *bulging*, which is not considered by some to be a form of herniation (**Fig. 7.13d**). The terms *protrusion* (**Fig. 7.13e**) and *extrusion* (**Fig. 7.13f**) are also commonly used in the context of disc herniation. A protrusion is present if the greatest distance between the edges of the disc material beyond the disc space is less than the distance between the edges of the base in the same plane. The base is the cross-sectional area of disc material at the outer margin of the disc space of origin, where disc material displaced beyond the disc space is continuous with disc material within the disc space. An extrusion is present when any one distance between the edges of the disc material

beyond the disc space is greater than the distance between the edges of the base (**Fig. 7.14**) or when there is no continuity between the disc space and the disc fragment. Extrusion may be further classified as sequestered and migrated. Sequestration is noted if the displaced disc material is completely discontinuous with the parent disc. Migration consists of displacement of disc material away from the site of extrusion, regardless of whether or not there is sequestration (**Fig. 7.15**).

Intravertebral herniation is a herniated disc in the craniocaudal direction through a defect in the vertebral body end plate. Herniations can also be described as contained or uncontained. Contained herniations are displacements of disc material that are retained by the outer annulus. Uncontained herniations are not retained by the outer annulus. Each abnormal presentation of disc pathology has specific features that can be detected with MRI (see the following section).

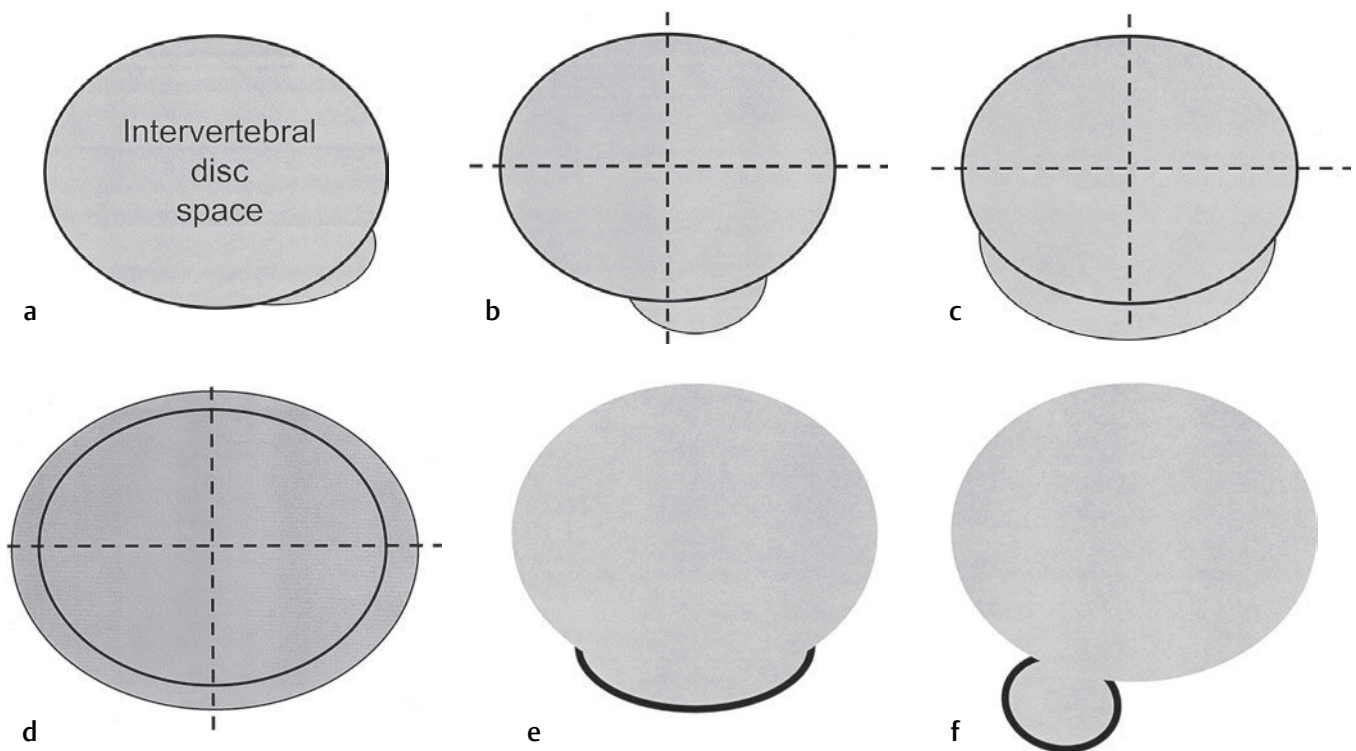


Fig. 7.13 Schematic drawings of disc herniation. In disc herniation, the interspace is defined, peripherally, by the edges of the vertebral ring apophyses, exclusive of osteophytic formations. **(a)** Localized extension of disc material beyond the intervertebral disc space, in a left posterior direction, which qualifies as a disc herniation. **(b)** By convention, a focal herniation involves <25% (90 degrees) of the disc circumference. **(c)** By convention, a broad-based herniation involves between 25% and 50% (90 to 180 degrees) of the disc circumference. **(d)** Symmetrical presence (or apparent presence) of disc tissue “circumferentially” (50% to 100%) beyond the edges of the ring apophyses may be described as a “bulging disc” or “bulging appearance” and is not considered a form of herniation. *Bulging* is a descriptive term for the shape of the disc contour and not a diagnostic category. **(e)** Protrusion (see definition in text). **(f)** Extrusion (see definition in text). (From Fardon DF, Milette PC. Nomenclature and classification of lumbar disc pathology. Recommendations of the Combined Task Forces of the North American Spine Society, American Society of Spine Radiology, and American Society of Neuroradiology. Spine 2001;26:E93–E113. Reprinted by permission.)

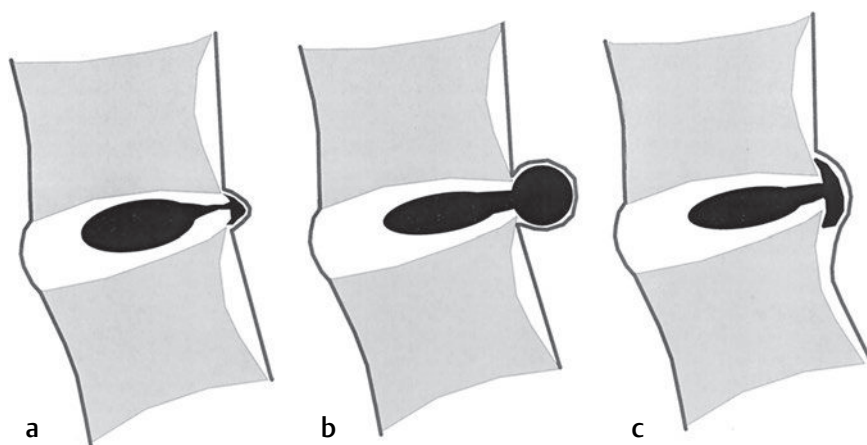
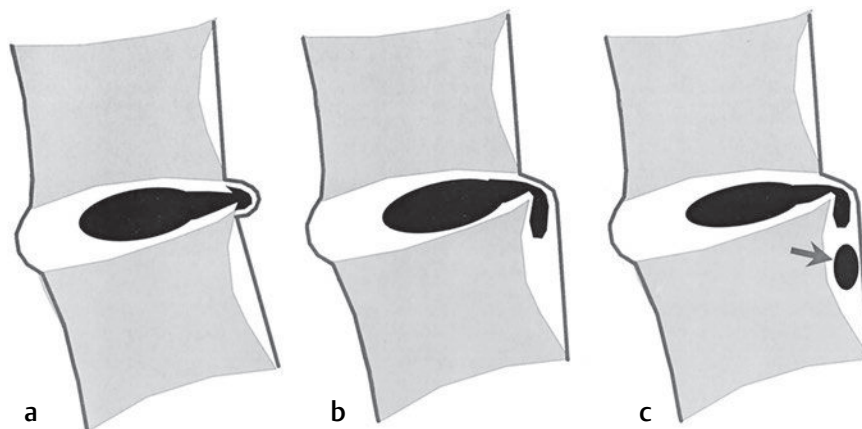


Fig. 7.14 Schematic drawings of protrusion and extrusion. When a relatively large amount of disc material is displaced, distinction between (a) protrusion and (b, c) extrusion is usually possible only on sagittal MR sections or sagittal CT reconstructions. (c) Although the shape of the displaced material is similar to that of a protrusion, the greatest craniocaudal diameter of the fragment is greater than the craniocaudal diameter of its base at the level of the parent disc, and the lesion therefore qualifies as an extrusion. In any situation, the distance between the edges of the base, which serves as reference for the definition of protrusion and extrusion, may differ from the distance between the edges of the aperture of the annulus, which cannot be assessed on CT images and is seldom appreciated on MR images. In the craniocaudal direction, the length of the base cannot exceed, by definition, the height of the intervertebral space. (From Milette PC. Classification, diagnostic imaging, and imaging characterization of a lumbar herniated disc. *Radiol Clin North Am* 2000;38:1267–1292. Reprinted by permission.)

Fig. 7.15 Schematic drawings of various types of posterior central herniations. (a) A small subligamentous herniation (or protrusion) without substantial disc material migration. (b) A subligamentous herniation with downward migration of disc material under the posterior longitudinal ligament. (c) A subligamentous herniation with downward migration of disc material and sequestered fragment (arrow). (From Milette PC. Classification, diagnostic imaging, and imaging characterization of a lumbar herniated disc. *Radiol Clin North Am* 2000;38:1267–1292. Reprinted by permission.)



■ Degenerative Conditions

Along with cervical degenerative disorders, lumbar degenerative disc disease and the associated stenosis are the most common indications for MRI of the spine. Most patients present with low back pain, lower extremity pain, or symptoms of neurogenic claudication. They usually have had at least 6 weeks of unsuccessful nonoperative management and often have already been evaluated with conventional radiography. The purpose of MRI in this situation is most frequently to evaluate for the presence or absence of spinal stenosis, disc herniation, and degenerative disc disease.

Lumbar spine degeneration typically includes a constellation of changes, such as degenerative disc

disease, arthritic and hypertrophic changes involving the facet joints, and hypertrophy of the ligamentum flavum (see Chapter 6, The Cervical Spine, for a discussion of inflammatory arthropathies, including ankylosing spondylitis). It is important to note that patients exhibiting MRI changes may not necessarily be symptomatic.^{35,36} A study of 33 asymptomatic, elite tennis players showed that 15.2% had normal MRI evaluations and 84.8% had abnormalities: 27.3% had pars lesions and 39.4% showed evidence of disc desiccation and bulging.³⁵ The high incidence of abnormal lumbar spine MRI studies was described by Boden et al³⁷ in 67 asymptomatic patients. A follow-up study of those 67 patients concluded that the MRI findings were not predictive of the development or duration of low back pain.³⁸

Discs and End Plates

Degenerative Disc Disease

As noted above, Fardon and Milette³⁰ have suggested the use of the terms *normal*, *spondylosis deformans*, and *intervertebral osteochondrosis* to describe the degenerative lumbar disc (**Fig. 7.12**). The specific changes seen on MRI correlate with the pathogenesis of degenerative disc disease, which results from the spectrum of changes that occur in the various parts of the vertebrodiscal complex. The nucleus pulposus becomes increasingly hypointense on T2-weighted images because of desiccation. An alternative finding is the intervertebral disc vacuum phenomenon secondary to a collection of intradiscal nitrogen, which manifests as a linear area of signal void on T1-weighted and T2-weighted sequences. Gradient-echo sequences may show this particular finding even better than do T1-weighted and T2-weighted images.³⁹ Early signs of disc degeneration on MRI include infolding of the anterior annulus and a hypointense central region—often seen before any loss of disc signal intensity—which may be associated with reproduction of pain at discography.³⁹ Advanced degeneration may present with a linear hyperintensity parallel to the end plate, which is thought to represent separation of the nucleus pulposus from the hyaline cartilage end plate.³⁹

Pfirrmann et al⁴⁰ introduced a grading system for lumbar degenerative disc disease based on MRI findings on sagittal T2-weighted images. This classification system describes five grades of progressively increasing degenerative disc disease. Its complexity may be the reason it is not commonly used by most clinicians. To summarize, the grading system describes the lumbar disc degenerative process as a continuum that progresses from a normal disc, to loss of the normal disc signal on T2-weighted images, to increasing loss of disc height, to degenerative end-plate changes and sclerosis.

Modic et al^{32,33} described signal changes within the vertebral body bone marrow and end plate adjacent to degenerating discs. The first finding in the sequence of changes is fibrovascular ingrowth that results in diminished signal intensity on T1-weighted images and a corresponding increase in signal intensity on T2-weighted images (type 1) (**Fig. 7.16**). The more chronic, type-2 changes involve a change from hematopoietic (red) to fatty (yellow) marrow, leading to relatively increased signal on T1-weighted images and slightly diminished signal intensity on T2-weighted images (**Fig. 7.17**). Type-3 changes consist of decreased signal intensity on T1-weighted and T2-weighted sequences and are associated with subchondral sclerosis on radiographs^{31,39} (**Fig. 7.18**). Among the three types of degenerative end-plate changes, type-1 changes have been found to have

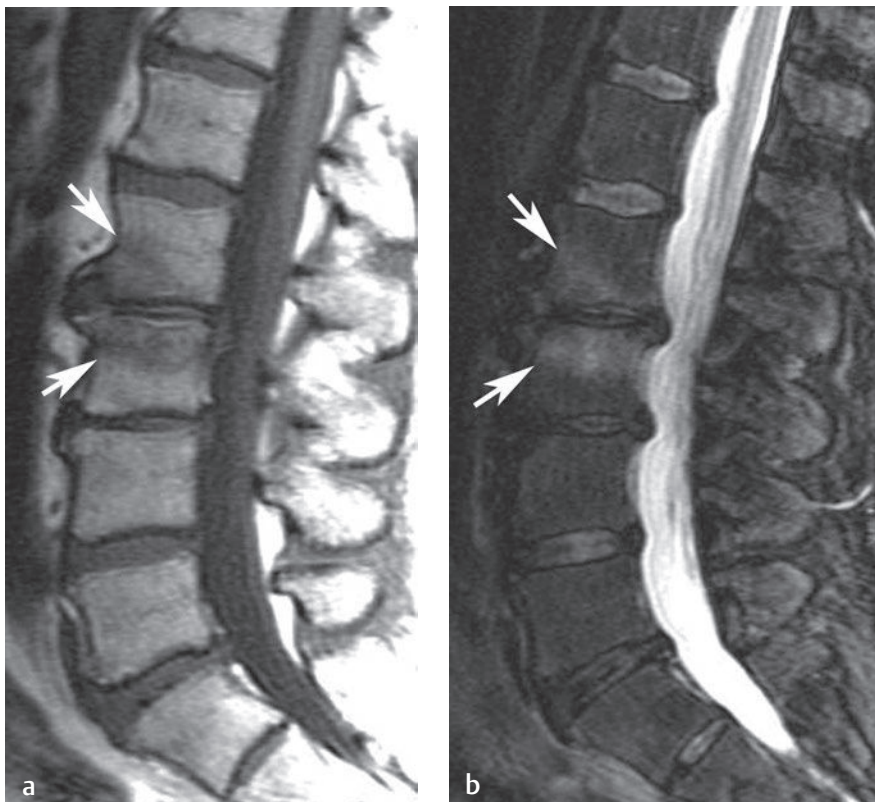


Fig. 7.16 Modic type-1 (fibrovascular) changes. Sagittal (a) T1-weighted and (b) fat-suppressed T2-weighted images show, at the L2-L3 level, the typical pattern (arrow on each) of decreased signal intensity on the T1-weighted image and increased signal on the T2-weighted image that is seen with Modic type-1 end-plate changes.[†]

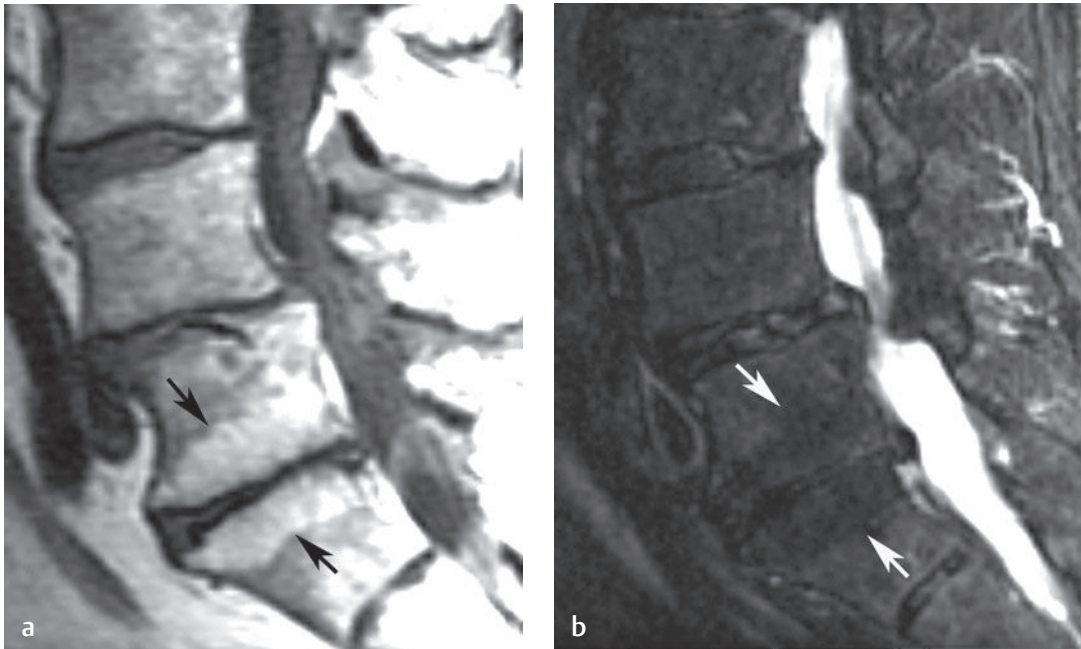


Fig. 7.17 Modic type-2 (fatty) changes. Sagittal (a) T1-weighted and (b) fat-suppressed T2-weighted images show, at the L5-S1 level, the typical pattern (arrows on each) of increased signal intensity on the T1-weighted image and decreased signal on the T2-weighted image that is seen with Modic type-2 end-plate changes. Note that degenerative changes and stenosis are also seen at other levels.[†]

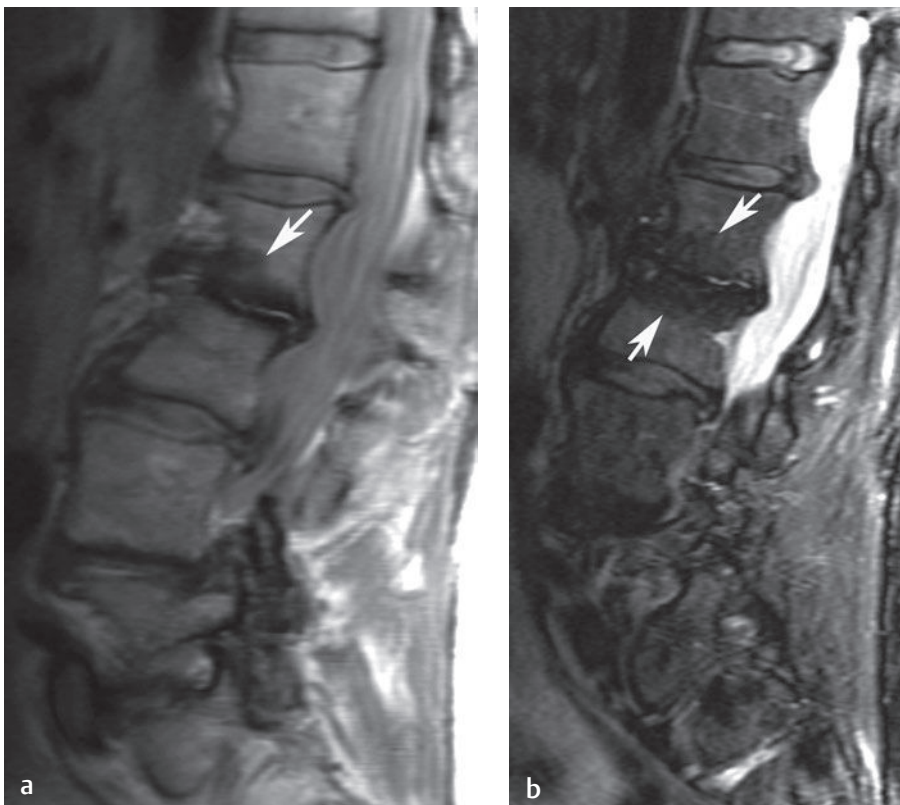


Fig. 7.18 Modic type-3 (sclerotic) changes. Sagittal (a) T1-weighted and (b) fat-suppressed T2-weighted images show, at the L2-L3 level, the typical pattern (arrow[s] on each) of decreased signal intensity that is seen with Modic type-3 end-plate changes. Note that degenerative changes are seen at other levels and that there is also evidence of lumbar scoliosis.[†]

the greatest correlation with the presence of discogenic back pain.^{34,41–43}

In addition to an assessment of the type of lumbar degenerative disc disease using the methods just described, one should also describe the degree of lumbar disc degeneration by noting the amount of disc space height loss (**Fig. 7.19**).

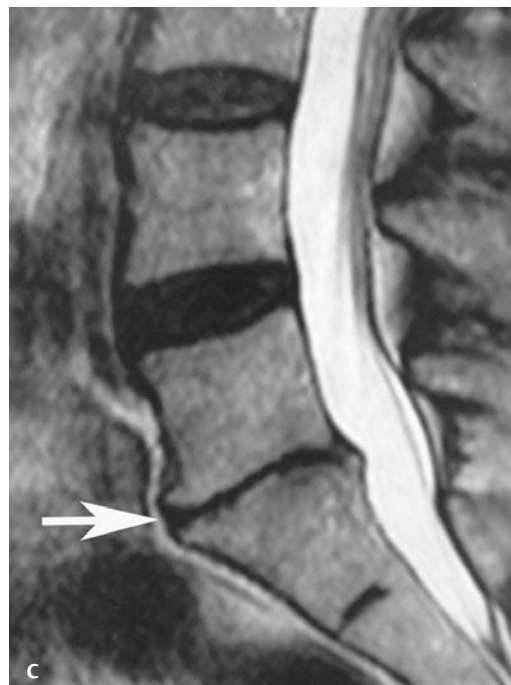
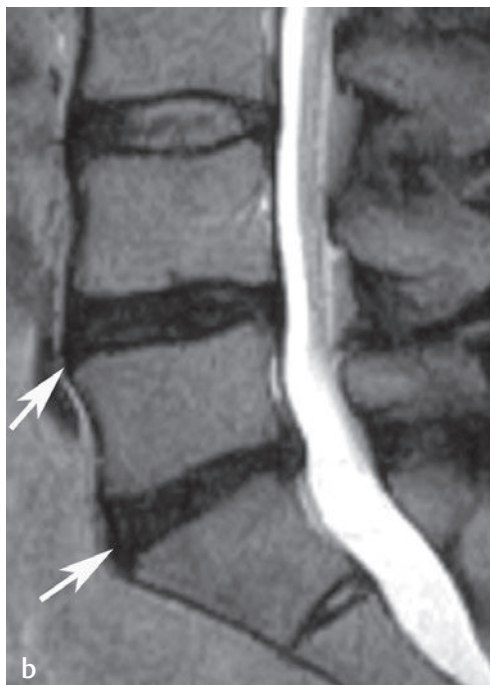


Fig. 7.19 Lumbar degenerative disc disease. The degree of disc T2-weighted signal and height loss should be evaluated and graded as (a) mild, (b) moderate, or (c) severe lumbar degenerative disc disease (arrow[s] on each).[†]

Annular Tears

Annular tears have a variable appearance on MRI, ranging from intermediate to high signal intensity on T2-weighted images. Studies have shown a correlation between high-signal-intensity annular tears in the lumbar spine and painful concordant annular tears seen at provocative discography.^{44,45} Some investigators have suggested that the inflammation associated with these annular tears results in irritation of the adjacent nerve root, potentially leading to radiculopathy without overt mechanical nerve root compression.⁴⁵ T2-weighted sequences have been used to show the following three types of annular tears:

- Concentric
- Radial
- Transverse

Concentric tears involve the entire extent of the annulus. Transverse tears occur at the periphery of the disc as a result of disruption of the Sharpey fibers. Radial tears extend from the nucleus through the annulus and may extend into the outer annulus, manifested on MRI as a high-intensity zone (**Fig. 7.9**). The high-intensity zone is defined as a focal area of high signal intensity within the posterior annulus of the degenerating disc, separate from the nucleus. These

high-intensity zones may also enhance after intravenous gadolinium administration.³⁹

Discography can be used to further evaluate patients with annular tears. In addition to the morphologic information provided on fluoroscopic images and on postdiscography CT, the patient's pain response can be used to help predict whether an annular tear or other degenerative pathology is the patient's pain generator.^{46,47} It is important to keep in mind, however, that the use of discography in the diagnosis of discogenic low back pain continues to be debated and is not uniformly accepted at all centers.

Lumbar Herniated Nucleus Pulposus

The terms used to describe the progressive states of herniated nucleus pulposus have been addressed previously (see the section on Nomenclature and Classification of Lumbar Disc Pathology). Shown here are the MRI appearances of each:

- Normal
- Bulge (**Fig. 7.20**)
- Protrusion (**Fig. 7.21**)
- Extrusion (**Fig. 7.22**)

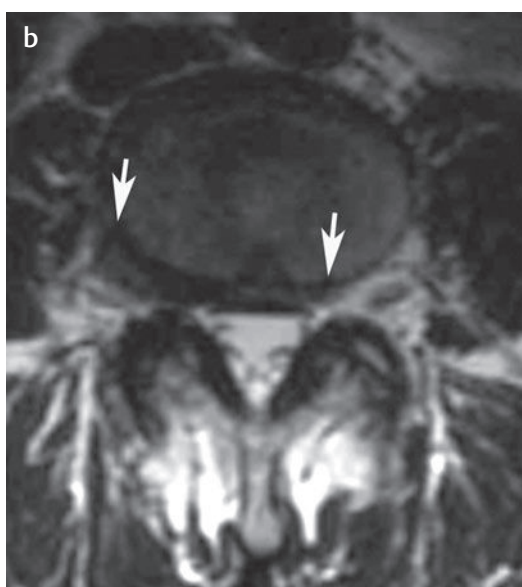


Fig. 7.20 Lumbar disc bulge. **(a)** Sagittal and **(b)** axial T2-weighted images show a right paracentral disc bulge that is asymmetric to the right, with extension into the right lateral recess and far laterally at the L4-L5 level (at arrow on **a** and between arrows on **b**).[†]



Fig. 7.21 Lumbar disc protrusion. **(a)** Sagittal and **(b)** axial T2-weighted images show a central disc protrusion at the L4-L5 level (arrow on each).[†]

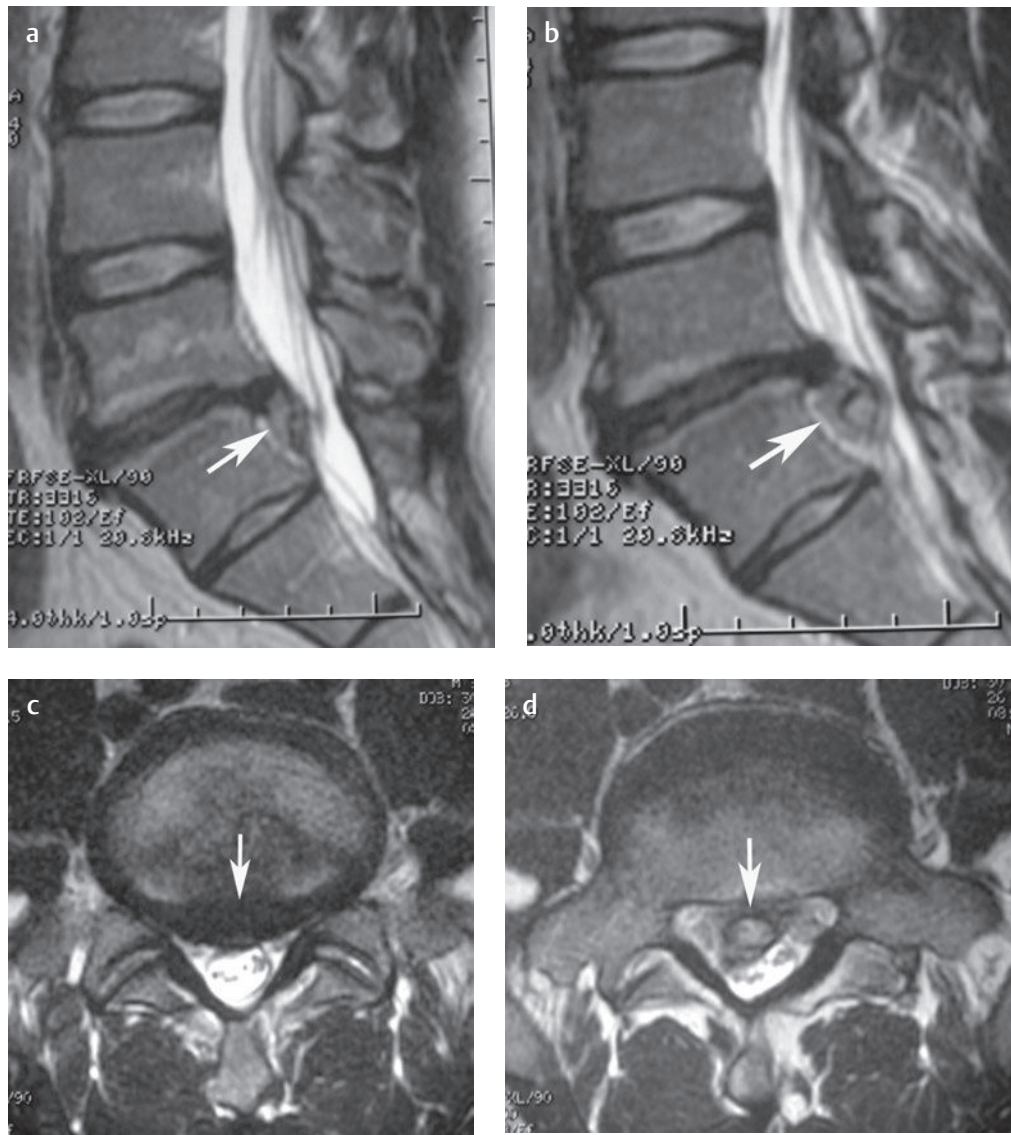


Fig. 7.22 Lumbar disc extrusion. **(a)** Midline sagittal and **(b)** parasagittal T2-weighted images show a large disc extrusion at the L4-L5 level and distal migration of the disc fragment (arrow on each) to behind the L5 vertebral body in a patient with transitional lumbosacral anatomy. Note the advanced degenerative disc disease at this level. **(c)** An axial T2-weighted image at the level of the L4-L5 disc shows what appears to be a central disc bulge (arrow). **(d)** However, an axial T2-weighted image at the L5 vertebral body level shows the disc extrusion (arrow).[†]

The status of the annulus provides insight into the status of a herniated disc. A disc protrusion is a herniation with an intact annulus, confined by the posterior longitudinal ligament. Extrusions occur when the nuclear material breaches the outer annular fibers. If herniated disc material becomes detached from the parent disc, it is termed *sequestered*. The sequestered fragment can migrate superiorly, inferiorly, or occasionally, posterior to the thecal sac. Intradural disc herniation is very rare.³⁹

It is often difficult to differentiate protrusion from extrusion. Several MRI signs may be used to aid this differentiation, including the following:

- If the AP diameter of the herniated disc is >50% of the spinal canal diameter, then an extrusion is present in >90% of cases.^{39,48}
- Examination of the base of the disc shows that a protrusion usually has a broad base against

the parent disc, broader than any other part of the hernia; an extrusion has a base that is narrower than the extruded material.

- Protrusions and extrusions can also be distinguished by their outlines. Protrusions are limited by the outer annular fibers and tend to have a smooth outline; in contrast, extrusions have a poorly defined outer margin.^{39,49}

When reviewing an MRI study that shows lumbar disc displacement, the clinician or radiologist should use the appropriate term to describe the morphology of the disc (bulge, protrusion, extrusion, sequestration) and should also describe several additional key characteristics of the disc pathology, including the following (see **Figs. 7.20** through **7.22** for examples of such descriptions):

- Level of the disc pathology
- Precise location relative to the disc space
- Size and degree of neural compression

With regard to location of the disc pathology, the axial and sagittal T2-weighted images should be carefully evaluated to determine the location of the disc protrusion or other pathology. The following terms should be used to describe the location of the protrusion (primarily based on the appearance of the axial T2-weighted image) (**Figs. 7.23** and **7.24**):

- **Central (Fig. 7.25)**
- **Posterolateral or lateral recess (Fig. 7.26)**
- **Foraminal (Fig. 7.27)**
- **Far lateral (Fig. 7.28)**

Of all lumbar disc herniations, 90% are central or paracentral (5% are foraminal and 5% are far lateral).⁵⁰ It should be noted that a typical posterolateral disc protrusion compresses the traversing nerve root, whereas a far-lateral disc protrusion compresses the exiting nerve root. Thus, for example, a posterolateral disc protrusion at the L4-L5 level will likely produce an L5 radiculopathy, whereas a far-lateral disc protrusion at the same level will likely produce an L4 radiculopathy.

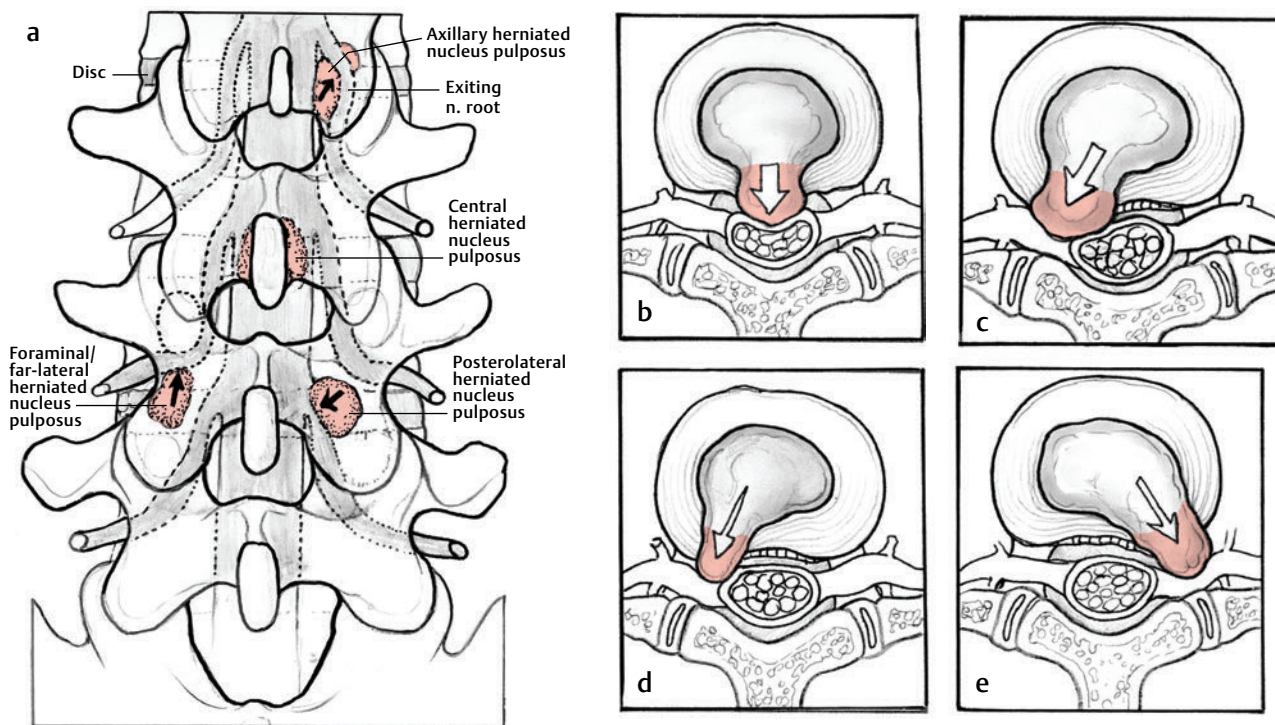


Fig. 7.23 Artist's sketches of types of herniated nucleus pulposus. (a) The posterior view shows their locations at the L2-L5 levels. The corresponding axial views show the (b) central, (c) posterolateral (paracentral), (d) lateral recess, and (e) far-lateral disc pathology. Each arrow indicates the direction of herniation. (Modified from Kerr SM, Patel DN, Vaccaro AR. Clinical features of herniated nucleus pulposus. In: Phillips FM, Laurysen C (eds). The Lumbar Intervertebral Disc. New York: Thieme, 2009:76–83. Reprinted by permission.)

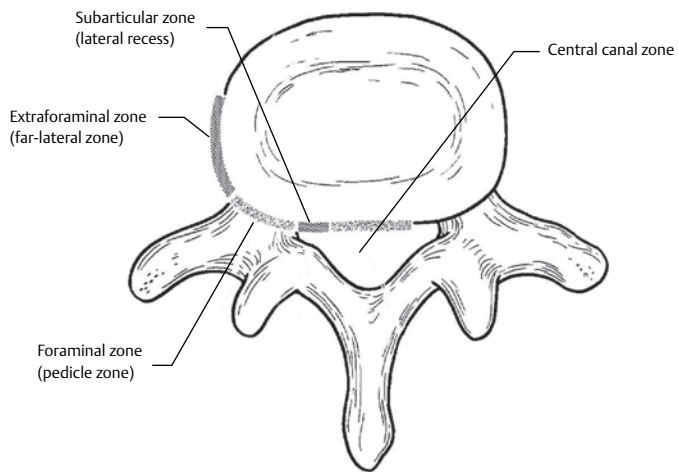


Fig. 7.24 Artist's sketch shows the anatomic "zones" identified on axial images. (From Wiltse LL, Berger PE, McCulloch JA. A system for reporting the size and location of lesions of the spine. *Spine* 1997;22:1534–1537. Reprinted by permission.)

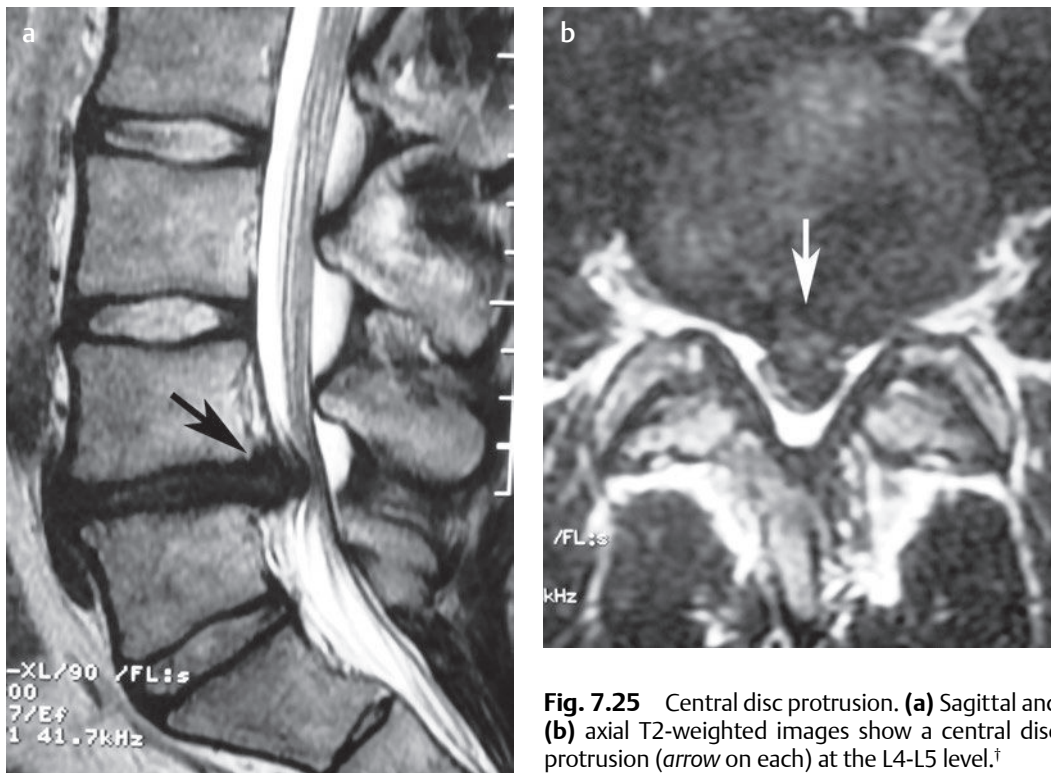


Fig. 7.25 Central disc protrusion. **(a)** Sagittal and **(b)** axial T2-weighted images show a central disc protrusion (arrow on each) at the L4-L5 level.[†]

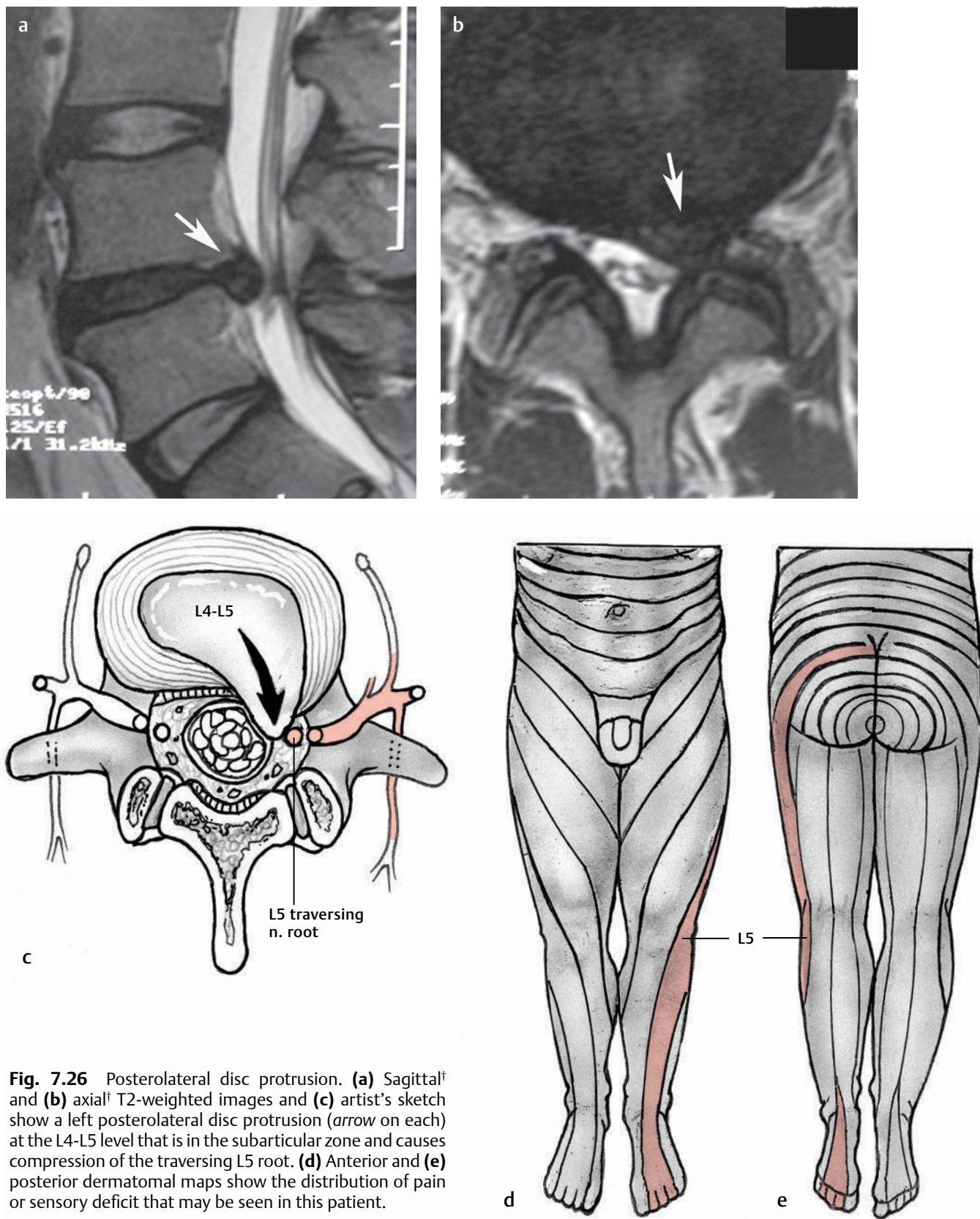


Fig. 7.26 Posterolateral disc protrusion. **(a)** Sagittal and **(b)** axial T2-weighted images and **(c)** artist's sketch show a left posterolateral disc protrusion (arrow on each) at the L4-L5 level that is in the subarticular zone and causes compression of the traversing L5 root. **(d)** Anterior and **(e)** posterior dermatomal maps show the distribution of pain or sensory deficit that may be seen in this patient.

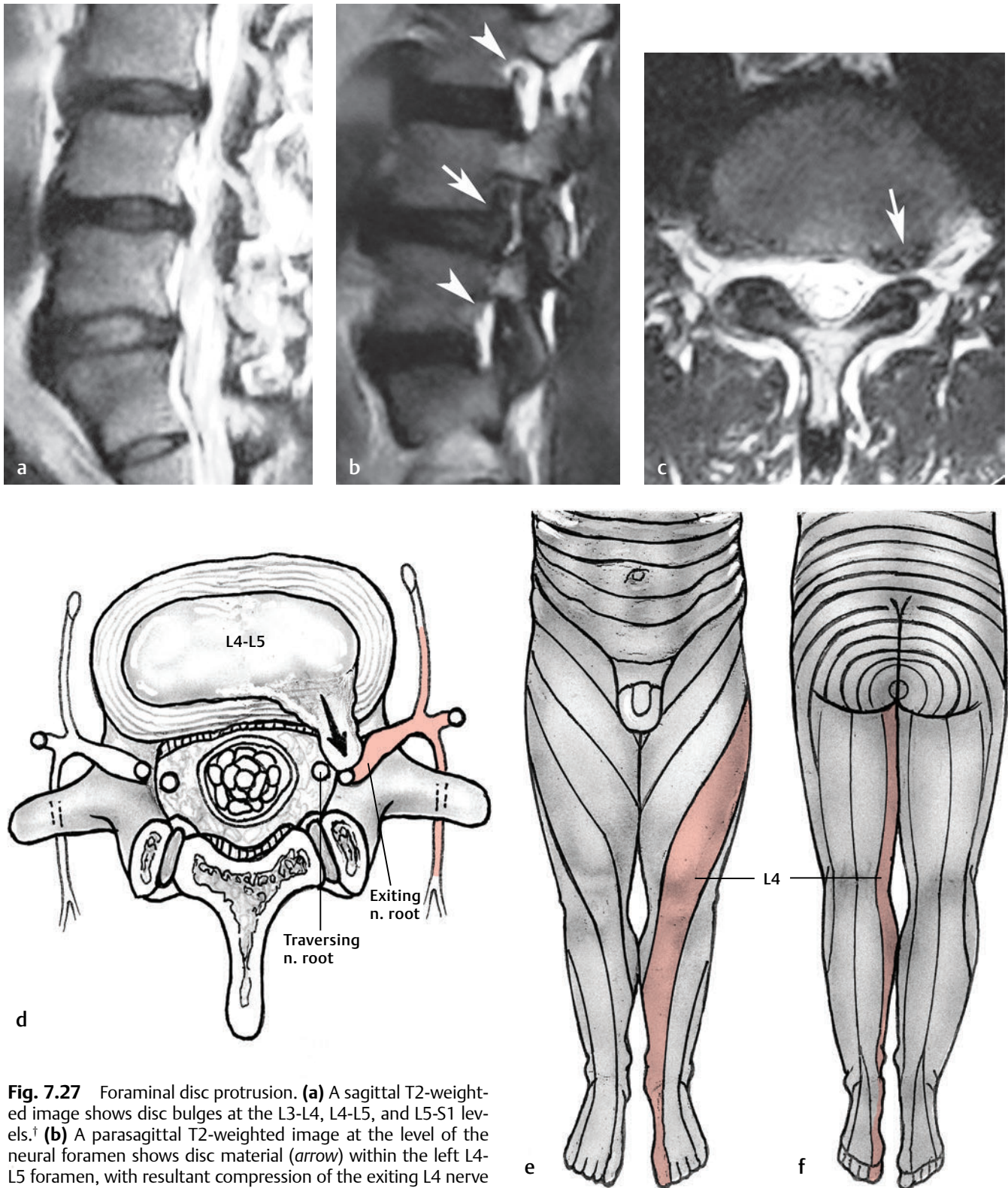
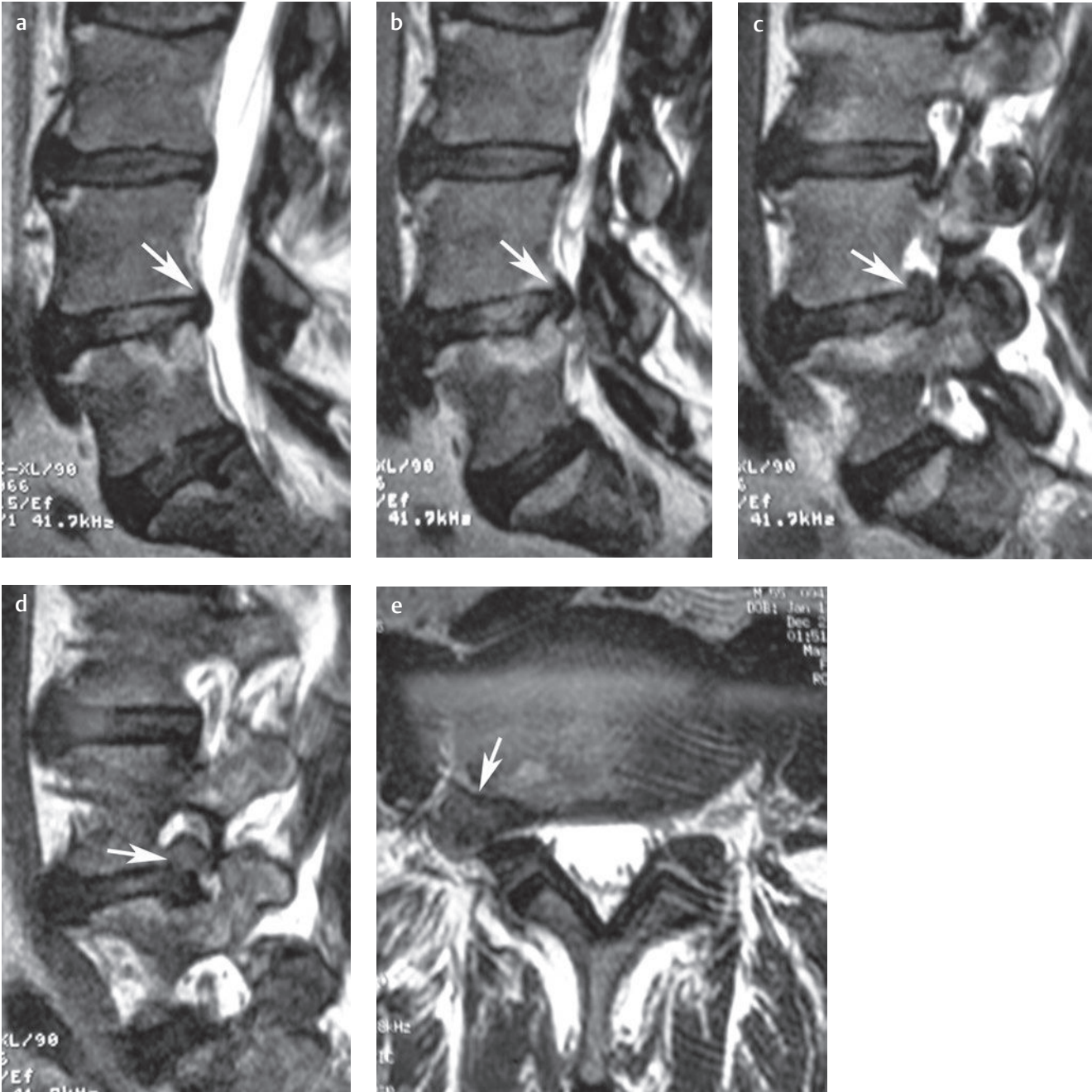


Fig. 7.27 Foraminal disc protrusion. **(a)** A sagittal T2-weighted image shows disc bulges at the L3-L4, L4-L5, and L5-S1 levels.[†] **(b)** A parasagittal T2-weighted image at the level of the neural foramen shows disc material (arrow) within the left L4-L5 foramen, with resultant compression of the exiting L4 nerve root.[†] Note the patency of the neural foramen at the L3-L4 and L5-S1 levels (arrowheads). **(c)** An axial T2-weighted image[†] and **(d)** artist's sketch at the L4-L5 level show a left-side disc protrusion (arrow) in the foraminal zone. **(e)** Anterior and **(f)** posterior dermatomal maps show the distribution of pain or sensory deficit that may be seen in this patient.



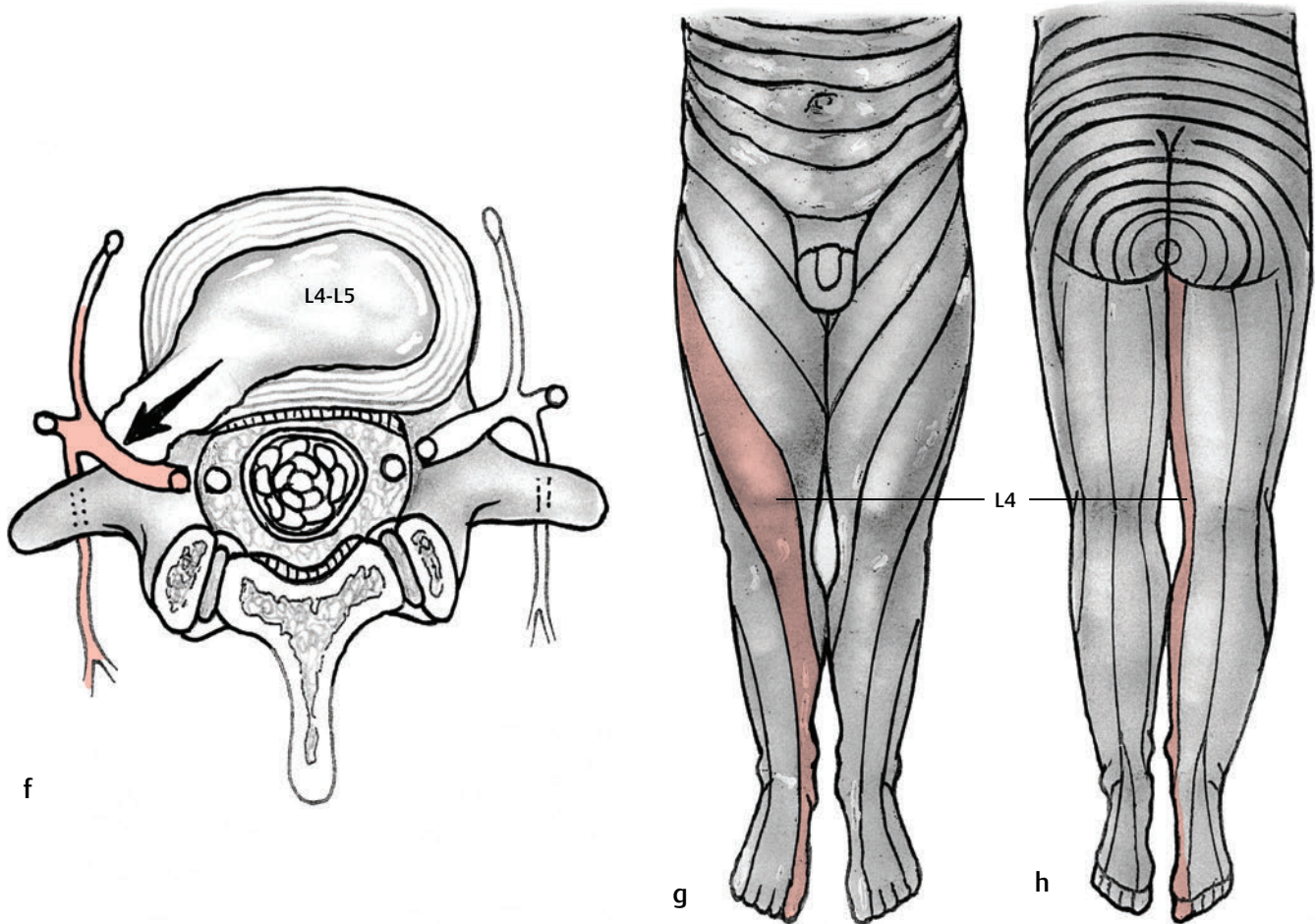


Fig. 7.28 Far-lateral disc protrusion. Sagittal T2-weighted images obtained in the (a) midline,[†] (b) a few millimeters lateral to midline,[†] (c) at the level of the pedicle,[†] and (d) lateral to the pedicle and foramen show a right-side far-lateral disc herniation that is seen primarily on d (arrow on each) at the L4-L5 level.[†] (e) The axial T2-weighted image (and [f] corresponding artist's sketch[†]) confirms that the disc protrusion is in the far-lateral zone (arrow) on the right side.[†] (g) Anterior and (h) posterior dermatomal maps show the distribution of pain or sensory deficit that may be seen in this patient.

Another characteristic of the disc pathology that should be evaluated is its expected consistency at surgery. Specifically, the spine surgeon will benefit from knowing whether the disc can be expected to be “soft” or “hard.” A soft disc protrusion consists primarily of nucleus pulposus, whereas hard disc pathology may consist of a chronic and desiccated disc protrusion or a posterior or posterolateral osteophyte (Fig. 7.29). T2-weighted images occasionally show increased signal within the disc protrusion, a finding that often correlates with a soft disc at surgery.

Thoracic Disc Herniation

Thoracic disc herniations are rare, constituting only 1% to 2% of all disc herniations.⁵¹ When they do occur, they are seen most often in the lower thoracic spine, likely the result of the increased mobility and load in this region. They can also be seen in association with Scheuermann disease. Sagittal T2-weighted images show thoracic disc herniations, and axial T2-weighted images allow additional characterization of the size, location, and morphology of the lesion (Fig. 7.30).

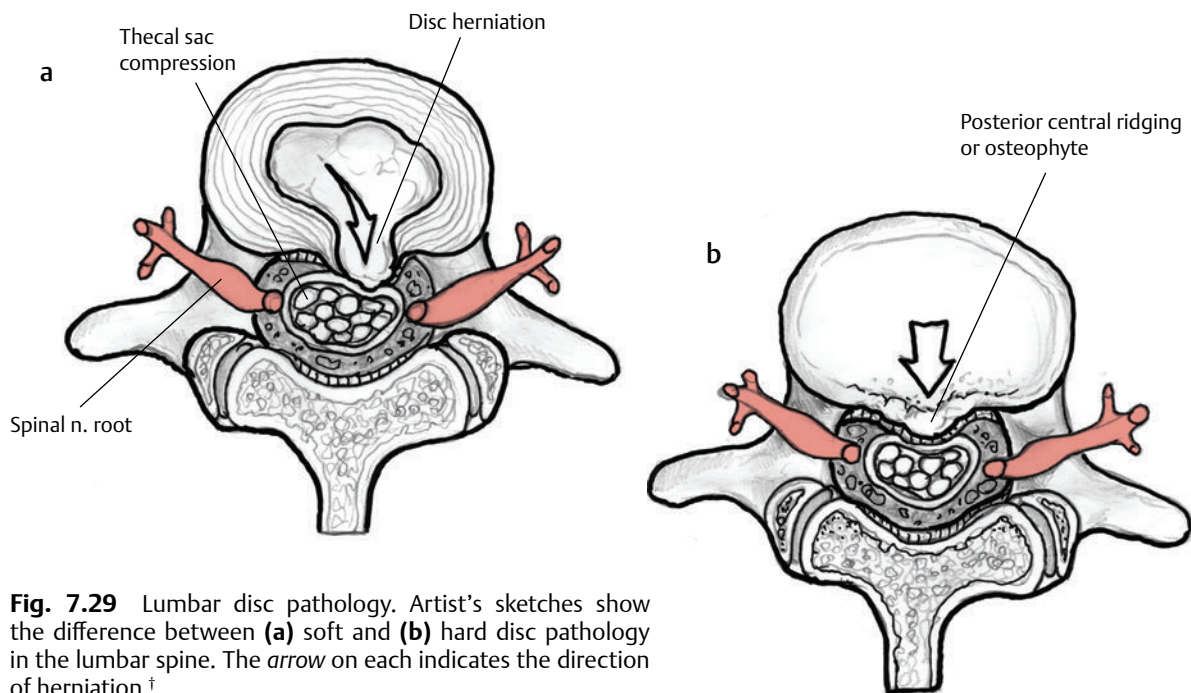


Fig. 7.29 Lumbar disc pathology. Artist's sketches show the difference between (a) soft and (b) hard disc pathology in the lumbar spine. The arrow on each indicates the direction of herniation.[†]

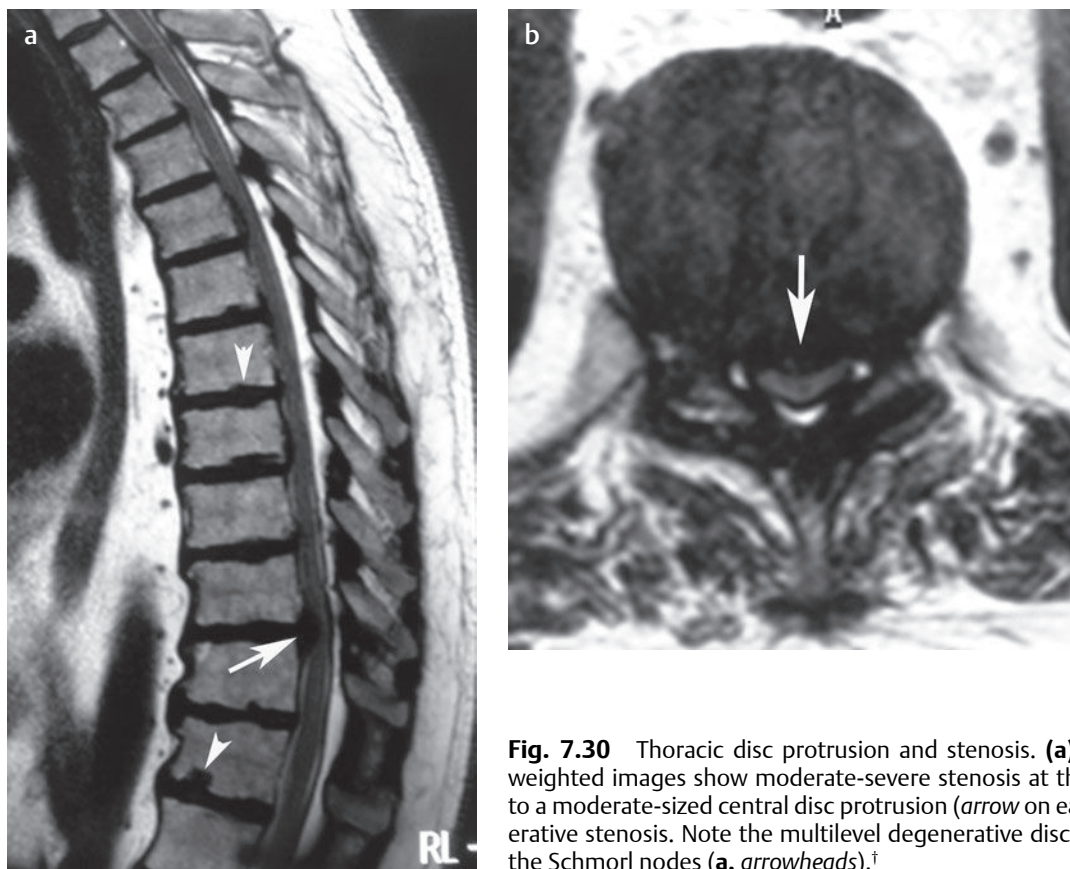


Fig. 7.30 Thoracic disc protrusion and stenosis. (a) Sagittal and (b) axial T2-weighted images show moderate-severe stenosis at the T10-T11 level secondary to a moderate-sized central disc protrusion (arrow on each) and underlying degenerative stenosis. Note the multilevel degenerative disc disease at other levels and the Schmorl nodes (a, arrowheads).[†]

Schmorl Nodes

Schmorl nodes represent herniations of the intervertebral disc through weak areas in the adjacent vertebral end plates and into the vertebral body.⁵² They are found most commonly in the thoracic and lumbar spine and occur in ~10% of the population, with no dependency on age or gender.⁵³ Scheuermann kyphosis is one of several processes that is associated with Schmorl nodes and premature disc degeneration. Patients may be asymptomatic or have nonspecific pain that may not be directly related to the presence of the Schmorl node. When symptoms are the result of the Schmorl node(s), the patient may present with axial back pain. MRI provides the optimal detection of Schmorl nodes (**Fig. 7.30**); they appear as extensions of disc material (with direct continuity with the disc) into the vertebral body, surrounded by a rim of low signal intensity secondary to reactive sclerosis.³⁹ Cases in which the Schmorl node is associated with increased T2-weighted signal in the adjacent bone marrow are more commonly associated with back pain and may represent an acute or subacute Schmorl node.^{50,54}

Facets

Facet Arthropathy

Although it is now accepted that the facet joints may be a cause of pain in the degenerated spine, it is difficult to associate them with a particular clinical syndrome.^{55–57} One of the earliest MRI findings of facet arthropathy is seen as fluidlike intraarticular signal intensity on sagittal or axial T2-weighted images (**Fig. 7.31**). Observation of such fluid within the facet joints suggests the potential for dynamic instability on flexion-extension radiographs and,

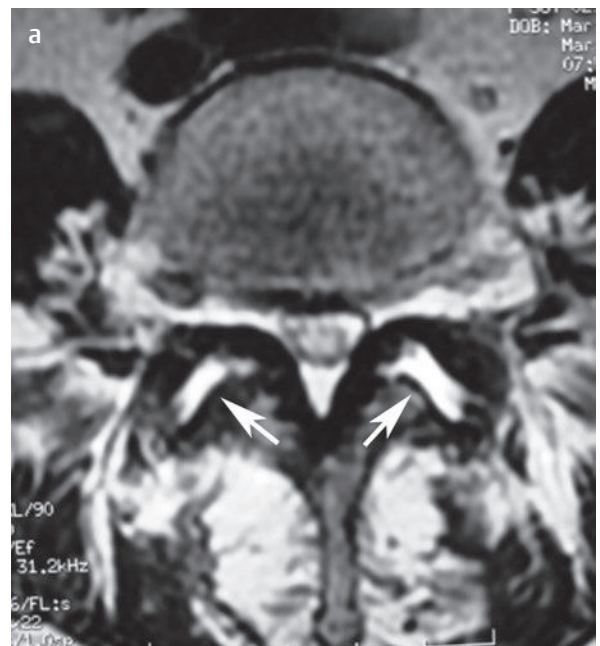
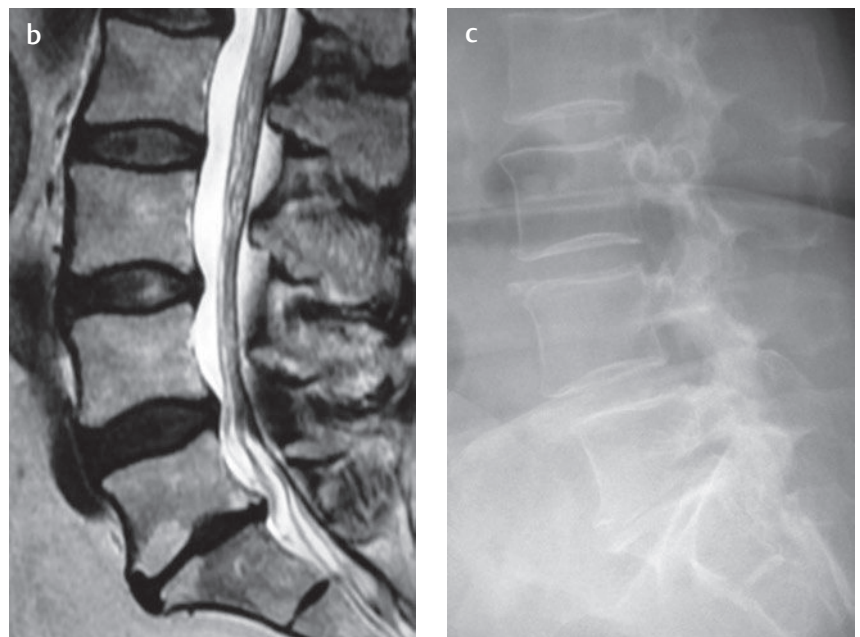


Fig. 7.31 Facet arthropathy and dynamic instability. **(a)** An axial T2-weighted image at the L4-L5 level shows bilateral facet arthropathy with fluid within and distending the L4-L5 facet joints (arrows). **(b)** A sagittal T2-weighted image (obtained with the patient in a supine position) shows evidence of stenosis at this level and also suggests the possibility of a subtle L4-L5 spondylolisthesis. Advanced degenerative disc disease is also seen at the L5-S1 level. **(c)** A standing lateral radiograph shows an obvious Meyerding grade-1 spondylolisthesis at the L4-L5 level. This series of images shows that degenerative changes and excessive fluid within the facet joints may be associated with instability; given that MRI is performed with the patient in the supine position, the spondylolisthesis may not be seen on the sagittal MR images.[†]



therefore, may affect the selection of surgical options for patients who demonstrate this finding.^{58,59} Renfrew and Heithoff²⁷ described a practical and simple way to assess facet arthropathy:

- **Mild:** mild undulation of the margins with small (1- to 3-mm) osteophytes, minimal subchondral sclerosis, mild narrowing of articular cartilage, and <25% increase in facet joint transverse dimension (**Fig. 7.32a**)
- **Moderate:** more pronounced changes, osteophytes up to 3 to 5 mm, and 25% to 50% increase in facet transverse dimension (**Fig. 7.32b**)

- **Severe:** additional progression of disease with near-complete loss of cartilage, osteophytes >5 mm, and joint width >50% of expected transverse dimension (**Fig. 7.32c**)

Facet joint hypertrophy may cause canal, subarticular recess, or foraminal stenosis and neural compromise. Effusions may also be seen within facet joints, reflecting synovitis from osteoarthritis or a synovial proliferative process in an inflammatory arthritis. Finally, asymmetric facet disease may predispose to degenerative disc disease and eventual scoliosis.⁶⁰⁻⁶²

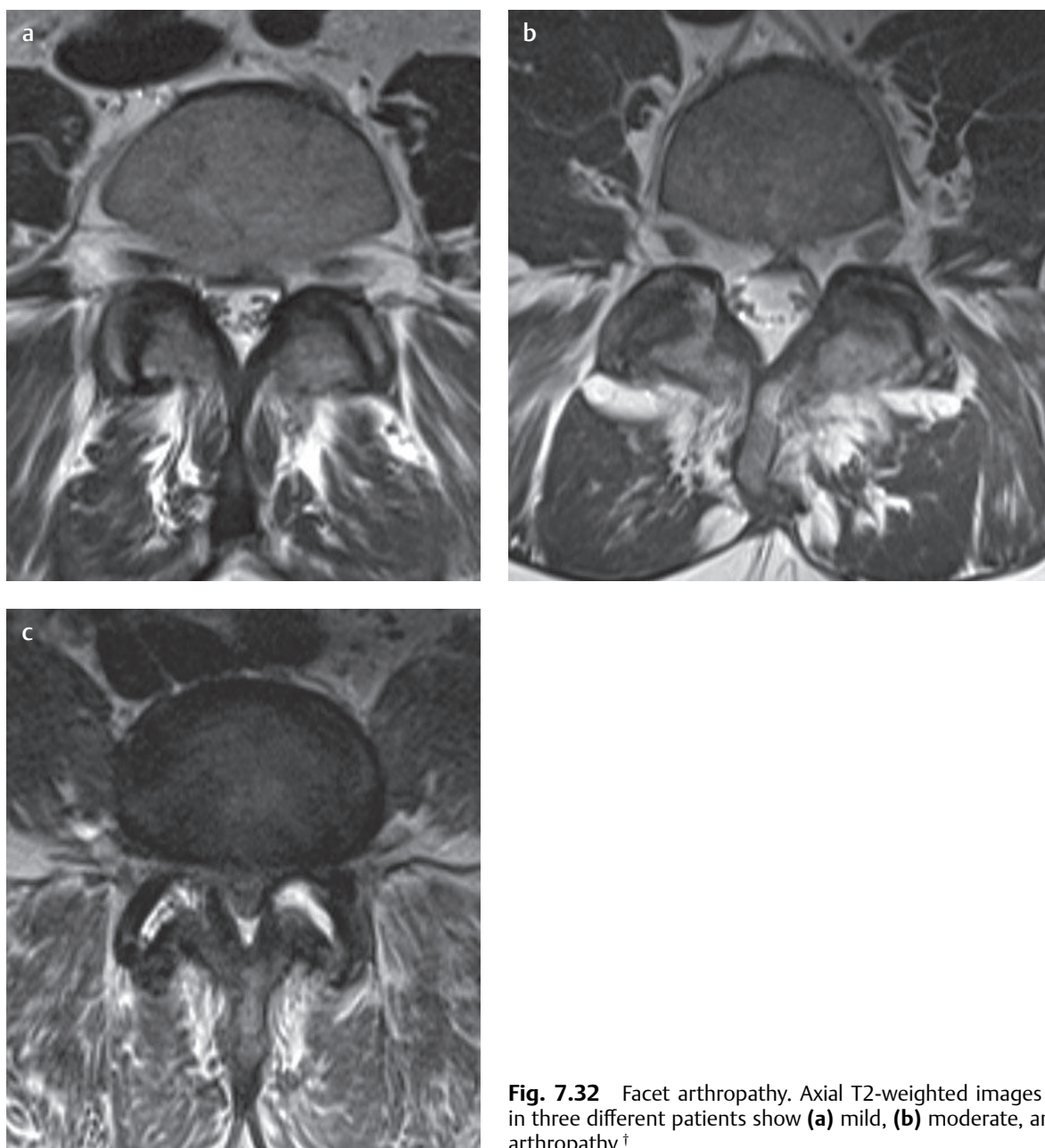


Fig. 7.32 Facet arthropathy. Axial T2-weighted images at the L4-L5 level in three different patients show (a) mild, (b) moderate, and (c) severe facet arthropathy.[†]

Synovial Cyst

A synovial cyst, which originates most commonly from lumbar facet joints, may also cause neural compression and may appear on a sagittal T2-weighted image as a hyperintense cyst with a hypointense rim (Fig. 7.33). T2-weighted MR images in the axial plane

show the degree of lateral recess stenosis. Neural foramen stenosis may arise from a reduction in the height of the neural foramen because of degenerative narrowing of the intervertebral disc space, facet joint hypertrophy and osteophyte formation, or posterolateral encroachment from the disc in the form of bulges, protrusions, and extrusions. This compression is

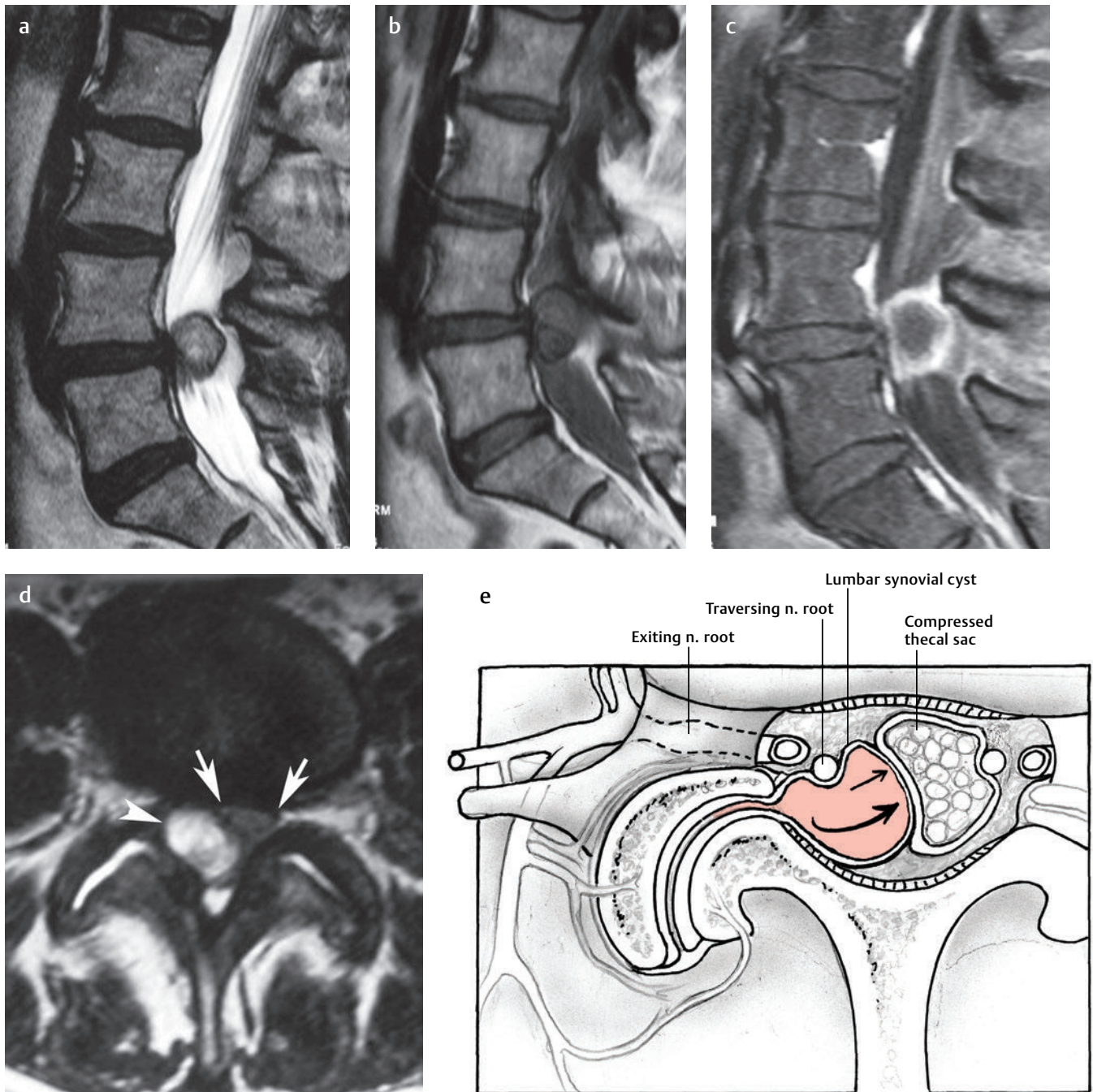


Fig. 7.33 Lumbar synovial cyst. Sagittal (a) T2-weighted,[†] (b) T1-weighted,[†] and (c) postgadolinium fat-suppressed T1-weighted[†] images show a large L4-L5 lesion compatible with a facet joint cyst when correlated with (d) the axial T2-weighted image. Note the intense peripheral enhancement of the lesion on c, the postgadolinium T1-weighted image. (d) The axial T2-weighted image shows that the cyst (arrowhead) likely originates from the right L4-L5 facet joint and that the thecal sac (between arrows) is severely compressed and shifted toward the left.[†] (e) An artist's sketch in the axial plane illustrates the findings seen in the preceding images.

evaluated best on far-lateral parasagittal T1-weighted and T2-weighted images that visualize the neural foramina in cross-section.⁶³ On occasion, synovial cysts may contain air or may calcify, in which case they may not have the typical bright fluid signal on T2-weighted images and may appear gray or dark on all sequences.

Lumbar Spinal Stenosis

The term *spinal stenosis* describes the compression of the neural elements in the spinal canal, lateral recesses, or neural foramina. The evaluation of patients with known or suspected lumbar spinal stenosis is one of the primary indications for MRI of the lumbar spine.^{64,65} Patients with lumbar stenosis typically present with combinations of radicular leg pain or weakness, neurogenic claudication, and low back pain. After nonoperative management fails for such patients and conventional radiographs have been obtained, MRI can be considered. The MR images should be evaluated to determine the degree (i.e., mild to severe), level (i.e., L1 to S1), and type (e.g., degenerative, congenital) of lumbar spinal stenosis.

The authors' suggested method for the assessment of lumbar spinal stenosis begins with a systematic evaluation of the midsagittal T2-weighted images. These images show the conus medullaris in the patient without scoliosis. The clinician or radi-

ologist should carefully trace the posterior margin of the vertebral bodies and intervening discs to ensure that there is no effacement of the CSF space. Next, the dorsal margin of the thecal sac should be evaluated on these images to evaluate for focal hypertrophy of the ligamentum flavum. This procedure should be repeated on the parasagittal T2-weighted images in each direction (left and right from center) to evaluate for lateral recess and foraminal stenosis. After the sagittal T2-weighted images have been evaluated, the axial T2-weighted images are sequentially evaluated from the sacrum toward the upper lumbar spine. Specifically, CSF should be seen ventral to the cauda equina, which is often displaced posteriorly within the spinal canal, given that most studies are obtained with the patient in a supine position. The lateral recess and foraminal region should be evaluated bilaterally at each level to rule out stenosis secondary to disc, facet, or ligamentum flavum pathology.

Spinal stenosis may involve the neural foramina, lateral recesses, or central canal of the lumbosacral spine and is usually developmental or acquired in nature. Developmental spinal stenosis, which constitutes ~15% of all cases of spinal stenosis, is hereditary-idiopathic or associated with disorders of skeletal growth.⁶³ MRI of the hereditary form shows minor hypoplasia of the posterior osseous arch of the vertebrae, short pedicles, and narrowing of the cross-sectional area of the central spinal canal (**Fig. 7.34**).

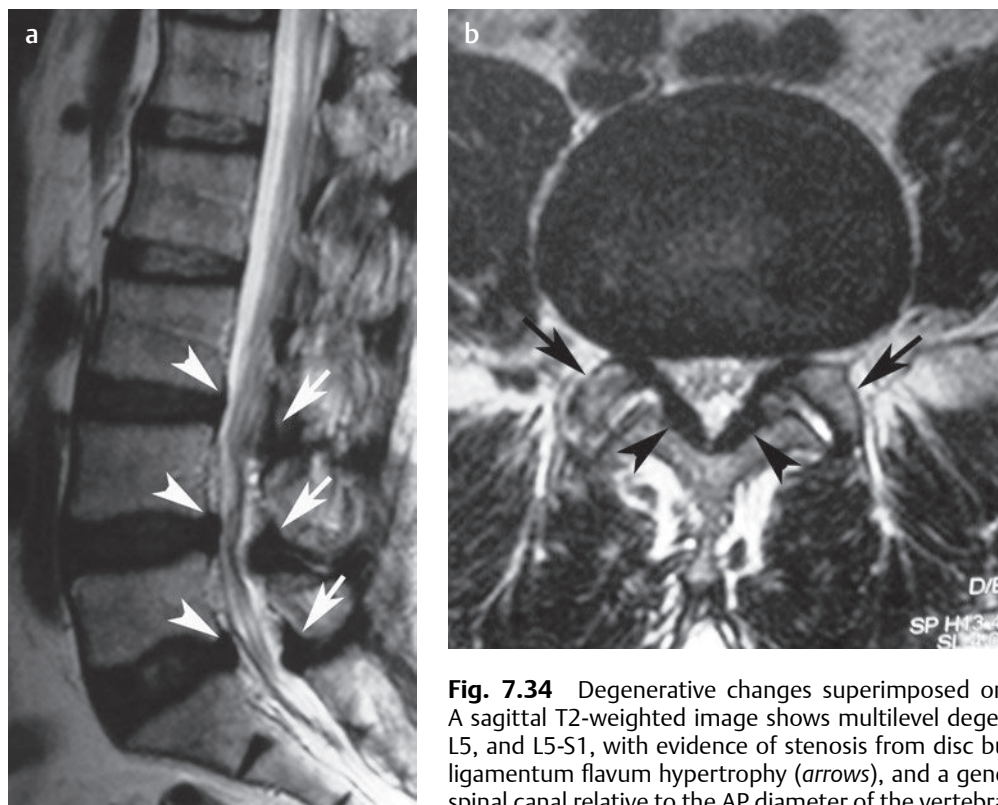


Fig. 7.34 Degenerative changes superimposed on congenital lumbar stenosis. **(a)** A sagittal T2-weighted image shows multilevel degenerative disc disease at L3-L4, L4-L5, and L5-S1, with evidence of stenosis from disc bulges at these levels (arrowheads), ligamentum flavum hypertrophy (arrows), and a generalized narrow appearance of the spinal canal relative to the AP diameter of the vertebral bodies. **(b)** An axial T2-weighted image at the L4-L5 level shows minimal to moderate stenosis secondary to underlying congenital stenosis with superimposed degenerative changes, including ligamentum flavum hypertrophy (arrowheads) and facet arthropathy (arrows).[†]

Sagittal images may show progressive narrowing of the AP dimension of the spine in the caudal direction, indicating developmental spinal stenosis.

Acquired central spinal canal stenosis may arise from hypertrophic or degenerative changes of the intervertebral discs, facet joints, or ligamentum flavum (**Fig. 7.35**). On MRI, central canal stenosis is characterized by compression of the thecal sac, best seen on sagittal and axial T2-weighted images. Fat-suppressed T2-weighted and STIR images provide a “myelographic effect,” in which the CSF is seen as bright signal anterior and posterior to the neural elements on sagittal and axial images. Effacement, discontinuity, or displacement of this CSF space is seen in patients with focal and concentric spinal stenosis (**Fig. 7.36**).

There are several objective measures of lumbar spinal stenosis.^{66,67} Hamanishi et al⁶⁶ found that a cross-sectional area of $<100 \text{ mm}^2$ at more than two of three lumbar intervertebral levels was highly as-

sociated with the presence of intermittent neurogenic claudication. Speciale et al⁶⁷ evaluated observer variability in assessing lumbar spinal stenosis on MRI in relation to cross-sectional spinal canal area and found only a fair level of agreement among the observers; however, they found that the ability of the various readers to predict the degree of central stenosis was high.

Another method for evaluating the degree of lumbar spinal stenosis and its potential for contribution to clinical symptoms is the “sedimentation sign,” a phenomenon named by Barz et al,⁶⁸ who also defined a positive sedimentation sign as an absence of sedimentation of nerve roots in patients with a diagnosis of lumbar spinal stenosis (**Figs. 7.37** and **7.38**). In patients without lumbar spinal stenosis, the lumbar nerve roots “sediment” to the dorsal part of the thecal sac (**Fig. 7.39**). Conversely, in patients with symptomatic and morphologic central lumbar stenosis, such sedimentation is rarely seen.⁶⁸

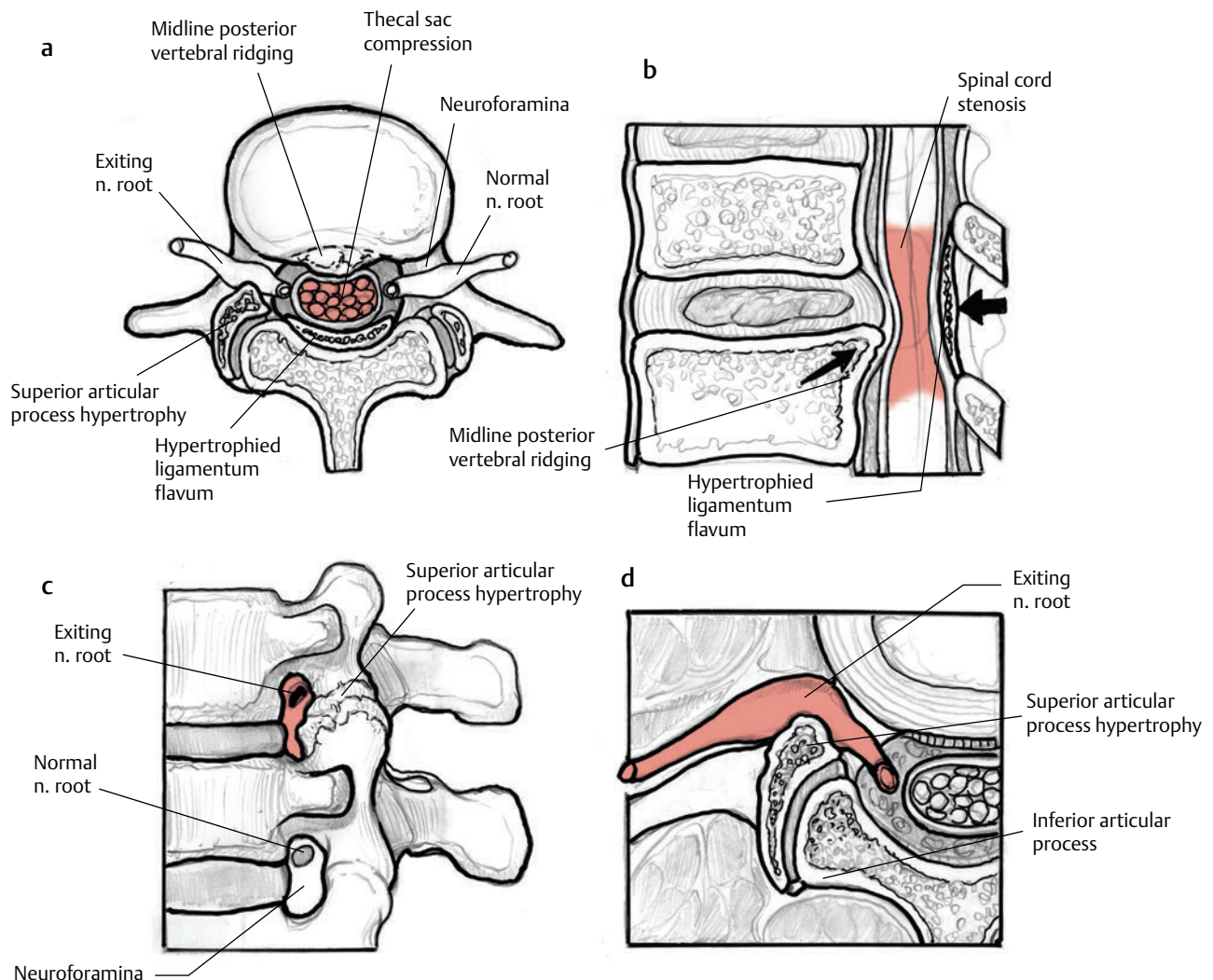


Fig. 7.35 Artist's sketches illustrating the anatomic changes that lead to lumbar stenosis. (a) An axial view. (b) A midline sagittal view. (c) A parasagittal view at the level of the neural foramina. (d) A magnified axial view shows the left lateral recess and foramen.[†]

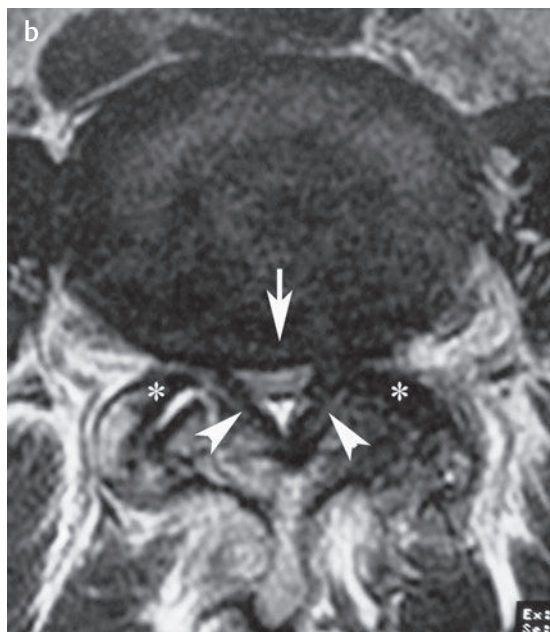
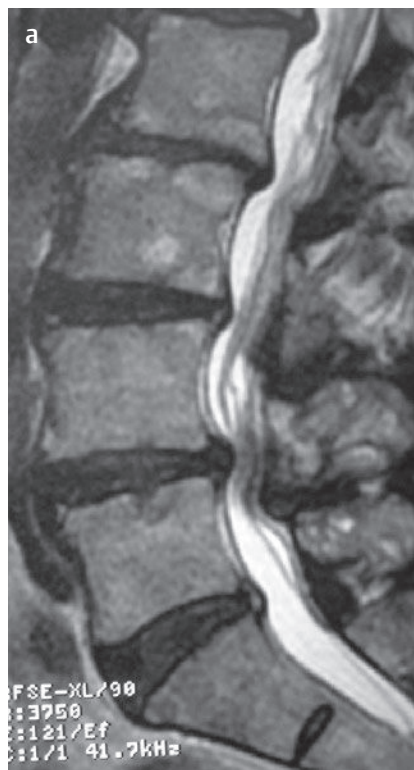


Fig. 7.36 Lumbar stenosis. **(a)** A sagittal T2-weighted image shows multilevel stenosis in the lumbar spine. **(b)** An axial T2-weighted image at the L4-L5 level shows moderate-severe stenosis secondary to contributions from a central disc bulge (arrow), ligamentum flavum hypertrophy (arrowheads), and facet arthropathy (asterisks).[†]

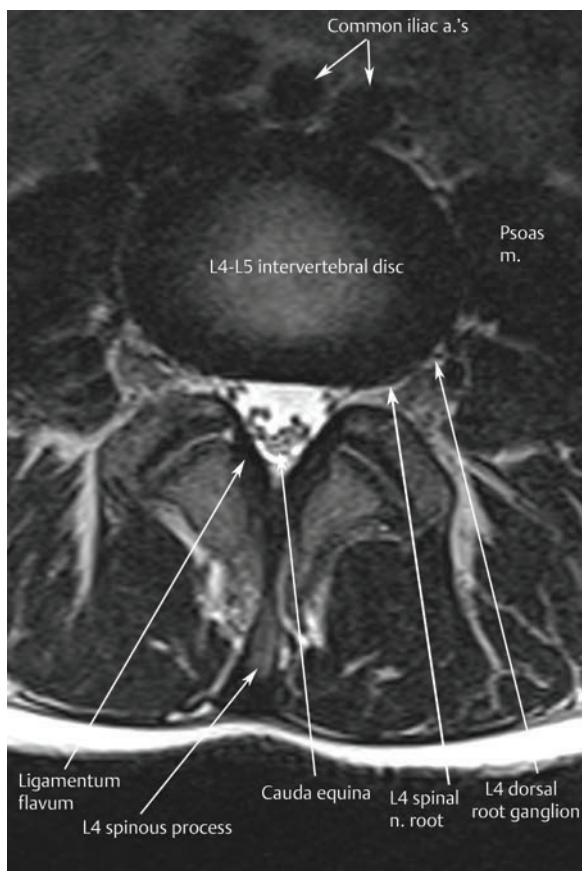


Fig. 7.37 An axial T2-weighted image of the lumbar spine at the L4-L5 level shows the cauda equina, L4 spinal nerve root, and L4 dorsal nerve root ganglion. Note the "sedimentation" of the nerve roots in the dorsal aspect of the thecal sac.[†]

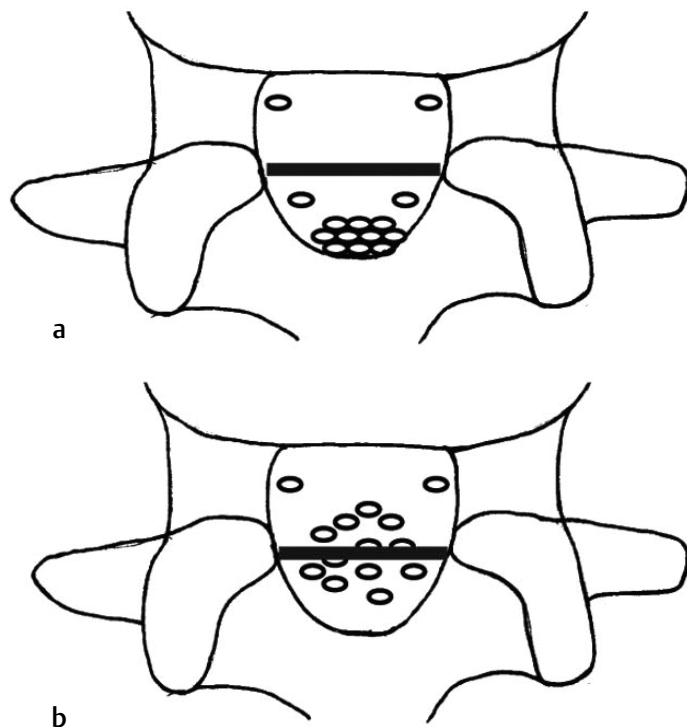


Fig. 7.38 An artist's sketch showing **(a)** negative and **(b)** positive sedimentation signs. (From Barz T, Melloh M, Staub LP, Lord SJ, Lange J, Roder CP, Theis JC, Merk HR. Nerve root sedimentation sign: evaluation of a new radiological sign in lumbar spinal stenosis. *Spine (Phila Pa 1976)* 2010;35(8):892–897. Reprinted by permission.)

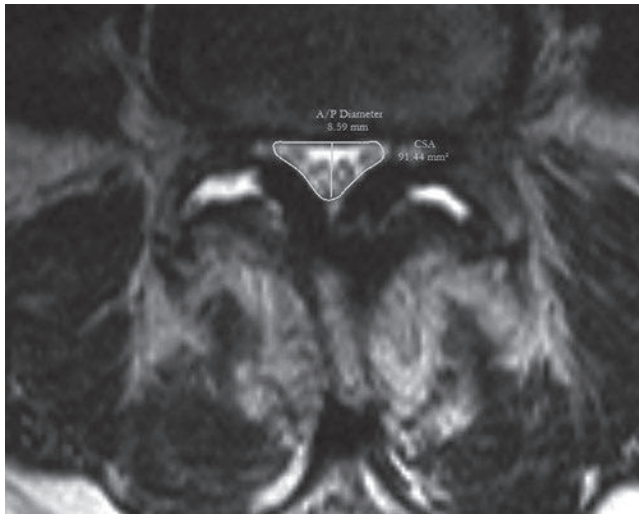


Fig. 7.39 An axial T2-weighted image of the lumbar spine shows the cross-sectional area and AP measurements and depicts a positive sedimentation sign. (From Fazal A, Yoo A, Bendo JA. Does the presence of the nerve root sedimentation sign on MRI correlate with the operative level in patients undergoing posterior lumbar decompression for lumbar stenosis? *Spine J.* 2013;13(8):837–842. Reprinted by permission.)

To show the clinical utility of the sedimentation sign and compare it with other, more traditional measures of lumbar stenosis, Fazal et al⁶⁹ performed a retrospective review of the preoperative MRI studies of 71 consecutive patients who presented with lumbar spinal stenosis and underwent a lumbar decompressive procedure. They evaluated several radiographic parameters, including the sedimentation sign, and found that the sedimentation sign was noted to be positive in 120 of 134 (89.5%) operated levels. Based on this and other findings, those authors suggested that the sedimentation sign allows physicians to evaluate the degree of spinal stenosis objectively and that the sign is most often present in patients who undergo lumbar decompressive surgery; they also found good degrees of correlation between the sedimentation sign and other radiographic parameters, including cross-sectional area, AP canal diameter, and degree of facet joint hypertrophy.⁶⁹

Although the formal measurements of lumbar stenosis on MRI just described are well known, most clinicians and radiologists tend to grade the degree of spinal stenosis as mild, moderate, or severe. The authors use the following terms and definitions:

- **Mild:** stenosis in which the canal begins to assume a triangular shape, the thecal sac is not compressed, and there is only minimal (<2 mm) thickening of the ligamentum flavum. The AP canal diameter is >75% of expected normal without nerve root crowding.

- **Moderate:** findings similar to those of mild stenosis but with compression and minimal flattening and deformity of the thecal sac. The AP canal diameter is between 50% and 75% of expected normal.
- **Severe:** advanced stenosis with very pronounced flattening and deformity of the thecal sac that is obvious on both sagittal and axial T2-weighted images. The ligamentum flavum is often thickened to >4 mm. The AP canal diameter is <50% of expected normal.

It should be noted that in some cases, canal narrowing can be downgraded if there is ample CSF surrounding the neural structures and upgraded if the surrounding CSF is scant. Similar terminology can be applied to grading stenosis in the subarticular recesses or foramina.

In addition to evaluating the degree of central and canal stenosis, the lateral recess, foraminal, and extraforaminal zones should also be specifically assessed (**Fig. 7.24**). Lateral recess and foraminal stenosis are most often the result of a combination of pathologies: facet arthropathy, ligamentum flavum hypertrophy, and disc bulge or protrusion. Specifically, hypertrophy of the superior articular process from the caudal level often leads to the development of foraminal stenosis. In addition, degenerative disc disease with the associated loss of disc height and subsequent loss of foraminal height and volume can lead to the development or exacerbation of foraminal stenosis from other degenerative pathologies. Many clinicians and radiologists evaluate for the presence of foraminal stenosis in the axial plane. However, parasagittal images are also quite useful in confirming the presence of foraminal stenosis (**Figs. 7.27** and **7.28**). The normal foramen has an ovoid configuration on parasagittal images (see Chapter 2, Normal Spine MRI Anatomy) where the superior aspect of the foramen contains the exiting nerve root and the inferior aspect of the foramen shows high signal intensity on both T1-weighted (from perineural fat) and T2-weighted (from CSF within the nerve root sleeve) images. On parasagittal images, patients with foraminal stenosis have progressive narrowing of the foramen, with resultant compression of the nerve root.

Cauda Equina Syndrome

Cauda equina syndrome is typically characterized by unilateral or bilateral sciatica, perianal or saddle anesthesia, bowel and bladder incontinence, and sensory and motor deficits in the lower extremities.⁷⁰ Often, it is caused by a space-occupying mass compressing against the cauda equina and/or conus medullaris. There can be numerous etiologies, including disc herniation, severe stenosis, trauma, tumor, or infection.^{71,72}

MRI is the preferred imaging modality for the evaluation of the patient with suspected cauda equina syndrome. MRI allows visualization of space-occupying lesions within the spinal canal as well as identification of compression of neural structures. Lumbar myelography with CT of the lumbar spine is indicated in patients who are unable to undergo MRI. Given that the treatment of cauda equina syndrome is urgent decompression, one of these imaging studies should be obtained without delay.

Spondylolisthesis

Spondylolisthesis is defined as anterior displacement of a vertebral body relative to the one caudal to it. Retrolisthesis is seen when the superior vertebral body is displaced posterior to the one caudal to it. Wiltse et al⁷³ classified lumbar spondylolisthesis on the basis of etiology: dysplastic, isthmic, degenerative, traumatic, iatrogenic, or pathologic. Meyerding⁷⁴ described the various degrees of forward slippage (from grade 1 to grade 4) based on a division of the superior surface of the lower vertebra into quarters (**Fig. 7.40**). According to this system, a complete slip of L5 on S1 is termed *spondyloptosis*. Each manifestation of spondylolisthesis has specific associated MRI findings.

The system of Wiltse et al⁷³ details the features of spondylolisthesis as follows:

- **Dysplastic spondylolisthesis:** may present with degeneration and pseudobulging of the lumbosacral disc, with potential compression of the cauda equina between the neural arch of L4 and the superoposterior aspect of the sacrum (for a slip at L5). A parasagittal T1-weighted SE image may show severe compression of the exiting L5 nerve root.
- **Isthmic spondylolisthesis:** sagittal T2-weighted images often show obvious spondylolisthesis at the L5-S1 level (**Fig. 7.41**). Parasagittal images at the level of the pedicle may show compression of the exiting L5 nerve root between the bulging L5-S1 disc and the undersurface of the L5 pedicle, along with reduction of foraminal height. The parasagittal images should also be scrutinized for the presence of a pars intraarticularis defect or reparative granulation tissue in that region; CT imaging may help confirm the presence of the pars defect.
- **Degenerative spondylolisthesis:** seen most commonly at the L4-L5 level. MRI can be used to evaluate narrowing of the central canal, lateral recesses, and neural foramina and compression of the cauda equina and exiting nerve roots. Facet joint cysts are not uncommon in the presence of degenerative spondylolisthesis. Sagittal and axial T2-weighted images delineate these entities clearly (**Fig. 7.42**).

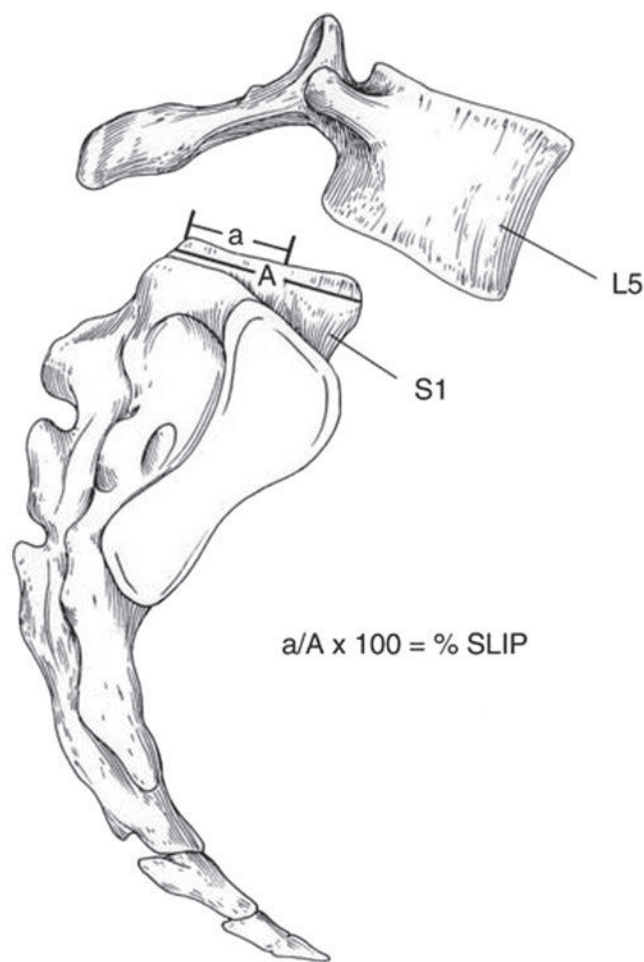


Fig. 7.40 An artist's sketch of the Meyerding classification, which is used to quantify the degree of spondylolisthesis. Grade 1 is 0% to 25% slip, grade 2 is 26% to 50% slip, grade 3 is 51% to 75% slip, and grade 4 is 76% to 99% slip. A = width of the superior end plate of S1, a = distance between the posterior edge of the inferior end plate of L5 and the posterior edge of the superior end plate of S1. (From Cavalier R, Herman MJ, Cheung EV, Pizzutillo PD. Spondylolysis and spondylolisthesis in children and adolescents. I. Diagnosis, natural history, and nonsurgical management. *J Am Acad Orthop Surg* 2006;14:417–424. This reprinted illustration was modified with permission from Herman MJ, Pizzutillo PD, Cavalier R. Spondylolysis and spondylolisthesis in the child and adolescent athlete. *Orthop Clin North Am* 2003;34:461–467. Reprinted by permission.)

- **Traumatic spondylolisthesis:** MRI shows the associated soft-tissue injury, which may include rupture of the intervertebral disc and posterior ligamentous complex, as seen with bilateral facet dislocation (**Fig. 7.10**).
- **Pathologic spondylolisthesis:** MRI shows very focal changes at the level of the pars intraarticularis based on the specific pathology involved.

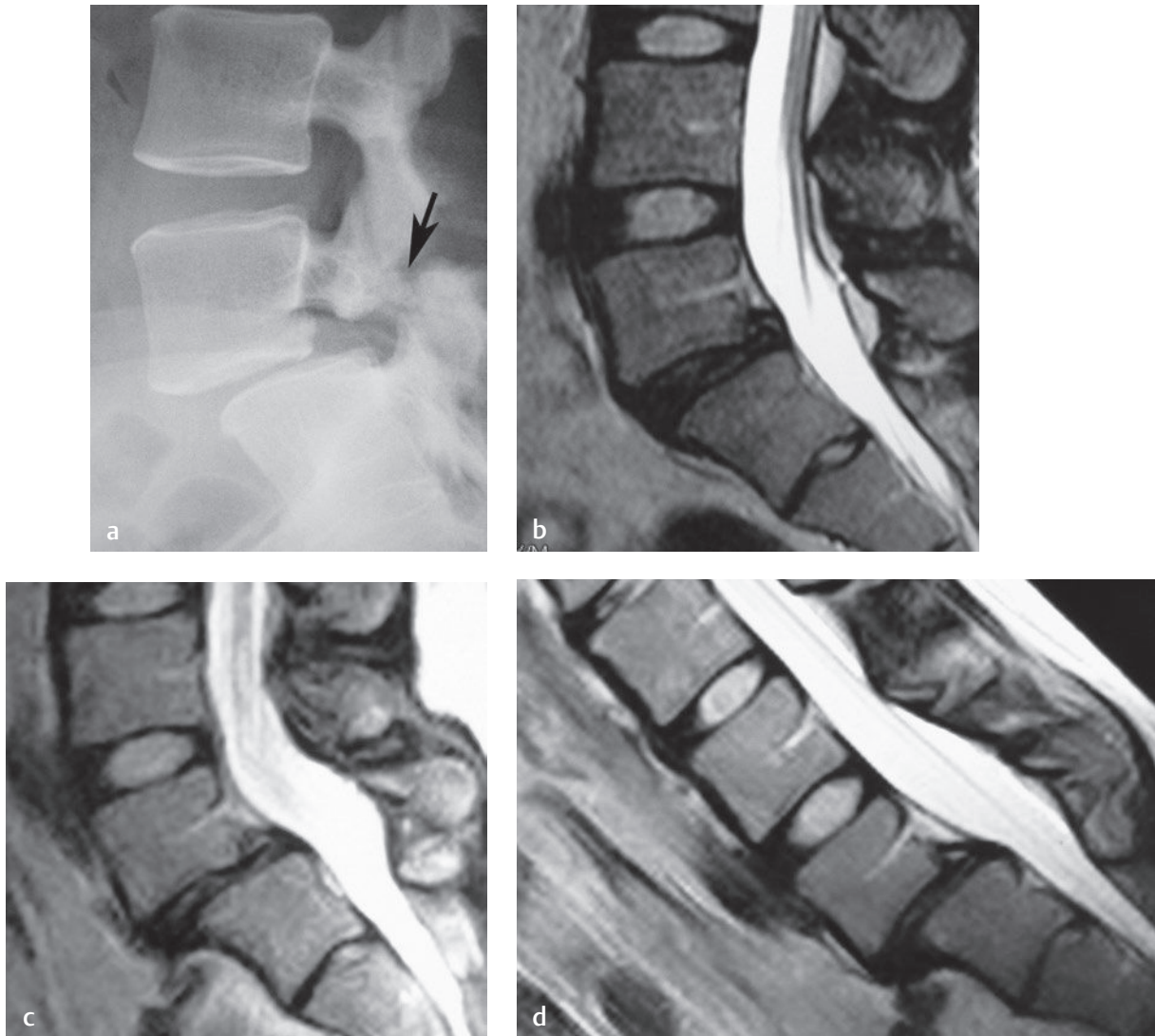


Fig. 7.41 Isthmic spondylolisthesis. **(a)** A lateral radiograph shows bilateral pars intraarticularis defects (*arrow*) at the L5-S1 level with Meyerding grade-2 spondylolisthesis. **(b)** A sagittal T2-weighted MR image obtained via a closed system with the same patient in a supine position shows grade-1 spondylolisthesis. **(c)** A sagittal T2-weighted MR image obtained via an open MRI system with the patient in a standing position shows that the spondylolisthesis progresses to grade 2. **(d)** A sagittal T2-weighted image obtained via an open MRI system with the patient in a flexed position shows that the grade-2 spondylolisthesis progresses compared with images in the **(c)** neutral and **(b)** supine positions.[†]

- **Iatrogenic spondylolisthesis:** may occur after laminectomy, facetectomy, and extensive resection of the facet joint and neural arch without fusion. MRI shows changes directly correlated to the specific areas altered during surgery.

Recently, the focus in spondylolisthesis has moved beyond the slippage of the vertebral bodies to include, among other issues, its etiologic factors and spinopelvic alignment. This change in focus has led to the development of more comprehensive classification systems that may be better at predicting progression of the disease, especially in younger individuals.⁷⁵⁻⁷⁷

Scoliosis

Scoliosis is a lateral curvature of the vertebral column in the coronal plane involving lateral and rotational vectors, and it may be associated with spinal cord or other neuronal abnormalities that are best visualized with MRI before operative intervention. The most common indication for MRI in patients with scoliosis is degenerative scoliosis. In this scenario, MRI is obtained to evaluate for the presence, degree, and levels of stenosis. Because of the unique challenge of obtaining contiguous visualization of the spinal canal

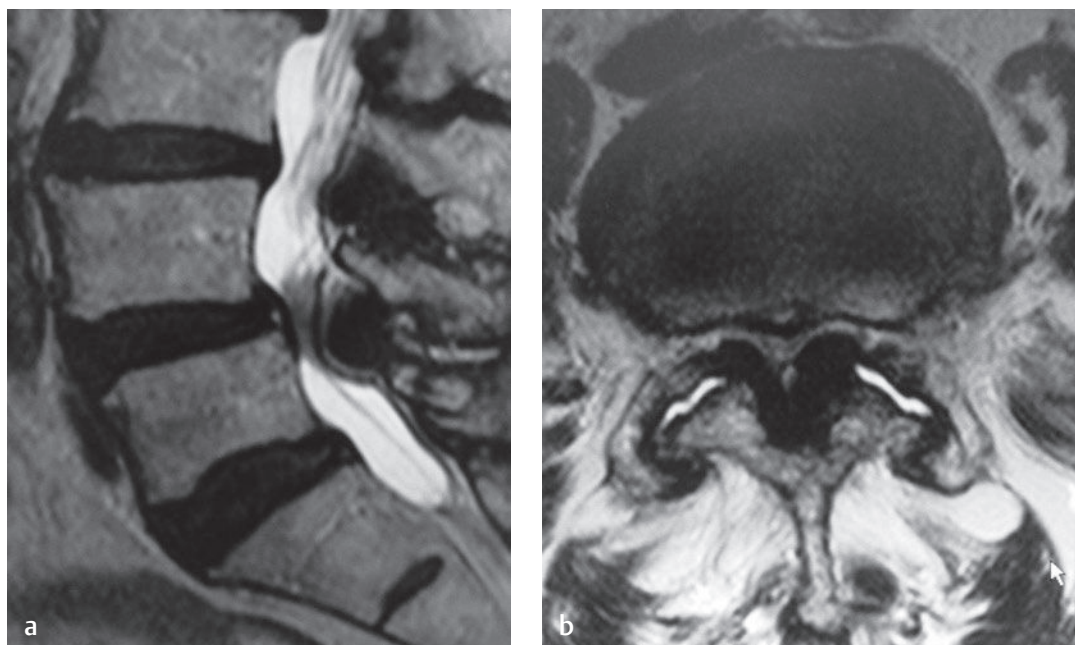


Fig. 7.42 Degenerative spondylolisthesis. **(a)** A sagittal T2-weighted image shows Meyerding grade-1 spondylolisthesis at the L4-L5 level with severe stenosis and evidence of a high-intensity zone at the posterior annulus of the L4-L5 disc. **(b)** An axial T2-weighted image shows severe stenosis from a central disc bulge, ligamentum flavum hypertrophy, and facet arthropathy.[†]

content in the scoliotic spine, specific protocols should be followed to obtain the best views. Redla et al⁷⁸ described the use of sagittal T1-weighted SE and T2-weighted FSE sequences, beginning from above the foramen magnum and including the brainstem down to the sacrum. However, for typical thoracolumbar scoliosis, MR images are obtained of the thoracic and lumbar spine only. When the curve is severe, sagittal sequences are obtained parallel to the two major portions of the curve and are planned from the coronal plane. Axial T1-weighted images are obtained through the apices of the curve, providing a second view of the cord. A coronal T1-weighted sequence also is obtained, especially to assess the vertebral bodies for congenital anomalies. In patients with degenerative stenosis, the sagittal and axial T2-weighted images should be evaluated in correlation with each other to determine the degree and type of stenosis at each level (**Fig. 7.43**). This information helps determine the levels for decompression in a patient who is being considered for surgical intervention.

Aside from the evaluation of the patient with lumbar degenerative scoliosis and suspected stenosis, the indications for MRI in patients with scoliosis have been the subject of debate (see Chapter 9, MRI of the Pediatric Spine). Although some studies have shown that routine MRI is not indicated for patients with adolescent idiopathic scoliosis who have a typical right

thoracic curve and who are neurologically intact,^{79–81} others have found a high incidence of spinal cord abnormalities (17.6% to 26%) in patients with infantile and juvenile forms of scoliosis.^{78,82} Those studies stressed the importance of MRI in children younger than 11 years old. Spinal cord abnormality is suggested by several physical examination findings, including a left thoracic curve, absent abdominal reflexes, lower limb neurologic deficits, and cutaneous stigmata of occult spinal dysraphism.⁷⁸

Specific MRI findings for abnormalities seen with scoliosis secondary to an underlying neurologic abnormality include the following:

- Tethered cord: thickened filum terminale and spinal lipoma, seen on sagittal T1-weighted SE and T2-weighted FSE images
- Syringohydromyelia: dissection of CSF through the cord substance, best seen on T2-weighted images with increased signal within the cord, sometimes associated with sacculation
- Diastematomyelia: a midline sagittal cleft of the spinal cord most commonly involving the lower thoracic and lumbar region, seen as two hemicords on MRI, with each having a single dorsal and ventral horn and a septum seen from the dorsal aspect of the vertebral body and extending into the cleft between the cords

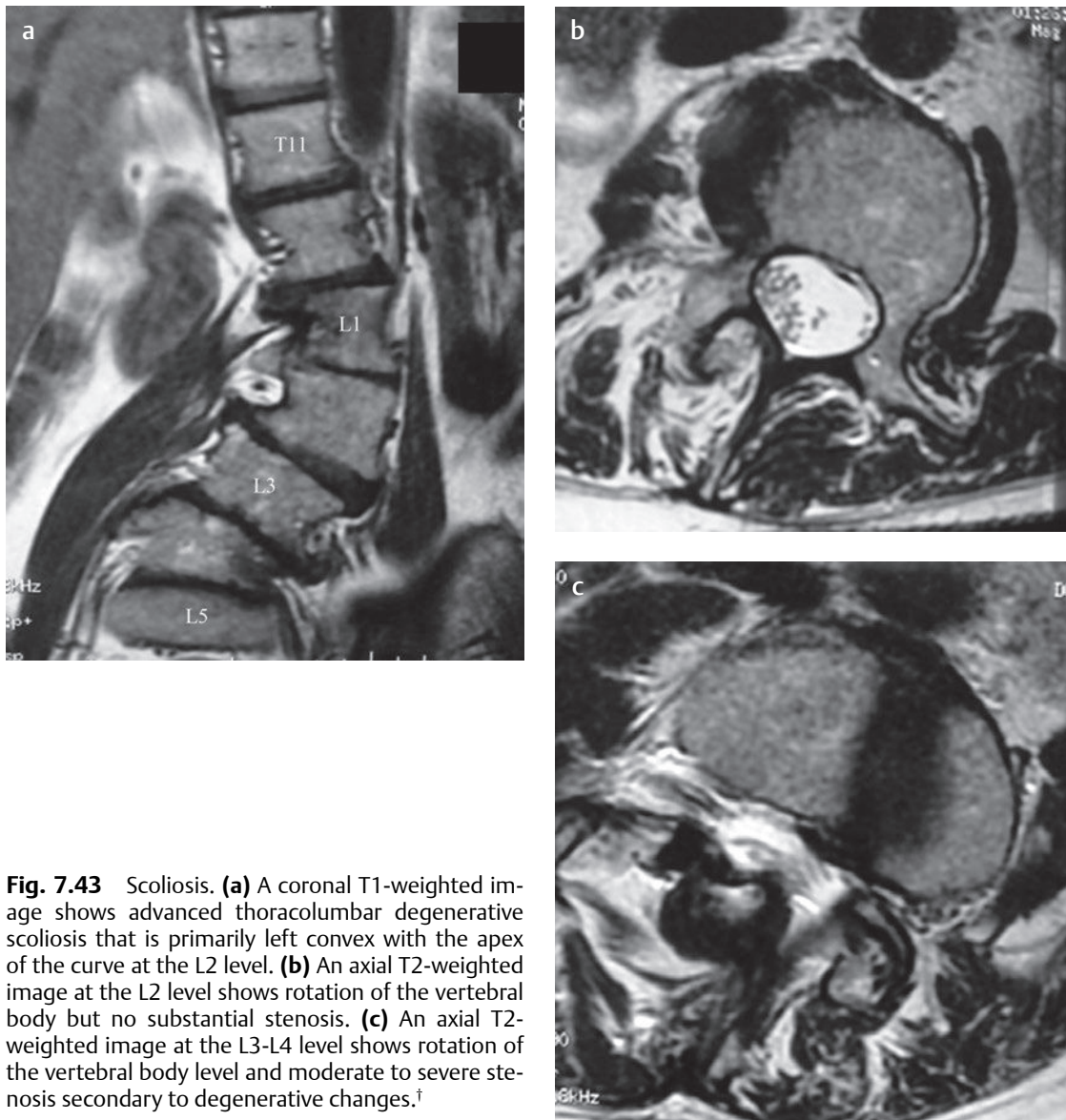


Fig. 7.43 Scoliosis. **(a)** A coronal T1-weighted image shows advanced thoracolumbar degenerative scoliosis that is primarily left convex with the apex of the curve at the L2 level. **(b)** An axial T2-weighted image at the L2 level shows rotation of the vertebral body but no substantial stenosis. **(c)** An axial T2-weighted image at the L3-L4 level shows rotation of the vertebral body level and moderate to severe stenosis secondary to degenerative changes.[†]

- Neurofibromatosis: a congenital condition that may show dural ectasia, pseudomeningocele, and neurofibromas on MRI
- Pars defects: a common occurrence in patients with developmental scoliosis; may occur in up to 6.2% of patients with idiopathic scoliosis⁸³

Epidural Lipomatosis

Epidural lipomatosis is a condition in which there is excessive deposition of fat in the epidural space that, in turn, leads to spinal stenosis and neural compression. The syndrome is primarily associated with excessive glucocorticoid levels, which

may be exogenous or endogenous but may also be spontaneous or idiopathic.^{84–86} In the lumbar spine, epidural fat surrounding and compressing the thecal sac is the key finding. In the thoracic spine, the presence of >6 mm of fat posterior to the cord is diagnostic. The characteristic feature of lumbar epidural lipomatosis is the presence of epidural tissue that follows the signal characteristics of subcutaneous fat on all pulse sequences, including fat-suppressed sequences (**Fig. 7.44**). The primary differential consideration includes an intraspinal lipoma, which is typically focal and is often located in the anterior thoracic spine.⁸⁷ Other epidural abnormalities tend to have a low T1-weighted signal and can be excluded.

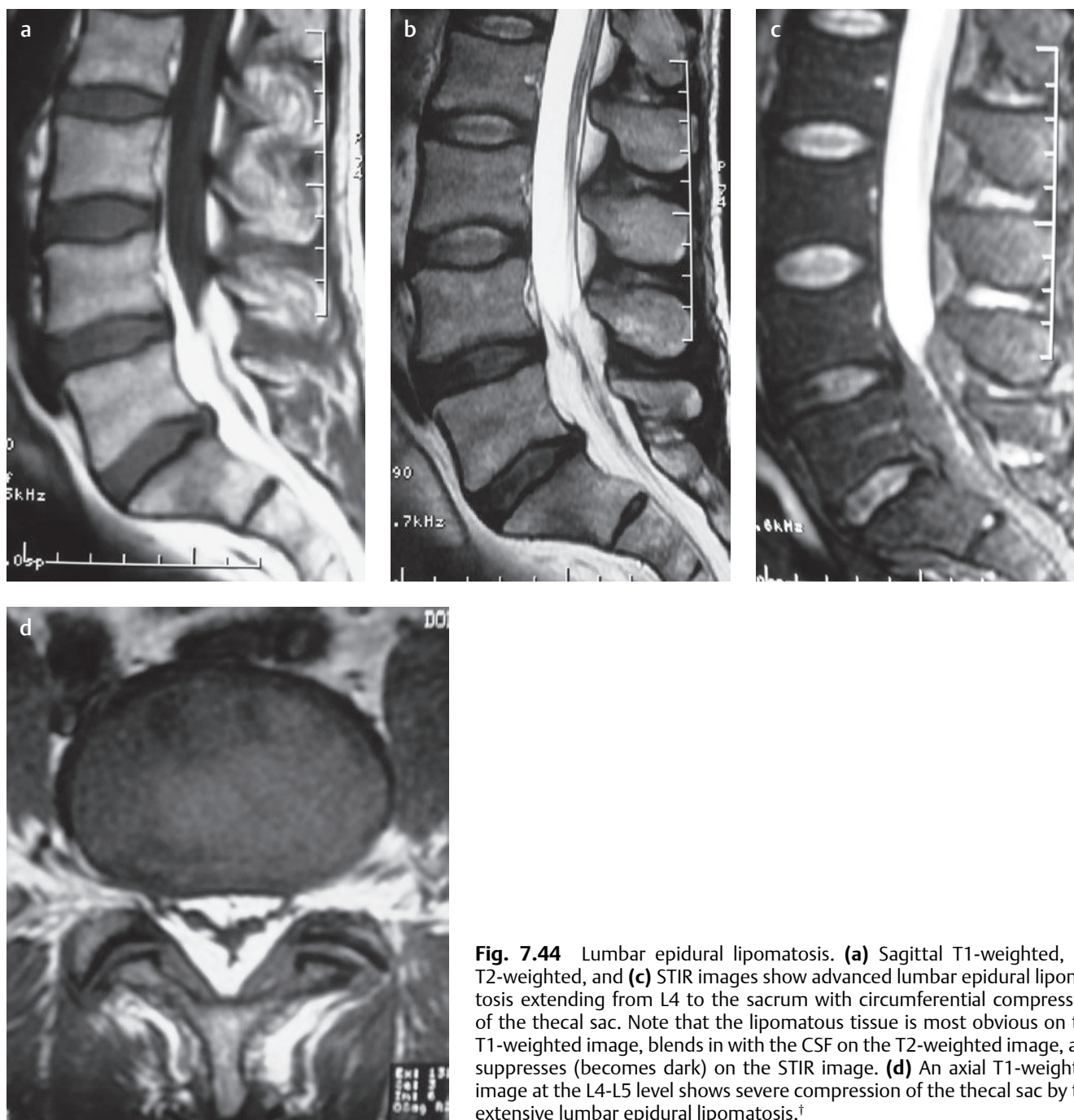


Fig. 7.44 Lumbar epidural lipomatosis. **(a)** Sagittal T1-weighted, **(b)** T2-weighted, and **(c)** STIR images show advanced lumbar epidural lipomatosis extending from L4 to the sacrum with circumferential compression of the thecal sac. Note that the lipomatous tissue is most obvious on the T1-weighted image, blends in with the CSF on the T2-weighted image, and suppresses (becomes dark) on the STIR image. **(d)** An axial T1-weighted image at the L4-L5 level shows severe compression of the thecal sac by the extensive lumbar epidural lipomatosis.[†]

■ Infectious Conditions

Vertebral Osteomyelitis

Cases of vertebral osteomyelitis comprise between 2% and 4% of all skeletal infections.^{88,89} MRI is usually regarded as the imaging modality of choice for the detection of this process, with a sensitivity of >82%

and a specificity of 53% to 94%.⁹⁰ Infection involving the vertebral body occurs through one of three primary routes⁹¹:

- Hematogenous (most common)
- Direct inoculation through surgery or penetrating trauma
- Contiguous spread from an adjacent soft-tissue infection

Hematogenous seeding occurs through nutrient arterioles of the vertebral bodies or by retrograde spread through the paravertebral venous plexus of Batson.⁹¹⁻⁹³ Infection then spreads from the vertebral body and marrow to the contiguous intervertebral disc and adjacent vertebral body, often sparing the central portion of the vertebral bodies.^{91,93}

The general MRI signal changes in patients with osteomyelitis include the following:

- Decreased signal intensity of the intervertebral disc and adjacent vertebral bodies, with

a discernible margin between the two on T1-weighted images

- Increased signal intensity of vertebral bodies adjacent to the involved disc on T2-weighted images
- An abnormal configuration and increased signal intensity of the intervertebral disc with loss of the nuclear cleft on T2-weighted images^{89,94} (**Fig. 7.45**).

Gadolinium enhancement may be seen in adjacent vertebral bodies. However, gadolinium may

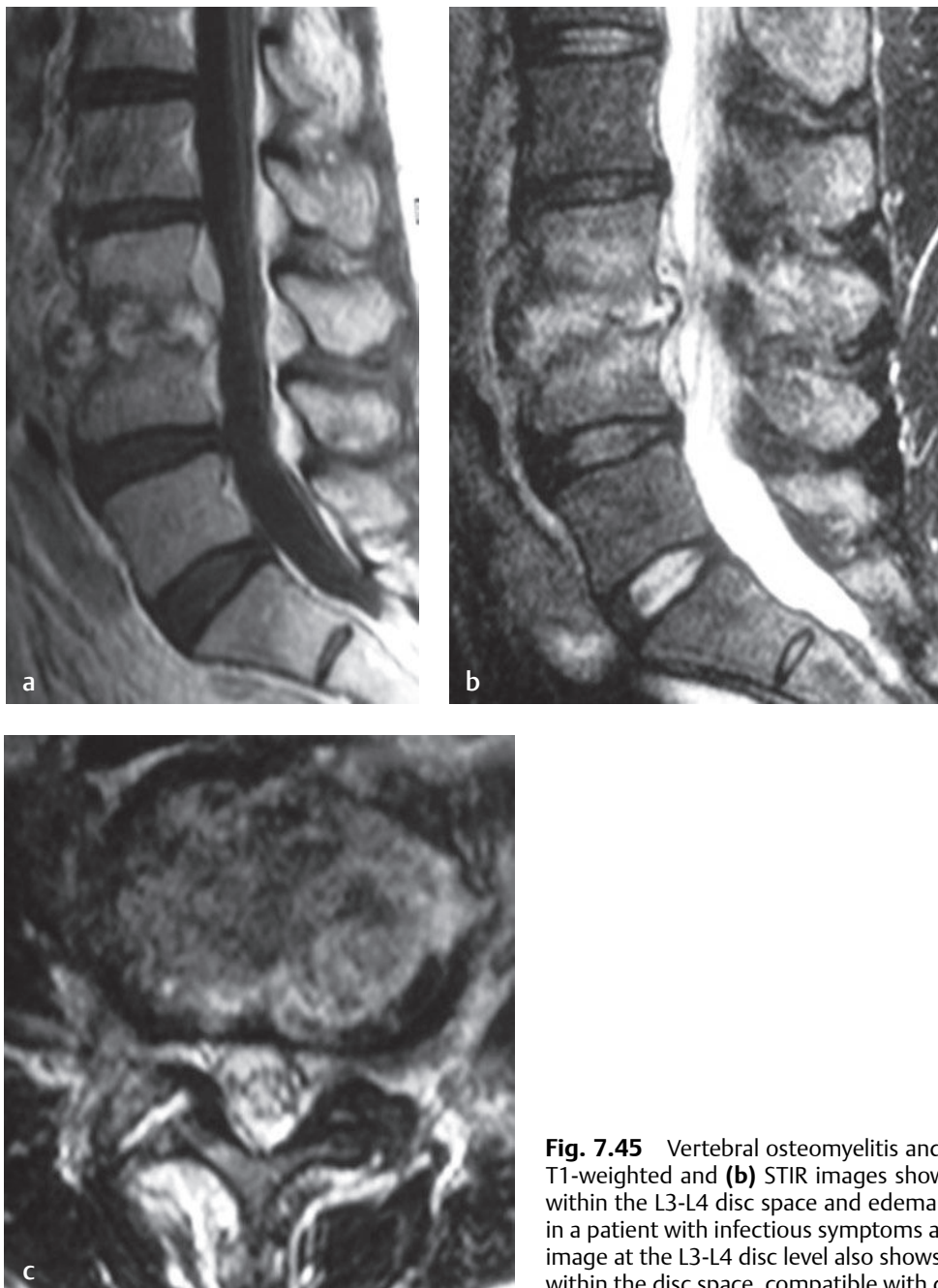


Fig. 7.45 Vertebral osteomyelitis and discitis. **(a)** Sagittal postgadolinium T1-weighted and **(b)** STIR images show enhancement and increased signal within the L3-L4 disc space and edema within the adjacent vertebral bodies in a patient with infectious symptoms and findings. **(c)** An axial T2-weighted image at the L3-L4 disc level also shows heterogeneous and increased signal within the disc space, compatible with discitis.[†]

also cause edematous marrow to blend in with the normal fatty marrow.⁹⁵ Combining fat-suppressed T1-weighted images with gadolinium contrast enhancement eliminates this problem.⁹⁴ STIR images may also be used for the MRI evaluation of osteomyelitis because they suppress the high signal intensity from fat and provide increased contrast.⁹⁶ STIR images are especially useful when combined with the anatomic detail from T1-weighted sequences.

The pattern of vertebral body involvement in vertebral osteomyelitis should be differentiated from that in patients with spinal tumors (see Chapter 8, Tumors of the Spine). Patients with vertebral osteomyelitis tend to have the epicenter of the pathologic change at the disc space, and those with tumors tend to have the epicenter at the vertebral body. In other words, infectious processes are based at and cross the disc space, whereas neoplastic processes are typically based in the vertebral body and do not cross the disc space.

Discitis

Disc infection often causes edema, which leads to hyperintensity of the disc and the end plate on T2-

weighted images; it also causes loss of definition of the vertebral end plates, inflammatory changes in the adjacent vertebral marrow, and gadolinium enhancement within the disc.^{39,97,98} In addition, it is not uncommon to have an associated paraspinal inflammatory mass.

Spondylodiscitis, which essentially is discitis with vertebral osteomyelitis, may be seen after lumbar disc surgery. It also may be seen after discography or myelography.⁹⁹ Postoperative spondylodiscitis is believed to occur in 0.1% to 3% of patients.⁹⁹ Intraoperative contamination usually is the most common mechanism for infection. The most common infecting organisms are *Staphylococcus epidermidis* and *Staphylococcus aureus*. MR images often show Modic type-1 changes at the level of the operated disc (vertebral end plate with decreased signal on T1-weighted images and increased signal intensity on T2-weighted images) and enhancement of the disc when contrast is used (**Fig. 7.46**). No enhancing tissue should be seen outside the intervertebral space. Normal vertebral bone marrow has low signal intensity on T1-weighted images and high signal intensity on T2-weighted and contrast-enhanced images.⁹⁹ If a rim of soft tissue around the affected intervertebral space is noted to enhance, concern about septic spondylodiscitis arises, which can be ruled out with disc biopsy.

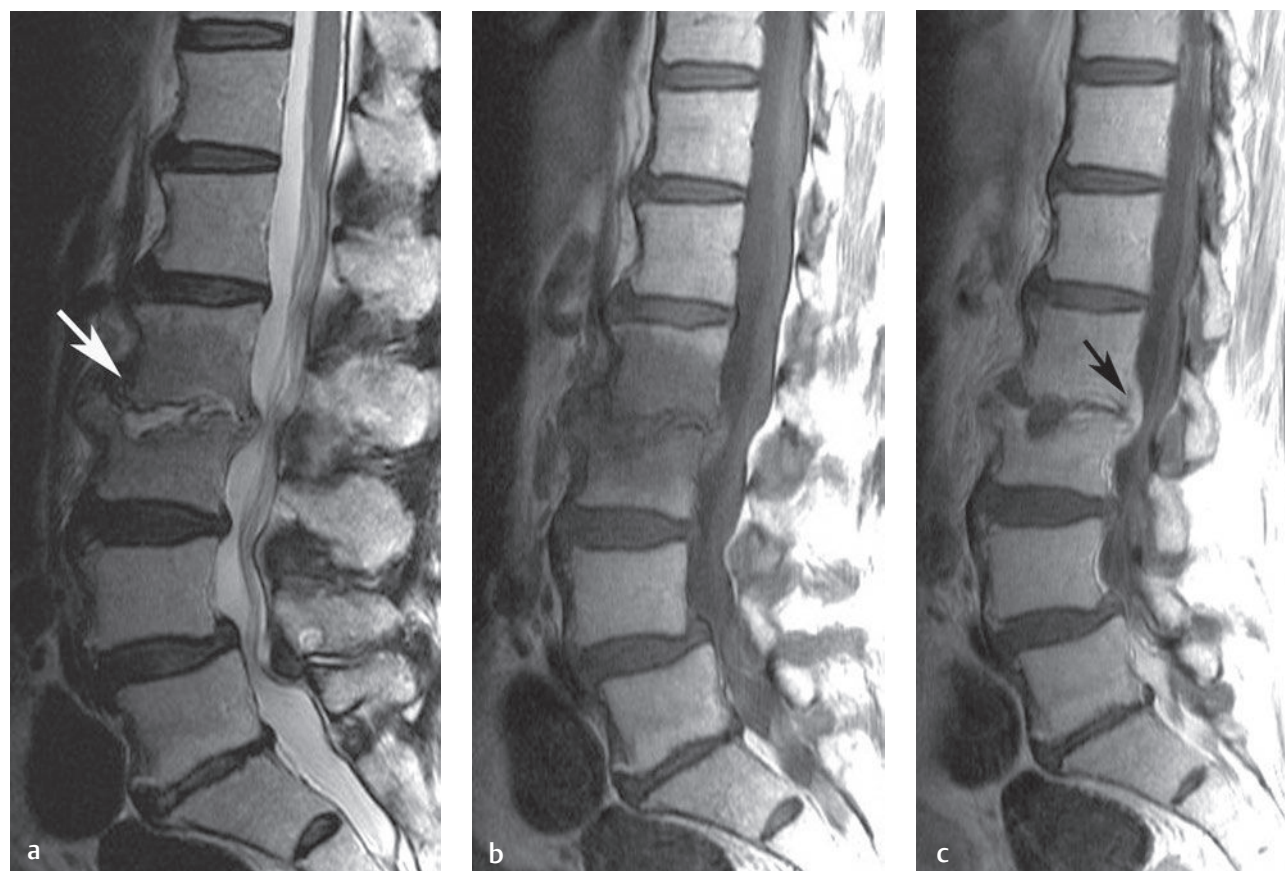


Fig. 7.46 Discitis. Sagittal (a) T2-weighted, (b) T1-weighted, and (c) postgadolinium T1-weighted images show the typical findings of discitis at the L2-L3 level (arrows on a and c). Note the increase in signal at the disc space on the T2-weighted image, the decrease in signal on the T1-weighted image, and the postgadolinium enhancement of the small epidural component (c, arrow).[†]

Epidural Abscess

An epidural abscess is a purulent epidural collection of material without involvement of the vertebral body or the disc space. Such collections are usually located anteriorly in the spinal canal and originate from the posterior aspect of the vertebral body and disc space. If the abscess originates from hematogenous sources, then it may be associated with a

positive blood culture. MRI is very sensitive in the detection of these abscesses.⁹⁵ MRI is also useful in visualizing phlegmon and epidural abscesses, which usually are isointense or hypointense compared with the spinal cord on T1-weighted images and which usually have high signal intensity on T2-weighted images^{96,99} (**Fig. 7.47**). The differentiation of epidural abscess and CSF may be difficult, necessitating gadolinium enhancement for better visualization. The

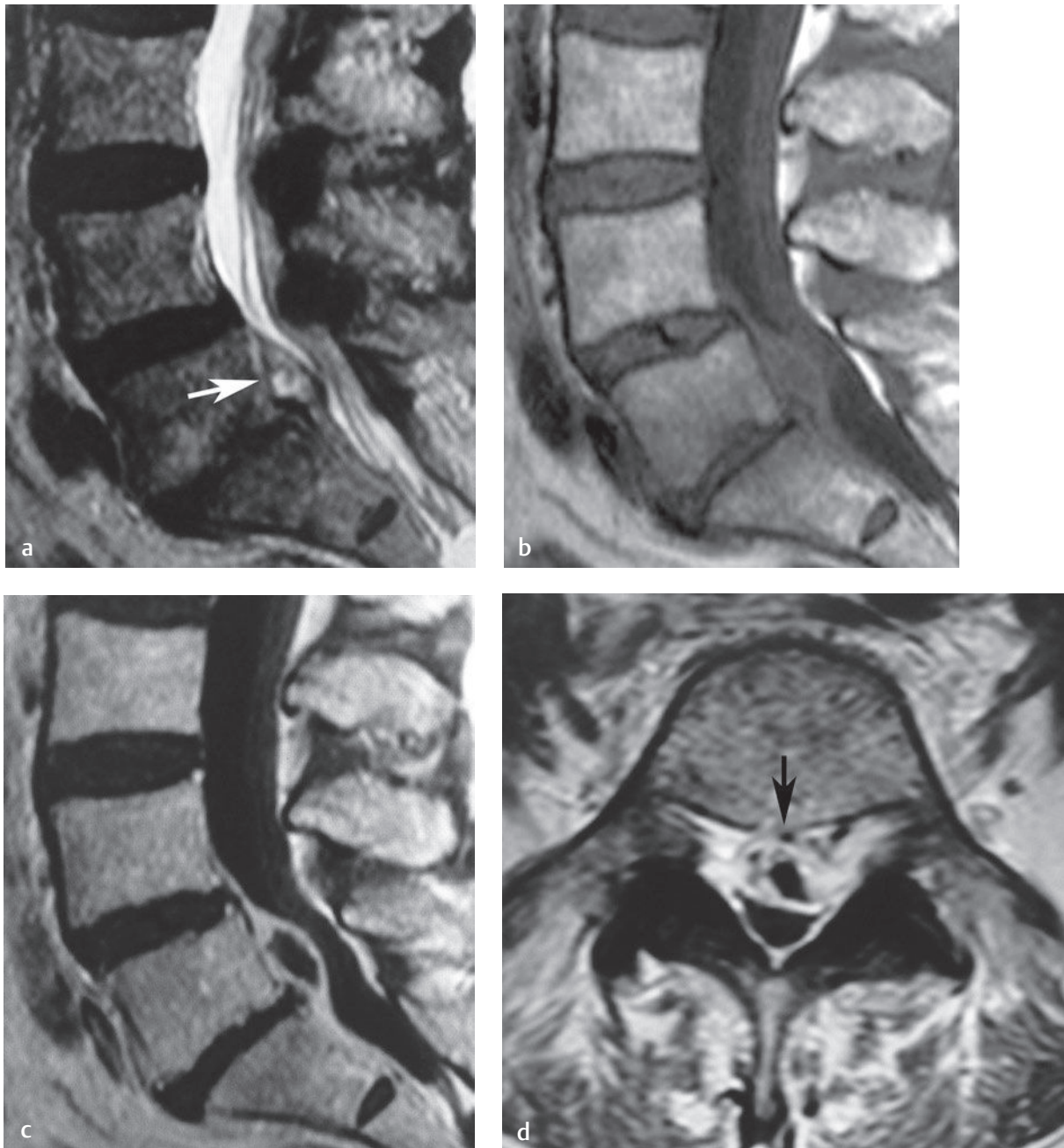


Fig. 7.47 Epidural abscess. **(a)** A sagittal T2-weighted image shows a ventral epidural collection (*arrow*) posterior to the L5 vertebral body in a patient with infectious symptoms and findings. **(b)** A sagittal T1-weighted image shows the same collection. **(c)** A sagittal postgadolinium T1-weighted image shows peripheral enhancement. **(d)** An axial postgadolinium T1-weighted image shows the ventral epidural collection (*arrow*), again with peripheral enhancement; the abscess is producing moderate to severe stenosis.[†]

high signal intensity of the enhancing mass can be distinguished easily from the lower signal intensity of the CSF and spine on T1-weighted images.⁹⁹ Sometimes fat suppression is necessary to differentiate an abscess from epidural fat.⁹⁹ Contrast enhancement also can aid in differentiating between epidural phlegmon and an abscess; dense homogeneous enhancement of the mass suggests phlegmon, whereas peripheral or ring enhancement of the mass suggests an abscess. Paraspinal abscesses, also well visualized with MRI, usually have low signal intensity on T1-weighted images, and they are commonly associated with swelling of the psoas on T1-weighted images and increased signal on T2-weighted images. Gadolinium-enhanced images provide additional abscess delineation.⁹⁹

Tuberculosis

Tuberculosis has reappeared in the developed world because of the emergence of acquired immune deficiency syndrome; 5% of all cases of tuberculosis affect the musculoskeletal system.¹⁰⁰

Tuberculosis usually results from hematogenous seeding. The rich vascular supply of the vertebral bodies makes the spine susceptible to infection. A vertebral body receives its blood supply inferiorly from the ascending branch of the posterior spinal artery and superiorly from the descending branch of this artery. These two arteries anastomose and create a network of vessels in the anterior epidural space. The network then leads to three or four arteries that enter the vertebral body through the nutrient foramen. Children are at an increased risk for discitis because they still have an arterial anastomosis between the vertebral end plate and the disc.¹⁰⁰ The intervertebral disc becomes less vascularized in adolescence. Arteries end within the vertebral bodies, which results in increased rates of infection within the bodies.¹⁰⁰

Tuberculous osteomyelitis usually involves the ventral trabecular bone marrow adjacent to the intervertebral disc, and it spreads via the anterior longitudinal ligament to adjacent vertebral bodies.⁹⁹ MRI signs of tuberculosis infection are hypointense signal on T1-weighted images and hyperintense signal on T2-weighted images seen in the subchondral tissue. There also may be a hyperintense signal within the disc on T2-weighted images (**Fig. 7.48**). As the disease progresses, it may lead to collapse of vertebral bodies, with an associated epidural abscess. Continuous destruction of the anterior cortices of single or contiguous vertebral bodies can lead to kyphotic deformity. Tuberculosis may also directly involve the spinal cord, a condition termed *tuberculosis myelitis*; it is usually seen in individuals <30 years old. MRI with gadolinium is the best imaging modality for this phenomenon.¹⁰⁰

It is not uncommon to see paraspinal involvement with abscess formation. In abscesses, gadolinium enhancement usually is seen only in the periphery, whereas granulation tissue enhances throughout. The observation of disc space sparing and enhancement of granulation tissue is highly suggestive of tuberculosis.⁹⁰

■ Postoperative MRI Findings

Previously, MRI had been considered to have limited use in evaluating the instrumented spine because of the resultant artifacts that were commonly seen. However, the introduction of titanium pedicle screws and specialized pulse sequences has improved the MRI visualization of the central spinal contents^{101–106} (see also Chapter 10, Advanced Techniques in Spine MRI). It is important to note that MRI may not always be the best imaging modality for the evaluation of the postoperative lumbar spine. Conventional radiographs are typically the starting point for the study of patients with an instrumented lumbar fusion, given that they enable the evaluation of overall spinal alignment, position of instrumentation, and evidence of fusion. CT may be best for more precise determination of the presence or absence of fusion, infection, loosening, and postoperative fluid collections. The addition of myelography to CT imaging provides excellent determination of the presence and degree of spinal stenosis, or its absence. MRI may be best for evaluating for the presence or absence of infection, postoperative fluid collection (such as hematoma or CSF), recurrent disc herniation, and residual or recurrent stenosis.¹⁰⁵

Surgical procedures in the spine are typically performed with the following goals in mind:

- Decompression of a stenotic spinal canal or neural foramen
- Removal of herniated disc material
- Stabilization and fusion of motion segments, for existing instability (such as spondylolisthesis, scoliosis, or posttraumatic injury) or after iatrogenic instability (such as with facetectomy or multilevel laminectomies)
- Excision of tumor or infection

Based on the type of surgery performed and the clinical scenario, the spine surgeon and radiologist can use MRI (and other imaging modalities) to evaluate for various postsurgical findings.

After Decompression without Instrumentation/Fusion

Almost all decompressive procedures in the lumbar spine are performed via a posterior approach. These procedures include a midline laminectomy and bilateral foraminotomies, hemilaminotomy with foraminotomy,

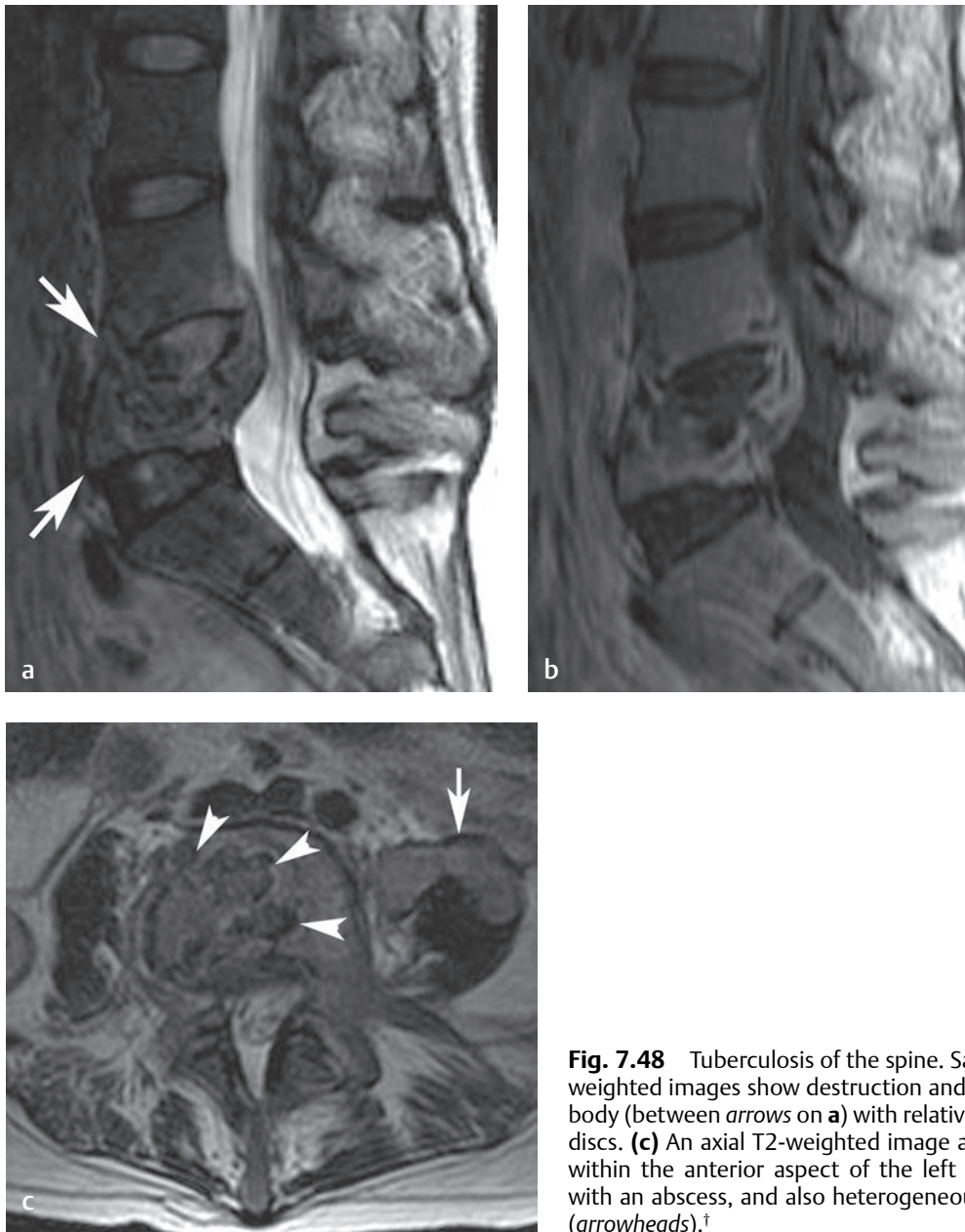


Fig. 7.48 Tuberculosis of the spine. Sagittal (a) T2-weighted and (b) T1-weighted images show destruction and partial collapse of the L5 vertebral body (between arrows on a) with relative preservation of the intervertebral discs. (c) An axial T2-weighted image at the L5 level shows signal change within the anterior aspect of the left psoas muscle (arrow), compatible with an abscess, and also heterogeneous signal within the vertebral body (arrowheads).[†]

and hemilaminotomy with discectomy. In most cases, careful review of the sagittal and axial images permits determination of the extent of bone removal during previous operations. Specifically, one should review the sagittal and axial T2-weighted images, follow the contour of the thecal sac, and look for focal areas of posterior expansion of the thecal sac or for regions of compression of the thecal sac by scar tissue or recurrent/residual disc fragments. The axial T1-weighted images (which show more osseous detail than do T2-weighted images) should be carefully reviewed for areas of postsurgical absence of the osseous structures (**Fig. 7.49**). If additional information may benefit the surgeon for preoperative planning, CT imaging may be considered.

After discectomy, specific changes may be noted around the affected area, depending on the length of time between surgery and the imaging study. At the level of the disc, a high-signal-intensity band extending from the nucleus pulposus to the side of annular disruption may be appreciated on T2-weighted images up to 2 months after surgery. Annular enhancement may also be seen. There also may be a component of disc height loss, depending on the aggressiveness of the discectomy. T1-weighted images show increased soft tissue within the anterior epidural space immediately after surgery; an epidural mass effect is observed in 80% of patients.¹⁰⁷ Anterior epidural soft-tissue edema with disruption of the

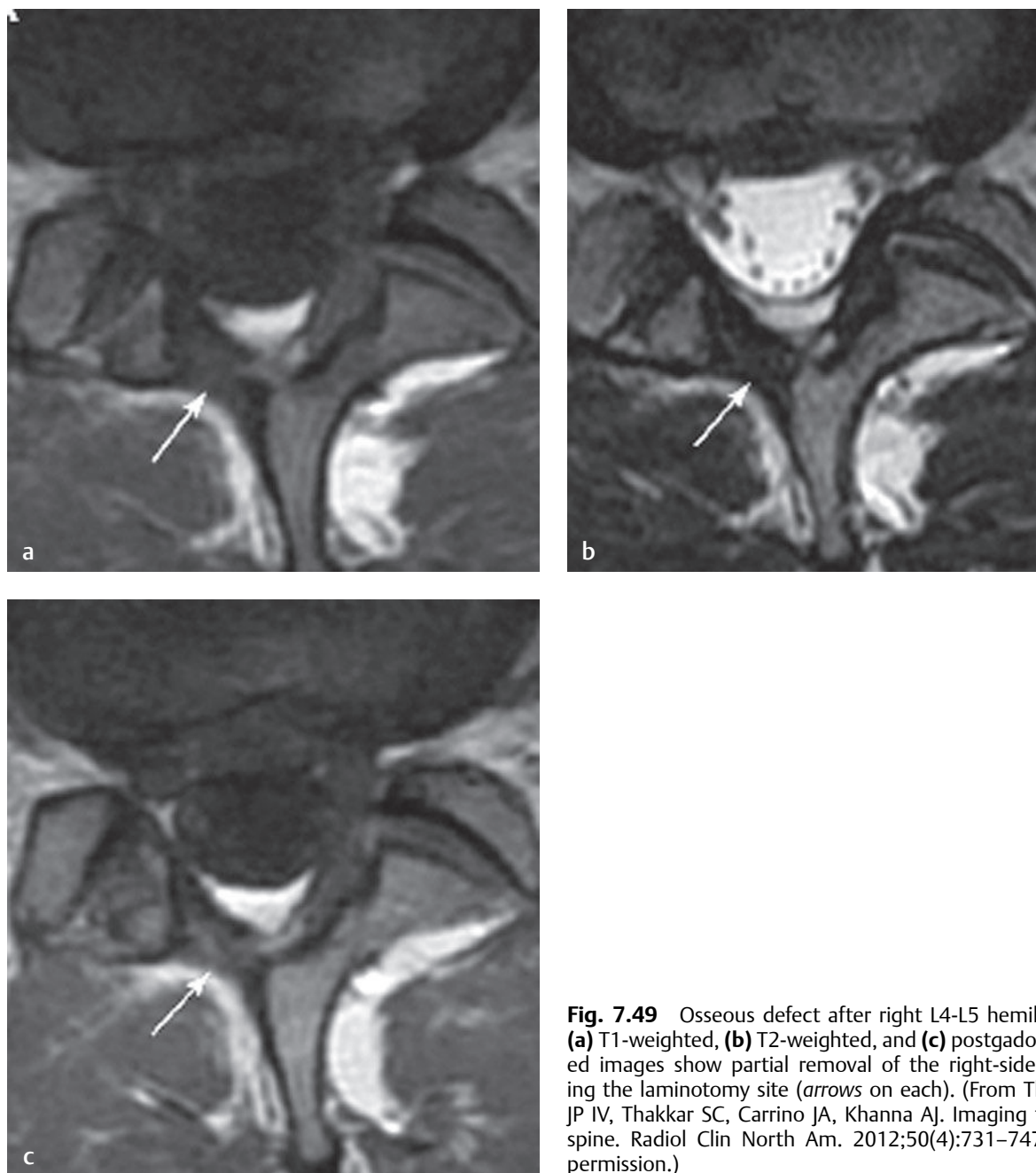


Fig. 7.49 Osseous defect after right L4-L5 hemilaminotomy. Axial (a) T1-weighted, (b) T2-weighted, and (c) postgadolinium T1-weighted images show partial removal of the right-side lamina, identifying the laminotomy site (arrows on each). (From Thakkar RS, Malloy JP IV, Thakkar SC, Carrino JA, Khanna AJ. Imaging the postoperative spine. *Radiol Clin North Am.* 2012;50(4):731–747. Reprinted with permission.)

posterior annular margin secondary to disc curettage can mimic the appearance of disc herniation. It can take from 2 to 6 months after surgery for a normal signal to return.^{108,109} One should use caution when evaluating MRI studies in the first 6 weeks after surgery because there may be a large amount of tissue disruption and edema, producing a mass effect on the anterior thecal sac.

Nerve root enhancement secondary to breakdown of the blood–nerve barrier is another common finding in the immediate postoperative period. This enhancement decreases by 3 months after surgery and

is virtually gone by 6 months.^{107,110} Posterior soft-tissue changes continue to be seen up to 3 months after surgery. These changes include disruption and edema of the paraspinal muscles, with low signal intensity on T1-weighted images and high signal intensity on T2-weighted images. An enhancing subcutaneous track may be seen with gadolinium enhancement. After 6 months, all of the acute postoperative changes secondary to hemorrhage and edema usually have resolved.¹⁰⁷ The remaining scar tissue shows low to intermediate signal intensity on T1-weighted imaging and hypointensity on T2-weighted imaging.

Unfortunately, recurrent disc herniation is a relatively common occurrence after surgery for a lumbar disc herniation. The reported range for the incidence of recurrent disc herniation is 2% to 18%, and a large meta-analysis has indicated the rate is 7% in patients who undergo limited discectomy and 3.5% in patients who undergo aggressive discectomy.¹¹¹ Another recent series found the incidence of recurrent lumbar disc herniation to be 7.1%.¹¹² MRI can be used to differentiate recurrent disc herniation from scar tissue.^{113–117} The importance of making the differentiation between recurrent disc hernia-

tion and scar tissue or epidural fibrosis lies in the fact that outcomes for revision surgery for recurrent disc herniation are substantially better than those for surgery in patients with only scar tissue and no recurrent disc herniation.^{118–122} MRI in patients with recurrent disc herniation shows a focal extradural lesion, typically in the posterolateral or lateral recess region, that has peripheral enhancement with a central area of nonenhancement on postgadolinium T1-weighted images (**Fig. 7.50**). Conversely, patients with epidural fibrosis show uniform enhancement of the epidural tissue.

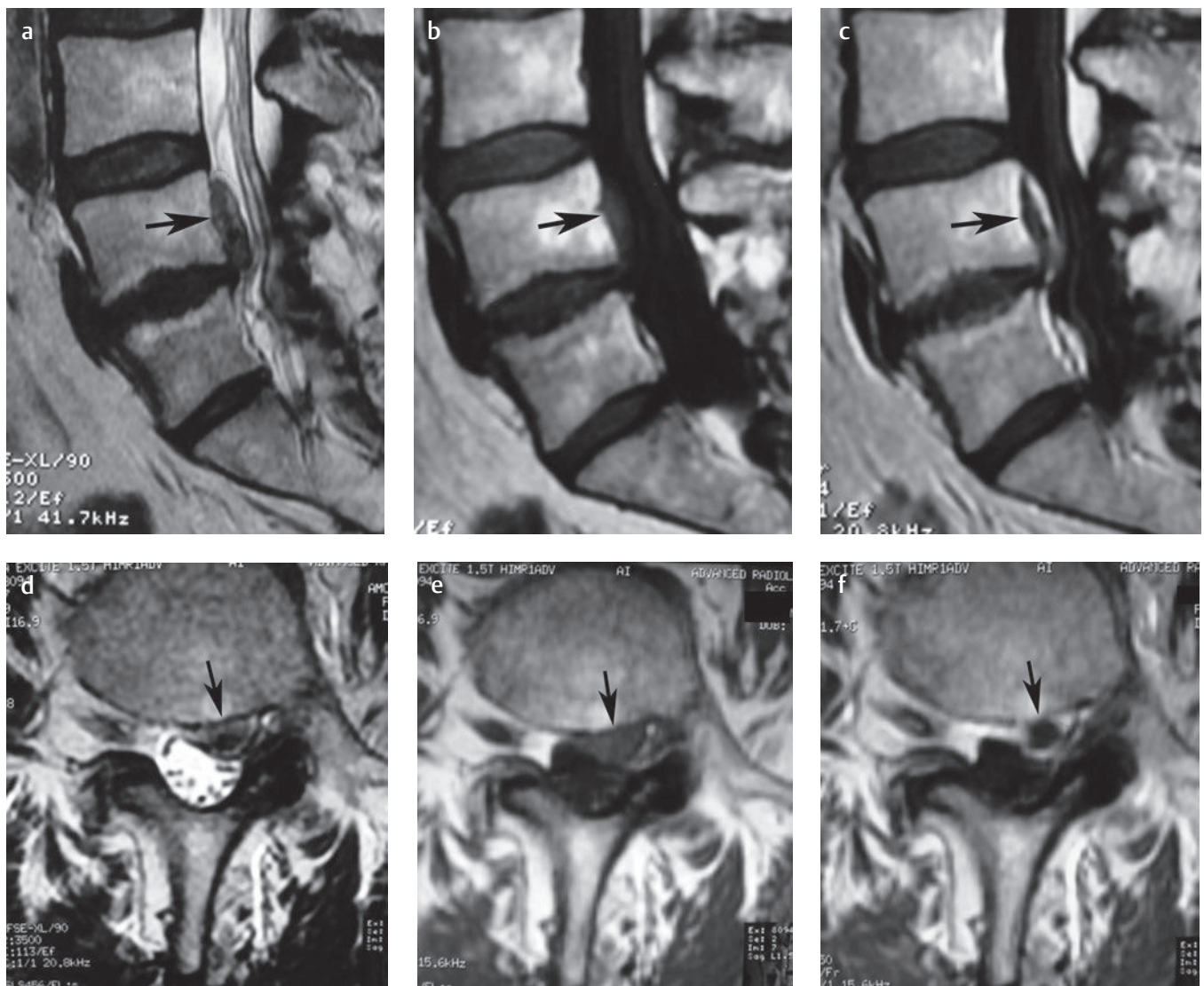


Fig. 7.50 Recurrent lumbar disc extrusion. Sagittal (a) T2-weighted, (b) T1-weighted, and (c) postgadolinium T1-weighted images in a patient with a history of L4-L5 discectomy show a large disc extrusion (arrow on each) that has migrated proximally and is located behind the L4 vertebral body. Note that the disc is difficult to see on b, the T1-weighted image, and shows peripheral enhancement on c, the postgadolinium T1-weighted image. Axial (d) T2-weighted, (e) T1-weighted, and (f) postgadolinium T1-weighted images at the L4-L5 level show the left paracentral extradural lesion (arrow on each), which appears to be disc material on d, the T2-weighted image, and shows peripheral enhancement on f, the postgadolinium T1-weighted image, compared with e, the pregadolinium T1-weighted image.[†]

After Instrumentation/Fusion

Stainless steel implants are considered superparamagnetic and produce the greatest degree of image degradation secondary to magnetic susceptibility artifacts.¹²² Titanium and tantalum spinal implants, which are not superparamagnetic, produce less artifact than does stainless steel. Even with conventional T2-weighted and T1-weighted pulse sequences, the central canal can be adequately visualized in patients with titanium pedicle screws. These images can enable the detection of postop-

erative fluid collections (such as hematoma, seroma, pseudomeningocele, and abscess) and can even accurately show the degree of thecal sac compression from these fluid collections. In addition, the degree of adjacent-level stenosis at levels above and below an instrumented lumbar fusion can be seen well on sagittal and axial T2-weighted images (**Fig. 7.51**).

The position of interbody fusion devices (such as those placed for transforaminal lumbar interbody fusion, posterior lumbar interbody fusion, and anterior lumbar interbody fusion) can also be assessed

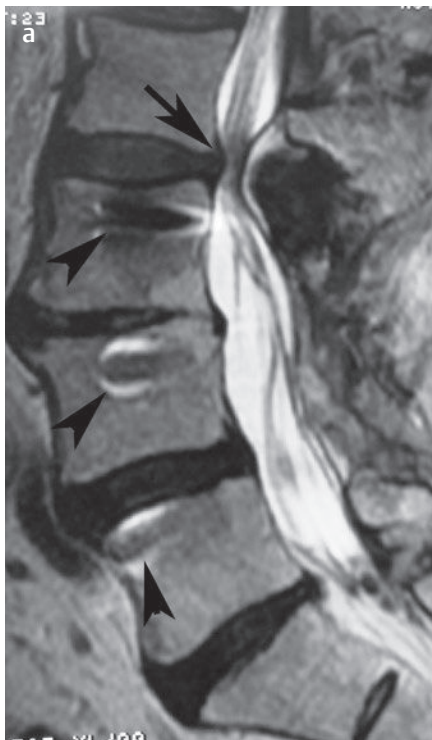
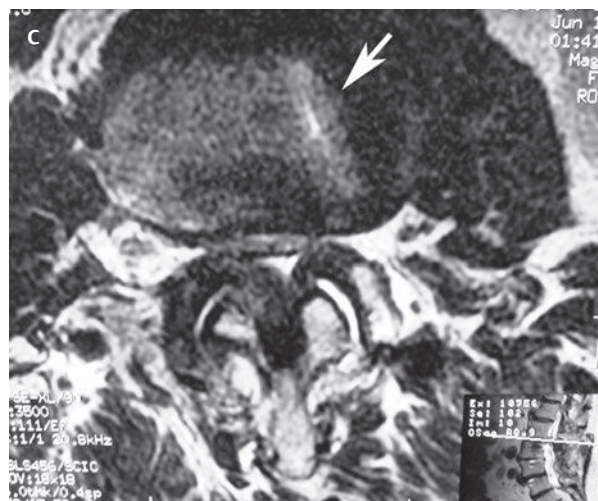
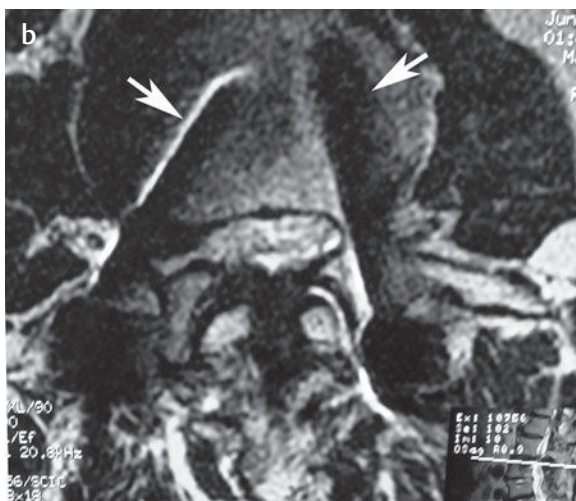


Fig. 7.51 Junctional lumbar stenosis above instrumented fusion. **(a)** A sagittal T2-weighted image shows junctional stenosis (*arrow*) at the L2-L3 level in a patient who has undergone L3-L5 laminectomy and instrumented fusion. Note the minimal artifact from the pedicle screws (*arrowheads*). **(b)** An axial T2-weighted image at the L3 pedicle screw level shows moderate to severe stenosis and also shows the pedicle screws (*arrows*). Note that the presence of the pedicle screws obscures the region of the lateral recess and foramen but does not prevent the evaluation of the status of the central canal. **(c)** An axial T2-weighted image at the L2-L3 level shows severe stenosis and only minimal residual artifact (*arrow*) from the pedicle screw below this level in the L3 vertebral body. Note the localizing sagittal image seen as an inset with each axial image (**b, c**).[†]



by MRI. These devices should be located within the confines of the interbody space, and the posterior aspect of the interbody device after a transforaminal or posterior lumbar interbody fusion procedure should be positioned within the posterior margin of the vertebral body. In cases of posterolateral graft extrusion

into the spinal canal or neural foramen, patients often present with severe radicular pain and/or weakness. MR images show the contours of the interbody device compressing the thecal sac or nerve root and the associated inflammatory changes and epidural fibrosis (**Fig. 7.52**).

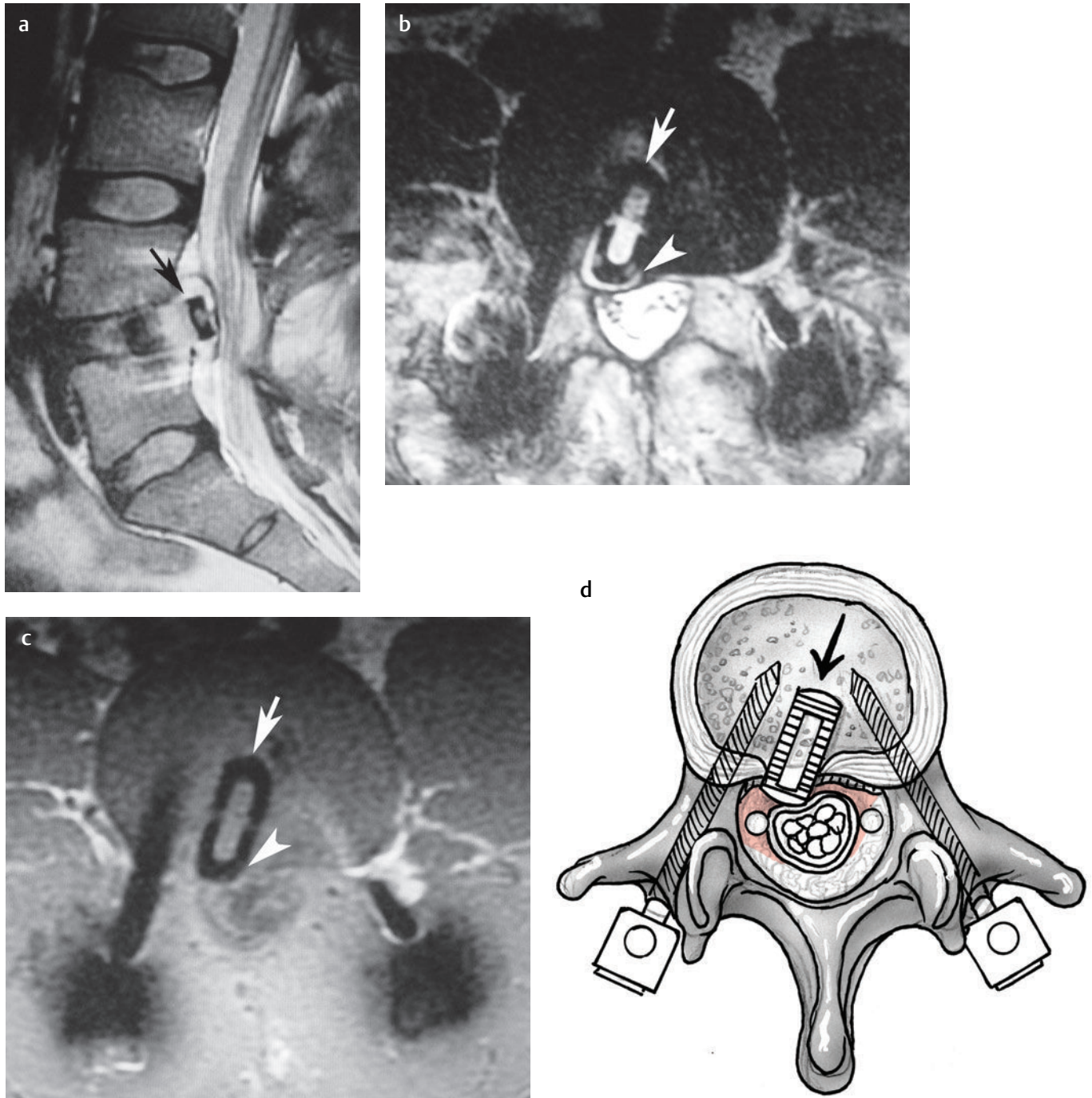


Fig. 7.52 Retropulsed interbody device. **(a)** A sagittal T2-weighted image shows retropulsion of an L4-L5 transforaminal interbody device (*arrow*) into the spinal canal.[†] An axial **(b)** T2-weighted image,[†] **(c)** T1-weighted image,[†] and **(d)** artist's sketch show that the interbody device (*arrow* on each) is retropulsed beyond the margin of the posterior vertebral body (*arrowhead* on **b** and **c**) and is producing right lateral recess stenosis.

Hematoma

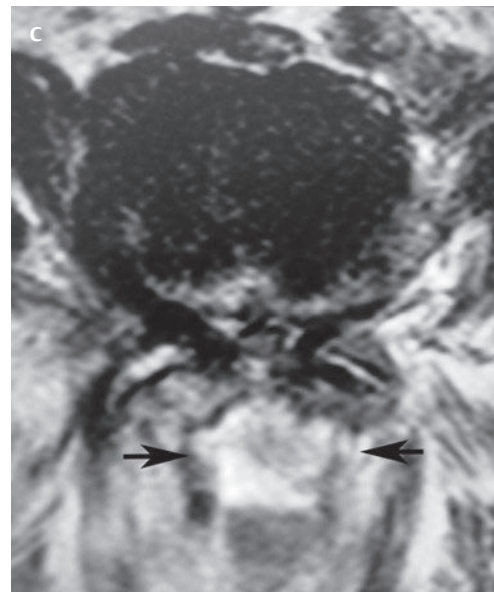
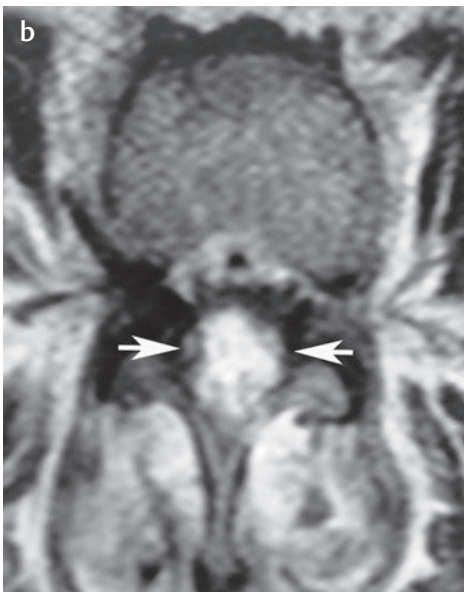
Postoperative epidural hematoma typically develops within a few days after a posterior lumbar surgery that includes decompression, and it can occur after “small” decompressive procedures, such as a microdiscectomy, as well as after larger procedures, such as multilevel laminectomy (**Fig. 7.53**) and posterior spinal fusion. Although CT is excellent for visualizing osseous detail and the precise location of spinal instrumentation relative to the spinal canal and neural foramen, MRI is superior for visualizing postoperative fluid collections (such as an epidural hematoma) and the size, location, and degree of compression of the thecal sac it produces.

Pseudomeningocele

A pseudomeningocele typically occurs in a patient who sustains a durotomy during an open surgical procedure or in a patient who undergoes resection of an intradural lesion. In both of these situations, there may be an incomplete closure of the dural opening, with resultant leakage of CSF into the operative site and posterior soft tissues. This collection of CSF is termed a *pseudomeningocele* because it is surrounded not by arachnoid and dura, but rather by a pseudomeninges of reactive fibrous tissue.¹²² Pseudomeningoceles typically are well circumscribed, communicate with the subarachnoid space, and contain fluid that matches



Fig. 7.53 Postoperative lumbar epidural hematoma. **(a)** A sagittal T2-weighted image shows a large and compressive fluid collection (between *arrows*) at the L3-L5 level in a patient after revision L4-L5 laminectomies. Axial T2-weighted images at the **(b)** L3-L4 and **(c)** L4-L5 levels show the hematoma (between *arrows* on each) and the associated compression of the thecal sac.[†]



the signal characteristics of CSF, which is homogeneous and has low signal intensity on T1-weighted images and high signal intensity on T2-weighted images (**Fig. 7.54**). Given that the pressure within a pseudomeningocele is often similar to that of the subarachnoid space, these collections often compress the thecal sac less than do postoperative epidural hematomas.¹²³

Arachnoiditis

Signs of arachnoiditis include central adhesion of the nerve roots within the thecal sac into a central clump of soft-tissue signal (pseudocord) instead of their normal feathery appearance (**Fig. 7.55**), peripheral adhesion of the nerve roots to the meninges (giving rise to an “empty” thecal sac sign), and an inflammatory mass that fills the thecal sac.¹²⁴ Various factors can lead to the development of arachnoiditis, including the trauma of the surgery itself, intradural blood after the repair of a durotomy, previous lumbar puncture, treated perioperative infection, and the previous use of myelographic contrast dye.¹²²

Summary

The typical MRI protocol of the lumbar spine for the evaluation of degenerative pathologies includes T2-weighted and T1-weighted images in both sagittal

and axial planes. However, imaging protocols of the lumbar spine for specific indications can vary among institutions and should be modified when specific diagnoses such as infection, recurrent disc herniation, and tumor are being considered.

The initial evaluation of patients with known or suspected lumbar spine injury begins with conventional radiographs and/or CT imaging, which provides greater osseous detail and may reveal fractures or details that are not detected with conventional radiography. MRI provides soft-tissue visualization that is superior to that of conventional radiography or CT and is useful for the assessment of spinal cord injury, ligamentous injury, degree of spinal stenosis, and additional fracture evaluation.

MRI is the preferred initial advanced imaging modality for the evaluation of symptomatic lumbar spine degeneration and is highly sensitive and specific for the detection of degenerative changes. Despite this high sensitivity and specificity, it is important to understand that radiographic and MRI abnormalities do not always correlate with a symptomatic degenerative lesion. Therefore, the spine surgeon or specialist must correlate the findings on MRI with the patient's history and physical examination. Degenerative conditions that can be evaluated on lumbar spine MRI include disc displacement, disc degeneration, spinal stenosis, and spondylolisthesis. The nomenclature used for describing lumbar disc pathology should be consistent and uniformly applied, as shown in Chapter 6, The Cervical Spine.

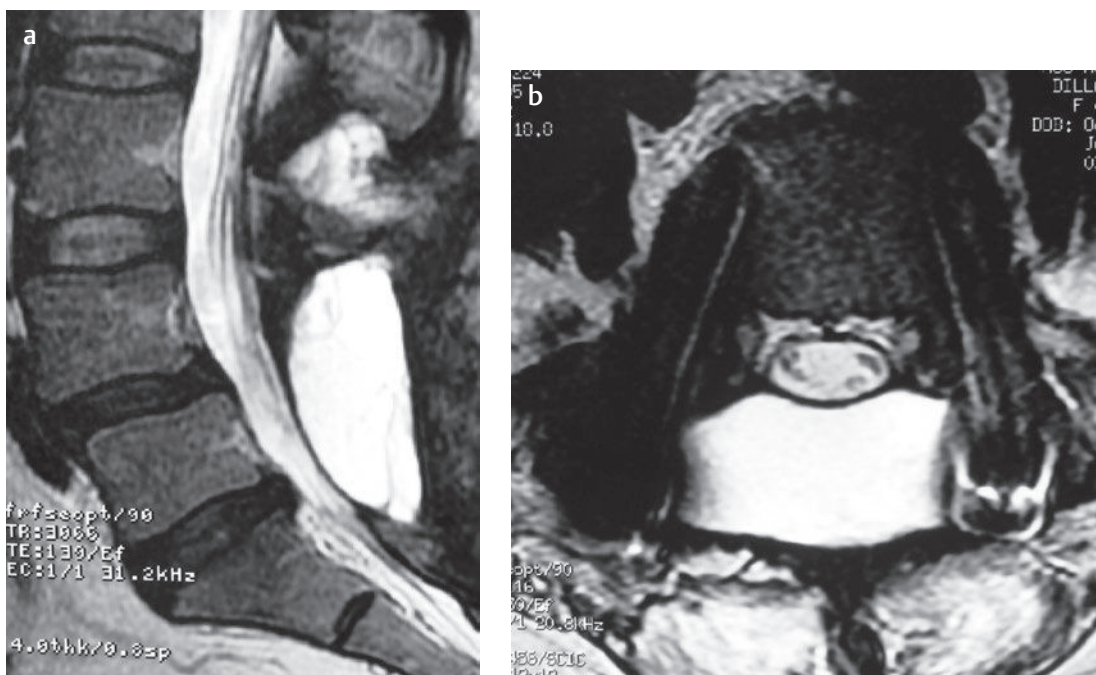


Fig. 7.54 Pseudomeningocele. **(a)** Sagittal and **(b)** axial T2-weighted images of a patient who sustained a durotomy during revision L4-S1 laminectomy and instrumented posterior fusion. The images show a well-circumscribed fluid collection that does not compress the thecal sac. Note that on **(b)** the axial image at the L5 level, the central canal can be well visualized in the presence of pedicle screws.[†]

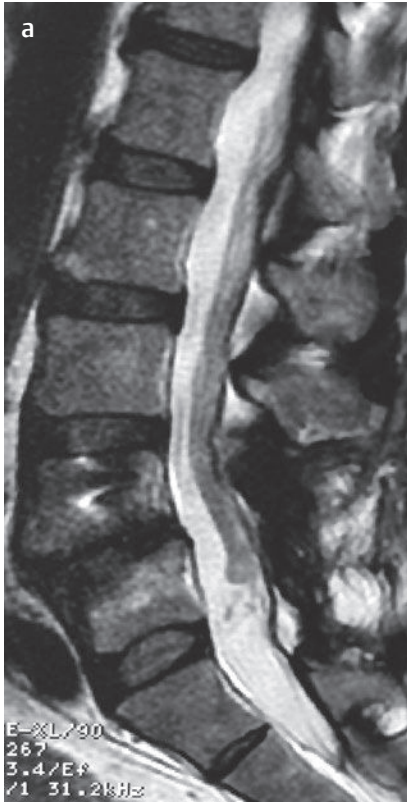
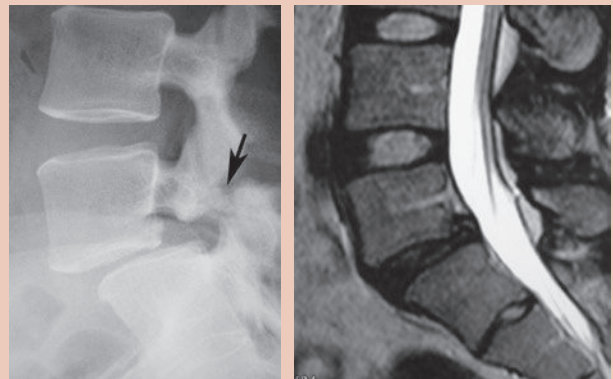


Fig. 7.55 Arachnoiditis. **(a)** Sagittal and **(b)** axial T2-weighted images of a patient after L4-L5 laminectomy and instrumented posterior fusion who had had several previous decompressive surgeries. Note the central adhesion of the nerve roots within the thecal sac into a central clump of soft-tissue signal (pseudocord) instead of their normal feathery appearance. **(b)** The axial image is at the L4-L5 level.[†]

Although the most common indication for MRI of the lumbar spine is the evaluation of degenerative conditions, this modality is also frequently and effectively used for the evaluation of patients with nondegenerative conditions such as trauma, infection, spinal tumors, various arthritides, and postoperative complications and findings.

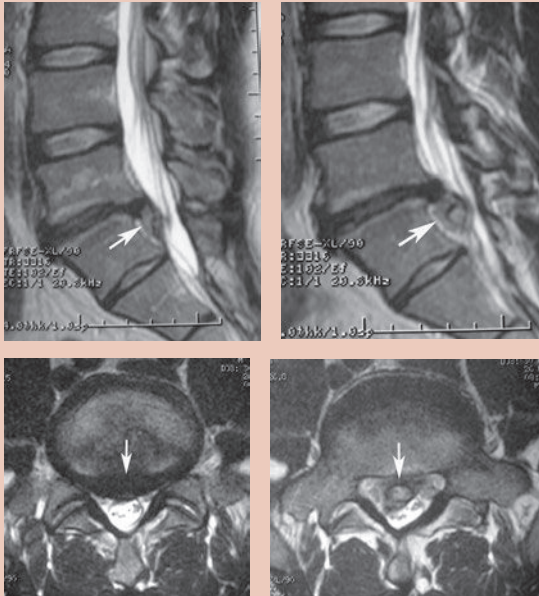
COMMON CLINICAL QUESTIONS

- Which of the following is *not* one of the criteria that the Thoracolumbar Injury Classification and Severity Score has recognized as being important in the evaluation of patients with thoracolumbar trauma?
 - Fracture morphology
 - Integrity of the posterior ligamentous complex
 - Neurologic status of the patient
 - Integrity of the middle column
 - C and D
- What type of spondylolisthesis is shown in the figures below?
 - Degenerative
 - Isthmic
 - Iatrogenic
 - Pathologic
 - Traumatic



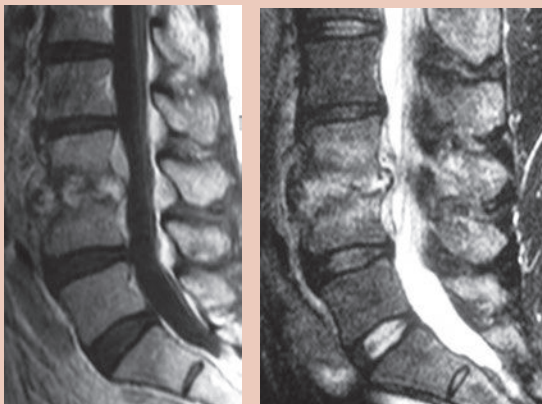
3. What type of disc pathology is seen in the images below?

A. Bulge
B. Protrusion
C. Extrusion
D. Sequestration
E. Synovial cyst



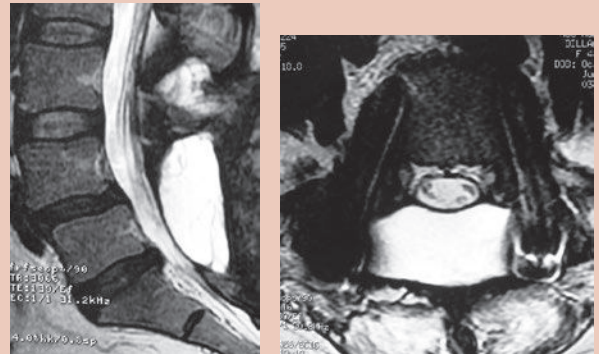
4. With what diagnosis are the images below most compatible?

A. Spinal tumor
B. Tuberculosis
C. Vertebral compression fracture
D. Discitis and osteomyelitis
E. These images are nondiagnostic, and a potential diagnosis cannot be suggested from this list without a biopsy.



5. What is the most likely diagnosis shown in the images below in a patient who has recently undergone a posterior lumbar surgical procedure?

A. Hematoma
B. Epidural abscess
C. Aneurysmal bone cyst
D. Pseudomeningocele
E. Myelomeningocele



References

- Melhem ER, Benson ML, Beauchamp NJ, Lee RR. Cervical spondylosis: three-dimensional gradient-echo MR with magnetization transfer. *AJNR Am J Neuroradiol* 1996;17(4):705–711 PubMed
- Denis F. The three column spine and its significance in the classification of acute thoracolumbar spinal injuries. *Spine (Phila Pa 1976)* 1983;8(8):817–831 PubMed
- Magerl F, Aebi M, Gertzbein SD, Harms J, Nazarian S. A comprehensive classification of thoracic and lumbar injuries. *Eur Spine J* 1994;3(4):184–201 PubMed
- McCormack T, Karaikovic E, Gaines RW. The load sharing classification of spine fractures. *Spine (Phila Pa 1976)* 1994;19(15):1741–1744 PubMed
- Vaccaro AR, Lehman RA Jr, Hurlbert RJ, et al. A new classification of thoracolumbar injuries: the importance of injury morphology, the integrity of the posterior ligamentous complex, and neurologic status. *Spine (Phila Pa 1976)* 2005;30(20):2325–2333 PubMed
- Patel AA, Vaccaro AR. Thoracolumbar spine trauma classification. *J Am Acad Orthop Surg* 2010;18(2):63–71 PubMed
- Joaquim AF, Fernandes YB, Cavalcante RAC, Fragoso RM, Honorato DC, Patel AA. Evaluation of the thoracolumbar injury classification system in thoracic and lumbar spinal trauma. *Spine (Phila Pa 1976)* 2011;36(1):33–36 PubMed
- Koh YD, Kim DJ, Koh YW. Reliability and validity of thoracolumbar injury classification and severity score (TLICS). *Asian Spine J* 2010;4(2):109–117 PubMed

9. Lewkonja P, Paolucci EO, Thomas K. Reliability of the thoracolumbar injury classification and severity score and comparison with the Denis classification for injury to the thoracic and lumbar spine. *Spine (Phila Pa 1976)* 2012;37(26):2161–2167 PubMed
10. Blankenbaker DG, De Smet AA, Vanderby R, McCabe RP, Koplin SA. MRI of acute bone bruises: timing of the appearance of findings in a swine model. *AJR Am J Roentgenol* 2008;190(1):W1–7 PubMed
11. Brown DB, Glaiberman CB, Gilula LA, Shimony JS. Correlation between preprocedural MRI findings and clinical outcomes in the treatment of chronic symptomatic vertebral compression fractures with percutaneous vertebroplasty. *AJR Am J Roentgenol* 2005;184(6):1951–1955 PubMed
12. Jung HS, Jee WH, McCauley TR, Ha KY, Choi KH. Discrimination of metastatic from acute osteoporotic compression spinal fractures with MR imaging. *Radiographics* 2003;23(1):179–187 PubMed
13. Kaplan PA, Orton DF, Asleson RJ. Osteoporosis with vertebral compression fractures, retropulsed fragments, and neurologic compromise. *Radiology* 1987;165(2):533–535 PubMed
14. Cuénod CA, Laredo JD, Chevret S, et al. Acute vertebral collapse due to osteoporosis or malignancy: appearance on unenhanced and gadolinium-enhanced MR images. *Radiology* 1996;199(2):541–549 PubMed
15. Panjabi MM, Thibodeau LL, Crisco JJ III, White AA III. What constitutes spinal instability? *Clin Neurosurg* 1988;34:313–339 PubMed
16. Wood KB, Khanna G, Vaccaro AR, Arnold PM, Harris MB, Mehdod AA. Assessment of two thoracolumbar fracture classification systems as used by multiple surgeons. *J Bone Joint Surg Am* 2005;87(7):1423–1429 PubMed
17. Bono CM, Vaccaro AR, Hurlbert RJ, et al. Validating a newly proposed classification system for thoracolumbar spine trauma: looking to the future of the thoracolumbar injury classification and severity score. *J Orthop Trauma* 2006;20(8):567–572 PubMed
18. Radcliff K, Su BW, Kepler CK, et al. Correlation of posterior ligamentous complex injury and neurological injury to loss of vertebral body height, kyphosis, and canal compromise. *Spine (Phila Pa 1976)* 2012;37(13):1142–1150 PubMed
19. Rihn JA, Anderson DT, Harris E, et al. A review of the TLICS system: a novel, user-friendly thoracolumbar trauma classification system. *Acta Orthop* 2008;79(4):461–466 PubMed
20. Young PC, Petersilge CA. MR imaging of the traumatized lumbar spine. *Magn Reson Imaging Clin N Am* 1999;7(3):589–602 PubMed
21. Carrino JA, Lurie JD, Tosteson ANA, et al. Lumbar spine: reliability of MR imaging findings. *Radiology* 2009;250(1):161–170 PubMed
22. Mitra D, Cassar-Pullicino VN, McCall IW. Longitudinal study of high intensity zones on MR of lumbar intervertebral discs. *Clin Radiol* 2004;59(11):1002–1008 PubMed
23. Peng B, Hou S, Wu W, Zhang C, Yang Y. The pathogenesis and clinical significance of a high-intensity zone (HIZ) of lumbar intervertebral disc on MR imaging in the patient with discogenic low back pain. *Eur Spine J* 2006;15(5):583–587 PubMed
24. Gundry CR, Heithoff KB. Epidural hematoma of the lumbar spine: 18 surgically confirmed cases. *Radiology* 1993;187(2):427–431 PubMed
25. Mochida K, Komori H, Okawa A, Muneta T, Haro H, Shinomiya K. Regression of cervical disc herniation observed on magnetic resonance images. *Spine (Phila Pa 1976)* 1998;23(9):990–995, discussion 996–997 PubMed
26. Watanabe N, Ogura T, Kimori K, Hase H, Hirasawa Y. Epidural hematoma of the lumbar spine, simulating extruded lumbar disk herniation: clinical, discographic, and enhanced magnetic resonance imaging features. A case report. *Spine (Phila Pa 1976)* 1997;22(1):105–109 PubMed
27. Renfrew DL, Heithoff KB. Degenerative disease. In: Renfrew DL, ed. *Atlas of Spine Imaging*. Philadelphia, PA: Saunders; 2003:11–128
28. Schellinger D, Manz HJ, Vidic B, et al. Disk fragment migration. *Radiology* 1990;175(3):831–836 PubMed
29. Flanders AE, Tartaglino LM, Friedman DP, Aquilone LF. Magnetic resonance imaging in acute spinal injury. *Semin Roentgenol* 1992;27(4):271–298 PubMed
30. Fardon DF, Milette PC. Nomenclature and classification of lumbar disc pathology. Recommendations of the Combined Task Forces of the North American Spine Society, American Society of Spine Radiology, and American Society of Neuroradiology. *Spine (Phila Pa 1976)* 2001;26(5):E93–E113 PubMed
31. Modic MT. Degenerative disc disease and back pain. *Magn Reson Imaging Clin N Am* 1999;7(3):481–491, viii PubMed
32. Modic MT, Masaryk TJ, Ross JS, Carter JR. Imaging of degenerative disk disease. *Radiology* 1988;168(1):177–186 PubMed
33. Modic MT, Ross JS. Lumbar degenerative disk disease. *Radiology* 2007;245(1):43–61 PubMed
34. Modic MT, Steinberg PM, Ross JS, Masaryk TJ, Carter JR. Degenerative disk disease: assessment of changes in vertebral body marrow with MR imaging. *Radiology* 1988;166(1 Pt 1):193–199 PubMed
35. Alyas F, Turner M, Connell D. MRI findings in the lumbar spines of asymptomatic, adolescent, elite tennis players. *Br J Sports Med* 2007;41(11):836–841, discussion 841 PubMed
36. Wassenar M, van Rijn RM, van Tulder MW, et al. Magnetic resonance imaging for diagnosing lumbar spinal pathology in adult patients with low back pain or sciatica: a diagnostic systematic review. *Eur Spine J* 2012;21(2):220–227 PubMed
37. Boden SD, Davis DO, Dina TS, Patronas NJ, Wiesel SW. Abnormal magnetic-resonance scans of the lumbar spine in asymptomatic subjects. A prospective investigation. *J Bone Joint Surg Am* 1990;72(3):403–408 PubMed
38. Borenstein DG, O'Mara JW Jr, Boden SD, et al. The value of magnetic resonance imaging of the lumbar spine to predict low-back pain in asymptomatic subjects: a seven-year follow-up study. *J Bone Joint Surg Am* 2001;83-A(9):1306–1311 PubMed
39. Morgan S, Saifuddin A. MRI of the lumbar intervertebral disc. *Clin Radiol* 1999;54(11):703–723 PubMed
40. Pfirrmann CWA, Metzendorf A, Zanetti M, Hodler J, Boos N. Magnetic resonance classification of lumbar intervertebral disc degeneration. *Spine (Phila Pa 1976)* 2001;26(17):1873–1878 PubMed
41. Thompson KJ, Dagher AP, Eckel TS, Clark M, Reinig JW. Modic changes on MR images as studied with provocative diskography: clinical relevance—a retrospective study of 2457 disks. *Radiology* 2009;250(3):849–855 PubMed
42. Toyone T, Takahashi K, Kitahara H, Yamagata M, Murakami M, Moriya H. Vertebral bone-marrow changes in degenerative lumbar disc disease. An MRI study of 74 patients

- with low back pain. *J Bone Joint Surg Br* 1994;76(5):757–764 PubMed
43. Weishaupt D, Zanetti M, Hodler J, et al. Painful lumbar disk derangement: relevance of endplate abnormalities at MR imaging. *Radiology* 2001;218(2):420–427 PubMed
 44. Aprill C, Bogduk N. High-intensity zone: a diagnostic sign of painful lumbar disc on magnetic resonance imaging. *Br J Radiol* 1992;65(773):361–369 PubMed
 45. Gundry CR, Fritts HM. Magnetic resonance imaging of the musculoskeletal system. Part 8. The spine, section 1. *Clin Orthop Relat Res* 1997;338:275–287 PubMed
 46. Stadnik TW, Lee RR, Coen HL, Neirynck EC, Buisseret TS, Osteaux MJ. Annular tears and disk herniation: prevalence and contrast enhancement on MR images in the absence of low back pain or sciatica. *Radiology* 1998;206(1):49–55 PubMed
 47. Yoshida H, Fujiwara A, Tamai K, Kobayashi N, Saiki K, Saotome K. Diagnosis of symptomatic disc by magnetic resonance imaging: T2-weighted and gadolinium-DTPA-enhanced T1-weighted magnetic resonance imaging. *J Spinal Disord Tech* 2002;15(3):193–198 PubMed
 48. Herzog RJ. The radiologic assessment for a lumbar disc herniation. *Spine (Phila Pa 1976)* 1996;21(24, Suppl):19S–38S PubMed
 49. Cassar-Pullicino VN. MRI of the ageing and herniating intervertebral disc. *Eur J Radiol* 1998;27(3):214–228 PubMed
 50. Malfair D, Beall DP. Imaging the degenerative diseases of the lumbar spine. *Magn Reson Imaging Clin N Am* 2007;15(2):221–238, vi PubMed
 51. Dietze DD Jr, Fessler RG. Thoracic disc herniations. *Neurosurg Clin N Am* 1993;4(1):75–90 PubMed
 52. Peng B, Wu W, Hou S, Shang W, Wang X, Yang Y. The pathogenesis of Schmorl's nodes. *J Bone Joint Surg Br* 2003;85(6):879–882 PubMed
 53. Hamanishi C, Kawabata T, Yosii T, Tanaka S. Schmorl's nodes on magnetic resonance imaging. Their incidence and clinical relevance. *Spine (Phila Pa 1976)* 1994;19(4):450–453 PubMed
 54. Wagner AL, Murtagh FR, Arrington JA, Stallworth D. Relationship of Schmorl's nodes to vertebral body endplate fractures and acute endplate disk extrusions. *AJNR Am J Neuroradiol* 2000;21(2):276–281 PubMed
 55. Jackson RP, Jacobs RR, Montesano PX. 1988 Volvo award in clinical sciences. Facet joint injection in low-back pain. A prospective statistical study. *Spine (Phila Pa 1976)* 1988;13(9):966–971 PubMed
 56. Revel M, Poiraudou S, Auleley GR, et al. Capacity of the clinical picture to characterize low back pain relieved by facet joint anesthesia. Proposed criteria to identify patients with painful facet joints. *Spine (Phila Pa 1976)* 1998;23(18):1972–1976, discussion 1977 PubMed
 57. Schwarzer AC, Aprill CN, Derby R, Fortin J, Kine G, Bogduk N. Clinical features of patients with pain stemming from the lumbar zygapophysial joints. Is the lumbar facet syndrome a clinical entity? *Spine (Phila Pa 1976)* 1994;19(10):1132–1137 PubMed
 58. Caterini R, Mancini F, Bisicchia S, Maglione P, Farsetti P. The correlation between exaggerated fluid in lumbar facet joints and degenerative spondylolisthesis: prospective study of 52 patients. *J Orthop Traumatol* 2011;12(2):87–91 PubMed
 59. Cho BY, Murovic JA, Park J. Imaging correlation of the degree of degenerative L4–5 spondylolisthesis with the corresponding amount of facet fluid. *J Neurosurg Spine* 2009;11(5):614–619 PubMed
 60. Boden SD, Riew KD, Yamaguchi K, Branch TP, Schellinger D, Wiesel SW. Orientation of the lumbar facet joints: association with degenerative disc disease. *J Bone Joint Surg Am* 1996;78(3):403–411 PubMed
 61. Farfan HF, Sullivan JD. The relation of facet orientation to intervertebral disc failure. *Can J Surg* 1967;10(2):179–185 PubMed
 62. Noren R, Trafimow J, Andersson GBJ, Huckman MS. The role of facet joint tropism and facet angle in disc degeneration. *Spine (Phila Pa 1976)* 1991;16(5):530–532 PubMed
 63. Jenkins JR. MR evaluation of stenosis involving the neural foramina, lateral recesses, and central canal of the lumbosacral spine. *Magn Reson Imaging Clin N Am* 1999;7(3):493–511, viii PubMed
 64. de Schepper EIT, Overvest GM, Suri P, et al. Diagnosis of lumbar spinal stenosis: an updated systematic review of the accuracy of diagnostic tests. *Spine (Phila Pa 1976)* 2013;38(8):E469–E481 PubMed
 65. Issack PS, Cunningham ME, Pumberger M, Hughes AP, Cammisa FP Jr. Degenerative lumbar spinal stenosis: evaluation and management. *J Am Acad Orthop Surg* 2012;20(8):527–535 PubMed
 66. Hamanishi C, Matukura N, Fujita M, Tomihara M, Tanaka S. Cross-sectional area of the stenotic lumbar dural tube measured from the transverse views of magnetic resonance imaging. *J Spinal Disord* 1994;7(5):388–393 PubMed
 67. Speciale AC, Pietrobon R, Urban CW, et al. Observer variability in assessing lumbar spinal stenosis severity on magnetic resonance imaging and its relation to cross-sectional spinal canal area. *Spine (Phila Pa 1976)* 2002;27(10):1082–1086 PubMed
 68. Barz T, Melloh M, Staub LP, et al. Nerve root sedimentation sign: evaluation of a new radiological sign in lumbar spinal stenosis. *Spine (Phila Pa 1976)* 2010;35(8):892–897 PubMed
 69. Fazal A, Yoo A, Bendo JA. Does the presence of the nerve root sedimentation sign on MRI correlate with the operative level in patients undergoing posterior lumbar decompression for lumbar stenosis? *Spine J* 2013;23(8):837–842 PubMed
 70. Buchner M, Schiltenswolf M. Cauda equina syndrome caused by intervertebral lumbar disk prolapse: mid-term results of 22 patients and literature review. *Orthopedics* 2002;25(7):727–731 PubMed
 71. Bagley CA, Gokaslan ZL. Cauda equina syndrome caused by primary and metastatic neoplasms. *Neurosurg Focus* 2004;16(6):11–18 PubMed
 72. Harrop JS, Hunt GE Jr, Vaccaro AR. Conus medullaris and cauda equina syndrome as a result of traumatic injuries: management principles. *Neurosurg Focus* 2004;16(6):19–23 PubMed
 73. Wiltse LL, Newman PH, Macnab I. Classification of spondylolysis and spondylolisthesis. *Clin Orthop Relat Res* 1976;117:23–29 PubMed
 74. Meyerding HW. Spondylolisthesis; surgical fusion of lumbosacral portion of spinal column and interarticular facets; use of autogenous bone grafts for relief of disabling backache. *J Int Coll Surg* 1956;26(5 Part 1):566–591 PubMed
 75. Hammerberg KW. New concepts on the pathogenesis and classification of spondylolisthesis. *Spine (Phila Pa 1976)* 2005;30(6, Suppl):S4–S11 PubMed

76. Mac-Thiong JM, Labelle H. A proposal for a surgical classification of pediatric lumbosacral spondylolisthesis based on current literature. *Eur Spine J* 2006;15(10):1425–1435 PubMed
77. Mac-Thiong JM, Labelle H, Parent S, et al. Reliability and development of a new classification of lumbosacral spondylolisthesis. *Scoliosis* 2008;3:19 PubMed
78. Redla S, Sikdar T, Saifuddin A. Magnetic resonance imaging of scoliosis. *Clin Radiol* 2001;56(5):360–371 PubMed
79. O'Brien MF, Lenke LG, Bridwell KH, Blanke K, Baldus C. Preoperative spinal canal investigation in adolescent idiopathic scoliosis curves > or = 70 degrees. *Spine (Phila Pa 1976)* 1994;19(14):1606–1610 PubMed
80. Slipman CW, Shin CH, Patel RK, et al. Etiologies of failed back surgery syndrome. *Pain Med* 2002;3(3):200–214, discussion 214–217 PubMed
81. Winter RB, Lonstein JE, Heithoff KB, Kirkham JA. Magnetic resonance imaging evaluation of the adolescent patient with idiopathic scoliosis before spinal instrumentation and fusion. A prospective, double-blinded study of 140 patients. *Spine (Phila Pa 1976)* 1997;22(8):855–858 PubMed
82. Lewonowski K, King JD, Nelson MD. Routine use of magnetic resonance imaging in idiopathic scoliosis patients less than eleven years of age. *Spine (Phila Pa 1976)* 1992;17(6, Suppl):S109–S116 PubMed
83. Fisk JR, Moe JH, Winter RB. Scoliosis, spondylolysis, and spondylolisthesis. Their relationship as reviewed in 539 patients. *Spine (Phila Pa 1976)* 1978;3(3):234–245 PubMed
84. Al-Khawaja D, Seex K, Eslick GD. Spinal epidural lipomatosis—a brief review. *J Clin Neurosci* 2008;15(12):1323–1326 PubMed
85. Badami JP, Hinck VC. Symptomatic deposition of epidural fat in a morbidly obese woman. *AJNR Am J Neuroradiol* 1982;3(6):664–665 PubMed
86. Gero BT, Chynn KY. Symptomatic spinal epidural lipomatosis without exogenous steroid intake. Report of a case with magnetic resonance imaging. *Neuroradiology* 1989;31(2):190–192 PubMed
87. St. Amour TE, Hodges SE, Laakman RW, Tamas DE. Epidural lipomas, angioliomas, and epidural lipomatosis. In: St. Amour TE, Hodges SC, Laakman RW, Tamas DE, eds. *MRI of the Spine*. New York, NY: Raven Press; 1994:501–507
88. Jaramillo-de la Torre JJ, Bohinski RJ, Kuntz C IV. Vertebral osteomyelitis. *Neurosurg Clin N Am* 2006;17(3):339–351, vii PubMed
89. Modic MT, Feiglin DH, Piraino DW, et al. Vertebral osteomyelitis: assessment using MR. *Radiology* 1985;157(1):157–166 PubMed
90. Vaccaro AR, Betz RR, Zeidman SM, Eds. *Principles and Practice of Spine Surgery*. St. Louis, MO: Mosby; 2003
91. Dagirmanjian A, Schils J, McHenry M, Modic MT. MR imaging of vertebral osteomyelitis revisited. *AJR Am J Roentgenol* 1996;167(6):1539–1543 PubMed
92. Batson OV. The vertebral vein system. *Caldwell lecture, 1956. Am J Roentgenol Radium Ther Nucl Med* 1957;78(2):195–212 PubMed
93. Ratcliffe JF. Anatomic basis for the pathogenesis and radiologic features of vertebral osteomyelitis and its differentiation from childhood discitis. A microarteriographic investigation. *Acta Radiol Diagn (Stockh)* 1985;26(2):137–143 PubMed
94. Dagirmanjian A, Schils J, McHenry MC. MR imaging of spinal infections. *Magn Reson Imaging Clin N Am* 1999;7(3):525–538 PubMed
95. Post MJD, Quencer RM, Montalvo BM, Katz BH, Eismont FJ, Green BA. Spinal infection: evaluation with MR imaging and intraoperative US. *Radiology* 1988;169(3):765–771 PubMed
96. Bertino RE, Porter BA, Stimac GK, Tepper SJ. Imaging spinal osteomyelitis and epidural abscess with short TI inversion recovery (STIR). *AJNR Am J Neuroradiol* 1988;9(3):563–564 PubMed
97. Brown R, Hussain M, McHugh K, Novelli V, Jones D. Discitis in young children. *J Bone Joint Surg Br* 2001;83(1):106–111 PubMed
98. Mahboubi S, Morris MC. Imaging of spinal infections in children. *Radiol Clin North Am* 2001;39(2):215–222 PubMed
99. Van Goethem JWM, Parizel PM, van den Hauwe L, Van de Kelft E, Verlooy J, De Schepper AMA. The value of MRI in the diagnosis of postoperative spondylodiscitis. *Neuroradiology* 2000;42(8):580–585 PubMed
100. Almeida A. Tuberculosis of the spine and spinal cord. *Eur J Radiol* 2005;55(2):193–201 PubMed
101. Berquist TH. Imaging of the postoperative spine. *Radiol Clin North Am* 2006;44(3):407–418 PubMed
102. Gundry CR, Fritts HM. Magnetic resonance imaging of the musculoskeletal system. Part 8. The spine, section 2. *Clin Orthop Relat Res* 1997;343:260–271 PubMed
103. Malik AS, Boyko O, Aktar N, Young WF. A comparative study of MR imaging profile of titanium pedicle screws. *Acta Radiol* 2001;42(3):291–293 PubMed
104. Rupp RE, Ebraheim NA, Wong FF. The value of magnetic resonance imaging of the postoperative spine with titanium implants. *J Spinal Disord* 1996;9(4):342–346 PubMed
105. Thakkar RS, Malloy JP IV, Thakkar SC, Carrino JA, Khanna AJ. Imaging the postoperative spine. *Radiol Clin North Am* 2012;50(4):731–747 PubMed
106. Viano AM, Gronemeyer SA, Haliloglu M, Hoffer FA. Improved MR imaging for patients with metallic implants. *Magn Reson Imaging* 2000;18(3):287–295 PubMed
107. Babar S, Saifuddin A. MRI of the post-discectomy lumbar spine. *Clin Radiol* 2002;57(11):969–981 PubMed
108. Annertz M, Jönsson B, Strömqvist B, Holtås S. Serial MRI in the early postoperative period after lumbar discectomy. *Neuroradiology* 1995;37(3):177–182 PubMed
109. Ross JS. Magnetic resonance imaging of the postoperative spine. *Semin Musculoskelet Radiol* 2000;4(3):281–291 PubMed
110. Grand CM, Bank WO, Balériaux D, Matos C, Levivier M, Brotchi J. Gadolinium enhancement of vertebral endplates following lumbar disc surgery. *Neuroradiology* 1993;35(7):503–505 PubMed
111. McGirt MJ, Ambrossi GLG, Datto G, et al. Recurrent disc herniation and long-term back pain after primary lumbar discectomy: review of outcomes reported for limited versus aggressive disc removal. *Neurosurgery* 2009;64(2):338–344, discussion 344–345 PubMed
112. Kim MS, Park KW, Hwang C, et al. Recurrence rate of lumbar disc herniation after open discectomy in active young men. *Spine (Phila Pa 1976)* 2009;34(1):24–29 PubMed

113. Bradley WG. Use of contrast in MR imaging of the lumbar spine. *Magn Reson Imaging Clin N Am* 1999;7(3): 439–457, vii PubMed
114. Bundschuh CV, Modic MT, Ross JS, Masaryk TJ, Bohlman H. Epidural fibrosis and recurrent disk herniation in the lumbar spine: MR imaging assessment. *AJR Am J Roentgenol* 1988;150(4):923–932 PubMed
115. Bundschuh CV, Stein L, Slusser JH, Schinco FP, Ladaga LE, Dillon JD. Distinguishing between scar and recurrent herniated disk in postoperative patients: value of contrast-enhanced CT and MR imaging. *AJNR Am J Neuroradiol* 1990;11(5):949–958 PubMed
116. Jinkins JR, Van Goethem JWM. The postsurgical lumbosacral spine. Magnetic resonance imaging evaluation following intervertebral disk surgery, surgical decompression, intervertebral bony fusion, and spinal instrumentation. *Radiol Clin North Am* 2001;39(1):1–29 PubMed
117. Sotiropoulos S, Chafetz NI, Lang P, et al. Differentiation between postoperative scar and recurrent disk herniation: prospective comparison of MR, CT, and contrast-enhanced CT. *AJNR Am J Neuroradiol* 1989;10(3): 639–643 PubMed
118. Bernard TN Jr. Repeat lumbar spine surgery. Factors influencing outcome. *Spine (Phila Pa 1976)* 1993; 18(15):2196–2200 PubMed
119. Fandiño J, Botana C, Viladrich A, Gomez-Bueno J. Reoperation after lumbar disc surgery: results in 130 cases. *Acta Neurochir (Wien)* 1993;122(1–2):102–104 PubMed
120. Herron L. Recurrent lumbar disc herniation: results of repeat laminectomy and discectomy. *J Spinal Disord* 1994;7(2):161–166 PubMed
121. Jönsson B, Strömqvist B. Repeat decompression of lumbar nerve roots. A prospective two-year evaluation. *J Bone Joint Surg Br* 1993;75(6):894–897 PubMed
122. Van Goethem JWM, Parizel PM, Jinkins JR. Review article: MRI of the postoperative lumbar spine. *Neuroradiology* 2002;44(9):723–739 PubMed
123. Radcliff KE, Morrison WB, Kepler C, et al. Distinguishing pseudomeningocele, epidural hematoma, and postoperative infection on postoperative MRI. *J Spinal Disord Tech* 2013; 10.1097/BSD.0b013e31828f9203 PubMed
124. Gundry CR, Fritts HM. Magnetic resonance imaging of the musculoskeletal system: the spine. *Clin Orthop Relat Res* 1998;346:262–278 PubMed

ANSWERS TO COMMON CLINICAL QUESTIONS

1. D

Explanation: The Thoracolumbar Injury Classification and Severity Score has recognized the importance of the following three factors when evaluating a patient with thoracolumbar trauma⁵: fracture morphology, integrity of the posterior ligamentous complex (stability or potential for neurologic compromise), and neurologic status of the patient.

2. B

Explanation: The lateral radiograph shows bilateral pars intraarticularis defects (*arrow*) at the L5-S1 level with Meyerding grade-1 spondylolisthesis, and the sagittal T2-weighted MR image shows the spondylolisthesis. The presence of the bilateral pars defects indicates that this is an isthmic spondylolisthesis, as described by Wiltse et al⁷³; this type is most commonly seen at the L5-S1 level but can also be seen at other levels.

3. C

Explanation: A disc herniation is defined as a localized displacement of disc contents beyond the borders of the intervertebral disc space. Most clinicians tend to describe disc pathology using the terms *bulge*, *protrusion*, *extrusion*, and *sequestration*. Although the last two terms are often used correctly, there seems to be a high degree of interobserver variability in the use of the first two terms. A protrusion is present if the greatest distance between the edges of the disc material beyond the disc space is less than the distance between the edges of the base in the same plane. The base is the cross-sectional area of disc material at the outer margin of the disc space of origin, where disc material displaced beyond the disc space is continuous with disc material within the disc space. An extrusion is present when any one distance between the edges of the disc material beyond the disc space is greater than the distance between the edges of the base or when there is no continuity between the disc space and the disc fragment. Extrusion may be further classified as sequestered and migrated. Sequestration is noted if the displaced disc material is completely discontinuous with the parent disc. Migration refers to displacement of disc material away from the site of extrusion, regardless of whether or not there is sequestration.

4. D

Explanation: The pattern of vertebral body involvement in patients with vertebral osteomyelitis should be differentiated from that in patients with spinal tumors. Patients with vertebral osteomyelitis tend to have the epicenter of the pathologic change at the disc space, and those with tumors tend to have the epicenter at the vertebral body. The increased signal seen within the L3-L4 disc and adjacent vertebral bodies on the sagittal postgadolinium T1-weighted (**a**) and sagittal STIR (**b**) images has its epicenter at the disc space and is, therefore, most compatible with discitis and vertebral osteomyelitis. A tumor would more likely “spare” the disc space, and tuberculous infection would likely do the same. The diagnosis of discitis and osteomyelitis may be confirmed with a CT-guided biopsy, which would enable identification of the pathogen and selection of the appropriate antibiotic therapy. The increased signal with a vertebral compression fracture is seen in the vertebral body at the site of the fracture in patients with acute or subacute fractures, and the adjacent disc has normal signal.

5. D

Explanation: These sagittal (**a**) and axial (**b**) T2-weighted images show a well-circumscribed fluid collection that does not compress the thecal sac in a patient who has undergone an L4-S1 laminectomy and instrumentation fusion procedure. A pseudomeningocele typically occurs in a patient who sustains a durotomy during an open surgical procedure or in a patient who undergoes resection of an intradural lesion. In both of these situations, there may be an incomplete closure of the dural opening, with resultant leakage of CSF into the operative site and posterior soft tissues. This collection of CSF is termed a *pseudomeningocele* because it is surrounded not by arachnoid and dura, but rather by a pseudomeninges of reactive fibrous tissue.¹²² Pseudomeningoceles typically are well circumscribed, communicate with the subarachnoid space, and contain fluid that matches the signal characteristics of CSF, which is homogeneous and has low signal intensity on T1-weighted images and high signal intensity on T2-weighted images. Given that the pressure within a pseudomeningocele is usually similar to that of the subarachnoid space, these collections usually compress the thecal sac less than do postoperative epidural hematomas.¹²³

8 Tumors of the Spine

Daniel M. Sciubba, Patricia L. Zadnik, Bruce A. Wasserman, and Ziya L. Gokaslan

CHAPTER OUTLINE

- I. Specialized Pulse Sequences and Imaging Protocols
- II. Extradural Tumors
 - A. Metastatic Disease
 - B. Primary Benign Tumors
 1. Vertebral Hemangioma
 2. Osteoid Osteoma
 3. Osteblastoma
 4. Giant Cell Tumor
 5. Osteochondroma
 6. Aneurysmal Bone Cyst
 7. Eosinophilic Granuloma
 - C. Primary Malignant Tumors
 1. Multiple Myeloma
 2. Solitary Bone Plasmacytoma
 3. Chordoma
 4. Sarcomas
 - a. Chondrosarcoma
 - b. Osteosarcoma/Osteogenic Sarcoma
 - c. Ewing Sarcoma
 - D. Other Tumors
 1. Neuroblastic Tumors
 2. Angiolipoma
 3. Lymphoma
- III. Intradural–Extramedullary Tumors
 - A. Meningioma
 - B. Schwannoma
 - C. Neurofibroma
 - D. Malignant Peripheral Nerve Sheath Tumor
 - E. Hemangiopericytoma
- IV. Intramedullary Tumors
 - A. Ependymoma and Low-Grade Astrocytoma
 - B. Hemangioblastoma
 - C. Intramedullary Metastases
- V. Summary

Spine tumors are traditionally classified by anatomic location into three compartments^{1–6}:

- Extradural
- Intradural–extramedullary
- Intramedullary

The extradural compartment consists of all structures outside the dura, including the osseous structures, the paravertebral region (including the paraspinal musculature), and the epidural space. Although orthopedic surgeons most commonly manage tumors of the extradural compartment, they must have an understanding of the other two compartments to provide comprehensive patient care and to communicate effectively with neurosurgical colleagues.

Spine tumors also are classified by type of origin as primary or metastatic. Although a large number of primary lesions may occur in the spinal cord, nerve roots, dura, and osseous spine, most lesions within the spine are metastatic tumors.^{7–9} Such lesions occur mostly in the extradural compartment, especially in the osseous structures. As systemic therapies for metastatic disease have improved and the life expectancy of such patients has increased, the incidence of metastatic spread to the spine has also increased.

Up to 40% of patients with cancer develop visceral or osseous metastases, and the spinal column is the most common site of osseous metastases.^{9–13} Prostate, lung, and breast cancer account for most of such lesions.^{3,6} Metastases can occur in any compartment of the spinal column, but the vertebral body is the site most commonly affected (~85% of occurrences), followed by the paravertebral region, epidural space, and intradural compartment.¹⁴ In addition, although all segments of the spine can be affected, such lesions occur most often in the thoracic spine (rate, ~70%), followed by the lumbar spine (20%) and then the cervical spine and sacrum (10%).¹⁴

Epidemiologic data suggest that most patients with suspected spine tumors are eventually shown to have metastatic (rather than primary) disease in the vertebral body (rather than in other locations)

and that metastatic and primary lesions (benign and malignant) can occur within any segment and compartment of the spine and in men or women of almost any age. Although most lesions have particular identifying characteristics, it is still imperative that, to arrive efficiently and effectively at the correct diagnosis of a spine tumor, the following steps are followed rigorously when reviewing imaging studies.^{1,2}

1. The compartment location of the lesion in the spinal column (extradural, intradural–extramedullary, or intramedullary) must be identified. Such localization may provide a narrowed differential diagnosis.
2. The clinician generates a preimaging differential diagnosis based on patient demographics and clinical characteristics, such as patient age, sex, medical history, and neurologic signs and symptoms (**Table 8.1**). Such a meticulous evaluation not only guides the type and location of such imaging but also provides substantial insight as to the true underlying pathology. In this way, imaging serves to corroborate or refute, rather than merely suggest, the previously hypothesized differential diagnosis.
3. The patient’s demographic information and clinical presentation are used to narrow the differential diagnosis. For instance, tumors that present in pediatric patients often are extremely rare in adults and vice versa. In addition, in patients with a history of cancer, neck pain or back pain should be assumed to be a symptomatic spinal metastasis until proven otherwise.
4. Various imaging modalities (conventional radiographs, CT, or MRI) can be used to narrow the differential to a working diagnosis. Although these steps may often lead the clinician

to the correct diagnosis, it should be noted that the working diagnosis based on current imaging techniques is not always accurate. For this reason, image-guided or open biopsy often has a role in obtaining a definitive diagnosis before the initiation of a proposed treatment plan (surgery, radiation therapy, chemotherapy, etc.).

MRI is the preferred imaging modality for evaluating most disorders of the spine, including spine tumors.^{15–19} MRI is more sensitive than conventional radiographs, CT, or bone scans in detecting primary malignant bone tumors and metastatic lesions in the spine.^{20,21} This increased sensitivity results from the fact that MRI provides superior resolution of soft-tissue structures, such as the intervertebral discs, spinal cord, nerve roots, meninges, and paraspinal musculature. In addition, MRI provides clarity at the osseous–soft-tissue interface, yielding precise anatomic detail of osseous compression or invasion of neural and paraspinal structures.

Despite this excellent anatomic and soft-tissue depiction, however, MRI is limited in its detection of calcifications and small osseous fragments⁶ and is subject to metal-induced artifact when used in the instrumented spine (usually with stainless steel or titanium), which may prohibit accurate assessment of neural compression and necessitate a fluoroscopic or CT myelogram for optimal evaluation. CT also provides superior osseous detail and permits resolution of calcification in areas within or around soft-tissue structures. Therefore, the ideal method of evaluating a patient with a suspected or known spinal mass involves a combination of conventional radiographs and/or CT imaging with MRI.

This chapter describes image interpretation techniques that permit identification of the compartment and the MRI appearance of the most common tumors

Table 8.1 Differential diagnosis of spine lesion by anatomic compartment†

Compartment	Malignant	Benign	Nontumorous Growths
Extradural	Metastases Myeloma Lymphoma Ewing sarcoma Osteosarcoma Chordoma Leukemia Chondrosarcoma	Hemangioma Aneurysmal bone cyst Giant cell tumor Osteoid osteoma Osteoblastoma Osteochondroma Eosinophilic granuloma	
Intradural extramedullary	Metastases Malignant nerve sheath tumors	Nerve sheath tumors Schwannoma Neurofibroma Meningioma Hemangiopericytoma Paraganglioma	Lipoma Epidermoid Dermoid Arachnoid cyst
Intramedullary	Astrocytoma Metastases	Astrocytoma Hemangioblastoma Ependymoma	

in each location, facilitating the systematic and efficient creation of a differential diagnosis (**Table 8.1**) for any spine tumor evaluated with MRI.

■ Specialized Pulse Sequences and Imaging Protocols

MRI protocols vary widely among institutions and in relation to the spinal region involved. Despite such variation, the MRI protocol for any patient suspected of having a spine tumor should include T1-weighted and T2-weighted images and gadolinium-enhanced studies in the axial and sagittal planes.^{2,22–24} Gadolinium enhancement often provides improved anatomic detail of spinal tumors and may supply signature clues to the underlying pathology.²² Because of the high signal intensity of fat within an adult's marrow on T1-weighted images, fat-suppression techniques are useful in evaluating osseous lesions that enhance with contrast.² Similarly, enhancing lesions in the epidural space are better seen with fat suppression, particularly in the lumbar spine in which the epidural space is composed primarily of fat. Gradient-echo sequences are not as useful in assessing spine tumors unless hemorrhage is suspected. On the other hand, diffusion-weighted imaging, which often reveals restricted diffusion in a vertebral body with a tumor, may be helpful in distinguishing benign and pathologic compression fractures.^{16,25} Consultation with a neuroradiologist generally is advisable for the selection of the ideal imaging protocol.

■ Extradural Tumors

Extradural masses typically arise from the osseous spine, intervertebral discs, and adjacent soft tissues. With MRI, the hallmark of such lesions is focal displacement of the thecal sac away from the mass, with an obliterated subarachnoid space and compressed spinal cord (**Fig. 8.1**). The dura often appears to be draped over the mass. The most common malignant extradural masses are metastases (**Fig. 8.2**), followed by primary malignant tumors of the spine.⁴ The most common benign extradural masses are degenerative and traumatic lesions, such as disc herniations, osteophytes, and fractures, followed by primary benign tumors of the spine.⁴ This chapter discusses extradural *neoplastic* lesions of the spine, both malignant and benign.

Metastatic Disease

The spinal column is the most common site of osseous metastases, and the most common extradural malignant spine tumors in adults are metastatic lesions.⁴ Autopsy studies reveal vertebral metastases

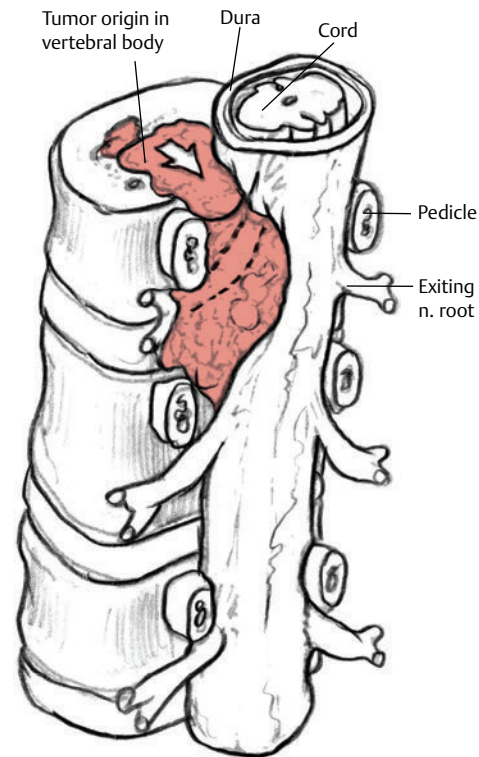


Fig. 8.1 An artist's sketch (posterior oblique view) depicts the characteristics of an extradural mass. The spinal cord and dura are displaced. The depicted mass extends from the vertebral body (arrow) into the extradural space.[†]

in up to 40% of patients with systemic cancer, with 5% of adults presenting with epidural spinal cord compression.^{8,10,13,26}

Most spine metastases in adults arise from lung, breast, and prostate cancer, followed less frequently by lymphoma, melanoma, renal cancer, sarcoma, and multiple myeloma.^{7,8} Approximately 5% of children with solid malignant tumors develop spinal metastases with cord compression.²⁷ In such cases, spine metastases most often are caused by Ewing sarcoma and neuroblastoma, followed by osteogenic sarcoma, rhabdomyosarcoma, Hodgkin disease, soft-tissue sarcoma, and germ cell tumors.²⁷

In adults, the initial site of metastatic tumor growth in the spine typically is the posterior vertebral body, followed by the epidural space and pedicle.²⁸ Conversely, metastatic tumors in children typically invade the spinal canal via the neural foramina, causing circumferential cord compression.⁷ Spinal metastases in the adult can occur at any level, but they usually involve the lower thoracic and lumbar spine because of the higher proportion of red bone marrow in those locations.^{20,28}

MRI is the method of choice for imaging metastatic spine disease because of its unparalleled ability to delineate epidural and paraspinal soft-tissue involvement. Imaging patterns of such lesions can reveal focal

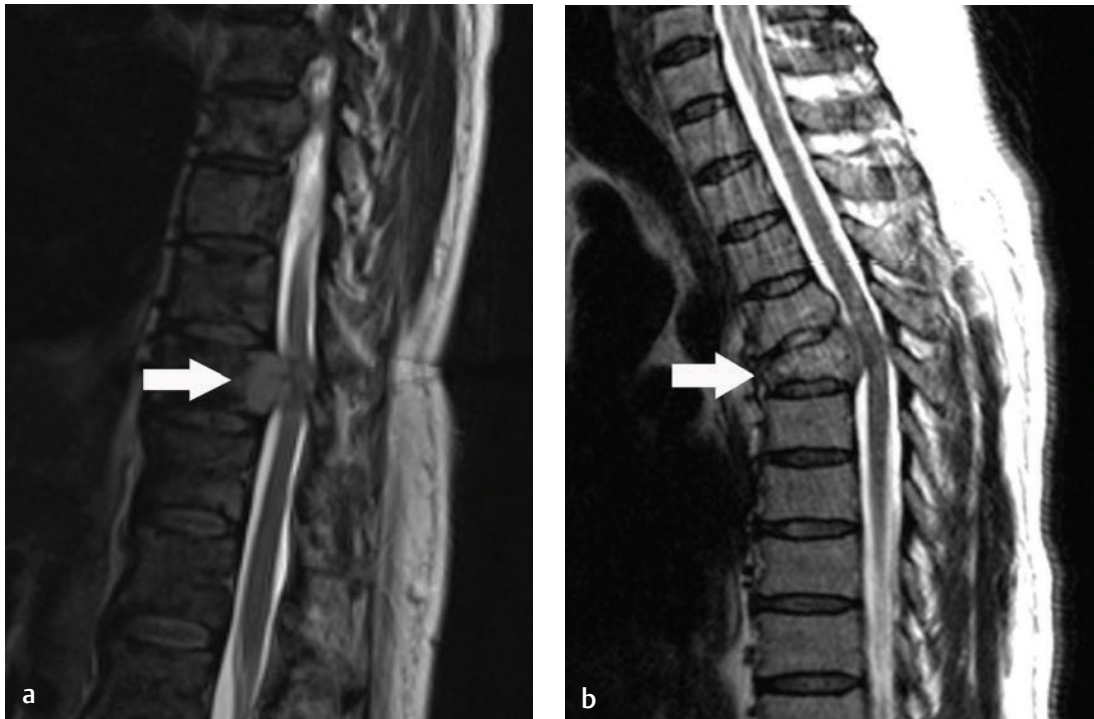


Fig. 8.2 Sagittal T2-weighted images of extradural metastatic lesions reveal compression and distortion of the underlying dura and spinal cord in two different patients. **(a)** Prostate metastasis (*arrow*) to the thoracic spine with epidural extension. **(b)** Non-small-cell lung cancer metastasis to the upper thoracic spine with epidural extension. Loss of vertebral body height is noted (*arrow*).

lytic, focal blastic/sclerotic, diffuse homogeneous, and diffuse inhomogeneous lesions.^{4,21,24,29,30} The most common pattern seen is multifocal lytic lesions, which are hypointense on T1-weighted images and hypo- to hyperintense on T2-weighted images (**Fig. 8.3**). Sclerotic lesions tend to be hypointense on both T1-weighted images and T2-weighted images. Diffuse homogeneous and inhomogeneous lesions are hypointense on T1-weighted images and hyperintense on T2-weighted images, although the signal pattern can be variable and depends on the degree of fatty marrow. Contrast enhancement of such lesions is extremely variable as well.

MRI also may be useful for distinguishing benign, osteoporotic fractures from pathologic, tumor-related fractures.^{16,25,31,32} Benign fractures typically have marrow signal intensity identical to that of neighboring normal vertebral bodies. Pathologic fractures are more hypointense on T1-weighted images and more hyperintense on T2-weighted images than are normal vertebral bodies.³¹ Additionally, diffusion-weighted images, combined with apparent diffusion coefficient mapping, often shows more extensive restricted diffusion with pathologic fractures than with osteoporotic fractures.² The identification of epidural or paraspinal soft-tissue involvement is also helpful for confirming a pathologic etiology.

Primary Benign Tumors

Benign primary tumors of the extradural compartment of the spine have characteristic MRI findings and patient demographics (**Table 8.2**) that help differentiate them from malignant lesions.

Vertebral Hemangioma

Vertebral hemangioma is the most common spinal axis tumor.^{32,33} This benign vascular tumor of the vertebral body, often discovered incidentally on imaging, can be associated with vertebral body collapse and epidural extension with spinal cord compression; on rare occasions, it may exhibit aggressive growth.^{34,35} MRI sequences of the typical (fatty) hemangioma show lesions that are hyperintense on T1-weighted and T2-weighted images, with robust contrast enhancement³⁶ (**Fig. 8.4**). Vertebral hemangiomas are one of the very few spinal tumors that show increased signal intensity on both T1-weighted and T2-weighted images. Occasionally, such lesions are more vascular and may appear isointense or hypointense on T1-weighted images, making them difficult to

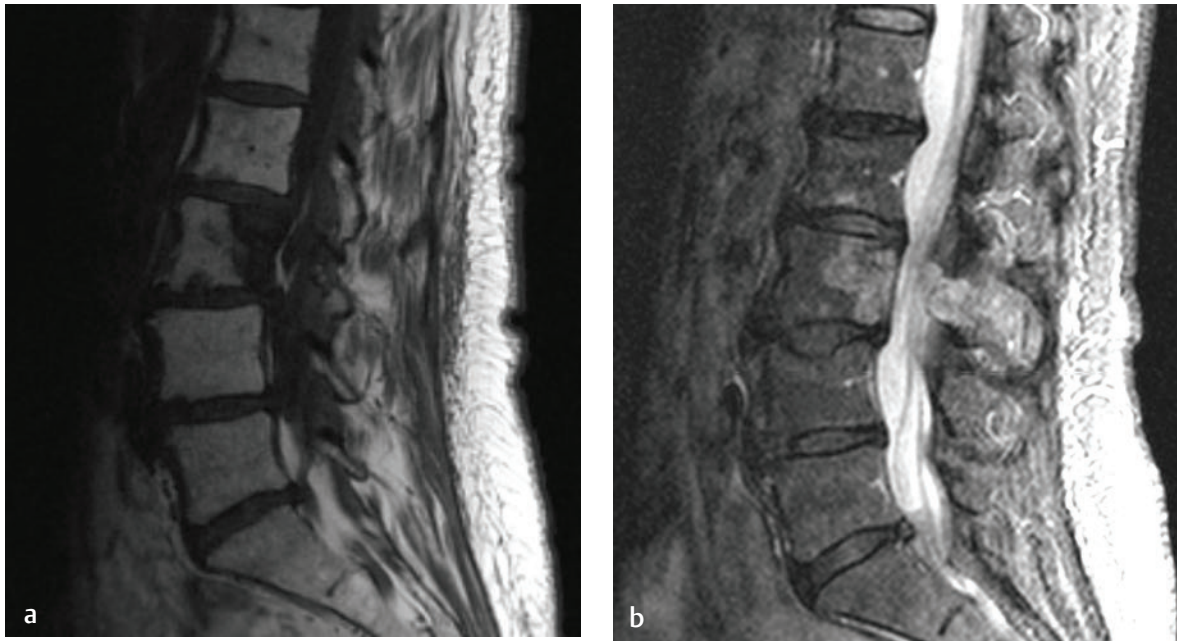


Fig. 8.3 Lumbar spine metastasis from breast carcinoma. **(a)** A sagittal T1-weighted image shows a hypointense lesion occupying the L3 vertebral body. **(b)** The disease extent is more evident on this sagittal fat-suppressed T2-weighted image.

Table 8.2 Benign primary tumors of the extradural compartment

Lesion	Location in Segment	Spinal Segment	Incidence	Age (years)	Imaging Clue
Hemangioma	Vertebral body	T, L > C	Most common	All	Bright on T1-weighted image
Osteoid osteoma	Neural arch	L, C > T	Common	10 to 20	Target lesion <2 cm
Osteoblastoma	Neural arch	C > L, T, S	Uncommon	<30	Expansile, lytic >2 cm
Giant cell tumor	Vertebral body	S >> C, T, L	Uncommon	20 to 50	Expansile, lytic, vascular
Osteochondroma	Spinous, transverse processes	C >> T, L	Rare in spine	5 to 30	Mushroom-shaped
Aneurysmal bone cyst	Neural arch	C, T > L, S	Rare	<20	Fluid-fluid levels, eggshell-like rims
Eosinophilic granuloma	Vertebral body	T > L, C	Rare	<15	Vertebra plana

Source: This table was published in Diagnostic Neuroradiology, Osborn AG (ed). Cysts, tumors, and tumorlike lesions of the spine and spinal cord, 876–918, Copyright Elsevier (1994). Adapted with permission.

Abbreviations: C, cervical; L, lumbar; S, sacral; T, thoracic

distinguish from metastases. Although CT images show the typical “polka dot” appearance on axial images and the typical “corduroy” or “jailhouse striation” pattern on sagittal images, as a result of the thickened trabeculae, MRI is the best modality for characterizing the epidural extent and cord compromise of aggressive lesions. Although such lesions primarily involve the vertebral body, 10% to 15% have concomitant involvement of the posterior elements.³³ Multiple lesions are seen in 25% to 30% of patients.³⁷

Osteoid Osteoma

This benign, osteoid-producing tumor, usually <1.5 cm in size, is often surrounded by a ring of sclerotic bone. Almost all of these lesions involve the neural arch, and most occur within the lumbar spine, followed by the cervical, thoracic, and sacral regions. Bone scintigraphy and CT are generally more helpful for detecting and characterizing these lesions than is MRI. The nidus is hypo- or isointense on T1-weighted

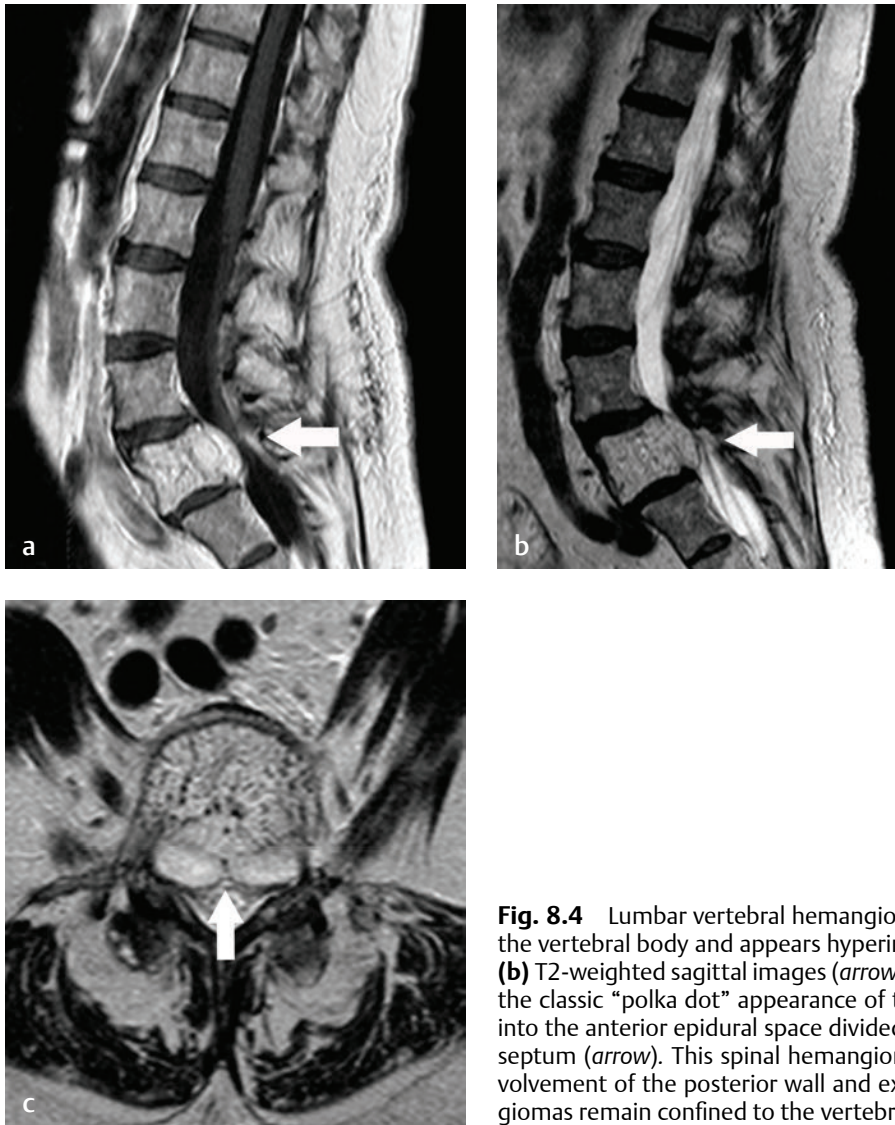


Fig. 8.4 Lumbar vertebral hemangioma. This asymptomatic lesion is centered in the vertebral body and appears hyperintense on **(a)** T1-weighted postcontrast and **(b)** T2-weighted sagittal images (arrow on each). **(c)** On axial T2-weighted imaging, the classic “polka dot” appearance of the vertebral body is noted, with infiltration into the anterior epidural space divided by a cleavage plane formed by the midline septum (arrow). This spinal hemangioma is somewhat atypical in that there is involvement of the posterior wall and extension into the spinal canal. Most hemangiomas remain confined to the vertebral body.

images and varies from hypo- to hyperintense on T2-weighted images, often with surrounding hyperintensity that likely is related to a local inflammatory response (**Fig. 8.5**).^{38–40} The rapid enhancement pattern, typically located within the nidus, is best seen on dynamic sequences (e.g., serial postcontrast images). The surrounding reactive zone enhances more slowly with such imaging. Of note, up to 70% of patients may present with scoliosis, related to muscle spasm, with concavity on the side of the tumor.⁴¹ Patients often report severe nighttime pain.⁴²

Osteoblastoma

Osteoblastomas, also known as giant osteoid osteomas, are similar histologically to osteoid osteomas

but are differentiated from them largely by size (>1.5 cm). Clinical symptoms also can help to distinguish these lesions: osteoblastomas cause a dull pain as opposed to the intense night pain caused by osteoid osteomas.^{43–45} Occasionally, osteoblastomas possess atypical features and behave aggressively.⁴⁵ Like osteoid osteomas, these lesions originate in the neural arch but exhibit greater mass expansion.⁴ Thus, they may be centered in the pedicle, lamina, transverse or spinous process, articular pillar, or pars interarticularis, with extension into the vertebral body. The lesion is hypo- or isointense on T1-weighted images and iso- or hyperintense on T2-weighted images, with extensive peritumoral edema (flare phenomenon); fluid–fluid levels are often present within the lesion (**Fig. 8.6**). Contrast enhancement is variable.⁴⁴

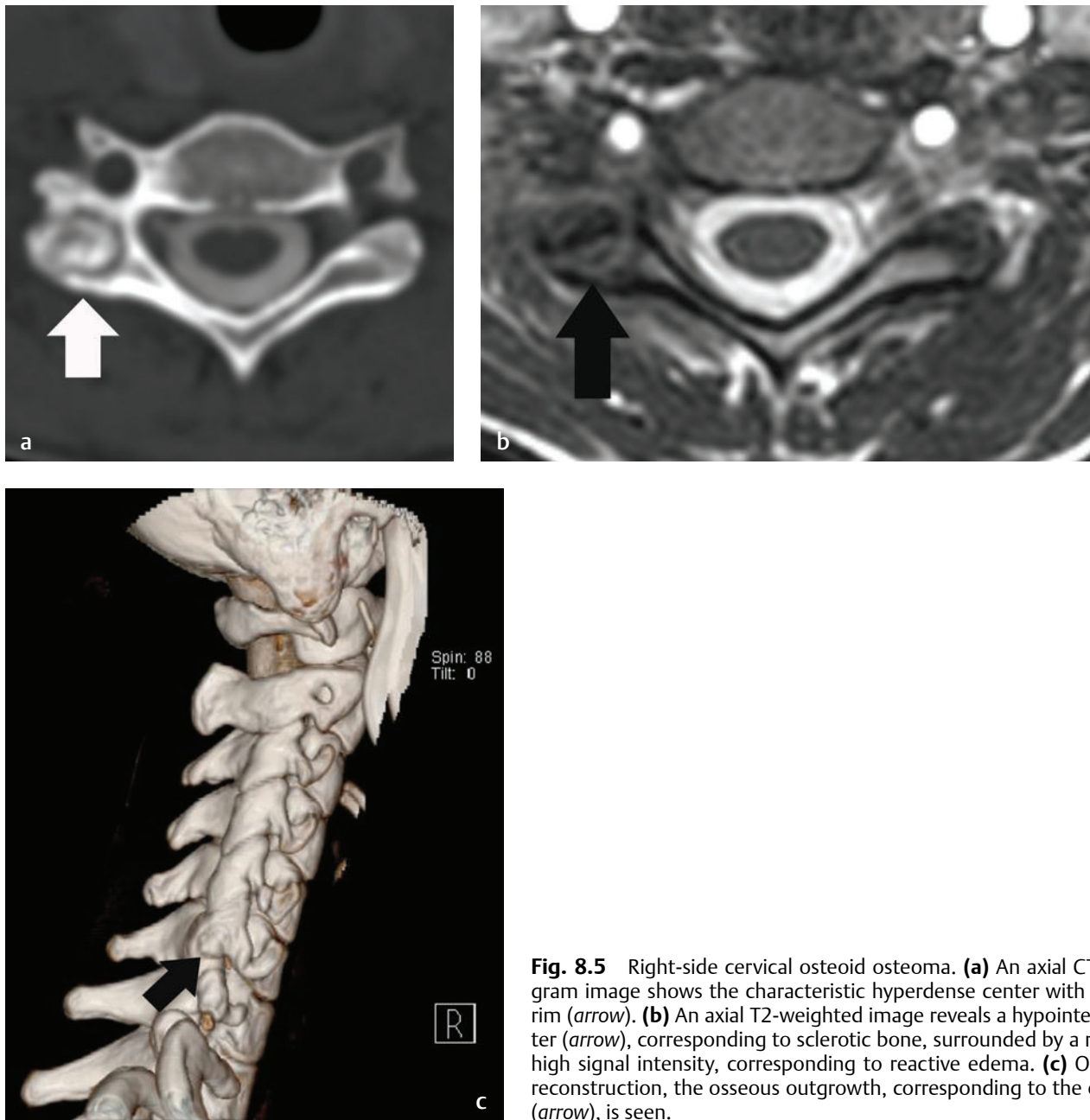


Fig. 8.5 Right-side cervical osteoid osteoma. **(a)** An axial CT myelogram image shows the characteristic hyperdense center with sclerotic rim (arrow). **(b)** An axial T2-weighted image reveals a hypointense center (arrow), corresponding to sclerotic bone, surrounded by a region of high signal intensity, corresponding to reactive edema. **(c)** On 3D CT reconstruction, the osseous outgrowth, corresponding to the osteoma (arrow), is seen.

Giant Cell Tumor

Giant cell tumors are locally aggressive, lytic tumors in the vertebral body and sacrum and are named for the osteoclast-like giant cells that are present on histology.^{32,46} Hemorrhage is common secondary to the hypervascular stroma of these lesions. MRI shows expansile lesions with hypo- to isointense signal on T1-weighted images and iso- to hyperintense signal on T2-weighted images (**Fig. 8.7**). Contrast enhancement often is heterogeneous, commonly surround-

ing areas of necrosis, blood, blood degradation products, and/or cystic cavities with fluid–fluid levels.⁴⁷ Such lesions can undergo sarcomatous transformation (10% of cases) to become malignant giant cell tumors,⁴⁶ and therefore patients with these tumors must be monitored with MRI or CT because of the risk of recurrence. It is important to note that the differential diagnosis of midline tumors in the sacrum includes giant cell tumor, chordoma, aneurysmal bone cyst, plasmacytoma, and metastases in adults and sacrococcygeal teratoma in children.¹⁴

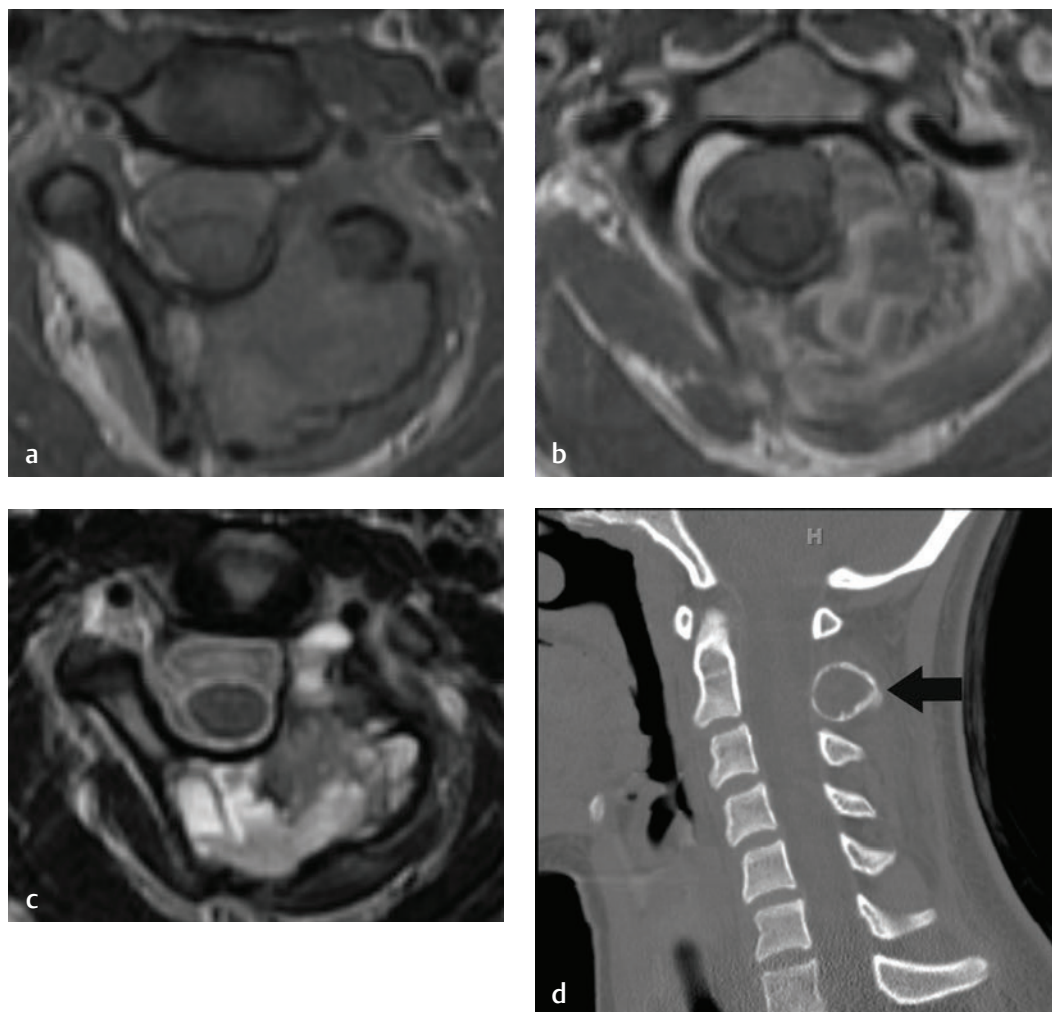


Fig. 8.6 Left-side cervical osteoblastoma. Axial (a) precontrast and (b) postcontrast T1-weighted images show a lesion similar to (but larger than) the osteoid osteoma shown in **Fig. 8.5**. The lesion shows heterogeneous contrast enhancement with infiltration into the epidural space. (c) An axial T2-weighted image also shows the lesion. (d) A sagittal CT reconstruction highlights the osseous destruction and expansion associated with the osteoblastoma in the spinous process (*arrow*).

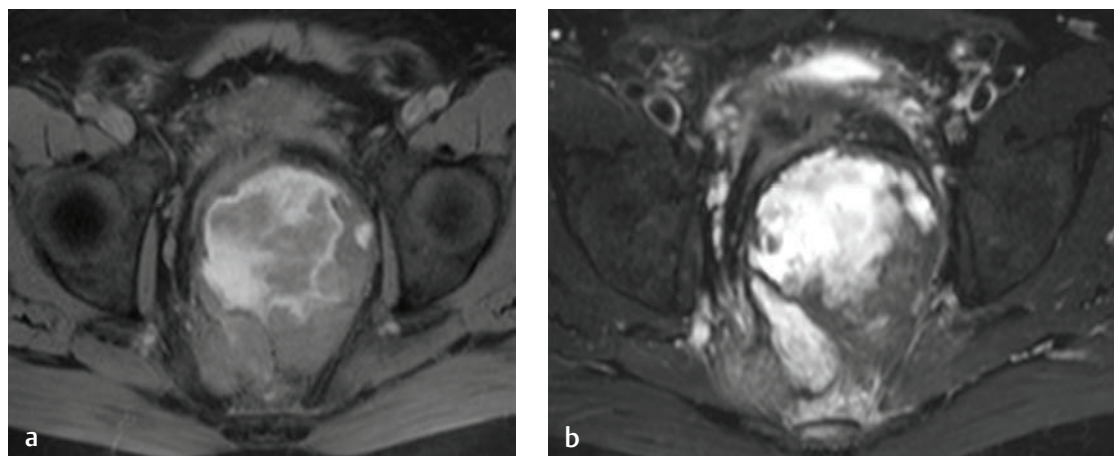


Fig. 8.7 Sacral giant cell tumor. This expansile lesion shows heterogeneous enhancement on (a) a coronal postcontrast T1-weighted image and high signal intensity on (b) an axial fat-suppressed T2-weighted image.

Osteochondroma

Osteochondroma, also known as osteocartilaginous exostosis, consists of cartilage-covered osseous protuberances with a medullary cavity that is contiguous with the parent bone.^{48,49} These lesions grossly appear to be cauliflower- or mushroom-shaped lesions with cartilaginous caps. Only 5% of these growths occur within the spine (compared with 85% in long-bone metaphyses), but when they do, they are located mostly in the cervical spine, particularly at C2.¹⁴ These lesions most commonly arise from the spinous and transverse processes, but they also may arise from the vertebral body. On T1-weighted and T2-weighted images, they appear as central hyperintense lesions surrounded by hypointense calcified cortex.⁵⁰ The cartilaginous cap is hypo- to isointense on T1-weighted images and iso- to hyperintense on T2-weighted images and exhibits peripheral enhancement of cartilage.⁴⁹ MRI is the preferred imaging modality for measuring the cartilaginous cap and determining the status of regional neural and musculoskeletal tissue. Thickening of the cap (>1 cm) should raise concern for malignant transformation to chondrosarcoma. CT may be used for evaluating the osseous structure of the lesion, confirming the contiguity of the medullary cavity with the parent bone, and evaluating for fractures.

Aneurysmal Bone Cyst

These lesions are expansile benign neoplasms containing thin-walled cavities filled with blood and blood products that occur most commonly in patients <20 years old. A substantial proportion of aneurysmal bone cysts are associated with preexisting osseous lesions, such as an osteoblastoma, giant cell tumor, chondroblastoma, nonsifying fibroma, or fibrous dysplasia.^{46,51–55} They arise in the neural arch, but most extend into the vertebral body. The classic presentation is a balloon-like expansile remodeling of bone, leaving a thinned “eggshell” cortex. On T1-weighted and T2-weighted images, the lesions appear as lobulated neural arch masses, commonly with extension into the vertebral body, epidural space, and adjacent vertebral bodies and ribs.⁵¹ Intratumoral cysts contain fluid–fluid levels secondary to blood breakdown products (**Fig. 8.8**), although visualization of these levels often requires the patient to be motionless for a few minutes before imaging. Contrast enhancement may be present at the periphery of the tumor and in the septations. Vertebral body collapse may occur secondary to the extensive vertebral body destruction associated with such lesions.

Eosinophilic Granuloma

This lytic lesion of the vertebral body classically presents with a single collapsed vertebral body (vertebra plana) in patients <10 years old (**Fig. 8.9**) and consists of a benign proliferation of Langerhans cell histiocytes. The lesions are hyperintense on T2-weighted images but present with variable intensity on T1-weighted images. Contrast enhancement is robust.^{4,56}

Primary Malignant Tumors

Multiple Myeloma

Multiple myeloma is the multifocal, metastatic, and systemic presentation of a solitary bone plasmacytoma (see next paragraph).⁵⁷ Like solitary bone plasmacytomas, focal lesions appear in the vertebral bodies with low to intermediate signal intensity on T1-weighted images compared with normal bone marrow, and they appear hyperintense on T2-weighted images. Postgadolinium enhancement is often present (**Fig. 8.10**). Multiple myeloma also is revealed on MRI by diffuse marrow involvement at multiple spinal levels.⁵⁸ Compared with other metastatic lesions, which usually have early pedicle involvement, multiple myeloma usually involves the pedicle late in the course of disease.¹⁴

Solitary Bone Plasmacytoma

Solitary plasmacytoma presents as a mass of monoclonal plasma cells from bone or soft tissue and may precede multiple myeloma by several years.⁵⁹ Clinical differentiation from multiple myeloma requires a biopsy-proven solitary lesion, the absence of other such lesions in the skeleton, and the absence of anemia, hypercalcemia, and renal involvement suggesting systemic myeloma.^{60–62} Such lesions are lytic, destructive, and often accompanied by compression fractures associated with soft-tissue masses and fractures that may lead to severe collapse (vertebra plana). T1-weighted images reveal a solitary lesion centered in the vertebral body that is hypo- or isointense compared with muscle and can show curvilinear low-signal areas and/or cortical infolding caused by end-plate fractures. In most cases, the posterior elements are involved, and neural compression is varied. T2-weighted images reveal heterogeneous signal within the lesion with focal hyperintensities. Mild to moderate diffuse contrast enhancement is common, and peripheral (rim) contrast enhancement is rare.⁶³ Scanning of the entire skeleton is mandatory to identify a secondary lesion, which occurs in the spine in one third of patients.^{14,64}

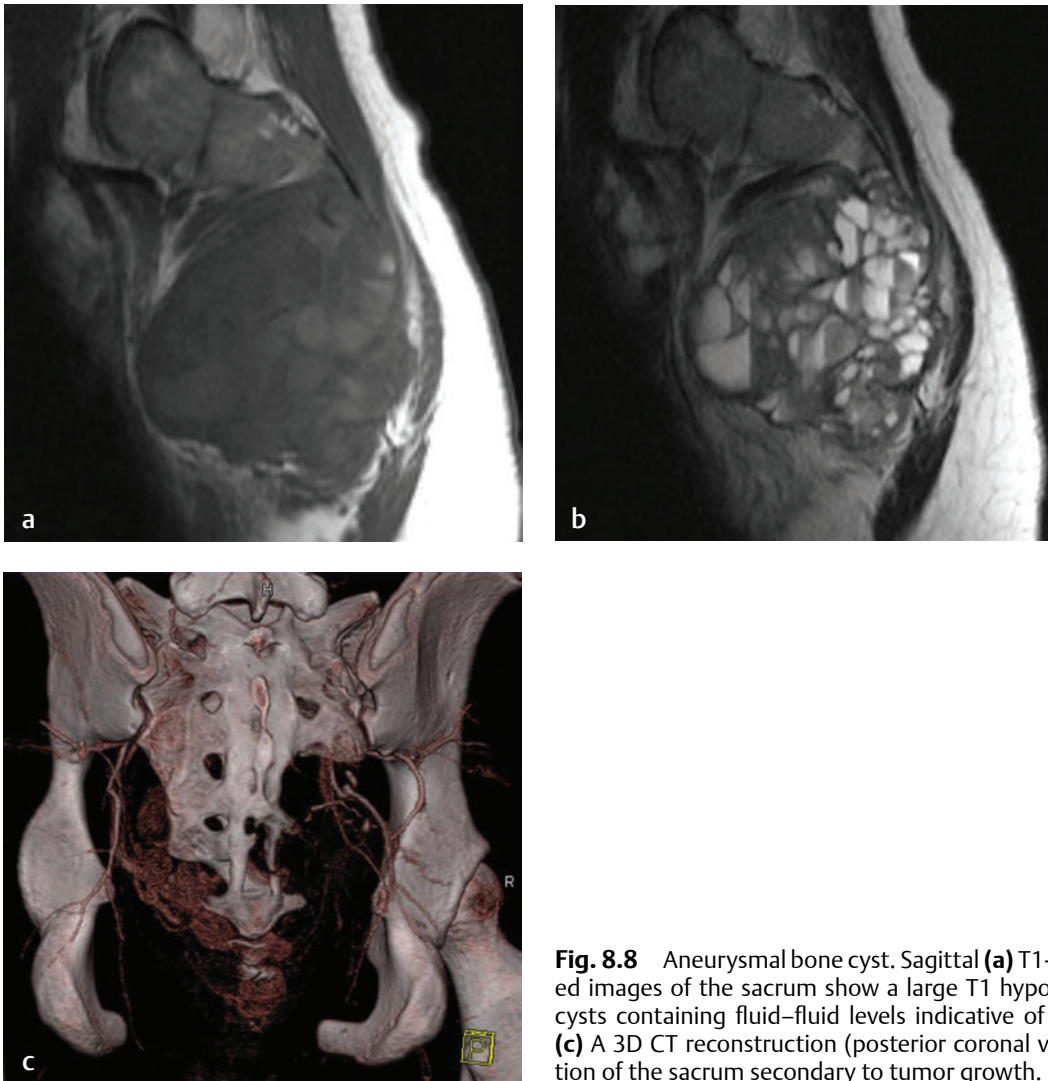


Fig. 8.8 Aneurysmal bone cyst. Sagittal (a) T1-weighted and (b) T2-weighted images of the sacrum show a large T1 hypointense tumor with multiple cysts containing fluid–fluid levels indicative of blood breakdown products. (c) A 3D CT reconstruction (posterior coronal view) shows osseous destruction of the sacrum secondary to tumor growth.

Chordoma

These malignant tumors arising from notochord remnants typically present in one of two histologic patterns. The more common type, known as a *typical chordoma*, is composed of lobules and sheets of physaliphorous cells, which contain intracytoplasmic vacuoles and abundant mucin.⁶⁵ The less common type contains cartilaginous foci and is termed *chondroid chordoma*.^{4,65} Chordomas present as lytic, destructive lesions arising in the midline of the spinal column at any location from clivus to coccyx, but they are found more commonly at the sacrococcygeal (50%) and sphenooccipital (clival) (35%) areas and less commonly in the vertebral body (15%).¹⁴ For lesions within the vertebral

bodies, a cervical location (particularly at C2) is most common, followed by lumbar and thoracic areas. Chordomas often are several centimeters in size at discovery, usually involve two or more adjacent vertebrae, and extend into the intervertebral discs, surrounding paravertebral soft tissues, and spinal canal. On T1-weighted images, the lesions are hypo- or isointense (compared with marrow). On T2-weighted images, lesions are hyperintense compared with intervertebral discs and CSF, secondary to the high intratumoral mucin content, and are septated by low-signal fibrous bands (**Fig. 8.11**). STIR or fat-suppressed T2-weighted images can help in defining borders with neighboring soft tissues. Contrast-enhanced images range from contrast blush to robust enhancement.^{66,67}

Fig. 8.9 A sagittal T2-weighted image of an eosinophilic granuloma shows the typical finding of a vertebra plana (*arrow*). In this case, there is also an epidural mass that displaces the spinal cord. Note the associated kyphotic deformity.[†]



Fig. 8.10 Multiple myeloma. **(a)** Mid-sagittal and **(b)** parasagittal T2-weighted images of the lumbar spine show multiple, well-circumscribed, high-signal-intensity lesions throughout the lumbar spine. The diagnosis of multiple myeloma can be confirmed by correlation with CT imaging and also with urine and serum protein electrophoresis.

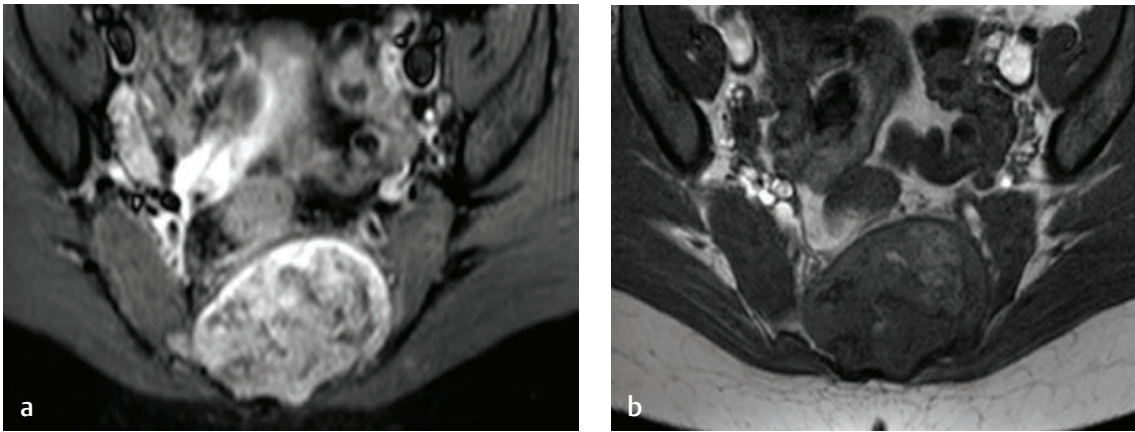


Fig. 8.11 This (a) axial fat-suppressed T2-weighted image of a sacral chordoma reveals a hyperintense lesion that has extended into the pelvis and left gluteal muscles. (b) The lesion appears mostly hypointense with focal regions of hyperintensity, likely representing hemorrhage or mucinous material on an axial T1-weighted image.

Sarcomas

Primary sarcomas include chondrosarcoma, osteosarcoma, and Ewing sarcoma, all of which involve the spine only occasionally. Primary fibrosarcomas of the spine are extremely rare.

Chondrosarcoma

These malignant, lytic tumors of chondrocytes are characterized by the formation of cartilaginous matrix, can occur as primary tumors or as malignant degeneration of osteochondromas and enchondromas, can cause cortical disruption, and can extend into surrounding soft tissues.^{68,69} Chondrosarcomas can occur wherever cartilage exists,⁷⁰ and ~5% occur in the spine.¹⁴ T2-weighted images reveal high signal intensity in areas of hyaline cartilage and low intensity in areas of mineralized matrix. T1-weighted images are helpful in delineating soft-tissue invasion. Contrast-enhanced images show strong enhancement of the septa with “ring and arc” patterns that delineate areas of hyaline cartilage, cystic mucoid tissue, and necrosis, all of which do not enhance with contrast (**Fig. 8.12**).⁷¹

Osteosarcoma/Osteogenic Sarcoma

Of all primary osteogenic sarcomas, 4% occur in the spine and sacrum, primarily in the posterior spinal elements.⁷² These malignant, lytic tumors of osteoblasts are characterized by the formation of immature, woven osteoid and can occur as primary tumors or as malignant degeneration in individuals with Paget disease, irradiated bone, or bone infarcts. These tumors present primarily in the vertebral bodies, commonly with extension into the posterior elements, and typically have focal areas of low signal

on all pulse sequences, secondary to matrix mineralization (**Fig. 8.13**).⁷³ In the telangiectatic form, T2-weighted images may show fluid–fluid levels.

Ewing Sarcoma

The spine is a rare site for Ewing sarcoma. When it does occur, it usually represents a metastatic tumor from another site of origin.⁴¹ Usually centered in the vertebral body or sacrum, Ewing sarcoma often causes a “moth-eaten” or permeative type of bone destruction rather than extensive bone loss.⁷⁴ Fifty percent of these lesions have an extraosseous, noncalcified soft-tissue mass.^{72,75} On T1-weighted images, these lesions are hypo- to isointense compared with surrounding bone marrow, and the cortex usually is preserved despite extraosseous tumor spread. On T2-weighted images, lesions are hyperintense. MRI is the ideal imaging study for delineating extension of soft-tissue mass. Because Ewing sarcoma is histologically a small, round cell tumor, it can be radiographically identical to primitive neuroectodermal tumors, Langerhans cell histiocytosis, lymphoma, leukemia, myeloma, and metastatic neuroblastoma. Ewing sarcoma may also have imaging characteristics similar to those of osteomyelitis. In addition, patients with Ewing sarcoma may present with vertebral body collapse, similarly to patients with Langerhans cell histiocytosis.⁷⁶

Other Tumors

Neuroblastic Tumors

These embryonal tumors, which are derived from neural crest cells, exist as a spectrum ranging from the most benign ganglioneuromas, to intermediate-differentiated ganglioneuroblastomas, to the most

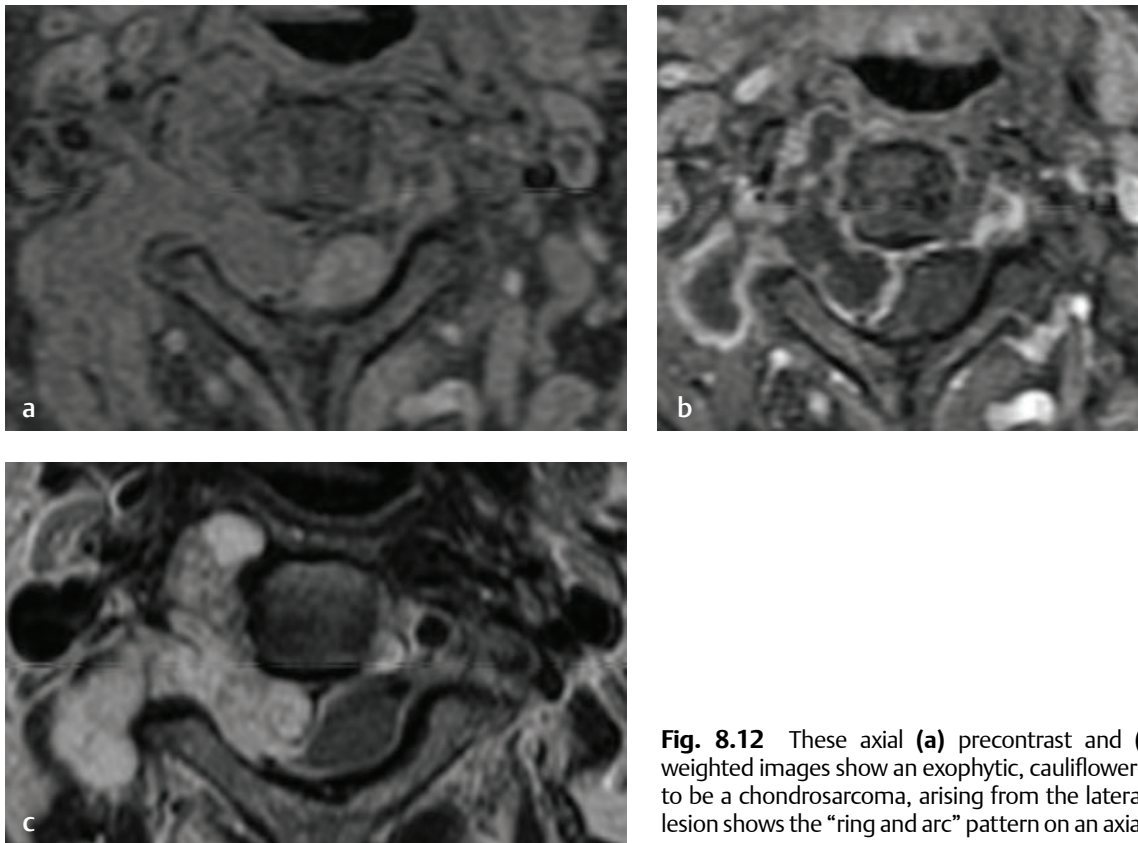


Fig. 8.12 These axial (a) precontrast and (b) postcontrast T1-weighted images show an exophytic, cauliflower-shaped lesion, found to be a chondrosarcoma, arising from the lateral mass of C2. (c) The lesion shows the “ring and arc” pattern on an axial T2-weighted image.

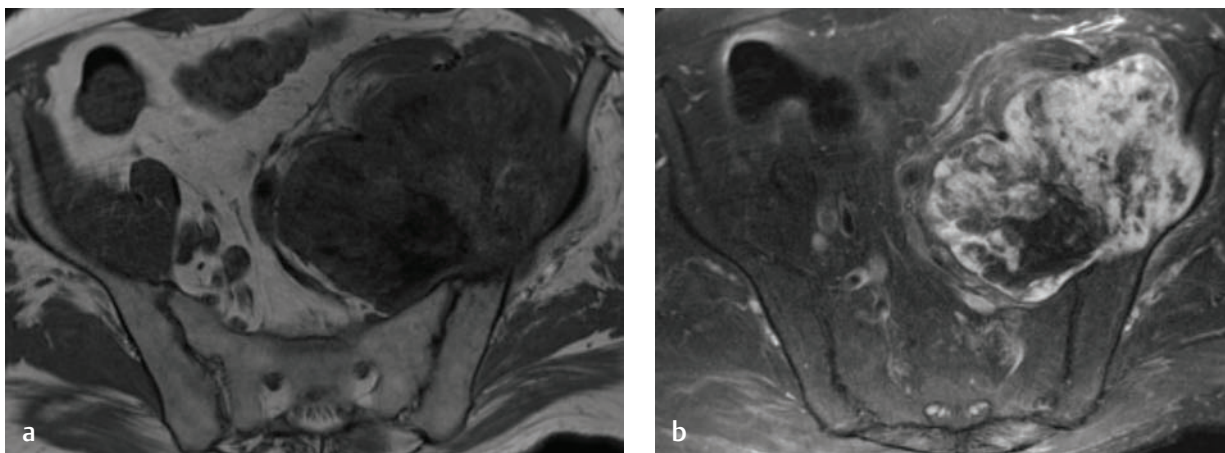


Fig. 8.13 Osteosarcoma. (a) An axial T1-weighted image of a left-side osteosarcoma of the sacrum and ilium. (b) The lesion is hyperintense on an axial postgadolinium, fat-suppressed T1-weighted image with a central hypointense, cystic/necrotic area.

malignant neuroblastomas. These tumors present almost exclusively in patients <10 years old and almost exclusively as abdominal or thoracic paraspinal masses with intraspinal extension.⁴ The lesions are typically large and extend through a widened neural foramen, creating dumbbell-shaped morphologies and compressing the spinal cord (**Fig. 8.14**).

The lesions are hypo- to isointense on T1-weighted images and hypo- to hyperintense on T2-weighted images. Although classically they present as paraspinal masses, they may appear as metastatic lesions within vertebral bodies. Contrast enhancement varies but often surrounds areas of internal hemorrhage or necrosis.^{77,78}

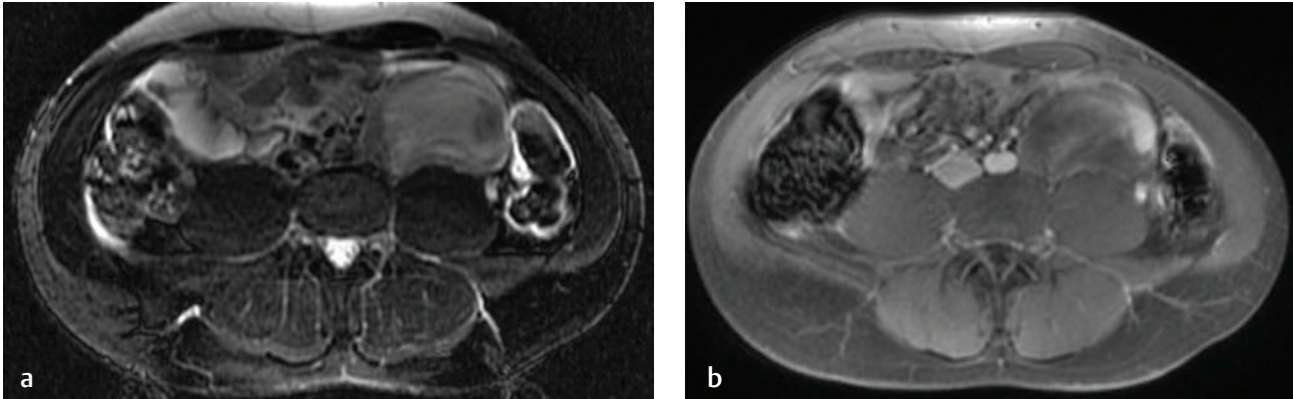


Fig. 8.14 Left-side paraspinal ganglioneuroma. **(a)** An axial T2-weighted fat-suppressed image shows a lesion adjacent to the vertebral body and anterior to the psoas muscle. The lesion is hyperintense compared with muscle. **(b)** An axial postgadolinium T1-weighted image shows the lesion to be isointense compared with muscle, with sparse intralesional and peripheral enhancement.

Angiolipoma

These benign lesions of adipose and vascular elements present in the spine primarily as epidural masses; they rarely present in an intramedullary location.⁷⁹ Because the lesions are composed of fat and vascular tissues, MRI shows heterogeneous signal intensity. On T1-weighted images, most lesions are hyperintense with iso- to hypointense areas around prominent vascular components. The lesion may appear heterogeneous on T2-weighted images, but it generally has high signal intensity. Therefore, fat-suppressed T1-weighted images with contrast are most useful for defining this lesion and often show heterogeneous enhancement. Interestingly, these lesions do not show vascular flow voids. These lesions may destroy adjacent bone in the anterior epidural space, although only rarely in the posterior epidural space.⁸⁰

Lymphoma

Lymphoreticular neoplasms present with variable imaging manifestations within the spine.^{81,82} All locations of the spine may be affected: epidural space (most common), osseous structures, lymphomatous meninges (within the subarachnoid space), and intramedullary (least common).¹⁴ Lymphomas of the spine are usually metastatic lesions, not primary lesions arising in the spine.⁸³ Only 3% to 4% of all malignant bone tumors are primary osseous lymphomas. In the spine, non-Hodgkin lymphoma is far more common than Hodgkin disease, and >80% of such lesions are of B-cell origin.⁸⁴

MRI is ideal for defining the spinal compartment within which the tumor resides. Epidural lesions are isointense on T1-weighted images and variable, but

often isointense or hyperintense compared with the spinal cord, on T2-weighted images (**Fig. 8.15**). Osseous lesions are hypointense compared with normal marrow on T1-weighted images and iso- to hyperintense on T2-weighted images. Leptomeningitic lymphomas result in thickening of the nerve roots, occasionally with focal nodules, which are isointense compared with the spinal cord on T1-weighted and T2-weighted images. Intramedullary masses show cord thickening that is isointense compared with the spinal cord on T1-weighted images and hyperintense with surrounding edema on T2-weighted images. Contrast-enhanced images show diffuse uniform enhancement regardless of the location, with a diagnostic accuracy of 99%.¹⁴

■ Intradural–Extramedullary Tumors

These lesions arise within the dura but not from within the spinal cord. Classic MRI findings include a widened ipsilateral subarachnoid space in which the cord and roots are displaced away from the mass (**Fig. 8.16**). Nerve sheath tumors (schwannomas and neurofibromas) and meningiomas account for >80% of such masses.⁸⁵

Meningioma

Most of these tumors are slow growing, benign (>95%), and based on the dura mater.⁸⁶ CT imaging may provide added detail because these tumors can calcify; however, MRI is still the ideal imaging modality.⁸⁶ Classically, the lesions are isointense compared with the spinal cord on T1-weighted images and

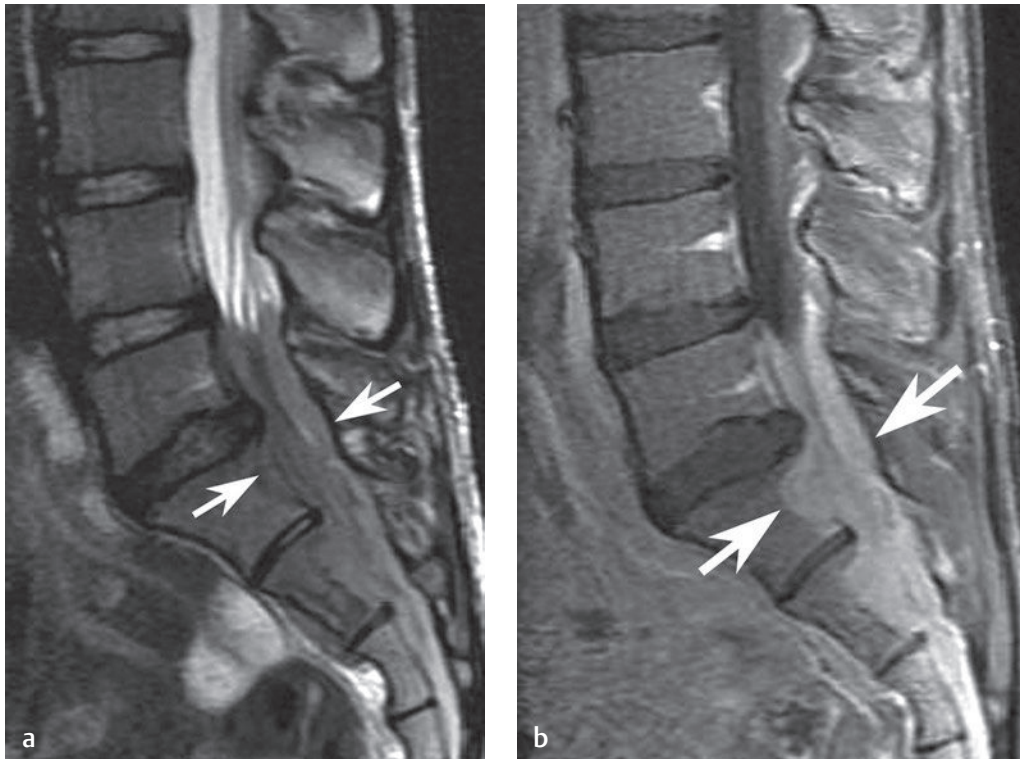


Fig. 8.15 Epidural B-cell lymphoma surrounding and compressing the caudal thecal sac in the lumbosacral spine. **(a)** On a sagittal T2-weighted image, the lesion is isointense compared with the nerve roots and fills the spinal canal, expanding the canal at S1 (arrows). **(b)** On a sagittal postgadolinium T1-weighted image, the lesion (arrows) shows robust enhancement.[†]

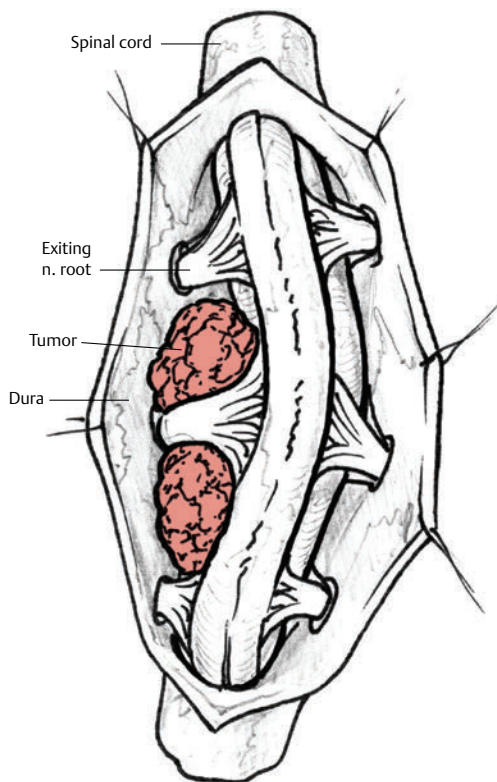


Fig. 8.16 An artist's sketch (dorsal view) depicts the imaging characteristics of an intradural-extramedullary mass.[†]

iso- to hyperintense on T2-weighted images (**Fig. 8.17**). Focal areas of hypointensity occur in the presence of calcifications or flow voids. Contrast-enhanced T1-weighted images show prominent enhancement, sometimes with a broad-based dural attachment (dural “tails”). Most lesions are solitary and occur most commonly in the thoracic spine (80%), followed by the cervical spine (16%) and lumbar spine (4%).^{87,88} Compared with nerve sheath tumors, which are usually anterolateral, meningiomas are usually located dorsal to the cord.^{87,88}

Schwannoma

These benign neoplasms of the peripheral nerve sheaths are the most common intradural-extramedullary masses and appear as well-circumscribed lesions that may be intradural-extramedullary (75%), completely extradural-paraspinal (15%), or intra- and extradural (dumbbell-shaped).⁴ T1-weighted images often show an iso- to hypointense lesion relative to the spinal cord that may be associated with adjacent osseous erosion, such as widening of the neural foramen or vertebral scalloping.^{89,90} In contrast to meningiomas, most schwannomas are hyperintense on T2-weighted images. Postgadolinium T1-weighted images show enhancement that may

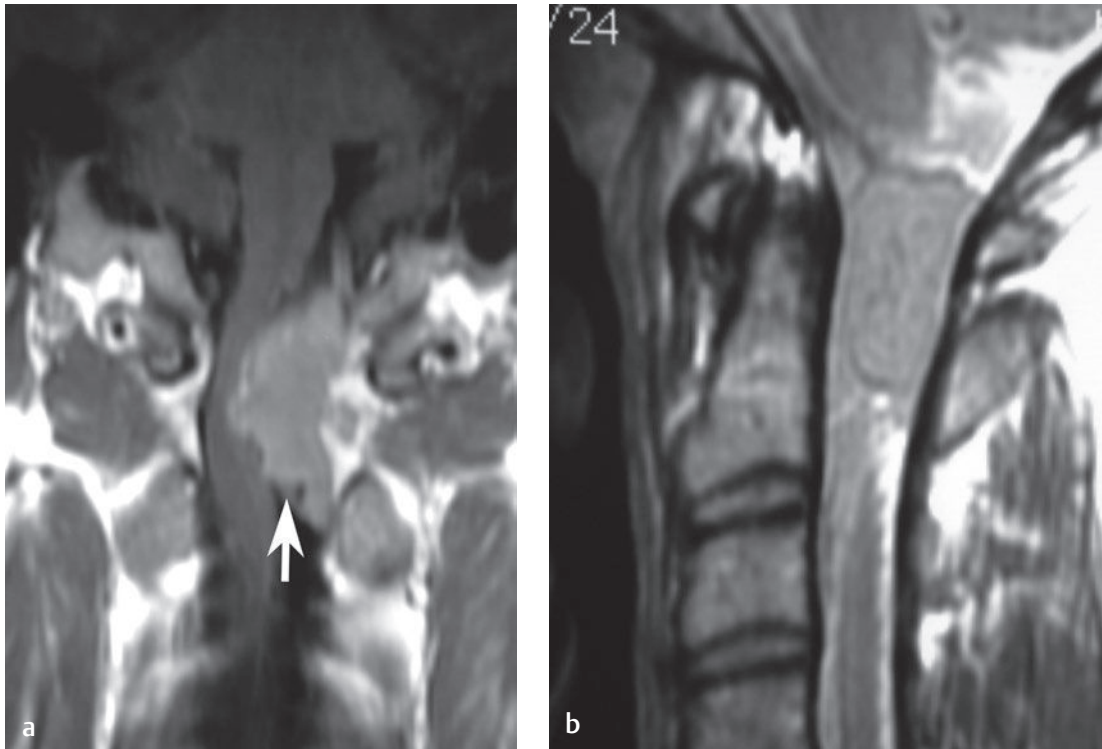


Fig. 8.17 Cervical meningioma. **(a)** A coronal postgadolinium T1-weighted image shows a widely dural-based lesion (*arrow*) that enhances and is hyperintense compared with the spinal cord. **(b)** On a sagittal T2-weighted image, the lesion is slightly hyperintense compared with the spinal cord, showing cord displacement and widening of the ipsilateral CSF space, characteristic of intradural–extramedullary lesions.[†]

be homogeneous, heterogeneous, or rim-enhancing around cystic areas (**Fig. 8.18**). Hemorrhage and cystic degeneration are more common with schwannomas than with neurofibromas. Solitary lesions are usually sporadic, but when these lesions occur at multiple concurrent sites, the diagnosis of neurofibromatosis type II should be considered.

Neurofibroma

These benign neoplasms of the peripheral nerve sheaths can present as focal, diffuse, or plexiform lesions. They can undergo transformation to malignant tumors. Neurofibromas have MRI characteristics (**Fig. 8.19**) similar to those of schwannomas, but they often occur as multiple lesions in a patient with the stigmata of familial neurofibromatosis⁹¹:

- Vertebral anomalies
- Meningoceles
- Dural ectasia
- Intramedullary astrocytomas
- Short-segment thoracic scoliosis or kyphosis
- Axillary or inguinal freckling
- Café-au-lait spots

- Optic glioma
- Lisch nodules (hamartomas of the iris) of neurofibromatosis type I

Therefore, if lesions that look like a schwannoma or neurofibroma on imaging occur in an individual with characteristics of neurofibromatosis type I, the lesions are likely to be neurofibromas, not schwannomas.⁹² Even when isolated, these lesions are usually associated with neurofibromatosis type I. Additionally, and unlike schwannomas, neurofibromas on T2-weighted images often have a peripheral area of high signal intensity surrounding a central area of low to intermediate signal intensity known as a *target sign*. Also unlike schwannomas, neurofibromas typically lack a cystic component.

Malignant Peripheral Nerve Sheath Tumor

These malignant spindle-cell sarcomas of neural origin involve the spinal roots, neural plexuses, peripheral nerves, and end organs and are divided into malignant schwannomas and neurofibrosarcomas. Approximately 50% to 60% are associated with neurofibromatosis

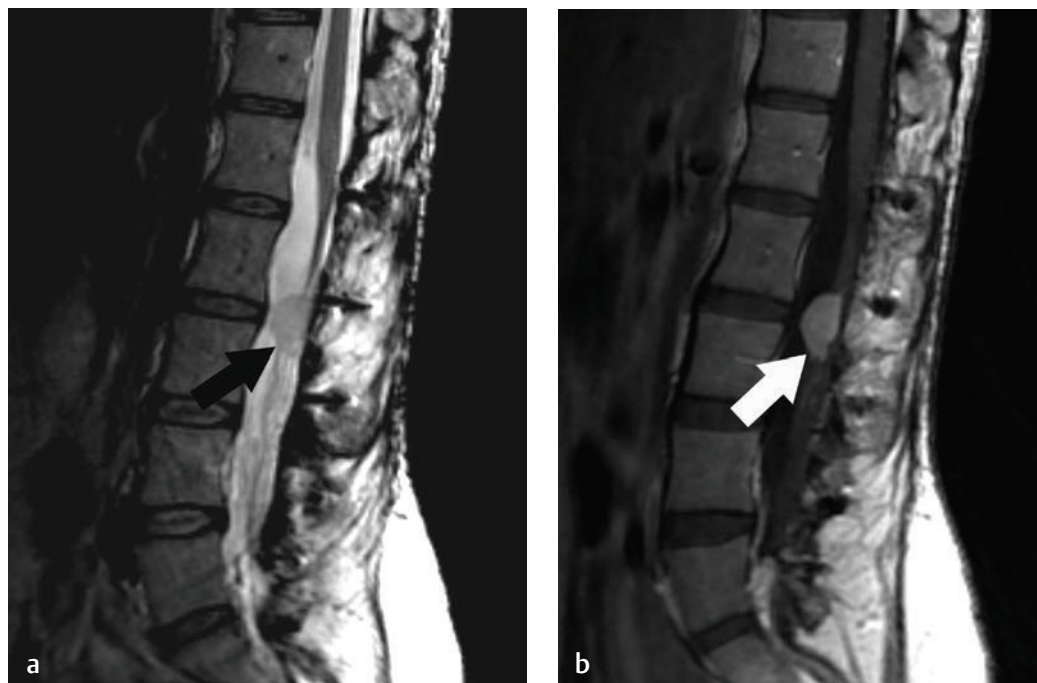


Fig. 8.18 Sagittal images of a schwannoma in the lumbar spine. **(a)** The lesion (arrow on each) is slightly hyperintense compared with the cord on a T2-weighted image and **(b)** shows strong homogeneous contrast enhancement with gadolinium on a T1-weighted image.

type I. They most commonly present as large (>5 cm), infiltrative, hemorrhagic, soft-tissue masses.⁸⁶ MRI is the preferred imaging modality. The lesions are hyperintense compared with surrounding fat on T2-weighted images and on STIR images, and isointense compared with muscle on T1-weighted images (**Fig. 8.20**). T1-weighted images with contrast show marked enhancement. Infiltration into surrounding soft tissue may lead to indistinct margins. Hemorrhage and necrosis within the mass may be seen, resulting in heterogeneous signal. Intradural-extramural masses often may show a dumbbell configuration with widening of the intervertebral foramina and erosion of the pedicles. Because of this characteristic, these lesions may be difficult to distinguish from benign spinal schwannomas. Therefore, a malignant peripheral nerve sheath tumor should be suspected in the presence of sudden growth in a preexisting schwannoma or neurofibroma.

Hemangiopericytoma

Although radiographically very similar to meningiomas, these dural-based lesions are hypervascular, more locally aggressive, and more prone to metastasis. They often erode and replace adjacent bone and exhibit large soft-tissue components. MRI

reveals multilobular masses hypointense on T1-weighted images and hyperintense on T2-weighted images.^{92,93} T1-weighted images with contrast and fat suppression show robust, homogeneous enhancement. Malignant meningiomas may look similar to hemangiopericytomas, but meningiomas often possess finger-like processes rather than the lobules of hemangiopericytomas.

■ Intramedullary Tumors

These lesions of the spinal cord itself account for 5% to 10% of all central nervous system tumors, 20% of intraspinal neoplasms in adults, and 30% to 35% of intraspinal neoplasms in children.¹⁴ More than 90% of these lesions are gliomas.⁹⁴ Of spinal cord gliomas, >95% are ependymomas and low-grade astrocytomas, with ependymomas being more common (60%) than astrocytomas (30%).^{14,95-97} In children, however, astrocytomas are more common.⁹⁸ The remaining lesions include hemangioblastomas and metastases, but these lesions are very rare.⁹⁹

MRI is the diagnostic procedure of choice in evaluating possible spinal cord tumors and myelopathy in general. Classic MRI findings show a diffuse, multi-segmental smoothly enlarged cord or filum terminale

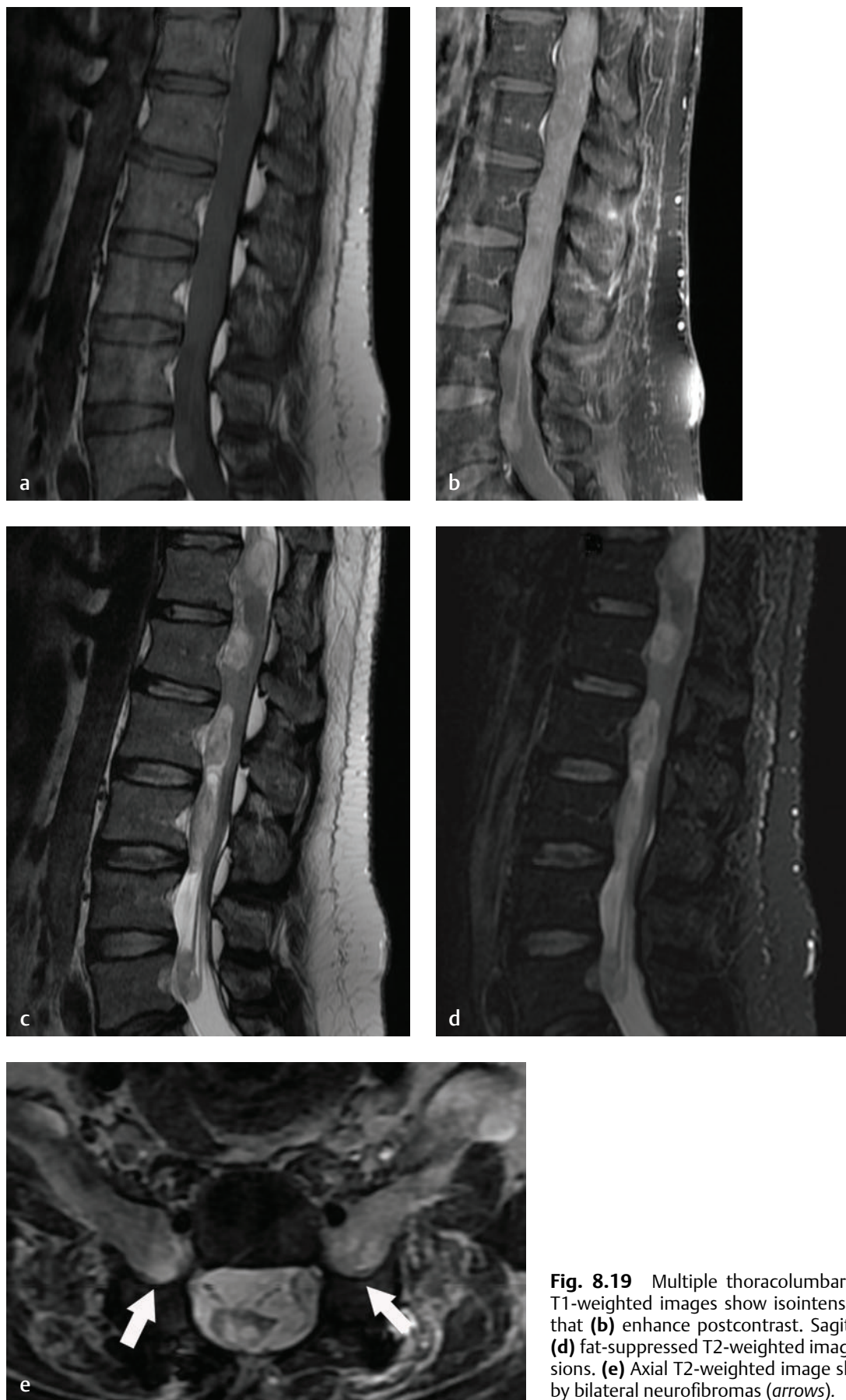


Fig. 8.19 Multiple thoracolumbar neurofibromas. Sagittal T1-weighted images show isointense lesions **(a)** precontrast that **(b)** enhance postcontrast. Sagittal **(c)** T2-weighted and **(d)** fat-suppressed T2-weighted images show hyperintense lesions. **(e)** Axial T2-weighted image shows foraminal widening by bilateral neurofibromas (arrows).

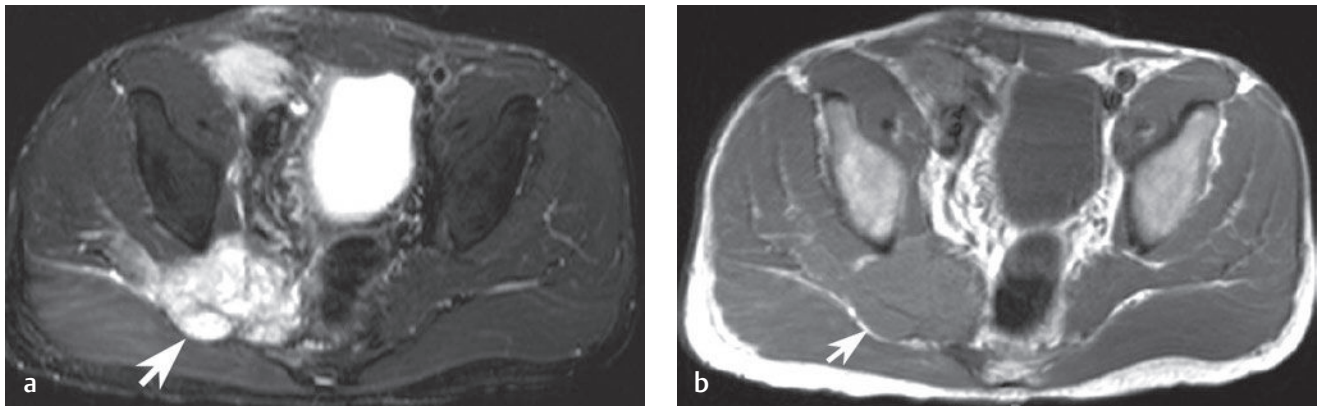


Fig. 8.20 Right-side sacral malignant peripheral nerve sheath tumor. Compared with muscle, the lesion (arrow on each) is (a) hyperintense on an axial fat-suppressed T2-weighted image and (b) isointense on an axial T1-weighted image.[†]

mass with gradual surrounding subarachnoid effacement. Many lesions are associated with syringomyelia, or cyst-like cavities within the cord, extending within the central canal of the cord, or eccentric to the canal in a longitudinal orientation (**Fig. 8.21**).

Ependymoma and Low-Grade Astrocytoma

Ependymomas and low-grade astrocytomas appear nearly identical on MRI.^{23,100} Widening of the cord secondary to infiltration and syringomyelia are most obvious on T2-weighted images, in which the hyperintense CSF signal is contrasted against the less intense cord signal. Additionally, such lesions typically possess high signal intensity on T2-weighted images. T1-weighted images usually reveal lesions that are iso- or hypointense relative to the surrounding spinal cord (**Fig. 8.22**).^{23,100}

Mixed-signal lesions are seen if hemorrhage (more typical of ependymomas), tumor necrosis, or cyst formation has occurred. With the administration of contrast, intramedullary tumors generally show robust enhancement, often in a nodular, peripheral, or heterogeneous pattern. Such lesions usually are located in the cervical and/or thoracic spinal cord.¹⁰¹ Ependymomas more commonly have a “cap sign,” referring to a focal hypointensity on T2-weighted images that appears in areas of hemosiderin at the cranial or caudal margin of the tumor. A helpful tool for learning to identify intramedullary spinal cord tumors, most specifically ependymomas, is recalling the five Cs:

- Central within the cord
- Cervical in location
- Contrast-enhancing
- (Associated with) cysts
- Cap sign

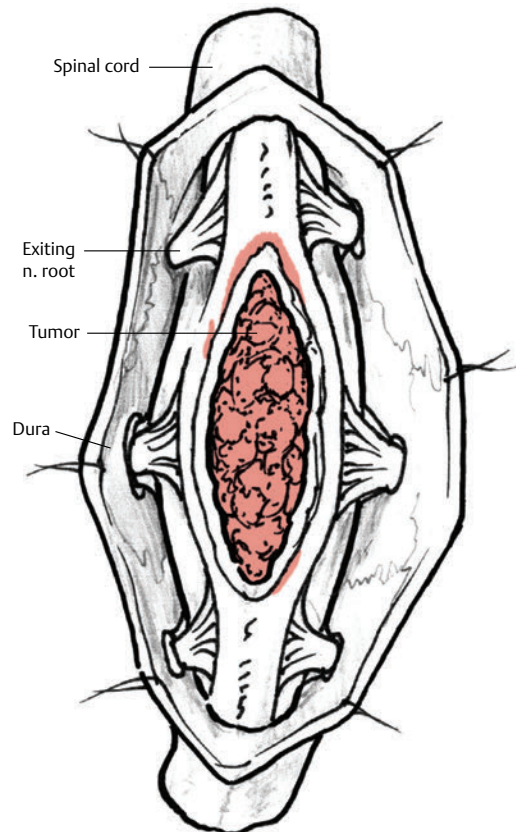


Fig. 8.21 An artist's sketch (dorsal view) depicts the characteristics of an intramedullary mass. The mass diffusely enlarges the cord over multiple spinal segments.[†]

Unlike cellular or mixed ependymomas, which most commonly occur in the cervical spine, myxopapillary ependymomas most often occur in the conus medullaris and filum terminale.^{102–104} Because

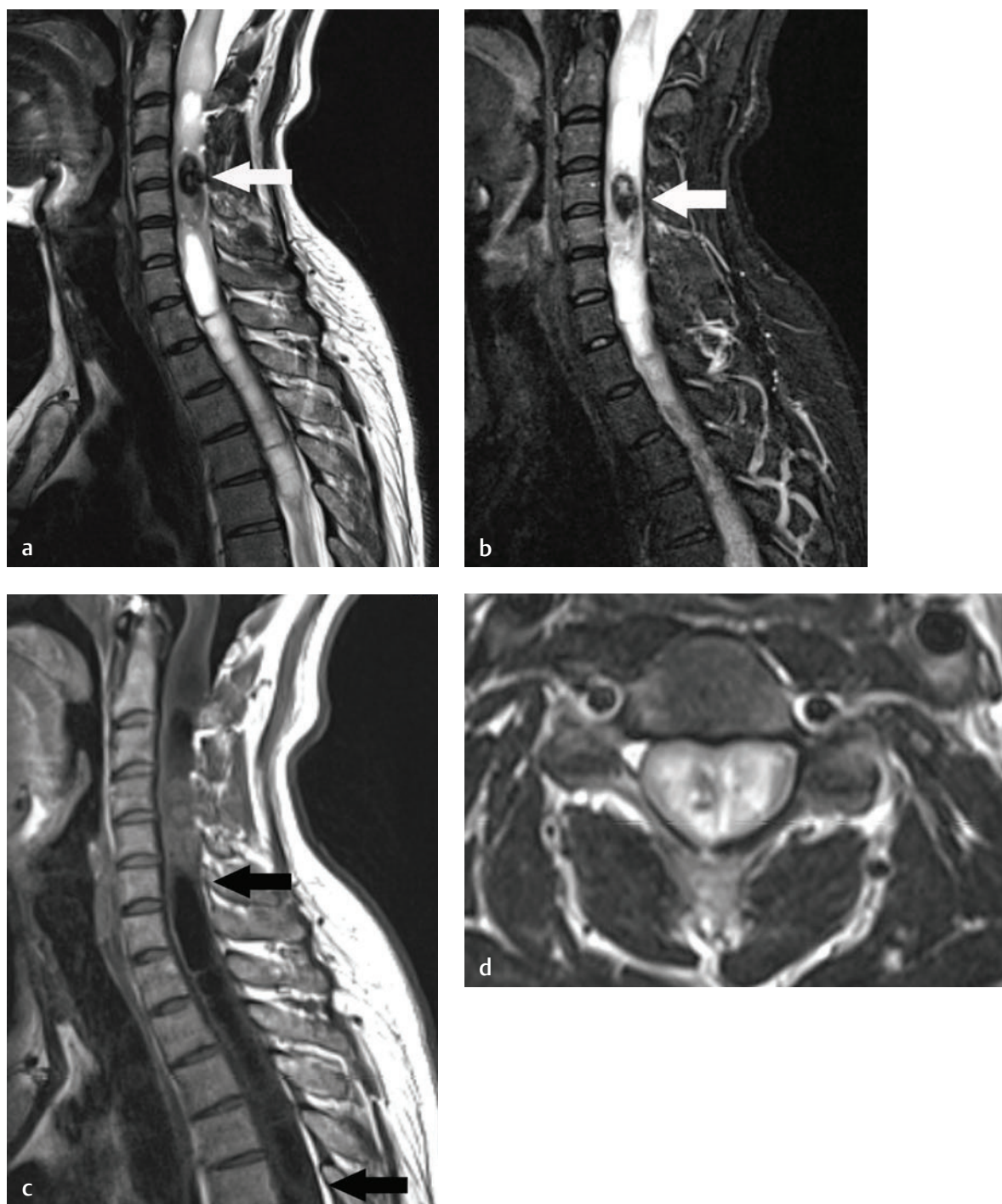


Fig. 8.22 Cervical ependymoma. Sagittal (a) T2-weighted and (b) STIR images show a large cervical ependymoma centered at C4-C5 but with abnormal cord signal extending from C2-C7. Note the hypointense hemosiderin “cap” (arrows on each). (c) A sagittal T1-weighted image shows that the tumor is located at C4-C5 and that the abnormal cord signal change extending below the lesion is secondary to the formation of a septated syrinx (between arrows). A syrinx also extends cranially from the lesion. (d) An axial T2-weighted image shows that the lesion is located within the spinal cord, which is seen as a thin sliver of low signal intensity surrounding the lesion.

these lesions typically are slow growing, vertebral body scalloping is common, with a large conus lesion that fills the entire lumbosacral thecal sac; the neural foramina also may be enlarged. Interestingly, although these lesions grow from ependymal cells of the conus and filum, making them intra-

medullary in origin, they most commonly appear like intradural–extramedullary masses because there is no widening of the cord at the level of the cauda equina. Therefore, CSF signal on T2-weighted images creates a meniscus-like sign around the lesion (**Fig. 8.23**).

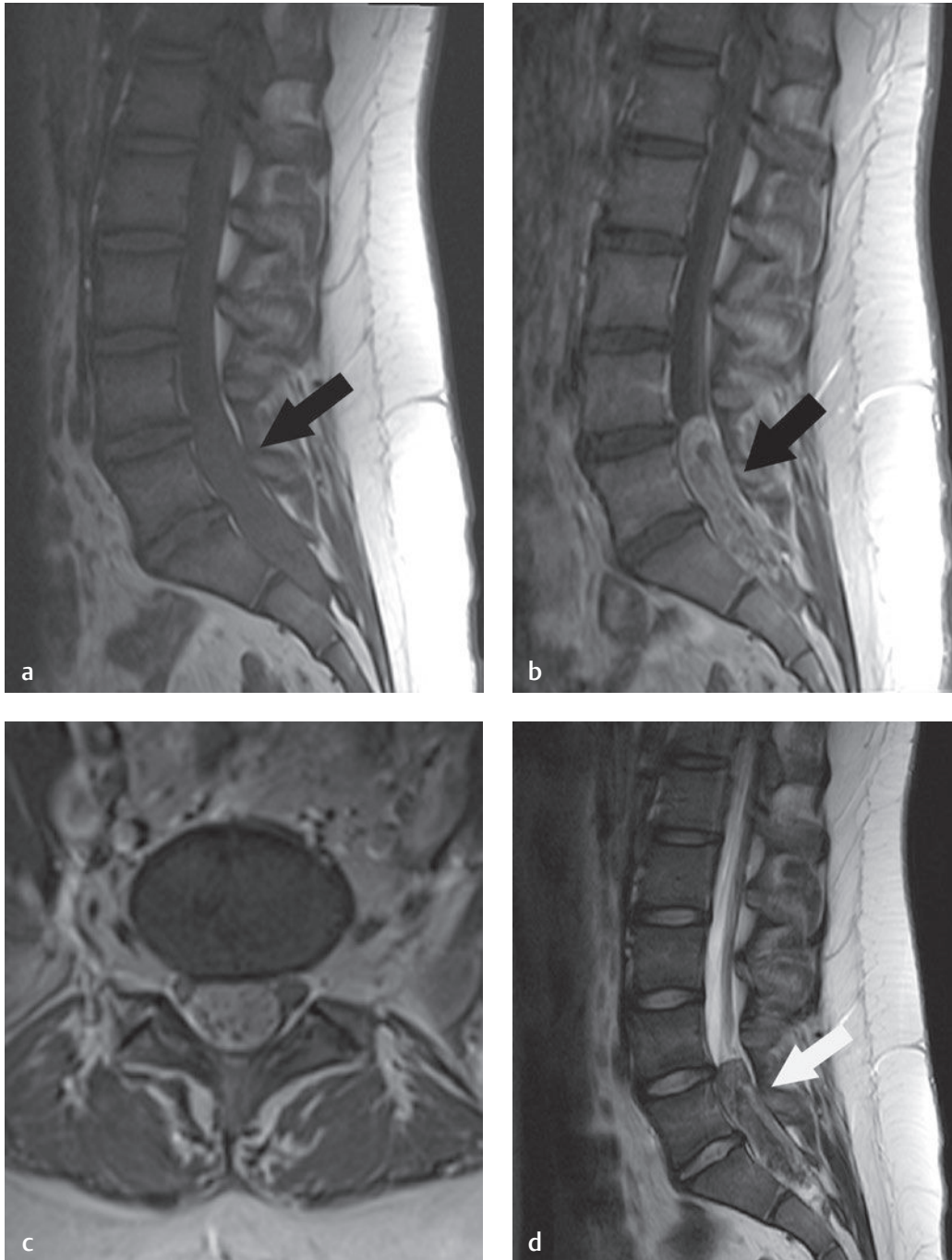


Fig. 8.23 Myxopapillary ependymoma of the lumbar region. **(a)** A sagittal T1-weighted precontrast image shows a hypointense lesion (*arrow*). **(b)** Sagittal and **(c)** axial T1-weighted postcontrast images reveal robust enhancement of the lesion (*arrow* on **b**). **(d)** A sagittal T2-weighted image shows the lesion (*arrow*) is heterogeneously hypointense. Although derived from the filum, ependymomas in this segment of the spine reside in the intradural–extramedullary compartment.

Parangliomas are rare tumors that most commonly present in the cauda equina, where they often are indistinguishable from myxopapillary ependymomas.⁸⁴ On MRI, these lesions are typically seen as well-defined areas of intense enhancement after contrast administration. Because of their high degree of vascularity, paragangliomas often show prominent foci of high-velocity signal loss (“flow voids”), corresponding to enlarged feeding arteries and/or draining veins.

Hemangioblastoma

Hemangioblastomas typically appear as highly vascular nodules within the *subpial* compartment; thus, they lie closer to the surface of the cord than do ependymomas and astrocytomas.¹⁰⁵ They are associated with extensive cyst formation that diffusely enlarges the cord in up to 70% of patients.¹⁰⁶ Because of the highly vascular nature of such lesions, robust homogeneous contrast enhancement within the tumor nodule is the rule, and MRI almost always shows prominent flow voids (**Fig. 8.24**). Multiple lesions can occur in the presence of von Hippel–Lindau syndrome, with rare extensive involvement of the leptomeninges, referred to as *leptomeningeal hemangioblastomatosis*.¹⁰⁷ When a spinal hemangioblastoma is suspected on MRI, it is advisable to image the entire central nervous system to exclude multiple lesions.

Intramedullary Metastases

Intramedullary metastases are rare, representing only 4% to 8.5% of all central nervous system metastases.¹⁴ Most spinal cord metastases are localized to the pia mater, in which they appear as a thin rim of enhancement along the cord surface on postcontrast T1-weighted images. In addition, edema out of proportion to a focal, small cord lesion suggests metastasis, even if isolated.¹⁰⁸ Primary malignancies accounting for such lesions are most commonly lung and breast carcinomas, lymphoma, leukemia, and melanoma.^{22,109} In 20% of patients, intramedullary metastasis is the first presentation of cancer for the patient.¹⁴

MRI with and without contrast can be quite helpful in distinguishing benign cysts or syrinxes from those associated with intramedullary tumors. Tumor cysts are smaller, more irregular, often eccentrically positioned within the cord, and almost always associated with an enhancing tumor, whereas benign cysts are rostral or caudal to the tumor, have smooth walls, cause symmetric cord expansion, and do not show contrast enhancement.¹¹⁰

Other lesions of the spinal cord that must be included in the differential diagnosis include autoimmune or inflammatory myelitis, cord ischemia or infarction, and arteriovenous malformations.⁴

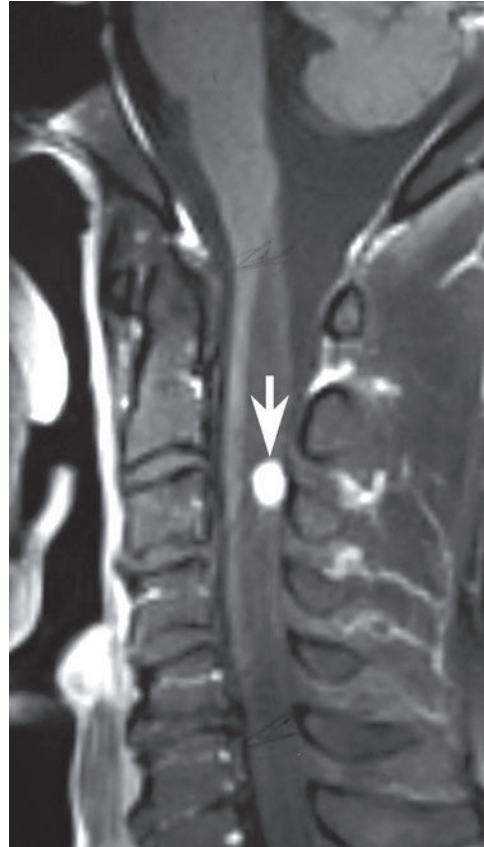


Fig. 8.24 A sagittal postgadolinium fat-suppressed T1-weighted image of a cervical hemangioblastoma reveals a small, eccentrically located robustly enhancing tumor nodule (arrow) associated with a large cervicothoracic syrinx.[†]

Summary

Anatomically, spine tumors are traditionally classified into extradural, intradural–extramedullary, or intramedullary locations. Although primary lesions may occur in the spinal cord, nerve roots, dura, and osseous spine, most lesions within the spine are metastatic tumors and typically^{7–9} occur in the osseous extradural compartment. Up to 40% of patients with cancer develop visceral or osseous metastases, and the spinal column is the most common site of osseous metastases. Proper diagnosis of spinal tumors involves identifying the compartment location, generating a preimaging differential diagnosis, incorporating patient information to narrow the differential diagnosis, and using various imaging modalities.

MRI is the preferred imaging modality for spinal tumors; it displays soft-tissue structures at a higher resolution than other modalities. Its unparalleled ability to delineate epidural and paraspinal soft-tissue involvement is particularly useful in the context of

metastatic spine disease. However, it poorly detects calcifications and small osseous fragments, and it can display metal-induced artifacts; therefore, it should be complemented by conventional radiographs and/or CT. Generally, the MRI protocol for any patient suspected of having a spine tumor should include T1-weighted and T2-weighted images and gadolinium-enhanced studies in the axial and sagittal planes. A neuroradiologist should be consulted to select the most fitting imaging protocol.

Extradural primary benign tumors have characteristic MRI and patient demographics that differentiate them from malignant tumors. Such primary benign tumors include hemangioma, osteoid osteoma, giant cell tumor, osteochondroma, aneurysmal bone cyst, and eosinophilic granuloma. Extradural primary malignant tumors include multiple myeloma, solitary bone plasmacytoma, chordoma, and sarcomas (chondrosarcoma, osteosarcoma/osteogenic sarcoma, Ewing sarcoma, and, very rarely, fibrosarcoma). Other extradural tumors include neuroblast, angiolioma, and lymphoma lesions.

Intradural-extramedullary lesions arise specifically from within the dura. For these tumors, MRI typically displays a widened ipsilateral subarachnoid space in which the cord and roots are displaced away from the mass. Nerve sheath tumors (schwannomas and neurofibromas) and meningiomas account for >80% of such masses. Other lesions include malignant peripheral nerve sheath tumor and hemangiopericytoma.

Intramedullary tumors grow from the spinal cord itself and account for 20% of intraspinal neoplasms in adults and 30% to 35% of intraspinal neoplasms in children. Nearly 90% of these tumors are gliomas (predominantly ependymomas and low-grade astrocytomas). Less common lesions include hemangioblastomas and metastases. On MRI, classic intramedullary lesions show a diffuse, multisegmental smoothly enlarged cord or filum terminale mass with gradual surrounding subarachnoid effacement. Many lesions are associated with syringomyelia, or cyst-like cavities within the cord, extending within the central canal of the cord or eccentric to the canal in a longitudinal orientation.

References

1. Gebauer GP, Farjoodi P, Sciubba DM, et al. Magnetic resonance imaging of spine tumors: classification, differential diagnosis, and spectrum of disease. *J Bone Joint Surg Am* 2008;90(Suppl 4):146–162 PubMed
2. Khanna AJ, Shindle MK, Wasserman BA, et al. Use of magnetic resonance imaging in differentiating compartmental location of spinal tumors. *Am J Orthop* 2005;34(10):472–476 PubMed
3. Masaryk TJ. Neoplastic disease of the spine. *Radiol Clin North Am* 1991;29(4):829–845 PubMed

COMMON CLINICAL QUESTIONS

1. All of the following features seen on MRI are associated with ependymoma *except*:
A. Central within the cord
B. Cervical in location
C. Osseous invasion
D. Contrast-enhancing
E. Associated with cysts
F. Cap sign
2. Ependymomas and astrocytomas appear nearly identical on MRI. True or false?
3. A 19-year-old woman presents to your office with 2 months of worsening buttock pain and right-side leg weakness. Pelvic MRI shows an expansile lesion with fluid–fluid levels. Her most likely diagnosis is:
A. Chordoma
B. Giant cell tumor
C. Metastatic breast cancer
D. Osteochondroma
4. Osteoid osteomas are larger than osteoblastomas. True or false?
5. Which of the following lesions are commonly identified in the neural arch?
A. Hemangioma
B. Osteoid osteoma
C. Aneurysmal bone cyst
D. Eosinophilic granuloma
E. B and C
F. None of the above

4. Osborn AG. Cysts, tumors, and tumorlike lesions of the spine and spinal cord. In: Osborn AG, ed. *Diagnostic Neuroradiology*. St. Louis, MO: Mosby; 1994:876–918
5. Seivick RJ, Wallace CJ. MR imaging of neoplasms of the lumbar spine. *Magn Reson Imaging Clin N Am* 1999;7(3):539–553, ix PubMed
6. Williams RS, Williams JP. Tumors. In: Rao KCVG, Williams JP, Lee BCP, Sherman JL, eds. *MRI and CT of the Spine*. Baltimore, MD: Williams & Wilkins; 1994:347–426
7. Cappuccino M, Bandiera S, Babbi L, et al. Management of bone metastases. *Eur Rev Med Pharmacol Sci* 2010;14(4):407–414 PubMed
8. Perrin RG, Laxton AW. Metastatic spine disease: epidemiology, pathophysiology, and evaluation of patients. *Neurosurg Clin N Am* 2004;15(4):365–373 PubMed
9. Sciubba DM, Petteys RJ, Dekutoski MB, et al. Diagnosis and management of metastatic spine disease. A review. *J Neurosurg Spine* 2010;13(1):94–108 PubMed
10. Constans JP, de Divitiis E, Donzelli R, Spaziente R, Meder JF, Haye C. Spinal metastases with neurological manifestations. Review of 600 cases. *J Neurosurg* 1983;59(1):111–118 PubMed

11. Eleraky M, Papanastassiou I, Vrionis FD. Management of metastatic spine disease. *Curr Opin Support Palliat Care* 2010;4(3):182–188 PubMed
12. Joyce D, O'Donoghue G, Kerin M. Metastatic breast disease: an all too common cause of back pain. *BMJ Case Rep* 2010;2010: 10.1136/bcr.10.2009.2388 PubMed
13. Kamholtz R, Sze G. Current imaging in spinal metastatic disease. *Semin Oncol* 1991;18(2):158–169 PubMed
14. Ross JS. Chondrosarcoma. In: Ross JS, Brant-Zawadzki M, Moore KR, et al, eds. *Diagnostic Imaging: Spine*. Salt Lake City, UT: Amirsys; 2004:IV-1-38–IV-1-41
15. Balériaux DLF. Spinal cord tumors. *Eur Radiol* 1999;9(7):1252–1258 PubMed
16. Pozzi G, Garcia Parra C, Stradiotti P, Tien TV, Luzzati A, Zerbi A. Diffusion-weighted MR imaging in differentiation between osteoporotic and neoplastic vertebral fractures. *Eur Spine J* 2012;21(Suppl 1):S123–S127 PubMed
17. Thawait SK, Marcus MA, Morrison WB, Klufas RA, Eng J, Carrino JA. Research synthesis: what is the diagnostic performance of magnetic resonance imaging to discriminate benign from malignant vertebral compression fractures? Systematic review and meta-analysis. *Spine (Phila Pa 1976)* 2012;37(12):E736–E744 PubMed
18. Umutlu L, Forsting M, Ladd ME. Ultrahigh-field magnetic resonance imaging: the clinical potential for anatomy, pathogenesis, diagnosis and treatment planning in neck and spine disease. *Neuroimaging Clin N Am* 2012;22(2):363–371, xii PubMed
19. Van Goethem JWM, van den Hauwe L, Ozsarlak O, De Schepper AMA, Parizel PM. Spinal tumors. *Eur J Radiol* 2004;50(2):159–176 PubMed
20. Algra PR, Bloem JL, Tissing H, Falke TH, Arndt JW, Verboom LJ. Detection of vertebral metastases: comparison between MR imaging and bone scintigraphy. *Radiographics* 1991;11(2):219–232 PubMed
21. Avrahami E, Tadmor R, Dally O, Hadar H. Early MR demonstration of spinal metastases in patients with normal radiographs and CT and radionuclide bone scans. *J Comput Assist Tomogr* 1989;13(4):598–602 PubMed
22. Chamberlain MC, Sandy AD, Press GA. Spinal cord tumors: gadolinium-DTPA-enhanced MR imaging. *Neuroradiology* 1991;33(6):469–474 PubMed
23. Sun B, Wang C, Wang J, Liu A. MRI features of intramedullary spinal cord ependymomas. *J Neuroimaging* 2003;13(4):346–351 PubMed
24. Switlyk MD, Hole KH, Skjeldal S, et al. MRI and neurological findings in patients with spinal metastases. *Acta Radiol* 2012;53(10):1164–1172 PubMed
25. Li KC, Poon PY. Sensitivity and specificity of MRI in detecting malignant spinal cord compression and in distinguishing malignant from benign compression fractures of vertebrae. *Magn Reson Imaging* 1988;6(5):547–556 PubMed
26. Tatsui H, Onomura T, Morishita S, Oketa M, Inoue T. Survival rates of patients with metastatic spinal cancer after scintigraphic detection of abnormal radioactive accumulation. *Spine (Phila Pa 1976)* 1996;21(18):2143–2148 PubMed
27. Byrne TN. Spinal cord compression from epidural metastases. *N Engl J Med* 1992;327(9):614–619 PubMed
28. Algra PR, Heimans JJ, Valk J, Nauta JJ, Lachniet M, Van Kooten B. Do metastases in vertebrae begin in the body or the pedicles? Imaging study in 45 patients. *AJR Am J Roentgenol* 1992;158(6):1275–1279 PubMed
29. Molina CA, Gokaslan ZL, Sciubba DM. Diagnosis and management of metastatic cervical spine tumors. *Orthop Clin North Am* 2012;43(1):75–87, viii–ix PubMed
30. Wald JT. Imaging of spine neoplasm. *Radiol Clin North Am* 2012;50(4):749–776 PubMed
31. Baker LL, Goodman SB, Perkasie I, Lane B, Enzmann DR. Benign versus pathologic compression fractures of vertebral bodies: assessment with conventional spin-echo, chemical-shift, and STIR MR imaging. *Radiology* 1990;174(2):495–502 PubMed
32. Thakur NA, Daniels AH, Schiller J, et al. Benign tumors of the spine. *J Am Acad Orthop Surg* 2012;20(11):715–724 PubMed
33. Yochum TR, Lile RL, Schultz GD, Mick TJ, Brown CW. Acquired spinal stenosis secondary to an expanding thoracic vertebral hemangioma. *Spine (Phila Pa 1976)* 1993;18(2):299–305 PubMed
34. Bandiera S, Gasbarrini A, De Iure F, Cappuccio M, Picci P, Boriani S. Symptomatic vertebral hemangioma: the treatment of 23 cases and a review of the literature. [in English and Italian] *Chir Organi Mov* 2002;87(1):1–15 PubMed
35. Urrutia J, Postigo R, Larrondo R, Martin AS. Clinical and imaging findings in patients with aggressive spinal hemangioma requiring surgical treatment. *J Clin Neurosci* 2011;18(2):209–212 PubMed
36. Baudrez V, Galant C, Vande Berg BC. Benign vertebral hemangioma: MR-histological correlation. *Skeletal Radiol* 2001;30(8):442–446 PubMed
37. Djindjian M, Nguyen JP, Gaston A, Pavlovitch JM, Poirier J, Awad IA. Multiple vertebral hemangiomas with neurological signs. Case report. *J Neurosurg* 1992;76(6):1025–1028 PubMed
38. Gangi A, Alizadeh H, Wong L, Buy X, Dietemann JL, Roy C. Osteoid osteoma: percutaneous laser ablation and follow-up in 114 patients. *Radiology* 2007;242(1):293–301 PubMed
39. Harish S, Saifuddin A. Imaging features of spinal osteoid osteoma with emphasis on MRI findings. *Eur Radiol* 2005;15(12):2396–2403 PubMed
40. Liu PT, Chivers FS, Roberts CC, Schultz CJ, Beauchamp CP. Imaging of osteoid osteoma with dynamic gadolinium-enhanced MR imaging. *Radiology* 2003;227(3):691–700 PubMed
41. Dorwart RH, LaMasters DL, Watanabe TJ. Tumors. In: Newton T, Potts D, eds. *Computed Tomography of the Spine and Spinal Cord*. San Anselmo, CA: Clavadel Press; 1983:115–147
42. Laurence N, Epelman M, Markowitz RI, Jaimes C, Jaramillo D, Chauvin NA. Osteoid osteomas: a pain in the night diagnosis. *Pediatr Radiol* 2012;42(12):1490–1501, quiz 1540–1542 PubMed
43. Boriani S, Amendola L, Bandiera S, et al. Staging and treatment of osteoblastoma in the mobile spine: a review of 51 cases. *Eur Spine J* 2012;21(10):2003–2010 PubMed
44. Boriani S, Capanna R, Donati D, Levine A, Picci P, Savini R. Osteoblastoma of the spine. *Clin Orthop Relat Res* 1992;278(278):37–45 PubMed
45. Harrop JS, Schmidt MH, Boriani S, Shaffrey CI. Aggressive “benign” primary spine neoplasms: osteoblastoma, aneurysmal bone cyst, and giant cell tumor. *Spine (Phila Pa 1976)* 2009;34(22, Suppl):S39–S47 PubMed
46. Luther N, Bilsky MH, Härtl R. Giant cell tumor of the spine. *Neurosurg Clin N Am* 2008;19(1):49–55 PubMed

47. Murphey MD, Nomikos GC, Flemming DJ, Gannon FH, Temple HT, Kransdorf MJ. From the archives of AFIP. Imaging of giant cell tumor and giant cell reparative granuloma of bone: radiologic-pathologic correlation. *Radiographics* 2001;21(5):1283–1309 PubMed
48. Lotfinia I, Vahedi P, Tubbs RS, Ghavame M, Meshkini A. Neurological manifestations, imaging characteristics, and surgical outcome of intraspinal osteochondroma. *J Neurosurg Spine* 2010;12(5):474–489 PubMed
49. Sharma MC, Arora R, Deol PS, Mahapatra AK, Mehta VS, Sarkar C. Osteochondroma of the spine: an enigmatic tumor of the spinal cord. A series of 10 cases. *J Neurosurg Sci* 2002;46(2):66–70, discussion 70 PubMed
50. Rodallec MH, Feydy A, Larousserie F, et al. Diagnostic imaging of solitary tumors of the spine: what to do and say. *Radiographics* 2008;28(4):1019–1041 PubMed
51. Boriani S, De Iure F, Campanacci L, et al. Aneurysmal bone cyst of the mobile spine: report on 41 cases. *Spine (Phila Pa 1976)* 2001;26(1):27–35 PubMed
52. Cebula H, Boujan F, Beaujeux R, Boyer P, Froelich S. [Giant cell tumor of the C2 colonized by an aneurysmal bone cyst. Report of case]. [in French] *Neurochirurgie* 2012;58(6):376–381 PubMed
53. Manaster BJ. *Skeletal Radiology*. Chicago, IL: Year Book Medical Publishers; 1989
54. Mankin HJ, Hornicek FJ, Ortiz-Cruz E, Villafuerte J, Gebhardt MC. Aneurysmal bone cyst: a review of 150 patients. *J Clin Oncol* 2005;23(27):6756–6762 PubMed
55. Wu Z, Yang X, Xiao J, et al. Aneurysmal bone cyst secondary to giant cell tumor of the mobile spine: a report of 11 cases. *Spine (Phila Pa 1976)* 2011;36(21):E1385–E1390 PubMed
56. Oguro K, Sakai H, Arai M, Igarashi T. Eosinophilic granuloma of bone: two case reports. *Brain Dev* 2013;35(4):372–375 PubMed
57. Bataille R, Harousseau JL. Multiple myeloma. *N Engl J Med* 1997;336(23):1657–1664 PubMed
58. Mouloupoulos LA, Dimopoulos MA, Alexanian R, Leeds NE, Libshitz HI. Multiple myeloma: MR patterns of response to treatment. *Radiology* 1994;193(2):441–446 PubMed
59. Holland J, Trenkner DA, Wasserman TH, Fineberg B. Plasmacytoma. Treatment results and conversion to myeloma. *Cancer* 1992;69(6):1513–1517 PubMed
60. Bolek TW, Marcus RB Jr, Mendenhall NP. Solitary plasmacytoma of bone and soft tissue. *Int J Radiat Oncol Biol Phys* 1996;36(2):329–333 PubMed
61. He MX, Zhu MH, Zhang YM, Fu QG, Wu LL. [Solitary plasmacytoma of spine: a clinical, radiologic and pathologic study of 13 cases]. [in Chinese] *Zhonghua Bing Li Xue Za Zhi* 2009;38(5):307–311 PubMed
62. Ota K, Tsuda T, Katayama N, et al. A therapeutic strategy for isolated plasmacytoma of bone. *J Int Med Res* 2001;29(4):366–373 PubMed
63. Shah BK, Saifuddin A, Price GJ. Magnetic resonance imaging of spinal plasmacytoma. *Clin Radiol* 2000;55(6):439–445 PubMed
64. Knobel D, Zouhair A, Tsang RW, et al. Prognostic factors in solitary plasmacytoma of the bone: a multicenter Rare Cancer Network study. *BMC Cancer* 2006;6:118 PubMed
65. Walcott BP, Nahed BV, Mohyeldin A, Coumans JV, Kahle KT, Ferreira MJ. Chordoma: current concepts, management, and future directions. *Lancet Oncol* 2012;13(2):e69–e76 PubMed
66. Boriani S, Weinstein JN, Biagini R. Primary bone tumors of the spine. Terminology and surgical staging. *Spine (Phila Pa 1976)* 1997;22(9):1036–1044 PubMed
67. Soo MYS. Chordoma: review of clinicoradiological features and factors affecting survival. *Australas Radiol* 2001;45(4):427–434 PubMed
68. Hsieh PC, Xu R, Sciubba DM, et al. Long-term clinical outcomes following en bloc resections for sacral chordomas and chondrosarcomas: a series of twenty consecutive patients. *Spine (Phila Pa 1976)* 2009;34(20):2233–2239 PubMed
69. Strike SA, McCarthy EF. Chondrosarcoma of the spine: a series of 16 cases and a review of the literature. *Iowa Orthop J* 2011;31:154–159 PubMed
70. Dorfman HD, Czerniak B. *Bone Tumors*. St. Louis, MO: Mosby; 1998
71. Aoki J, Sone S, Fujioka F, et al. MR of enchondroma and chondrosarcoma: rings and arcs of Gd-DTPA enhancement. *J Comput Assist Tomogr* 1991;15(6):1011–1016 PubMed
72. Crim J. Osteosarcoma. In: Ross JS, Brant-Zawadzki M, Moore KR, et al, eds. *Diagnostic Imaging: Spine*. Salt Lake City, UT: Amirsys; 2004:IV-1-42–IV-1-45
73. Bramwell VHC. Osteosarcomas and other cancers of bone. *Curr Opin Oncol* 2000;12(4):330–336 PubMed
74. Boriani S, Amendola L, Corghi A, et al. Ewing's sarcoma of the mobile spine. *Eur Rev Med Pharmacol Sci* 2011;15(7):831–839 PubMed
75. Crim J. Ewing sarcoma. In: Ross JS, Brant-Zawadzki M, Moore KR, et al, eds. *Diagnostic Imaging: Spine*. Salt Lake City, UT: Amirsys; 2004:IV-1-50–IV-1-53
76. Boyko OB, Cory DA, Cohen MD, Provisor A, Mirkin D, DeRosa GP. MR imaging of osteogenic and Ewing's sarcoma. *AJR Am J Roentgenol* 1987;148(2):317–322 PubMed
77. Lonergan GJ, Schwab CM, Suarez ES, Carlson CL. Neuroblastoma, ganglioneuroblastoma, and ganglioneuroma: radiologic-pathologic correlation. *Radiographics* 2002;22(4):911–934 PubMed
78. Sofka CM, Semelka RC, Kelekis NL, et al. Magnetic resonance imaging of neuroblastoma using current techniques. *Magn Reson Imaging* 1999;17(2):193–198 PubMed
79. Guzey FK, Bas NS, Ozkan N, Karabulut C, Bas SC, Turgut H. Lumbar extradural infiltrating angiolipoma: a case report and review of 17 previously reported cases with infiltrating spinal angiolipomas. *Spine J* 2007;7(6):739–744 PubMed
80. Oge HK, Söylemezoglu F, Rousan N, Ozcan OE. Spinal angiolipoma: case report and review of literature. *J Spinal Disord* 1999;12(4):353–356 PubMed
81. De Fino C, Arena V, Hohaus S, Di Iorio R, Bozzoli V, Mirabella M. Intravascular large B-cell lymphoma presenting as slowly progressive paraparesis with normal MRI features. *J Neurol Sci* 2012;314(1-2):171–174 PubMed
82. Thornton E, Krajewski KM, O'Regan KN, Giardino AA, Jagannathan JP, Ramaiya N. Imaging features of primary and secondary malignant tumours of the sacrum. *Br J Radiol* 2012;85(1011):279–286 PubMed
83. Katzman GL. Lymphoma. In: Ross JS, Brant-Zawadzki M, Moore KR, et al, eds. *Diagnostic Imaging: Spine*. Salt Lake City, UT: Amirsys; 2004:IV-1-54–IV-1-57
84. Koeller KK, Rosenblum RS, Morrison AL. Neoplasms of the spinal cord and filum terminale: radiologic-pathologic correlation. *Radiographics* 2000;20(6):1721–1749 PubMed
85. Li MH, Holtás S, Larsson EM. MR imaging of intradural extramedullary tumors. *Acta Radiol* 1992;33(3):207–212 PubMed

86. Burger PC, Shcethauer BW, Vogel FS. *Surgical Pathology of the Nervous System and Its Coverings*. Philadelphia, PA: Churchill Livingstone; 2002
87. Cohen-Gadol AA, Zikel OM, Koch CA, Scheithauer BW, Krauss WE. Spinal meningiomas in patients younger than 50 years of age: a 21-year experience. *J Neurosurg* 2003;98(3, Suppl):258–263 PubMed
88. Naderi S. Spinal meningiomas. *Surg Neurol* 2000;54(1):95 PubMed
89. Conti P, Pansini G, Mouchaty H, Capuano C, Conti R. Spinal neurinomas: retrospective analysis and long-term outcome of 179 consecutively operated cases and review of the literature. *Surg Neurol* 2004;61(1):34–43, discussion 44 PubMed
90. Murphey MD, Smith WS, Smith SE, Kransdorf MJ, Temple HT. Imaging of musculoskeletal neurogenic tumors: radiologic-pathologic correlation. *Radiographics* 1999;19(5):1253–1280 PubMed
91. Uhlmann EJ, Plotkin SR. Neurofibromatosis. *Adv Exp Med Biol* 2012;724:266–277 PubMed
92. Akhaddar A, Chakir N, Amarti A, et al. Thoracic epidural hemangiopericytoma. Case report. *J Neurosurg Sci* 2002;46(2):89–92, discussion 92 PubMed
93. Ackerman PD, Khaldi A, Shea JF. Intradural hemangiopericytoma of the thoracic spine: a case report. *Spine J* 2011;11(7):e9–e14 PubMed
94. Brant-Zawadzki M. Astrocytoma, spinal cord. In: Ross JS, Brant-Zawadzki M, Moore KR, et al, eds. *Diagnostic Imaging: Spine*. Salt Lake City, UT: Amirsys; 2004: IV-1-102–IV-1-105
95. Harrop JS, Ganju A, Groff M, Bilsky M. Primary intramedullary tumors of the spinal cord. *Spine (Phila Pa 1976)* 2009;34(22, Suppl):S69–S77 PubMed
96. Houten JK, Cooper PR. Spinal cord astrocytomas: presentation, management and outcome. *J Neurooncol* 2000;47(3):219–224 PubMed
97. Parsa AT, Chi JH, Acosta FL Jr, Ames CP, McCormick PC. Intramedullary spinal cord tumors: molecular insights and surgical innovation. *Clin Neurosurg* 2005;52:76–84 PubMed
98. Smith AB, Soderlund KA, Rushing EJ, Smirniotopolous JG. Radiologic-pathologic correlation of pediatric and adolescent spinal neoplasms: Part 1, Intramedullary spinal neoplasms. *AJR Am J Roentgenol* 2012;198(1):34–43 PubMed
99. Houten JK, Weiner HL. Pediatric intramedullary spinal cord tumors: special considerations. *J Neurooncol* 2000;47(3):225–230 PubMed
100. Lowe GM. Magnetic resonance imaging of intramedullary spinal cord tumors. *J Neurooncol* 2000;47(3):195–210 PubMed
101. McCormick PC, Torres R, Post KD, Stein BM. Intramedullary ependymoma of the spinal cord. *J Neurosurg* 1990;72(4):523–532 PubMed
102. Bagley CA, Kothbauer KF, Wilson S, Bookland MJ, Epstein FJ, Jallo GI. Resection of myxopapillary ependymomas in children. *J Neurosurg* 2007;106(4, Suppl Pediatrics):261–267 PubMed
103. Bagley CA, Wilson S, Kothbauer KF, Bookland MJ, Epstein F, Jallo GI. Long term outcomes following surgical resection of myxopapillary ependymomas. *Neurosurg Rev* 2009;32(3):321–334, discussion 334 PubMed
104. Sonneland PRL, Scheithauer BW, Onofrio BM. Myxopapillary ependymoma. A clinicopathologic and immunocytochemical study of 77 cases. *Cancer* 1985;56(4):883–893 PubMed
105. Pruksakorn P, Siwanuwatn R, Snabboon T. Spinal hemangioblastoma. *Am J Med Sci* 2011;342(3):240 PubMed
106. Murota T, Symon L. Surgical management of hemangioblastoma of the spinal cord: a report of 18 cases. *Neurosurgery* 1989;25(5):699–707, discussion 708 PubMed
107. Chu BC, Terae S, Hida K, Furukawa M, Abe S, Miyasaka K. MR findings in spinal hemangioblastoma: correlation with symptoms and with angiographic and surgical findings. *AJNR Am J Neuroradiol* 2001;22(1):206–217 PubMed
108. Reddy P, Sathyanarayana S, Acharya R, Nanda A. Intramedullary spinal cord metastases: case report and review of literature. *J La State Med Soc* 2003;155(1):44–45 PubMed
109. Soga K, Irioka T, Yano T, Mizusawa H. Intramedullary spinal cord metastasis with a longitudinally extensive spinal cord lesion. *Intern Med* 2011;50(7):795–796 PubMed
110. Brunberg JA, DiPietro MA, Venes JL, et al. Intramedullary lesions of the pediatric spinal cord: correlation of findings from MR imaging, intraoperative sonography, surgery, and histologic study. *Radiology* 1991;181(2):573–579 PubMed

ANSWERS TO COMMON CLINICAL QUESTIONS

1. C
Explanation: The MRI features of ependymoma include a central location within the spinal cord, predilection for the cervical spine, postgadolinium contrast enhancement, association with cysts, and the cap sign, as described in this chapter.
2. True
Explanation: Ependymomas and astrocytomas have nearly identical appearances on MRI. Therefore, they are typically differentiated by biopsy.
3. B
Explanation: Of the options listed, giant cell tumor is the most compatible with the MRI characteristics and age of the patient. Aneurysmal bone cyst would be another consideration but is not provided as an option in this question.
4. False
Explanation: Osteoid osteomas are similar to but smaller than osteoblastomas. A size of 1.5 cm is typically used as the threshold to differentiate between these two diagnoses.
5. E
Explanation: Osteoid osteomas and aneurysmal bone cysts are commonly identified in the neural arch (posterior elements). Aneurysmal bone cysts typically originate in the neural arch and then extend into the vertebral body. Hemangiomas and eosinophilic granulomas are typically seen in the vertebral body.

9 MRI of the Pediatric Spine

A. Jay Khanna, Bruce A. Wasserman, and Paul D. Sponseller

CHAPTER OUTLINE

- I. Specialized Pulse Sequences and Imaging Protocols
- II. Pediatric Sedation Protocols
- III. Normal Pediatric MRI Anatomy
 - A. Adolescents and Adults
 - B. Children
 - 1. Differences between the Pediatric and Adult Spine
 - 2. Full-Term Infant
 - 3. Age: 3 Months
 - 4. Age: 2 Years
 - 5. Age: 10 Years
 - C. Conus Medullaris
- IV. Pathologic Processes Involving the Pediatric Spine
 - A. Infection
 - B. Trauma
- V. Imaging of Spinal Dysraphism
 - A. Chiari Malformations
 - B. Tethered Cord Syndrome
- VI. Controversies with MRI of the Pediatric Spine
 - A. Scoliosis
 - B. Evaluation of the Tethered Cord Syndrome
 - C. Imaging in the Presence of Implants

■ Specialized Pulse Sequences and Imaging Protocols

Standard pulse sequences for spinal imaging include SE T1-weighted and FSE T2-weighted images. The FSE technique enables the acquisition of T2-weight-

ed images without prolonged imaging times. T1-weighted images enable the evaluation of anatomic detail, including that of the osseous structures and soft tissues. T2-weighted images are primarily used to evaluate the spinal cord and enhance lesion conspicuity. Because CSF is bright on T2-weighted images and the spinal cord retains its intermediate signal, the T2-weighted images maximize the CSF to neural tissue contrast and therefore enable optimal delineation of the spinal cord and nerve roots. T2-weighted images are very sensitive to pathologic changes in tissue, including any processes in which cells and the extracellular matrix have increased water content. This pathologic change is usually shown as an increase in signal intensity on T2-weighted images, which increases the conspicuity of most pathologic processes affecting the spine.

Open MRI systems are becoming more frequently used, especially for pediatric imaging. Although these systems often have significantly lower field strengths than closed magnets and thus usually produce studies of inferior overall quality, the open environment provides young patients with access to their parents and makes the experience less intimidating for patients with claustrophobia. Open systems are also helpful for procedures that might benefit from MRI guidance. When possible, however, the authors recommend that MR imaging be performed using closed 1.5-T or 3-T MRI systems.

■ Pediatric Sedation Protocols

Formal sedation is often required for the successful MRI evaluation of the pediatric patient, and multiple studies and reviews have evaluated and recommended specific sedation protocols.^{1,2} The American Academy of Pediatrics has published guidelines for the elective sedation of pediatric patients,^{3,4} but compliance

with these guidelines is not mandatory. The American Academy of Pediatrics has stated that careful medical screening and patient selection by knowledgeable medical personnel are needed to exclude patients at high risk for life-threatening hypoxia.³ Also, monitoring using their guidelines is necessary for the early detection and management of life-threatening hypoxia.⁴ The American Academy of Pediatrics recommends that, before an examination in which sedation is to be used, children up to 3 years old should ingest nothing by mouth for 4 hours, and children 3 to 6 years old should ingest nothing by mouth for 6 hours.³

Although multiple protocols exist for the specific administration of various medications for pediatric sedation and although practices vary among institutions, a few agents are essential for most sedation protocols. Oral chloral hydrate is recommended for children <18 months old. However, the use of oral chloral hydrate is controversial because of its variable absorption, paradoxical effects, and nonstandardized dosing regimen. Older or larger children usually receive intravenous pentobarbital with or without fentanyl. Although some studies have reported the successful administration of sedation by trained nurses,^{1,2} patients who may benefit from the expertise of an anesthesiologist include those with substantial comorbidities, such as the following:

- Cardiopulmonary disease
- Skeletal dysplasias
- Neuromuscular disease
- Abnormal airway anatomy

An important consideration after sedation for pediatric MRI is the need for strict adherence to established discharge criteria, including the following⁵:

- Return to baseline vital signs
- Level of consciousness close to baseline
- Ability to maintain a patent airway

Because of the potential risks associated with anesthesia and sedation in the young patient, there is a trend toward referring pediatric patients who require sedation to hospitals with pediatric anesthesiologists. Alternate techniques include sleep deprivation and rapid, segmental scanning; the latter permits the acquisition of high-quality images without the use of sedation. The surgeon referring pediatric patients for MR images of the spine should be familiar with the sedation protocols and level of expertise at the selected facilities. It is important to note that sedation protocols vary greatly from institution to institution and that no protocol is 100% safe, which emphasizes the need for monitoring, careful patient selection, and evaluation. The authors advise consultation with the pediatric anesthesiologists at the referring physician's institution when sedating patients for MRI studies.

■ Normal Pediatric MRI Anatomy

To better understand and predict the MRI appearance of pathologic processes involving the spine, one should have a basic understanding of the normal MRI anatomy.⁶ Because most orthopaedic surgeons are more familiar with the normal anatomy of the adolescent (**Fig. 9.1**) and adult spines than with that of the pediatric spine, the salient points of the former two are presented first as a framework for understanding and differentiating the pediatric spine (for a full discussion of the adult spine anatomy, see Chapter 2, Normal Spine MRI Anatomy).

Adolescents and Adults

The lumbar spine is the most frequently imaged region in both children and adults. The lumbar spinal canal transitions from a round appearance in its proximal portion to a more triangular one distally. The lumbar facet joints are covered with 2 to 4 mm of hyaline cartilage. This cartilage can be nicely visualized on FSE pulse sequences and with gradient-echo pulse sequences. The epidural space and ligaments should also be carefully evaluated. The epidural fat is seen as high signal intensity on T1-weighted images; the ligamentum flavum shows minimally higher T1-weighted signal than the other ligaments. The conus medullaris, usually located at the L1-L2 level, is best seen as a regional enlargement of the spinal cord on the sagittal images. The filum terminale extends from the conus medullaris to the distal thecal sac. The traversing nerve roots pass distally from the conus medullaris and extend anteriorly and laterally. These nerve roots exit laterally underneath the pedicle and into the neural foramen. The intervertebral disc, consisting of the cartilaginous end plates, annulus fibrosus, and the nucleus pulposus, normally shows increased T2 signal in its central portion. It is important to note that CSF pulsations often create artifacts that degrade the image in the lumbar spine; those artifacts must not be mistaken for a pathologic process.

Evaluation of the cervical spine begins with the vertebral bodies. A mild lordosis is noted on sagittal images. On axial images, the spinal canal is triangular, with the base located anteriorly. It is important to note the normal variant dark band at the base of the dens that represents a remnant of the subdental synchondrosis; it should not be mistaken for a fracture. In adults, the facet joints are small and triangular, whereas in children they are relatively larger and flat. The spinal cord is elliptical in cross-section in the cervical spine. It is important to recognize that there is a difference in signal between the normal gray and white matter of the spinal cord. This signal

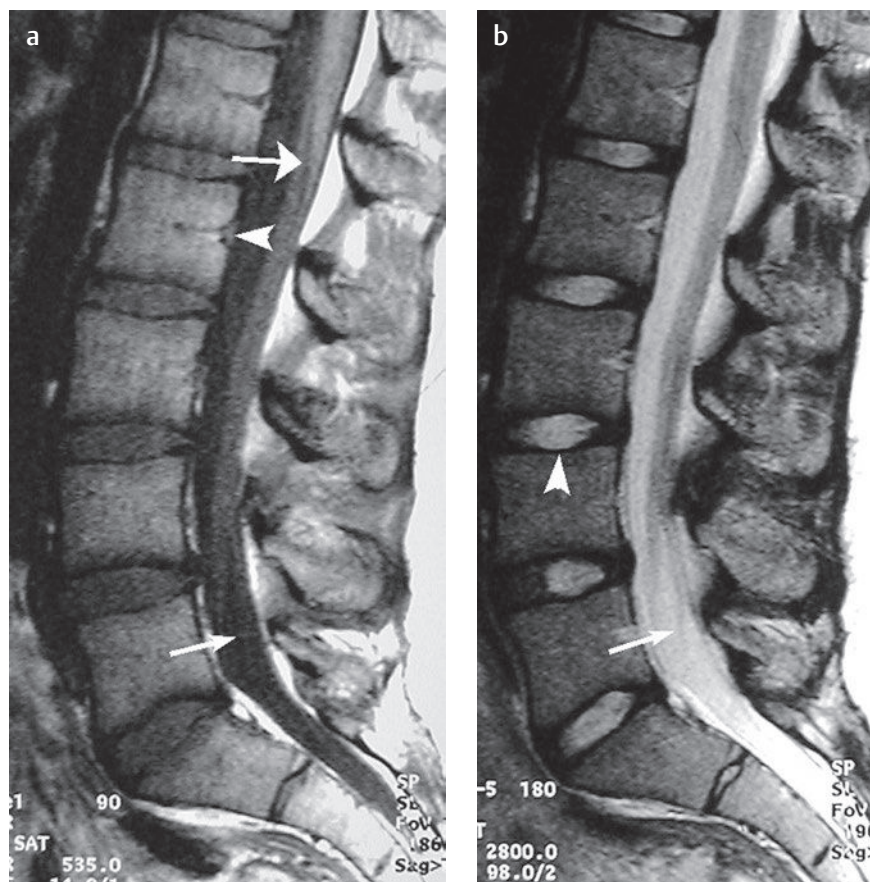


Fig. 9.1 Normal lumbar spine in a 16-year-old girl. **(a)** A sagittal T1-weighted image shows dark CSF (arrow with small head), the conus medullaris terminating at the L1-L2 level (arrow with large head), and the basivertebral channel (arrowhead). Note the normal rectangular appearance of the vertebral bodies and the lumbar lordosis. **(b)** A sagittal T2-weighted image shows bright CSF (arrow) and a bright nucleus pulposus (arrowhead).

heterogeneity should not be mistaken for intramedullary pathology. The intervertebral discs are similar in appearance to, but smaller than, those seen at the thoracic and lumbar levels. An important anatomic feature of the cervical spine is the prominent epidural venous plexus, which is not present in the thoracic or lumbar spine.

The thoracic vertebral bodies are relatively constant in size, and the spinal canal is relatively round. Abundant epidural fat is present posteriorly, but there is less anteriorly than in the lumbosacral region. The cord is more round than in the cervical or lumbar regions, and the cord segment lies between two and three levels above the corresponding vertebral body. The intervertebral discs are thinner than the discs in the lumbar spine. The appearance of the CSF is more variable in the thoracic spine than that in the lumbar region because of more prominent CSF pulsations, but it is most commonly seen as a region of low signal dorsal to the spinal cord on T1-weighted images. This artifact is often most severe at the apex of curves, including the thoracic kyphosis. Techniques are available for minimizing this artifact, including gating to the pulse or cardiac cycle.

Children

Differences between the Pediatric and Adult Spine

Understanding the normal adult and adolescent spine leads to appreciation of the dynamic development of the pediatric spine. The MRI appearance of the growing spine is quite complex. Multiple substantial changes occur in the vertebral ossification center and the intervertebral discs that markedly alter the overall appearance of the spine, especially between infancy and 2 years of age.⁷ In general, the vertebral ossification centers are incompletely ossified early in childhood, and the discs are thicker and have higher water content than those in the adult. The spinal canal and neural foramina are larger, and there is less curvature. In addition, the overall signal intensity of the vertebral bodies is lower than that of the adult spine on T1-weighted images because of the abundance of red (hematopoietic) marrow relative to yellow (fat) marrow in the pediatric, adolescent, and young adult spine.

By understanding the MRI appearance of this development process, the clinician is better equipped to differentiate normal from pathologic states. Sze et al⁷ have characterized the MRI evolution of the pediatric spine between infancy and 2 years of age, and Goske et al⁶ have described this dynamic process through the age of 10 years (see details later).

Full-Term Infant

In the newborn, the overall size of the vertebral body is small relative to the spinal canal, and the spinal cord ends at approximately the L2 level. The lumbar spine does not show the usual lordosis and is straight. The vertebral bodies show markedly low signal intensity on T1-weighted images, with a thin central hyperintense band that likely represents the basivertebral plexus. The spongy bone of the ossification center is ellipsoidal rather than rectangular and is often mistaken for a disc. The intervertebral disc is relatively narrow and often contains a thin, bright central band on T2-weighted images that represents the notochordal remnants.

Age: 3 Months

At 3 months, the osseous component of the vertebral body has increased and the amount of hyaline cartilage has decreased, with a resultant rectangular appearance to the vertebral bodies. The ossification centers begin to increase in signal intensity, starting at the end plates and progressing centrally. The neural foramina have not substantially changed at this age, remaining relatively large and ovoid in shape.

Age: 2 Years

At 2 years, the spine has begun to show its normal curvature, most likely because of the effects of weight bearing (**Fig. 9.2**). The ossified portion of the vertebral body increases substantially in size and begins to assume its adult appearance, with near-complete ossification of the pedicles and the articular processes. The disc space and nucleus pulposus become longer and thinner. The cartilaginous end plate has decreased in size and is often difficult to identify. The neural foramen also begins to take its adult appearance as its inferior portion narrows.

Age: 10 Years

At 10 years, the spinal curvature resembles that of an adult (**Fig. 9.3**). The ossification of the vertebral bodies and posterior elements is nearly complete, with a resultant decrease in the spinal canal diameter.

The vertebral bodies also develop concave superior and inferior contours. The nucleus pulposus becomes smaller at this age and spans approximately half of the disc space in the sagittal plane. The neural foramina continue to narrow inferiorly.

Conus Medullaris

The spinal cord extends to the inferior aspect of the osseous spinal column in early fetal life.⁶ Because of the more rapid longitudinal growth of the vertebral bodies relative to the spinal cord, the conus medullaris is repositioned in the upper lumbar spine by birth. It is important to note the location of the conus medullaris on every pediatric spine MRI study (**Figs. 9.1** and **9.2**). A conus level below the L2-L3 interspace in children >5 years old is abnormal and indicates possible tethering.^{8,9} Saifuddin et al¹⁰ reviewed the MRI findings of 504 normal adult spines and found that the average conus position was the lower third of L1 (range, middle third of T12 to the upper third of L3).

■ Pathologic Processes Involving the Pediatric Spine

Infection

Infectious processes involving the pediatric spine include osteomyelitis, discitis, epidural abscess, and paraspinal abscess.^{11–13} In general, the MRI signal characteristics of infection include a region of low T1 signal intensity and high T2 signal intensity in bone and soft tissue.

MRI is more sensitive than conventional radiographs or CT and is more specific than nuclear scintigraphy in identifying vertebral osteomyelitis.^{14,15} MRI provides the optimal means of imaging osteomyelitis (**Fig. 9.4**). Marrow edema can be detected on STIR images, and enhancement of the disc and adjacent vertebral bodies on postgadolinium, fat-suppressed T1-weighted images helps to confirm the diagnosis. The specificity of MRI for infection is higher in children than in adults because one of the primary confounding findings, degenerative arthritis, can be removed from the differential diagnosis. A key concept in both children and adults is differentiating osteomyelitis from neoplastic disease. An important characteristic that may help make this differentiation is the fact that infectious processes are more likely to cross intervertebral discs than are neoplastic conditions (**Fig. 9.5**).

Discitis, seen as a disruption of the normally well-defined disc-vertebral borders on T1-weighted images and as an increase in signal of the disc on

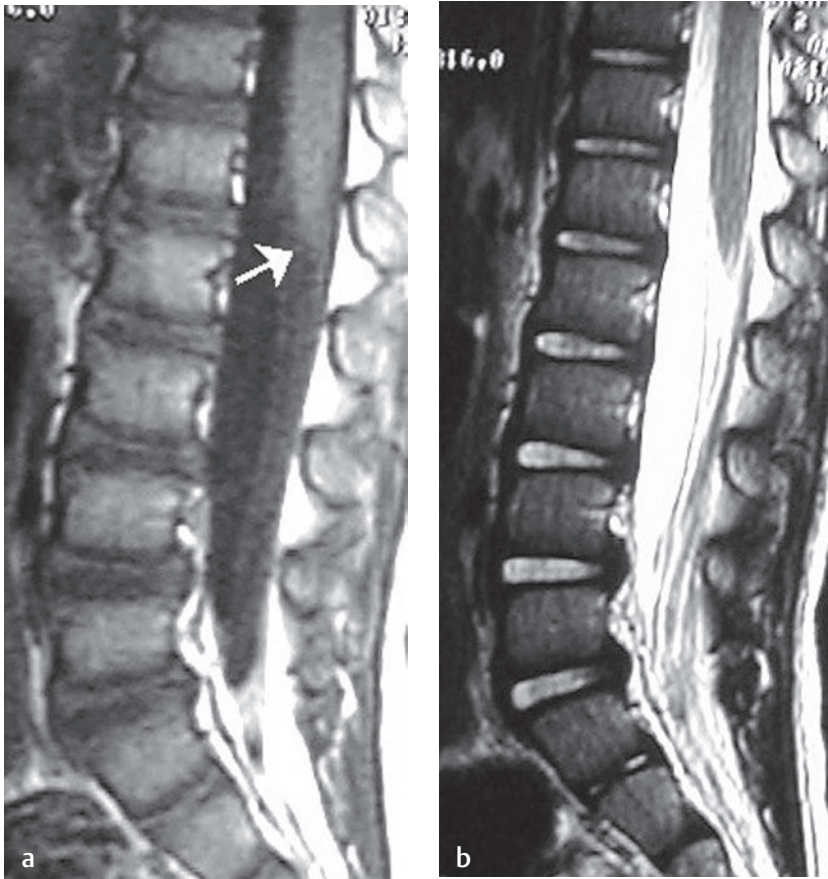
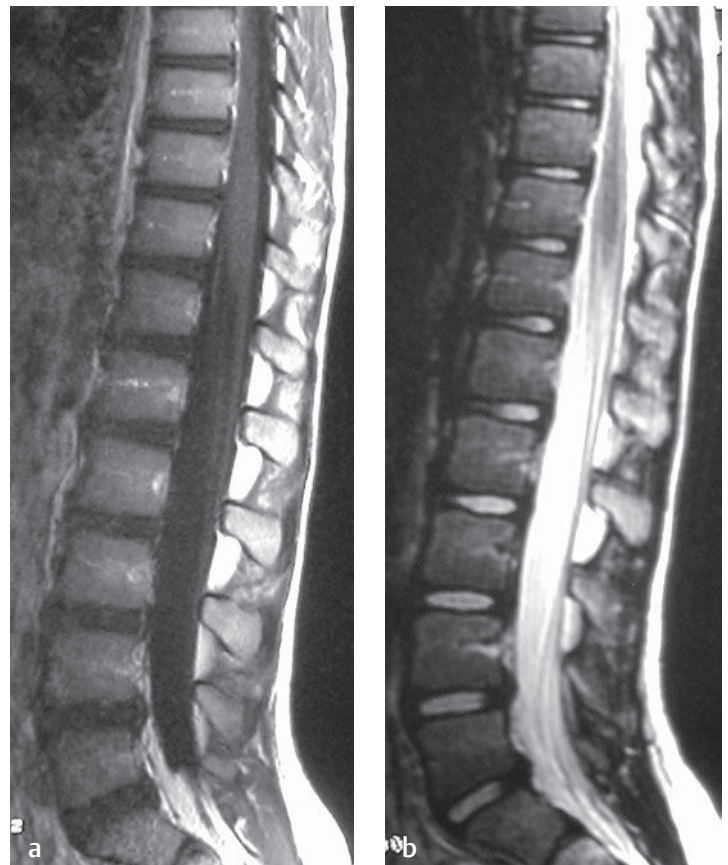


Fig. 9.2 Normal lumbar spine in a 2-year-old boy. **(a)** A sagittal T1-weighted image shows rectangular vertebral bodies and a wide, thin intervertebral disc. Note that the conus medullaris terminates at the L1-L2 level (*arrow*). **(b)** A sagittal T2-weighted image shows increased disc signal compared with that seen on the T1-weighted image.

Fig. 9.3 This 10-year-old girl has a normal lumbar spine with normal lordosis. **(a)** A sagittal T1-weighted image. **(b)** A sagittal T2-weighted image. Note that the posterior elements are well formed, with a resultant decrease in the canal diameter.



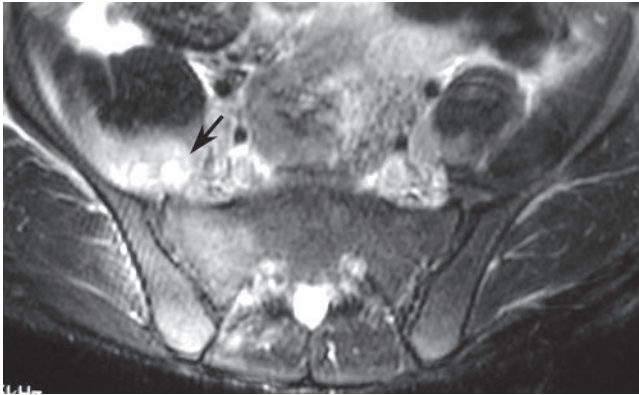


Fig. 9.4 This axial T2-weighted image in a 15-year-old boy with infectious symptoms and complaints of low back pain shows increased T2-weighted signal in the region of the right sacroiliac joint and an associated soft-tissue component at the anterior aspect of the joint (arrow), compatible with a sacroiliac joint infection.

T2-weighted images,¹² may obliterate the horizontal cleft within the intervertebral disc normally seen on T2-weighted images (**Fig. 9.6**). The abnormal signal seen in infectious discitis is classically associated with surrounding soft-tissue inflammation and reactive end-plate changes. Compared with adult patients, pediatric patients are more likely to develop primary discitis because of increased blood supply to the disc. Adults are more likely to develop infectious discitis after surgery or from contiguous spread from primary end-plate osteomyelitis.

Epidural abscesses are rare, but when they do develop, it is usually after surgery or vertebral osteomyelitis. The diagnosis of epidural abscesses can be made in the patient who has a collection in the epidural space and a clinical history that supports infection.¹¹ Gadolinium-enhanced T1-weighted images often show a peripheral rim of enhancement that represents the abscess wall.

Trauma

An important role of MRI is to evaluate for the presence of neural injury in the pediatric patient who has sustained substantial trauma to the spine and who has an abnormal neurologic examination or is unresponsive. The initial evaluation is performed with conventional radiographs, which are often normal. MRI evaluation may then be performed to evaluate for osseous, ligamentous, intervertebral disc, cord, and nerve root injury. Although CT enables better evaluation of osseous detail and displaced fractures, MRI enables improved evaluation of nondisplaced fractures because of its ability to detect marrow signal

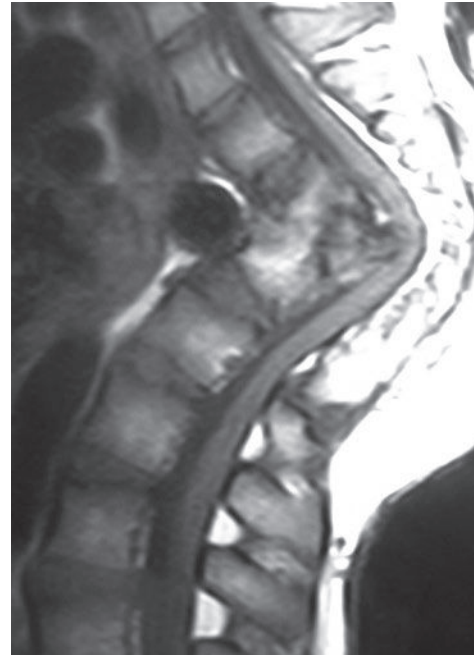


Fig. 9.5 In this 16-year-old girl with a history of tuberculosis, a sagittal T1-weighted image shows destruction of three consecutive mid-thoracic vertebral bodies with associated kyphosis and gibbus deformity, compatible with tuberculous osteomyelitis.

abnormalities (**Fig. 9.6**). MRI is also useful in its ability to help determine the age of the fracture and to evaluate for posttraumatic myelopathy. MRI, however, is not the optimal method for evaluating spondylolysis. CT offers increased spatial resolution and the ability to define accurately the osseous defect, whereas radionuclide imaging can show increased radiotracer activity in the region of the defect.

With regard to acute disc herniation in the pediatric age group, it is important to note that this herniation represents more of a fracture with a hinge-like displacement of fibrocartilage and displacement of the entire disc and vertebral end plate than extrusion of a disc fragment, as is seen in the adult population.¹⁶ Such avulsion fractures are often occult on conventional radiographs and are better detected with CT and MRI.¹⁶ Axial MR images shows the fracture fragment as an area of low signal intensity protruding into the spinal canal, and the sagittal images show a low signal intensity region in the shape of a Y or 7 on all pulse sequences.¹⁶

Spinal cord injury without radiographic abnormality is an established entity seen after pediatric spine trauma.^{17,18} The characteristic hypermobility and ligamentous laxity of the pediatric osseous cervical and thoracic spine predispose children to a spinal cord injury without radiographic abnormality-type

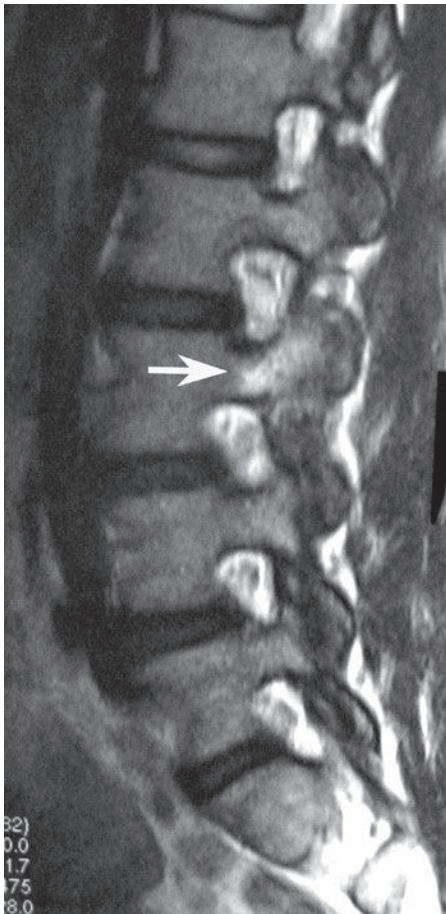


Fig. 9.6 In this 12-year-old boy with persistent low back pain and normal radiographs, a parasagittal T2-weighted image shows an area of increased signal (*arrow*) within the region of the pars intraarticularis, compatible with edema from an acute or subacute nondisplaced pars intraarticularis fracture.

injury.¹⁷ The elasticity of the osseous pediatric spine as well as the relatively large size of the head enable deformation of the musculoskeletal structures beyond physiologic limits, which results in cord trauma followed by spontaneous reduction of the spine.¹⁷

As with other types of spinal cord injuries, the most important predictor of outcome is the severity of neurologic injury. A patient with a complete neurologic deficit after spinal cord injury without radiographic abnormality has a poor prognosis for recovery of neurologic function. The role of MRI in spinal cord injury without radiographic abnormality syndrome is to define the degree of neural injury, rule out occult fractures and subluxation that may require surgical intervention, and evaluate for the presence of ligamentous injury. The T2-weighted and STIR images¹⁹ should show increased signal in the cord or vertebral body. The increased T2 signal in the cord is compatible with edema and can range from a partial, reversible contusion to complete transection of the cord.

■ Imaging of Spinal Dysraphism

Spinal dysraphism is a general term used to describe a wide range of anomalies resulting from incomplete fusion of the midline mesenchyme, bone, and neural elements. The osseous abnormalities consist of defects within the neural arch with partial or complete absence of the spinous processes, laminae, or other components of the posterior elements. MRI has been shown to be the best modality for the evaluation of spinal dysraphism.^{20–22}

To better understand the MRI of spinal dysraphism, it is important to have a basic knowledge of its various types. A classification system has been proposed that permits the systematic evaluation of a patient with a suspected spinal dysraphism (**Table 9.1**).²¹ By using this clinical classification system, the differential diagnosis can be rapidly narrowed to one of three categories: spinal dysraphism with a non-skin-covered back mass, spinal dysraphism with a skin-covered back mass, and spinal dysraphism with no back mass. The final diagnosis can then be selected from the identified category based on the lesion's MRI characteristics.

Myelomeningoceles represent a common type of spina bifida, the most common form of spinal dysraphism (**Fig. 9.7**). It most often presents as a non-skin-covered back mass in the lumbosacral region, although it can also be seen at higher levels. This mass may or may not be covered by leptomeninges containing a variable amount of neural tissue. The sac herniates through a defect in the posterior elements of the spine. The spinal cord usually contains a dorsal cleft, is splayed open, and is often tethered within the sac.²¹ Progressive scoliosis is seen in 66% of patients; Arnold-Chiari type-II malformation, in 90% to 99%; diastematomyelia, in 30% to 40%; and syringohydromyelia, in 40% to 80%.²³ Scarring can occur at the surgical site after sac closure, and it is important to monitor these patients for the signs and symptoms of the tethered cord syndrome.

Of the entities presenting with a skin-covered back mass in the presence of spinal dysraphism, lipomeningocele is the most common. The lipomeningocele consists of lipomatous tissue that is continuous with the subcutaneous tissue of the back and also insinuates through the dysraphic defect and dura and into the spinal canal. The spinal cord often contains a dorsal defect at the level of the lipomatous tissue and may be tethered at this level. The essential MRI feature of this lesion is that the lipomatous tissue matches the signal characteristics of subcutaneous fat on all pulse sequences, including fat-suppressed pulse sequences.

Occult spinal dysraphism presents without a back mass and includes many entities (**Table 9.1**). Diastematomyelia is characterized by a sagittal splitting of the spinal cord, conus medullaris, or filum terminale into two segments, often in the thoracic or lumbar

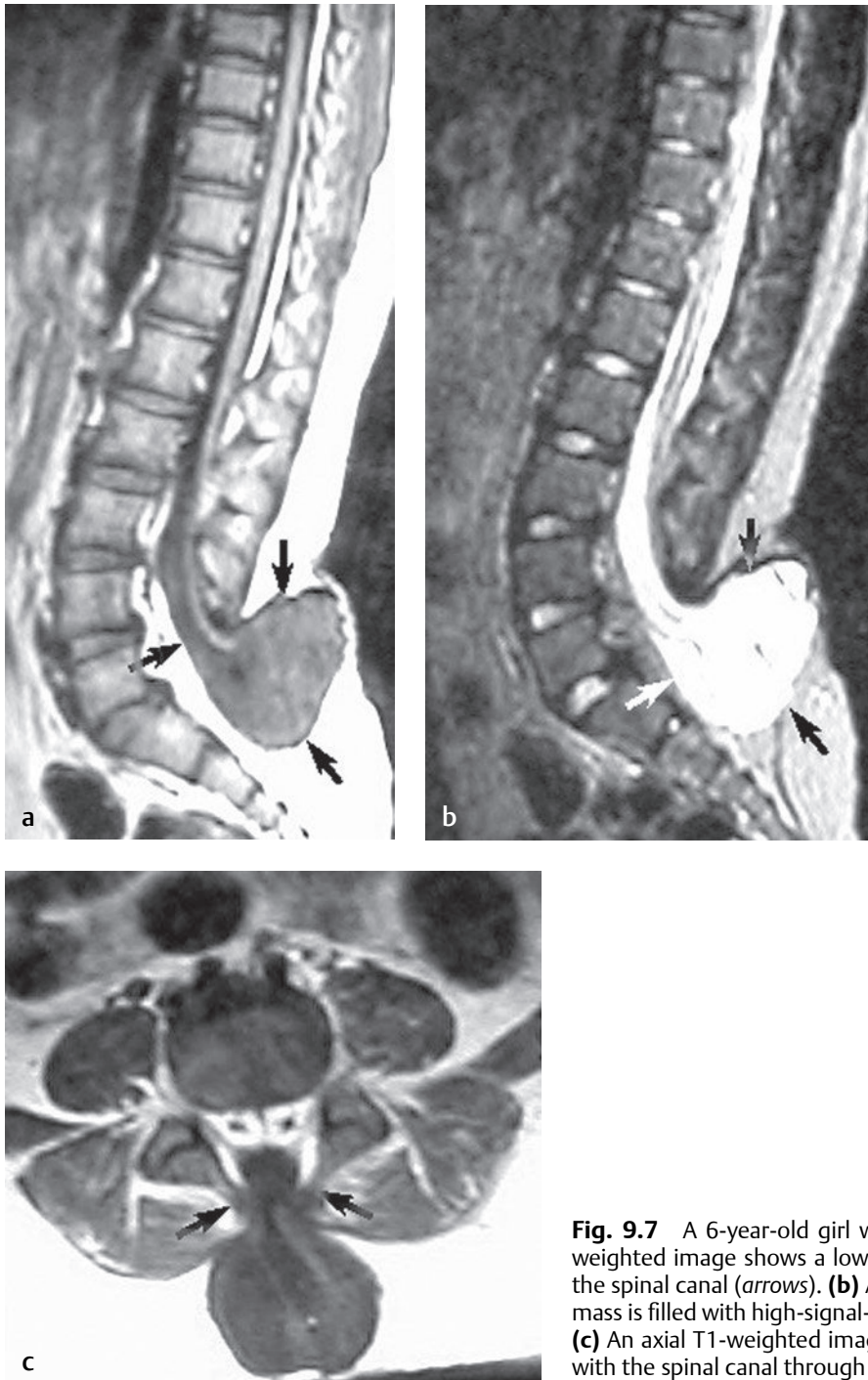


Fig. 9.7 A 6-year-old girl with a myelomeningocele. **(a)** A sagittal T1-weighted image shows a low back mass contiguous with the contents of the spinal canal (arrows). **(b)** A sagittal T2-weighted image shows that the mass is filled with high-signal-intensity fluid, compatible with CSF (arrows). **(c)** An axial T1-weighted image confirms the communication of the mass with the spinal canal through a defect in the posterior elements (arrows).

spine. The dural tube and arachnoid are undivided in approximately half of the patients; in such patients, clinical findings are rare, and surgery is not indicated. In the other half, the dural tube and arachnoid are completely or partially split at the level of the spinal cord cleft, which results in tethering of the cord and subsequent clinical symptoms. Coronal T1-weighted and T2-weighted images best define the sagittal split in the cord; the findings should be confirmed on axial images. The osseous spur or fibrous band that occurs between

each hemicord appears dark on T1-weighted and T2-weighted images and can be better visualized on CT.

Another important entity often seen in patients with spinal dysraphism is syringohydromyelia, or syrinx (**Fig. 9.8**). A syrinx is a longitudinal cavity within the spinal cord that may or may not communicate with the central canal. Multiple theories exist to explain the etiology of a syrinx, including developmental and trauma-, inflammation-, ischemia-, and pressure-related causes. Sagittal MR images show a linear low

Table 9.1 Classification of spinal dysraphism

Category	Types
Spinal dysraphism with a non-skin-covered back mass	Myelomeningocele Myelocele
Spinal dysraphism with a skin-covered back mass	Lipomeningocele Myelocystocele Simple posterior meningocele
Spinal dysraphism without a back mass	Diastematomyelia Dorsal dermal sinus Intradural lipoma Tight filum terminale Anterior sacral meningocele Lateral thoracic meningocele Hydromyelia Split notochord syndrome Caudal regression syndrome

[This table was published in Magnetic Resonance Imaging Clinics of North America, 4, Byrd SE, Darling CF, McLone DG, Tomita T, MR imaging of the pediatric spine, 797–833, Copyright Elsevier (1996).]

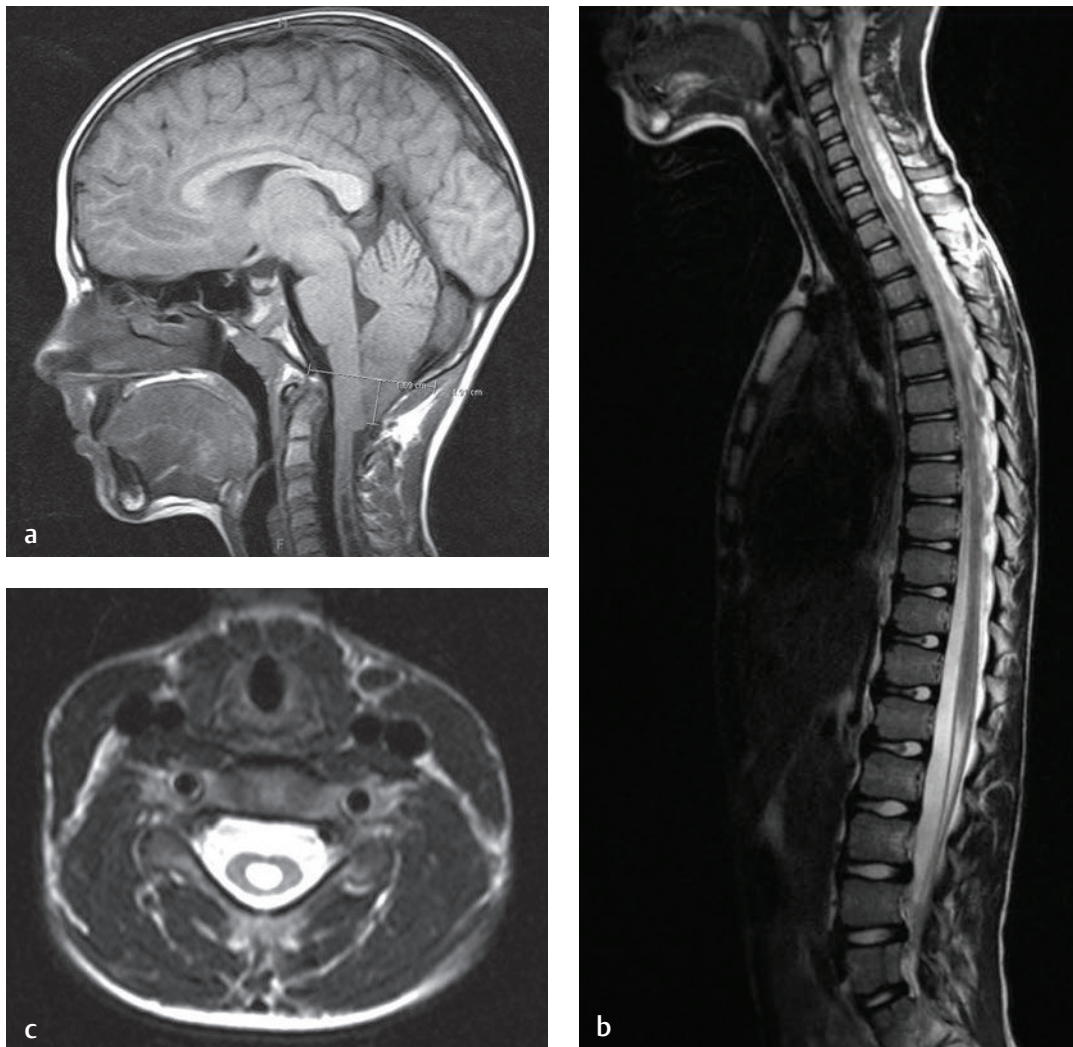


Fig. 9.8 A 9-year-old boy with a large syrinx of the cervical spine. **(a)** A sagittal T1-weighted image of the brain and upper cervical spine showing an Arnold Chiari type-I malformation and a syrinx of the upper cervical spine (lines showing 4.91 cm of cerebellar tonsil ectopia below the level of the foramen magnum). **(b)** A sagittal T2-weighted image of the entire spine showing a large syrinx extending from C4-C7. **(c)** An axial T2-weighted image at the C6 level confirms that the syrinx is located in the center of the spinal cord.

T1 signal intensity and high T2 signal intensity within the parenchyma of the spinal cord. Identification of a syrinx is sometimes an indication for contrast administration to exclude an underlying enhancing lesion.

Chiari Malformations

Chiari malformations are frequently seen in patients with spinal dysraphism. Chiari type-I malformations consist of cerebellar tonsillar ectopia, in which the cerebellar tonsils extend below the level of the foramen magnum. The commonly quoted measurement for the degree of herniation of the tonsils below the foramen magnum is 5 mm. Mikulis et al²⁴ reported a variation by age in the upper limit of normal: 6 mm in the first decade of life, 5 mm in the second and third decades, and 3 mm by the ninth decade. In Chiari type-I malformations, the brainstem is spared, and the fourth ventricle remains in its normal location. Chiari type-I malformations are associated with syringohydromyelia,²⁵ craniovertebral junction anomalies, and basilar invagination. Chiari type-II malformations are more advanced and consist of downward displacement of the brainstem and inferior cerebellum into the cervical spinal canal, with a decrease in the size of the posterior fossa.

Tethered Cord Syndrome

The tethered cord syndrome, an important problem, is seen in a substantial number of patients with spinal dysraphism, especially those who have undergone surgical closure of the defect.^{26,27} During fetal life, the spinal cord extends to the sacrococcygeal level. Because of the more rapid growth of the vertebral column after birth, the cord ascends to the L1-L2 level in the newborn. During the formation of a spinal dysraphic defect such as myelomeningocele, the open neural elements often attach to the peripheral ectoderm, resulting in spinal cord tethering. After surgical closure of the sac, there is a tendency for the spinal cord to become adherent at the repair site. As the child grows, this adherence may result in tethering of the cord and prevention of cephalad cord migration, with eventual symptoms. Thus, tethered cord should be ruled out as the potential cause of any deterioration in neurologic function in patients with spinal dysraphic and related conditions, including the following:

- Myelomeningoceles
- Myeloceles
- Lipomeningoceles
- Diastematomyelia

MRI has been proposed as the initial, and possibly the only, imaging modality for a patient with a suspected tethered spinal cord.⁹ The sagittal images should be evaluated to determine the level of the conus medullaris (**Fig. 9.9**). A conus level below the

L2-L3 interspace in children >5 years old is abnormal and an indication of possible tethering.^{8,9} In addition, the tethered cord is often displaced posteriorly in the spinal canal. Other findings include lipoma or scar tissue within the epidural space and increased thickness of the filum terminale.⁹

It is important to note that although MRI can determine if a spinal cord is anatomically tethered, these findings should be correlated with the patient's symptoms and serial physical examinations before surgical release is considered.

■ Controversies with MRI of the Pediatric Spine

As with any diagnostic test, there remain several areas for which the use of MRI of the pediatric spine is controversial, including the specific indications for the following:

- Imaging of scoliosis
- Imaging of tethered cord syndrome
- Imaging in the presence of spinal instrumentation

Scoliosis

Idiopathic scoliosis most often presents with a right-side lower thoracic curve. The purpose of MRI in the imaging of scoliosis is to detect intraspinal pathology, which is most frequently associated with left lower thoracic curves, an abnormal neurologic examination, and a young age at presentation.²⁸⁻³³ Do et al²⁹ concluded that MRI is not indicated before spinal arthrodesis in a patient with an adolescent idiopathic scoliosis curve pattern and normal physical and neurologic examinations.

One particular area of controversy is the pediatric patient with back pain in the presence of scoliosis. In the authors' experience, young patients with typical idiopathic scoliosis often complain of intermittent and vague back pain at some point during their clinical course. In a retrospective study of 2,442 patients, Ramirez et al³⁴ found that a left thoracic curve or an abnormal neurologic examination was most predictive of an underlying pathologic condition. They found a significant association between back pain and an age of >15 years, skeletal maturity, postmenarchal status, and a history of injury. Their conclusion was that it is unnecessary to perform extensive diagnostic studies on every patient with scoliosis and back pain. Based on clinical experience and a review of the literature, the current authors recommend obtaining an MRI in patients with scoliosis with a left lower thoracic curve, abnormal neurologic findings, infantile scoliosis, or juvenile scoliosis. Because coronal images are especially useful in evaluating patients with scoliosis, they should be a part of the routine imaging protocol.

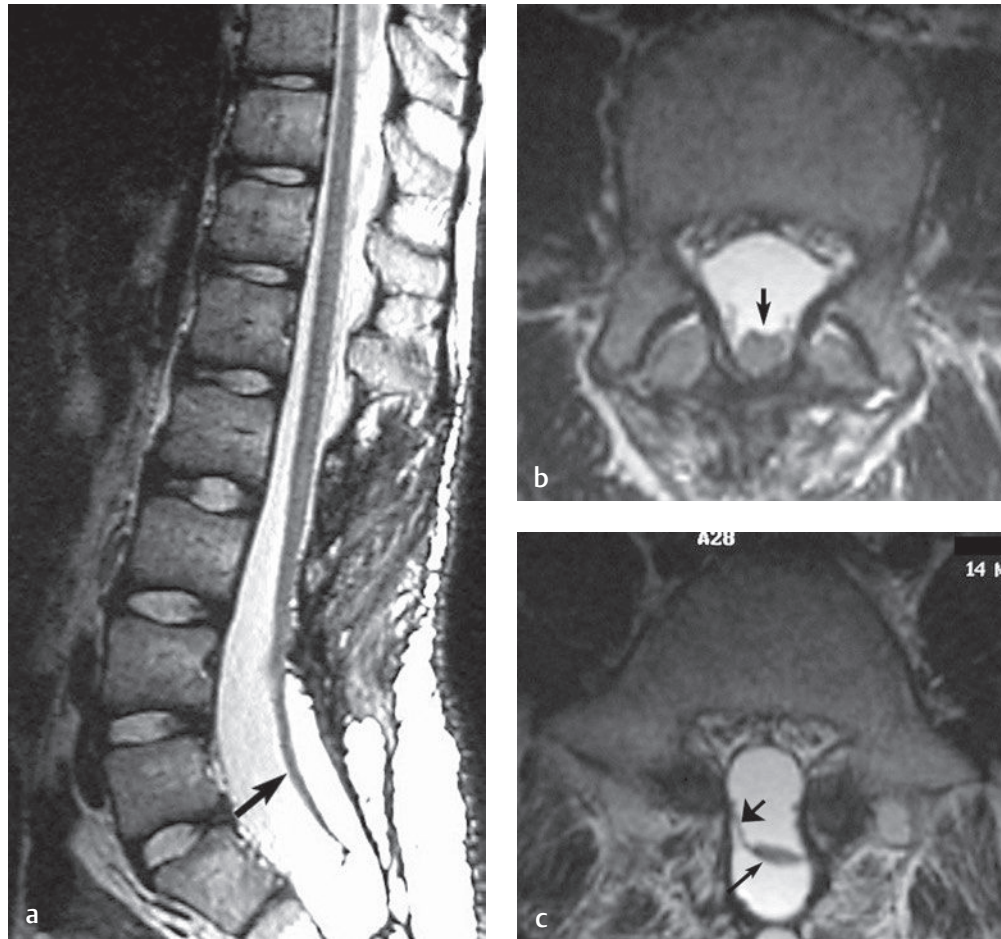


Fig. 9.9 This 14-year-old boy had a history of lipomeningocele. After surgical resection, he developed bowel and bladder dysfunction and new lower extremity paresthesias. **(a)** A sagittal T2-weighted image shows the cord to extend to approximately the L4 level and the filum terminale to extend to the S1 level (arrow), compatible with a tethered cord syndrome. **(b)** An axial T2-weighted image at the L4 level shows the cord to be located posteriorly within the thecal sac (arrow). **(c)** An axial T2-weighted image at the L5 level shows the placode (arrow with a small head) with a right-side nerve root coursing anteriorly and laterally (arrow with a large head).

Evaluation of the Tethered Cord Syndrome

As mentioned previously, the imaging of the tethered cord syndrome remains controversial. A dilemma arises when the MRI findings of tethered cord syndrome are noted and a decision with regard to non-operative versus operative treatment has to be made. It is important to remember that although anatomic tethering of the cord can be easily identified by MRI, the determining factor for surgical intervention are the clinical history and examination, preferably obtained on a serial basis.

Imaging in the Presence of Implants

MRI of the spine in the presence of instrumentation is generally safe but limited because image artifacts produced by implants vary in degree based

on the type of metal used and the pulse sequence used. Titanium produces less image degradation from artifact because it is less ferromagnetic than stainless steel.^{35,36} However, with appropriate imaging techniques, clinically useful information can be safely obtained in the presence of both types of implants.³⁷ Specialized pulse sequences can help reduce the degree of tissue-obscuring artifact produced by spinal hardware and improve image quality compared with conventional T1-weighted SE pulse sequences.³⁸ For example, the metal-artifact-reduction pulse sequence has been shown to substantially reduce the amount of tissue-obscuring artifact produced by spinal hardware.³⁸ The current authors use MRI to evaluate pediatric spines with stainless steel or titanium implants (**Fig. 9.10**), but the fact that the latter produces substantially less artifact affects the implant choice for a patient who may require follow-up MRI evaluation.

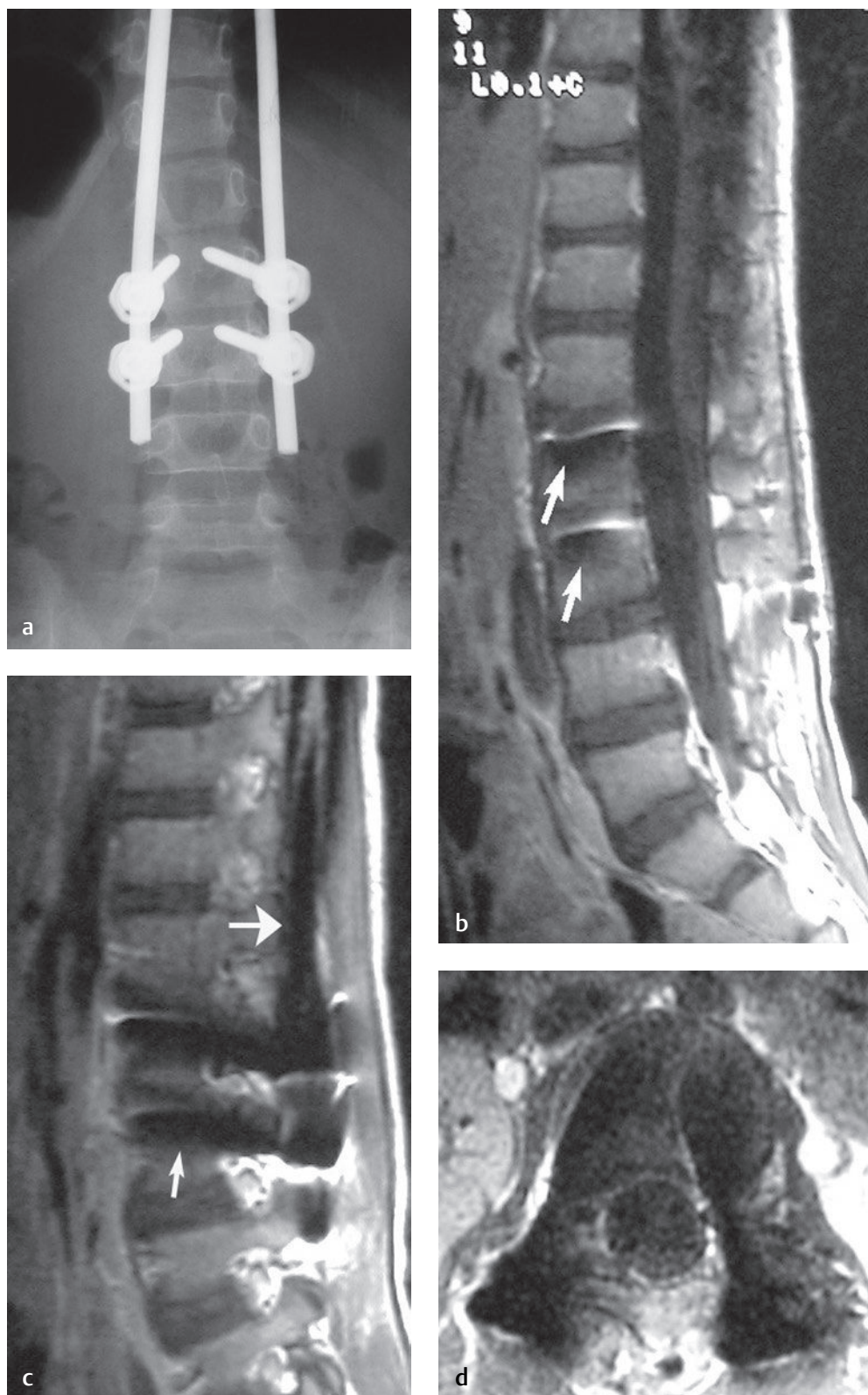


Fig. 9.10 A 6-year-old boy with a history of high-grade astrocytoma underwent resection, multilevel laminectomy, and posterior spinal arthrodesis from T4-L3 with titanium pedicle screws, hooks, and rods. **(a)** An AP radiograph 6 weeks after surgery. **(b)** A midline sagittal post-gadolinium T1-weighted image enables visualization of the canal contents with only minimal artifact from the pedicle screws (arrows). **(c)** A parasagittal postgadolinium T1-weighted image shows a rod (arrow with a large head) and a pedicle screw (arrow with a small head), neither of which substantially degrades the image. **(d)** An axial postgadolinium T1-weighted image also shows the pedicle screws and a patent spinal canal.

COMMON CLINICAL QUESTIONS

- Pediatric patients with which of the following diagnoses may benefit from the expertise of an anesthesiologist when undergoing MRI examination of the spine?
 - Cardiopulmonary disease
 - Skeletal dysplasias
 - Neuromuscular disease
 - Abnormal airway anatomy
 - All of the above
- At what age does the spine begin to show its normal curvature (i.e., lumbar lordosis)?
 - At birth
 - 3 months
 - 2 years
 - 10 years
 - 16 years
- What is the typical location of the conus medullaris on a sagittal T2-weighted image of the lumbar spine in a patient who is ≥ 5 years old?
 - T11
 - L1-L2
 - L3
 - L3-L4
 - The lumbosacral junction (L5-S1)
- What is the most common type of spinal dysraphism?
 - Diastematomyelia
 - Lipomenigocele
 - Myelocele
 - Caudal regression syndrome
 - Myelomeningocele
- Which of the following is NOT an indication for MR imaging of the spine in a pediatric patient with scoliosis?
 - Low back pain
 - Left lower thoracic curve
 - Abnormal neurologic findings
 - Infantile scoliosis
 - Juvenile scoliosis

References

- Beebe DS, Tran P, Bragg M, Stillman A, Truwitt C, Belani KG. Trained nurses can provide safe and effective sedation for MRI in pediatric patients. *Can J Anaesth* 2000;47(3):205–210 PubMed
- Sury MR, Hatch DJ, Deeley T, Dicks-Mireaux C, Chong WK. Development of a nurse-led sedation service for paediatric magnetic resonance imaging. *Lancet* 1999;353(9165):1667–1671 PubMed
- American Academy of Pediatrics Committee on Drugs. Guidelines for monitoring and management of pediatric patients during and after sedation for diagnostic and therapeutic procedures. *Pediatrics* 1992;89(6 Pt 1):1110–1115 PubMed
- Vade A, Sukhani R, Dolenga M, Habisohn-Schuck C. Chloral hydrate sedation of children undergoing CT and MR imaging: safety as judged by American Academy of Pediatrics guidelines. *AJR Am J Roentgenol* 1995;165(4):905–909 PubMed
- Malviya S, Voepel-Lewis T, Prochaska G, Tait AR. Prolonged recovery and delayed side effects of sedation for diagnostic imaging studies in children. *Pediatrics* 2000;105(3):E42 PubMed
- Goske MJ, Modic MT, Yu S. Pediatric spine: normal anatomy and spinal dysraphism. In: Modic MT, Masaryk TJ, Ross JS, eds. *Magnetic Resonance Imaging of the Spine*. St. Louis: Mosby-Year Book; 1994:352–387
- Sze G, Baierl P, Bravo S. Evolution of the infant spinal column: evaluation with MR imaging. *Radiology* 1991;181(3):819–827 PubMed
- Barson AJ. The vertebral level of termination of the spinal cord during normal and abnormal development. *J Anat* 1970;106(Pt 3):489–497 PubMed
- Moufarrij NA, Palmer JM, Hahn JF, Weinstein MA. Correlation between magnetic resonance imaging and surgical findings in the tethered spinal cord. *Neurosurgery* 1989;25(3):341–346 PubMed
- Saifuddin A, Burnett SJD, White J. The variation of position of the conus medullaris in an adult population. A magnetic resonance imaging study. *Spine (Phila Pa 1976)* 1998;23(13):1452–1456 PubMed
- Auletta JJ, John CC. Spinal epidural abscesses in children: a 15-year experience and review of the literature. *Clin Infect Dis* 2001;32(1):9–16 PubMed
- du Lac P, Panuel M, Devred P, Bollini G, Padovani J. MRI of disc space infection in infants and children. Report of 12 cases. *Pediatr Radiol* 1990;20(3):175–178 PubMed
- Modic MT, Feiglin DH, Piraino DW, et al. Vertebral osteomyelitis: assessment using MR. *Radiology* 1985;157(1):157–166 PubMed
- Fernandez M, Carrol CL, Baker CJ. Discitis and vertebral osteomyelitis in children: an 18-year review. *Pediatrics* 2000;105(6):1299–1304 PubMed
- Miller GM, Forbes GS, Onofrio BM. Magnetic resonance imaging of the spine. *Mayo Clin Proc* 1989;64(8):986–1004 PubMed
- Banerian KG, Wang AM, Samberg LC, Kerr HH, Wesolowski DP. Association of vertebral end plate fracture with pediatric lumbar intervertebral disk herniation: value of CT and MR imaging. *Radiology* 1990;177(3):763–765 PubMed
- Kriss VM, Kriss TC. SCIWORA (spinal cord injury without radiographic abnormality) in infants and children. *Clin Pediatr (Phila)* 1996;35(3):119–124 PubMed
- Pang D, Pollack IF. Spinal cord injury without radiographic abnormality in children—the SCIWORA syndrome. *J Trauma* 1989;29(5):654–664 PubMed
- Henry M, Scarlata K, Riesenburger RI, et al. Utility of STIR MRI in pediatric cervical spine clearance after trauma. *J Neurosurg Pediatr* 2013;12(1):30–36 PubMed
- Altman NR, Altman DH. MR imaging of spinal dysraphism. *AJNR Am J Neuroradiol* 1987;8(3):533–538 PubMed
- Byrd SE, Darling CF, McLone DG, Tomita T. MR imaging of the pediatric spine. *Magn Reson Imaging Clin N Am* 1996;4(4):797–833 PubMed

22. Huisman TAGM, Rossi A, Tortori-Donati P. MR imaging of neonatal spinal dysraphia: what to consider? *Magn Reson Imaging Clin N Am* 2012;20(1):45–61 PubMed
23. Modic MT, Yu S. Normal anatomy. In: Modic MT, Masaryk TJ, Ross JS, eds. *Magnetic Resonance Imaging of the Spine*. St. Louis: Mosby-Year Book; 1994:37–79
24. Mikulis DJ, Diaz O, Egglin TK, Sanchez R. Variance of the position of the cerebellar tonsils with age: preliminary report. *Radiology* 1992;183(3):725–728 PubMed
25. Strahle J, Muraszko KM, Kapurch J, Bapuraj JR, Garton HJL, Maher CO. Chiari malformation Type I and syrinx in children undergoing magnetic resonance imaging. *J Neurosurg Pediatr* 2011;8(2):205–213 PubMed
26. Hall WA, Albright AL, Brunberg JA. Diagnosis of tethered cords by magnetic resonance imaging. *Surg Neurol* 1988;30(1):60–64 PubMed
27. Heinz ER, Rosenbaum AE, Scarff TB, Reigel DH, Drayer BP. Tethered spinal cord following meningocele repair. *Radiology* 1979;131(1):153–160 PubMed
28. Diab M, Landman Z, Lubicky J, et al. Use and outcome of MRI in the surgical treatment of adolescent idiopathic scoliosis. *Spine (Phila Pa 1976)* 2011;36(8):667–671 PubMed
29. Do T, Fras C, Burke S, Widmann RF, Rawlins B, Boachie-Adjei O. Clinical value of routine preoperative magnetic resonance imaging in adolescent idiopathic scoliosis. A prospective study of three hundred and twenty-seven patients. *J Bone Joint Surg Am* 2001;83(4):577–579 PubMed
30. Evans SC, Edgar MA, Hall-Craggs MA, Powell MP, Taylor BA, Noordeen HH. MRI of 'idiopathic' juvenile scoliosis. A prospective study. *J Bone Joint Surg Br* 1996;78(2):314–317 PubMed
31. Gupta P, Lenke LG, Bridwell KH. Incidence of neural axis abnormalities in infantile and juvenile patients with spinal deformity. Is a magnetic resonance image screening necessary? *Spine (Phila Pa 1976)* 1998;23(2):206–210 PubMed
32. Mejia EA, Hennrikus WL, Schwend RM, Emans JB. A prospective evaluation of idiopathic left thoracic scoliosis with magnetic resonance imaging. *J Pediatr Orthop* 1996;16(3):354–358 PubMed
33. Schwend RM, Hennrikus W, Hall JE, Emans JB. Childhood scoliosis: clinical indications for magnetic resonance imaging. *J Bone Joint Surg Am* 1995;77(1):46–53 PubMed
34. Ramirez N, Johnston CE II, Browne RH. The prevalence of back pain in children who have idiopathic scoliosis. *J Bone Joint Surg Am* 1997;79(3):364–368 PubMed
35. Rudisch A, Kremser C, Peer S, Kathrein A, Judmaier W, Daniaux H. Metallic artifacts in magnetic resonance imaging of patients with spinal fusion. A comparison of implant materials and imaging sequences. *Spine (Phila Pa 1976)* 1998;23(6):692–699 PubMed
36. Rupp R, Ebraheim NA, Savolaine ER, Jackson WT. Magnetic resonance imaging evaluation of the spine with metal implants. General safety and superior imaging with titanium. *Spine (Phila Pa 1976)* 1993;18(3):379–385 PubMed
37. Lyons CJ, Betz RR, Mesgarzadeh M, Revesz G, Bonakdarpour A, Clancy M. The effect of magnetic resonance imaging on metal spine implants. *Spine (Phila Pa 1976)* 1989;14(7):670–672 PubMed
38. Chang SD, Lee MJ, Munk PL, Janzen DL, MacKay A, Xiang QS. MRI of spinal hardware: comparison of conventional T1-weighted sequence with a new metal artifact reduction sequence. *Skeletal Radiol* 2001;30(4):213–218 PubMed

ANSWERS TO COMMON CLINICAL QUESTIONS

1. E
Explanation: Although several studies have reported the successful administration of sedation by trained nurses, pediatric patients with each of the diagnoses listed here may benefit from the expertise of an anesthesiologist when undergoing a MRI examination of the spine.
2. C
Explanation: The spine has usually begun to show its normal curvature (i.e., lumbar lordosis) by 2 years of age, most likely because of the effects of weightbearing.
3. B
Explanation: A conus level below the L2-L3 interspace in children >5 years old is abnormal and indicates possible tethering. A review of the MRI findings of 504 normal adult spines found that the average conus position was the lower third of L1 (range, middle third of T12 to the upper third of L3).¹⁰
4. E
Explanation: Myelomeningocele is the most common form of spinal dysraphism. It most often presents as a non-skin-covered back mass in the lumbosacral region, although it can also be seen at higher levels. This mass may or may not be covered by leptomeninges containing a variable amount of neural tissue. The sac herniates through a defect in the posterior elements of the spine.
5. A
Explanation: One particular area of controversy for obtaining MRI is the pediatric patient with back pain in the presence of scoliosis. In the current authors' experience, young patients with typical idiopathic scoliosis often complain of intermittent and vague back pain at some point during their clinical course, and at least one large study has found that MRI is not indicated before spinal arthrodesis in a patient with an adolescent idiopathic scoliosis curve pattern and a normal physical and neurologic examination.

Special Conditions

10 Advanced Techniques in Spine MRI

Joseph P. Gjolaj and John A. Carrino

CHAPTER OUTLINE

- I. Magnets and Imaging Equipment
 - A. 3.0-T Magnets
 - B. Parallel Imaging
 - C. Open-Bore MRI
 - D. Intraoperative MRI
- II. Positional, Load-Bearing, or Dynamic (Functional) Imaging
- III. Novel Pulse Sequences
- IV. MRI in the Presence of Metallic Implants
- V. MRI-Guided Interventions
 - A. Musculoskeletal Biopsy
 - B. Cryotherapy
 - C. Pain Management
- VI. Summary

Although imaging for spinal disease typically begins with radiographs, CT, or conventional MRI, there are several advanced MRI techniques that have proven useful for the evaluation of the early manifestations, preoperative planning, and postoperative analysis of subtle and complex pathology. In addition, advanced MRI techniques may be helpful in narrowing a differential diagnosis, addressing a specific clinical question, or evaluating a finding detected on another imaging study. This chapter focuses on techniques in spinal MRI that are increasingly used to assist clinical problem solving.

■ Magnets and Imaging Equipment

3.0-T Magnets

High-field-strength MRI systems, typically with magnetic field strengths of 3.0 T, are becoming widely available in the clinical setting. The higher intrinsic

signal-to-noise ratio of high-field-strength MRI can be used to improve imaging speed or resolution, but there are changes in relaxation time at 3.0 T and increased artifacts to consider. Nevertheless, 3.0-T MRI offers the opportunity to explore physiologic imaging of spinal anatomy with greater definition (**Fig. 10.1**).

Intrinsic signal-to-noise ratio is a function of the strength of the magnetic field, the volume of the tissue being imaged, and the RF coils used. All else being equal, 3.0 T should provide twice the intrinsic signal-to-noise ratio of 1.5 T, but this goal is not achieved clinically for several reasons. The FDA and manufacturers have mandated the use of power-monitoring systems for 3.0-T MRI systems because of the increased risk of RF burns. The more problematic sequences are FSE/TSE and short-TR SE (T1-weighted) sequences. Because motion, chemical shift, and susceptibility artifacts from metallic implants are increased at 3.0 T, postoperative imaging may be more problematic at higher field strengths, although there are advancements with metal artifact reduction sequences.

Imaging speed is improved with higher field strength; therefore, it is theoretically possible to acquire images up to four times faster at 3.0 T than at 1.5 T while maintaining a comparable signal-to-noise ratio. In actuality, given the number of different considerations, it is typical to image only twice as fast with 3.0 T as with 1.5 T. Image acquisition time at 3.0 T may be optimized by minimizing the number of signal averages, increasing TR to account for longer T1 relaxation, using a higher receiver bandwidth for non-FSE sequences, and using small echo spacing for FSE/TSE sequences. As previously mentioned, the increase in signal-to-noise ratio at 3.0 T may be used to improve spatial resolution of images acquired by producing thinner and more numerous sections (**Fig. 10.2**).¹⁻³

High-resolution 3D imaging of the whole spine is also an advantage of 3.0-T imaging, with an increased signal-to-noise ratio compared with 1.5-T imaging.⁴ The signal gain at 3.0 T can be used to further increase

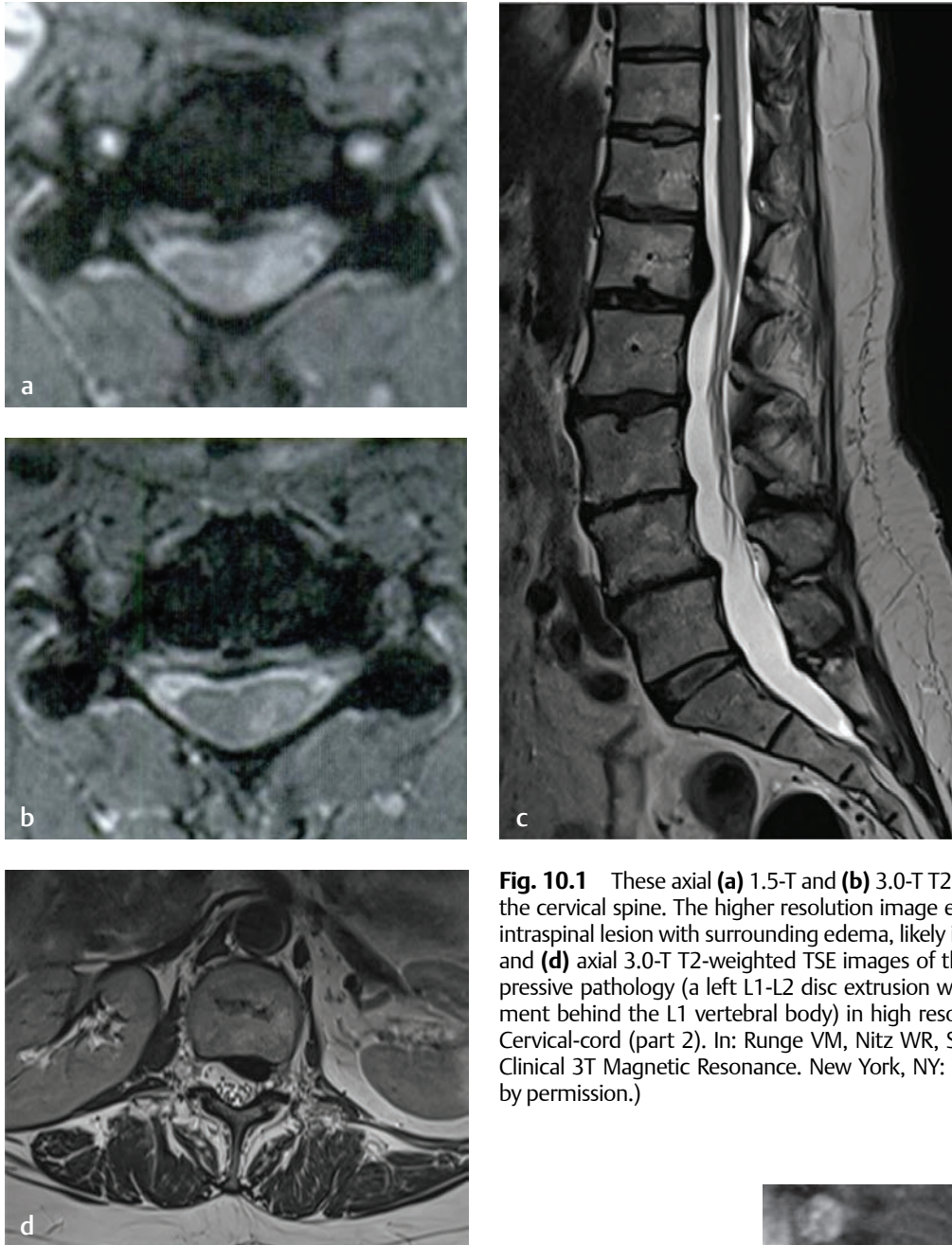
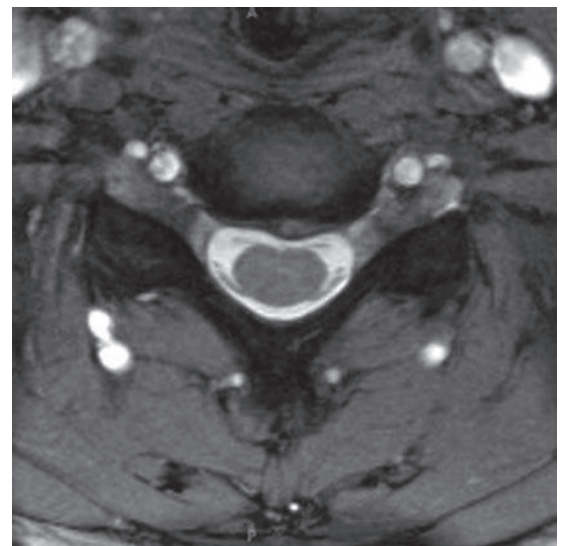


Fig. 10.1 These axial **(a)** 1.5-T and **(b)** 3.0-T T2-weighted gradient-echo images of the cervical spine. The higher resolution image enables the identification of a small intraspinal lesion with surrounding edema, likely inflammatory in nature. **(c)** Sagittal and **(d)** axial 3.0-T T2-weighted TSE images of the lumbar spine show neural compressive pathology (a left L1-L2 disc extrusion with proximal migration of the fragment behind the L1 vertebral body) in high resolution. **(a and b):** From Runge VM. Cervical-cord (part 2). In: Runge VM, Nitz WR, Schmeets SH, Shoenberg SO (Eds). Clinical 3T Magnetic Resonance. New York, NY: Thieme; 2007:114–115. Reprinted by permission.)

Fig. 10.2 An axial T2*-weighted (a T2-like image [bright fluid] created with a gradient-echo rather than an SE technique) 3.0-T image at the C4-C5 level of the spine shows a high signal-to-noise ratio with high spatial resolution, providing excellent visualization of the ventral and dorsal roots in addition to a small central disc protrusion.[†]



spatial resolution, which makes exceptionally detailed imaging possible (**Fig. 10.3**). However, pronounced interpatient variability of signal-to-noise ratio at 3.0 T has been reported and is thought to be a result of nonhomogeneous RF deposition as a result of dielectric effects; however, these effects are more prominent in abdominal imaging.⁴

Parallel Imaging

Parallel imaging is a relatively new class of techniques capable of substantially increasing the imaging speed of MRI. Parallel imaging involves using spatial information inherent in the elements of an RF coil array to allow a reduction in the number of time-consuming, phase-encoded steps required during a scan. Parallel imaging, therefore, imposes particular hardware requirements. Coil arrays must be used with separate preamplifiers and receivers for each individual element and with appropriate decoupling networks to decrease cross-talk between elements. Although these techniques may be used to some degree with existing coil arrays, many tailored array geometries have been designed specifically for parallel imaging. Parallel imaging techniques may be applied to any existing pulse sequence to reduce imaging time or increase spatial resolution. Resultant time savings can

then be used to add modifications that would otherwise prohibitively lengthen a pulse sequence. Recent technical advances and increased availability have placed parallel imaging in widespread clinical use.

Increased imaging speeds do come with a well-defined signal-to-noise ratio penalty, which must be taken into account when developing protocols. Nevertheless, for sequences with sufficient baseline signal-to-noise ratio, parallel imaging can offer substantial benefits. There is great synergy with 3D volumetric acquisitions and high-field-strength MRI systems (higher signal-to-noise ratio), which facilitates a shift toward rapid, volumetric image acquisitions. Recently, major vendors of MRI scanners have implemented versions of parallel imaging in several commercial systems.⁵

Open-Bore MRI

To accommodate the needs of a larger patient population, including athletes and bariatric patients, open-bore MRI has been developed. This new technology needs to be coupled with other technologies to improve off-isocenter imaging,⁶ enabling numerous positioning options (such as lateral decubitus), reduced levels of claustrophobia, and the ability to perform functional imaging, with all of the benefits of high-field-strength 3.0-T imaging.

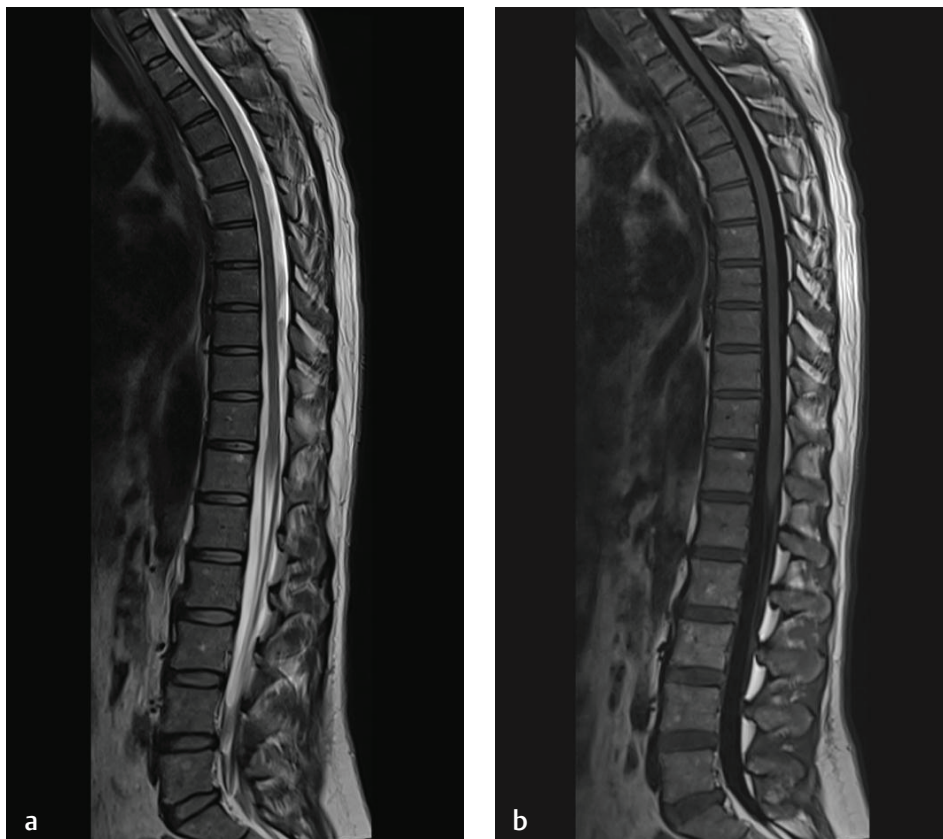


Fig. 10.3 High-resolution 3D imaging of the whole spine using 3.0-T MR imaging with a 24-channel matrix coil. **(a)** A sagittal T2-weighted TSE image (3-mm slice thickness) acquired in two 32-cm field-of-view steps with 5 min, 36 sec total acquisition time. **(b)** A sagittal T1-weighted turbo inversion recovery image (3-mm slice thickness) acquired in two 32-cm field-of-view steps with 9 min, 8 sec total acquisition time, with the parallel acquisition technique, an MRI method that combines signals from several coil elements to reconstruct an image, thereby shortening the total acquisition time or improving the signal-to-noise ratio.

Intraoperative MRI

New operating suites have been designed that incorporate MRI scanners, enabling a patient undergoing surgery to be imaged intraoperatively. Careful architectural planning and MRI-compatible surgical and anesthesia equipment make this new technique possible, which has been primarily used in neurosurgery. The value of such information has been shown to outweigh the cost of time necessary for image acquisition.⁷ Low-field-strength open MRI units are common because of their lower cost and more flexible integration into the operative suite.⁸ However, image quality is improved with high-field-strength closed magnets; such systems have been mounted on ceilings of neurosurgical operating rooms to image the brain.⁸ Intraoperative MRI has the capacity to detect residual tumor during a difficult resection, define complex anatomy during orthopedic procedures, and assess for complications. Although the potential for this technique is great, additional studies are needed to define the role of this technology in an orthopedic setting.

■ Positional, Load-Bearing, or Dynamic (Functional) Imaging

Positional, load-bearing, or dynamic (functional) imaging of the spine may be useful in certain contexts when imaging in the supine position has not fully revealed relevant pathology. Available options for imaging the spine include the supine, supine with axial loading (simulated weight bearing), seated, and standing upright positions.

Simulated weight bearing is performed by applying an axial load during supine imaging, which may be accomplished by having the patient wear a hardened plastic vest (DynaWell L-Spine, DynaWell, Billdal, Sweden).⁹ This device, which is free of material that would disturb the magnetic field in the MRI scanner, is strapped over the patient's shoulders and upper chest. The patient's feet are placed against the footplate of a compression device, which is attached to two adjustable cords, one on each side of the vest. By tightening the cords to a desired measured load (up to 50% of body weight), it is possible to provide compression that is similar to that of upright posture. This axially loaded position may reveal pathologies such as spondylolisthesis (**Fig. 10.4**), kyphosis, and disc herniations that are otherwise not seen in a supine position (**Fig. 10.5**).

MRI in the seated position is possible in a specially designed, vertically open intraoperative 0.5-T

magnet (Signa SP, General Electric Medical Systems, Milwaukee, WI) configured as a double bore with a 60-cm gap, which has been likened to a "double donut."¹⁰ Although this device is no longer commercially available, it is still in use and offers several advantages compared with conventional MRI. By placing a seat for the patient between the "donuts" in the center of the bore, this MRI allows imaging of the lumbar spine in neutral, flexion, and extension positions for a seated patient, providing a form of dynamic imaging. The seated position provides an axial load that may reproduce back pain symptoms for some patients. This type of imaging has shown physiologic changes of the spinal canal; for example, the cross-sectional area of the spinal canal and neural foramina is smallest in the extended position (**Fig. 10.6**). Conventional MRI may show abnormalities that may take on greater importance because of encroachment or neural impingement on dynamic load-bearing (seated) sequences.

Another option for functional musculoskeletal imaging is upright, weight-bearing, dynamic-kinetic MRI of the spine. A specifically designed 0.6-T magnet (Stand-Up MRI, Fonar Corporation, Melville, NY)¹¹ enables imaging of the standing patient. This system is applicable for imaging the cervical, thoracic, and lumbar spine. This scanner is useful for normal positional and kinetic images, for showing position-related disc protrusions in the spine worsening with extension, and for showing fluctuating positional foraminal and central spinal stenosis in the spine between recumbent and upright neutral positions. This type of imaging has led to a concept of fluctuating kinetic central spinal stenosis (fluctuating fluid disc herniation) that can be shown only by imaging in various upright positions (**Fig. 10.7**). Although a cervical spine MRI in the recumbent position may show posterior osteophytes, an upright MRI with cervical extension may reveal cord compression.

Back pain often occurs in weight-bearing situations, so positional imaging has great potential for showing pathology that may be subtle or inconspicuous on conventional supine MRI. However, the role of imaging the hip, knee, and ankle under an axial load has not been fully investigated. If supine-simulated weight-bearing techniques become validated, traditional magnets can be used without having to deploy new, costly, space-occupying devices.¹² Additional studies comparing simulated weight-bearing and upright imaging are needed to determine whether new magnets are required for this purpose. Load-bearing and dynamic imaging may not be necessary to show relevant pathology for all patients; patient selection criteria need to be developed so that this technology can be applied appropriately.

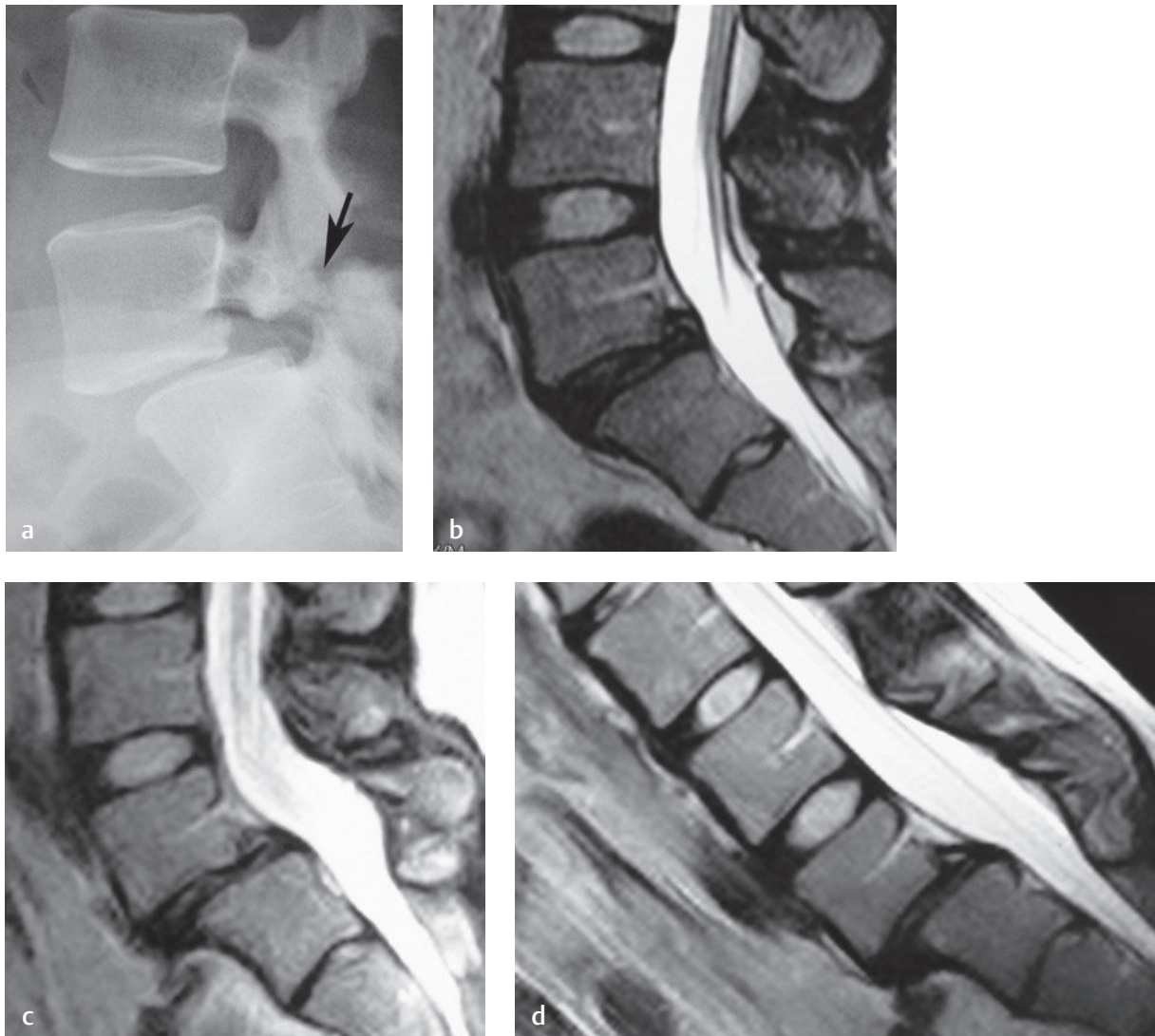


Fig. 10.4 Isthmic spondylolisthesis. **(a)** A lateral radiograph shows bilateral pars interarticularis defects (*arrow*) at the L5-S1 level with Meyerding grade-2 spondylolisthesis. **(b)** A sagittal T2-weighted MR image obtained on a closed system with the same patient in a supine position shows a grade-1 spondylolisthesis. **(c)** A sagittal T2-weighted MR image obtained on an open MRI system with the patient in a standing position shows that the spondylolisthesis progresses to grade-2. **(d)** A sagittal T2-weighted image obtained on an open MRI system with the patient in a flexed position shows that the grade-2 spondylolisthesis progresses compared with images in the **(c)** neutral and **(b)** supine positions.[†]

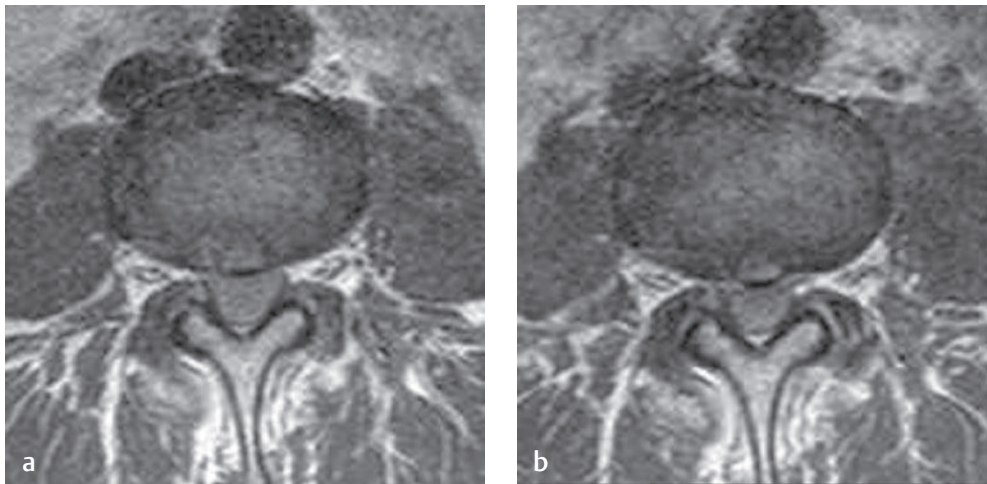


Fig. 10.5 Load-bearing spine imaging: simulated weight-bearing paradigm. These axial T1-weighted images were obtained at the level of the intervertebral disc in a conventional horizontal-bore 1.5-T MRI scanner with the use of a specially designed compression device (DynaWell Corp.) in a patient with neurogenic claudication. **(a)** A view without axial loading shows a mild disc bulge without substantial stenosis. **(b)** A view with axial loading shows a focal protrusion-type disc herniation and increasing stenosis.[†] (Courtesy of Per Lennart Westesson, MD, PhD, DDS, University of Rochester Medical Center, Rochester, NY.)

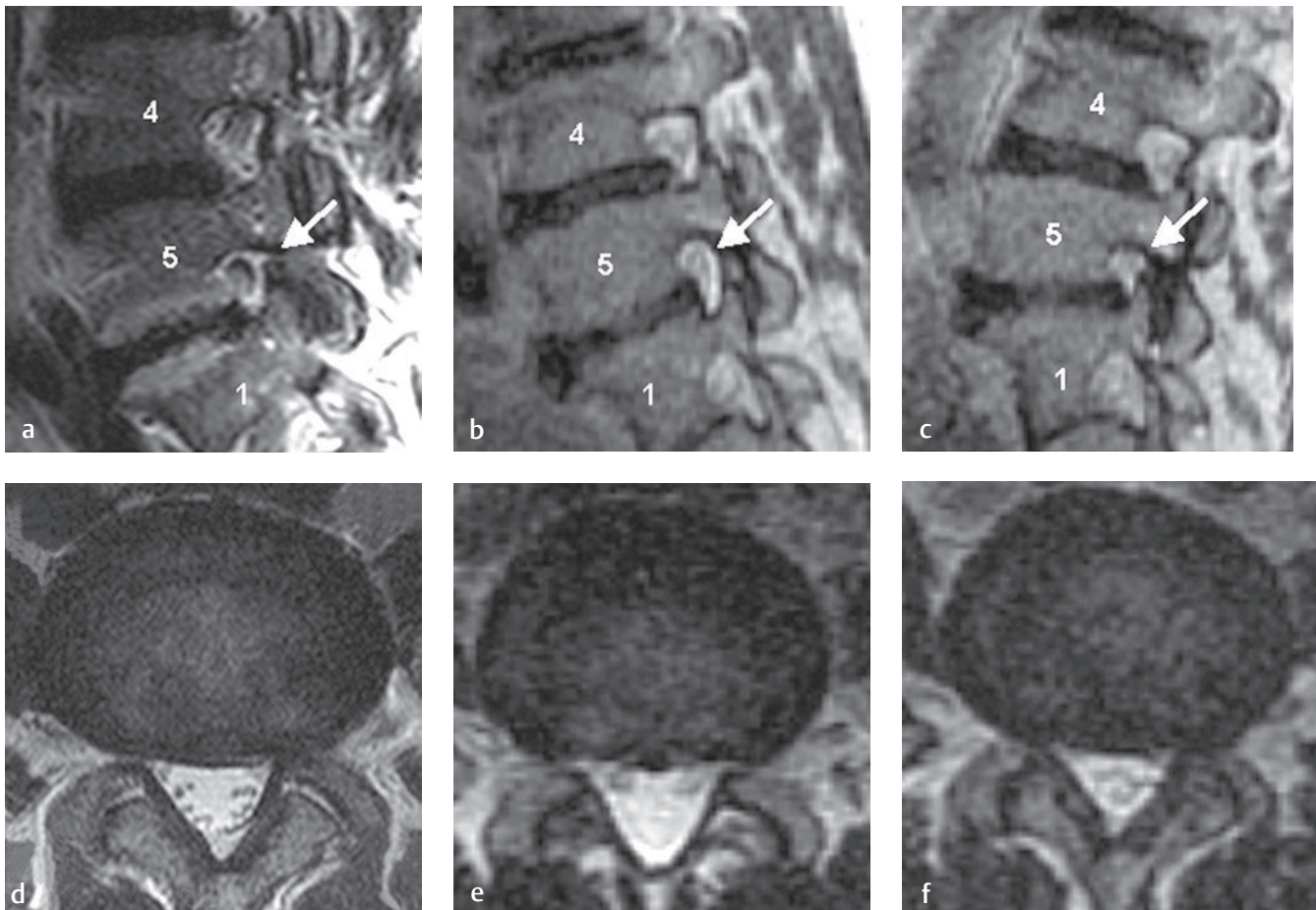


Fig. 10.6 Load-bearing spine imaging: seated positional paradigm. These **(a–c)** sagittal and **(d–f)** axial T2-weighted images were obtained in a specially designed vertically open 0.5-T MRI scanner (General Electric Medical Systems). The patient was seated and images were acquired in **(a, d)** neutral, **(b, e)** flexion, and **(c, f)** extension positions. **(a)** The L5-S1 foramen shows a slight foraminal stenosis with deformity of the epidural fat (*arrow*) on the conventional image. **(b)** This image obtained with the patient in seated flexion shows improvement, with increased epidural fat surrounding the exiting nerve (*arrow*). **(c)** This image obtained with the patient in seated extension shows a marked foraminal stenosis at the L5-S1 foramen, with epidural fat only partially surrounding the nerve root present (*arrow*). The cross-sectional area of the dural sac increased from **(d)** 150 mm² in the supine position to **(e)** 170 mm² in upright (seated) flexion and **(f)** decreased to 110 mm² in upright (seated) extension. These images reveal that spinal canal and neural canal dimensions are position dependent.[†] (Courtesy of Dominik Weishaupt, MD, Institute of Diagnostic Radiology, University Hospital, Zurich, Switzerland.)

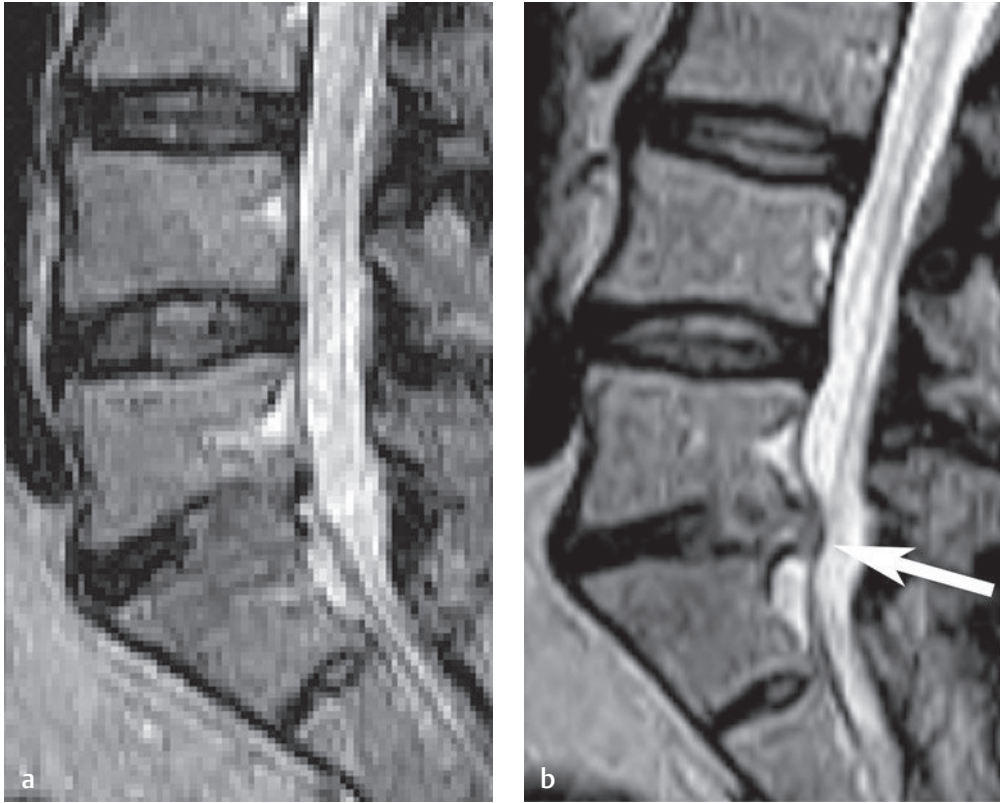


Fig. 10.7 Load-bearing spine imaging: standing positional paradigm. These sagittal T2-weighted views were obtained in a specially designed open 0.6-T magnet that allows both horizontal (recumbent) and vertical (upright) imaging (Fonar Corp.). This patient had recurrent radiculopathy 8 months after partial discectomy, with symptoms only when upright. **(a)** A supine image shows no focal contour abnormality at L5-S1. **(b)** An upright-neutral image reveals a posterior disc herniation at the L5-S1 level, elevating the posterior longitudinal ligament (*arrow*), which was not visible on the supine image.[†] (Courtesy of J. Randy Jenkins, MD, FACR, FEC, Downstate Medical Center, State University of New York, Brooklyn, NY.)

■ Novel Pulse Sequences

Although often useful, conventional musculoskeletal MRI pulse sequences may yield nonspecific findings. Several new imaging techniques may help narrow a differential diagnosis and further characterize a disease entity. For example, in- and out-of-phase chemical-shift imaging uses an MR artifact to determine whether there is a loss of normal marrow fat by an infiltrative process. Normal marrow and benign entities (such as vertebral fractures, hemangiomas, or Schmorl nodes) show loss of signal on out-of-phase images, which is not seen in neoplastic processes (**Fig. 10.8**). Chemical-shift sequences are therefore useful for determining whether heterogeneous marrow signal on T1-weighted images reflects tumor involvement or benign processes in the axial skeleton.^{13,14}

Diffusion-weighted imaging is based on the Brownian motion of water molecules in tissues. Pathologic processes typically restrict spontaneous diffusion of water; the degree of diffusion can then be

imaged to differentiate benign from malignant processes in the musculoskeletal system. This technique can show the extent of tumor necrosis and is used to differentiate tumor recurrence from posttreatment signal changes. Diffusion-weighted imaging is especially helpful for characterizing soft-tissue tumors because of the inherent contrast from high water diffusion in muscle. Diffusion-weighted imaging can also differentiate malignant from benign vertebral compression fractures because a benign fracture exhibits greater diffusion and bone-marrow edema.¹⁵

MR spectroscopy can assess the malignant potential of a lesion by evaluating its metabolic constituents. Because it represents an element of cell membranes, choline is present to a greater degree in malignant lesions, serving as a marker for increased cell turnover.¹⁶ Hydrogen 1 (1H) or proton MR spectroscopy can be used to measure relative quantities of choline, which requires selecting a volumetric region of interest. Each region of interest can be located with dynamic gadolinium-enhanced imaging by defining regions of a tumor with early enhancement. Commercially available software then provides spectroscopic data, whereby

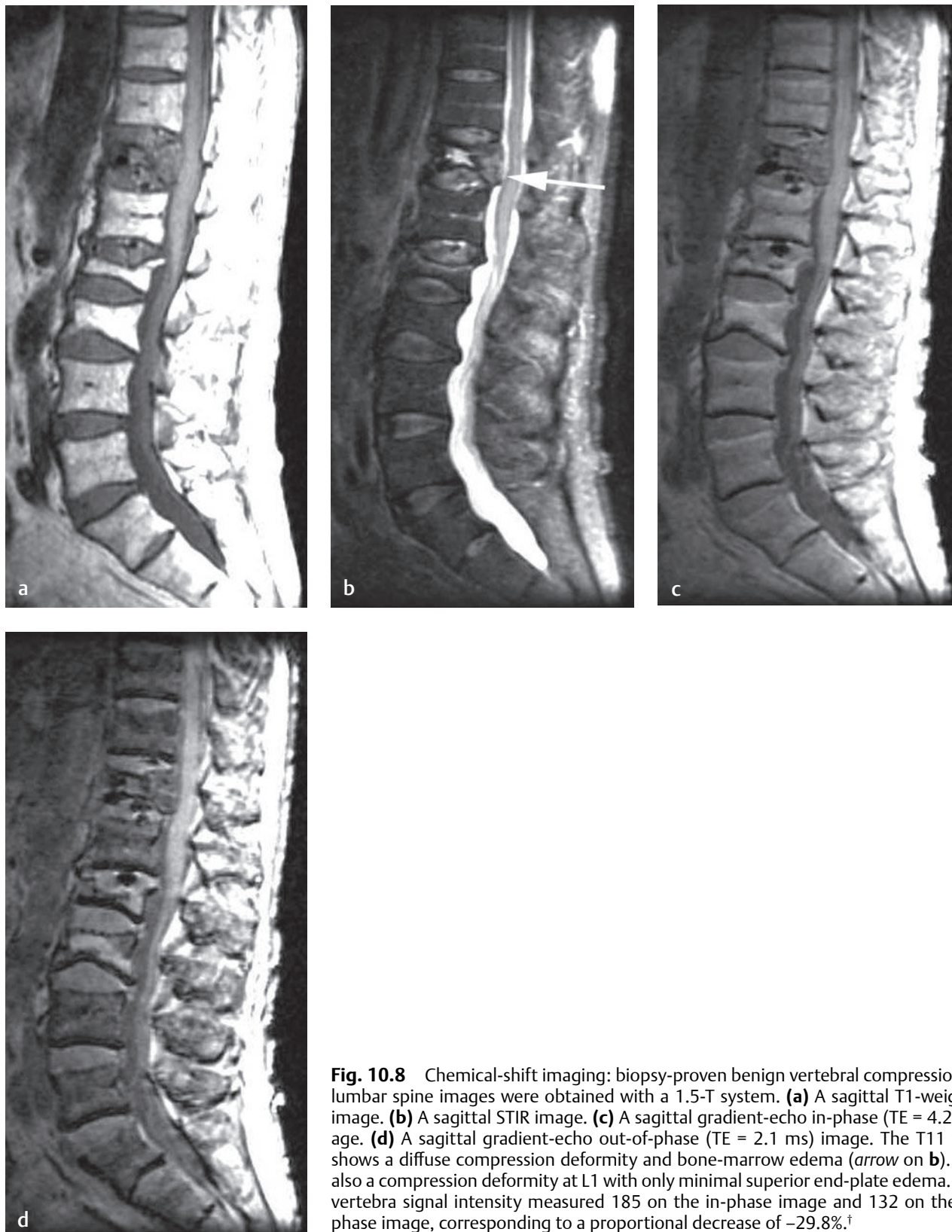


Fig. 10.8 Chemical-shift imaging: biopsy-proven benign vertebral compression. These lumbar spine images were obtained with a 1.5-T system. **(a)** A sagittal T1-weighted SE image. **(b)** A sagittal STIR image. **(c)** A sagittal gradient-echo in-phase (TE = 4.2 ms) image. **(d)** A sagittal gradient-echo out-of-phase (TE = 2.1 ms) image. The T11 vertebra shows a diffuse compression deformity and bone-marrow edema (arrow on **b**). There is also a compression deformity at L1 with only minimal superior end-plate edema. The T11 vertebra signal intensity measured 185 on the in-phase image and 132 on the out-of-phase image, corresponding to a proportional decrease of -29.8% .[†]

the relative amount of choline within a region of interest is measured at a peak of 3.2 ppm. MR-spectroscopy-based studies have shown that pathologically proven malignant lesions contain a significantly greater amount of choline than adjacent tissue.^{17–19} MR spectroscopy, therefore, has the potential to provide a noninvasive method for evaluating the malignant potential of tumors.

Another novel imaging strategy, termed BLADE (Siemens Healthcare, Malvern, PA) or PROPELLER (GE Healthcare, Buckinghamshire, United Kingdom), has been shown to be effective in reducing a variety of artifacts. This imaging sequence is performed by oversampling the central part of k-space; in conjunction with high-resolution 3.0-T imaging, it is useful for reducing various forms of artifact, especially those caused by motion. It has been shown to be superior to the TSE sequence when applied to T2-weighted images where motion or other forms of artifact are a concern.^{20,21} However, because the acquisition time is typically longer and the TEs are constrained, this technique is not compatible with all pulse sequences (Fig. 10.9).

■ MRI in the Presence of Metallic Implants

Susceptibility artifacts from metallic spinal implants have historically limited the usefulness of MRI in the postoperative setting. Although radiography, conventional myelography, and nuclear medicine studies are

accessible and cost-effective, these imaging modalities have limited sensitivity and specificity for common postoperative clinical questions. With adjustments to routine pulse sequences, MRI can be a tool for the evaluation of postoperative conditions, with improved visualization of periprosthetic tissues.

Metallic objects cause local magnetic field distortions, which lead to varying degrees of misregistration and characteristic artifacts that are worsened at higher magnetic field strengths. Titanium and tantalum implants create substantially less artifact than does stainless steel.^{22,23} Appropriate patient positioning and imaging protocols can dramatically reduce such artifacts; for example, such artifacts are reduced when the long axis of a metallic object is parallel to the long axis of the magnet. Metallic interference with the local magnetic field limits the usefulness of fat-suppression techniques; STIR sequences avoid this problem and are preferred for generating T2-weighted images.²⁴ Additionally, FSE/TSE sequences are typically less susceptible to metallic artifacts than are conventional SE techniques.²⁵ Smaller fields of view also help to limit the influence of metallic objects.²⁶

View angle tilting and slice encoding for metal artifact correction are two novel sequence acquisition schemes that can reduce metal artifact within MR imaging.²⁷ View angle tilting is typically implemented into a TSE sequence and can compensate for in-plane distortions by applying an additional readout gradient along the slice-selective direction. As a consequence of using two separate effects, view angle tilting may cause blurring of the image. Using

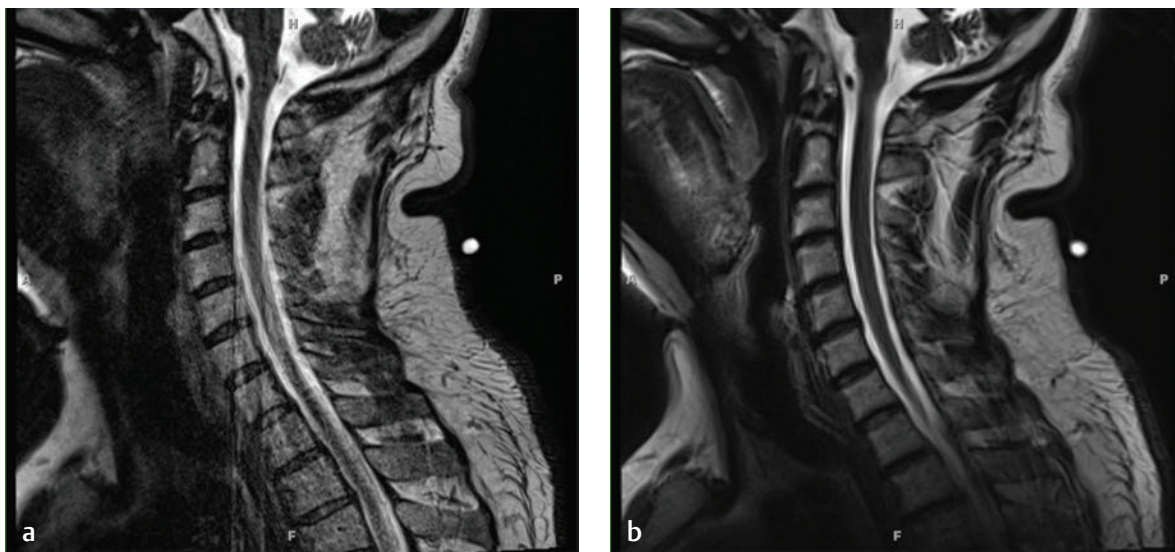


Fig. 10.9 Motion artifact in the cervical spine on sagittal T2-weighted images using 3.0-T MRI in the (a) TSE versus (b) BLADE (Siemens Healthcare) sequences. Motion artifact is substantially reduced as a result of using the BLADE sequence.

high resolution and thin slices may reduce the image blurring that can be seen with view angle tilting. Slice encoding for metal artifact correction is also based on a 2D TSE sequence with an additional encoding dimension applied to correct through-plane distortions. This technique is similar to a 3D scan in that each slice is also phase-encoded in the third dimension. Although slice encoding for metal artifact correction can reduce through-plane artifact, this technique is time-consuming and thus may not be appropriate for routine MRI examinations.

The diagnostic accuracy of metallic artifact reduction sequences compared with that of conventional MRI techniques is well established. Artifact reduction sequences are particularly important for imaging the spine, where key findings are routinely missed without appropriate imaging protocols.^{28,29} MRI serves as an extremely useful problem-solving technique in the presence of metallic hardware, particularly when clinical suspicion is high and radiography is negative or equivocal (**Fig. 10.10**).

■ MRI-Guided Interventions

The use of MRI for image-guided musculoskeletal interventions has increased in popularity over the past several years. The number and types of MRI-

guided interventions have increased and likely will continue to do so.³⁰⁻³² Current applications include the following:

- Musculoskeletal lesion biopsy procedures³²
- Cryoablation procedures³³
- Pain management techniques, such as sacroiliac joint injections, discography, transforaminal epidural injection, selective nerve block, sympathetic block, celiac plexus block, and facet joint cryotherapy neurotomies^{30,31}

Musculoskeletal Biopsy

MRI is a useful imaging technique for musculoskeletal lesion biopsy because of its excellent depiction of bone and soft-tissue pathology.^{32,33} It is particularly helpful for the following:

- Lesions adjacent to critical structures best seen with MRI (**Fig. 10.11**)
- Lesions for which characterization of the internal composition, such as a region of necrosis, is important in terms of obtaining a diagnostic specimen^{32,33}

In many respects, open interventional MRI systems offer many of the advantages of ultrasound and CT, such as ultrasound's real-time visualization of tissue and CT's excellent visualization of bone.³⁴

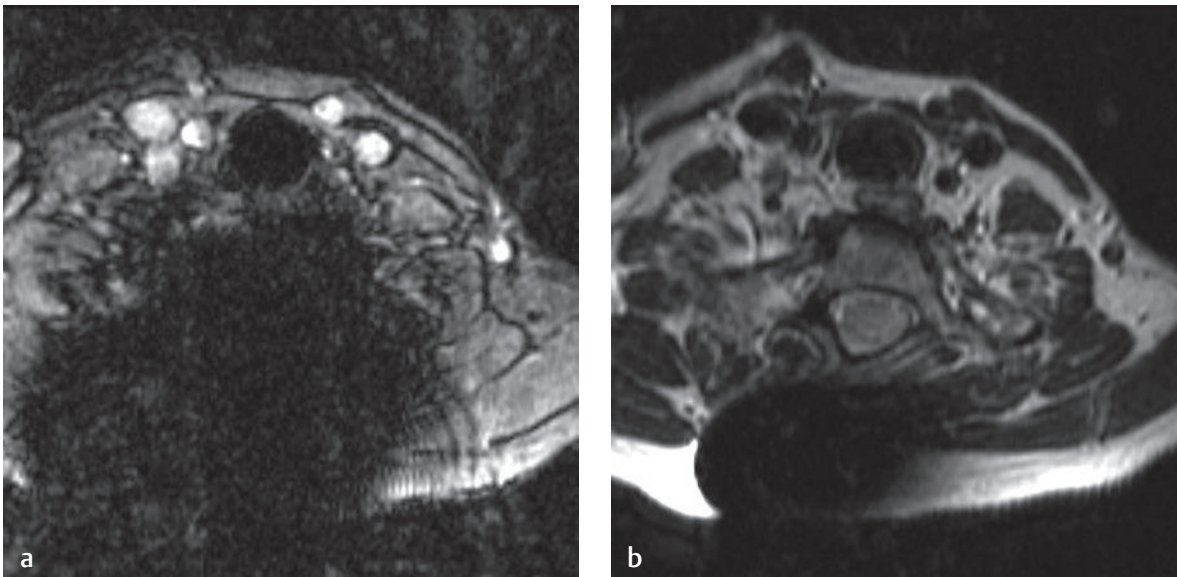


Fig. 10.10 MRI in the presence of metallic implants. This patient had posterior spinal fixation at the T1 vertebral level. **(a)** An axial gradient-echo T2*-weighted image (a T2-like image [bright fluid] created with a gradient-echo rather than a SE technique) shows a large signal void obscuring the spinal canal. **(b)** An axial T2-weighted image with FSE/TSE technique at the same level in the same patient during the same imaging examination minimizes the susceptibility artifact from the metallic implants and substantially reduces the signal void so that the spinal canal contents are visible.[†]

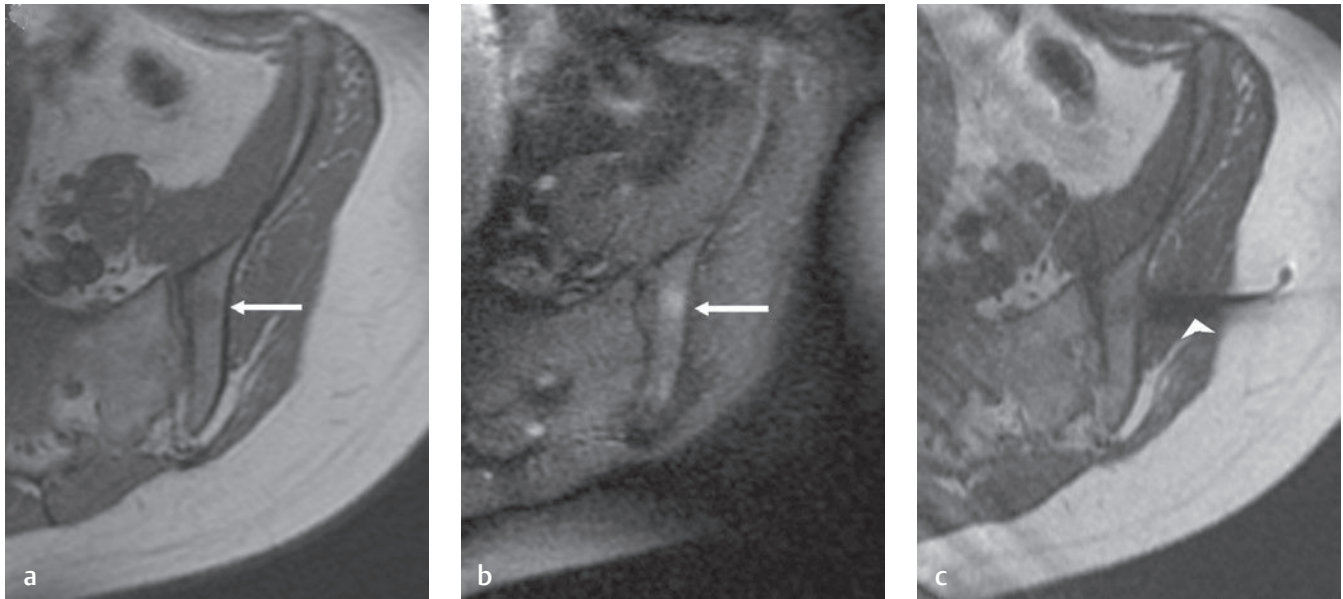


Fig. 10.11 Interventional MRI biopsy. This 38-year-old pregnant woman at 23 weeks of gestation who had a history of breast cancer presented with left hip pain. The preprocedure axial **(a)** T1-weighted FSE and **(b)** STIR images both show a small lesion (<1 cm) in the left ilium (*arrow* on each). **(c)** An intraprocedural axial T1-weighted FSE image with the patient in the right lateral decubitus position shows the trephine needle (*arrowhead*) positioned on the cortex at the level of the lesion. The specimen showed metastatic breast cancer.[†]

Cryotherapy

MR-guided cryotherapy of soft-tissue and bone metastases has been shown to be a safe and effective technique, and it can provide excellent local tumor control and pain relief in the appropriate clinical setting.³³ The efficacy of MR-guided cryotherapy is based on the fact that MRI is sensitive to temperature changes within tissue and that cryoablated tissue is easily recognized (and approximates tissue death) on standard MRI pulse sequences. Cryoablated tissue produces a signal void on standard pulse sequences and has been referred to as an *ice ball*³³ (**Fig. 10.12**). MRI-guided percutaneous cryotherapy reduces morbidity by using a percutaneous approach, and it offers the advantage of estimating the volume of tissue ablation during the procedure.³³

Pain Management

MR-guided interventions have also been shown to be safe and effective when used for numerous pain management techniques, including the following:

- Sacroiliac joint injections
- Discography
- Transforaminal epidural injection
- Selective nerve block
- Sympathetic block
- Celiac plexus block
- Facet joint cryotherapy neurotomies^{30,31}

The excellent depiction of soft-tissue structures provides a distinct advantage when isolating nerves and facet joints for injections.

Summary

Advanced MR imaging includes equipment and techniques that have become increasingly helpful in diagnosing and treating spinal pathologies. Higher resolution spinal imaging and increased imaging speed are now possible as 3.0-T MRI becomes more widely available. 3.0-T MRI has also facilitated the introduction and utilization of other advanced MRI techniques.

Advanced MRI techniques that help increase the speed of spinal imaging include parallel imaging techniques, which use spatial information inherent in the elements of an RF coil array to enable a reduction in the number of time-consuming, phase-encoded steps required during a typical scan. This increased imaging speed is further improved with the use of 3.0-T MRI.

Advanced MRI equipment, such as intraoperative MRI and open-bore MRI, has also contributed to improved spinal interventions. More complex spinal procedures have been facilitated by the introduction of intraoperative MRI. Open-bore MRI can accommodate larger patients, can reduce claustrophobia, enables functional or dynamic imaging, and offers

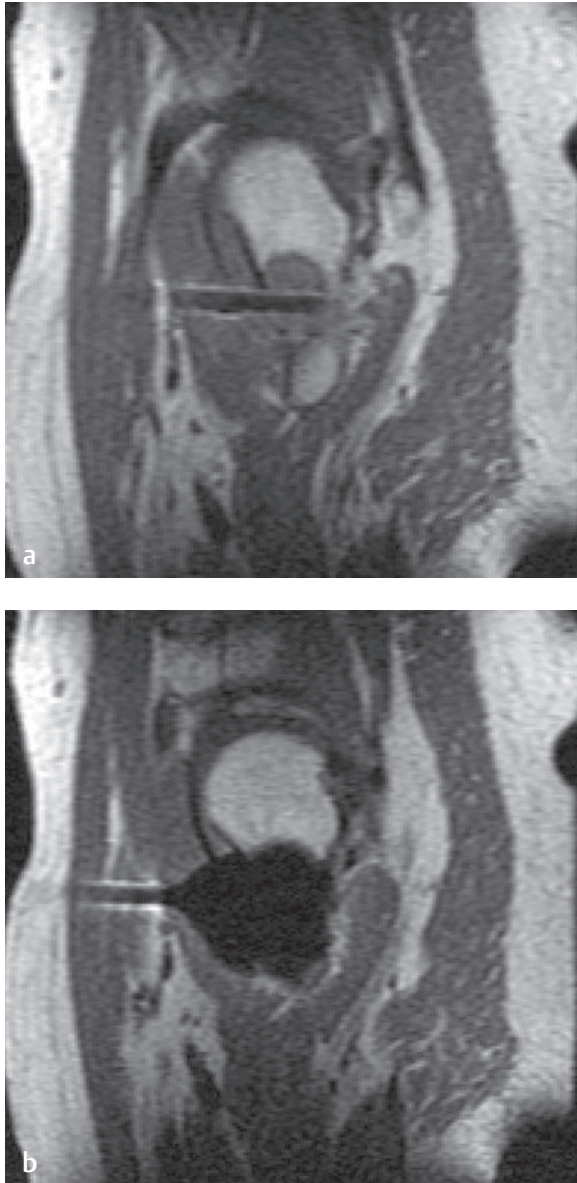


Fig. 10.12 Interventional MRI: cryotherapy. This 50-year-old man had renal cell carcinoma metastatic to the proximal right femur. **(a)** A sagittal T1-weighted image shows a cryotherapy needle in the hypointense metastasis in the region of the right lesser trochanter. **(b)** A sagittal T1-weighted image shows an elliptical signal void of the ice ball, representing the treatment zone. Critical structures avoided were the femoral nerve, femoral vessels, and iliopsoas tendon attachment.[†]

numerous positioning options such as simulated weight bearing and upright positions.

In addition to the parallel imaging techniques previously mentioned, other advanced MRI techniques include novel pulse sequences. MR spectroscopy is a novel pulse sequence that may provide a

noninvasive method for evaluating the malignant potential of spinal tumors. Other novel pulse sequences have effectively reduced artifact from motion (BLADE or PROPELLER) or metallic spinal implants (view angle tilting or slice encoding for metal artifact correction).

Finally, MRI-guided interventions are advanced spinal techniques with diagnostic and therapeutic applications such as musculoskeletal lesion biopsy procedures, cryoablation procedures, and pain management techniques, including sacroiliac joint injections, discography, transforaminal injections, selective nerve and sympathetic blocks, and facet joint cryotherapy neurotomies.

COMMON CLINICAL QUESTIONS

1. Clinically, 3.0-T MRI provides twice the intrinsic signal-to-noise ratio of 1.5-T MRI. True or false?
2. Parallel imaging provides what advantages over conventional MR imaging techniques?
 - A. Increased resolution
 - B. Decreased metal artifact
 - C. Increased imaging speed
 - D. Decreased motion artifact
3. All of the following are options for positioning during spinal MR imaging, except which one?
 - A. Supine
 - B. Supine with axial loading (simulated weight bearing)
 - C. Seated
 - D. Prone
 - E. Standing upright positions
4. Studies of MR spectroscopy have shown that pathologically proven malignant lesions contain significantly greater amounts of choline than adjacent tissue. True or false?
5. Which of the following implant materials creates the most metal artifact during MRI?
 - A. Titanium
 - B. Stainless steel
 - C. Tantalum
 - D. Ceramic
6. All of the following are MRI-guided interventions, except which one?
 - A. Musculoskeletal lesion biopsy
 - B. RF ablation procedures
 - C. Pain management procedures
 - D. Cryoablation procedures

References

- Ramnath RR. 3T MR imaging of the musculoskeletal system (Part I): considerations, coils, and challenges. *Magn Reson Imaging Clin N Am* 2006;14(1):27–40 PubMed
- Takahashi M, Uematsu H, Hatabu H. MR imaging at high magnetic fields. *Eur J Radiol* 2003;46(1):45–52 PubMed
- Tanenbaum LN. Clinical 3T MR imaging: mastering the challenges. *Magn Reson Imaging Clin N Am* 2006;14(1):1–15 PubMed
- Rodegerdts EA, Boss A, Riemarzik K, et al. 3D imaging of the whole spine at 3T compared to 1.5T: initial experiences. *Acta Radiol* 2006;47(5):488–493 PubMed
- Wiesinger F, Van de Moortele PF, Adriany G, De Zanche N, Ugurbil K, Pruessmann KP. Potential and feasibility of parallel MRI at high field. *NMR Biomed* 2006;19(3):368–378 PubMed
- Siemens Medical. Siemens True-Form Magnet and Gradient Design. Available at http://www.medical.siemens.com/siemens/it_IT/gg_mr_FBAs/files/brochures/skyra_brochures/110927_TrueForm_Magnet_Gradient_design_brochure_FINAL.pdf. Accessed on April 29, 2013
- Lewin JS, Nour SG, Meyers ML, et al. Intraoperative MRI with a rotating, tiltable surgical table: a time-use study and clinical results in 122 patients. *AJR Am J Roentgenol* 2007;189(5):1096–1103 PubMed
- Jolesz FA. Future perspectives for intraoperative MRI. *Neurosurg Clin N Am* 2005;16(1):201–213 PubMed
- DynaWell. Simulate upright position in CT and MRI using the DynaWell L-spine compression device. Available at <http://www.dynawell.biz>. Accessed on April 29, 2013
- Wipro GE. Healthcare. Signa SP/i 0.5T. Available at <http://www.gehealthcare.com/in/en/rad/mri/products/spi/index.html>. Accessed on March 28, 2007
- Fonar Corporation. The upright MRI. Available at <http://www.fonar.com/standup.htm>. Accessed on March 28, 2007
- Shellock FG. Functional assessment of the joints using kinematic magnetic resonance imaging. *Semin Musculoskelet Radiol* 2003;7(4):249–276 PubMed
- Maas M, Akkerman EM, Venema HW, Stoker J, Den Heeten GJ. Dixon quantitative chemical shift MRI for bone marrow evaluation in the lumbar spine: a reproducibility study in healthy volunteers. *J Comput Assist Tomogr* 2001;25(5):691–697 PubMed
- Maas M, van Kuijk C, Stoker J, et al. Quantification of bone involvement in Gaucher disease: MR imaging bone marrow burden score as an alternative to Dixon quantitative chemical shift MR imaging—initial experience. *Radiology* 2003;229(2):554–561 PubMed
- Baur A, Stäbler A, Brüning R, et al. Diffusion-weighted MR imaging of bone marrow: differentiation of benign versus pathologic compression fractures. *Radiology* 1998;207(2):349–356 PubMed
- Aboagye EO, Bhujwala ZM. Malignant transformation alters membrane choline phospholipid metabolism of human mammary epithelial cells. *Cancer Res* 1999;59(1):80–84 PubMed
- Fayad LM, Bluemke DA, McCarthy EF, Weber KL, Barker PB, Jacobs MA. Musculoskeletal tumors: use of proton MR spectroscopic imaging for characterization. *J Magn Reson Imaging* 2006;23(1):23–28 PubMed
- Subhawong TK, Wang X, Durand DJ, et al. Proton MR spectroscopy in metabolic assessment of musculoskeletal lesions. *AJR Am J Roentgenol* 2012;198(1):162–172 PubMed
- Wang CK, Li CW, Hsieh TJ, Chien SH, Liu GC, Tsai KB. Characterization of bone and soft-tissue tumors with in vivo ¹H MR spectroscopy: initial results. *Radiology* 2004;232(2):599–605 PubMed
- Dietrich TJ, Ulbrich EJ, Zanetti M, Fucentese SF, Pfirrmann CWA. PROPELLER technique to improve image quality of MRI of the shoulder. *AJR Am J Roentgenol* 2011;197(6):W1093–1100 PubMed
- Fellner C, Menzel C, Fellner FA, et al. BLADE in sagittal T2-weighted MR imaging of the cervical spine. *AJNR Am J Neuroradiol* 2010;31(4):674–681 PubMed
- Burtscher IM, Owman T, Romner B, Ståhlberg F, Holtås S. Aneurysm clip MR artifacts. Titanium versus stainless steel and influence of imaging parameters. *Acta Radiol* 1998;39(1):70–76 PubMed
- Wang JC, Yu WD, Sandhu HS, Tam V, Delamarter RB. A comparison of magnetic resonance and computed tomographic image quality after the implantation of tantalum and titanium spinal instrumentation. *Spine (Phila PA 1976)* 1998;23(15):1684–1688 PubMed
- Viano AM, Gronemeyer SA, Haliloglu M, Hoffer FA. Improved MR imaging for patients with metallic implants. *Magn Reson Imaging* 2000;18(3):287–295 PubMed
- Guerhazi A, Miaux Y, Zaim S, Peterfy CG, White D, Genant HK. Metallic artefacts in MR imaging: effects of main field orientation and strength. *Clin Radiol* 2003;58(4):322–328 PubMed
- Lee MJ, Kim S, Lee SA, et al. Overcoming artifacts from metallic orthopedic implants at high-field-strength MR imaging and multi-detector CT. *Radiographics* 2007;27(3):791–803 PubMed
- Ai T, Padua A, Goerner F, et al. SEMAC-VAT and MSVAT-SPACE sequence strategies for metal artifact reduction in 1.5T magnetic resonance imaging. *Invest Radiol* 2012;47(5):267–276 PubMed
- Rudisch A, Kremser C, Peer S, Kathrein A, Judmaier W, Daniaux H. Metallic artifacts in magnetic resonance imaging of patients with spinal fusion. A comparison of implant materials and imaging sequences. *Spine (Phila PA 1976)* 1998;23(6):692–699 PubMed
- Tartaglino LM, Flanders AE, Vinitski S, Friedman DP. Metallic artifacts on MR images of the postoperative spine: reduction with fast spin-echo techniques. *Radiology* 1994;190(2):565–569 PubMed
- Carrino JA, Blanco R. Magnetic resonance—guided musculoskeletal interventional radiology. *Semin Musculoskelet Radiol* 2006;10(2):159–173 PubMed
- Carrino JA, Jolesz FA. MRI-guided interventions. *Acad Radiol* 2005;12(9):1063–1064 PubMed
- Carrino JA, Khurana B, Ready JE, Silverman SG, Winalski CS. Magnetic resonance imaging—guided percutaneous biopsy of musculoskeletal lesions. *J Bone Joint Surg Am* 2007;89(10):2179–2187 PubMed
- Tuncali K, Morrison PR, Winalski CS, et al. MRI-guided percutaneous cryotherapy for soft-tissue and bone metastases: initial experience. *AJR Am J Roentgenol* 2007;189(1):232–239 PubMed
- Silverman SG, Collick BD, Figueira MR, et al. Interactive MR-guided biopsy in an open-configuration MR imaging system. *Radiology* 1995;197(1):175–181 PubMed

ANSWERS TO COMMON CLINICAL QUESTIONS

1. False.
Explanation: Although 3.0-T MRI *theoretically* provides twice the intrinsic signal-to-noise ratio of 1.5-T MRI, the actual or clinically applicable signal-to-noise ratio is limited by FDA-mandated power-monitoring systems to reduce the risk of RF burns.
2. C
Explanation: Parallel imaging increases the MRI speed by using spatial information that is inherent in the RF coil array to reduce the number of phase-encoded steps required during a scan, which can be a time-consuming step during conventional MR imaging.
3. D
Explanation: Prone positioning is not a typical positioning option during spinal MRI because of the inherent decline in pulmonary function experienced by most patients while lying prone for extended periods of time.
4. True
Explanation: MR spectroscopy has the potential to provide a noninvasive method for evaluating the malignant potential of tumors because of its ability to differentiate malignant lesions from normal adjacent tissues based on the choline content.
5. B
Explanation: Because stainless steel is a ferromagnetic material, it produces more metallic artifact with MRI than do titanium and tantalum. Ceramic is a nonmetallic substance.
6. B
Explanation: RF ablation procedures are not MRI-guided interventions because these procedures require the use of equipment that is not MRI-compatible.

11 Correlation of MRI with Other Imaging Studies

Shivani Ahlawat, Uma Srikumaran, A. Jay Khanna, and Laura M. Fayad

CHAPTER OUTLINE

- I. MRI
- II. Conventional Radiography
- III. CT
- IV. Myelography, CT Myelography
- V. Discography
- VI. Nuclear Scintigraphy
- VII. PET
- VIII. Summary

Although the preceding chapters have focused on MRI of the spine, it is important for the clinician to recognize that other imaging modalities play an important role in the evaluation of patients with spine disorders. These other commonly used imaging modalities include conventional radiography, CT, nuclear scintigraphy, and PET. Discography, conventional radiographic myelography, and CT myelography are less commonly used because of the wide availability and contrast resolution of MRI. When the clinician is evaluating the patient for a particular disease process, a basic understanding of the strengths and weaknesses of these modalities is important in deciding which imaging study to request and evaluate for the patient. For many patients, one or more imaging modalities will be superior to MRI alone. In addition, after the patient has been evaluated with an MRI study, the other imaging modalities may provide additional anatomic or physiologic information that can help narrow the differential diagnosis and guide treatment.

■ MRI

MRI provides excellent visualization of the tissues in the musculoskeletal system in multiple planes because of its high contrast resolution compared with

other modalities. One of its major advantages is that the multiple pulse sequences (see Chapter 1, Essentials of MRI Physics and Pulse Sequences) enable the detection of soft-tissue and bone-marrow abnormalities with great sensitivity (**Fig. 11.1**). In general terms, an MRI study is often obtained to evaluate the water content of tissues because most acute and subacute abnormalities result in free extracellular fluid. MR pulse sequences use the magnetization and relaxation properties of protons to assess and differentiate various tissue types. Tissues that contain large amounts of water (e.g., CSF) are bright on fluid-sensitive sequences, and tissues that contain small amounts of water (e.g., cortical bone) are dark on all pulse sequences. Structures that contain little or no water are not well assessed by MRI. For example, the lung volume has a large proportion of air; therefore, although MRI is an advanced technique, it is rarely, if ever, used for the evaluation of tumors and other abnormalities of the lung parenchyma. Cortical bone also has a low water content, and therefore MRI is relatively limited (compared with CT, for example) for the evaluation of cortical osseous structures. The preceding chapters discuss specific indications for MRI and the conditions that can be effectively evaluated using this imaging modality.

■ Conventional Radiography

As most clinicians have learned throughout their training, conventional radiographs are often the initial step in the evaluation of a patient who has (or is suspected of having) a spine disorder. Conventional radiographs are obtained via the use of ionizing irradiation. The radiation beam is attenuated by structures between the image intensifier and the film cassette. Structures with high density (e.g., cortical bone, metallic implants) block a larger amount of the radiation and thus leave a white region on the film. Structures with lower density (e.g., air, subcutaneous

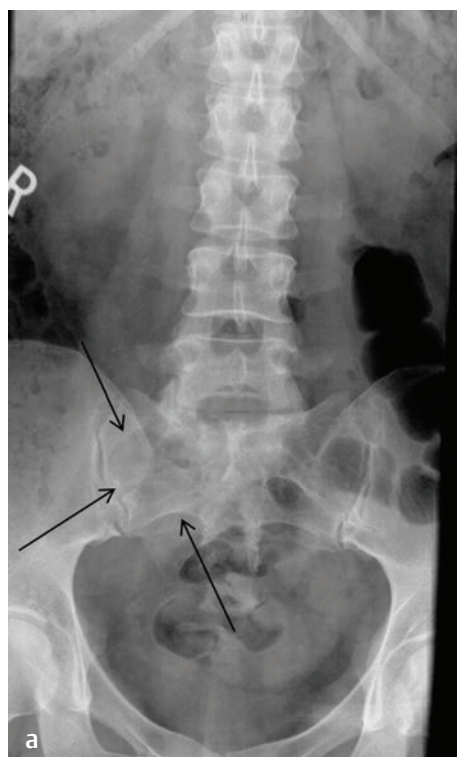
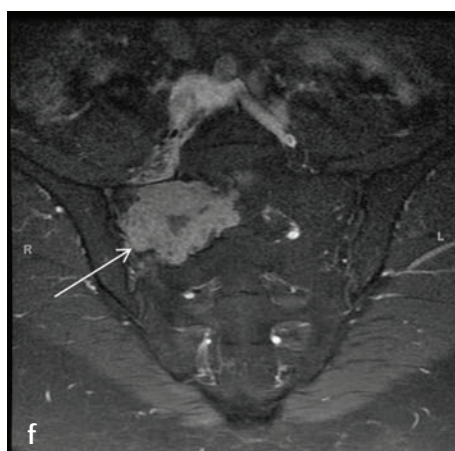
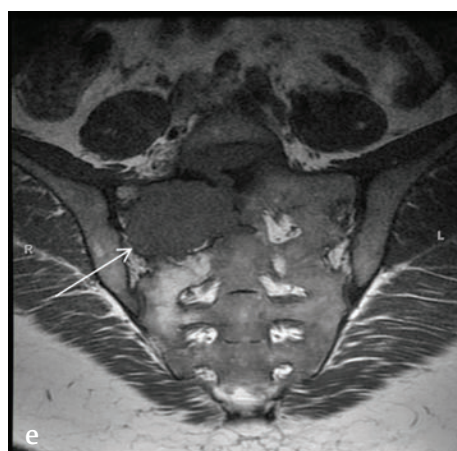
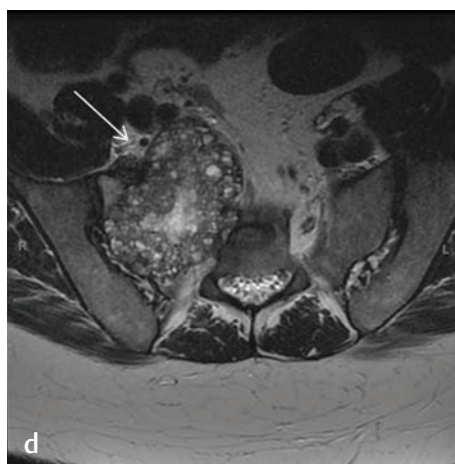
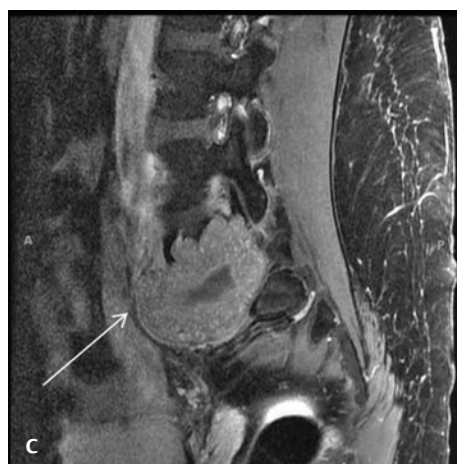
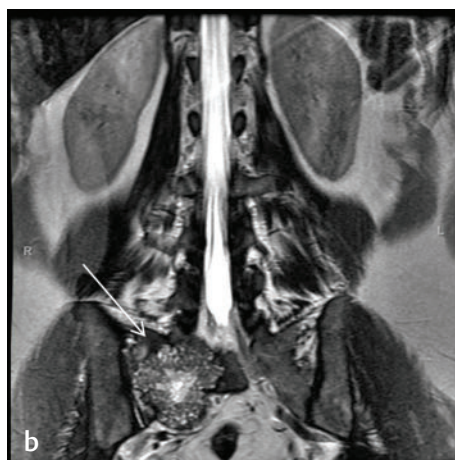


Fig. 11.1 MRI: excellent soft-tissue contrast. **(a)** This AP radiograph of the lumbar spine was obtained in a young patient for the evaluation of pain. The subtle lytic lesion in the right hemisacrum (*arrows*) can be difficult to differentiate from adjacent bowel loops. **(b–d)** The patient had a subsequent MRI study that showed a large soft-tissue mass (*arrow on each*) with fluid–fluid levels extending into the presacral tissues and sparing the spinal canal. **(e)** Axial precontrast and **(f)** postcontrast T1-weighted images with fat saturation reveal the enhancing soft-tissue component (*arrow on each*).



tissues) block less radiation and thus leave a dark or gray region on the film.

Conventional radiographs are easily available and are good for the evaluation of osseous detail. This modality is also exceptionally time- and cost-effective. The large field of view enables the study of glob-

al deformities, for example, in a patient with a spine deformity such as scoliosis or kyphosis (**Fig. 11.2**). On the other hand, conventional radiographs do not provide optimal visualization of the soft-tissue structures such as ligaments, intervertebral discs, and the spinal cord. Radiographs are also less

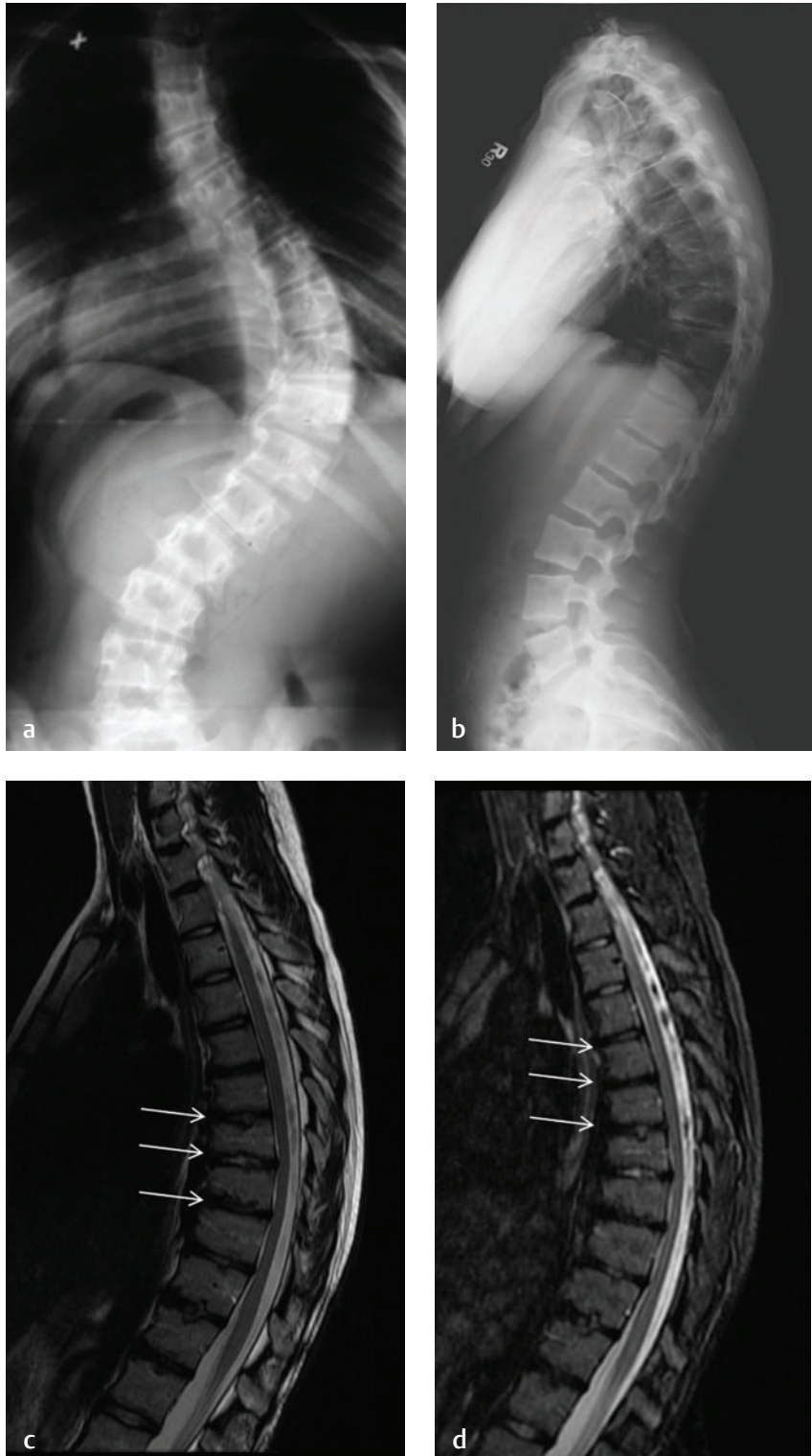


Fig. 11.2 Conventional radiographs: visualization of local and global deformity. **(a)** A PA radiograph of the spine shows a large right thoracic scoliosis. **(b)** A lateral radiograph of the spine of another patient shows subtle increased mid-thoracic kyphosis and end-plate irregularities. Because of pain, an MRI study, including sagittal **(c)** T2-weighted and **(d)** STIR images, of the thoracic spine was obtained, which better delineated end-plate irregularities and multilevel disc desiccation and herniation (arrows on each) in this young patient, consistent with Scheuermann disease.

sensitive than CT or MRI for the evaluation of osseous destruction and involvement of the bone marrow. As an example, a 30% decrease in bone mass is often required before osteoporosis can be appreciated on radiographs.^{1,2} Conventional radiography is often the study of choice for the initial evaluation of a patient with a traumatic injury of the spine. However, conventional radiographs are less valuable in the evaluation of a patient with low back pain, neck pain, or spinal stenosis.

Conventional radiographs are also extremely useful for the preoperative evaluation of patients undergoing spine surgery. For example, preoperative radiographs facilitate evaluation of spinal alignment and localization of the level of abnormality. This information can then be correlated with intraoperative radiographs or fluoroscopy to confirm the operative level, hardware placement, and deformity correction. In the absence of red flags such as recent trauma, osteoporosis, or age >70 years, conventional radio-

graphs also play a role in the initial evaluation of back or neck pain. Additional evaluation or advanced imaging is warranted if there is clinical suspicion of malignancy or infection.^{3,4} Radiographs have a role in evaluation of alignment, instability, and scoliosis and in the postoperative evaluation of instrumentation and fusion (**Fig. 11.3**).

Flexion and extension radiography is often used to assess dynamic spinal stability; MR and CT imaging are typically performed with the patient in the supine position (**Fig. 11.4**).

By flexion-extension radiography, the prevalence of unstable ligamentous injury in trauma patients has been estimated at 0.9%; however, by MRI, one investigation reported a much higher estimated prevalence of 23%.⁵ Because MRI does not directly assess stability, the implications for structural integrity of the spine remain unknown.⁵ The limitations of flexion and extension radiography include incomplete or ambiguous findings in many patients.^{6,7}

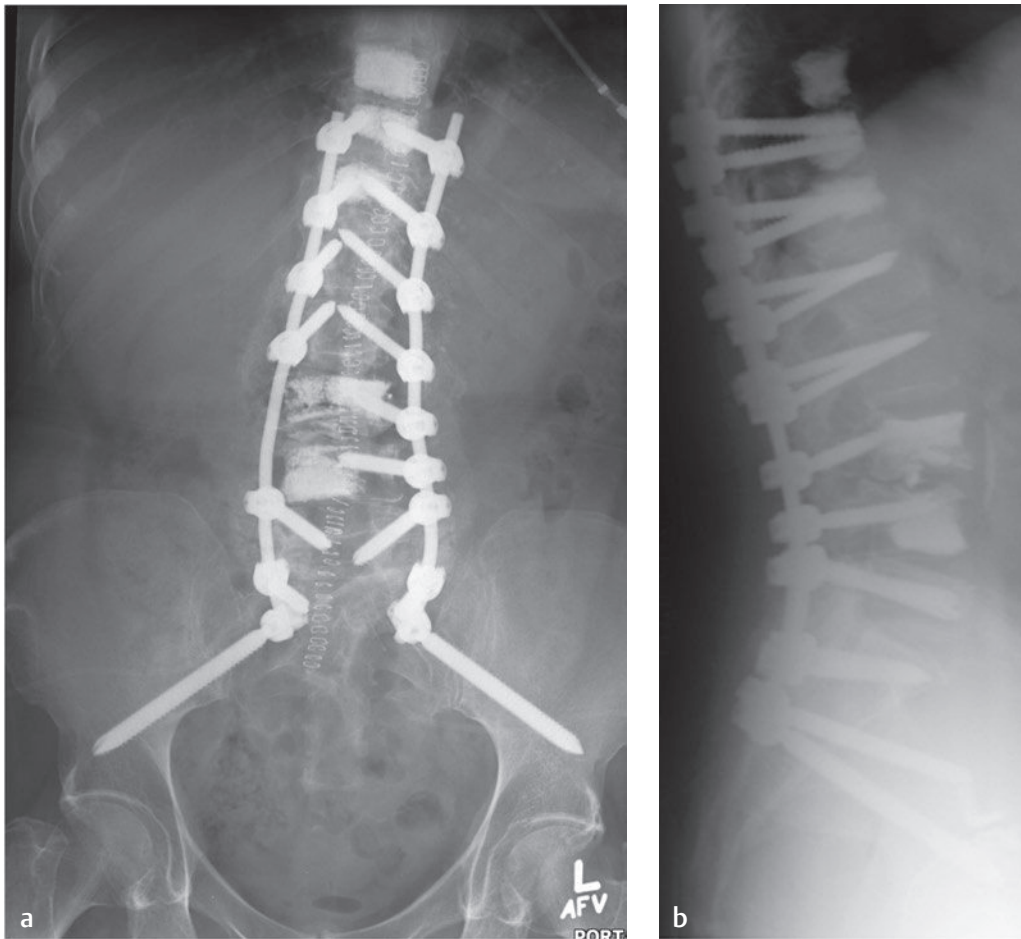


Fig. 11.3 Conventional radiographs of a patient with a history of osteoporosis who underwent revision surgery for thoracolumbar scoliosis and stenosis. **(a)** AP and **(b)** lateral images show an instrumented fusion from T11 to the pelvis with screw augmentation with polymethylmethacrylate cement at the T11 and T12 levels and prophylactic vertebroplasty at the T10 level. The vertebroplasties at the L3 and L4 levels had been performed previously.

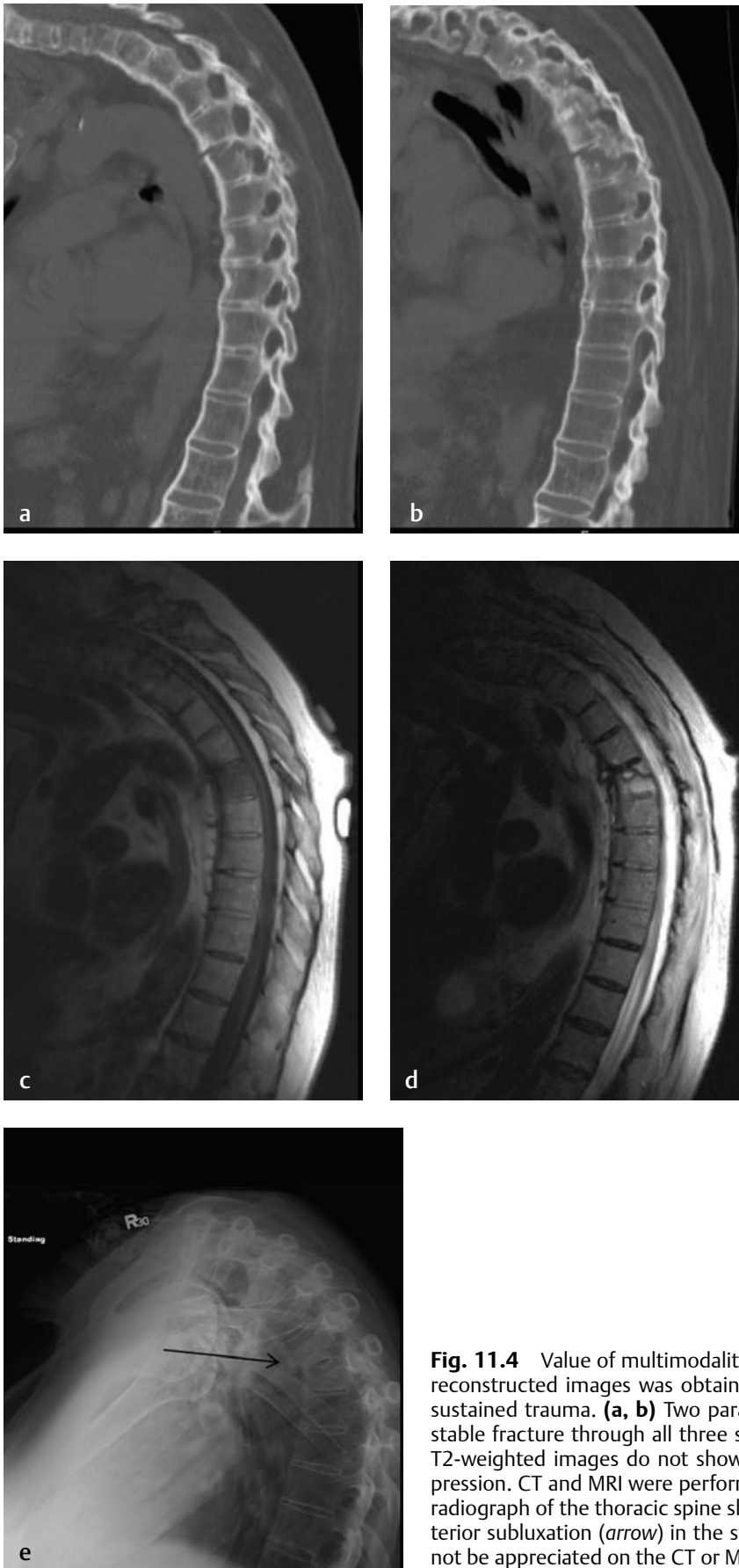


Fig. 11.4 Value of multimodality imaging. Noncontrast CT imaging with sagittal reconstructed images was obtained in a patient with ankylosing spondylitis who sustained trauma. **(a, b)** Two parasagittal reconstructed CT images show the unstable fracture through all three spinal columns. **(c)** Sagittal T1-weighted and **(d)** T2-weighted images do not show epidural hemorrhage, cord contusion, or compression. CT and MRI were performed in the supine position. **(e)** A standing lateral radiograph of the thoracic spine shows the unstable nature of the fracture with anterior subluxation (arrow) in the standing position; the dynamic component could not be appreciated on the CT or MR images.

Furthermore, flexion and extension radiographs do not facilitate treatment and may lead to increased cost and prolonged cervical immobilization.⁷ Many recommend that MRI should be used whenever the integrity of ligaments is in question and that flexion and extension radiography may be useful in evaluating potential ligamentous injury in patients who have equivocal MRI examinations. These radiographic techniques would be most appropriate when the MRI has shown abnormal signal in spinal ligaments without definite disruption.

■ CT

CT images, which are acquired based on principles similar to those used for conventional radiography, can be considered multiplanar high-resolution conventional radiography because the radiation is transmitted through the patient in multiple planes, which permits the acquisition of a large-volume dataset. Unlike conventional radiography, in which the images are acquired in one plane, this dataset can be manipulated using computer software algorithms to provide images in any plane. In addition, current-generation multidetector CT scanning devices allow for the acquisition of very large volumes of data in incredibly small amounts of time (for example, 10 seconds or less), a particularly valuable asset in the pediatric and trauma patient populations.³

With regard to its use for patients with known or suspected spine pathology, CT is most valuable in the assessment of osseous detail. CT is also useful for characterizing osseous abnormalities in areas where the use of conventional radiography is less reliable, such as the OCJ, cervicothoracic junction, sacrum, and pelvis. Although CT does not provide physiologic information about the status of the various tissues (except for limited cases in which an intravenous contrast is used), it does provide excellent spatial resolution (**Fig. 11.5**). This modality is particularly useful for imaging the axial skeleton and for evaluating the extent of osseous lesions.^{8–10} With the development of multiplanar 3D reconstructions, CT imaging provides additional guidance in preoperative planning, fracture assessment and classification, and the evaluation of complex deformities.^{11,12} Although CT images provide excellent osseous detail and can precisely localize fracture extent and fragmentation (information that can guide operative intervention), as a general rule, they do not provide high enough contrast resolution for optimal evaluation of the soft tissues, such as ligaments.⁸

CT has a dominant role in the setting of spine trauma, particularly in unconscious, intubated patients. CT has a much higher sensitivity and speci-

ficity than lateral radiographs in evaluating unstable cervical spine injuries.¹³ CT with multiplanar reformatted sagittal and coronal planes is useful for depicting osseous structural problems such as spondylolysis, fracture, scoliosis, and stenosis and for the postsurgical evaluation of bone graft integrity, surgical fusion, and instrumentation placement.¹⁴ CT can also assist in preoperative planning for surgical procedures, including those in conjunction with image guidance systems, which are now gaining more widespread adoption.

Future directions for CT include dual-energy CT imaging.¹⁵ Dual-energy CT systems are equipped with two X-ray tubes, enabling simultaneous acquisition at two different energy levels; therefore, they can extract information and characterize the chemical composition of material according to the differential X-ray photon energy-dependent attenuation of the compounds being examined at the two different energy levels.

■ Myelography, CT Myelography

Conventional myelography was the mainstay of lumbar herniated disc diagnosis for decades. It is now usually combined with postmyelography CT. The combined study is complementary to conventional CT or MRI and is occasionally more accurate in diagnosing disc herniation, but it suffers the disadvantage of requiring lumbar puncture and intrathecal contrast injection.^{16–19} Other disadvantages include risk of bleeding, headache, nausea, allergy, and decreased seizure threshold. Conventional myelography may, however, also be useful in surgical planning, especially for patients who have contraindications to MRI, such as patients with nerve stimulators or pacemakers.

■ Discography

Discography may have a role in localizing the source of back pain that is indeterminate by less invasive studies and in clarifying the diagnosis for patients with multifocal abnormalities on MRI.²⁰ Although radiographs, MRI, and postinjection CT images may depict nonspecific aging or degenerative changes, the injection itself may reproduce or provoke the patient's pain, which may have diagnostic value. Limitations include the necessity of disc space injections, variability of patient response, and limited specificity.^{21–23} A recent correlative MRI and discography study found Modic type-1 signal intensity changes on MRI to have a high positive predictive value in the identification of a pain generator at

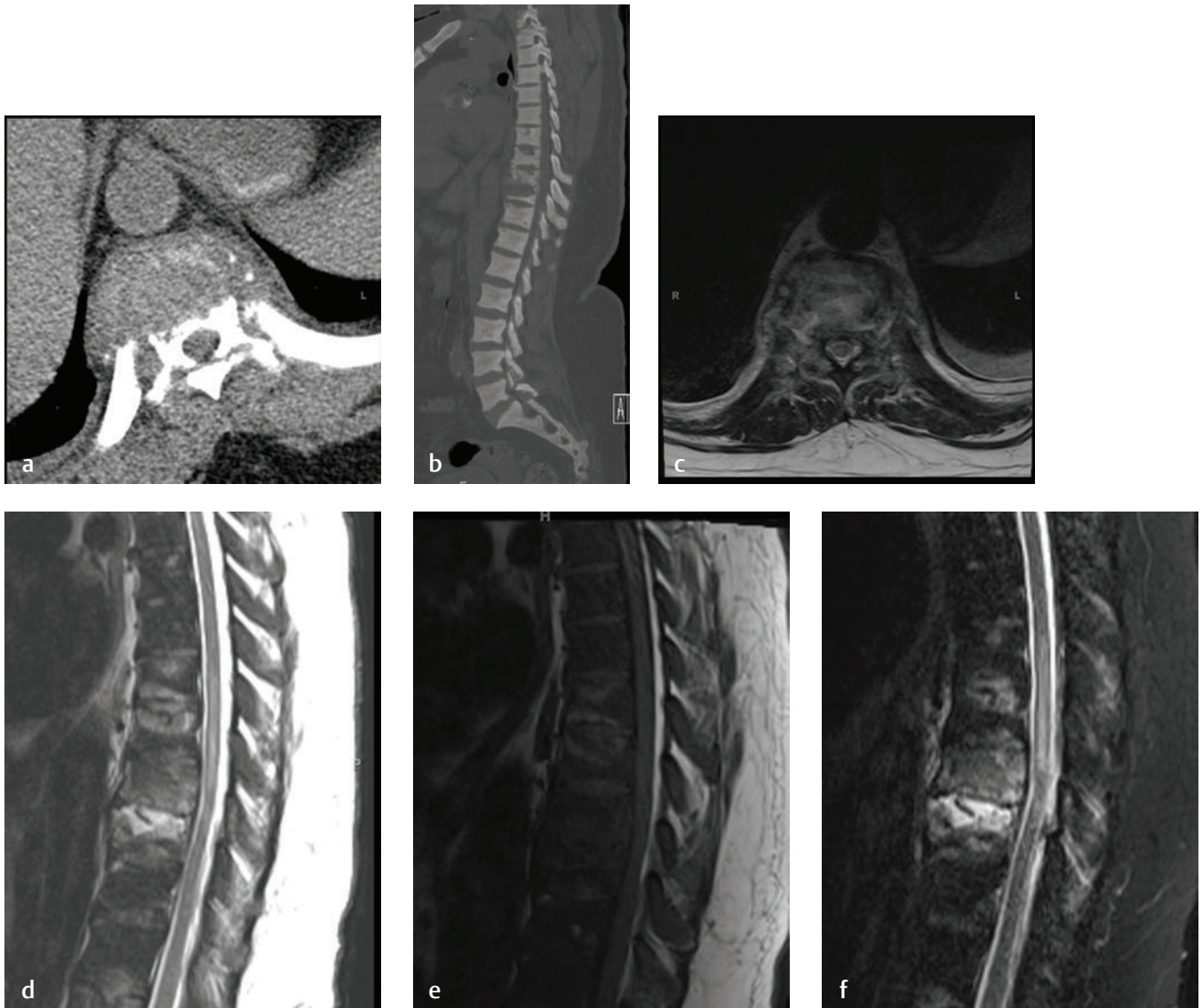


Fig. 11.5 CT: evaluation of axial skeleton. Noncontrast CT was obtained in a patient on hemodialysis with septicemia and acute onset bilateral lower extremity paralysis. Initial radiographs were not helpful because of the patient's body habitus. **(a)** An axial CT image in a soft-tissue window reveals a paravertebral soft-tissue mass. **(b)** A sagittal CT image shows diffuse spine sclerosis with end-plate destruction in the lower thoracic spine. The constellation of clinical and imaging findings suggested discitis and osteomyelitis. **(c)** An axial T2-weighted image shows bilateral paravertebral extension, whereas **(d)** the sagittal T2-weighted image shows intramedullary cord edema in addition to frank fluid signal in the affected intervertebral disc space. **(e)** A sagittal T1-weighted image shows diffusely hypointense or dark vertebral bodies, whereas **(f)** the sagittal STIR image accentuates the fluid signal in the affected intervertebral disc. The constellation of findings suggested a diagnosis of infection. The patient underwent percutaneous CT-guided biopsy, which confirmed discitis and osteomyelitis.

discography.²⁴ Of note, a recent 10-year matched cohort study by Carragee et al²⁵ examined disc degeneration in patients with and without baseline discography. Those authors showed that discography resulted in accelerated disc degeneration, new disc herniation, disc height loss, and intervertebral desiccation over a 10-year follow-up compared with matched controls. They advised careful risk-benefit analysis before recommending disc puncture for diagnostic purposes.²⁵

■ Nuclear Scintigraphy

Although the foregoing imaging studies all provide excellent anatomic information, they are relatively limited in their abilities to provide high-quality physiologic information, specifically information related to bone turnover. In this regard, the imaging modality of choice is three-phase bone scintigraphy. For a bone scan, the patient is injected with technetium-99m

phosphate or another radiopharmaceutical agent that emits gamma rays. Subsequently, the patient is placed under a scintillation camera to detect the presence and distribution of the radiotracer activity. The typical three-phase bone scan acquires the radiotracer activity information in the following phases:

- Angiographic phase
- Blood-pool phase
- Delayed or bone phase

Each of these phases provides different information. In the angiographic phase, increased uptake is found in areas of mature blood vessels. The second (soft-tissue) or blood-pool phase shows areas of neovascularity, such as with acute inflammation or vascular neoplasms. In the delayed or bone phase, the radiotracer has had time to adsorb to newly formed crystals at the site of bone turnover.^{26,27}

The advantages of bone scans are that they provide physiologic information regarding bone (more specifically, mineral turnover) and have the capability of surveying the entire body and detecting lesions early in their course. Their disadvantages are that the images are nonspecific and provide very poor spatial and anatomic resolution. Thus, the general thought is that with a bone scan, one is trading the anatomic detail provided by other imaging studies for physiologic information regarding the metabolic activity in the bone. Fortunately, in this era, systems have been developed that, in combination with CT scanning, allow functional metabolic imaging and anatomic location to occur simultaneously. The indications for scintigraphy include evaluation of osseous lesions, usually metastatic disease, benign and malignant primary tumors, metabolic disorders, infection, and vertebral compression fractures.^{26,28–30} Specifically, different findings in the phases of a three-phase bone scan can help differentiate a patient with osteomyelitis from one with soft-tissue infection without osseous involvement.^{29,31}

In the setting of osteomyelitis, conventional radiographs are the initial study of choice, but additional imaging modalities are often required for a definitive diagnosis because osteomyelitis is not detectable by radiography until ~40% bone destruction has occurred. MRI and nuclear scintigraphy can provide greater diagnostic sensitivity and specificity: MRI is exquisitely sensitive to the presence of bone-marrow edema, can show associated soft-tissue involvement, and is considered the imaging modality of choice for

the early detection of osteomyelitis. Nuclear scintigraphy has an advantage in that it can quickly reveal other areas of involvement, a particularly important advantage for the pediatric patient, who may have multiple sites of infection.³¹ It is important to note that when bone turnover is exceptionally high, such as in a patient with multiple myeloma and other lytic processes, conventional bone scan techniques may result in false-negative findings.^{32,33}

Nuclear scintigraphy can also be used to help determine the age or physiologic activity of vertebral compression and other fractures^{34–36} (**Fig. 11.6**). In such cases, nuclear scintigraphy may be indicated in patients for whom MRI is contraindicated, such as those with claustrophobia or non-MRI-compatible pacemakers and defibrillators. The bone scan is a moderately sensitive test for detecting the presence of tumor, infection, and occult fractures of the vertebrae but not for specifying the diagnosis.

■ PET

As does nuclear scintigraphy, PET facilitates the evaluation of the physiologic activity in the tissues, in this case, glucose metabolism. Specifically, the patient is injected with a marker, ¹⁸F-FDG, which emits (ultimately) gamma rays and is concentrated in tissues based on the rate of glucose metabolism. The most common indication for positron emission scanning is for the evaluation of malignant metastases or tumor recurrence (**Fig. 11.7**).^{37,38} Based on a meta-analysis comparing ¹⁸F-FDG PET to CT, MRI, and bone scan for the diagnosis of bone metastases, ¹⁸F-FDG PET had a sensitivity (approaching 90%) similar to that of MRI on a per-lesion and per-patient basis.³⁹ An additional retrospective study compared MRI with ¹⁸F-FDG-PET/CT in the differential diagnosis of benign and malignant vertebral compression fractures and found that, when MRI findings are equivocal, ¹⁸F-FDG-PET/CT can be considered as an adjunctive diagnostic method for differentiating malignant and benign spine compression fractures.⁴⁰ In comparison with MRI, ¹⁸F-FDG-PET/CT showed slightly higher sensitivity and lower specificity.⁴⁰ The combined technique of PET and CT has been advocated for use in diagnostically difficult cases of adolescent back pain.⁴¹ The strength of this technique lies in the combination and correlation of functional data with the anatomic data.

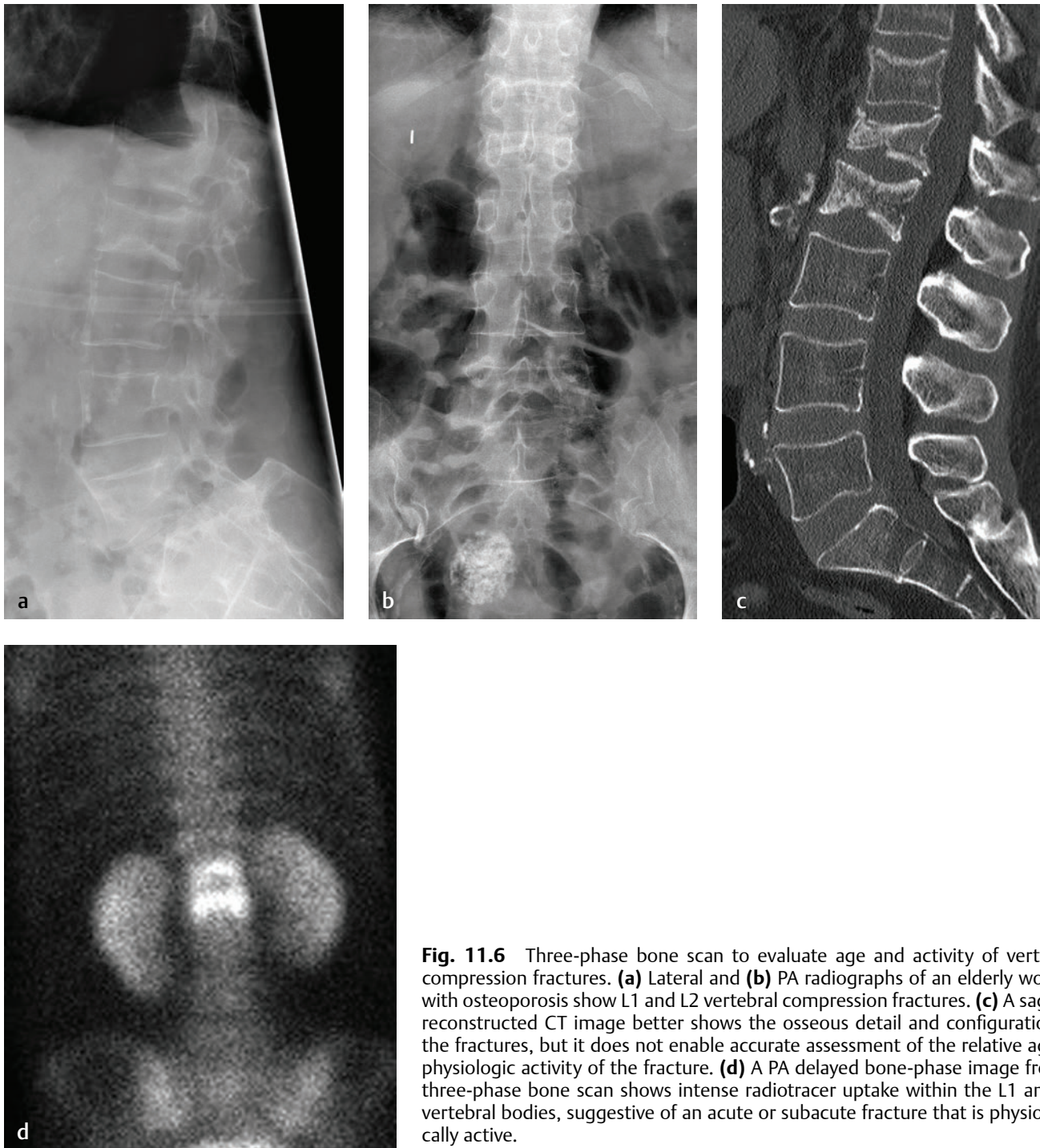


Fig. 11.6 Three-phase bone scan to evaluate age and activity of vertebral compression fractures. **(a)** Lateral and **(b)** PA radiographs of an elderly woman with osteoporosis show L1 and L2 vertebral compression fractures. **(c)** A sagittal reconstructed CT image better shows the osseous detail and configuration of the fractures, but it does not enable accurate assessment of the relative age or physiologic activity of the fracture. **(d)** A PA delayed bone-phase image from a three-phase bone scan shows intense radiotracer uptake within the L1 and L2 vertebral bodies, suggestive of an acute or subacute fracture that is physiologically active.

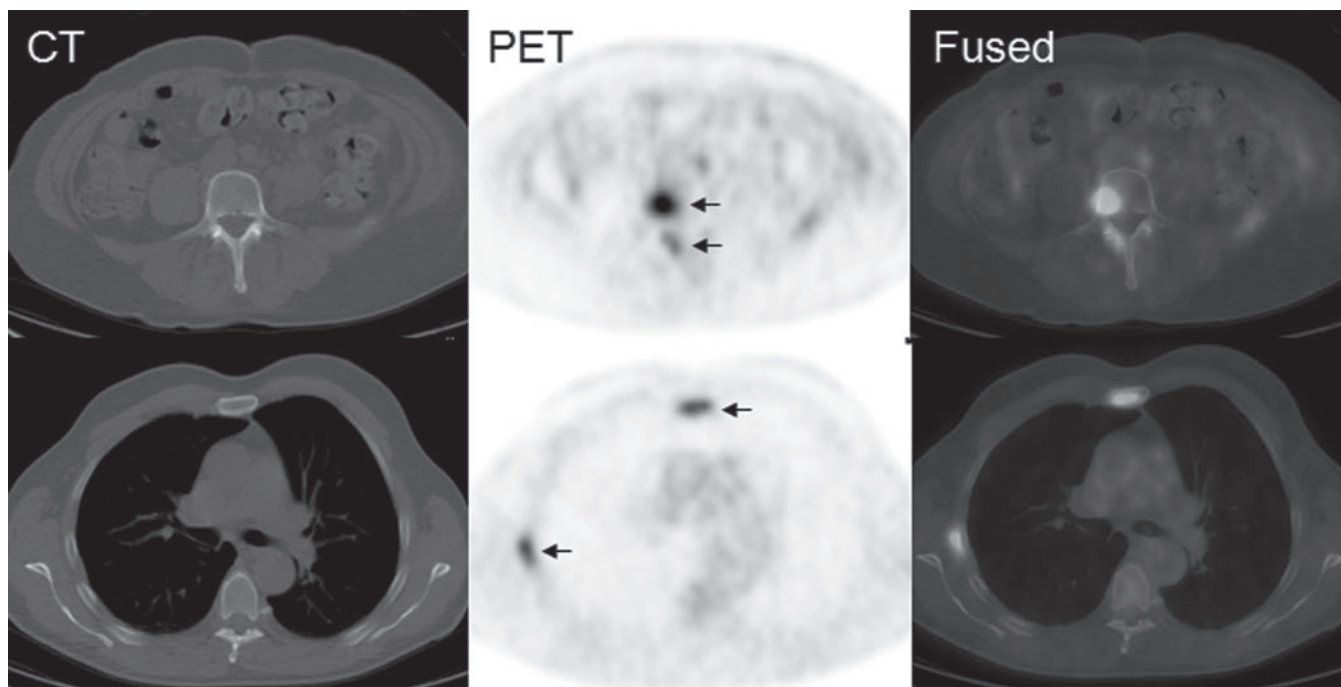


Fig. 11.7 A 50-year-old man had bladder transitional cell carcinoma. This PET/CT image shows foci of intense fluorodeoxyglucose activity fusing a lumbar vertebra and pedicle, the sternum, and a right rib (*arrows*). Despite the lack of abnormality on the corresponding CT image, these findings are most consistent with osseous metastases.[†]

■ Summary

For the appropriate evaluation of a patient with musculoskeletal disease, it is important for clinicians to use all of the imaging tools and modalities in their armamentarium. Efficacy, cost, availability, and patient limitations all play roles in imaging modality selection. In most cases, most of the

clinically important information can be obtained with conventional radiographs and MRI. However, for selected patients, the clinician must make the decision to request other imaging studies, such as CT, nuclear scintigraphy, and PET, as they are indicated. With time, one can expect improvements in technology and the development of new imaging modalities that can be integrated into diagnosis and treatment algorithms.

COMMON CLINICAL QUESTIONS

1. Which of the following is an ideal modality for initial follow-up of a postoperative patient who has undergone a lumbar decompression and posterior spinal fusion with instrumentation?
 - A. CT
 - B. MRI
 - C. Conventional radiography
 - D. PET/CT scan
2. CT is the best imaging modality for the evaluation of patients with known or suspected spinal neoplasms. True or false?
3. Which of the following is an ideal modality in the assessment of spinal stenosis in a patient who cannot undergo MRI?
 - A. Radiography
 - B. Conventional myelography
 - C. CT myelography
 - D. Discography
4. Which of the following is an ideal modality for initial diagnostic assessment of an obtunded patient in the setting of trauma?
 - A. Radiography
 - B. Flexion-extension radiography
 - C. MRI
 - D. CT
5. What is the most common indication for PET imaging in patients with known or suspected spinal pathology?
 - A. Evaluation of isthmic spondylolisthesis
 - B. Evaluation of infection
 - C. Evaluation of status of fusion
 - D. Evaluation of malignant metastases or tumor recurrence
 - E. Evaluation of degree of osteoporosis

References

1. Kamholtz R, Sze G. Current imaging in spinal metastatic disease. *Semin Oncol* 1991;18(2):158–169 PubMed
2. Steinbach HL. The roentgen appearance of osteoporosis. *Radiol Clin North Am* 1964;2:191–207 PubMed
3. Agency for Health Care Policy and Research. Acute low back problems in adults: assessment and treatment. *Clin Pract Guidel Quick Ref Guide Clin* 1994;(14):iii–iv, 1–25 PubMed
4. State of Florida Agency for Health Care Administration. Universe of Florida Patients with Low Back Pain or Injury: Medical Practice Guidelines. Tallahassee, FL: State of Florida Agency for Health Care Administration; 1996
5. Sliker CW, Mirvis SE, Shanmuganathan K. Assessing cervical spine stability in obtunded blunt trauma patients: review of medical literature. *Radiology* 2005;234(3):733–739 PubMed
6. Duane TM, Cross J, Scarcella N, et al. Flexion-extension cervical spine plain films compared with MRI in the diagnosis of ligamentous injury. *Am Surg* 2010;76(6):595–598 PubMed
7. Duane TM, Scarcella N, Cross J, et al. Do flexion extension plain films facilitate treatment after trauma? *Am Surg* 2010;76(12):1351–1354 PubMed
8. Fayad LM, Bluemke DA, Fishman EK. Musculoskeletal imaging with computed tomography and magnetic resonance imaging: when is computed tomography the study of choice? *Curr Probl Diagn Radiol* 2005;34(6):220–237 PubMed
9. Fayad LM, Johnson P, Fishman EK. Multidetector CT of musculoskeletal disease in the pediatric patient: principles, techniques, and clinical applications. *Radiographics* 2005;25(3):603–618 PubMed
10. Genant HK, Wilson JS, Bovill EG, Brunelle FO, Murray WR, Rodrigo JJ. Computed tomography of the musculoskeletal system. *J Bone Joint Surg Am* 1980;62(7):1088–1101 PubMed
11. Geijer M, El-Khoury GY. MDCT in the evaluation of skeletal trauma: principles, protocols, and clinical applications. *Emerg Radiol* 2006;13(1):7–18 PubMed
12. Wilson JS, Korobkin M, Genant HK, Bovill EG Jr. Computed tomography of musculoskeletal disorders. *AJR Am J Roentgenol* 1978;131(1):55–61 PubMed
13. Brohi K, Healy M, Fotheringham T, et al. Helical computed tomographic scanning for the evaluation of the cervi-

- cal spine in the unconscious, intubated trauma patient. *J Trauma* 2005;58(5):897–901 PubMed
14. Williams AL, Gornet MF, Burkus JK. CT evaluation of lumbar interbody fusion: current concepts. *AJNR Am J Neuroradiol* 2005;26(8):2057–2066 PubMed
 15. Nicolaou S, Liang T, Murphy DT, Korzan JR, Ouellette H, Munk P. Dual-energy CT: a promising new technique for assessment of the musculoskeletal system. *AJR Am J Roentgenol* 2012;199(5, Suppl):S78–S86 PubMed
 16. Jackson RP, Cain JE Jr, Jacobs RR, Cooper BR, McManus GE. The neuroradiographic diagnosis of lumbar herniated nucleus pulposus: II. A comparison of computed tomography (CT), myelography, CT-myelography, and magnetic resonance imaging. *Spine (Phila Pa 1976)* 1989;14(12):1362–1367
 17. Kent DL, Haynor DR, Larson EB, Deyo RA. Diagnosis of lumbar spinal stenosis in adults: a metaanalysis of the accuracy of CT, MR, and myelography. *AJR Am J Roentgenol* 1992;158(5):1135–1144 PubMed
 18. Modic MT, Masaryk T, Boumphrey F, Goormastic M, Bell G. Lumbar herniated disk disease and canal stenosis: prospective evaluation by surface coil MR, CT, and myelography. *AJR Am J Roentgenol* 1986;147(4):757–765 PubMed
 19. Shafaie FF, Wippold FJ II, Gado M, Pilgram TK, Riew KD. Comparison of computed tomography myelography and magnetic resonance imaging in the evaluation of cervical spondylotic myelopathy and radiculopathy. *Spine (Phila Pa 1976)* 1999;24(17):1781–1785
 20. Manchikanti L, Glaser SE, Wolfer L, Derby R, Cohen SP. Systematic review of lumbar discography as a diagnostic test for chronic low back pain. *Pain Physician* 2009;12(3):541–559 PubMed
 21. Carragee EJ, Lincoln T, Parmar VS, Alamin T. A gold standard evaluation of the “discogenic pain” diagnosis as determined by provocative discography. *Spine (Phila Pa 1976)* 2006;31(18):2115–2123
 22. Manchikanti L, Singh V, Pampati V, et al. Provocative discography in low back pain patients with or without somatization disorder: a randomized prospective evaluation. *Pain Physician* 2001;4(3):227–239 PubMed
 23. Shah RV, Everett CR, McKenzie-Brown AM, Sehgal N. Discography as a diagnostic test for spinal pain: a systematic and narrative review. *Pain Physician* 2005;8(2):187–209 PubMed
 24. Thompson KJ, Dagher AP, Eckel TS, Clark M, Reinig JW. Modic changes on MR images as studied with provocative diskography: clinical relevance—a retrospective study of 2457 disks. *Radiology* 2009;250(3):849–855 PubMed
 25. Carragee EJ, Don AS, Hurwitz EL, Cuellar JM, Carrino J, Herzog R. 2009 ISSLS Prize Winner: Does discography cause accelerated progression of degeneration changes in the lumbar disc: a ten-year matched cohort study. *Spine (Phila Pa 1976)* 2009;34(21):2338–2345
 26. Abdel-Dayem HM. The role of nuclear medicine in primary bone and soft tissue tumors. *Semin Nucl Med* 1997;27(4):355–363 PubMed
 27. Deutsch AL, Coel MN, Mink JH. Imaging of stress injuries to bone. Radiography, scintigraphy, and MR imaging. *Clin Sports Med* 1997;16(2):275–290 PubMed
 28. Alazraki NP. Radionuclide imaging in the evaluation of infections and inflammatory disease. *Radiol Clin North Am* 1993;31(4):783–794 PubMed
 29. El-Maghraby TAF, Moustafa HM, Pauwels EKJ. Nuclear medicine methods for evaluation of skeletal infection among other diagnostic modalities. *Q J Nucl Med Mol Imaging* 2006;50(3):167–192 PubMed
 30. Greenspan A, Stadalnik RC. A musculoskeletal radiologist's view of nuclear medicine. *Semin Nucl Med* 1997;27(4):372–385 PubMed
 31. Santiago Restrepo C, Giménez CR, McCarthy K. Imaging of osteomyelitis and musculoskeletal soft tissue infections: current concepts. *Rheum Dis Clin North Am* 2003;29(1):89–109 PubMed
 32. Ghanem N, Lohrmann C, Engelhardt M, et al. Whole-body MRI in the detection of bone marrow infiltration in patients with plasma cell neoplasms in comparison to the radiological skeletal survey. *Eur Radiol* 2006;16(5):1005–1014 PubMed
 33. Mulligan ME. Myeloma update. *Semin Musculoskelet Radiol* 2007;11(3):231–239 PubMed
 34. Fernandez-Ulloa M, Klostermeier TT, Lancaster KT. Orthopaedic nuclear medicine: the pelvis and hip. *Semin Nucl Med* 1998;28(1):25–40 PubMed
 35. Masala S, Schillaci O, Massari F, et al. MRI and bone scan imaging in the preoperative evaluation of painful vertebral fractures treated with vertebroplasty and kyphoplasty. *In Vivo* 2005;19(6):1055–1060 PubMed
 36. Maynard AS, Jensen ME, Schweickert PA, Marx WF, Short JG, Kallmes DF. Value of bone scan imaging in predicting pain relief from percutaneous vertebroplasty in osteoporotic vertebral fractures. *AJNR Am J Neuroradiol* 2000;21(10):1807–1812 PubMed
 37. Bastiaannet E, Groen H, Jager PL, et al. The value of FDG-PET in the detection, grading and response to therapy of soft tissue and bone sarcomas; a systematic review and meta-analysis. *Cancer Treat Rev* 2004;30(1):83–101 PubMed
 38. Feldman F, van Heertum R, Manos C. 18FDG PET scanning of benign and malignant musculoskeletal lesions. *Skeletal Radiol* 2003;32(4):201–208 PubMed
 39. Yang HL, Liu T, Wang XM, Xu Y, Deng SM. Diagnosis of bone metastases: a meta-analysis comparing ¹⁸FDG PET, CT, MRI and bone scintigraphy. *Eur Radiol* 2011;21(12):2604–2617 PubMed
 40. Cho WI, Chang UK. Comparison of MR imaging and FDG-PET/CT in the differential diagnosis of benign and malignant vertebral compression fractures. *J Neurosurg Spine* 2011;14(2):177–183 PubMed
 41. Ovadia D, Metser U, Lievshitz G, Yaniv M, Wientroub S, Even-Sapir E. Back pain in adolescents: assessment with integrated 18F-fluoride positron-emission tomography-computed tomography. *J Pediatr Orthop* 2007;27(1):90–93 PubMed

ANSWERS TO COMMON CLINICAL QUESTIONS

1. C
Explanation: The initial and routine follow-up of a patient who has undergone a lumbar decompression and instrumented fusion is best performed with conventional radiographs. This imaging modality enables the evaluation of instrumentation position, spinal alignment, and status of fusion. An MRI may be obtained if recurrent or residual neural compression is suspected, such as in the case of an epidural hematoma. A CT scan may allow for the optimal evaluation of the osseous structures and implant (such as pedicle screw) malposition.
2. False
Explanation: MRI is the best modality for the evaluation of patients with known or suspected spinal neoplasms because of its excellent ability to show contrast between soft-tissue structures such as neoplastic tissue, neural elements, and CSF.
3. C
Explanation: CT myelography is the ideal imaging modality for the assessment of spinal stenosis in a patient who cannot undergo MRI because the intrathecal contrast agent enables excellent depiction of the spinal canal and neural foramina and any spinal stenosis that may result from extradural compressive elements such as degenerative changes.
4. D
Explanation: CT is ideal for the initial evaluation of the obtunded patient in the setting of trauma because it is almost always immediately available and provides optimal evaluation of the osseous structures. If CT imaging is negative or there is concern for ligamentous injury, MRI can be obtained. Flexion-extension radiography should not be attempted in obtunded patients because of the potential for neurologic injury.
5. D
Explanation: The most common indication for positron emission scanning is the evaluation of malignant metastases or tumor recurrence. PET imaging facilitates the evaluation of the physiologic activity in the tissues, specifically glucose metabolism. Isthmic spondylolisthesis is best evaluated with single photon emission CT imaging. Spinal infections are best evaluated by MRI, often with gadolinium contrast enhancement. Fusion status is best evaluated by CT. The degree of osteoporosis is best evaluated by dual-energy X-ray absorptiometry scanning.

12 MRI Safety Considerations for the Referring Clinician

Monica D. Watkins and Bruce A. Wasserman

CHAPTER OUTLINE

- I. Physiologic Effects of the Magnetic Field
 - A. Static Magnetic Fields
 - B. Time-Varying Magnetic Fields
- II. Metallic Substances
 - A. Field Distortion
 - B. Metallic Objects in Magnetic Fields
 - C. Implant Safety Profiles
 - 1. Unsafe
 - 2. Conditionally Safe
 - 3. Safe Devices
 - D. Superficial Metal
 - E. External Metallic Objects
- III. Pregnancy
- IV. Contrast
 - A. Nephrogenic Systemic Fibrosis
 - B. Pregnancy and Contrast
 - C. Other Special Populations and Contrast
- V. Claustrophobia
- VI. Summary

The field of MRI continues to evolve, and as it does, so does the physician's understating of what can be done to maintain a standard of minimal risk for the patient. In an effort to improve diagnostic capabilities, clinicians investigate the use of magnets with higher field strengths but have to balance progress against any potential adverse biologic consequences. Rapid advances in the type and number of medical implant devices mandate increasing research to maintain MRI as a safe diagnostic procedure. In addition, judicious use of contrast media has become increasingly important to avoid potentially lethal consequences. Although the MRI center is usually responsible for safety screening, the referring physi-

cian can minimize the chance of an adverse effect by being aware of important contraindications to MRI and of safety concerns that might put an individual at risk. This chapter reviews these issues and provides guidelines for maximizing safety.

■ Physiologic Effects of the Magnetic Field

Within the MRI scanner, a patient is exposed to magnetic fields from two sources. The first is the baseline static magnetic field that aligns hydrogen atoms within the body. The second source comes from far weaker time-varying magnetic fields created by a RF field generator with receiver coils that rapidly switch on and off to identify the location of the hydrogen nuclei for generating images. The strength of these magnetic fields is measured in gauss (G) or tesla (T) units; 1 T equals 10,000 G. For comparison, the strength of the earth's magnetic field is 0.6 G.¹ The static magnetic field of a clinical MRI scanner generally ranges from 0.5 to 3.0 T, although there are human magnets up to 11.7 T in the research arena. The FDA has guidelines, last updated in 2010,² for the exposure of patients to static and time-varying magnetic fields.

Static Magnetic Fields

Currently, the FDA approves clinical imaging using a static magnetic field strength of up to 4.0 T for patients <1 month old and up to 8.0 T for older patients.² Many studies have evaluated the potential biologic effects of a static magnetic field, and there has been no clear evidence of deleterious effects.³ Although there have been concerns about an elevation of skin and core body temperatures induced by the magnetic field, investigators have concluded that harmful heating does not occur in human subjects.^{4,5}

Reversible electrocardiogram changes (e.g., an increase in the amplitude of the T wave or a nonspecific wave form) secondary to the conductive nature of blood have been noted with field strength up to 8 T.⁶

However, this “magnetohydrodynamic effect” has not been associated with a clinically adverse effect. Transient increase of systolic blood pressure by 3.6 mm Hg has been noted at 8 T in some patients.⁷

At strengths of 4 T, patients may experience transient reversible biologic effects, such as nausea (which may be caused by stimulation of the vestibulolabyrinthine complex) or a flashing light sensation (magnetophosphenes, thought to be caused by direct excitation of the optic nerves or retina, by changing magnetic fields, or by rapid eye movements).⁸

Time-Varying Magnetic Fields

Time-varying magnetic fields or gradient magnetic fields can induce current in the body, which can have two possible biologic effects: heating and neuromuscular stimulation. With significant exposure, body temperatures have been shown to rise, although tingling or tapping sensations and minor temperature changes (i.e., <0.6 degrees C) have been described.⁹ The FDA has suggested guidelines to limit the risk of these effects and ensure heat dissipation by restricting the strength of time-varying magnetic fields.² The intensity of the RF energy absorbed by tissue is termed the specific absorption rate and is measured in watts per kilogram. The FDA reports that specific absorption rates of ≤ 3 W/kg for the head, ≤ 4 W/kg (averaged) for the rest of the body, and ≤ 8.0 W/kg for any 1 g of tissue pose no substantial risk.² Usually, higher specific-absorption-rate exposures are a concern with faster pulse sequences.

■ Metallic Substances

Field Distortion

Image quality depends on the ability to maintain homogeneity of the magnetic field surrounding the patient. Metallic artifacts can result in misregistered spatial information or signal loss, leading to image distortion. Magnetic materials have an inherent ability to disturb the uniformity of magnetic fields used for imaging, thereby causing artifacts. The three types of magnetic materials—ferromagnetic, paramagnetic, and diamagnetic—differ in this ability and, thus, cause varying degrees of artifacts. Of these three, ferromagnetic materials (e.g., iron, nickel, and martensitic stainless steel) concentrate and retain magnetism the most, resulting in severe distortion of the images. Paramagnetic or weakly

ferromagnetic materials (e.g., platinum) have a minimal effect on magnetic field homogeneity and result in less image distortion. Diamagnetic materials (e.g., zinc, gold, and copper) do not affect or affect only minimally the static or local magnetic field homogeneity.

Metallic Objects in Magnetic Fields

The clinical value of an MRI examination in a patient with metallic hardware generally depends on the proximity of the hardware to the site of interest. For example, one can anticipate limited evaluation of neural foramina adjacent to an anterior cervical fusion or an inability to detect an epidural abscess adjacent to pedicle screw instrumentation. However, there are multiple techniques that can be applied to limit artifact during scanning. Myelography remains a viable alternative for the postoperative spine. CT also is a valuable alternative in postoperative patients, particularly in conjunction with myelography.

In addition to causing distortion of images, some metallic foreign bodies or surgical implants can move or generate heat in the presence of a magnetic field, possibly leading to injury or death.^{10,11} For this reason, each patient must be screened for metallic objects within the body, usually with a verbal interview and a written checklist.

Of particular concern are metallic foreign bodies within the orbit that may dislodge and rupture the globe or damage the optic nerve. To the authors' knowledge, there is only one reported case of a patient who suffered a vitreous hemorrhage, caused by a dislodged metal fragment (2.0×3.5 mm), that led to blindness.¹²

Although it is standard for MRI facilities to pre-screen for metallic orbital foreign bodies, methods of accomplishing this screening vary. Conventional radiographs of the orbits are said to detect metallic fragments as small as $0.1 \times 0.1 \times 0.1$ mm. However, there is debate over which patients should be referred for conventional radiographs. Many MRI centers obtain orbital radiographs of patients with an occupational history of welding, but some experts advocate obtaining them only if the patient is aware of a previous orbital exposure to metal without removal of the fragment by an ophthalmologist.¹³ At the authors' institutions, patients with a history of working with metal undergo screening orbital conventional radiographs. Alternatively, review of a previous CT scan, including the entirety of the orbits, is often considered sufficient.

In addition to assessing for orbital foreign bodies, the clinician should question the patient regarding any history of metallic foreign bodies such as bullet fragments, pellets, and shrapnel that could potentially move and cause local damage. Although most

tested ammunition is made from nonferrous material, it may have traces of ferromagnetic components, whereas most shrapnel is ferromagnetic.¹⁴ It is important to gain information as to whether these foreign bodies are near other vital structures, such as the lungs or spinal cord. For example, bullet fragments in the spinal canal in a patient without complete cord injury contraindicate MRI because they may be ferromagnetic.

Implant Safety Profiles

The FDA requires testing of all implants to evaluate their safety profiles and classify them as MRI unsafe, conditionally safe, or safe. The list of these devices is extensive and constantly changing, especially as more objects are tested at 3 T and higher, precluding a complete review of these devices in this chapter. A regularly updated list of reviewed implants and devices is available online at <http://www.MRIsafety.com>.

Unsafe

It is important to be aware of the devices that most commonly contraindicate MRI scanning, including the following:

- Implantable medication infusion pumps
- Ferromagnetic aneurysm clips (e.g., stainless steel)
- Pacemakers/implantable defibrillators
- Neurostimulation systems
- Brain stimulators
- Cochlear implants
- Spine/bone fusion stimulators
- Swan-Ganz thermodilution catheters
- Poppen-Blaylock carotid artery clamps
- Tissue expanders

Certain models of some of these devices, such as implantable cardiac defibrillators, cardiac pacemakers, neurostimulation systems, deep brain stimulators, spinal/bone fusion stimulators, and cochlear implants, have been developed specifically for MRI scanning or may be scanned under strict criteria on a case-by-case basis, taking into consideration the manufacturers' restrictions and the relative risk versus benefit of the study.^{15–21} An orchestrated effort between the referring specialist and radiologist might be needed with informed consent of the patient.

Of note, the Starr-Edwards Model Pre-6000 heart valve prosthesis (Baxter Healthcare, Santa Ana, CA) is now designated as conditionally MRI safe, although previously it was thought to be an absolute contraindication to an MRI examination.²²

In the past, residual epicardial pacing wires were also considered to be a contraindication to MRI. However, the current consensus is that such patients may undergo MRI if the wires are cut short (flush with skin) and there are no loops of wire outside the patient. Again, consultation with the patient's cardiologist may be necessary.²³ Retained intracardiac pacing leads remain a contraindication.²⁴

Programmable cerebral spinal shunt valves may need to be reset after MRI scanning. In general, external and implantable insulin pumps should be removed before entering the scanner.

Conditionally Safe

Devices that are conditionally safe for MRI are implants that may be scanned if certain guidelines are satisfied. These devices include weakly magnetic intravascular filters, stents, and coils. MRI of patients with such devices may require a waiting period of 6 to 8 weeks after implantation to ensure that movement of the device caused by the magnetic field does not disturb its implantation onto the vessel wall.^{25,26} The evolving list of all such devices is beyond the scope of this chapter, but in general, one should acquire additional information (e.g., brand name of the device and date of implantation) for patients who have undergone recent placement of such devices. Most MRI centers require documentation of this information before scanning is allowed.

Safe Devices

Devices that are safe for MRI are those known to produce no clinically significant hazard in the MRI environment. In general, these devices have no electronically or magnetically activated components, are made from a nonferromagnetic material (such as titanium or nitinol), and may undergo MRI scanning at ≤ 1.5 T immediately after implantation.^{27,28} Many of these devices have been tested in the 3-T environment. It is important to obtain the brand name of the device from patients (who may have the package insert) or from their records. Furthermore, it is helpful for the surgeon to provide the patient with a written record of the device name so the patient can present this information at the time of a scan and avoid delays and unnecessary cancellations if this information is otherwise inaccessible to the MRI technologists. Safe devices also include orthopedic implants firmly placed within the bone because, although they may be weakly magnetic, they do not dislodge or generate substantial heat.

Superficial Metal

There are safety concerns not only with internal metallic devices but also with skin surface metal, such as medicine patches containing a metal foil, surgical staples, tattoos, or permanent cosmetics that could cause skin burns. It is standard practice to remove transdermal medicine patches containing metallic foil at the time of an MRI. Tope and Shellock²⁹ reviewed the results of a questionnaire given to 1032 patients with cosmetic tattoos. Only two patients experienced any sensory consequences (i.e., “slight tingling” or a “burning” sensation). These sensations are thought to be caused by heating from iron oxide or other metal-based pigment. The FDA Center for Food Safety and Applied Nutrition, Office of Cosmetics and Colors fact sheet states, “The risks of avoiding an MRI when your doctor has recommended one are likely to be much greater than the risk of complications from the interaction between the MRI and tattoo or permanent makeup.”³⁰ Most practices agree that an ice pack or cold compress can be applied during scanning to the site of the tattoo, permanent cosmetics, or surgical staples to reduce the chance of thermal injury.

External Metallic Objects

In addition to precautions about internal foreign bodies, MRI centers screen for external metallic devices that may become projectiles in the MRI suite. Injuries and death have occurred when large metallic objects, such as a ferrous oxygen tank, have been brought into the MRI suite.^{31–33} Even small objects that may not seem dangerous to many patients, such as jewelry or hairpins, can become projectiles and cause injury. It is standard procedure to ask patients to remove such objects and to empty their pockets.

Pregnancy

There have long been theoretical concerns that the electromagnetic fields of MRI could disrupt cell division at any stage of pregnancy. Because cell division is more rapid in the first trimester, scanning at this time bears a greater potential risk. However, the current consensus of the American College of Radiology is that “no special consideration is recommended for the first, versus any other trimester in pregnancy.”¹⁷ MRI during pregnancy continues to be obtained on a case-by-case basis, weighing the risk and benefit for each examination. The American College of Radiology outlines that the radiologist should confer with the referring physician and document that:

“1. The information requested from the MR study cannot be acquired by means of nonionizing means (e.g., ultrasonography); 2. The data is needed to potentially affect the care of the patient or fetus during the pregnancy; 3. The referring physician believes that it is not prudent to wait until the patient is no longer pregnant to obtain this data.”¹⁷ In almost all institutions, written, informed consent is obtained.

Contrast

MRI contrast agents are often used in the postoperative patient to evaluate for infection or scar tissue, in patients with known or suspected spinal tumors, and for MR angiography of the carotid and peripheral arteries. The gadolinium ion contains seven unpaired electrons in the outer shell, providing a large magnetic moment. This paramagnetic property enhances the relaxation rates of nearby water protons. Although gadolinium itself is toxic, chelation with other substances makes it nontoxic and usable as a contrast agent. Over time, within the body, the free gadolinium ion can dissociate from its chelate. Normally, the amount of free ions is low because of rapid clearance through the kidney.

In addition to screening for the specific populations listed in the following paragraphs, it is important to obtain a patient’s allergy history, especially with regard to whether the patient had a reaction to gadolinium contrast previously and, if so, the nature of that reaction. A history of a mild reaction (such as hives) to gadolinium generally requires premedication with prednisone and diphenhydramine. A history of reactions as severe as respiratory or circulatory compromise is a contraindication to the use of MRI contrast. An adverse reaction to MRI contrast is rare and generally expected to occur in <1% of patients.³⁴ Reactions range from headache to weakness and, very rarely, anaphylaxis.³⁴

Clinicians and radiologists are often faced with the decision to give gadolinium contrast to a patient with a history of an allergy to ionic contrast agents, such as those used for CT. Studies have shown that patients with a history of an ionic contrast allergy are at a higher risk for a reaction, as are those with asthma and multiple medication allergies.^{34,35} Often, MRI centers will require consent from such patients before giving contrast, and some centers may require that the patient be premedicated. In addition to premedication, a gadolinium contrast agent that differs from the one that elicited the previous reaction can be used if a future contrast-enhanced MRI scan is deemed clinically important.

Nephrogenic Systemic Fibrosis

Nephrogenic systemic fibrosis is a progressive and sometimes fatal disease seen in patients with reduced renal function who have received gadolinium contrast. The disease results in fibrosis of the skin and connective tissues throughout the body, including muscles of the extremities or abdomen, the diaphragm, and pulmonary vessels. The exact mechanism is unknown; however, it is speculated that decreased renal clearance results in accumulating free ion levels and toxicity to the tissues. Gadolinium has been detected in the soft tissues of several patients with nephrogenic systemic fibrosis who were exposed to it as a radiographic contrast agent, supporting its association with this disease.³⁶ The efficacy of hemodialysis to help prevent the disease is still unknown.

Originally it was thought that nephrogenic systemic fibrosis could occur in patients with less severe renal dysfunction and with superimposed liver disease, such as with hepatorenal syndrome or in a perioperative liver transplant period. Hepatic disease in and of itself, in the absence of acute or chronic kidney disease, is no longer considered a risk factor for nephrogenic systemic fibrosis. By current estimations, patients with an eGFR of <30 mL/min/ 1.73 m² have a 1% to 7% chance of developing nephrogenic systemic fibrosis after one or more exposures to gadolinium.³⁷

Since it was first described, there have been at least 380 confirmed cases of nephrogenic systemic fibrosis listed in an international pathology registry,³⁸ with more reported cases elsewhere.³⁹ Nephrogenic systemic fibrosis has been associated with the following FDA-approved gadolinium agents: Gadavist (Bayer Healthcare Pharmaceuticals, Berlin, Germany), Magnevist (Bayer Healthcare Pharmaceuticals), Multihance (Bracco Diagnostics, Singen, Germany), Omniscan (GE Healthcare, Oslo, Norway), Optimark (Mallinckrodt, St. Louis, MO), and Prohance (Bracco Diagnostics). In the most recent update from the FDA in 2010, Magnevist, Omniscan, and Optimark were associated with a higher risk of nephrogenic systemic fibrosis than the other agents and consequently are contraindicated in patients with an eGFR of <30 mL/min/ 1.73 m².⁴⁰

The American College of Radiology warns against using gadolinium contrast agents in patients with an eGFR of <45 mL/min/ 1.73 m² and in patients with acute kidney injury, regardless of calculated eGFR, because there could be rapid fluctuations in kidney function.³⁷ In most institutions, the benefits of the gadolinium administration are weighed against the risk for patients with eGFRs between 30 and 60 mL/min/ 1.73 m². At the

authors' institutions, a creatinine/eGFR measurement is currently obtained for patients at risk for renal dysfunction, including those ≥ 60 years old or with a history of diabetes, those with renal disease or transplantation, and those with hepatorenal syndrome.

Pregnancy and Contrast

In pregnant patients, contrast agents cross the placenta, enter the fetal collecting system, and then are excreted into the amniotic fluid. To the authors' knowledge, no studies show the clearance rate of MRI contrast agents in the fetus, but it is possible that a chelated gadolinium agent could stay within the amniotic fluid long enough to allow toxic free ions to accumulate. Gadolinium-based intravenous MR contrast is labeled by the FDA as a category C medication; that is, there is a lack of controlled studies with which to evaluate the effects. Contrast is generally not administered to pregnant patients unless the potential benefit outweighs its risks and unless written, informed consent has been obtained.^{37,41} The theoretic risk of free ion accumulation is smaller if the agent is administered toward the end of gestation in the third trimester, leaving less time for dissociation and accumulation of free ions before fetus delivery.

When a breastfeeding mother receives contrast, it is expected that most of the contrast will have cleared by 24 h, leaving minimal residual contrast ($<1\%$) to be excreted into the breast milk.^{37,41} Although this is a low residual, a breastfeeding mother should be given information about abstaining from breastfeeding for 24 h and to pump and discard breast milk for this time period.

Other Special Populations and Contrast

Other patient populations have a theoretic risk of toxicity from gadolinium, although no direct clinical evidence has been established. For example, patients with elevated levels of copper (such as those with Wilson disease) or zinc may have increased free ion accumulation after contrast administration because these metals may compete with gadolinium for the chelate. Previous studies have shown that fully deoxygenated sickle erythrocytes align perpendicular to the magnetic field.^{42,43} It has been suspected that this alignment could be exacerbated by the administration of gadolinium, possibly leading to the slowing of flow and vasoocclusive crisis in patients with sickle cell disease.^{42,43} However, to the authors' knowledge, there is no documented clinical evidence to suggest that these agents can precipitate a sickle cell crisis.³⁷

■ Claustrophobia

The key to obtaining an informative MRI study is a cooperative patient who is able to remain still for the duration of the examination. Scanning an uncooperative patient often leads to poor image quality with motion artifact, and it increases the anxiety level of the individual for future examinations. It is important to identify claustrophobic patients who may be unable to tolerate the examination and to determine whether sedation is needed. In some cases, patients' fears and anxieties may be alleviated by being told they can communicate with the technicians via an intercom and can stop the examination if needed. A benzodiazepine, such as diazepam, may be used to sedate a nervous patient, with additional monitoring provided by the nursing staff. Occasionally, a patient may be unable to tolerate imaging, even with sedation. In such cases, an open (unenclosed) or wide-bore MRI examination might be best. However, image quality may be sacrificed in this procedure because of the lower field strength of some of these open/semi-open MRI systems.

■ Summary

Although MRI facilities are mandated to present patients with a prescreening checklist, the referring physician can prevent the need to reschedule the patient or abort the procedure by beginning the screening process and alleviating some of the concerns or fears the patient may have regarding the examination. It is imperative that physicians be familiar with the few absolute contraindications to MRI and identify patients for whom additional information is needed. Furthermore, brief questions to screen for claustrophobia, pregnancy, and known gadolinium contrast allergy, combined with identifying potential safety hazards via knowledge of the patient's history that might put the patient at risk during an examination, can facilitate obtaining the most informative and the safest study possible.

COMMON CLINICAL QUESTIONS

- Which is correct regarding image quality in the MRI scanner?
 - The static magnetic field aligns oxygen atoms within the body.
 - A homogenous magnetic field surrounding the patient is needed for optimal image quality.
 - Platinum causes more distortion in the magnetic field than iron.
 - The baseline static magnetic field of the MRI scanner is weaker than the time-varying magnetic fields applied during the examination.
- All of the following implants are absolute contraindications to MRI scanning except:
 - Stainless steel brain aneurysm clips
 - Swan-Ganz thermodilution catheters
 - Bilateral rod and pedicle screw spine fixation
 - Poppen-Blaylock carotid artery clamps
- Regarding pregnant/postpartum patients:
 - A pregnant patient may be scanned only in the third trimester.
 - Contrast agents do not enter the amniotic fluid.
 - A patient must stop breastfeeding for 1 week after receiving intravenous gadolinium.
 - Written informed consent is usually obtained before a pregnant patient enters the scanner.
- Which of the following is true regarding gadolinium contrast agents?
 - Most gadolinium contrast agents are processed mainly through the liver.
 - A patient who has had an adverse reaction to gadolinium contrast with hives should not receive contrast again.
 - Patients with a history of a reaction to ionic contrast for a CT scan and multiple medicine allergies are at a higher risk for having a reaction to gadolinium administration.
 - Twenty percent of patients will have an adverse reaction to gadolinium contrast.
- Which is true regarding nephrogenic systemic fibrosis?
 - It can be cured with dialysis.
 - Gadolinium has been identified in the soft tissue of patients with nephrogenic systemic fibrosis.
 - It is typically seen in patients with an eGFR of 50 to 70 mL/min/1.73 m².

References

- Westbrook C, Roth CK, Talbot J. MRI safety. In: *MRI in Practice*. 3rd ed. Oxford: Blackwell Publishing; 2005:329–351
- U. S. Food and Drug Administration. Guidance for industry and FDA staff: criteria for significant risk investigations of magnetic resonance diagnostic devices. Available at <http://www.fda.gov/MedicalDevices/DeviceRegulationandGuidance/GuidanceDocuments/ucm072686.htm>. Accessed July 17, 2013
- Schenck JF. Health effects and safety of static magnetic fields. In: Shellock FG, ed. *Magnetic Resonance Procedures: Health Effects and Safety*. Boca Raton, FL: CRC Press; 2001:1–29
- Shellock FG, Schaefer DJ, Crues JV. Exposure to a 1.5-T static magnetic field does not alter body and skin temperatures in man. *Magn Reson Med* 1989;11(3):371–375 PubMed
- Shellock FG, Schaefer DJ, Gordon CJ. Effect of a 1.5 T static magnetic field on body temperature of man. *Magn Reson Med* 1986;3(4):644–647 PubMed
- Chakeres DW, Kangarlu A, Boudoulas H, Young DC. Effect of static magnetic field exposure of up to 8 tesla on sequential human vital sign measurements. *J Magn Reson Imaging* 2003;18(3):346–352 PubMed
- Chakeres DW, de Vocht F. Static magnetic field effects on human subjects related to magnetic resonance imaging systems. *Prog Biophys Mol Biol* 2005;87(2-3):255–265 PubMed
- Schenck JF, Dumoulin CL, Redington RW, Kressel HY, Elliott RT, McDougall IL. Human exposure to 4.0-tesla magnetic fields in a whole-body scanner. *Med Phys* 1992;19(4):1089–1098 PubMed
- Shellock FG, Crues JV. MR procedures: biologic effects, safety, and patient care. *Radiology* 2004;232(3):635–652 PubMed
- Boutin RD, Briggs JE, Williamson MR. Injuries associated with MR imaging: survey of safety records and methods used to screen patients for metallic foreign bodies before imaging. *AJR Am J Roentgenol* 1994;162(1):189–194 PubMed
- Klucznik RP, Carrier DA, Pyka R, Haid RW. Placement of a ferromagnetic intracerebral aneurysm clip in a magnetic field with a fatal outcome. *Radiology* 1993;187(3):855–856 PubMed
- Kelly WM, Paglen PG, Pearson JA, San Diego AG, Soloman MA. Ferromagnetism of intraocular foreign body causes unilateral blindness after MR study. *AJNR Am J Neuroradiol* 1986;7(2):243–245 PubMed
- Seidenwurm DJ, McDonnell CH III, Raghavan N, Breslau J. Cost utility analysis of radiographic screening for an orbital foreign body before MR imaging. *AJNR Am J Neuroradiol* 2000;21(2):426–433 PubMed
- Teitelbaum GP, Yee CA, Van Horn DD, Kim HS, Colletti PM. Metallic ballistic fragments: MR imaging safety and artifacts. *Radiology* 1990;175(3):855–859 PubMed
- Dyer RK Jr, Nakmali D, Dormer KJ. Magnetic resonance imaging compatibility and safety of the SOUNDTEC Direct System. *Laryngoscope* 2006;116(8):1321–1333 PubMed
- Jung W, Zvereva V, Hajredini B, Jäckle S. Safe magnetic resonance image scanning of the pacemaker patient: current technologies and future directions. *Europace* 2012;14(5):631–637 PubMed
- Kanal E, Barkovich AJ, Bell C, et al. ACR guidance document on MR safe practices: 2013. *J Magn Reson Imaging* 2013;37(3):501–530 PubMed
- Martinelli M. Magnetic resonance imaging and cardiac implantable electronic devices: safety barrier overtaken—is the image quality the current target? *Heart Rhythm* 2013;10(6):873–874 PubMed
- Nazarian S, Hansford R, Roguin A, et al. A prospective evaluation of a protocol for magnetic resonance imaging of patients with implanted cardiac devices. *Ann Intern Med* 2011;155(7):415–424; W-121–W-122 PubMed
- Santini L, Forleo GB, Santini M; World Society of Arrhythmias. Evaluating MRI-compatible pacemakers: patient data now paves the way to widespread clinical application? *Pacing Clin Electrophysiol* 2013;36(3):270–278 PubMed
- Sommer T, Naehle CP, Yang A, et al. Strategy for safe performance of extrathoracic magnetic resonance imaging at 1.5 tesla in the presence of cardiac pacemakers in non-pacemaker-dependent patients: a prospective study with 115 examinations. *Circulation* 2006;114(12):1285–1292 PubMed
- Shellock FG. Heart valve prostheses and annuloplasty rings. In: *Reference Manual for Magnetic Resonance Safety, Implants, and Devices: 2007 Edition*. Los Angeles, CA: Biomedical Research Publishing Group; 2007:224–226
- Hartnell GG, Spence L, Hughes LA, Cohen MC, Saouaf R, Buff B. Safety of MR imaging in patients who have retained metallic materials after cardiac surgery. *AJR Am J Roentgenol* 1997;168(5):1157–1159 PubMed
- Shellock FG. Epicardial pacing leads and intracardiac pacing leads. In: *Reference Manual for Magnetic Resonance Safety, Implants, and Devices: 2013 Edition*. Los Angeles, CA: Biomedical Research Publishing Group; 2013:36–38
- Shellock FG, Shellock VJ. Metallic stents: evaluation of MR imaging safety. *AJR Am J Roentgenol* 1999;173(3):543–547 PubMed
- Teitelbaum GP, Bradley WG Jr, Klein BD. MR imaging artifacts, ferromagnetism, and magnetic torque of intravascular filters, stents, and coils. *Radiology* 1988;166(3):657–664 PubMed
- Pride GL Jr, Kowal J, Mendelsohn DB, Chason DP, Fleckenstein JL. Safety of MR scanning in patients with nonferromagnetic aneurysm clips. *J Magn Reson Imaging* 2000;12(1):198–200 PubMed
- Shellock FG. Section II: MR procedures and implants, devices, and materials. In: *Reference Manual for Magnetic Resonance Safety, Implants, and Devices: 2007 Edition*. Los Angeles: Biomedical Research Publishing Group; 2007:125–315
- Tope WD, Shellock FG. Magnetic resonance imaging and permanent cosmetics (tattoos): survey of complications and adverse events. *J Magn Reson Imaging* 2002;15(2):180–184 PubMed
- United States Health Care Administration. Tattoos and Permanent Makeup. Rockville, MD: U.S. Food and Drug Administration; 2006
- Chaljub G, Kramer LA, Johnson RF III, Johnson RF Jr, Singh H, Crow WN. Projectile cylinder accidents resulting from the presence of ferromagnetic nitrous oxide or oxygen tanks in the MR suite. *AJR Am J Roentgenol* 2001;177(1):27–30 PubMed
- Colletti PM. Size “H” oxygen cylinder: accidental MR projectile at 1.5 tesla. *J Magn Reson Imaging* 2004;19(1):141–143 PubMed
- United States Health Care Administration—Center for Devices and Radiological Health. MRI safety. Available at <http://www.fda.gov/cdrh/safety/mrisafety.html>. Accessed on May 7, 2013
- Dillman JR, Ellis JH, Cohan RH, Strouse PJ, Jan SC. Frequency and severity of acute allergic-like reactions to gadolinium

- ium-containing IV contrast media in children and adults. *AJR Am J Roentgenol* 2007;189(6):1533–1538 PubMed
35. Nelson KL, Gifford LM, Lauber-Huber C, Gross CA, Lasser TA. Clinical safety of gadopentetate dimeglumine. *Radiology* 1995;196(2):439–443 PubMed
 36. High WA, Ayers RA, Chandler J, Zito G, Cowper SE. Gadolinium is detectable within the tissue of patients with nephrogenic systemic fibrosis. *J Am Acad Dermatol* 2007;56(1):21–26 PubMed
 37. ACR Committee on Drugs and Contrast Media. ACR Manual on Contrast Media: Version 8. Available at <http://www.acr.org/~media/ACR/Documents/PDF/QualitySafety/Resources/Contrast%20Manual/FullManual.pdf>. Accessed on May 2, 2012
 38. Cowper SE. Nephrogenic systemic fibrosis (The International Center for Nephrogenic Systemic Fibrosis Research [ICNSFR] website), 2001–2013. Available at <http://www.icnsfr.org>. Accessed on July 17, 2013
 39. Krefting I. Gadolinium-based contrast agents (GB-CAs) and the NSF Risk: Regulatory Update. Available at <http://www.fda.gov/downloads/AdvisoryCommittees/CommitteesMeetingMaterials/Drugs/PeripheralandCentralNervousSystemDrugsAdvisoryCommittee/UCM241072.pdf>. Accessed on July 17, 2013
 40. U.S. Food and Drug Administration. Information for health-care professionals: gadolinium-based contrast agents for magnetic resonance imaging (marketed as Magnevist, MultiHance, Omniscan, OptiMARK, ProHance). Available at <http://www.fda.gov/Drugs/DrugSafety/PostmarketDrugSafetyInformationforPatientsandProviders/ucm142884.htm>. Accessed on May 2, 2013
 41. Kubik-Huch RA, Gottstein-Aalame NM, Frenzel T, et al. Gadopentetate dimeglumine excretion into human breast milk during lactation. *Radiology* 2000;216(2):555–558 PubMed
 42. Brody AS, Embury SH, Mentzer WC, Winkler ML, Gooding CA. Preservation of sickle cell blood-flow patterns during MR imaging: an in vivo study. *AJR Am J Roentgenol* 1988;151(1):139–141 PubMed
 43. Brody AS, Sorette MP, Gooding CA, et al. AUR Memorial Award. Induced alignment of flowing sickle erythrocytes in a magnetic field. A preliminary report. *Invest Radiol* 1985;20(6):560–566 PubMed

ANSWERS TO COMMON CLINICAL QUESTIONS

1. B
Explanation: The key to image quality is homogeneity within the magnetic field. Ferromagnetic materials such as iron result in the greatest distortion of images. The patient is exposed to two magnetic fields within the scanner environment: the stronger is the baseline static field, and the weaker is the time-varying or gradient magnetic field. The static magnetic field aligns hydrogen atoms within the body.
2. C
Explanation: Metallic objects implanted firmly in bone are not at risk for movement during scanning, although they can result in substantial distortion of images.
3. D
Explanation: After MRI scanning is determined to be a medical necessity, written informed consent is typically obtained. There are theoretical concerns that MRI could disrupt cell division at any stage in pregnancy and that, because cell division is more rapid in the first trimester, there would be a greater potential risk. However, on a case-by-case basis, weighing the risks and benefits, patients in all trimesters can be scanned. Contrast agents do enter the amniotic fluid and are administered to pregnant patients in rare circumstances. Typically, a breastfeeding mother is given the option to abstain from breastfeeding /discard breast milk for 24 h after IV gadolinium contrast.
4. C
Explanation: In general, patients with multiple medicine allergies, including previous ionic CT contrast dye allergy, are at a higher risk for reaction to gadolinium administration. Patients who have a history of isolated hives (i.e., no shortness of breath or anaphylaxis), can receive gadolinium again after premedication, typically with prednisone and diphenhydramine. Less than 1% of patients who receive gadolinium will have an adverse reaction. Gadolinium contrast dyes are primarily excreted through the kidney.
5. B
Explanation: Nephrogenic systemic fibrosis results in progressive fibrosis of the skin and connective tissue throughout the body in patients who have received gadolinium contrast and have reduced renal function. It can be fatal and is without a known cure. Gadolinium has been detected in the soft tissues. Patients typically have an eGFR of <30 mL/min/1.73 m².

Glossary

Abbreviation	Definition
2D	two-dimensional
3D	three-dimensional
AP	anteroposterior
CSF	cerebrospinal fluid
CT	computed tomography
eGFR	estimated glomerular filtration rate
FDA	Food and Drug Administration
^{18}F -FDG	2-deoxy-2- (^{18}F) fluoro-D-glucose
FSE	fast spin echo
MR	magnetic resonance
MRI	magnetic resonance imaging
OCJ	occipitocervical junction
PA	posteroanterior
PET	positron emission tomography
RA	rheumatoid arthritis
RF	radiofrequency
SE	spin echo
STIR	short tau (or T1) inversion recovery
TE	echo time
TR	repetition time
TSE	turbo-spin echo

Index

An “f” or “t” after a page number indicates a figure or table, respectively.

1.5-T magnets, 253
3.0-T magnets, 253, 254f, 255

A

abscess, epidural
 cervical, 144–145
 lumbar, 195–196, 195f
 pediatric, 242f
acquired immune deficiency syndrome, 146
acute transverse myelopathy, 146
adolescent spine anatomy, 238–240, 239f
AIDS. *See* acquired immune deficiency syndrome
Allen-Ferguson classification system, 113, 114f
amyloidosis, 149
aneurysmal bone cyst, 97–98, 219, 220f
angiography. *See* MR angiography
angioliipoma, 224
ankylosing spondylitis, 121f, 149
annular fissure, 62
 images, 12f, 63f
annular tear, 131f, 166, 166f, 171–172, 172f
annulus, 20
arachnoiditis, 203, 204f
arteries, 25, 31–32, 32f, 33f
 of the lumbar spine, 31f
 of the thoracic spine, 24f
 of the upper cervical spine, 31f
 vertebral artery, 30f
 injury, 124, 126f
arthritis. *See* psoriatic arthritis; rheumatoid arthritis
artifacts, in MRI, 14–15, 17f, 261–262, 262f
astrocytoma, low-grade, 229, 231–232
atlantoaxial instability, 124, 125f
atlantooccipital dissociation, 121, 123
atlas (C1)
 congenital anomalies, 93
 trauma, 101, 101f, 123
axis (C2)
 congenital anomalies, 93–94
 trauma, 101, 101f, 123, 123f

B

bacterial infections, of the spinal cord, 146, 148
Bergman ossicle, 94
biopsy, musculoskeletal, MR-guided, 262
bone cyst, aneurysmal, 97–98, 219, 220f
bone marrow, 10f

bone scans, 273–274, 275
burst fracture
 cervical, 122f
 thoracolumbar, 162

C

C5 nerve root, 48–49, 50f, 52f
C6 nerve root, 49, 51f, 52f
C7 nerve root, 52, 54f
C8 nerve root, 55, 55f
calcium pyrophosphate dihydrate deposition disease, 149
cauda equina syndrome, 187–188
cerebrospinal fluid (CSF), 12f, 24, 69
cervical disc radiculopathy, 47–48
cervical scoliosis, 39
cervical spine
 anatomy, 33, 35f, 36f, 238–239
arthropathies
 amyloidosis, 149
 ankylosing spondylitis, 149
 calcium pyrophosphate dihydrate deposition disease, 149
 gout, 149
 psoriatic arthritis, 149
 RA, 148–149, 148f
degenerative conditions
 disc disease, 129, 130f, 130t
 disc displacement. *See* disc displacement
 imaging techniques, 129
fractures, 115f, 122f
imaging, 15f, 35f, 36f, 36–39
imaging protocols, 111–112, 150
infections
 discitis, 143–144, 144f
 epidural abscess, 144–145
 generally, 142–143
 intradural, 145
 osteomyelitis, 143–144, 144f
 postoperative, 144
MRI
 axial, 38–39
 coronal, 39
 sagittal, 36–37
myelopathies
 acute transverse, 146
 bacterial infections, 146, 148
 granulomatous infections, 146, 148
 human immunodeficiency virus, 146

cervical spine
 myelopathies (*continued*)
 multiple sclerosis plaques, 146, 147f
 nitrous oxide poisoning, 148
 parasitic infections, 146, 148
 subacute necrotizing, 146
 vacuolar, 146
 viral infections, 146
 vitamin B12 deficiency, 148
 stenosis, 136f, 139f
 acquired, 136, 137t
 congenital, 136, 137f, 137t
 contributing factors, 138f
 degenerative, 136, 137f
 measures of, 138, 140, 140f, 141f
 MRI findings, 138
 T2-weighted images, review of, 70, 72, 73f, 74f, 75f
 trauma
 axial load injuries, 119, 121, 122f
 burst fracture, 122f
 characterization of, 124–125
 classification, 113, 114f
 evaluation, 113t
 facet dislocation, 117, 117f, 118f
 hyperextension injuries, 118–119, 120f, 121f
 hyperflexion injuries, 113, 116f, 117–118, 119f
 imaging protocols, 112–113
 ligament injuries, 127–129, 128f
 OCJ injuries, 121–124
 penetrating trauma, 124
 vertebral artery injury, 124, 126f
 tumors. *See* tumors
 Chamberlain's line, 87, 88t, 89f, 90f
 Chiari malformations
 pediatric, 246
 type-I, 93f, 94, 95f
 type-II, 89f, 94, 95f
 type-III, 96
 type-IV, 96
 child(ren), spinal anatomy. *See also* pediatric spine
 age 2 years, 240, 241f
 age 3 months, 240
 age 10 years, 240, 241f
 infant, full-term, 240
 chondrosarcoma, 222, 223f
 chordoma, 97, 220, 222
 claustrophobia, 285
 clivus canal angle, 88t
 coccyx, 43
 computed tomography (CT), 272, 273f
 contrast-enhanced imaging, 14
 conus medullaris, 240
 conventional radiography, 267–272
 cranial settling, 96–97, 96f
 craniometry, of the OCJ, 87–88, 88t
 cryotherapy, MR-guided, 263

CSF (cerebrospinal fluid), 12f, 24, 69
 CT (computed tomography), 272, 273f

D

Denis three-column concept, 158, 160, 161f
 dermatome map, 53
 diabetes, spinal infection with, 143
 diastematomyelia, 190
 disc
 anatomy, 20
 dessication, 12f, 46f
 disease, degenerative
 cervical, 129, 130f
 lumbar, 168, 169, 171f
 displacement
 anatomy, 131
 bulge, 132f, 172, 172f
 disc-ridge complex, 132
 extrusion, 133f, 168f, 172, 173f, 174
 protrusion, 15f, 132f, 168f, 172, 172f, 174, 175f, 176f, 177f, 178f–179f
 soft vs hard, 132, 133f, 179
 herniation
 central, 63
 morphology, 47f, 180f
 recurrent, 15f
 pathology, 47, 179, 180f
 prevalence, 45, 179
 recurrent, 199, 199f
 lesions, 166
 pathology
 nomenclature, 164–168
 herniations, 166–167, 166f, 167f, 168f
 spondylosing deformans, 166f
 rupture, 120f
 discitis
 cervical, 143–144, 144f
 imaging choices, 143
 lumbar, 193f, 194, 194f
 pediatric, 240, 242
 discogenic axial back pain, 61–62
 discography, 272–273
 Down syndrome, 101, 101f, 102f
 dynamic (functional) imaging, 256
 dysraphism, spinal, 243–246, 245t

E

echo time (TE), 7–8
 end plate, 20
 end-plate changes, degenerative, 62
 Modic type-I, 62, 62f, 169, 169f
 Modic type-II, 62, 169, 170f
 Modic type-III, 62, 169, 170f
 eosinophilic granuloma, 219, 221f
 ependymoma, 98, 100f, 229, 230f, 231–232, 231f

epidural
 abscess
 cervical, 144–145
 lumbar, 195–196, 195f
 pediatric, 242f
 fibrosis, 16f
 hematomas
 postoperative, 202, 202f
 thoracolumbar, 162–163
 lipomatosis, lumbar, 11f, 191, 192f
 space, anatomy, 24
 Ewing sarcoma, 222

F

facet joint
 anatomy, 25, 30f
 arthropathy, 181–182, 181f, 182f
 Renfrew and Heithoff classification, 182, 182f
 dislocations, 117, 117f, 118f
 synovitis, 64f
 Fardon and Milette classification, 169
 fibrosis, epidural, 16f
 foramina, spinal, anatomy, 25
 Fourier analysis, 5
 fractures, 115f, 116f, 122f, 123, 123f, 162

G

gadolinium contrast, 14, 283–284
 giant cell tumor, 97, 217, 218f
 Gibbs phenomenon, 112
 glial tumors, 98
 gout, 149
 gradient coils, 7
 gradient-echo images
 3D, 14
 advantages, 10t, 13
 disadvantages, 10t, 13
 sequence, 7–8, 8f
 granuloma, eosinophilic, 219, 221f
 granulomatous infections, of the spinal cord, 146, 148

H

Harris technique, 101, 103f
 hemangioblastoma, 98, 232, 232f
 hemangioma, 97, 214–215, 216f
 hemangiopericytoma, 98, 227
 hematomas, epidural
 postoperative, 202, 202f
 thoracolumbar, 162–163
 hemilaminotomy, MRI after, 198f
 herniated nucleus pulposus. *See* nucleus pulposus, herniated
 high-intensity zones, 62, 164f

human immunodeficiency syndrome myelopathy, 146

I

implants, metallic, MRI and, 261–262, 262f, 281–283
 infant(s), spinal anatomy. *See also* pediatric spine
 age 3 months, 240
 full-term, 240
 intermediate-weighted images, 10t
 intervertebral discs. *See* disc
 intervertebral osteochondrosis, 166f
 intradural infections, 145
 intramedullary metastases, 232
 intraoperative MRI, 256
 inversion time (TI), 8

J

Jefferson burst fracture, 123
 juvenile RA, 149

K

Klippel-Feil syndrome, 96

L

L4 nerve root, 59, 59f
 L5 nerve root, 60, 60f
 Larmor equation, 5, 6f, 7
 leptomeningeal infection, spinal, 145
 ligaments, spinal
 anatomy, 25, 27f, 28f
 cervical injuries, 127–129, 128f
 posterior ligamentous complex, evaluation of, 161, 162f
 posterior longitudinal ligament, ossification of, 134f–135f
 tears, 118, 119f
 limbus vertebra, 20f
 lipomatosis, epidural, 11f, 191, 192f
 lipomeningocele, 243
 low-grade astrocytoma, 229, 231–232
 lumbar disc radiculopathy, 56, 57f, 58–61, 58f
 lumbar spine. *See also* thoracolumbar spine
 anatomy, 39, 56, 238
 annular tears, 131f, 166, 166f, 171–172, 172f
 cauda equina syndrome, 187–188
 disc degeneration, 168–171
 disc displacement
 bulge, 172, 172f
 extrusion, 172, 173f, 174
 protrusion, 172, 172f, 174, 175f, 176f, 177f, 178f–179f
 soft vs hard, 179

lumbar spine (*continued*)
 disc herniation
 morphology, 180f
 pathology, 179, 180f
 prevalence, 179
 disc pathology, 164–168
 epidural lipomatosis, 11f, 191, 192f
 facet arthropathy, 181–182, 181f, 182f
 herniated nucleus pulposus, 57f, 172–174, 175f, 176f, 177f, 178f, 179, 179f, 180f
 infections
 discitis, 193f, 194, 194f
 epidural abscess, 195–196, 195f
 osteomyelitis, 192–194
 spondylodiscitis, 194
 tuberculosis, 196, 197f
 MRI
 axial, 41–42, 42f
 coronal, 42
 postoperative findings, 196–203
 sagittal, 40, 40f, 41f
 nomenclature, 164–168
 scoliosis
 imaging protocols, 189–190
 MRI findings, 190–191, 191f
 spondylolisthesis
 Meyerding classification, 188, 188f, 189f
 MRI findings, 188–189
 Wiltse classification, 188–189, 190f
 stenosis, 168, 185f, 186f
 developmental, 184, 185
 hereditary, 184, 184f
 measures of, 185
 sedimentation sign, 185, 186f, 187, 187f
 synovial cysts, 183–184, 183f
 T2-weighted images, review of, 72, 76, 76f, 77f, 78f
 lymphoma, 224, 225f

M

magnetic dipoles, 3, 4f
 magnetic field effects, 280–281
 magnetic resonance imaging. *See* MRI
 malignant peripheral nerve sheath tumor, 226–227, 229f
 McGregor's line, 87–88, 88t, 89f
 McRae's line, 88, 88t, 89f
 meningioma, 98, 224–225, 226f
 metallic objects
 MRI and, 261–262, 262f, 281–283
 safety profiles, 282–283
 metastasis, 213–214, 214f, 232
 Meyerding classification, 188, 188f, 189f
 Modic end-plate changes
 type-I, 62, 62f, 169, 169f
 type-II, 62, 169, 170f
 type-III, 62, 169, 170f
 MR (magnetic resonance) angiography, 70, 112

MR (magnetic resonance)-guided interventions
 cryotherapy, 263
 musculoskeletal biopsy, 262, 263f
 pain management, 263
 MRI (magnetic resonance imaging)
 artifacts, 14–15, 17f, 261–262, 262f
 axial, 38–39
 and claustrophobia, 285
 contrast agents, 283–284
 coronal, 39
 dynamic, 256
 fundamentals, 3–9, 16–17
 intraoperative, 256
 load bearing, 256, 257f, 258f, 259f
 with metallic implants, 261–262, 262f
 positional, 256
 and pregnancy, 283, 284
 pulse sequences, 7–9, 9f, 10t, 69, 259, 260f, 261
 sagittal, 36–37
 studies, review of, 68–69. *See also* T1-weighted images; T2-weighted images
 systems
 3.0-T magnets, 253, 254f, 255
 open-bore, 255
 parallel imaging, 255
 multiple myeloma, 219, 221f
 multiple sclerosis, 146, 147f
 muscles, paraspinal, 32–33, 34f
 musculoskeletal biopsy, MR-guided, 262
Mycobacterium tuberculosis, 143
 myelography, 272
 myelomalacia, 127f
 myeloma, multiple, 219, 221f
 myelomeningoceles, 243, 244f
 myelopathies. *See* cervical spine, myelopathies

N

nephrogenic systemic fibrosis (NSF), 284
 nerve roots. *See specific nerve roots*
 nerve sheath tumor, malignant peripheral, 226–227, 229f
 nerves, spinal, anatomy, 25, 29f
 neuroblastic tumors, 222–223, 224f
 neurofibroma, 98, 226, 228f
 neurofibromatosis, 191
 neurologic examination, 46–47
 nitrous oxide poisoning, 148
 NSF (nephrogenic systemic fibrosis), 284
 nuclear scintigraphy, 273–274, 275
 nucleus pulposus, herniated, 57f, 172–174, 175f, 176f, 177f, 178f, 179, 179f, 180f

O

occipitocervical junction (OCJ)
 acquired conditions
 basilar impression, 96

cranial settling, 96–97, 96f
 tumors, 97–98, 99f, 100f
 anatomy, 88, 91
 atlantoaxial dissociation, 124, 125f
 atlantooccipital dissociation, 121, 123
 atlas trauma, 123
 axis trauma, 123, 123f
 congenital anomalies
 of the atlas, 93
 of the axis, 93–94
 Chiari malformations. *See* Chiari malformations
 Klippel-Feil syndrome, 96
 of the occiput, 91–92
 os odontoideum, 36f, 94, 94f
 craniometry, 87–88, 88t
 Down syndrome, 101, 101f, 102f
 imaging protocols, 88, 91
 trauma
 to the atlas, 101, 105f
 to the axis, 101, 105f
 Harris technique, 101, 103f
 occipitocervical, 101
 Powers ratio, 101, 103f
 spondylolisthesis, 106
 tumors. *See* tumors
 OCJ. *See* occipitocervical junction
 odontoid fracture, type-II, 123, 123f
 os odontoideum, 36f, 94, 94f
 ossification of the posterior longitudinal ligament,
 134f–135f
 osteoblastoma, 97–98, 216, 216f, 218f
 osteochondritis, 166f
 osteochondroma, 219
 osteogenic sarcoma, 222
 osteoid osteoma, 97–98, 215–216, 217f
 osteomyelitis
 cervical, 143–144, 144f
 imaging choices, 143
 lumbar, 192–194

P

pain, biochemical basis of, 46
 pain management injections, MR-guided, 263
 pannus formation, 92f, 142
 parallel imaging, 255
 parasitic infections, of the spinal cord, 146, 148
 paraspinal muscles, 32–33, 34f
 pars defect, 191
 pediatric spine
 and adult spine, differences between, 239–240
 anatomy, 238–240, 239f
 Chiari malformations, 246
 conus medullaris, 240, 241f
 imaging protocols, 237
 with implants, imaging controversies, 247, 248f
 infections, 240, 242, 242f
 MRI, controversies with, 246–247

sedation protocols, 237–238
 spinal dysraphism, 243–246, 245t
 Chiari malformations, 246
 tethered cord syndrome, 246, 247f
 trauma, 242–243, 243f
 PET (positron emission tomography), 274, 276f
 plasmacytoma, solitary bone, 219
 platybasia, 90f
 positron emission tomography (PET), 274, 276f
 postoperative infections, 144
 postoperative MRI findings
 after decompression without instrumentation/
 fusion, 196–199
 after hemilaminotomy, 198f
 after instrumentation/fusion, 200–201
 arachnoiditis, 203, 204f
 hematoma, 202, 202f
 pseudomeningocele, 202–203, 203f
 recurrent disc herniations, 199, 199f
 retropulsed interbody device, 201f
 Powers ratio, 101, 103f
 pregnancy, MRI and, 283, 284
 pseudomeningocele, 202–203, 203f
 psoriatic arthritis, 149

Q

quadrangular fracture, 116f

R

RA. *See* rheumatoid arthritis
 radiography, conventional, 267–272
 Ranawat's criterion, 88, 88t, 89f
 Renfrew and Heithoff classification, 182, 182f
 repetition time (TR), 8
 RF (radio frequency) pulse, 5, 6f, 7f
 rheumatoid arthritis (RA)
 cervical spine involvement, 141–142, 142f,
 148–149, 148f
 pannus formation, 92f, 142
 cranial settling, 96–97, 96f
 juvenile, 149
 spinal infections, 143

S

S1 nerve root, 60–61, 61f
 sacroiliac joint, 43, 43f
 sacrum, 42
 sarcomas, 97, 222
 Ewing, 222
 osteogenic, 222
 osteosarcoma, 222, 223f
 Scheuermann disease, 179
 Schmorl nodes
 anatomy, 20, 181
 images, 24f

schwannoma, 98, 99f, 225–226, 227f
 scoliosis
 cervical spine involvement, 39
 imaging protocols, 189–190
 MRI, controversies with, 246–247
 MRI findings, 190–191, 191f
 sedation protocols, in pediatric MRI, 237–238
 SEMAC (slice encoding for metal artifact correction), 261–262
 Sharpey fibers, 20
 short tau (or T1) inversion recovery (STIR) images, 8, 11f, 13, 69, 70f
 signal localization, 7
 slice encoding for metal artifact correction, 261–262
 solitary bone plasmacytoma, 219
 spinal column, anatomy, 19
 spinal cord
 anatomy, 25, 26f, 28f, 38f
 infections, 146, 148
 spinal stability, assessment of
 Denis three-column concept, 158, 160, 161f
 posterior ligamentous complex, 161
 spinal stenosis
 cervical, 136f, 139f
 acquired, 136, 137t
 congenital, 136, 137f, 137t
 contributing factors, 138f
 degenerative, 136, 137f
 measures of, 138, 140, 140f, 141f
 MRI findings, 138
 lumbar, 168, 185f, 186f
 developmental, 184, 185
 hereditary, 184, 184f
 measures of, 185
 sedimentation sign, 185, 186f, 187, 187f
 spin-down orientation, 3, 4f
 spine anatomy, 19–33
 spin echo (SE) sequence, 7–8, 8f
 spin-up orientation, 3, 4f
 spondylodiscitis, 194
 spondylolisthesis
 Meyerding classification, 188, 188f, 189f
 MRI findings, 188–189
 in the OCJ, 106
 Wiltse classification, 188–189, 190f
 spondylosing deformans, 166f
Staphylococcus aureus, 143
 STIR (short tau [or T1] inversion recovery) images, 8, 11f, 13, 69, 70f
 subacute necrotizing myelopathy, 146
 Subaxial Injury Classification (SLIC) system, 113, 115t
 synovial cysts, 183–184, 183f
 syringohydromyelia (syrinx), 190, 244, 245f, 246

T

T1 recovery, 5, 7
 T1-weighted images
 advantages, 9, 10t, 11
 disadvantages, 10t, 11
 fat-suppressed, 13, 69
 postcontrast, 70, 71f, 80
 review of, 69, 79, 80f
 standard, 9, 11
 T2* relaxation, 5, 7
 T2 relaxation, 5, 7
 T2-weighted images
 advantages, 10t, 11–12
 disadvantages, 10t, 12–13
 fat-suppressed, 10t, 13, 69, 70f, 79–80, 81f
 pattern recognition, 76, 78–79
 review of, 69, 73–79
 Tarlov cysts, 24f
 TE. *See* echo time
 tethered cord syndrome, 246, 247f
 MRI, controversies with, 247
 thoracic spine. *See also* thoracolumbar spine
 anatomy, 39, 239
 vertebral bodies, 23f
 Thoracolumbar Injury Classification and Severity Score, 157, 157f, 158t
 thoracolumbar spine. *See also* lumbar spine;
 thoracic spine
 burst fracture, 162, 164f
 disc pathology, 162
 dislocation, 163–164, 165f
 epidural hematomas, 162
 imaging protocols, 155–156
 neural compromise, assessment of, 161–162
 translation, 163–164
 trauma
 classification of, 157
 evaluation of, 156, 156t
 fracture morphology, 157–158, 159f, 160f
 spinal stability, 158, 160–162
 TI. *See* inversion time
 TR. *See* repetition time
 trauma. *See specific anatomy*
 tuberculosis, 196, 197f
 tumors
 cervical spine, 145–146
 diagnosis, 212t
 extradural, 97, 215t
 aneurysmal bone cyst, 97–98, 219, 220f
 angiolioma, 224
 chondrosarcoma, 222, 223f
 chordoma, 97, 220, 222
 eosinophilic granuloma, 219, 221f
 Ewing sarcoma, 222

giant cell, 97, 217, 218*f*
 hemangioma, 97, 214–215, 216*f*
 lymphoma, 224, 225*f*
 metastasis, 213–214, 214*f*
 multiple myeloma, 219, 221*f*
 neuroblastic tumors, 222–223, 224*f*
 osteoblastoma, 97–98, 216, 216*f*, 218*f*
 osteochondroma, 219
 osteogenic sarcoma, 222
 osteoid osteoma, 97–98, 215–216, 217*f*
 osteosarcoma, 222, 223*f*
 sarcomas, 97, 222
 solitary bone plasmacytoma, 219
 generally, 211–212
 imaging protocols, 213
 imaging studies, 212
 intradural–extramedullary, 225*f*
 hemangiopericytoma, 98, 227
 malignant peripheral nerve sheath tumor,
 226–227, 229*f*
 meningioma, 98, 224–225, 226*f*
 neurofibroma, 98, 226, 228*f*
 schwannoma, 98, 99*f*, 225–226, 227*f*
 intramedullary, 227, 229, 229*f*
 ependymoma, 98, 100*f*, 229, 230*f*, 231–232,
 231*f*
 glial tumors, 98
 hemangioblastoma, 98, 232, 232*f*

intramedullary metastases, 232
 low-grade astrocytoma, 229, 231–232
 of the OCJ, 97–98, 99*f*, 100*f*
 prevalence, 211–212

V

vacuolar myelopathy, 146
 vertebral artery injury, 124, 126*f*
 vertebral bodies
 anatomy of, 20
 cervical, 21*f*
 lumbar, 22*f*
 thoracic, 23*f*
 vertebral fracture, 15*f*
 view angle tilting, 261–262
 viral infections, of the spinal cord, 146
 vitamin B12 deficiency, 148
 voxels, 7

W

Wackenheim's clivus baseline, 87, 88*t*, 89*f*, 90*f*
 Welcher's basal angle, 88, 88*t*, 90*f*

Z

zygapophyseal joint (z-joint), 25

